

Mollicutes: from evolution to pathogenesis, volume II

Edited by

Glenn Francis Browning, Chih-Horng Kuo, Florence Tardy,
Meghan May and Christine Citti

Published in

Frontiers in Microbiology
Frontiers in Genetics



FRONTIERS EBOOK COPYRIGHT STATEMENT

The copyright in the text of individual articles in this ebook is the property of their respective authors or their respective institutions or funders. The copyright in graphics and images within each article may be subject to copyright of other parties. In both cases this is subject to a license granted to Frontiers.

The compilation of articles constituting this ebook is the property of Frontiers.

Each article within this ebook, and the ebook itself, are published under the most recent version of the Creative Commons CC-BY licence. The version current at the date of publication of this ebook is CC-BY 4.0. If the CC-BY licence is updated, the licence granted by Frontiers is automatically updated to the new version.

When exercising any right under the CC-BY licence, Frontiers must be attributed as the original publisher of the article or ebook, as applicable.

Authors have the responsibility of ensuring that any graphics or other materials which are the property of others may be included in the CC-BY licence, but this should be checked before relying on the CC-BY licence to reproduce those materials. Any copyright notices relating to those materials must be complied with.

Copyright and source acknowledgement notices may not be removed and must be displayed in any copy, derivative work or partial copy which includes the elements in question.

All copyright, and all rights therein, are protected by national and international copyright laws. The above represents a summary only. For further information please read Frontiers' Conditions for Website Use and Copyright Statement, and the applicable CC-BY licence.

ISSN 1664-8714
ISBN 978-2-8325-5546-0
DOI 10.3389/978-2-8325-5546-0

About Frontiers

Frontiers is more than just an open access publisher of scholarly articles: it is a pioneering approach to the world of academia, radically improving the way scholarly research is managed. The grand vision of Frontiers is a world where all people have an equal opportunity to seek, share and generate knowledge. Frontiers provides immediate and permanent online open access to all its publications, but this alone is not enough to realize our grand goals.

Frontiers journal series

The Frontiers journal series is a multi-tier and interdisciplinary set of open-access, online journals, promising a paradigm shift from the current review, selection and dissemination processes in academic publishing. All Frontiers journals are driven by researchers for researchers; therefore, they constitute a service to the scholarly community. At the same time, the *Frontiers journal series* operates on a revolutionary invention, the tiered publishing system, initially addressing specific communities of scholars, and gradually climbing up to broader public understanding, thus serving the interests of the lay society, too.

Dedication to quality

Each Frontiers article is a landmark of the highest quality, thanks to genuinely collaborative interactions between authors and review editors, who include some of the world's best academicians. Research must be certified by peers before entering a stream of knowledge that may eventually reach the public - and shape society; therefore, Frontiers only applies the most rigorous and unbiased reviews. Frontiers revolutionizes research publishing by freely delivering the most outstanding research, evaluated with no bias from both the academic and social point of view. By applying the most advanced information technologies, Frontiers is catapulting scholarly publishing into a new generation.

What are Frontiers Research Topics?

Frontiers Research Topics are very popular trademarks of the *Frontiers journals series*: they are collections of at least ten articles, all centered on a particular subject. With their unique mix of varied contributions from Original Research to Review Articles, Frontiers Research Topics unify the most influential researchers, the latest key findings and historical advances in a hot research area.

Find out more on how to host your own Frontiers Research Topic or contribute to one as an author by contacting the Frontiers editorial office: frontiersin.org/about/contact

Mollicutes: from evolution to pathogenesis, volume II

Topic editors

Glenn Francis Browning — The University of Melbourne, Australia

Chih-Horng Kuo — Institute of Plant and Microbial Biology, Academia Sinica, Taiwan

Florence Tardy — Agence Nationale de Sécurité Sanitaire de l'Alimentation, de l'Environnement et du Travail (ANSES), France

Meghan May — University of New England, United States

Christine Citti — Institut National de recherche pour l'agriculture, l'alimentation et l'environnement (INRAE), France

Citation

Browning, G. F., Kuo, C.-H., Tardy, F., May, M., Citti, C., eds. (2024). *Mollicutes: from evolution to pathogenesis, volume II*. Lausanne: Frontiers Media SA.
doi: 10.3389/978-2-8325-5546-0

Table of contents

- 06 **Genital Mycoplasmas and Biomarkers of Inflammation and Their Association With Spontaneous Preterm Birth and Preterm Prelabor Rupture of Membranes: A Systematic Review and Meta-Analysis**
Nathalia M. Noda-Nicolau, Ourlad Alzeus G. Tantengco, Jossimara Poletti, Mariana C. Silva, Giovana F. C. Bento, Geovanna C. Cursino, Camila Marconi, Ronald F. Lamont, Brandie D. Taylor, Márcia G. Silva, Daniel Jupiter and Ramkumar Menon
- 23 **The *Mycoplasma* spp. 'Releasome': A New Concept for a Long-Known Phenomenon**
Patrice Gaurivaud and Florence Tardy
- 42 **Molecular Tools for Typing *Mycoplasma pneumoniae* and *Mycoplasma genitalium***
Roger Dumke
- 55 **High Prevalence of *Mycoplasma penetrans* in *Chlamydia trachomatis* Positive Rectal Samples From Men: A Brief Report**
Inmaculada Pérez-Prieto, Axel Skafte-Holm and Jørgen Skov Jensen
- 59 **MycoWiki: Functional annotation of the minimal model organism *Mycoplasma pneumoniae***
Christoph Elfmann, Bingyao Zhu, Tiago Pedreira, Ben Hoßbach, Maria Lluch-Senar, Luis Serrano and Jörg Stülke
- 69 ***Mycoplasma bovis* inhibits autophagy in bovine mammary epithelial cells via a PTEN/PI3K-Akt-mTOR-dependent pathway**
Maolin Xu, Yang Liu, Tuerdi Mayinuer, Yushan Lin, Yue Wang, Jian Gao, Dong Wang, John P. Kastelic and Bo Han
- 82 **Antimicrobial susceptibilities and mechanisms of resistance of commensal and invasive *Mycoplasma salivarium* isolates**
Li Xiao, Arthur H. Totten, Donna M. Crabb, Thomas Prescott Atkinson and Ken B. Waites
- 93 **The attenuated *Mycoplasma bovis* strain promotes apoptosis of bovine macrophages by upregulation of CHOP expression**
Hui Zhang, Siyi Lu, Jin Chao, Doukun Lu, Gang Zhao, Yingyu Chen, Huanchun Chen, Muhammad Faisal, Liguang Yang, Changmin Hu and Aizhen Guo
- 109 **Iodixanol density gradients as an effective phytoplasma enrichment approach to improve genome sequencing**
Bianca Rodrigues Jardim, Lucy T. T. Tran-Nguyen, Cherie Gambley, Brendan Rodoni and Fiona E. Constable

- 125 **Multilocus sequence typing of diverse phytoplasmas using hybridization probe-based sequence capture provides high resolution strain differentiation**
Karolina Pusz-Bochenska, Edel Perez-Lopez, Tyler J. Wist, Harvinder Bennypaul, Daniel Sanderson, Margaret Green and Tim J. Dumonceaux
- 141 **Isolation and structure of the fibril protein, a major component of the internal ribbon for *Spiroplasma* swimming**
Yuya Sasajima, Takayuki Kato, Tomoko Miyata, Akihiro Kawamoto, Keiichi Namba and Makoto Miyata
- 153 **Virulence factors of *Mycoplasma synoviae*: Three genes influencing colonization, immunogenicity, and transmissibility**
Sara M. Klose, Oluwadamilola S. Omotainse, Sahar Zare, Paola K. Vaz, Parisa Armat, Pollob Shil, Nadeeka Wawegama, Anna Kanci Condello, Denise O'Rourke, Jillian F. Disint, Daniel M. Andrews, Gregory J. Underwood, Chris J. Morrow, Marc S. Marenda and Amir H. Noormohammadi
- 164 **Immune profiling of experimental murine mastitis reveals conserved response to mammary pathogenic *Escherichia coli*, *Mycoplasma bovis*, and *Streptococcus uberis***
Peleg Schneider, Hagit Salamon, Nathalie Weizmann, Einat Nissim-Eliraz, Inna Lysnyansky and Nahum Y. Shpigel
- 176 **Genotyping of *Mycoplasma pneumoniae* strains isolated in Japan during 2019 and 2020: spread of p1 gene type 2c and 2j variant strains**
Tsuyoshi Kenri, Tsutomu Yamazaki, Hitomi Ohya, Michio Jinnai, Yoichiro Oda, Sadasaburo Asai, Rikako Sato, Nobuhisa Ishiguro, Tomohiro Oishi, Atsuko Horino, Hiroyuki Fujii, Toru Hashimoto, Hiroshi Nakajima and Keigo Shibayama
- 189 **Phenotypic and genetic insights into efflux pump mechanism in *Mycoplasma anserisalpingitidis***
Eszter Zsófia Nagy, Áron Botond Kovács, Enikő Wehmann, Katinka Bekő, Dorottya Földi, Krisztián Bányai, Zsuzsa Kreizinger and Miklós Gyuranecz
- 202 **Establishment of a *Mycoplasma hyorhinis* challenge model in 5-week-old piglets**
Dorottya Földi, Zsófia Eszter Nagy, Nikolett Belec, Levente Szeredi, József Földi, Anna Kollár, Miklós Tenk, Zsuzsa Kreizinger and Miklós Gyuranecz
- 213 **An atypical GdpP enzyme linking cyclic nucleotide metabolism to osmotic tolerance and gene regulation in *Mycoplasma bovis***
Xifang Zhu, Eric Baranowski, Zhiyu Hao, Xixi Li, Gang Zhao, Yaqi Dong, Yingyu Chen, Changmin Hu, Huanchun Chen, Christine Citti, Aiping Wang and Aizhen Guo

- 225 ***Mycoplasma synoviae* LP78 is a fibronectin/plasminogen binding protein, putative adhesion, and potential diagnostic antigen**
Shuizhong Han, Ying Wang, Lizhen Wang, Wenchang, Bo Wen, Junyang Fang, Xiaolan Hou, Xuefeng Qi and Jingyu Wang
- 239 ***Mesoplasma florum*: a near-minimal model organism for systems and synthetic biology**
Dominick Matteau, Anthony Duval, Vincent Baby and Sébastien Rodrigue
- 253 **Identification of *Mycoplasma pneumoniae* proteins interacting with NOD2 and their role in macrophage inflammatory response**
Yongyu Wang, Chunji Ma, Xiujing Hao, Weili Wang, Haixia Luo and Min Li



Genital Mycoplasmas and Biomarkers of Inflammation and Their Association With Spontaneous Preterm Birth and Preterm Prelabor Rupture of Membranes: A Systematic Review and Meta-Analysis

OPEN ACCESS

Edited by:

Glenn Francis Browning,
The University of Melbourne, Australia

Reviewed by:

Marian Kacerovsky,
University Hospital Hradec Králové,
Czechia
Alessandra Sensini,
Italian Association of Clinical
Microbiologists, Italy

*Correspondence:

Ramkumar Menon
ra2menon@utmb.edu

† These authors have contributed
equally to this work and share first
authorship

Specialty section:

This article was submitted to
Infectious Agents and Disease,
a section of the journal
Frontiers in Microbiology

Received: 21 January 2022

Accepted: 07 March 2022

Published: 30 March 2022

Citation:

Noda-Nicolau NM,
Tantengco OAG, Poletti J, Silva MC,
Bento GFC, Cursino GC, Marconi C,
Lamont RF, Taylor BD, Silva MG,
Jupiter D and Menon R (2022) Genital
Mycoplasmas and Biomarkers
of Inflammation and Their Association
With Spontaneous Preterm Birth
and Preterm Prelabor Rupture
of Membranes: A Systematic Review
and Meta-Analysis.
Front. Microbiol. 13:859732.
doi: 10.3389/fmicb.2022.859732

Nathalia M. Noda-Nicolau^{1†}, Ourlad Alzeus G. Tantengco^{2,3†}, Jossimara Poletti^{4†},
Mariana C. Silva¹, Giovana F. C. Bento¹, Geovanna C. Cursino¹, Camila Marconi⁵,
Ronald F. Lamont^{6,7}, Brandie D. Taylor², Márcia G. Silva¹, Daniel Jupiter⁸ and
Ramkumar Menon^{2*}

¹ Department of Pathology, Botucatu Medical School, Universidade Estadual Paulista, Botucatu, Brazil, ² Division of Basic and Translational Research, Department of Obstetrics and Gynecology, The University of Texas Medical Branch at Galveston, Galveston, TX, United States, ³ Department of Biochemistry and Molecular Biology, College of Medicine, University of the Philippines Manila, Manila, Philippines, ⁴ Graduate Program in Biomedical Sciences, Universidade Federal da Fronteira Sul, Passo Fundo, Brazil, ⁵ Department of Basic Pathology, Setor de Ciências Biológicas, Universidade Federal do Paraná, Curitiba, Brazil, ⁶ Research Unit of Gynaecology and Obstetrics, Department of Gynecology and Obstetrics, Institute of Clinical Research, University of Southern Denmark, Odense, Denmark, ⁷ Division of Surgery, Northwick Park Institute for Medical Research, University College London, London, United Kingdom, ⁸ Department of Preventive Medicine and Community Health, University of Texas Medical Branch, Galveston, TX, United States

Genital mycoplasmas (GM), such as *Mycoplasma hominis*, *Mycoplasma genitalium*, *Ureaplasma parvum*, and *Ureaplasma urealyticum* are commonly associated with spontaneous preterm labor (SPTL), spontaneous preterm birth (PTB), and preterm prelabor rupture of membranes (PPROM). This study determined the association between GM and such adverse pregnancy outcomes. We searched for studies published 1980–2019 in MEDLINE, EMBASE, and Web of Science. Studies were eligible when GM was detected during pregnancy. We included 93 and 51 studies in determining the prevalence and the inflammatory biomarkers associated with GM, respectively, using the "metafor" package within R. The protocol was registered with PROSPERO (registration no. CRD42016047297). Women with the studied adverse pregnancy outcomes had significantly higher odds of presence with GM compared to women who delivered at term. For PTB, the odds ratios were: *M. hominis* (OR: 2.25; CI: 1.35–3.75; I^2 : 44%), *M. genitalium* (OR: 2.04; CI: 1.18–3.53; I^2 : 20%), *U. parvum* (OR: 1.75; CI: 1.47–2.07; I^2 : 0%), *U. urealyticum* (OR: 1.50; CI: 1.08–2.07; I^2 : 58%). SPTL had significantly higher odds with *M. hominis* (OR: 1.96; CI: 1.19–3.23; I^2 : 1%) or *U. urealyticum* (OR: 2.37; CI: 1.20–4.70; I^2 : 76%) compared to women without SPTL. Women with PPRM had significantly higher odds with *M. hominis* (OR: 2.09; CI: 1.42–3.08; I^2 : 0%) than women without PPRM. However, our subgroup analysis based on the diagnostic test and the sample used for detecting GM showed a higher prevalence of GM in maternal samples than in fetal samples. GM presence of the cervix and vagina

was associated with lower odds of PTB and preterm labor (PTL). In contrast, GM presence in the AF, fetal membrane, and placenta was associated with increased odds of PTB and PTL. However, genital mycoplasmas may not elicit the massive inflammation required to trigger PTB. In conclusion, GM presence in the fetal tissues was associated with significantly increased odds of PTB and PTL.

Keywords: inflammatory cytokines, *Mycoplasma* species, pregnancy, preterm birth, *Ureaplasma* species, pregnancy adverse outcomes

INTRODUCTION

The onset of labor before 37 weeks of gestation, defined as spontaneous preterm labor (SPTL), that may lead to preterm birth (PTB), along with the preterm prelabor rupture of the membranes (PPROM), characterized by the rupture of membranes before labor that occurs before 37 weeks of pregnancy, are two major complications of pregnancies affecting ~11% of all pregnancies worldwide (Chawanpaiboon et al., 2019).

Microbial invasion of the amniotic cavity (MIAC) followed by intraamniotic inflammation is associated with most cases of SPTL, PTB, and PPROM. Approximately 50% of all PTBs, defined as births that occur before 37 weeks of gestation, and 20–40% of PPROM have an infectious and inflammatory association (Jacobsson et al., 2003; Menon and Fortunato, 2007; Romero et al., 2015). Furthermore, MIAC and intraamniotic infection and inflammation are associated with histologic chorioamnionitis, funisitis, and systemic fetal inflammatory response during pregnancy (Romero et al., 2011; Kacerovsky et al., 2013b). MIAC is often detected as a single bacterial infection (Stranik et al., 2021). However, polymicrobial bacterial are documented in the amniotic cavity and associated with poor perinatal prognosis in preterm labor (PTL) (Yoneda et al., 2016). In this context, the most common of which are *Ureaplasma* and *Mycoplasma*, collectively known as genital mycoplasmas (Taylor-Robinson and Lamont, 2010; Tantengco and Yanagihara, 2019). Conversely, the literature on the use of prophylactic antibiotics to prevent PTB is confusing (Lamont, 2015). The use of antibiotics has not successfully reduced global rates of PTB or PPROM. Ambiguity concerning the effectiveness of antibiotic interventions and reducing the risk of PTB and PPROM can be attributed to several factors (Oh et al., 2019; Tanaka et al., 2019; Kacerovsky et al., 2020): (i) although there is an association between MIAC and/or intraamniotic inflammation with PTB and PPROM, an infectious etiology and the kinetics of intraamniotic infection and inflammation is difficult to determine; (ii) microbial load, polymicrobial nature and sites of microbial localization are critical in determining mechanistic events that can lead to PTB or PPROM; (iii) various underlying pathologies associated with fetomaternal uterine tissues that can compromise both antimicrobial and innate immune defense can cause MIAC, which might be a secondary condition; (iv) inflammation and inflammatory mediators generated in response to MIAC are not homogeneous.

Mechanistic models have not helped the derivation of management strategies because they may be indefinite in

determining the contribution of pathogens to the pathways of PTB and PPROM. Our *in vitro* models have shown that the fetal inflammatory response differs based on polymicrobial combinations and their respective load (Noda-Nicolau et al., 2016; Poletini et al., 2018). Combinations of *Gardnerella vaginalis* and genital mycoplasmas produced distinct and load-dependent inflammatory profiles. A combination of high loads of *G. vaginalis* and a low load of genital mycoplasmas caused an immense fetal inflammatory response (Noda-Nicolau et al., 2016). Conversely, a high mycoplasma load and low *G. vaginalis* load produced a balanced inflammatory response with a robust anti-inflammatory response. Therefore, genital mycoplasmas at various loads and combinations are less proinflammatory than *G. vaginalis* (Noda-Nicolau et al., 2016).

Nonetheless, other studies have shown that *Ureaplasma parvum* can cause maternal T cell activation (Friedland et al., 2016). *In vivo*, animal models have shown that vaginal or intraamniotic infection inoculation of mycoplasmas can trigger SPTL (Motomura et al., 2020; Pavlidis et al., 2020). All these models have indicated several pathophysiologic aspects of PTB induced by microbes. However, these models have limitations and do not accurately mimic MIAC or intraamniotic inflammation seen in humans. These studies can be improved, and better mechanistic information can be generated if we have better knowledge from clinical studies concerning the prevalence of infection, infectious agents, and data on inflammatory mediators correlated with infection.

To synthesize knowledge and improve our understanding of the role of genital mycoplasmas in MIAC and intraamniotic inflammation contributing to SPTL, PTB, and PPROM, a comprehensive systematic review (SR) and meta-analysis (MA) was conducted. Fetal, neonatal, and postpartum maternal complications due to these microorganisms were not a part of this study. This study determined the prevalence of genital mycoplasma presence in PTB and PPROM. We also checked any association between the genital mycoplasmas and SPTL, PTB, and PPROM. Lastly, we evaluated the potential biomarkers associated with genital mycoplasma presence in SPTL, PTB, and PPROM.

MATERIALS AND METHODS

Eligibility Criteria, Information Sources, Search Strategy

An SR was conducted according to the PRISMA statement (Liberati et al., 2009) and performed using three biomedical

literature databases, MEDLINE, EMBASE, and Web of Science, selecting relevant studies concerning mycoplasma presence and preterm labor regardless of delivery at term or preterm (SPTL), SPTL followed by PTB (PTB), or preterm prelabor rupture of the membranes (PPROM). We sought studies between 1980 and 2019 using the following terms: *Ureaplasma urealyticum* OR *U. parvum* OR *Mycoplasma hominis* OR *Mycoplasma genitalium* AND pregnancy. This study was supported by the Strategic Research Commitment fund from the University of Texas Medical Branch at Galveston, UTMB, and 1R01HD100729 (NIH/NICHD) to R Menon.

Study Selection

Case-control, cross-sectional, prospective, and retrospective cohort studies were considered eligible in this SR, presenting the following criteria: subjects were pregnant women with the target outcomes either SPTL that leads to preterm birth (PTB) or PPRM; detection of genital mycoplasma presence in either maternal or fetal biological compartments during pregnancy. Cross-sectional studies were used in estimating the pooled prevalence of genital mycoplasma among patients with PTL, PTB, and PPRM. On the other hand, case-control and cohort studies were used in determining the association between genital mycoplasma and PTL, PTB, and PPRM.

Reviews, editorials, letters, case reports, conferences, summaries, books, opinions, *in vitro* studies, studies of diagnostics methodologies, and studies in animal models were excluded, and a search for unpublished studies was not performed. Other characteristics of excluded studies were maternal exposure to infection(s) caused by genital mycoplasmas during pregnancy was not directly measured but mentioned as a possible pathogen; infection by genital mycoplasmas in term infants; only term deliveries; PTB caused by other associated complications, such as preeclampsia, intrauterine growth restriction, stillbirth, diabetes, placental abruption, multiple pregnancies; the full-text of the study was not written in English, Portuguese, Spanish or French.

Data Extraction

Two authors (NN-N and MGS) independently performed the screening of the records, first by titles and then by abstracts. Full-text analysis was performed by seven authors (NN-N, JP, OT, MCS, GB, GC, and CM) for articles that fulfilled the predetermined selection criteria for this SR. Discrepancies between the reviewers were discussed until consensus was reached. For each included study, we extracted the following primary data: author's names, year of publication, type of study, the country where the study was conducted, study objective and design; the total number of participants, the pregnancy outcome, number of cases and controls (when applicable), gestational age or trimester at the time of sample collection, source of the biological sample, species of genital Mycoplasma detected, methodology used to identify genital mycoplasmas, the method for detecting inflammatory biomarkers, type of samples used for biomarker analysis and analytical approaches. The data collected were compared and discussed by the reviewers, and disagreements were resolved by consensus.

Assessment of Risk of Bias

Six authors (NN-N, JP, OT, MCS, GB, and GC) assessed the quality of each included study, which was evaluated according to a set of parameters defined for this review using the Newcastle Ottawa Scale for case-control, cohort, and cross-sectional studies (Wells et al., 2013; Lo et al., 2014). The criteria for quality assessment are shown in **Supplementary Tables 1–3**.

Data Synthesis and Statistical Analysis

A meta-analysis (MA) was carried out using random-effects models to determine the prevalence of genital mycoplasma with SPTL, PTB, and PPRM, considering all types of studies. For association analysis, only case-control and cohort studies were included. Forest and funnel plots were produced. A *p*-value of <0.05 was considered statistically significant. Higgins I^2 was used to assess heterogeneity with I^2 value of >50% regarded as high heterogeneity. All analyses were performed using the "metafor" package within R (R Core Team, 2020).

RESULTS

Study Selection

We identified 4699 articles, and after the screening process, we retained 121 articles and included these in the qualitative synthesis of this SR (**Figure 1**). This included 93 articles showing the prevalence and association of genital mycoplasma and adverse pregnancy outcomes, including SPTL, PTB, and PROM, and 51 articles reporting the levels of inflammatory biomarkers in pregnant women with genital mycoplasma and women with any of these adverse pregnancy outcomes. Excluded studies are described in **Supplementary Table 4**.

Study Characteristics

Genital Mycoplasma and Adverse Pregnancy Outcomes

Of the 93 articles that reported genital mycoplasma presence associated with SPTL, PTB, and PPRM, 61 were cross-sectional studies, while 32 were case-control and cohort studies (**Supplementary Figure 1**). Of the cross-sectional studies, 23 had PTB as an outcome, 28 on SPTL, and 27 on PPRM. Among the case-control and cohort studies, 24 studies had PTB as the primary outcome, ten on SPTL, and only two on PPRM. Specific details of the included studies are shown in **Supplementary Tables 5, 6**.

Most of the studies on the association of genital mycoplasma presence with adverse pregnancy outcomes were from Europe (33/93), North America (30/93), and Asia (22/93). There were few studies from Africa (2/93), Australia (3/93), and South America (3/93) (**Figure 2A** and **Supplementary Tables 5, 6**). There was a continuous increase in published articles on this topic from 1984 to the present (**Figure 2B**). PTB is the most common pregnancy outcome associated with genital mycoplasma presence (47/93), followed by SPTL (38/93) and PPRM (29/93) (**Figure 2C** and **Supplementary Tables 5, 6**). The samples used and the

diagnostic test to detect genital mycoplasma presence varied across different studies. The most used sample was amniotic fluid (AF) (40/93) and vaginal samples (34/93), while culture (47/93) and nucleic acid amplification test (NAAT)/polymerase chain reaction (PCR) test (29/93) were the most common diagnostic method used for genital mycoplasma diagnosis (Figures 2D,E and Supplementary Tables 5, 6). The time of collection of these samples varied between studies, given that the most common time of collection was at the time of labor and delivery (33/93). Still, other studies collected samples as early as the first trimester (9/93), while some studies collected samples postpartum (8/93) (Figure 2F and Supplementary Tables 5, 6). This difference in the timing of sample collection may have biased the associations made between genital mycoplasma presence and adverse pregnancy outcomes.

Most of the included studies in this SR only detected one species of genital mycoplasma with *U. urealyticum* being the most studied, followed by *M. hominis*. There were fewer studies that focused on *M. genitalium* and *U. parvum*. Several studies detected co-infection of different species of genital mycoplasmas, mainly *U. urealyticum* and *M. hominis* co-infection (Figure 2G). Further details of the included studies are shown in Supplementary Tables 5, 6.

Genital Mycoplasma and Inflammatory Biomarkers

The studies on the levels of the inflammatory biomarker among pregnant women with genital mycoplasma presence were mainly from Europe (25/51), North America (12/51), and Asia (11/51). There were only two studies from Australia, one from South America, and none from Africa (Figure 3A and Supplementary Tables 7, 8). The number of studies in this field progressively increased since the first publication in 1992 (Figure 3B). Most of the inflammatory biomarkers detected in the studies included in this SR were proinflammatory cytokines such as IL-6, IL-8, C-reactive protein (CRP), tumor necrosis factor (TNF)- α , IL-1 β , matrix metalloproteinase (MMP)-8, triggering receptor expressed on myeloid cells (TREM)-1, IL-1 α , and MMP-9. IL-10 was the only anti-inflammatory cytokine included in the panel of inflammatory biomarkers detected in four studies included in this SR (Jacobsson et al., 2009; Kacerovsky et al., 2012, 2013a; Payne et al., 2014; Figure 3C). These biomarkers were collected from different samples, including AF (35/51), maternal blood (5/51), and umbilical cord blood samples (5/51) (Figure 3D). ELISA was the most used assay in detecting inflammatory biomarkers (Figure 3E), and the samples used for detecting these biomarkers were usually collected during the 2nd and 3rd trimester of pregnancy (Figure 3F). Most of the studies only collected single samples and no follow-up samples. Further details of the included studies are shown in Supplementary Tables 7, 8.

We performed a MA to determine the levels of different inflammatory biomarkers among pregnant women with and without genital mycoplasma presence. However, MA was not feasible due to the lack of sufficient studies that could be combined. Factors included heterogeneity in the set of inflammatory biomarkers, the diagnostic method used and reporting of inflammatory biomarker levels. There were also

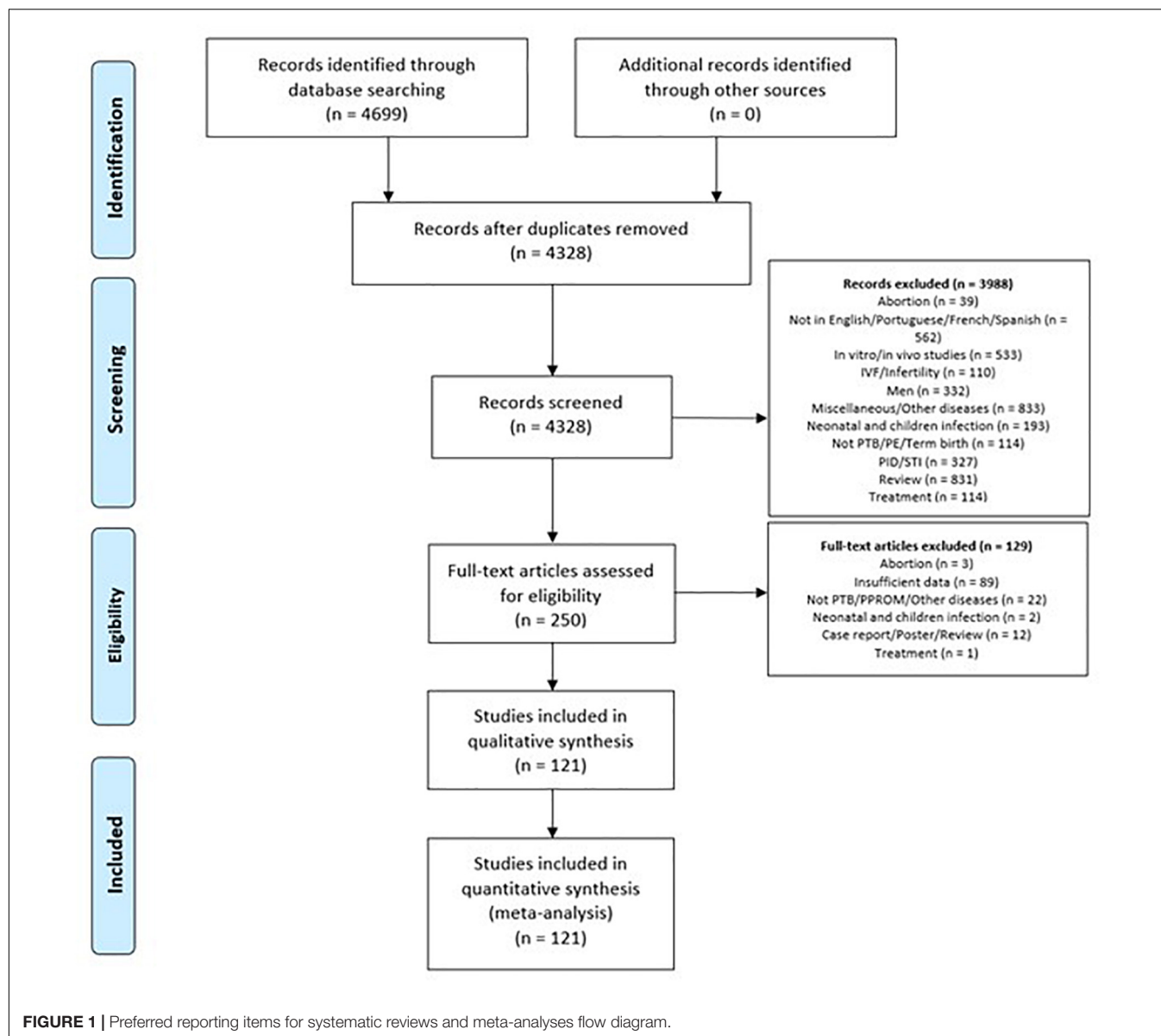
considerable differences in the type of samples used and the time of collection. Accordingly, we created a qualitative synthesis table (Supplementary Tables 7, 8) listing all the inflammatory biomarkers detected in pregnant patients with genital mycoplasma colonization.

We observed that pregnant women who experienced SPTL, PTB, and PPROM had significantly higher inflammatory biomarkers than those with term delivery (Supplementary Table 7). Specifically, cervicovaginal fluid concentrations of IL-1 α , IL-1 β , IL-6, RANTES, and TNFr1 and AF concentration of IL-6, IL-8, MMP-8, and TNF α were elevated in women with PTB. For women in SPTL, cervicovaginal fluid concentrations of IL-6 and IL-8 and AF levels of IL-1 α , IL-1 β , IL-6, and IL-8 were significantly elevated compared to women who gave birth at term. Women with PPROM had substantially higher levels of CRP in maternal serum, IL-6 and IL-8 in the vaginal fluid, IL-6, IL-8, and TNF α in cord blood samples, and C-C Motif Chemokine Ligand (CCL)-2 gene, CCL-3 gene, CRP, intercellular adhesion molecules (ICAM)-1, IL-6, IL-8, IL-10, MMP-8, and TNF α in the AF (Supplementary Table 7).

Among those women with adverse pregnancy outcomes, we also observed detection of *Mycoplasma* spp. or *Ureaplasma* spp. during pregnancy was associated with a significant increase in several proinflammatory biomarkers, including CRP, IL-6, IL-8, MMP-8, MMP-9, and TREM-1. However, one study also reported a significant increase in IL-10, an anti-inflammatory cytokine (Kacerovsky et al., 2013a). We then looked at studies reporting the inflammatory biomarker levels associated with each species of genital mycoplasmas. There were no studies on the concentration of inflammatory biomarkers in pregnant women infected with *M. genitalium*. Several studies reported significantly higher levels of IL-1 β , IL-4, IL-6, and IL-16 from the AF samples of pregnant women diagnosed with *M. hominis* presence than uninfected women. One study also reported a positive correlation between *U. parvum* load and IL-8 levels from the AF samples of pregnant women who delivered preterm (Kasper et al., 2010). Conversely, *U. urealyticum* presence among pregnant women was also associated with significantly higher AF levels of IL-1 β , IL-6, MMP-8, and TNF α compared to uninfected pregnant women (Supplementary Table 8).

Risk of Bias of Included Studies

Regarding the quality of the included studies, we observed that most of the cross-sectional studies were assessed as satisfactory (17/74), good (33/74), and very good quality papers (20/74). Only four studies were evaluated as unsatisfactory due to low sample size, lack of description on the assessment of pregnancy outcomes, and the analysis did not control for confounding factors. For cohort and case-control studies, most of the papers were assessed as satisfactory (4/47), good (30/47), or very good quality (12/47). Only one paper was evaluated as unsatisfactory due to the low sample size and lack of operational definitions of primary outcomes. However, those unsatisfactory papers were retained in the analysis, as their results regarding



mycoplasma prevalence or biomarkers did not influence our study (Supplementary Tables 1–3).

Synthesis of Results

The Pooled Prevalence of Genital Mycoplasma Presence

The pooled prevalence of genital mycoplasma presence are reported by pregnancy outcome: among women with PTB, *U. parvum* had the highest prevalence of 0.28 (CI: 0.04–0.53; I^2 : 94%), followed by *U. urealyticum* with a proportion of 0.26 (CI: 0.18–0.34; I^2 : 98%), *M. hominis* at 0.10 (CI: 0.01–0.18; I^2 : 99%), and *M. genitalium* at 0.03 (CI: 0.01–0.05; I^2 : 0%) (Figure 4). Among women with SPTL, *U. urealyticum* was the most common with a proportion of 0.19 (CI: 0.10–0.28; I^2 : 99%), followed by *U. parvum* (0.13; CI: 0.03–0.23; I^2 : 70%), *M. hominis* (0.06; CI: 0.02–0.10; I^2 : 98%), and *M. genitalium* (0.01; CI: -0.02–0.03; I^2 :

0%) (Figure 5). For women with PPROM, *U. urealyticum* was also the most prevalent with a proportion of 0.27 (CI: 0.19–0.35; I^2 : 94%), followed by *U. parvum* (0.15; CI: -0.06–0.36; I^2 : 94%), and *M. hominis* (0.01; CI: 0.01–0.02; I^2 : 27%). There were no studies that reported on the prevalence of *M. genitalium* among women with PPROM (Figure 6).

We then performed a subgroup analysis based on the type of sample used, and the methods used to detect genital mycoplasma. We observed differences in the prevalence of genital mycoplasmas based on the diagnostic methods used. *U. parvum* had a higher prevalence in studies that used PCR tests, while *U. urealyticum* had a higher prevalence in studies that used the culture method for detection (Supplementary Table 9). We also observed that most genital mycoplasmas had a higher pooled prevalence in studies that used maternal samples such as cervical and vaginal samples compared to studies that used fetal

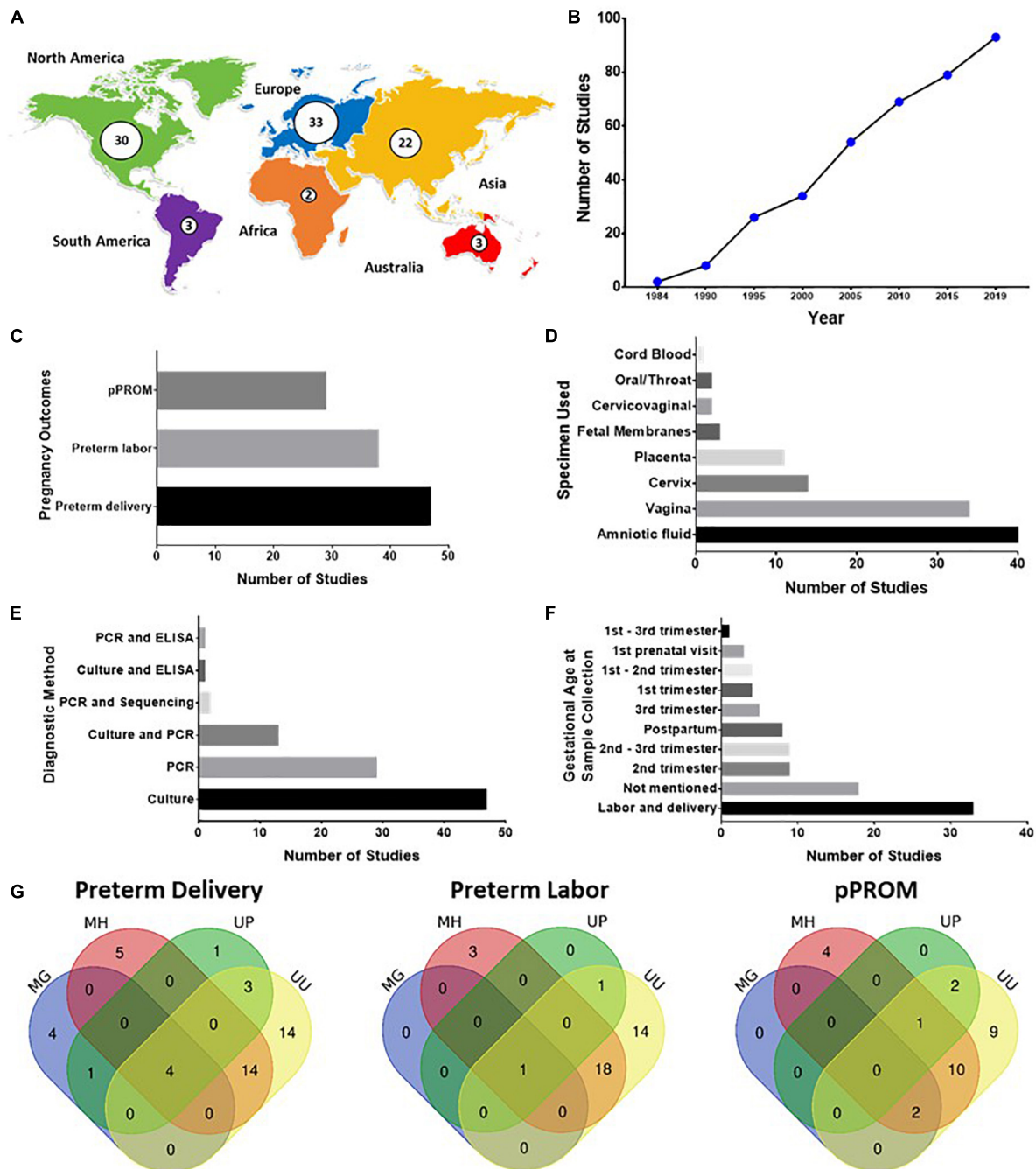


FIGURE 2 | (A–G) Summary of studies on the association of genital Mycoplasma infection with preterm birth. **(A)** Geographical distribution of published studies on genital Mycoplasma and preterm birth. **(B)** Cumulative count of published studies in genital Mycoplasma and preterm birth. **(C)** Types of pregnancy outcomes studied. **(D)** Samples used for diagnosing genital Mycoplasma infections **(E)** Diagnostic method used for detecting genital Mycoplasma infections **(F)** Gestational age of patients during the time of sample collection for diagnosing genital Mycoplasma infections. **(G)** Venn diagrams depicting the combination of different genital Mycoplasma species detected from patients with spontaneous preterm labor (SPTL), preterm birth (PTB), and preterm prelabor rupture of membranes (PPROM).

samples such as amniotic fluid, fetal membrane, and placenta (Supplementary Table 10).

To determine the prevalence of polymicrobial presence among women with adverse pregnancy outcomes, we retrieved all articles that reported co-infection with at least two species of

genital mycoplasmas. We have presented a qualitative synthesis of data in Supplementary Table 11. Only co-infection with *M. hominis* and *U. urealyticum* were reported in previous studies. For women with PTB, the reported prevalence was 0.05 (Goldenberg et al., 2008). Based on seven studies, the proportion

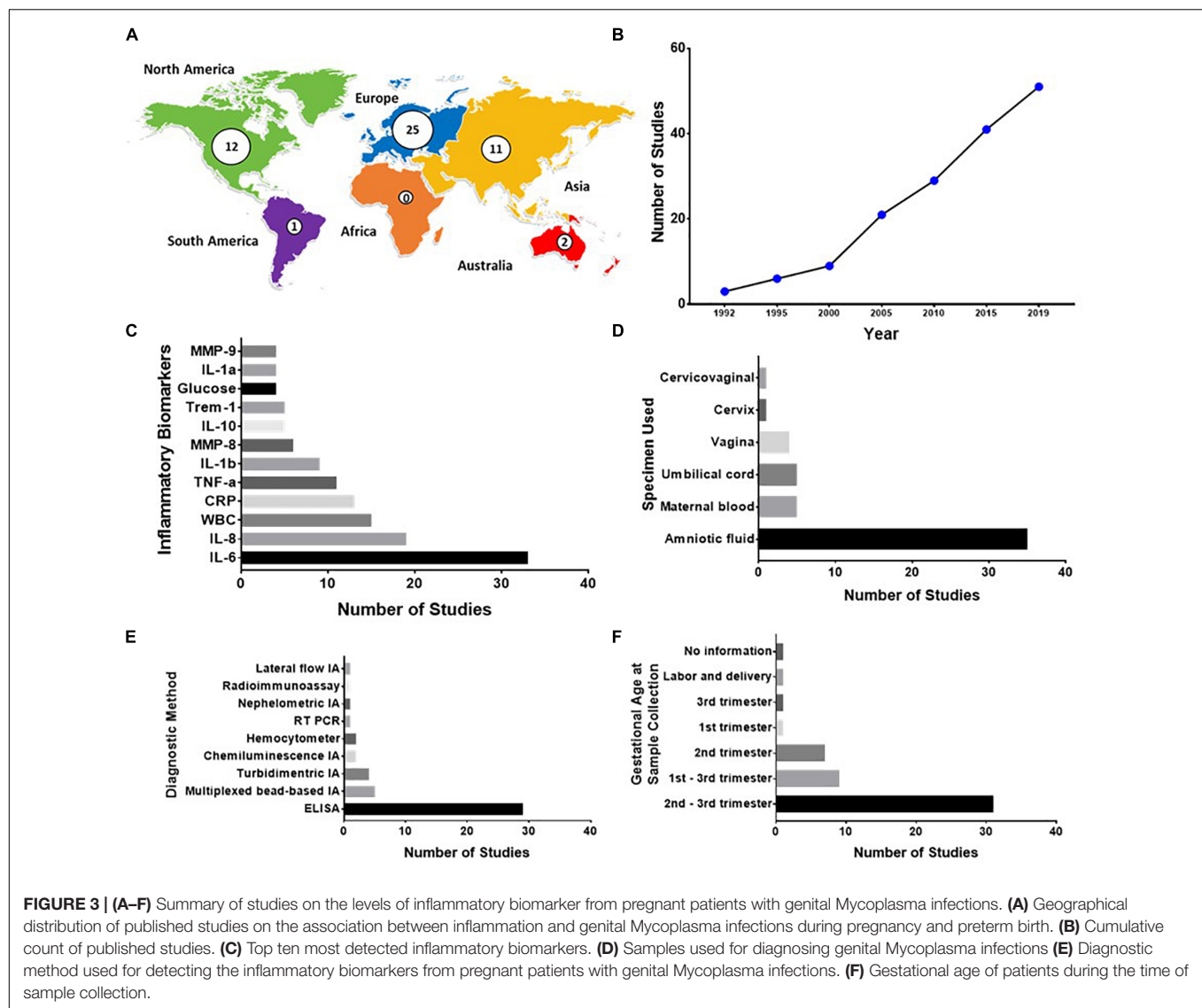


FIGURE 3 | (A–F) Summary of studies on the levels of inflammatory biomarker from pregnant patients with genital *Mycoplasma* infections. **(A)** Geographical distribution of published studies on the association between inflammation and genital *Mycoplasma* infections during pregnancy and preterm birth. **(B)** Cumulative count of published studies. **(C)** Top ten most detected inflammatory biomarkers. **(D)** Samples used for diagnosing genital *Mycoplasma* infections **(E)** Diagnostic method used for detecting the inflammatory biomarkers from pregnant patients with genital *Mycoplasma* infections. **(F)** Gestational age of patients during the time of sample collection.

of *M. hominis* and *U. urealyticum* co-infection ranged from 0 to 0.19 (Gravett et al., 1986; Romero et al., 1992b; Watts et al., 1992; Horowitz et al., 1995; Holst et al., 2005; Kim et al., 2012; Lee et al., 2013). Conversely, the proportion of *M. hominis* and *U. urealyticum* co-infection among women with PPRM ranged from 0.09 to 0.16 (Romero et al., 1992c; Grattard et al., 1995; Horowitz et al., 1995).

Association of Genital Mycoplasma Presence With Adverse Pregnancy Outcomes

To determine whether genital mycoplasma presence is associated with adverse pregnancy outcomes, we performed a MA for all case-control and cohort studies with reported odds ratio for genital mycoplasma infection and adverse pregnancy outcomes. Women with PTB had significantly higher odds of presence of with all four *Mycoplasmas* species than women who delivered at term. The highest odds ratio was for *M. hominis* (OR: 2.25; CI: 1.35–3.75; I^2 : 44%), followed by *M. genitalium* (OR: 2.04; CIL

1.18–3.53; I^2 : 20%), *U. parvum* (OR: 1.75; CI: 1.47–2.07; I^2 : 0%), and *U. urealyticum* (OR: 1.50; CI: 1.08–2.07; I^2 : 58%) (Figure 7).

Women who experienced SPTL had significantly higher odds of *M. hominis* (OR: 1.96; CI: 1.19–3.23; I^2 : 1%) or *U. urealyticum* (OR: 2.37; CI: 1.20–4.70; I^2 : 76%) presence compared to women who did not experience SPTL (Figure 8A). Based on two studies, women with PPRM had significantly higher odds of colonization with *M. hominis* (OR: 2.09; CI: 1.42–3.08; I^2 : 0%) than pregnant women without PPRM. These two studies were conducted in the Czech Republic and the USA (Minkoff et al., 1984; Kacerovský et al., 2009). They used cervical or vaginal fluid collected either at admission for rupture of membranes or during the first prenatal visit, and genital mycoplasmas were detected by culture. The result for *U. urealyticum* (OR: 3.31; CI: 0.35–31.51; I^2 : 96%) was equivocal and did not reach statistical significance (Figure 8B). No studies reported the odds ratio for *M. genitalium* and *U. parvum* presence in women with SPTL and PPRM.

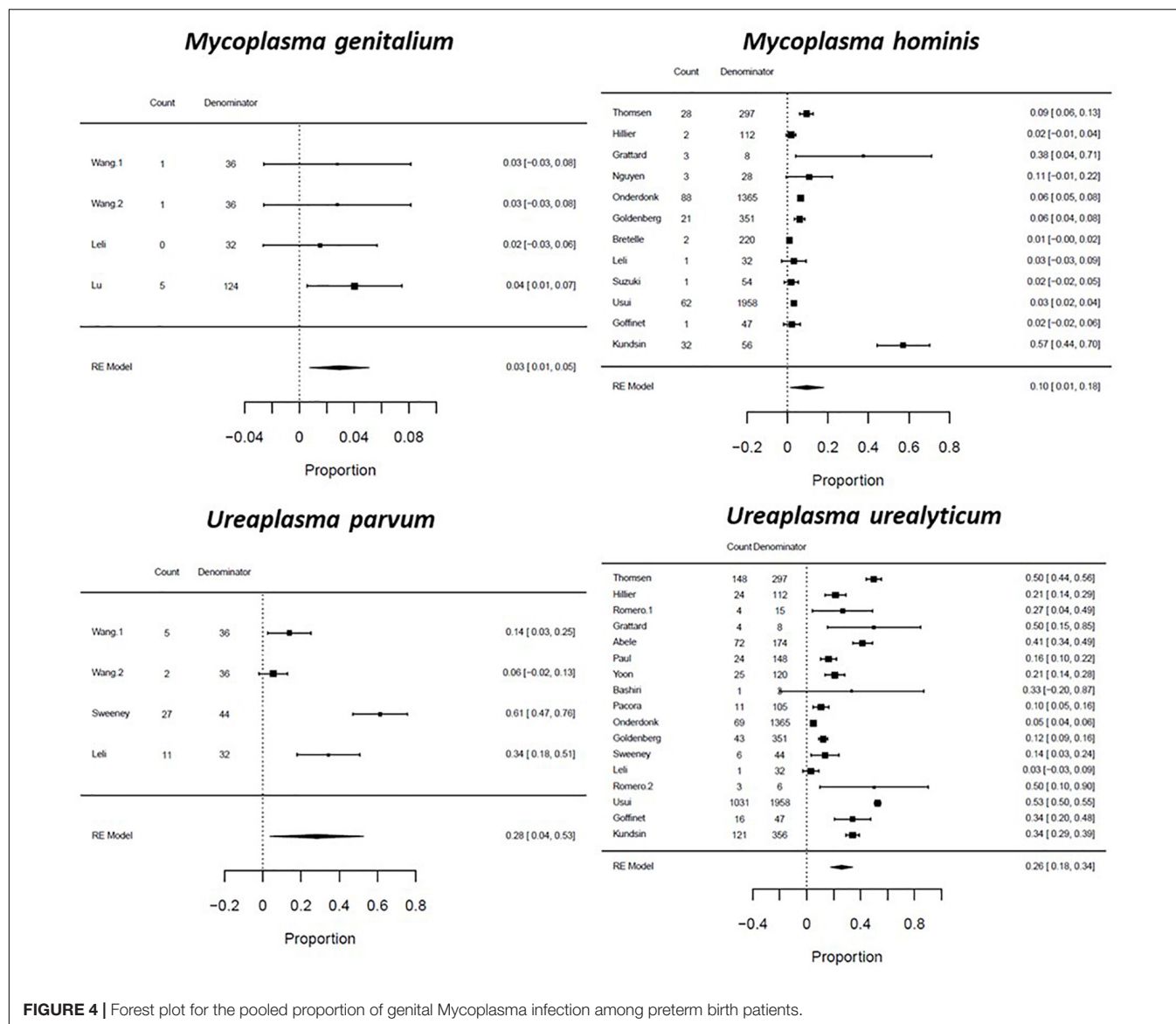


FIGURE 4 | Forest plot for the pooled proportion of genital Mycoplasma infection among preterm birth patients.

We performed subgroup analysis on the association of genital mycoplasma with adverse pregnancy outcomes based on the diagnostic method used to detect genital mycoplasmas. The pooled ORs for studies that used culture-based detection methods showed significantly higher odds of PTB and PPROM than studies that used PCR-based detection methods. *M. hominis* and *U. urealyticum* presence were significantly associated with 2.84- and 1.57-times increased odds of PTB, respectively. Only *M. hominis* presence showed significantly increased odds of PPROM, but not *U. urealyticum* (Table 1). We also performed subgroup analysis based on the sample used. We generally observed a higher pooled OR for studies that detected genital mycoplasmas in fetal tissues than in studies that used maternal tissues. For example, the presence of *U. parvum* and *U. urealyticum* in fetal samples had 2.08- and 1.55-times increased odds of PTB. In comparison, *U. parvum* and *U. urealyticum* colonization in the maternal samples was

associated with 1.77- and 1.45-times increased odds of PTB. Moreover, *M. hominis* presence of the fetal tissues was associated with 4.35-times increased odds of PTL, whereas *M. hominis* colonization of the maternal tissues was only associated with 1.72-times increased odds of PTL. Lastly, only *M. hominis* and not *U. urealyticum* colonization of the maternal tissues was associated with increased odds of PPROM (2.07-times) (Table 2).

DISCUSSION

Main Findings

This SR and MA showed a 28% prevalence of *U. parvum* mycoplasmas among women with PTB, 19% prevalence of *U. urealyticum* in SPTL, and 27% in women with PPROM. We also showed that detection of genital mycoplasmas was significantly associated with a one to two-fold higher risk for

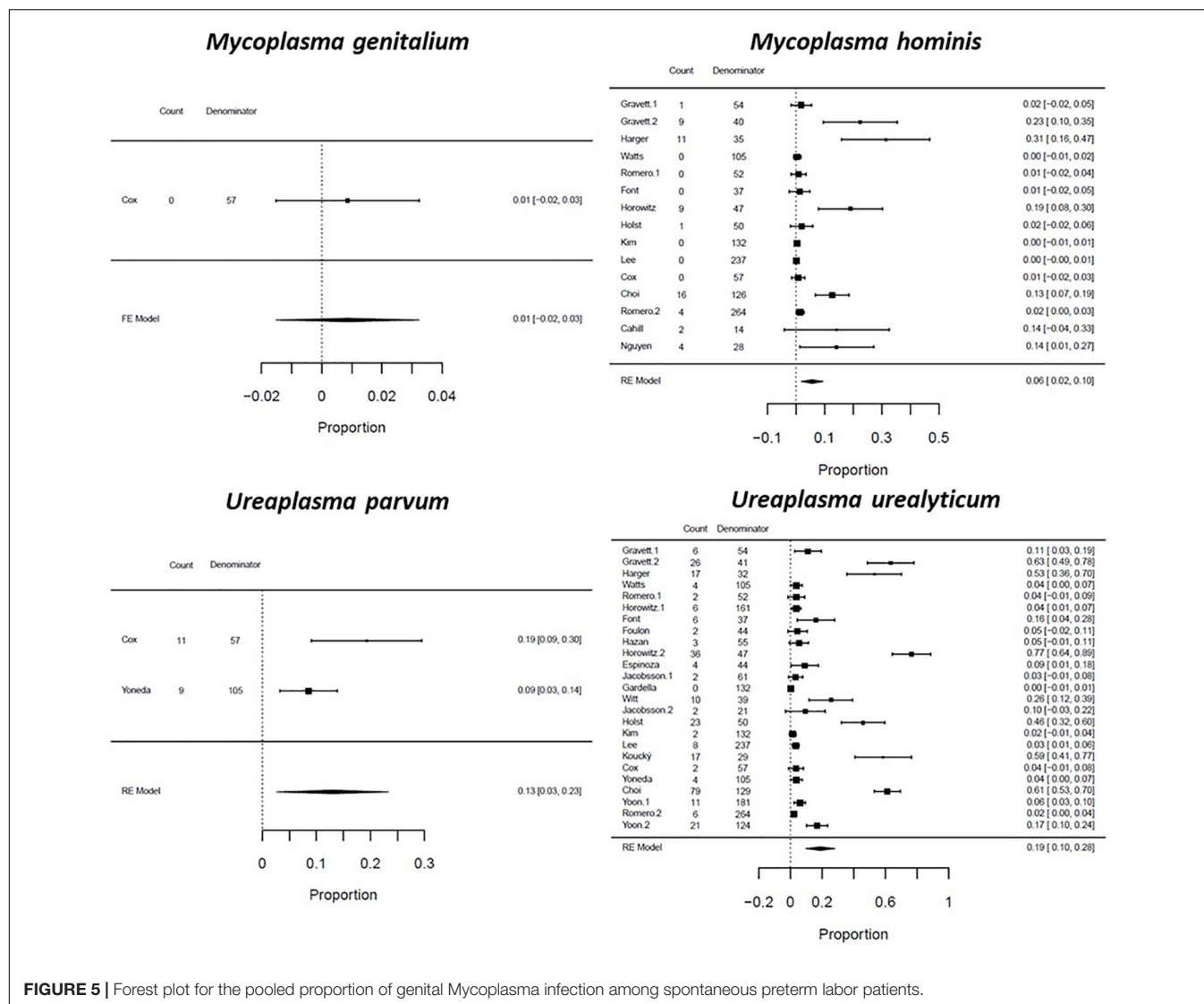


FIGURE 5 | Forest plot for the pooled proportion of genital Mycoplasma infection among spontaneous preterm labor patients.

PTB and a two to three-fold higher risk for SPTL and PPROM. However, after subgroup analysis, the prevalence and the association between genital mycoplasma and adverse pregnancy outcomes changes depending on the diagnostic test and the sample used. We observed that genital mycoplasmas have a higher prevalence in maternal samples than fetal samples. Genital mycoplasma presence of the cervix and vagina was associated with lower odds of PTB and PTL.

In contrast, colonization of the AF, fetal membrane, and the placenta was associated with higher odds of PTL. In addition, the association (odds ratio) of GM with adverse pregnancy outcomes changed after subgroup analysis (Tables 1, 2). This further adds to the growing evidence that genital mycoplasma presence in the cervix and the vagina is insufficient to promote preterm birth. Unless the cervix is compromised, it will serve as a barrier protecting the fetus in the intraamniotic cavity (Motomura et al., 2020; Pavlidis et al., 2020). Genital mycoplasma in the cervicovaginal space may promote a mild inflammatory response

to prime the cervical tissues to mount an immune response to potentially pathogenic organisms that may try to ascend to the amniotic cavity (Tantengco and Menon, 2022).

Ascending genital mycoplasma to the fetal side very well may cause adversity during pregnancy as the presence in the amniotic cavity or invasion of the fetal organs can mount a massive fetal inflammatory response that can cause SPTL and PTB. This is unlikely for infections limited to the maternal side alone. We propose that the fetal inflammatory response is the final trigger to promote genital mycoplasma-induced PTB, while maternal inflammation due to GM presence helps maintain immunologic homeostasis during pregnancy and promote fetoplacental growth.

Our data partly corroborate the results of two recent SRs, which showed that *M. genitalium*, but not *M. hominis*, *U. urealyticum*, or *U. parvum* was significantly associated with PTB (Lis et al., 2015; Ma et al., 2021). Those SRs analyzed only three articles reporting PTB with *M. hominis* or *U. urealyticum*

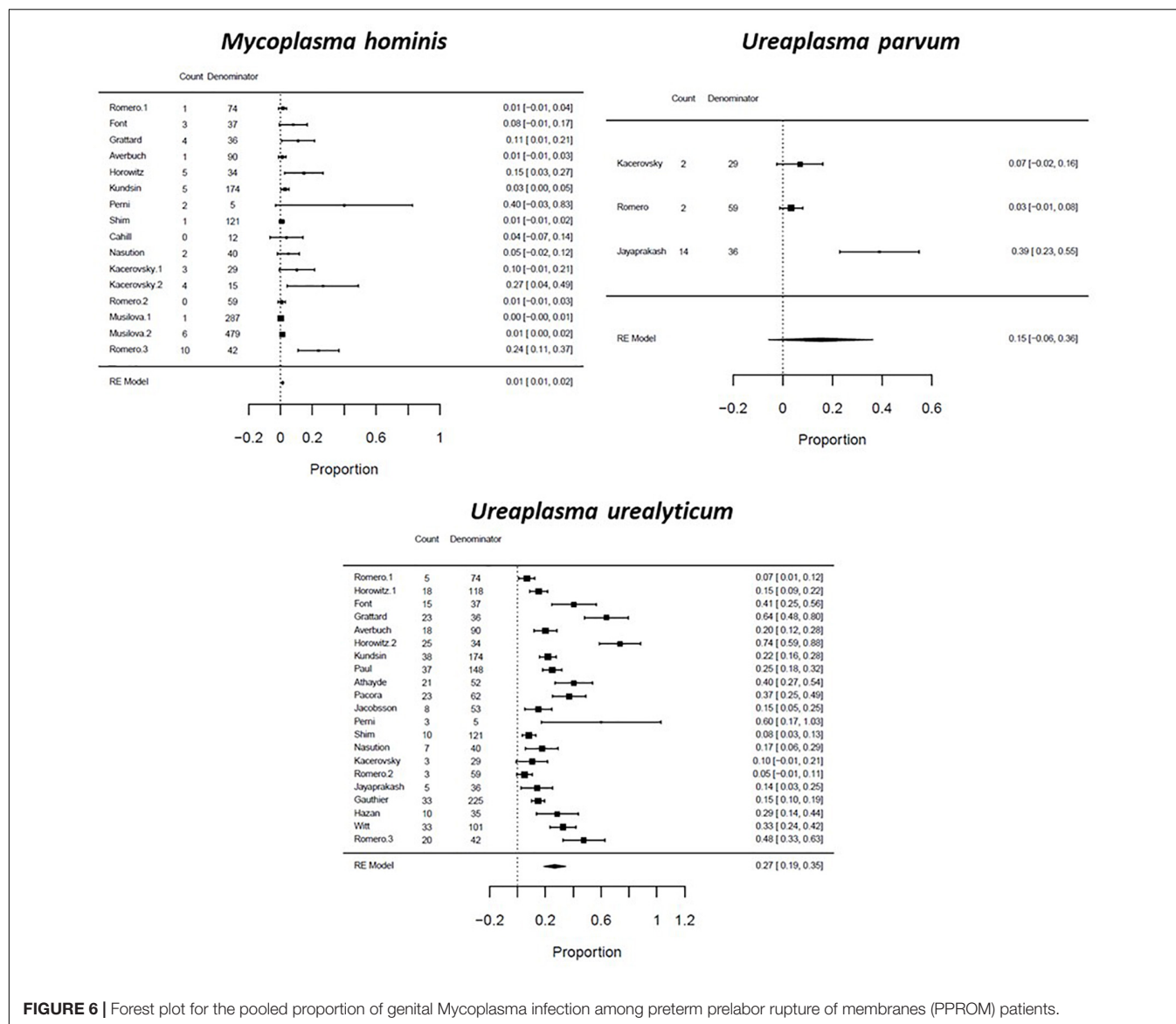


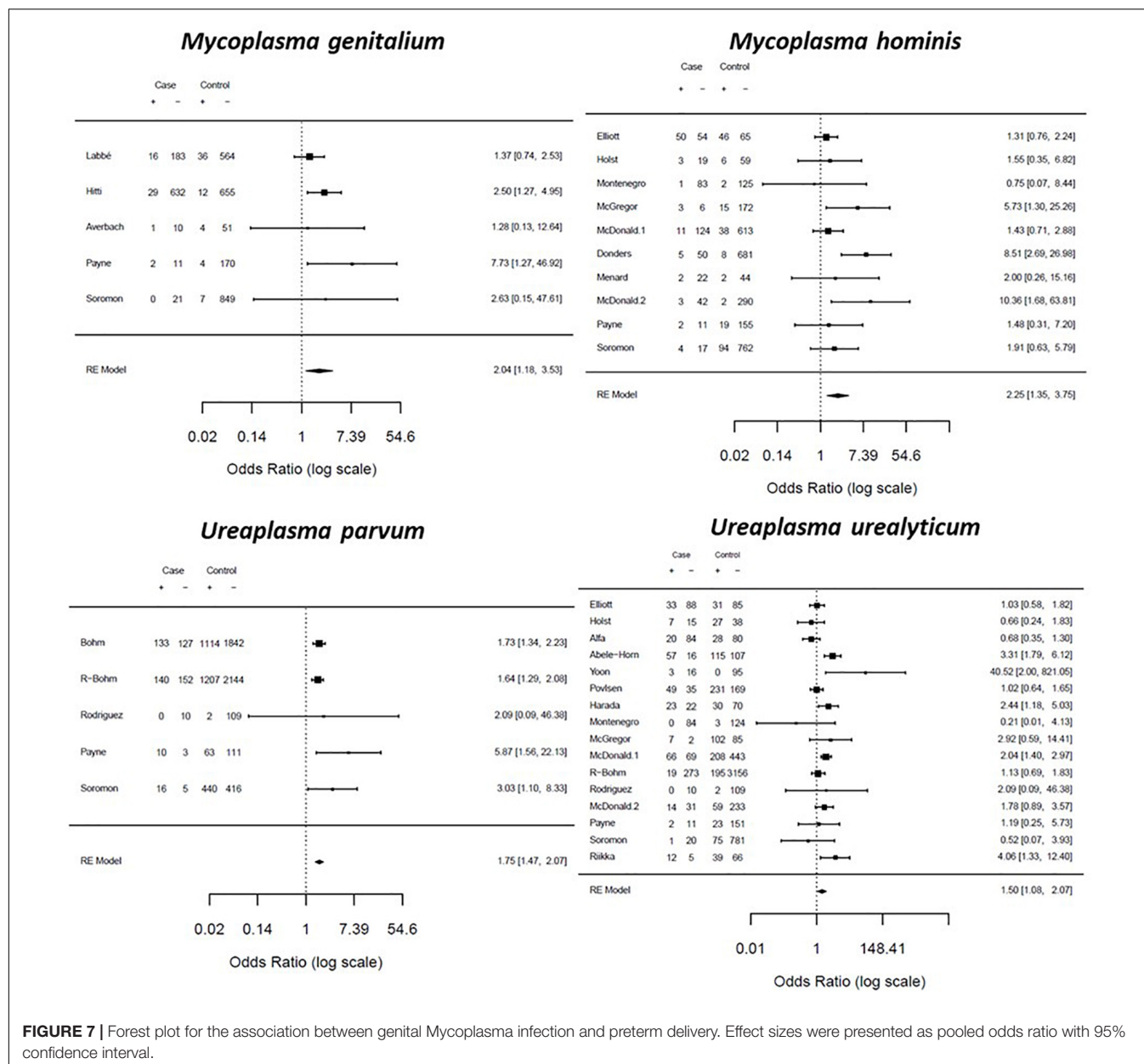
FIGURE 6 | Forest plot for the pooled proportion of genital Mycoplasma infection among preterm prelabor rupture of membranes (PPROM) patients.

presence and one article regarding *U. parvum*. At the same time, our SR also included more recent papers and retrieved respectively 10, 16, and 5 articles reporting an association between these microorganisms and PTB. It is also important to highlight that one of the two referred SRs included only studies based on NAATs to detect genital mycoplasmas. In contrast, our SR had studies that used other diagnostic tests such as culture and PCR-based tests.

Strengths and Limitations

Most of the included studies were from Europe (33/93) or North American (30/93). This limited number of studies from some regions, such as low- and middle-income countries, impaired an estimative of a global prevalence and a more reliable association between the genital mycoplasmas and adverse pregnancy outcomes. Therefore, more studies are required in these regions, especially following a recent SR that showed a

higher prevalence of *M. genitalium* infection in the general population in developing countries compared to developed countries (Baumann et al., 2018). Based on cross-sectional studies, the prevalence of *M. hominis* among women with SPTL or PTB was >10% in AF samples from United States (Gravett et al., 1986) and Switzerland (Nguyen et al., 2004), in vaginal samples from United States (Gravett et al., 1986; Harger et al., 1991), Israel (Horowitz et al., 1995), and Korea (Choi et al., 2012), and in fetal membranes from United Kingdom (Cahill et al., 2005). With PPROM, over 10% prevalence of *M. hominis* was reported in vaginal samples from France (Grattard et al., 1995) and Israel (Horowitz et al., 1995), in AF samples from United States (Perni et al., 2004) and Czech Republic (Kacerovsky et al., 2014), and cord blood samples from Czech Republic (Kacerovsky et al., 2014). In contrast, the prevalence of *U. urealyticum* in SPTL and/or PTB was more than 30% in AF samples from United States (Gravett et al., 1986;



Athayde et al., 2000; Romero et al., 2019) and Israel (Horowitz et al., 1995; Bashiri et al., 1999), in vaginal samples from United States (Gravett et al., 1986; Harger et al., 1991), Israel (Holst et al., 1994), France (Grattard et al., 1995; Goffinet et al., 2003), Germany (Abele-Horn et al., 1997), Korea (Choi et al., 2012), Japan (Usui et al., 2002), Denmark/England (Thomsen et al., 1984), and Czech Republic (Koucký et al., 2016), while more than 30% of *U. urealyticum* in PPROM was reported in AF samples from United States (Romero et al., 1992a; Font et al., 1995; Athayde et al., 2000; Pacora et al., 2000; Perni et al., 2004), Israel (Horowitz et al., 1995), and Austria (Witt et al., 2005), in vaginal samples in France (Grattard et al., 1995), and placenta in Austria (Witt et al., 2005). These data demonstrate that the most prevalent microorganisms have

been reported in diverse populations. This review observed significant associations in only two studies from low-income countries. These data demonstrate that the most prevalent microorganisms have been reported in diverse populations. This review observed significant associations in only two studies from low-income countries.

Analyses of cord blood cultures in the Alabama Preterm Birth Study demonstrated that 27.9% of samples from non-white women and 16.8% from white women were positive for *U. urealyticum* and/or *M. hominis* (Goldenberg et al., 2008). There was also a lower prevalence of *M. hominis* in white women, albeit that *U. urealyticum* presence was unrelated to ethnicity (Witt et al., 2005). Racial or ethnic disparities in adverse pregnancy outcomes associated with the genital mycoplasmas

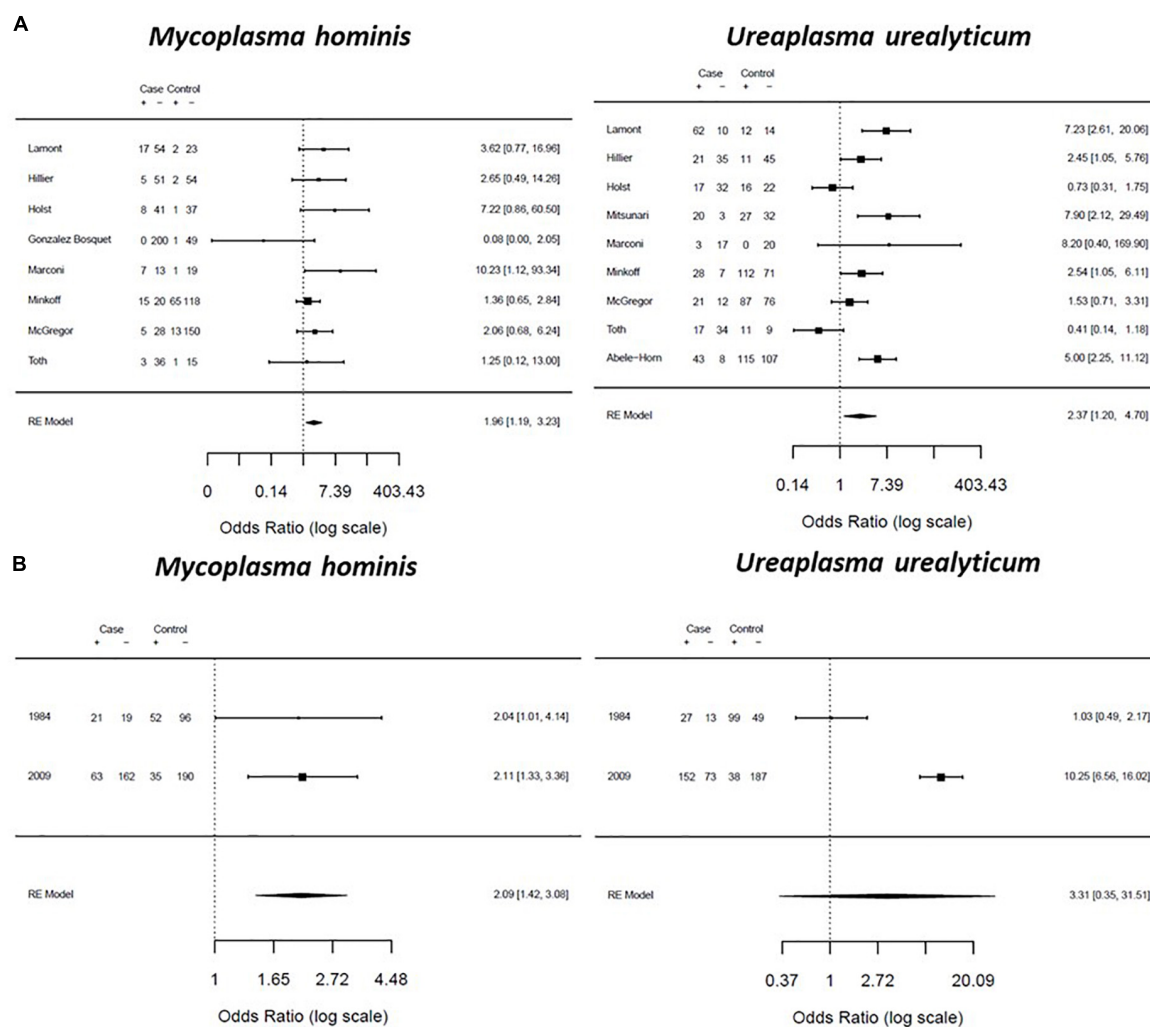


FIGURE 8 | Forest plot for the association between genital Mycoplasma infection and preterm labor (A) and preterm prelabor rupture of membranes (PPROM) (B). Effect sizes were presented as pooled odds ratio with 95% confidence interval.

are difficult to establish based on current data as many studies do not report population ethnicity and we strongly recommend inclusion of race/ethnicity of populations in future studies to determine the contribution of racial and genetic factors in the determination of risk.

The relationship between intraamniotic infection and adverse pregnancy outcomes has been examined extensively over the last four decades. In this MA we were able to confirm the prevalence and importance of the genital mycoplasmas in SPTL, PTB and PPROM. The human *Ureaplasma* spp. are divided into *U. urealyticum* and *U. parvum* with 14 known serotypes. In the raw prevalence analysis, ureaplasmas were predominant in the three studied outcomes and was more prevalent in SPTL and PPROM, while *U. parvum* showed a higher prevalence in PTB. Based on *in vitro* models (Novy et al., 2009; Motomura et al., 2020) and *in vivo* (Shimizu et al., 2008; Novy et al., 2009; Dando et al., 2012; Uchida et al., 2013), it has been argued that infection of *Ureaplasma* and or its antigens may

elicit a fetal inflammatory response contributing to PTB, which supports our findings.

Polymicrobial presence demonstrated in PTB (Thomsen et al., 1984; Elliott et al., 1990; McGregor et al., 1990; Hillier et al., 1991; McDonald et al., 1992, 1994; Holst et al., 1994; Grattard et al., 1995; Kundsins et al., 1996; Usui et al., 2002; Goffinet et al., 2003; Goldenberg et al., 2008; Onderdonk et al., 2008; Montenegro et al., 2019), SPTL (Minkoff et al., 1984; Gravett et al., 1986; Lamont et al., 1987; Hillier et al., 1988; Romero et al., 1989, 1992c; McGregor et al., 1990; Harger et al., 1991; Toth et al., 1992; Watts et al., 1992; Holst et al., 1994, 2005; Font et al., 1995; Horowitz et al., 1995; Marconi et al., 2011; Choi et al., 2012; Kim et al., 2012; Lee et al., 2013), and PPROM (Minkoff et al., 1984; Romero et al., 1992b,c; Averbuch et al., 1995; Font et al., 1995; Grattard et al., 1995; Horowitz et al., 1995; Kundsins et al., 1996; Perni et al., 2004; Shim et al., 2005; Nasution et al., 2007), was mostly based on a combination of *U. urealyticum* and *M. hominis* (Ma et al., 2021). Co-infections

TABLE 1 | Subgroup analysis of the association (odds ratio) of genital mycoplasma with preterm birth (PTB), preterm labor (PTL), and preterm prelabor rupture of membranes (PPROM) based on the diagnostic method used to detect genital mycoplasma.

Genital mycoplasma	Culture		PCR	
	OR	95% CI	OR	95% CI
Preterm birth				
<i>M. genitalium</i>	–	–	2.04	1.18–3.52
<i>M. hominis</i>	2.84	1.02–2.40	1.64	0.75–3.59
<i>U. parvum</i>	–	–	1.75	1.47–2.07
<i>U. urealyticum</i>	1.57	1.02–2.40	1.32	0.83–2.12
Preterm labor				
<i>M. genitalium</i>	–	–	–	–
<i>M. hominis</i>	1.78	0.08–1.08	10.23	0.11–4.54
<i>U. parvum</i>	–	–	–	–
<i>U. urealyticum</i>	1.96	–0.05–1.40	7.95	0.86–3.28
Preterm prelabor rupture of membrane				
<i>M. genitalium</i>	–	–	–	–
<i>M. hominis</i>	2.09	1.42–3.08	–	–
<i>U. parvum</i>	–	–	–	–
<i>U. urealyticum</i>	3.31	0.35–31.50	–	–

TABLE 2 | Subgroup analysis of the association (odds ratio) of genital mycoplasma with preterm birth (PTB), preterm labor (PTL), and preterm prelabor rupture of membranes (PPROM) based on the specimen used to detect genital mycoplasma.

Genital mycoplasma	Fetal sample		Maternal sample		Both samples	
	OR	95% CI	OR	95% CI	OR	95% CI
Preterm birth						
<i>M. genitalium</i>	–	–	2.04	1.18–3.52	–	–
<i>M. hominis</i>	0.75	0.07–8.44	2.37	1.39–4.04	–	–
<i>U. parvum</i>	2.08	0.09–46.06	1.74	1.47–2.07	–	–
<i>U. urealyticum</i>	1.55	0.22–11.12	1.45	1.09–1.94	3.31	1.79–6.12
Preterm labor						
<i>M. genitalium</i>	–	–	–	–	–	–
<i>M. hominis</i>	4.35	1.14–16.59	1.72	1.01–2.91	–	–
<i>U. parvum</i>	–	–	–	–	–	–
<i>U. urealyticum</i>	2.68	1.18–6.09	1.94	0.77–4.90	5.00	2.25–11.12
Preterm prelabor rupture of membrane						
<i>M. genitalium</i>	–	–	–	–	–	–
<i>M. hominis</i>	–	–	2.09	1.42–3.08	–	–
<i>U. parvum</i>	–	–	–	–	–	–
<i>U. urealyticum</i>	–	–	3.31	0.35–31.50	–	–

were also associated with decreased gestational age at birth and birth weight, and a significant increase in the incidence of histologic chorioamnionitis (Kwak et al., 2014). However, most of these studies examined only genital mycoplasmas. They did not examine other more virulent Gram-negative or positive associated with mycoplasmas, which may have biased some reports and conclusions.

One of the limitations of this SR is the heterogeneity shown by the large I^2 values from our MA. This may be due to

several factors, such as the variability in the source and timing of biological samples and diagnostic methods for detecting genital mycoplasma.

Interpretation

Like other organisms associated with SPTL, PTB, or PPROM such as *G. vaginalis*, quantitative analysis of the genital mycoplasmas may be more important than simply the presence or absence of the organism, whether detected by cultivation-dependent or independent techniques (Lamont et al., 2020). Using cultivation-dependent technology in women delivering between 26 and 34 completed weeks of gestation, 80 and 24% of those in SPTL were colonized by *U. urealyticum* and *M. hominis*, respectively. In contrast, women who were not in SPTL but delivered electively for maternal-fetal indications such as preeclampsia or intrauterine growth restriction at the same gestational age, 46 and 8%, were colonized by *U. urealyticum* and *M. hominis*, respectively. The qualitative analysis was statistically significantly different for *U. urealyticum* ($p < 0.01$) but not for *M. hominis*. Nevertheless, when only heavy presence of *M. hominis* was considered [$>10^5$ color change units (the unit of quantity at the time)], 13 women in the study group (18%) and none of the controls were identified ($p < 0.05$), suggesting that it was not the presence or absence of the organism that was important but the quantity present (Lamont et al., 1987). This was also supported by various *in vitro* and *in vivo* studies showing a dose-dependent increase in inflammation and PTB rate with higher doses of *Ureaplasma* spp. infections (Glaser et al., 2017, 2018; Motomura et al., 2020; Tantengco et al., 2021).

Only specific subtypes of the genital mycoplasmas are pathogenic. Using molecular-based techniques, it was found that *Ureaplasma* species consist of 14 serovars from two biovars. The majority of human *Ureaplasma* isolates belong to *U. parvum* (biovar 1), comprising four serovars (the predominant biovar in patients with genital tract infections), with *U. urealyticum* (biovar 2) containing ten serovars isolated much less often. However, the data are limited and conflicted because of the difficulties with traditional genotyping methods (Dhawan et al., 2012). This may be relevant to the confusion about the role of ureaplasmas in adverse outcomes of pregnancy.

The most common method of identifying microbes reported was culture, followed by PCR. Both these approaches are used for both qualitative and quantitative detection of bacteria. Most recent studies used molecular detection of genital mycoplasma instead of culture, as only four studies used microbiological culture after 2010 (Kim et al., 2012; Lee et al., 2013; Wang et al., 2013; Suzuki et al., 2018). Accordingly, detection of genital mycoplasmas may have been underestimated in former studies as the detection rate of mycoplasmas by PCR is higher than that by cultivation (Choi et al., 2012). Molecular analysis has the advantage of differentiating mycoplasma species and allowing the bacterial load to be measured, although bacterial load was reported only in a few included studies. The microbial load can alter the type of biomarker and their quantities (Flores-Herrera et al., 2012; Noda-Nicolau et al., 2016). Sample collections for mycoplasma detection were mainly performed at

admission with clinical indications of labor and/or at the time of labor and delivery.

One of the objectives of this study was to determine the association between the genital mycoplasmas and adverse pregnancy outcomes with specific inflammatory biomarkers. However, the data were too heterogeneous to perform a MA. It is still unclear if the genital mycoplasmas can mount a proinflammatory surge that can lead to adverse pregnancy outcomes. Most biomarker studies examined only proinflammatory markers, and few studies report anti-inflammatory mediators. Among PPRM patients, Oh et al. (2010) have demonstrated higher maternal blood WBC and CRP during mycoplasma AF positivity, mainly *Ureaplasma* spp. (Oh et al., 2010).

Conversely, one major study examined 26 proteins in AF and reported several anti-inflammatory markers (IL-10, sTNFR1, sIL-6r) elevated in cases associated with the genital mycoplasmas, also predominantly by *Ureaplasmas* (Cobo et al., 2012). *In vitro* models have suggested that unbiased analysis of pro- and anti-inflammatory markers is required to determine the actual role of diverse mycoplasmas in inducing an inflammatory response during pregnancy (Noda-Nicolau et al., 2016; Polettini et al., 2018). Some genital mycoplasmas such as *Ureaplasma* spp. may present themselves as proxies for other virulent microbial pathogens such as *E. coli*, Group B streptococcus (GBS), or *Gardnerella* species. Therefore, genital mycoplasma might be insufficient to cause SPTL and PTB but can assist other pathogens or modify the tissue environment in a polymicrobial situation.

CONCLUSION

This SR raises several questions related to the pathogenic role of the genital mycoplasmas, and the MA found an association with specific adverse pregnancy outcomes between a single pathogen or in mycoplasmas combination. However, ambiguity remains concerning independent contributions by various genital mycoplasmas and adverse pregnancy outcomes. This ambiguity is derived from a lack of evidence on the precise location of the infection (fetal vs. maternal), microbial load (most reports

on load are based on amplified microbial nucleic acid), and detection timing. This SR also evaluated biomarkers, and we report that the genital mycoplasmas are poor immunogens and do not generate the quantity of inflammatory mediators like those of other pathogens. However, this conclusion may depend on their load, location and polymicrobial presence. Our own *in vitro* studies have shown that poor immunogenicity by these microbes in human fetal membranes as well as in the cervix (Noda-Nicolau et al., 2016; Tantengco et al., 2021, 2022). These results suggest that the association between the genital mycoplasmas and adverse pregnancy outcomes might not be strong enough to warrant universal antimicrobial intervention. Intervention to prevent PTB may not be recommended but based on several factors such as the infectious agent, polymicrobial etiology, knowledge of the most virulent pathogen, bacterial load and location, and subsequent neonatal morbidity intervention strategies may be indicated and tailored to the patient's needs.

AUTHOR CONTRIBUTIONS

RM: conception of the work and funding. NN-N and MGS: data collection. NN-N, MGS, JP, CM, MCS, GB, GC, and OT: data extraction. NN-N, JP, OT, MCS, GB, and GC: quality assessment and drafting the manuscript. JP: meta-analysis. RM, RL, and BT: critical revision of the manuscript. All authors reviewed and approved the final version of the manuscript.

FUNDING

This work was supported by the Strategic Research Commitment fund from UTMB and a grant “1R01HD100729” from NIH/NICHD to RM, and CAPES International Cooperation Program (Grant/Award Number: PGCI 028/2012) to MGS.

SUPPLEMENTARY MATERIAL

The Supplementary Material for this article can be found online at: <https://www.frontiersin.org/articles/10.3389/fmicb.2022.859732/full#supplementary-material>

REFERENCES

- Abele-Horn, M., Wolff, C., Dressel, P., Pfaff, F., and Zimmermann, A. (1997). Association of *Ureaplasma urealyticum* biovars with clinical outcome for neonates, obstetric patients, and gynecological patients with pelvic inflammatory disease. *J. Clin. Microbiol.* 35, 1199–1202. doi: 10.1128/jcm.35.5.1199-1202.1997
- Athayde, N., Romero, R., Maymon, E., Gomez, R., Pacora, P., Yoon, B. H., et al. (2000). Interleukin 16 in pregnancy, parturition, rupture of fetal membranes, and microbial invasion of the amniotic cavity. *Am. J. Obstet. Gynecol.* 182, 135–141. doi: 10.1016/S0002-9378(00)70502-3
- Averbuch, B., Mazor, M., Shoham-Vardi, I., Chaim, W., Vardi, H., Horowitz, S., et al. (1995). Intra-uterine infection in women with preterm premature rupture of membranes: maternal and neonatal characteristics. *Eur. J. Obstet. Gynecol. Reprod. Biol.* 62, 25–29. doi: 10.1016/0301-2115(95)02176-8
- Bashiri, A., Horowitz, S., Huleihel, M., Hackmon, R., Dukler, D., and Mazor, M. (1999). Elevated concentrations of interleukin-6 in intra-amniotic infection with *Ureaplasma urealyticum* in asymptomatic women during. *Acta Obstet. Gynecol. Scand.* 78, 379–382. doi: 10.1080/j.1600-0412.1999.780506.x
- Baumann, L., Cina, M., Egli-Gany, D., Goutaki, M., Halbeisen, F. S., Lohrer, G. R., et al. (2018). Prevalence of *Mycoplasma genitalium* in different population groups: systematic review and meta-analysis. *Sex. Transm. Infect.* 94, 255–262. doi: 10.1136/sextrans-2017-053384
- Cahill, R. J., Tan, S., Dougan, G., O'Gaora, P., Pickard, D., Kennea, N., et al. (2005). Universal DNA primers amplify bacterial DNA from human fetal membranes and link *Fusobacterium nucleatum* with prolonged preterm membrane rupture. *Mol. Hum. Reprod.* 11, 761–766. doi: 10.1093/molehr/gah234
- Chawanpaiboon, S., Vogel, J. P., Moller, A. B., Lumbiganon, P., Petzold, M., Hogan, D., et al. (2019). Global, regional, and national estimates of levels of preterm birth in 2014: a systematic review and modelling analysis. *Lancet Glob. Heal.* 7, e37–e46. doi: 10.1016/S2214-109X(18)30451-0

- Choi, S. J., Park, S. D., Jang, I. H., Uh, Y., and Lee, A. (2012). The prevalence of vaginal microorganisms in pregnant women with preterm labor and preterm birth. *Ann. Lab. Med.* 32, 194–200. doi: 10.3343/alm.2012.32.3.194
- Cobo, T., Kacerovsky, M., Palacio, M., Hornychova, H., Hougaard, D. M., Skogstrand, K., et al. (2012). Intra-amniotic inflammatory response in subgroups of women with preterm prelabor rupture of the membranes. *PLoS One* 7:e43677. doi: 10.1371/journal.pone.0043677
- Dando, S. J., Nitsos, I., Kallapur, S. G., Newnham, J. P., Polglase, G. R., Pillow, J. J., et al. (2012). The role of the multiple banded antigen of *Ureaplasma parvum* in intra-amniotic infection: major virulence factor or decoy? *PLoS One* 7:29856. doi: 10.1371/journal.pone.0029856
- Dhawan, B., Malhotra, N., Sreenivas, V., Rawre, J., Khanna, N., Chaudhry, R., et al. (2012). *Ureaplasma* serovars & their antimicrobial susceptibility in patients of infertility & genital tract infections. *Indian J. Med. Res.* 136, 991–996.
- Elliott, B., Brunham, R. C., Laga, M., Piot, P., Ndinya-Achola, J. O., Maitha, G., et al. (1990). Maternal Gonococcal Infection as a Preventable Risk Factor for Low Birth Weight. *J. Infect. Dis.* 161, 531–536. doi: 10.1093/infdis/161.3.531
- Flores-Herrera, H., García-López, G., Díaz, N. F., Molina-Hernández, A., Osorio-Caballero, M., Soriano-Becerril, D., et al. (2012). An experimental mixed bacterial infection induced differential secretion of proinflammatory cytokines (IL-1 β , TNF α) and proMMP-9 in human fetal membranes. *Placenta* 33, 271–277. doi: 10.1016/j.placenta.2012.01.007
- Font, G. E., Gauthier, D. W., Meyer, W. J., Myles, T. D., Janda, W., and Bieniarz, A. (1995). Catalase activity as a predictor of amniotic fluid culture results in preterm labor or premature rupture of membranes. *Obstet. Gynecol.* 85, 656–658. doi: 10.1016/0029-7844(95)00026-N
- Friedland, Y. D., Lee-Pullen, T. F., Nathan, E. A., Watts, R., Keelan, J. A., Payne, M. S., et al. (2016). T cell cytokine responses to stimulation with *Ureaplasma parvum* in pregnancy. *J. Reprod. Immunol.* 116, 93–97. doi: 10.1016/j.jri.2016.03.002
- Glaser, K., Silwedel, C., Fehrholz, M., Henrich, B., Waaga-Gasser, A. M., Claus, H., et al. (2018). *Ureaplasma* isolates stimulate proinflammatory CC chemokines and matrix metalloproteinase-9 in neonatal and adult monocytes. *PLoS One* 13, 1–17. doi: 10.1371/journal.pone.0194514
- Glaser, K., Silwedel, C., Fehrholz, M., Waaga-Gasser, A. M., Henrich, B., Claus, H., et al. (2017). *Ureaplasma* Species differentially modulate pro- and anti-inflammatory cytokine responses in newborn and adult human monocytes pushing the state toward pro-inflammation. *Front. Cell. Infect. Microbiol.* 7, 1–15. doi: 10.3389/fcimb.2017.00484
- Goffinet, F., Maillard, F., Mihoubi, N., Kayem, G., Papiernik, E., Cabrol, D., et al. (2003). Bacterial vaginosis: prevalence and predictive value for premature delivery and neonatal infection in women with preterm labour and intact membranes. *Eur. J. Obstet. Gynecol. Reprod. Biol.* 108, 146–151. doi: 10.1016/s0301-2115(02)00423-2
- Goldenberg, R. L., Andrews, W. W., Goepfert, A. R., Faye-Petersen, O., Cliver, S., Carlo, W. A., et al. (2008). The Alabama Preterm Birth Study: umbilical cord blood *Ureaplasma urealyticum* and *Mycoplasma hominis* cultures in very preterm newborns. *Am. J. Obstet. Gynecol.* 198, e1–e43. doi: 10.1038/jid.2014.371
- Grattard, F., Soleihac, B., De Barbeyrac, B., Bebear, C., Seffert, P., and Pozzetto, B. (1995). Epidemiologic and molecular investigations of genital mycoplasmas from women and neonates at delivery. *Pediatr. Infect. Dis. J.* 14, 853–858. doi: 10.1097/00006454-199510000-00007
- Gravett, M. G., Hummel, D., Eschenbach, D. A., and Holmes, K. K. (1986). Preterm labor associated with subclinical amniotic fluid infection and with bacterial vaginosis. *Obstet. Gynecol.* 67, 229–237. doi: 10.1097/00006250-198602000-00013
- Harger, J. H., Meyer, M. P., Amortegui, A., Macpherson, T. A., Kaplan, L., and Mueller-Heubach, E. (1991). Low incidence of positive amniotic fluid cultures in preterm labor at 27–32 weeks in the absence of clinical evidence of chorioamnionitis. *Obstet. Gynecol.* 77, 228–234. doi: 10.1097/00006250-199102000-00013
- Hillier, S. L., Krohn, M. A., Kiviat, N. B., Watts, D. H., and Eschenbach, D. A. (1991). Microbiologic causes and neonatal outcomes associated with chorioamnion infection. *Am. J. Obstet. Gynecol.* 165, 955–961. doi: 10.1016/0002-9378(91)90447-y
- Hillier, S. L., Martius, J., Krohn, M., Kiviat, N., Holmes, K. K., and Eschenbach, D. A. (1988). A case-control study of chorioamnion infection and histologic chorioamnionitis in prematurity. *N. Engl. J. Med.* 319, 972–978. doi: 10.1056/NEJM198810133191503
- Holst, E., Goffeng, A. R., and Andersch, B. (1994). Bacterial vaginosis and vaginal microorganisms in idiopathic premature labor and association with pregnancy outcome. *J. Clin. Microbiol.* 32, 176–186. doi: 10.1128/jcm.32.1.176-186.1994
- Holst, R. M., Mattsby-Baltzer, I., Wennerholm, U. B., Hagberg, H., and Jacobsson, B. (2005). Interleukin-6 and interleukin-8 in cervical fluid in a population of Swedish women in preterm labor: Relationship to microbial invasion of the amniotic fluid, intra-amniotic inflammation, and preterm delivery. *Acta Obstet. Gynecol. Scand.* 84, 551–557. doi: 10.1111/j.0001-6349.2005.00708.x
- Horowitz, S., Horowitz, J., Mazor, M., Porath, A., and Glezerman, M. (1995). *Ureaplasma urealyticum* cervical colonization as a marker for pregnancy complications. *Int. J. Gynecol. Obstet.* 48, 15–19. doi: 10.1016/0020-7292(94)02236-4
- Jacobsson, B., Aaltonen, R., Rantakokko-Jalava, K., Morken, N.-H., and Alanen, A. (2009). Quantification of *Ureaplasma urealyticum* DNA in the amniotic fluid from patients in PTL and pPROM and its relation to inflammatory cytokine levels. *Acta Obstet. Gynecol. Scand.* 88, 63–70. doi: 10.1080/00016340802572646
- Jacobsson, B., Mattsby-Baltzer, I., Andersch, B., Bokström, H., Holst, R.-M., Nikolaitchouk, N., et al. (2003). Microbial invasion and cytokine response in amniotic fluid in a Swedish population of women with preterm prelabor rupture of membranes. *Acta Obstet. Gynecol. Scand.* 82, 423–431. doi: 10.1034/j.1600-0412.2003.00157.x
- Kacerovsky, M., Cobo, T., Andrys, C., Musilova, I., Drahosova, M., Hornychova, H., et al. (2013b). The fetal inflammatory response in subgroups of women with preterm prelabor rupture of the membranes. *J. Matern. Neonatal Med.* 26, 795–801. doi: 10.3109/14767058.2013.765404
- Kacerovsky, M., Celec, P., Vlkova, B., Skogstrand, K., Hougaard, D. M., Cobo, T., et al. (2013a). Amniotic fluid protein profiles of intraamniotic inflammatory response to *Ureaplasma* spp. and other bacteria. *PLoS One* 8, 6–12. doi: 10.1371/journal.pone.0060399
- Kacerovsky, M., Pavlovsky, M., and Tosner, J. (2009). Preterm premature rupture of the membranes and genital mycoplasmas. *Acta medica* 52, 117–120. doi: 10.14712/18059694.2016.115
- Kacerovsky, M., Pliskova, L., Bolehovska, R., Skogstrand, K., Hougaard, D. M., Tsiartas, P., et al. (2012). The impact of the microbial load of genital mycoplasmas and gestational age on the intensity of intraamniotic inflammation. *Am. J. Obstet. Gynecol.* 206, e1–e342. doi: 10.1016/j.ajog.2012.01.004
- Kacerovsky, M., Pliskova, L., Menon, R., Kutova, R., Musilova, I., Maly, J., et al. (2014). Microbial load of umbilical cord blood *Ureaplasma* species and *Mycoplasma hominis* in preterm prelabor rupture of membranes. *J. Matern. Neonatal Med.* 27, 1627–1632. doi: 10.3109/14767058.2014.887068
- Kacerovsky, M., Romero, R., Stepan, M., Stranik, J., Maly, J., Pliskova, L., et al. (2020). Antibiotic administration reduces the rate of intraamniotic inflammation in preterm prelabor rupture of the membranes. *Am. J. Obstet. Gynecol.* 223, e1–e114. doi: 10.1016/j.ajog.2020.01.043
- Kasper, D. C., Mechtler, T. P., Reischer, G. H., Witt, A., Langgartner, M., Pollak, A., et al. (2010). The bacterial load of *Ureaplasma parvum* in amniotic fluid is correlated with an increased intrauterine inflammatory response. *Diagn. Microbiol. Infect. Dis.* 67, 117–121. doi: 10.1016/j.diagmicrobio.2009.12.023
- Kim, S. M., Romero, R., Lee, J., Lee, S. M., Park, C.-W., Park, J. S., et al. (2012). The frequency and clinical significance of intra-amniotic inflammation in women with preterm uterine contractility but without cervical change: do the diagnostic criteria for preterm labor need to be changed? *J. Matern. Fetal. Neonatal Med.* 25, 1212–1221. doi: 10.3109/14767058.2011.629256
- Koucký, M., Malíčková, K., Cindrová-Davies, T., Smíšek, J., Vráblíková, H., Černý, A., et al. (2016). Prolonged progesterone administration is associated with less frequent cervicovaginal colonization by *Ureaplasma urealyticum* during pregnancy - Results of a pilot study. *J. Reprod. Immunol.* 116, 35–41. doi: 10.1016/j.jri.2016.04.285
- Kundsinn, R. B., Leviton, A., Allred, E. N., and Poulin, S. A. (1996). *Ureaplasma urealyticum* infection of the placenta in pregnancies that ended prematurely. *Obstet. Gynecol.* 87, 122–127. doi: 10.1016/0029-7844(95)00376-2
- Kwak, D. W., Hwang, H. S., Kwon, J. Y., Park, Y. W., and Kim, Y. H. (2014). Co-infection with vaginal *Ureaplasma urealyticum* and *Mycoplasma hominis* increases adverse pregnancy outcomes in patients with preterm labor or

- preterm premature rupture of membranes. *J. Matern. Neonatal Med.* 27, 333–337. doi: 10.3109/14767058.2013.818124
- Lamont, R. F. (2015). Advances in the Prevention of Infection-Related Preterm Birth. *Front. Immunol.* 6:566. doi: 10.3389/fimmu.2015.00566
- Lamont, R. F., Taylor-Robinson, D., Wigglesworth, J. S., Furr, P. M., Evans, R. T., and Elder, M. G. (1987). The role of mycoplasmas, ureaplasmas and chlamydiae in the genital tract of women presenting in spontaneous early preterm labour. *J. Med. Microbiol.* 24, 253–257. doi: 10.1099/00222615-24-3-253
- Lamont, R. F., van den Munckhof, E. H., Luef, B. M., Vinter, C. A., and Jørgensen, J. S. (2020). Recent advances in cultivation-independent molecular-based techniques for the characterization of vaginal eubiosis and dysbiosis. *Fac. Rev.* 9:21. doi: 10.12703/r/9-21
- Lee, S. Y., Park, K. H., Jeong, E. H., Oh, K. J., Ryu, A., and Kim, A. (2013). Intra-amniotic infection/inflammation as a risk factor for subsequent ruptured membranes after clinically indicated amniocentesis in preterm labor. *J. Korean Med. Sci.* 28, 1226–1232. doi: 10.3346/jkms.2013.28.8.1226
- Liberati, A., Altman, D. G., Tetzlaff, J., Mulrow, C., Gøtzsche, P. C., Ioannidis, J. P. A., et al. (2009). The PRISMA statement for reporting systematic reviews and meta-analyses of studies that evaluate health care interventions: explanation and elaboration. *PLoS Med.* 6:e1000100. doi: 10.1371/journal.pmed.1000100
- Lis, R., Rowhani-Rahbar, A., and Manhart, L. E. (2015). Mycoplasma genitalium Infection and Female Reproductive Tract Disease: a Meta-analysis. *Clin. Infect. Dis.* 61, 418–426. doi: 10.1093/cid/civ312
- Lo, C. K.-L., Mertz, D., and Loeb, M. (2014). Newcastle-Ottawa Scale: comparing reviewers' to authors' assessments. *BMC Med. Res. Methodol.* 14:45. doi: 10.1186/1471-2288-14-45
- Ma, C., Du, J., Dou, Y., Chen, R., Li, Y., Zhao, L., et al. (2021). The associations of genital Mycoplasmas with female infertility and adverse pregnancy outcomes?: a systematic review and meta-analysis. *Reprod. Sci.* 2021:399. doi: 10.1007/s43032-020-00399-w
- Marconi, C., de Andrade Ramos, B. R., Peraçoli, J. C., Donders, G. G. G., and da Silva, M. G. (2011). Amniotic fluid interleukin-1 beta and interleukin-6, but not interleukin-8 correlate with microbial invasion of the amniotic cavity in preterm labor. *Am. J. Reprod. Immunol.* 65, 549–556. doi: 10.1111/j.1600-0897.2010.00940.x
- McDonald, H. M., O'Loughlin, J. A., Jolley, P., Vigneswaran, R., and McDonald, P. J. (1992). Prenatal microbiological risk factors associated with preterm birth. *Br. J. Obstet. Gynaecol.* 99, 190–196. doi: 10.1111/j.1471-0528.1992.tb14497.x
- McDonald, H. M., O'Loughlin, J. A., Jolley, P. T., Vigneswaran, R., and McDonald, P. J. (1994). Changes in vaginal flora during pregnancy and association with preterm birth. *J. Infect. Dis.* 170, 724–728. doi: 10.1093/infdis/170.3.724
- McGregor, J. A., French, J. I., Richter, R., Franco-Buff, A., Johnson, A., Hillier, S., et al. (1990). Antenatal microbiologic and maternal risk factors associated with prematurity. *Am. J. Obstet. Gynecol.* 163, 1465–1473. doi: 10.1016/0002-9378(90)90607-9
- Menon, R., and Fortunato, S. J. (2007). Infection and the role of inflammation in preterm premature rupture of the membranes. *Best Pract. Res. Clin. Obstet. Gynaecol.* 21, 467–478. doi: 10.1016/j.bpobgyn.2007.01.008
- Minkoff, H., Grunebaum, A. N., Schwarz, R. H., Feldman, J., Cummings, M., Crombleholme, W., et al. (1984). Risk factors for prematurity and premature rupture of membranes: a prospective study of the vaginal flora in pregnancy. *Am. J. Obstet. Gynecol.* 150, 965–972. doi: 10.1016/0002-9378(84)90392-2
- Montenegro, D. A., Borda, L. F., Neuta, Y., Gómez, L. A., Castillo, D. M., Loyo, D., et al. (2019). Oral and uro-vaginal intra-amniotic infection in women with preterm delivery: a case-control study. *J. Investig. Clin. Dent.* 10:e12396. doi: 10.1111/jicd.12396
- Motomura, K., Romero, R., Xu, Y., Theis, K. R., Galaz, J., Winters, A. D., et al. (2020). Intra-Amniotic Infection with Ureaplasma parvum Causes Preterm Birth and Neonatal Mortality That Are Prevented by Treatment with Clarithromycin. *MBio* 11:20. doi: 10.1128/mBio.00797-20
- Nasution, T. A., Cheong, S. F., Lim, C. T., Leong, E. W. K., and Ngeow, Y. F. (2007). Multiplex PCR for the detection of urogenital pathogens in mothers and newborns. *Malays. J. Pathol.* 29, 19–24.
- Nguyen, D. P., Gerber, S., Hohlfeld, P., Sandrine, G., and Witkin, S. S. (2004). Mycoplasma hominis in mid-trimester amniotic fluid: Relation to pregnancy outcome. *J. Perinat. Med.* 32, 323–326. doi: 10.1515/JPM.2004.060
- Noda-Nicolau, N. M., Poletti, J., Peltier, M. R., da Silva, M. G., and Menon, R. (2016). Combinations and loads of bacteria affect the cytokine production by fetal membranes: an in vitro study. *Am. J. Reprod. Immunol.* 76, 504–511. doi: 10.1111/aji.12596
- Novy, M. J., Duffy, L., Axthelm, M. K., Sadowsky, D. W., Witkin, S. S., Gravett, M. G., et al. (2009). Ureaplasma parvum or Mycoplasma hominis as sole pathogens cause chorioamnionitis, preterm delivery, and fetal pneumonia in rhesus macaques. *Reprod. Sci.* 16, 56–70. doi: 10.1177/1933719108325508
- Oh, K. J., Lee, S. E., Jung, H., Kim, G., Romero, R., and Yoon, B. H. (2010). Detection of ureaplasmas by the polymerase chain reaction in the amniotic fluid of patients with cervical insufficiency. *J. Perinat. Med.* 38, 261–268. doi: 10.1515/jpm.2010.040
- Oh, K. J., Romero, R., Park, J. Y., Lee, J., Conde-Agudelo, A., Hong, J.-S., et al. (2019). Evidence that antibiotic administration is effective in the treatment of a subset of patients with intra-amniotic infection/inflammation presenting with cervical insufficiency. *Am. J. Obstet. Gynecol.* 221, e1–e140. doi: 10.1016/j.ajog.2019.03.017
- Onderdonk, A. B., Delaney, M. L., DuBois, A. M., Allred, E. N., and Leviton, A. (2008). Detection of bacteria in placental tissues obtained from extremely low gestational age neonates. *Am. J. Obstet. Gynecol.* 198, e1–e7. doi: 10.1016/j.ajog.2007.05.044
- Pacora, P., Maymon, E., Gervasi, M. T., Gomez, R., Edwin, S. S., Yoon, B. H., et al. (2000). Lactoferrin in intrauterine infection, human parturition, and rupture of fetal membranes. *Am. J. Obstet. Gynecol.* 183, 904–910. doi: 10.1067/mob.2000.108882
- Pavlidis, I., Spiller, O. B., Sammut Demarco, G., MacPherson, H., Howie, S. E. M., Norman, J. E., et al. (2020). Cervical epithelial damage promotes Ureaplasma parvum ascending infection, intrauterine inflammation and preterm birth induction in mice. *Nat. Commun.* 11, 1–12. doi: 10.1038/s41467-019-14089-y
- Payne, M. S., Feng, Z., Li, S., Doherty, D. A., Xu, B., Li, J., et al. (2014). Second trimester amniotic fluid cytokine concentrations, Ureaplasma sp. colonisation status and sexual activity as predictors of preterm birth in Chinese and Australian women. *BMC Pregn. Childb.* 14:340. doi: 10.1186/1471-2393-14-340
- Perni, S. C., Vardhana, S., Korneeva, I., Tuttle, S. L., Paraskevas, L. R., Chasen, S. T., et al. (2004). Mycoplasma hominis and Ureaplasma urealyticum in midtrimester amniotic fluid: Association with amniotic fluid cytokine levels and pregnancy outcome. *Am. J. Obstet. Gynecol.* 191, 1382–1386. doi: 10.1016/j.ajog.2004.05.070
- Poletti, J., Peltier, M. R., Noda-Nicolau, N. M., Menon, R., and da Silva, M. G. (2018). Polybacterial stimulation suggests discrete IL-6/IL-6R signaling in human fetal membranes: Potential implications on IL-6 bioactivity. *J. Reprod. Immunol.* 126, 60–68. doi: 10.1016/j.jri.2018.02.007
- R Core Team (2020). *R: A language and environment for statistical computing*. Vienna: R Core Team.
- Romero, R., Espinoza, K., Goncalves, L. F., Kusanovic, J. P., Friel, L., and Hassan, S. (2011). The role of inflammation and infection in preterm birth. *Semin. Reprod. Med.* 38, 385–406. doi: 10.1016/j.clp.2011.06.003
- Romero, R., Gomez-Lopez, N., Winters, A. D., Jung, E., Shaman, M., Bieda, J., et al. (2019). Evidence that intra-amniotic infections are often the result of an ascending invasion - A molecular microbiological study. *J. Perinat. Med.* 47, 915–931. doi: 10.1515/jpm-2019-0297
- Romero, R., Mazar, M., Brandt, F., Sepulveda, W., Avila, C., Cotton, D. B., et al. (1992b). Interleukin-1 alpha and interleukin-1 beta in preterm and term human parturition. *Am. J. Reprod. Immunol.* 27, 117–123. doi: 10.1111/j.1600-0897.1992.tb00737.x
- Romero, R., Mazar, M., Sepulveda, W., Avila, C., Copeland, D., and Williams, J. (1992c). Tumor necrosis factor in preterm and term labor. *Am. J. Obstet. Gynecol.* 166, 1576–1587. doi: 10.1016/0002-9378(92)91636-O
- Romero, R., Gonzalez, R., Sepulveda, W., Brandt, F., Ramirez, M., Sorokin, Y., et al. (1992a). Infection and labor. VIII. Microbial invasion of the amniotic cavity in patients with suspected cervical incompetence: prevalence and clinical significance. *Am. J. Obstet. Gynecol.* 167, 1086–1091. doi: 10.1016/s0002-9378(12)80043-3
- Romero, R., Miranda, J., Chaemsaitong, P., Chaiworapongsa, T., Kusanovic, J. P., Dong, Z., et al. (2015). Sterile and microbial-associated intra-amniotic inflammation in preterm prelabor rupture of membranes. *J. Matern. Neonatal Med.* 28, 1394–1409. doi: 10.3109/14767058.2014.958463

- Romero, R., Sirtori, M., Oyarzun, E., Avila, C., Mazor, M., Callahan, R., et al. (1989). Infection and labor. V. Prevalence, microbiology, and clinical significance of intraamniotic infection in women with preterm labor and intact membranes. *Am. J. Obstet. Gynecol.* 161, 817–824. doi: 10.1016/0002-9378(89)90409-2
- Shim, S.-S., Romero, R., Jun, J. K., Moon, K. C., Kim, G., and Yoon, B. H. (2005). C-reactive protein concentration in vaginal fluid as a marker for intra-amniotic inflammation/infection in preterm premature rupture of membranes. *J. Matern. neonatal Med. Off. J. Eur. Assoc. Perinat. Med. Fed. Asia Ocean. Perinat. Soc. Int. Soc. Perinat. Obstet.* 18, 417–422. doi: 10.1080/14786430500362231
- Shimizu, T., Kida, Y., and Kuwano, K. (2008). *Ureaplasma parvum* lipoproteins, including MB antigen, activate NF- κ B through TLR1, TLR2 and TLR6. *Microbiology* 154, 1318–1325. doi: 10.1099/mic.0.2007/016212-0
- Stranik, J., Kacerovsky, M., Andrys, C., Soucek, O., Bolehovska, R., Holeckova, M., et al. (2021). Intra-amniotic infection and sterile intra-amniotic inflammation are associated with elevated concentrations of cervical fluid interleukin-6 in women with spontaneous preterm labor with intact membranes. *J. Matern. Neonatal Med.* 2021, 1–9. doi: 10.1080/14767058.2020.1869932
- Suzuki, Y., Horie, K., Yada, Y., Kono, Y., Hirashima, C., Usui, R., et al. (2018). Vaginal *Ureaplasma* species increase chorioamnionitis in very preterm infants with preterm premature rupture of the membranes at < 28 weeks of gestation. *Eur. J. Clin. Microbiol. Infect. Dis.* 37, 2371–2380.
- Tanaka, S., Tsumura, K., Nakura, Y., Tokuda, T., Nakahashi, H., Yamamoto, T., et al. (2019). New antibiotic regimen for preterm premature rupture of membrane reduces the incidence of bronchopulmonary dysplasia. *J. Obstet. Gynaecol. Res.* 2019, 1–7. doi: 10.1111/jog.13903
- Tantengco, O. A. G., Kechichian, T., Vincent, K. L., Pyles, R. B., Medina, P. M. B., and Menon, R. (2021). Inflammatory response elicited by *Ureaplasma parvum* colonization in human cervical epithelial, stromal, and immune cells. *Reproduction* 163, 1–10. doi: 10.1530/REP-21-0308
- Tantengco, O. A. G., and Menon, R. (2022). Breaking Down the Barrier: The Role of Cervical Infection and Inflammation in Preterm Birth. *Front. Glob. Women's Heal.* 2:777643. doi: 10.3389/fgwh.2021.777643
- Tantengco, O. A. G., Richardson, L., Radnaa, E., Kammala, A. K., Kechichian, T., Ganguly, E., et al. (2022). Cervix-on-a-chip for investigating ascending *Ureaplasma parvum* infection in pregnancy. *Am. J. Obstet. Gynecol.* 226, S12–S13. doi: 10.1016/j.ajog.2021.11.068
- Tantengco, O. A. G., and Yanagihara, I. (2019). Current understanding and treatment of intra-amniotic infection with *Ureaplasma* spp. *J. Obstet. Gynaecol. Res.* 2019:14052. doi: 10.1111/jog.14052
- Taylor-Robinson, D., and Lamont, R. F. (2010). Mycoplasmas in pregnancy. *Br. J. Obstet. Gynaecol.* 118, 164–174. doi: 10.1111/j.1471-0528.2010.02766.x
- Thomsen, A. C., Taylor-Robinson, D., Hansen, K. B., Furr, P. M., Ross, J. M., Milton, P. J., et al. (1984). The infrequent occurrence of Mycoplasmas in amniotic fluid from women with intact fetal membranes. *Acta Obstet. Gynecol. Scand.* 63, 425–429. doi: 10.3109/00016348409156697
- Toth, K. S., Letchworth, A. T., Noble, A. D., and Williams, M. (1992). The significance of infection in the aetiology of preterm labour. A prospective controlled study. *J. Obstet. Gynaecol.* 12, 94–99. doi: 10.3109/01443619209013603
- Uchida, K., Nakahira, K., Mimura, K., Shimizu, T., De Seta, F., Wakimoto, T., et al. (2013). Effects of *Ureaplasma parvum* lipoprotein multiple-banded antigen on pregnancy outcome in mice. *J. Reprod. Immunol.* 100, 118–127. doi: 10.1016/j.jri.2013.10.001
- Usui, R., Ohkuchi, A., Matsubara, S., Izumi, A., Watanabe, T., Suzuki, M., et al. (2002). Vaginal lactobacilli and preterm birth. *J. Perinat. Med.* 30, 458–466. doi: 10.1515/JPM.2002.072
- Wang, X., Buhimschi, C. S., Temoin, S., Bhandari, V., Han, Y. W., and Buhimschi, I. A. (2013). Comparative microbial analysis of paired amniotic fluid and cord blood from pregnancies complicated by preterm birth and early-onset neonatal sepsis. *PLoS One* 8:566131. doi: 10.1371/journal.pone.0056131
- Watts, D. H., Krohn, M. A., Hillier, S. L., and Eschenbach, D. A. (1992). The association of occult amniotic fluid infection with gestational age and neonatal outcome among women in preterm labor. *Obstet. Gynecol.* 79, 351–357. doi: 10.1097/00006250-199203000-00005
- Wells, G., Shea, B., O'Connell, D., Peterson, J., Welch, V., Losos, M., et al. (2013). *The Newcastle-Ottawa Scale (NOS) for assessing the quality of nonrandomised studies in meta-analyses*. Available online at: http://www.ohri.ca/programs/clinical_epidemiology/oxford.asp [Accessed January 21, 2021]
- Witt, A., Berger, A., Gruber, C. J., Petricevic, L., Apfalter, P., and Husslein, P. (2005). IL-8 concentration in maternal serum, amniotic fluid and cord blood in relation to different pathogens within the amniotic cavity. *J. Perinat. Med.* 33, 22–26. doi: 10.1515/JPM.2005.003
- Yoneda, N., Yoneda, S., Niimi, H., Ueno, T., Hayashi, S., Ito, M., et al. (2016). Polymicrobial Amniotic Fluid Infection with Mycoplasma/Ureaplasma and Other Bacteria Induces Severe Intra-Amniotic Inflammation Associated with Poor Perinatal Prognosis in Preterm Labor. *Am. J. Reprod. Immunol.* 75, 112–125. doi: 10.1111/aji.12456

Conflict of Interest: The authors declare that the research was conducted in the absence of any commercial or financial relationships that could be construed as a potential conflict of interest.

Publisher's Note: All claims expressed in this article are solely those of the authors and do not necessarily represent those of their affiliated organizations, or those of the publisher, the editors and the reviewers. Any product that may be evaluated in this article, or claim that may be made by its manufacturer, is not guaranteed or endorsed by the publisher.

Copyright © 2022 Noda-Nicolau, Tantengco, Poletini, Silva, Bento, Cursino, Marconi, Lamont, Taylor, Silva, Jupiter and Menon. This is an open-access article distributed under the terms of the Creative Commons Attribution License (CC BY). The use, distribution or reproduction in other forums is permitted, provided the original author(s) and the copyright owner(s) are credited and that the original publication in this journal is cited, in accordance with accepted academic practice. No use, distribution or reproduction is permitted which does not comply with these terms.



The *Mycoplasma* spp. ‘Releasome’: A New Concept for a Long-Known Phenomenon

Patrice Gaurivaud* and Florence Tardy

Anses, Laboratoire de Lyon, VetAgro Sup, UMR Mycoplasmoses Animales, Université de Lyon, Lyon, France

OPEN ACCESS

Edited by:

Iain Sutcliffe,
Northumbria University,
United Kingdom

Reviewed by:

Glenn Francis Browning,
The University of Melbourne, Australia
Steven Philip Djordjevic,
University of Technology Sydney,
Australia
Katarzyna Dudek,
National Veterinary Research Institute
(NVRI), Poland

*Correspondence:

Patrice Gaurivaud
patrice.gaurivaud@anses.fr

Specialty section:

This article was submitted to
Evolutionary and Genomic
Microbiology,
a section of the journal
Frontiers in Microbiology

Received: 12 January 2022

Accepted: 14 March 2022

Published: 15 April 2022

Citation:

Gaurivaud P and Tardy F (2022)
The *Mycoplasma* spp. ‘Releasome’:
A New Concept for a Long-Known
Phenomenon.
Front. Microbiol. 13:853440.
doi: 10.3389/fmicb.2022.853440

The bacterial secretome comprises polypeptides expressed at the cell surface or released into the extracellular environment as well as the corresponding secretion machineries. Despite their reduced coding capacities, *Mycoplasma* spp. are able to produce and release several components into their environment, including polypeptides, exopolysaccharides and extracellular vesicles. Technical difficulties in purifying these elements from the complex broth media used to grow mycoplasmas have recently been overcome by optimizing growth conditions and switching to chemically defined culture media. However, the secretion pathways responsible for the release of these structurally varied elements are still poorly described in mycoplasmas. We propose the use of the term ‘releasome,’ instead of secretome, to refer to molecules released by mycoplasmas into their environment. The aim of this review is to more precisely delineate the elements that should be considered part of the mycoplasmal releasome and their role in the interplay of mycoplasmas with host cells and tissues.

Keywords: secretome, polysaccharide, *Mycoplasma*, extracellular vesicles, exoproteome

INTRODUCTION

The term bacterial secretome was coined in the very beginning of the 21st century (Tjalsma et al., 2000) to describe “the components of machineries for protein secretion and the native secreted proteins,” with a primary focus on the secretion systems, i.e., machineries, involved in membrane translocation. Since then, the definition of the secretome has been regularly revised to focus more on the final localization of the secreted proteins and their potential distinct associated functions (Desvaux et al., 2009; Armengaud et al., 2012; Monteiro et al., 2021). The concept of the secretome now includes surface-exposed proteins (surface proteome), proteins released as free (not cell-attached) into the bacterial environment (exoproteome) and proteins embedded in extracellular vesicles (proteovesiculome) (Monteiro et al., 2021). The bacterial secretome plays a range of roles in interactions with the host (including adhesion, invasion, immune evasion and modulation), nutrient acquisition, and interactions between bacterial cells. Some of these interactions are positive, like biofilm formation, while others can be negative, like competition (Chagnot et al., 2013; Sharma et al., 2017; Tommassen and Arenas, 2017; Hernandez et al., 2020). Many of the proteins involved in virulence are found in the secretome, and characterizing these proteins is essential to understanding host-pathogen interactions and ultimately to developing a suitable disease control strategy (Dwivedi et al., 2016). However, although most of the extant literature has focused on secreted proteins, other polymers, like polysaccharides, are also exported by bacteria and fulfill different functions, depending on their final location, i.e., either cell-attached or not (Desvaux et al., 2009; Woodward and Naismith, 2016). Here we propose to (i) broaden the concept of the bacterial secretome to include non-polypeptide molecules like polysaccharides and

more complex elements like extracellular vesicles (EV), and to (ii) rename this broader group of components *releasome* in order to take account of the gaps in knowledge about secretion machineries in some bacterial models (which is especially true for mycoplasmas) and to alter the focus exclusively to non-cell-attached elements released by living cells.

Polysaccharides are long-chain polymers composed of sugar units linked by glycosidic bonds. Extracellular polysaccharides either are attached to the cell and form a capsule or a slime layer around the cell, or are secreted as cell-free polysaccharides into the bacterium's immediate environment. The generic term *exopolysaccharides* was proposed in 1972 to describe these two extracellular localizations (Sutherland, 1972). Many studies on exopolysaccharides fail to clearly specify their precise localization (free vs. cell-attached). However, it is essential to make a distinction between cell-linked and cell-free exopolysaccharides, as the two forms may play different roles in host interactions. The methodology used for purification provides clues about the type of exopolysaccharides under study: cell-linked polysaccharides are purified from washed cell pellets, while cell-free polysaccharides are purified from cell-free supernatants. In this review, for purposes of clarification, we use the acronym for cell-attached polysaccharides (CPS) that can form a capsule or a slime around the cell, and we use the term exopolysaccharides (EPS) strictly to refer to cell-free polysaccharides. The fact the composition and structure of the polysaccharide moiety might be identical with a single shared biosynthesis pathway (Woodward and Naismith, 2016) can make it difficult to distinguish between CPS and EPS: for instance, stresses can release CPS into the environment (Sutherland, 1985; Cerning, 1990; Llobet et al., 2008), and structures such as biofilms can make it difficult to assess cell attachment.

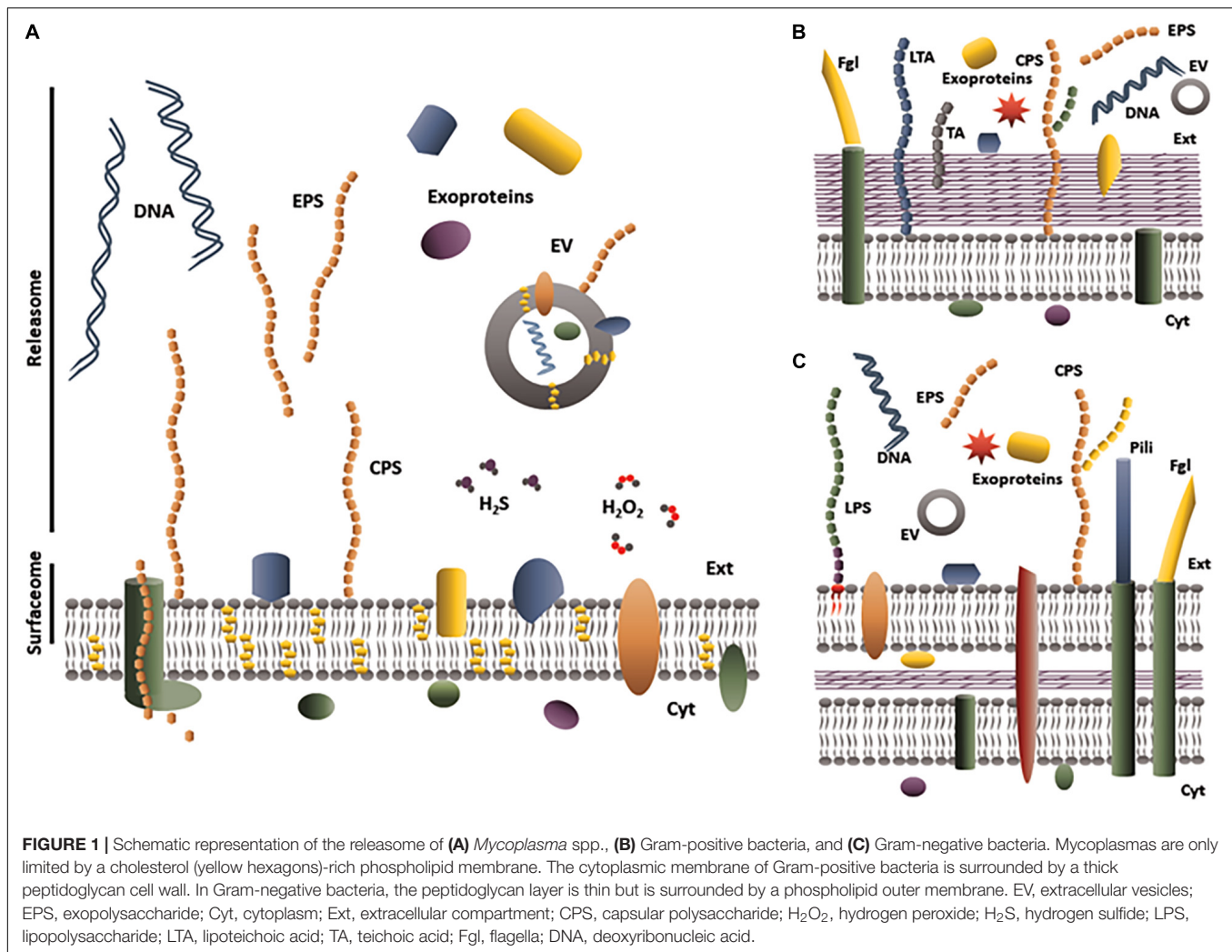
Extracellular vesicles are the most complex structures of the releasome, as they are composed of lipids, proteins, glycoconjugates and nucleic acids. Their composition reflects their biogenesis from the cell (Kim et al., 2015; Toyofuku et al., 2019). Bacterial EV are defined as non-replicative, membranous spherical structures with a size ranging from 20–400 nm that are secreted by viable cells (Deatherage et al., 2009; Toyofuku et al., 2019).

Figure 1 summarizes all potential components included in the releasome to date, i.e., a subset of polypeptides (whatever the secretion pathways) plus polysaccharides, EV, nucleic acids and metabolites (such as H₂O₂ or H₂S) released into the extracellular milieu. The releasome definition is particularly suitable for bacteria of the genus *Mycoplasma*, for which secretion systems are poorly known or poorly predictable *in silico* (Zubair et al., 2020a). Mycoplasmas, i.e., bacteria belonging to the genus *Mycoplasma* (*M.*), are small (300–800 nm diameter), wall-less bacteria with only a phospholipid, cholesterol-rich bilayer membrane surrounding the cytoplasm (**Figure 1A**, in contrast to panels B,C which show Gram+ or Gram– bacteria, respectively). Released molecules are ‘just’ translocated through the cytoplasmic membrane, which is a simpler situation than in the Gram+ and Gram– bacteria (Desvaux et al., 2009). Because of their small genome, coding for less than 1000 proteins, and the paucity of their metabolic pathways, mycoplasmas are

considered the simplest bacteria able to replicate in an acellular medium (Razin et al., 1998). The first evidence of cell-free molecules released by mycoplasmas is historically related to the first culture (in 1898) of *M. mycoides* subsp. *mycoides*, the causal agent of contagious bovine pleuropneumonia (CBPP) (Nocard and Roux, 1898). The authors used a collodion bag containing broth inoculated with serous pulmonary fluid from a CBPP-diseased cow and placed into a peritoneal cavity of a rabbit. Mycoplasmas were able to survive and grow inside this non-permissive host because the collodion bag was permeable to host-released nutrients but offered protection against the rabbit immune system (Bove, 1999). Their work also found evidence that the collodion bag released a mycoplasma-produced component that induced necrosis in the surrounding tissues and might have contributed to cachexia in the rabbit (Lloyd, 1966). Other studies in the 1960s–1970s demonstrated some cell-free molecules released by mycoplasmas, such as polysaccharides or antigens recovered from the body fluids of CBPP-infected animals (Plackett et al., 1963; Gourlay, 1965), nanosized globular elements observed by microscopy in *M. pneumoniae* broth cultures (Eng and Froholm, 1971), and uncharacterized molecules that had cytotoxic activity in the supernatant of *M. bovis genitalium* cultures (Afshar, 1967). However, investigators at the time were unable to precisely identify the chemical structure of these elements, as they were unable to purify them from components of the complex growth medium or from body fluids. These experimental bottlenecks have recently been eased through various strategies that are covered in the first part of this review. In the second part, we propose an updated picture of the known composition and role of three main components of the releasome—exoproteins, EPS, and EV—in *Mycoplasma* spp. This concerns only components released into supernatants of mycoplasma growth medium alone or in interaction with host cells. Cellular invasion by mycoplasmas have been described for several species, including *M. hyopneumoniae* (Raymond et al., 2018b), *M. bovis* (Burki et al., 2015), *M. genitalium* (McGowin et al., 2009), *M. fermentans* (Yavlovich et al., 2004a), and *M. pneumoniae* (Yavlovich et al., 2004b) and the phenomenon is likely to be widespread. However, components released by mycoplasmas once in this cytoplasmic compartment of the host cell have not been studied thus far. Molecular mechanisms leading to the release of exoproteins, EPS and EV will not be covered here except for purpose of understanding the potential dual localization of molecules. The third and final section discusses the role of the mycoplasmal releasome.

EXPERIMENTAL BOTTLENECKS TO CHARACTERIZING THE RELEASOME OF MYCOPLASMAS IN VITRO

Molecules found free in a bacterial growth medium can have 3 distinct origins: (i) they could be brought by some complex components of the medium itself (such as serum, for instance), (ii) they could be released as a result of cell lysis during the different growth phases or purification processes, or (iii) they

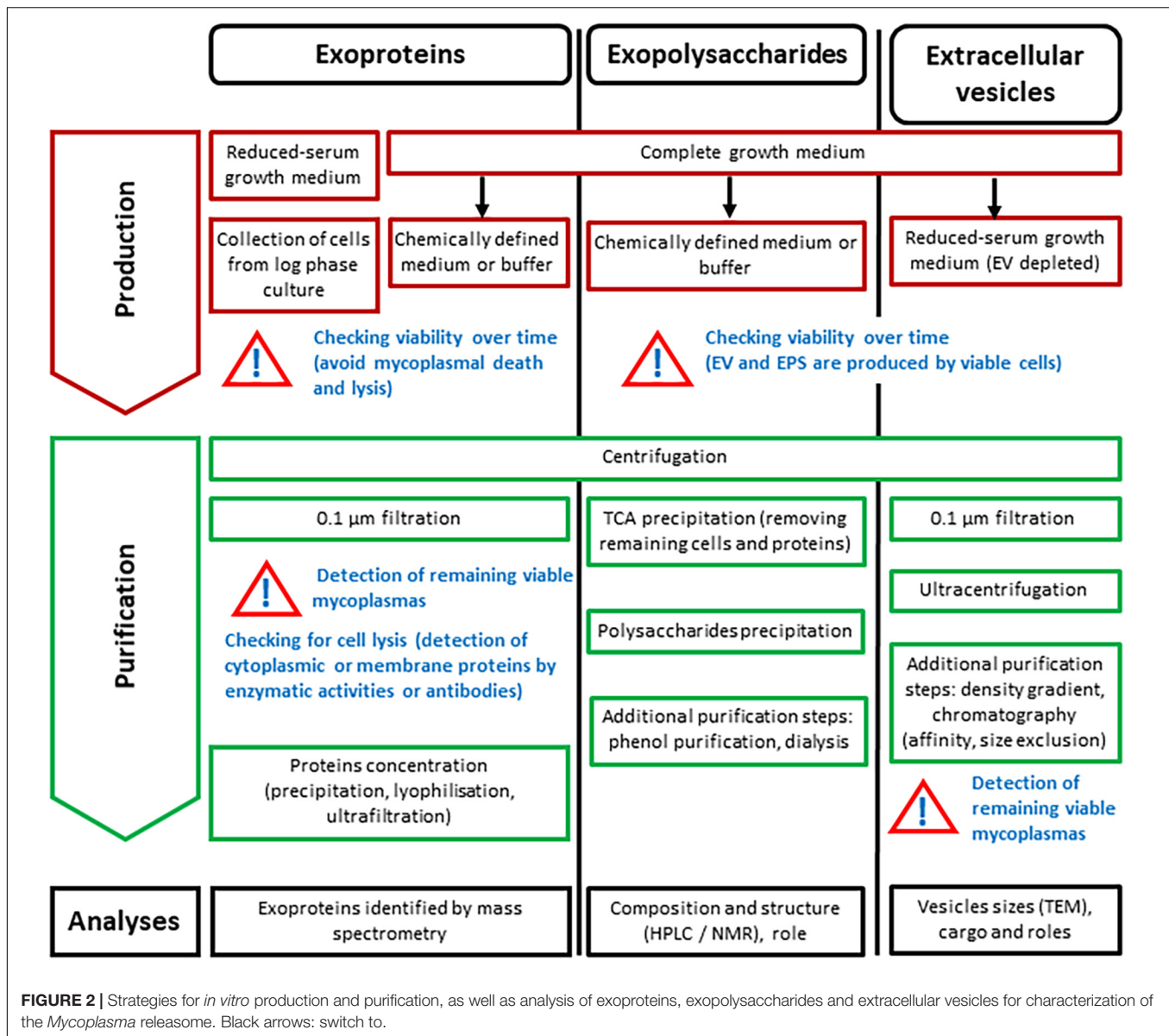


could be actively secreted or “simply” released (in the absence of known secretion machineries) by the bacterium. The release corresponds to the third category only, and one of the main experimental difficulties is to distinguish this category from the two others. Interference from medium components and from non-specific release of mycoplasma components (due to cell lysis in the different growth phases or harsh purification processes) varies between the different classes of molecules (proteins, polysaccharides, membrane vesicles) and the methodology used for their characterization (**Figure 2**). Exoproteins are usually identified by mass spectrometry, exopolysaccharides are identified by HPLC and NMR, and EV are first observed by TEM, and their composition is characterized using various biochemical techniques. *In vitro* characterization of the release necessitates a fine balance between placing mycoplasmas in the conditions where they actually release components (whether or not related to the total biomass produced) and finding experimental conditions that enable detection or purification of these components from the culture supernatant. The composition of the culture medium, the growth time before harvest, and the potential interspecies or interstrain diversity also need to be considered, as they can

substantially influence the composition of the release (Bertin et al., 2015; Monteiro et al., 2021; Olaya-Abril et al., 2021).

Exoproteome

Two recent papers have summarized the experimental bottlenecks and strategies for purification of the mycoplasma exoproteome (Zubair et al., 2020a; Zhang et al., 2021). The authors pointed out that the high polypeptide concentrations in the growth media contributed by components such as serum dramatically jeopardizes the purification of proteins released by mycoplasmas, as is the case for exoproteins from eukaryotic cells that require serum for growth (Armengaud et al., 2012). Indeed, the 20% serum supplementation, usually used in mycoplasma medium, adds up to 12 g of proteins/L, which is dramatically more than the 2 mg of mycoplasma biomass/L reached by *M. hyopneumoniae* under optimized growth conditions (Hwang et al., 2010). A simple solution is to lower the relative concentrations of serum, as has been done to study the exoproteome of *M. hyopneumoniae*/*M. flocculare* (Paes et al., 2017) and *M. bovis* (Zubair et al., 2020b). However, such modifications of the growth medium dramatically affect the



growth of mycoplasmas (Paes et al., 2017; Zubair et al., 2020b). Another strategy is to employ an ultrafiltration process to remove polypeptides from the growth medium prior to use. Voros et al. assessed the exoproteome of *M. capricolum* subsp. *capricolum* grown in a 10 kDa filtered complex medium (Voros et al., 2015). This process depletes proteins with a molecular weight greater than 10 kDa, but it comes at a risk of also removing lipids and cholesterol, which are essential for mycoplasma growth. However, the ultra-filtered medium nevertheless allowed residual growth of *M. capricolum* subsp. *capricolum* (Voros et al., 2009). Another method for bypassing this problem is to use a two-step approach (Figure 2), i.e., first, to produce a reasonable quantity of viable mycoplasma cells using complex growth media, and then to transfer the cells into a chemically defined medium with a reduced protein concentration (Ganter et al., 2019) or in an isotonic buffer like PBS (Zhang et al., 2021). Transferring

mycoplasmas from a complex to a simpler medium requires centrifugation and washing steps that are associated with a risk of cell lysis and consequently release of cytoplasmic proteins. In a medium allowing growth (complete or serum-reduced), mycoplasmas can be harvested during the log phase, assuming that no cell lysis occurs. When mycoplasmas are incubated in a medium other than those allowing growth, the viability of the mycoplasmas over the incubation time needs to be checked, for instance by plating aliquots onto solid media and counting colonies (Ganter et al., 2019; Zhang et al., 2021; Figure 2).

Centrifugation of mycoplasma cells is an essential step in the process of purifying exoproteins from the broth supernatant (Figure 2). However, even at 15000 g, viable mycoplasmas may remain in the supernatant (Hopfe et al., 2004). Increasing centrifuge force to completely remove floating cells (Zubair et al., 2020b) might not be the best solution, as it could damage the cells

and result in cell lysis (Razin et al., 1973). A preferred solution would be to filter the supernatant through a 0.1- μ m filter before characterizing the exoproteome. While 0.2- μ m filters can stop mycoplasma cells they do not completely remove all mycoplasma species (Gaurivaud et al., 2018). An agar plate count of viable mycoplasmas remaining in the supernatant is an easily performed control, but ensuring the total absence of viable mycoplasma cells is highly dependent on the test sample seeded on the agar plate. The control of potential cell lysis during purification could be ensured by detecting cytoplasmic or membrane proteins in supernatants using antibodies or assays for cytoplasmic enzymes such as lactate dehydrogenase (Voros et al., 2015) or hexokinase (Minion et al., 1993). However, caution is warranted when interpreting the results, as some moonlighting proteins expected to be cytoplasmic or membrane-bound can also be released into the extracellular environment as discussed below. For the same reason, the extracellular localization of a specific protein needs to be double-checked to confidently exclude any contamination by cell proteins during the exoproteome purification process. Protein localization is done either by detecting their enzymatic activities if feasible [e.g., extracellular nucleases; (Yamamoto et al., 2017)], or by using specific antibodies (Djordjevic et al., 2004; Zhang et al., 2016; Li et al., 2019). Such tests can be performed directly in complex medium and are less influenced by the contamination from cell lysis associated with transfer to a defined medium.

Exopolysaccharides

As with the exoproteome, a complex growth medium is not suitable for mycoplasma EPS purification (Bertin et al., 2013). Serum and yeast extracts contained in the growth medium contribute high concentrations of exogenous polysaccharides that hamper purification of the mycoplasma polysaccharides. Because very low quantities of EPS are produced by mycoplasmas [a maximum of 50 mg/L for *M. mycoides* subsp. *mycoides* (Bertin et al., 2013), while *Klebsiella* or *Acinetobacter* spp. can produce up to 6 g/L (Bryan et al., 1986)], partial depletion of exogenous polysaccharides is not sufficient, so the alternative is to use a defined culture medium that is totally devoid of polysaccharides. The effort to develop serum-free defined media started in the 1960s (Tourtellotte et al., 1964) with the aim of determining mycoplasma nutrient requirements more precisely (e.g., preferred carbon sources) and studying their general metabolism [e.g., sugar biosynthesis pathways; (Yus et al., 2009; Jordan et al., 2013)]. However, although defined culture media enable control of substrate concentrations, they remain difficult to produce and use even today, and have not been optimized for all mycoplasma species. A simpler alternative consists of using serum-free eukaryotic cell culture media such as CMRL, which contains only glucose as a carbon source—a strategy we previously used to purify polysaccharides secreted by mycoplasmas belonging to the *M. mycoides* cluster (Bertin et al., 2013, 2015) and by *M. agalactiae* (Gaurivaud et al., 2016). In culture media used for eukaryotic cell growth, mycoplasmas may maintain a degree of viability, but are unable to grow. Therefore, to reach a satisfactory biomass, mycoplasmas have to be first grown in a complex medium, with cells pelleted and washed

before being transferred into the defined eukaryotic cell medium (Figure 2). During incubation in CMRL, mycoplasmas remain viable and metabolically active for a period of time, with the duration dependent on the species. Polysaccharides are produced by viable mycoplasma cells, and so a viability time-course has to be checked before purification of the polysaccharides (Figure 2). However, even if some mycoplasmas are lysed in the process, this does not result in non-specific release of CPS (Bertin et al., 2013). After incubation, mycoplasma cells are removed by centrifugation. A supplementary 0.1- μ m filtration step is not essential, as the remaining cells and proteins in the supernatant are removed by trichloroacetic acid precipitation (Figure 2). Finally, the polysaccharides are precipitated with acetone or ethanol. The level of purification can be increased by adding a further step, such as dialysis, to remove free hexoses, which interfere with the sugar composition measured by HPLC, and phenol treatment to remove biologically active small peptides (Totte et al., 2015).

Antibodies raised against polysaccharides are a good screening tool to help track the purification process or detect EPS in biological fluids (Bertin et al., 2015). However, they are not easily produced, as large amounts of purified polysaccharides conjugated to a carrier protein are required.

Extracellular Vesicles

The ultracentrifugation step necessary to collect EV produced in a complex growth medium often results in an unwanted non-specific adsorption of albumin and immunoglobulins from the serum onto the surface of the vesicles, thus jeopardizing purification. The same difficulties are met during purification of exosomes from blood (Caradec et al., 2014). Reducing the serum and yeast extract concentrations is a good option, as it limits this 'co-precipitation' and also induces a nutritional stress conducive to vesicles formation and shedding (Klimentova and Stulik, 2015). This approach has been used for EV purification from *Mycoplasma* spp. and species of another close genus also belonging to the class *Mollicutes*, *Acholeplasma* (Chernov et al., 2011; Gaurivaud et al., 2018; Figure 2). Other stresses favoring EV production might be considered, such as iron deprivation through the use of chelators (Madsen et al., 2006; Martinez-Torro et al., 2020). Serum contains eukaryotic membrane vesicles that have to be removed before preparing the growth medium in order to ensure they are not co-purified with the EV (Kornilov et al., 2018). *In vitro*, EV are only produced by viable mycoplasma cells, and we demonstrated previously that lysed, heat-killed cells do not produce non-specific EV-like vesicles (Gaurivaud et al., 2018). A viability control is therefore necessary during experiments to produce EV.

Before ultracentrifugation of the broth medium supernatant to collect the EV, a preliminary 0.1- μ m filtration is advisable to remove small mycoplasma cells that could still be in suspension after elimination of the pelleted cells (Figure 2). However, this filtration step could also remove some of the large vesicles and hence select a sub-population of EV (Konoshenko et al., 2018), as there is a clear size overlap between small cells and large vesicles (Gaurivaud et al., 2018).

Once pelleted, EV can be further purified using density gradients (sucrose, OptiprepTM) or chromatography, as described for Gram-positive and Gram-negative bacterial vesicles (Kim et al., 2015; Klimentova and Stulik, 2015). This supplementary purification step has already been validated for *Acholeplasma laidlawii* (Chernov et al., 2014) and could be used for *Mycoplasma* spp., where it would help to remove any residual mycoplasma cells that might interfere with characterization of the polypeptides (by MS) and the DNA content (by PCR) of the purified EV.

KNOWN ELEMENTS OF THE MYCOPLASMAL RELEASOME

Exoproteome

Mycoplasma exoproteomes have been a recent focus of research and these studies have benefited from the considerable developmental advances in other bacterial models (Zubair et al., 2020a). The first partial exoproteome was obtained in 2012 for *M. synoviae* (Rebollo Couto et al., 2012), followed by those of *M. hyopneumoniae*, *M. flocculare*, *M. bovis* and *M. capricolum* subsp. *capricolum* cultivated in axenic conditions (Voros et al., 2015; Paes et al., 2017; Zubair et al., 2020b; Zhang et al., 2021). Another study explored the exoproteome produced by swine mycoplasmas in interaction with their host cells (Leal Zimmer et al., 2019). However, relevant studies remain scarce and are not readily comparable because of the use of different methodological approaches (strains, culture conditions, purification steps). Because of these problems with comparability, we have focused only on exoproteins that have a specific, detectable function (Table 1).

Nucleases

Nucleases are easy to detect *in vitro* by visualization of DNA hydrolysis. For instance, DNA can be embedded into a solid matrix, either agar growth medium or a polyacrylamide gel, and its hydrolysis results in a clear halo around colonies or a clear band after electrophoretic migration of the nuclease (Minion et al., 1993; Sharma et al., 2015; Zhang et al., 2016; Yamamoto et al., 2017). Extracellular nucleases have been suspected in mycoplasmas since 1993, when Minion et al. demonstrated degradation of linear DNA by mycoplasma-free supernatants obtained after incubation of several mycoplasma species in a nuclease assay buffer (Minion et al., 1993). More recently, DNA degradation around *M. pneumoniae* colonies indicated the secretion of an extracellular nuclease, which was found by mutagenesis to be the MPN491 nuclease (Yamamoto et al., 2017). Other extracellular proteins with nuclease activity *in vitro* have been reported, including the P40 protein of *M. penetrans*, as demonstrated using zymography (Bendjennat et al., 1997), and the MAM superantigen of *M. arthritidis*, as demonstrated by degradation of genomic DNA (Diedershausen et al., 2007). Homologs of these nucleases have also been detected in the cytoplasmic membrane of other species, but their extracellular localization has yet not been investigated (Sharma et al., 2015).

Specific antibodies can be used to detect and localize nucleases. An example is the Mhp597 nuclease of *M. hyopneumoniae*, an ortholog of *M. pneumoniae* MPN491, which was detected in the growth medium supernatant by western blotting using specific antibodies (Li et al., 2019).

Although less straightforward, bulk proteomics data can be examined to detect potential nucleases in the cell environment. For instance, several nucleases have been identified by MS in the exoproteome purified from cell-free culture supernatants [e.g., Mhp7448_0580 (homolog of Mhp597) and MBOV_RS02825] or in the supernatant of a swine tracheal cell line infected with *M. hyopneumoniae* (Zhang et al., 2016; Paes et al., 2017; Leal Zimmer et al., 2019; Table 1).

Once secreted into the mycoplasmal environment, extracellular nucleases could participate in (i) nutrient scavenging (through degradation of the DNA released by cell lysis during the infection process) or in (ii) host evasion through hydrolysis of the neutrophil extracellular traps (NET), which are DNA networks produced by neutrophils that can trap and kill pathogens. NET evasion has been shown *in vitro* for two important lung pathogens, *M. bovis* in cattle (by nuclease MBOV_RS02825) and *M. pneumoniae* in humans (with nuclease MPN491) (Zhang et al., 2016; Yamamoto et al., 2017). The inactivation/deletion of the gene coding MPN491 resulted in a reduced survival of *M. pneumoniae* in the presence of neutrophils *in vitro* as well as *in vivo* in a mouse nasal infection model. In the most recent example, poor survival of a mutant was associated with its inability to degrade NETs induced by *Escherichia coli* lipopolysaccharides (Yamamoto et al., 2017).

Proteases

Extracellular proteases produced by lung-colonizing ruminant mycoplasmas have been demonstrated by measuring the degradation of fluorescent casein in culture supernatants and observing clearer digestion areas around colonies on casein-enriched solid medium (Allam et al., 2010; Ganter et al., 2019). Zymography and mutagenesis experiments further showed that *M. mycoides* subsp. *capri* MMCAP2_0241 and *M. capricolum* subsp. *capricolum* MCAP_0240, which both belong to the S41 peptidase family, are the main extracellular peptidases of these two species (Allam et al., 2010, 2012; Ganter et al., 2019). By zymography, the apparent molecular mass of these polypeptidases was estimated to be 55 kDa, in contrast with the 75 kDa molecular mass predicted from the sequences of the corresponding genes. Two predicted transmembrane domains at the N- and C-terminal ends suggest a potential membrane localization of the native proteins that may be cleaved, by endoproteolysis for example, to be released into the medium (Ganter et al., 2019).

Sequence analysis and function prediction have identified several peptidases in the exoproteome of *M. capricolum* subsp. *capricolum* (Voros et al., 2015) and *M. bovis* (Zubair et al., 2020b), as well as in the supernatant of cells infected with *M. hyopneumoniae* and *M. flocculare* (Leal Zimmer et al., 2019; Table 1).

In other bacterial models, such as *Staphylococcus* (*S.*) *aureus*, extracellular proteases are involved in nutrient acquisition,

TABLE 1 | Non-exhaustive list of exoproteins with known functions released by *Mycoplasma* (sub)species.

Proteins	Identification	Species	Strains	Mnemonic/accession number	Culture conditions	Detection in extracellular environment	References
Nucleases	Ca ²⁺ /Mg ²⁺ nuclease	<i>M. hyopneumoniae</i>	V11	Mhp597	Complete growth medium	Western blotting	Li et al., 2019
			7448	MHP7448_0580	Serum reduced medium	Exoproteome	Paes et al., 2017
			J	MHJ_0581	Infected cells (serum free medium)	Exoproteome	Leal Zimmer et al., 2019
	Endonuclease/exonuclease	<i>M. bovis</i>	HB0801	MBOV_RS02825	Complete growth medium	Western blotting	Zhang et al., 2016
	Mg ²⁺ nuclease	<i>M. pneumoniae</i>	M129	MPN491	Complete growth medium	Zymography	Yamamoto et al., 2017
	Lipoprotein P40	<i>M. penetrans</i>	GTU-54-6A1	MYPE4380	Complete growth medium	Zymography	Bendjennat et al., 1997
	Superantigen	<i>M. arthritis</i>	PG6	Marth_orf036	Complete growth medium	Lymphocytes proliferation	Atkin et al., 1994
Peptidases	S41 family peptidase	<i>M. mycoides</i> subsp. <i>capri</i>	95010	MMCAP2_0241	Complete growth medium	Casein hydrolysis	Ganter et al., 2019
		<i>M. capricolum</i> subsp. <i>capricolum</i>	Ckid	MCAP_0240	Complete growth medium	Casein hydrolysis	Ganter et al., 2019
	Putative peptidase DUF31	<i>M. bovirhinis</i>	MV5	MBVR141_0224	Complete growth medium	Casein hydrolysis	Ganter et al., 2019
	Oligoendopeptidase F	<i>M. capricolum</i> subsp. <i>capricolum</i>	Ckid	MCAP_0193	Serum reduced medium	Exoproteome	Voros et al., 2015
		<i>M. hyopneumoniae</i>	7448	AAZ53887.2	Infected cells (serum free medium)	Exoproteome	Leal Zimmer et al., 2019
		<i>M. flocculare</i>	ATCC 27716	ENX51111.1	Infected cells (serum free medium)	Exoproteome	Leal Zimmer et al., 2019
		<i>M. bovis</i>	HB0801	Mbov_0133	Serum reduced medium	Exoproteome	Zubair et al., 2020b
	Zinc metalloprotease, putative	<i>M. capricolum</i> subsp. <i>capricolum</i>	Ckid	MCAP_0804	Serum reduced medium	Exoproteome	Voros et al., 2015
	Dipeptidase, putative	<i>M. capricolum</i> subsp. <i>capricolum</i>	Ckid	MCAP_0420	Serum reduced medium	Exoproteome	Voros et al., 2015
	Cytosol aminopeptidase	<i>M. capricolum</i> subsp. <i>capricolum</i>	Ckid	MCAP_0127; MCAP_0195	Serum reduced medium	Exoproteome	Voros et al., 2015
	Aminopeptidase	<i>M. flocculare</i>	ATCC 27716	WP_002557776.1	Infected cells (serum free medium)	Exoproteome	Leal Zimmer et al., 2019
		<i>M. hyopneumoniae</i>	J	AAZ44217.1	Infected cells (serum free medium)	Exoproteome	Leal Zimmer et al., 2019
	Leucyl aminopeptidase	<i>M. hyopneumoniae</i>	7448	AAZ53831.2	Infected cells (serum free medium)	Exoproteome	Leal Zimmer et al., 2019
		<i>M. flocculare</i>	ATCC 27716	WP_002557977.1	Infected cells (serum free medium)	Exoproteome	Leal Zimmer et al., 2019
		<i>M. bovis</i>	HB0801	Mbov_0789; Mbov_0673	Serum reduced medium	Exoproteome	Zubair et al., 2020b
	XAA-PRO aminopeptidase	<i>M. hyopneumoniae</i>	7448	AAZ54021.1	Infected cells (serum free medium)	Exoproteome	Leal Zimmer et al., 2019
	Peptidase M24 family protein	<i>M. flocculare</i>	ATCC 27716	WP_002557496.1	Infected cells (serum free medium)	Exoproteome	Leal Zimmer et al., 2019
	Clp protease ATP-binding subunit	<i>M. bovis</i>	HB0801	Mbov_0703	Serum reduced medium	Exoproteome	Zubair et al., 2020b
Lipases	Lipase MilA	<i>M. bovis</i>	PG45	MBOVPG45_0710	Complete growth medium	Western blotting	Adamu et al., 2020
			HB0801	ADR24994.1	Serum reduced medium	Exoproteome	Zubair et al., 2020b
	Lipase P65	<i>M. hyopneumoniae</i>	7448	AAZ54018.1	Serum reduced medium; Infected cells (serum free medium)	Exoproteome	Paes et al., 2017; Leal Zimmer et al., 2019
			J	AAZ44739.1	Infected cells (serum free medium)	Exoproteome	Leal Zimmer et al., 2019
	Triacyl glycerol lipase	<i>M. bovis</i>	HB0801	Mbov_0558	Serum reduced medium	Exoproteome	Zubair et al., 2020b
Adhesins	Protein P97	<i>M. hyopneumoniae</i>	7448	MHP7448_0198; MHP7448_0108	Serum reduced medium; Infected cells (serum free medium)	Exoproteome	Paes et al., 2017; Leal Zimmer et al., 2019

(Continued)

TABLE 1 | (Continued)

Proteins	Identification	Species	Strains	Mnemonic/accession number	Culture conditions	Detection in extracellular environment	References
	Protein 102	<i>M. hyopneumoniae</i>	J	AAZ44197.1	Infected cells (serum free medium)	Exoproteome	Leal Zimmer et al., 2019
		<i>M. hyopneumoniae</i>	7448	MHP7448_0199; MHP7448_0107	Serum reduced medium; Infected cells (serum free medium)	Exoproteome	Paes et al., 2017; Leal Zimmer et al., 2019
		<i>M. hyopneumoniae</i>	J	AAZ44196.1; AAZ44286.1	Infected cells (serum free medium)	Exoproteome	Leal Zimmer et al., 2019
		<i>M. hyopneumoniae</i>	232	ND	Complete growth medium	Immunoelectron microscopy	Djordjevic et al., 2004; Adams et al., 2005
	P216 surface protein	<i>M. flocculare</i>	ATCC 27716	MFC_00475	Serum reduced medium	Exoproteome	Paes et al., 2017
		<i>M. flocculare</i>	ATCC 27716	MFC_00848	Serum reduced medium	Exoproteome	Paes et al., 2017
		<i>M. hyopneumoniae</i>	7448	AAZ53862.1	Infected cells (serum free medium)	Exoproteome	Leal Zimmer et al., 2019
			J	AAQ11195.1	Infected cells (serum free medium)	Exoproteome	Leal Zimmer et al., 2019
	ABC transporter xylose-binding lipoprotein	<i>M. hyopneumoniae</i>	7448	MHP7448_0604	Serum reduced medium; Infected cells (serum free medium)	Exoproteome	Paes et al., 2017; Leal Zimmer et al., 2019
		<i>M. flocculare</i>	ATCC 27716	ENX51036.1	Infected cells (serum free medium)	Exoproteome	Leal Zimmer et al., 2019
		<i>M. hyopneumoniae</i>	J	AAZ44690.2	Infected cells (serum free medium)	Exoproteome	Leal Zimmer et al., 2019
	46K surface antigen precursor	<i>M. hyopneumoniae</i>	7448	AAZ53879.1	Infected cells (serum free medium)	Exoproteome	Leal Zimmer et al., 2019
			J	POC0J8.1	Infected cells (serum free medium)	Exoproteome	Leal Zimmer et al., 2019
		<i>M. flocculare</i>	ATCC 27716	WP_002557638.1	Infected cells (serum free medium)	Exoproteome	Leal Zimmer et al., 2019
Others proteins	Pyruvate dehydrogenase E1, beta subunit	<i>M. synoviae</i>	53	gij 144575045	Buffer	Exoproteome	Rebollo Couto et al., 2012
		<i>M. hyopneumoniae</i>	J	AAZ44204.1	Infected cells (serum free medium)	Exoproteome	Leal Zimmer et al., 2019
	Enolase	<i>M. synoviae</i>	53	gij 71894034	Buffer	Exoproteome	Rebollo Couto et al., 2012
		<i>M. capricolum</i> subsp. <i>capricolum</i>	Ckid	MCAP_0213	Serum reduced medium	Exoproteome	Voros et al., 2015
		<i>M. hyopneumoniae</i>	7448	AAZ53624.1	Infected cells (serum free medium)	Exoproteome	Leal Zimmer et al., 2019
			J	AAZ44333.1	Infected cells (serum free medium)	Exoproteome	Leal Zimmer et al., 2019
	Chaperone protein DnaK	<i>M. flocculare</i>	ATCC 27716	WP_002557541.1	Infected cells (serum free medium)	Exoproteome	Leal Zimmer et al., 2019
		<i>M. bovis</i>	HB0801	Mbov_0482	Serum reduced medium	Exoproteome	Zubair et al., 2020b
		<i>M. synoviae</i>	53	gij 71894366	Buffer	Exoproteome	Rebollo Couto et al., 2012
		<i>M. hyopneumoniae</i>	7448	AAZ53444.1	Infected cells (serum free medium)	Exoproteome	Leal Zimmer et al., 2019
			J	AAZ44157.1	Infected cells (serum free medium)	Exoproteome	Leal Zimmer et al., 2019
	Elongation factor EF-Tu	<i>M. flocculare</i>	ATCC 27716	WP_002557920.1	Infected cells (serum free medium)	Exoproteome	Leal Zimmer et al., 2019
		<i>M. synoviae</i>	53	gij 71894677	Buffer	Exoproteome	Rebollo Couto et al., 2012
		<i>M. hyopneumoniae</i>	7448	AAZ53889.1	Infected cells (serum free medium)	Exoproteome	Leal Zimmer et al., 2019
			J	AAZ44610.1	Infected cells (serum free medium)	Exoproteome	Leal Zimmer et al., 2019
	Lipoprotein P280	<i>M. flocculare</i>	ATCC 27716	WP_002557626.1	Infected cells (serum free medium)	Exoproteome	Leal Zimmer et al., 2019
		<i>M. bovis</i>	HB081	AFM51648.1	Complete growth medium	Western blotting	Zhao et al., 2021
		<i>M. hyopneumoniae</i>	J	AAZ44125.1	Infected cells (serum free medium)	Exoproteome	Leal Zimmer et al., 2019
			7448	AAZ53412.1	Infected cells (serum free medium)	Exoproteome	Leal Zimmer et al., 2019
	glyceraldehyde 3-phosphate dehydrogenase	<i>M. flocculare</i>	ATCC 27716	MFC_00829	Serum reduced medium	Exoproteome	Paes et al., 2017

Selected proteins have a known function and their extracellular localization has been demonstrated (either experimentally or because they are found in the exoproteome of several species/strains or conditions). ND, not done.

bacterial dissemination and immune evasion (Tam and Torres, 2019). In mycoplasmas, their precise roles have yet to be defined, with a few exceptions. For instance, in *M. hyopneumoniae* the endopeptidase F and the XAA-pro aminopeptidase degrade immunologically active peptides (see below), and the cell-free form of aminopeptidase AAZ44217.1 is involved in adhesion to plasminogen and heparin (Robinson et al., 2013). Extracellular peptidases of *M. capricolum* subsp. *capricolum* MCAP_0240 may have a direct or indirect role in cell surface shaving and thus modulate adhesion and immune invasion, as deletion mutants had a modified surface proteome (Ganter et al., 2019).

Lipases

Chromogenic substrates, such as 2-naphthyl caprylate and 2-naphthyl butyrate, have made it possible to detect lipase activity in the supernatant of *M. capricolum* subsp. *capricolum* cultures (Voros et al., 2015), but the corresponding protein has not yet been identified. Lipase activity has also been detected in two immunodominant surface proteins, the P65 lipoprotein of *M. hyopneumoniae* (Schmidt et al., 2004) and the *M. bovis* MilA protein (Wawegama et al., 2014), using assays based on hydrolysis of lipid substrates such as O-dilauryl-rac-glycero-3-glutaric acid resorufin ester, *p*-nitrophenyl caproate or *p*-nitrophenyl palmitate. Western blotting further demonstrated that one of them, the *M. bovis* MilA lipase, is released into the culture supernatant (Adamu et al., 2020) and it has also been found in the exoproteome of *M. bovis* strain HB0801 (Zubair et al., 2020b). In contrast, the P65 lipase of *M. hyopneumoniae* was not directly shown to be extracellular, but has been found in the exoproteomes of *M. hyopneumoniae* strains J and 7448 obtained from culture supernatants (Paes et al., 2017) and from the supernatant of infected cells (Leal Zimmer et al., 2019; **Table 1**).

In other bacteria, such as *S. aureus*, secreted extracellular lipases are involved in a broad spectrum of functions, including acquisition of lipids from the host (Delekta et al., 2018), immune evasion (Chen and Alonzo, 2019), biofilm formation, and host cell invasion (Nguyen et al., 2018). The dual potential localization—i.e., extracellular as well as cell-attached—of MilA in mycoplasmas complicates research into its function(s) (Adamu et al., 2020). MilA seems to be essential, as *M. bovis* growth is inhibited by anti-MilA antibodies, and screening of *M. bovis* transposon libraries has failed to detect a MilA mutant (Sharma et al., 2014; Josi et al., 2019; Adamu et al., 2020). Cell-free recombinant MilA has been shown to bind lipid and heparin, suggesting a putative role in the processing and transport of lipids and in adhesion to the extracellular matrix (Adamu et al., 2020).

Adhesins

Dozens of mycoplasma proteins have the capacity to bind to host cells or to components of the host extracellular matrix such as actin, fibronectin and glycosaminoglycans. Several of these adhesins or adhesion-related proteins, although classically described as cell surface-associated (and belonging to the surfaceome), are regularly identified in the exoproteome of several mycoplasma species (**Table 1**).

For instance, the P102 adhesin of *M. hyopneumoniae* has been shown, by immunoelectron microscopy after experimental infection of swine, to be localized either within mycoplasma cells or distant from them and directly attached to respiratory cilia of the experimentally infected swine (Djordjevic et al., 2004; Adams et al., 2005). P102-homologs have been identified in the exoproteomes of *M. hyopneumoniae* and *M. flocculare* (Paes et al., 2017; Leal Zimmer et al., 2019; **Table 1**). Other adhesins have been found in the exoproteome of *M. hyopneumoniae*, *M. flocculare* and *M. synoviae*, but no role has yet been firmly defined for them as released proteins (**Table 1**). A reasonable hypothesis could be that the release of adhesins from the mycoplasma cell could promote mycoplasma dispersion by limiting their adhesion to host cells and tissues, as described for other bacteria (Coutte et al., 2003). They could also be blocking anti-adhesin antibody binding to the cell, but this has yet to be demonstrated.

However, it is becoming increasingly evident that adhesins and other proteins could also play a role in degradation of the host extracellular matrix (ECM) by binding to plasminogen. This is the case for *M. hyopneumoniae* adhesin P102 (Seymour et al., 2012; Leal Zimmer et al., 2020). Binding of P102 to plasminogen resulted in increased conversion of plasminogen into plasmin, a serine protease able to degrade the ECM either directly or through activation of other enzymes, such as metalloproteases (Seymour et al., 2012). This strategy of ECM degradation by subversion of the host plasmin system is used by many other bacteria to invade and spread (Lahteenmaki et al., 2005). Non-adhesin proteins that could also contribute to degradation of the ECM include the glycolytic enzyme glyceraldehyde-3-P-dehydrogenase (GAPDH) in *M. hyorhinis* (Wang et al., 2021), the chaperone protein DnaK, GAPDH and subunit E1 α of the pyruvate dehydrogenase complex (PDHB), another enzyme involved in carbon metabolism, in *M. pneumoniae* (Grundel et al., 2016; Hagemann et al., 2017), the enzyme enolase, which catalyzes the interconversion of phosphoenolpyruvate into 2-phosphoglycerate in *M. bovis* (Song et al., 2012), and the elongation factor EF-Tu, which orchestrates transport of aminoacylated tRNA to the ribosome, in *M. pneumoniae* and *M. hyopneumoniae* (Widjaja et al., 2017). These proteins have been found in the exoproteome of mycoplasmas (**Table 1**).

Disruptors of Host-Cell Metabolism

The cell-free form of the chaperone protein DnaK from *M. fermentans* was also shown to be taken up by the host cells and localize in the cytoplasm, the perinuclear space and the nucleus (Benedetti et al., 2020). Once in the cell, DnaK interacts with several host proteins, including those involved in DNA repair, like PARP1 (poly-ADP ribose polymerase-1) and USP10 (ubiquitin carboxyl-terminal hydrolase protein-10). The interaction with USP10 in turn leads to a reduction in P53 activity, which is known to have an anti-oncogenic effect (Zella et al., 2018; Benedetti et al., 2020). For bacteria, this is a way to redirect host-cell metabolism to facilitate bacterial growth (Siegl and Rudel, 2015). Using immunoprecipitation techniques with an anti-P53 monoclonal antibody, Zella et al. identified other mycoplasma proteins able to interact with P53, one of which was

the glycolytic enzyme enolase (Zella et al., 2018), which has been found in the exoproteome of five mycoplasma species (Table 1).

Modulators of Host Immune Response

A western blotting study recently confirmed that the MbovP280 protein, predicted *in silico* to be secreted, was effectively released by *M. bovis* cells cultured for 36 h (Zhao et al., 2021). The secreted MbovP280 protein was further shown to bind to and induce the apoptosis of bovine macrophages through a complex signaling pathway (Zhao et al., 2021). However, the effect of a recombinant protein was greater than that of whole cells expressing MbovP280. Apoptotic activity has also been described for mycoplasmal extracellular proteins with other main roles. For instance, the nucleases P40 in *M. penetrans*, Mhp597 in *M. hyopneumoniae* and RS_02825 in *M. bovis* induce apoptosis in human lymphocytes (Bendjennat et al., 1999), in swine kidney epithelial cells (Li et al., 2019), and in bovine macrophages via the NFkB p65 pathway (Zhang et al., 2016), respectively. Extracellular nucleases can also play a role in modulation of cytokine production. *M. hyopneumoniae* Mhp597 nuclease has been shown to suppress INF γ secretion and stimulate IL1, IL8 and TNF secretion in macrophages (Li et al., 2019). This is an important finding, as INF γ is a first-line protection against viral infection. The MAM superantigen of *M. arthritidis* has also been shown to modulate cytokine release (Mu et al., 2000). In addition to nucleases, some proteases may also have immunomodulatory effects. *M. hyopneumoniae* endopeptidase F and XAA pro-aminopeptidase, which are both found in the exoproteome (Table 1), have recently been shown to be involved in the degradation of peptides that play a role in innate immunity (Jarocki et al., 2019). These data have started to demonstrate a role of the mycoplasma releasome in evasion of the immune system and modulation of its activity, which are two important features of mycoplasma virulence (Leal Zimmer et al., 2020; Askar et al., 2021; Jiang et al., 2021; Yiwen et al., 2021).

Gaps and Perspectives

The combination of (i) numerous potential experimental biases (failure to pellet some mycoplasma cells, cell lysis during the purification protocol, and so on), (ii) the high proportion (circa 30%) of hypothetical proteins with no associated function found in exoproteomes, (iii) the extent of moonlighting activity in mycoplasma proteins, and (iv) underpowered *in silico* prediction capacity (Zhao et al., 2021) means that further studies complementary to studies characterizing the core exoproteome are necessary to confirm the extracellular localization of the exoproteins and decipher their role. With the growing interest in mycoplasma exoproteins, the mycoplasma community would welcome a consensus methodology guideline to improve the quality of results and enable valuable comparisons of exoproteomes between species. For instance, specific labeling of newly synthesized proteins using new methodologies such as bioorthogonal non-canonical amino acid tagging and proximity labeling (Shin et al., 2019; Sukumaran et al., 2021) could be helpful to distinguish the exoproteome of mycoplasmas from proteins contained in a complex environment. This includes complex growth medium, the cytoplasmic compartment in case

of intracellular mycoplasmas, or different host sites occupied by mycoplasmas in the course of infection [for example *M. hyopneumoniae* has been detected in the heart, kidneys, liver and spleen of pigs (Le Carrou et al., 2006; Marois et al., 2007; Woolley et al., 2012)].

Studies addressing the role of exoproteins in the interplay with the host are also essential. As the generation and use of mycoplasma mutants is still limited, approaches based on recombinant proteins are increasingly being used (Bendjennat et al., 1999; Zhang et al., 2016; Yamamoto et al., 2017; Zhao et al., 2021), but they can sometimes exaggerate the actual role of a protein because of the high concentrations tested, which do not correspond to the actual quantities secreted by the cell (Zhao et al., 2021).

The mycoplasma community is starting to gain a global picture of the role of exoproteome interactions with host cells and with components of the host extracellular matrix and how it shapes immune evasion or modulation. However, the exoproteome composition is likely to vary over time, depending on the host context and the time since infection. Variability in exoproteome composition between species, and potentially between strains, might also explain some of the variability in virulence.

Last but not least, although some *Sec* genes have been identified *in silico* (Staats et al., 2007), further investigation is needed into the mechanisms involved in protein release by *Mycoplasma* spp. For instance, surface shaving via proteases could contribute to the release of exoproteins from the cell-surface, highlighting the tight connection between the surfaceome and the releasome (Raymond et al., 2013; Jarocki et al., 2015, 2019; Tacchi et al., 2016; Berry et al., 2017; Ganter et al., 2019; Machado et al., 2020). Other non-classical protein release mechanisms have been suggested such as explosive cell events or ghost cells formation (Raymond et al., 2018a). Those could contribute to free into the extracellular medium membrane or cytoplasmic proteins (Wang et al., 2013).

Exopolysaccharides

Composition and Structure

Mycoplasma exopolysaccharides were first reported in the 1930s, when Kurotchkin described a carbohydrate released by *M. mycoides* subsp. *mycoides* into the culture medium and the blood of animals with acute CBPP (Kurotchkin, 1937; Kurotchkin and Benaradsky, 1938). It was then of unknown composition and structure, but cross-reacted serologically with the *M. mycoides* subsp. *mycoides* capsular polysaccharide (Plackett et al., 1963), which is composed of galactose and named galactan (Plackett and Buttery, 1958). By the 1960s, it was clear that *M. mycoides* subsp. *mycoides* produced both a CPS and an EPS, with a shared antigenic signature recognized by the same antibodies. Despite several efforts, purification of the EPS from culture supernatants remained thwarted by difficulties in eliminating contamination from polysaccharides, such as glycogen, contained in the growth medium (Plackett et al., 1963; Hudson et al., 1967). It was only in 2013 that Bertin et al. eliminated contamination with medium-associated polysaccharides by transferring PPLO-grown

M. mycoides subsp. *mycoides* cells into CMRL, a defined cell culture medium with no polysaccharides and only glucose as a carbon source (Bertin et al., 2013). CMRL was shown to sustain mycoplasmal metabolism but not growth (Bertin et al., 2013). An EPS, in free form in the spent CMRL, was purified and its composition and structure were shown by NMR and HPLC to be identical to the polysaccharide moiety of the capsular galactan described 50 years earlier (Bertin et al., 2013). This identity explained the immunological cross-reactivity between the EPS and CPS, but was limited to the polysaccharide moiety, as galactan CPS contains a lipid anchor (Buttery and Plackett, 1960) that is not present when the galactan is released from the cells (Bertin et al., 2013).

Other EPS were identified among the members of the *M. mycoides* cluster using the same purification method: a β -(1 \rightarrow 2)-glucopyranose was detected in the culture supernatant of *M. capricolum* subsp. *capricolum*, *M. capricolum* subsp. *capripneumoniae* and *M. leachii* (Bertin et al., 2015; **Table 2**), and weak exopolysaccharide release was detected *in vitro* from the two serovars of *M. mycoides* subsp. *capri* (Bertin et al., 2015; Gaurivaud et al., 2016). Interestingly, the two serovars of the goat pathogen *M. mycoides* subsp. *capri* secreted two different polysaccharides: serovar LC (large colony) produced galactan and serovar capri produced β -(1 \rightarrow 6)-glucopyranose. Both EPS were homopolysaccharides with no ramification and no chemical modifications. However, not all mycoplasmal polysaccharides are as simple. The EPS isolated from *M. pneumoniae* biofilms, for instance, is composed of galactose and N-acetyl glucosamine (Simmons et al., 2013; **Table 2**).

All these EPS were also detected as CPS (**Table 2**). However, the presence of a CPS does not guarantee secretion of the corresponding EPS, as shown by the β -(1 \rightarrow 6)-glucopyranose of *M. agalactiae*, which was only detected as a CPS (Gaurivaud et al., 2016; **Table 2**). Other CPS have been detected in *M. feriruminatoris*, which is able to produce a galactan and a β -(1 \rightarrow 6)-glucopyranose CPS (Ambroset et al., 2017), and in *M. genitalium* (Daubenspeck et al., 2020) and *M. pulmonis* (Daubenspeck et al., 2009; **Table 2**). However, their release as EPS has not been demonstrated to date.

Exopolysaccharides Biosynthesis

In *M. mycoides* subsp. *mycoides*, the galactan is not secreted concomitantly as CPS and EPS *in vitro*, but rather alternatively by phenotypic variants undergoing phase variation (Bertin et al., 2013). One variant secreted a galactan CPS but no EPS, whereas the other one was not capsulated but produced a galactan EPS. This phenomenon was reversible and was shown to be related to the expression of a permease of the glucose-phosphoenolpyruvate phosphotransferase system (PTS) undergoing on/off phase variation (Gaurivaud et al., 2004; Bertin et al., 2013). The PTS system is a well-established sugar transport system, but also regulates carbon metabolism in bacteria (Deutscher et al., 2014) and has already been shown to regulate polysaccharide synthesis in *Vibrio cholerae* (Houot et al., 2010). One group posited glucose PTS system-mediated regulation of a glycosyltransferase possibly involved in attachment of the polysaccharide moiety to the membrane lipid

anchor (Bertin et al., 2013), but the regulatory and attachment mechanisms have yet to be demonstrated.

A complete biosynthesis pathway involving a membrane glycosyltransferase belonging to the synthase family (Whitney and Howell, 2013), and catalyzing both polymerization and transfer of the galactan of *M. mycoides* subsp. *mycoides* in its CPS or EPS across the cytoplasmic membrane, has been proposed based on *in silico* data (Bertin et al., 2013). The role of synthases in mycoplasma polysaccharide synthesis was also demonstrated using a functional genomics approach for the synthesis of the *M. agalactiae* β -(1 \rightarrow 6)-glucopyranose (Gaurivaud et al., 2016). Among the many glycosyltransferases identified in mycoplasmal genomes, synthases are easily identified as they have 4 or 7 transmembrane domains and a cytoplasmic loop bearing the glycosyltransferase-active sites (Gaurivaud et al., 2016). The number of transmembrane domains may be linked to substrate specificity and the structure of the resulting polymer. Synthases have been predicted *in silico* for 14 *Mycoplasma* species, which suggests that several other polysaccharides have yet to be identified (Gaurivaud et al., 2016). In contrast, no synthesis pathway has been identified for the polysaccharides produced by *M. pulmonis*, *M. genitalium* or *M. pneumoniae* (Daubenspeck et al., 2009, 2020). However, an ABC transporter pathway (Schmid, 2018) has been suggested for *M. pulmonis*, as the mutation of two ABC permease genes was associated with a loss of polysaccharide production (Daubenspeck et al., 2009).

Role in Host Interactions

In mycoplasmas, as in other bacterial models, CPS are known to be involved in the modulation of cytoadherence (Bolland and Dybvig, 2012) and in protection against phagocytosis (Shaw et al., 2013) and against the bactericidal activity of the complement system (Bolland et al., 2012; Gaurivaud et al., 2014). In contrast, with the exception of circulating galactan in the body fluids of animals experiencing CBPP, the role of mycoplasmal EPS has been under-researched. Intravenous injection of galactan purified from *M. mycoides* subsp. *mycoides* culture supernatant into calves resulted in an increase of pulmonary arterial blood pressure and a transient apnea (Buttery et al., 1976). However, in its EPS form, the galactan did not induce any fever and did not affect the susceptibility of calves to subsequent subcutaneous infection with *M. mycoides* subsp. *mycoides* (Hudson et al., 1967; Buttery et al., 1976). However, these results need to be interpreted with caution, as the purified galactan was shown to contain peptides (Hudson et al., 1967; Buttery et al., 1976). This ambiguity was overcome recently by Totte et al. (2015) who used a high-purity-grade galactan obtained from *M. mycoides* subsp. *mycoides* supernatant, checked by SDS PAGE and NMR, to examine its effect on immune cells. Pure galactan failed to activate naive lymphocytes but induced IL-10 release by bovine macrophages, thus echoing the observation of peak IL-10 1–2 weeks after experimental infection of cattle with *M. mycoides* subsp. *mycoides* (Sacchini et al., 2012). Moreover, the purified free galactan was able to reduce the release of pro-inflammatory cytokines by macrophages in response to *Escherichia coli* lipopolysaccharide (Totte et al., 2015). These observations indicated that, overall, the galactan EPS acts as

an immunosuppressor by inhibiting pro-inflammatory cytokines and increasing the IL-10 secretion that depresses T-cell responses (Totte et al., 2015).

Polysaccharides are a major constituent of biofilm matrices, where they play roles in binding different components and in physical resistance to stress or stratification of the biofilm structure (Limoli et al., 2015). Both CPS and EPS could contribute to biofilm formation in mycoplasmas. For instance, in *M. pulmonis*, different types of expressed dominant polysaccharides changed the propensity of strains to form a biofilm (Daubenspeck et al., 2009). Similarly, in *M. pneumoniae*, the volume, texture, robustness and internal structure of the biofilm was shown to differ between two strains (of different type), depending on how loosely or tightly the polysaccharides were attached to the mycoplasma cell (Simmons et al., 2013). This could ultimately completely modify the role of the resulting biofilm in virulence and chronicity of infection.

Gaps and Perspectives

Although extracellular polysaccharides have been detected in several *Mycoplasma* species, only three polymers have had

their structure elucidated thus far. This relatively low rate of structural characterization may be attributable to the necessity of purifying a high quantity (approximately 1 mg) of material for structure analyses by HPLC and NMR, which could be technically challenging depending on the species, culture conditions and overall complexity of the exopolysaccharide structure (e.g., biofilms) (Table 2).

Clear identification of the pathways involved in the synthesis of galactan, β -(1 \rightarrow 6)-glucopyranose and β -(1 \rightarrow 2)-glucopyranose has been helpful for *in silico* screening of other species for their potential to produce polysaccharides. However, for *M. pulmonis*, *M. genitalium* and *M. pneumoniae*, the EPS biosynthesis pathways have yet to be deciphered. In *M. pulmonis*, random transposon mutagenesis identified the role of two genes coding for ABC transporters, but failed to find the glycosyltransferase catalyzing the polymerization. This suggests that polymerization of the polysaccharides could be an essential function for mycoplasmas. Other mutations in genes involved in polysaccharide biosynthesis were shown to have an adverse effect on cell viability: for example, a mutation in the UDP galactofuranose mutase gene of *M. mycoides* subsp. *capri* reduced

TABLE 2 | List of *Mycoplasma* (sub)species producing exopolysaccharides.

Species	Hosts	Strains	Culture conditions	Tools	Polysaccharides		Biosynthesis pathways	CPS/EPS	References
					Composition	Structures			
<i>M. pneumoniae</i>	Human	M129	Biofilm	GC	Galactose, GlcNac	ND	ND	EPS	Simmons et al., 2013
		UAB PO1	Biofilm	GC	Galactose, GlcNac	ND	ND	CPS	Simmons et al., 2013
<i>M. mycoides</i> subsp. <i>mycoides</i>	Bovine	V5	Cell grown in complex medium	Biochemical and optical methods	Galactose	β -(1 \rightarrow 6)-galactofuranose	Synthase	CPS	Plackett and Buttery, 1958, 1964
		Afadé	Cell incubated in CMRL-medium	HPLC, NMR, MAb	Galactose	β -(1 \rightarrow 6)-galactofuranose	Synthase	CPS/EPS	Bertin et al., 2013, 2015
<i>M. mycoides</i> subsp. <i>capri</i> serovar <i>capri</i>	Caprine	PG3 ^T	Cell grown in complex medium	HPLC, NMR	Glucose	β -(1 \rightarrow 6)-glucopyranose	Synthase	CPS/EPS	Gaurivaud et al., 2016
<i>M. mycoides</i> subsp. <i>capri</i> serovar LC	Caprine	95010	Cell grown in complex medium	MAb	Galactose	β -(1 \rightarrow 6)-galactofuranose	Synthase	CPS/EPS	Bertin et al., 2015
<i>M. capricolum</i> subsp. <i>capricolum</i>	Caprine	7714	Cell grown in complex medium	MAb	Glucose	β -(1 \rightarrow 2)-glucopyranose	Synthase	CPS/EPS	Bertin et al., 2015
<i>M. capricolum</i> subsp. <i>capripneumoniae</i>	Caprine	Ambosa	Cell grown in complex medium	MAb	Glucose	β -(1 \rightarrow 2)-glucopyranose	Synthase	CPS/EPS	Bertin et al., 2015
<i>M. leachii</i>	Bovine	PG50 ^T	Cell incubated in CMRL-medium	HPLC, NMR	Glucose	β -(1 \rightarrow 2)-glucopyranose	Synthase	EPS	Bertin et al., 2015
			Cell grown in complex medium	MAb	Glucose	β -(1 \rightarrow 2)-glucopyranose	Synthase	CPS	Bertin et al., 2015
<i>M. agalactiae</i>	Caprine	14628	Cell grown in complex medium	HPLC, NMR, MAb	Glucose	β -(1 \rightarrow 6)-glucopyranose	Synthase	CPS	Gaurivaud et al., 2016
<i>M. feriruminatoris</i>	Ibex	15568	Cell grown in complex medium	HPLC, NMR, MAb	Glucose, galactose	β -(1 \rightarrow 6)-glucopyranose, β -(1 \rightarrow 6)-galactofuranose	Synthase	CPS	Ambroset et al., 2017

ND, not determined; MAb, monoclonal antibody; HPLC, high pressure liquid chromatography; NMR, nuclear magnetic resonance; CPS, cell-linked polysaccharide; EPS, exopolysaccharide; GlcNac, N-acetylglucosamine; PNAG, Poly-N-acetylglucosamine; T, type strain; GC, gas chromatography.

the membrane integrity of the cells (Schieck et al., 2016). The genes involved in polysaccharide attachment to the cell surface and the membrane anchor have not yet been identified.

A final crucial point is that we are still a long way from identifying the roles of EPS and their level of secretion *in vivo*. The example of galactan illustrates that, despite having the same polysaccharide moiety, CPS and EPS have two different roles: protection of the cell (CPS) and suppression of inflammation (EPS). This has some similarity with the moonlighting proteins of mycoplasmas that play different roles depending on their localization. Phase variation between capsulated variants and uncapsulated variants secreting EPS is thought to be involved in the adaptation of *M. mycoides* subsp. *mycoides* to changing environments during host colonization (Gaurivaud et al., 2014), but this hypothesis has yet to be validated *in vivo*.

Extracellular Vesicles

First Observations

Extracellular vesicles are the least investigated elements of the mycoplasmal releasome. Membranous particles, with a diameter of 75 to 210 nm, were first observed in the 1960s by electron microscopy in mycoplasma cultures during studies of cell ultrastructure and cellular division (Domermuth et al., 1964; Hummeler et al., 1965). More recently, using a classical method for EV purification, similar nanosized particles were observed by TEM in *Acholeplasma laidlawii* and several *Mycoplasma* species (Chernov et al., 2011; Gaurivaud et al., 2018). The diameters of these particles ranged from 30 to 170 nm, although a few larger particles of around 200 nm were also observed for *M. mycoides* subsp. *mycoides* (Gaurivaud et al., 2018). Although the shapes and sizes of these particles were typical of classical prokaryotic EV, further evidence was needed to definitively confirm that they were EV: they had to be (i) non-replicative, (ii) surrounded by a lipid bilayer, (iii) produced by viable cells, and (iv) contain cytoplasmic proteins in order to prove that the particle was not just a circularization/reassembly of membrane fragments (Thery et al., 2018). They were shown to meet the first three criteria (Gaurivaud et al., 2018), but the fourth criterion—internal protein contents of the EV—has not yet been assessed. However, TEM images of mycoplasma cultures clearly showed EV budding from cells, suggesting that they are not the result of reassembling membrane fragments nor of an aberrant division of small mycoplasma cells (Hummeler et al., 1965; Gaurivaud et al., 2018).

Production of vesicles by exploding bacterial cells has been described recently for *Bacillus* spp. (Toyofuku et al., 2019). The “explosion” results from the expression of an autolysin, i.e., a peptidoglycan hydrolyzing enzyme. After the degradation of the cell-wall, the cell is lysed because of the high intracellular pressure [10 atm for *Bacillus* (Rojas and Huang, 2018)]. Subsequent reassembly of bacterial membrane debris can generate vesicles. However, these vesicles differ from surface-budding EV with respect to their composition (Toyofuku et al., 2019). Explosive cell-lysis events leading to membrane vesicles formation were once observed for *M. hyopneumoniae* cells embedded in a biofilm produced *in vitro* (Raymond et al., 2018a). Comparison of size,

structure and cargo composition (expected to be random in case of explosive cells) between EV and vesicles produced from explosive cell events would certainly shed new light onto their respective roles.

Bacterial EV are involved in an array of processes, including stress responses, cell communication, and protein secretion (Kim et al., 2015; Coelho and Casadevall, 2019). Several proteins involved in host interactions have been identified in the proteome of EV membranes in three species, including pathogens of both domestic animals (*M. mycoides* subsp. *mycoides* and *M. agalactiae*) and humans (*M. fermentans*) (Gaurivaud et al., 2018). Of all the putative virulence factors found in EV membranes, DnaK is one of the most abundant proteins (Gaurivaud et al., 2018) and this protein has also been detected in host cells (Zella et al., 2018) (see earlier). Secretion through EV and delivery into the host cells could be used by mycoplasmas that are devoid of other more classical secretion systems. Secretion of proteins through EV confers both protection of the cargo molecules against degradation and an efficient transport system able to deliver high concentrations of cargo molecules to the cells (Coelho and Casadevall, 2019; McMillan and Kuehn, 2021).

Bacterial EV could be involved in nutrient acquisition, as recently described for iron acquisition by EV of *Mycobacterium tuberculosis* and *Pseudomonas (P.) aeruginosa* (Prados-Rosales et al., 2014; Lin et al., 2017). These bacteria are able to scavenge the iron sequestered by EV, and because of their dissemination over long distances, EV are assumed to supply nutrients to bacteria localized at different infection sites. Given that nutrient binding proteins, such as those belonging to ABC transporter systems, have been identified in the EV membranes of mycoplasmas (Gaurivaud et al., 2018), EV could participate in nutrient acquisition, which is a crucial feature for these biosynthetically limited bacteria.

Gaps and Perspectives

Data on the biogenesis, composition and role of mycoplasmal EV are scarce. Despite the considerable efforts made to date, there is still a need to further optimize the purification of EV (Thery et al., 2018) and completely eliminate the small-sized mycoplasma cells observed in the purified material from some species (Gaurivaud et al., 2018). A second gap to address is to complete the characterization of the EV composition and, crucially, their cytoplasmic content. The presence of polypeptides, nucleic acids, DNA and RNA within EV has not been yet assessed. A method that can directly assess the presence of DNA or RNA inside EV has been proposed recently (Bitto et al., 2017).

Extracellular vesicles secretion is energetically expensive for bacteria (McMillan and Kuehn, 2021) and may be even more expensive for the small-sized (300–800 nm diameter) mycoplasmas (Razin et al., 1998), which produce EV of 30–170 nm diameter. This raises the question of the fitness burden that EV release might represent for mycoplasmas, which needs to be compensated for by beneficial roles of EV release. Remodeling mycoplasmas membrane by vesicle production could be a rapid mechanism to maintain membrane integrity and its adaptation to changing environments, as it is described for other bacteria (McMillan and Kuehn, 2021). Deciphering

the cargo composition of EV, and an in-depth comparison of virulence factors in the vesicle membranes (Gaurivaud et al., 2018) with those of parental cells, would certainly help define these beneficial roles. Selective cargo packaging, i.e., preferential exclusion or selection of vesicle cargo, has already been demonstrated in enterotoxigenic *Escherichia coli* during stress (Orench-Rivera and Kuehn, 2021). EV produced by explosive-cell events [observed for *M. hyopneumoniae* biofilm *in vitro* (Raymond et al., 2018a)] carry different cargo than classical EV and may have different roles (Toyofuku et al., 2019; McMillan and Kuehn, 2021) such as release of “public goods” useful for the bacterial community inside the biofilm (Turnbull et al., 2016).

The *in vitro* use of cellular models to study EV release and cytotoxicity or their effect on immunity compared to mycoplasmas alone would bring further insights into their role. Similarly, experimental infection of animals could provide information about the potential long-distance dissemination of mycoplasmal EV (Stentz et al., 2018).

Extracellular vesicles-based vaccines could also hold promise for use in mycoplasmosis control as it has been shown for other bacterial diseases (Jiang et al., 2019; Behrens et al., 2021). However, the presence of proinflammatory lipoproteins in the mycoplasmal EV membrane and the yield rate and cost of *in vitro* EV production remain technical and economic bottlenecks, although they could be solved by expressing extracellular virulence factors within heterologous EV systems (Carvalho et al., 2019; Stentz et al., 2022).

Other Components of the Releasome

In addition to the three main elements of the releasome (exoproteins, EPS, and EV), mycoplasmas can also release other molecules, including DNA and byproducts of mycoplasmal metabolism. Further insights into the biology of mycoplasmas came from the recent demonstration within *M. hyopneumoniae* of morphological variants called ‘large cell variants’ (LCV) with inherent membrane instability and hence a capacity to release their cytoplasmic content, notably extracellular DNA by cell lysis leading to the formation of ghost cells and to explosive cell events (Raymond et al., 2018a). As extracellular DNA is necessary for biofilm formation on abiotic surfaces, Raymond et al. proposed that mycoplasmas could be self-sufficient in providing this DNA through LCV lysis. The contribution of LCV cell lysis to the final composition of the releasome has yet to be further defined.

Two byproducts of mycoplasmal metabolism, hydrogen peroxide and hydrogen sulfide, have drawn attention because of their potential cytotoxicity. Hydrogen sulfide is produced during cysteine catabolism by cysteine desulfurase/desulphydrase encoded by the *HapE* gene, which is found in many mycoplasmas (Grosshennig et al., 2016). Hydrogen peroxide is produced through glycerol metabolism by L- α -glycerophosphate oxidase or peroxide hydrogen NADH oxidase, and many mycoplasmas are able to produce it (Khan et al., 2005; Blotz and Stulke, 2017; Zhao et al., 2017). These two metabolites are considered virulence factors because of their capacity to damage their host cells (Blotz and Stulke, 2017). Hydrogen sulfide produced by *M. pneumoniae* has hemolytic activity (Grosshennig et al., 2016). Hydrogen peroxide, a known virulence factor of *Streptococcus*

pneumoniae (Gonzales et al., 2021), may be a virulence factor in several *Mycoplasma* species (Pilo et al., 2005; Hames et al., 2009; Zhu et al., 2019). In addition, hydrogen peroxide could prevent growth of competing bacteria (Herrero et al., 2016), thus offering an advantage in niche colonization.

CONCLUSION

Mycoplasmas actively release a wide variety of molecules and elements—from metabolites to proteins, polysaccharides, DNA and EV—into their environment. Not all these elements are associated with a known secretion system, but their common extracellular localization provides grounds for gathering them together under the general term of *releasome*. Besides molecules and elements actively released by living cells, cell lysis leading to formation of ghost cells and explosive cells event could be a mechanism for generating a certain releasome in a biofilm context (Raymond et al., 2018a).

Characterization of the releasome of *Mycoplasma* spp. began with the first culture of a mycoplasma, in 1898. To parallel with other bacteria, the first extracellular elements searched for were toxins and other virulence factors. Despite the methodological bottlenecks of the time, proteases, lipases and nucleases in the extracellular environment were detected early on, but the corresponding secretion machineries and their substrates were not identified. With time, another difficulty has arisen, as most of the released elements or parts of them (for instance, the polysaccharide moiety of cell-linked galactan or the external region of membrane proteases) also have a cell-localized counterpart that could have a different function, highlighting the tight connection between the releasome and the surfaceome. EVs have an important role in the releasome as they can contain proteins, polysaccharides and DNA in a protected environment. The physical form (free vs. EV-associated) of various elements of the releasome may modify their role, as has been described for LPS-induced activation of the inflammasome in *P. aeruginosa* (Bitto et al., 2018).

Data collected for the purpose of this review show that the elements of the releasome are now recognized as playing important roles in nutrient acquisition, adhesion to and invasion of host cells, and immune system modulation and evasion. However, a better understanding of the global role and dynamics of the releasome hinges on studying the balance of its different components (proteins, polysaccharides, metabolites and EV) at a precise time point after infection of the host, in different host sites, in specific physiological states of mycoplasmas, including their intracellularly.

Further advances in deciphering the releasome of mycoplasmas will bring further knowledge and hypotheses about the interplay between mycoplasmas and their hosts and help to progress identification of new molecules involved in virulence or cytoplasmic or membrane molecules that have different roles once they are released from the cell. Such virulence factors are not included in current inactivated vaccines. Moreover, exoproteome modifications have been observed after *in vitro* serial passage (Zhang et al., 2021), which indicates that

the release of passage-attenuated vaccine strains may differ from that of virulent field strains. Ultimately, experiments are needed to assess the benefit of adding release components to current vaccines.

DEFINITIONS

Release: set of not cell-attached molecules (proteins, polysaccharides, DNA and metabolites) and elements (EV) released by a living cell into its extracellular environment, whatever the release/secretion mechanism, but excluding release by cell lysis and contamination by medium components. As opposed to the secretome, the machinery of secretion may be unknown.

Secretome: classically defined as the set of proteins and their corresponding secretion systems allowing translocation through the membrane from the inside to the outside of the cell. This implies that the secretion systems are known.

Exoprotein: a protein released by viable mycoplasmas into their environment. This excludes cell-attached proteins (surfaceome).

Exoproteome: set of exoproteins secreted by a cell in a defined time and environment.

Extracellular vesicle (EV): nanosized, membranous spherical structure produced from viable cells by budding. EVs are composed of a part of the membrane and cytoplasm of the

parental cell, but cargo selection means that their composition is not the same as the parental cell.

Cell-linked polysaccharide (CPS): polysaccharide covalently linked to the cell surface. The resulting polymer remains attached to the cell where it can form a capsule or a slime layer around the cells. CPS are purified from washed cells.

Exopolysaccharide (EPS): polysaccharide non-covalently linked to the cell surface and released free in the culture supernatant or within the host. Such polysaccharides are purified *in vitro* from a cell-free supernatant.

AUTHOR CONTRIBUTIONS

PG and FT conceptualized, wrote the first manuscript draft, and revised the manuscript. All authors have read and approved the final version of the manuscript.

ACKNOWLEDGMENTS

We would like to thank the many students who participated in laboratory experiments behind some of the data assembled for this review: Monika Gjorgjieva, Khadidja Berrouane, Victoria Mari, Quentin Granjon, Marie Guillot, Alexandre Chassard, Alexandre Villard, Clothilde Bertin, and Sarah Ganter. We are very grateful to Laure Beven for critically reading this manuscript.

REFERENCES

- Adams, C., Pitzer, J., and Minion, F. C. (2005). *In vivo* expression analysis of the P97 and P102 paralog families of *Mycoplasma hyopneumoniae*. *Infect. Immun.* 73, 7784–7787. doi: 10.1128/IAI.73.11.7784-7787.2005
- Adamu, J. Y., Wawegama, N. K., Kanci Condello, A., Marendia, M. S., Markham, P. F., Browning, G. F., et al. (2020). *Mycoplasma bovis* membrane protein MilA is a multifunctional lipase with novel lipid and glycosaminoglycan binding activity. *Infect. Immun.* 88:e00945–19. doi: 10.1128/IAI.00945-19
- Afshar, A. (1967). The growth of *Mycoplasma bovis* in cell cultures. *J. Gen. Microbiol.* 47, 103–110. doi: 10.1099/00221287-47-1-103
- Allam, A. B., Brown, M. B., and Reyes, L. (2012). Disruption of the S41 peptidase gene in *Mycoplasma mycoides capri* impacts proteome profile, H(2)O(2) production, and sensitivity to heat shock. *PLoS One* 7:e51345. doi: 10.1371/journal.pone.0051345
- Allam, A. B., Reyes, L., Assad-Garcia, N., Glass, J. I., and Brown, M. B. (2010). Enhancement of targeted homologous recombination in *Mycoplasma mycoides* subsp. *capri* by inclusion of heterologous recA. *Appl. Environ. Microbiol.* 76, 6951–6954. doi: 10.1128/AEM.00056-10
- Ambroset, C., Pau-Roblot, C., Game, Y., Gaurivaud, P., and Tardy, F. (2017). Identification and characterization of *Mycoplasma feriruminatoris* sp. nov. strains isolated from Alpine ibex: a 4th species in the *Mycoplasma mycoides* cluster hosted by non-domesticated ruminants? *Front. Microbiol.* 8:939. doi: 10.3389/fmicb.2017.00939
- Armengaud, J., Christie-Oleza, J. A., Clair, G., Malard, V., and Duport, C. (2012). Exoproteomics: exploring the world around biological systems. *Expert Rev. Proteomics* 9, 561–575. doi: 10.1586/epr.12.52
- Askar, H., Chen, S., Hao, H., Yan, X., Ma, L., Liu, Y., et al. (2021). Immune evasion of *Mycoplasma bovis*. *Pathogens* 10:297. doi: 10.3390/pathogens10030297
- Atkin, C. L., Wei, S., and Cole, B. C. (1994). The *Mycoplasma arthritidis* superantigen MAM: purification and identification of an active peptide. *Infect. Immun.* 62, 5367–5375. doi: 10.1128/iai.62.12.5367-5375.1994
- Behrens, F., Funk-Hilsdorf, T. C., Kuebler, W. M., and Simmons, S. (2021). Bacterial membrane vesicles in pneumonia: from mediators of virulence to innovative vaccine candidates. *Int. J. Mol. Sci.* 22:3858. doi: 10.3390/ijms22083858
- Bendjennat, M., Blanchard, A., Loutfi, M., Montagnier, L., and Bahraoui, E. (1997). Purification and characterization of *Mycoplasma penetrans* Ca2+/Mg2+-dependent endonuclease. *J. Bacteriol.* 179, 2210–2220. doi: 10.1128/jb.179.7.2210-2220.1997
- Bendjennat, M., Blanchard, A., Loutfi, M., Montagnier, L., and Bahraoui, E. (1999). Role of *Mycoplasma penetrans* endonuclease P40 as a potential pathogenic determinant. *Infect. Immun.* 67, 4456–4462. doi: 10.1128/IAI.67.9.4456-4462.1999
- Benedetti, F., Cocchi, F., Latinovic, O. S., Curreli, S., Krishnan, S., Munawwar, A., et al. (2020). Role of *Mycoplasma* chaperone DnaK in cellular transformation. *Int. J. Mol. Sci.* 21:1311. doi: 10.3390/ijms21041311
- Berry, I. J., Jarocki, V. M., Tacchi, J. L., Raymond, B. B. A., Widjaja, M., Padula, M. P., et al. (2017). N-terminomics identifies widespread endoproteolysis and novel methionine excision in a genome-reduced bacterial pathogen. *Sci. Rep.* 7:11063. doi: 10.1038/s41598-017-11296-9
- Bertin, C., Pau-Roblot, C., Courtois, J., Manso-Silvan, L., Tardy, F., Poumarat, F., et al. (2015). Highly dynamic genomic loci drive the synthesis of two types of capsular or secreted polysaccharides within the *Mycoplasma mycoides* cluster. *Appl. Environ. Microbiol.* 81, 676–687. doi: 10.1128/AEM.02892-14
- Bertin, C., Pau-Roblot, C., Courtois, J., Manso-Silvan, L., Thiaucourt, F., Tardy, F., et al. (2013). Characterization of free exopolysaccharides secreted by *Mycoplasma mycoides* subsp. *mycoides*. *PLoS One* 8:e68373. doi: 10.1371/journal.pone.0068373
- Bitto, N. J., Baker, P. J., Dowling, J. K., Wray-McCann, G., De Paoli, A., Tran, L. S., et al. (2018). Membrane vesicles from *Pseudomonas aeruginosa* activate the noncanonical inflammasome through caspase-5 in human monocytes. *Immunol. Cell Biol.* 96, 1120–1130. doi: 10.1111/imcb.12190
- Bitto, N. J., Chapman, R., Pidot, S., Costin, A., Lo, C., Choi, J., et al. (2017). Bacterial membrane vesicles transport their DNA cargo into host cells. *Sci. Rep.* 7:7072. doi: 10.1038/s41598-017-07288-4
- Blotz, C., and Stulke, J. (2017). Glycerol metabolism and its implication in virulence in *Mycoplasma*. *FEMS Microbiol. Rev.* 41, 640–652. doi: 10.1093/femsre/fux033

- Bolland, J. R., and Dybvig, K. (2012). *Mycoplasma pulmonis* Vsa proteins and polysaccharide modulate adherence to pulmonary epithelial cells. *FEMS Microbiol. Lett.* 331, 25–30. doi: 10.1111/j.1574-6968.2012.02551.x
- Bolland, J. R., Simmons, W. L., Daubenspeck, J. M., and Dybvig, K. (2012). Mycoplasma polysaccharide protects against complement. *Microbiology (Reading)* 158(Pt. 7), 1867–1873. doi: 10.1099/mic.0.058222-0
- Bove, J. M. (1999). The one-hundredth anniversary of the first culture of a mollicute, the contagious bovine peripneumonia microbe, by Nocard and Roux, with the collaboration of Borrel, Salimbeni, and Dujardin-Baumetz. *Res. Microbiol.* 150, 239–245. doi: 10.1016/s0923-2508(99)80048-5
- Bryan, B. A., Linhardt, R. J., and Daniels, L. (1986). Variation in composition and yield of exopolysaccharides produced by *Klebsiella* sp. strain K32 and *Acinetobacter calcoaceticus* BD4. *Appl. Environ. Microbiol.* 51, 1304–1308. doi: 10.1128/aem.51.6.1304-1308.1986
- Burki, S., Gaschen, V., Stoffel, M. H., Stojilkovic, A., Frey, J., Kuehni-Boghenbor, K., et al. (2015). Invasion and persistence of *Mycoplasma bovis* in embryonic calf turinate cells. *Vet. Res.* 46:53. doi: 10.1186/s13567-015-0194-z
- Buttery, S. H., and Plackett, P. (1960). A specific polysaccharide from *Mycoplasma mycoides*. *J. Gen. Microbiol.* 23, 357–368. doi: 10.1099/00221287-23-2-357
- Buttery, S. H., Lloyd, L. C., and Titchen, D. A. (1976). Acute respiratory, circulatory and pathological changes in the calf after intravenous injections of the galactan from *Mycoplasma mycoides* subsp. *mycoides*. *J. Med. Microbiol.* 9, 379–391. doi: 10.1099/00222615-9-4-379
- Caradec, J., Kharmate, G., Hosseini-Beheshti, E., Adomat, H., Gleave, M., and Guns, E. (2014). Reproducibility and efficiency of serum-derived exosome extraction methods. *Clin. Biochem.* 47, 1286–1292. doi: 10.1016/j.clinbiochem.2014.06.011
- Carvalho, A. L., Miquel-Clopes, A., Wegmann, U., Jones, E., Stentz, R., Telatin, A., et al. (2019). Use of bioengineered human commensal gut bacteria-derived microvesicles for mucosal plague vaccine delivery and immunization. *Clin. Exp. Immunol.* 196, 287–304. doi: 10.1111/cei.13301
- Cerning, J. (1990). Exocellular polysaccharides produced by lactic acid bacteria. *FEMS Microbiol. Rev.* 7, 113–130. doi: 10.1111/j.1574-6968.1990.tb04883.x
- Chagnot, C., Zorngani, M. A., Astruc, T., and Desvaux, M. (2013). Proteinaceous determinants of surface colonization in bacteria: bacterial adhesion and biofilm formation from a protein secretion perspective. *Front. Microbiol.* 4:303. doi: 10.3389/fmicb.2013.00303
- Chen, X., and Alonzo, F. III (2019). Bacterial lipolysis of immune-activating ligands promotes evasion of innate defenses. *Proc. Natl. Acad. Sci. U.S.A.* 116, 3764–3773. doi: 10.1073/pnas.1817248116
- Chernov, V. M., Chernova, O. A., Mouzykantov, A. A., Efimova, I. R., Shaymardanova, G. F., Medvedeva, E. S., et al. (2011). Extracellular vesicles derived from *Acholeplasma laidlawii* PG8. *ScientificWorldJournal* 11, 1120–1130. doi: 10.1100/tsw.2011.109
- Chernov, V. M., Mouzykantov, A. A., Baranova, N. B., Medvedeva, E. S., Grygorieva, T. Y., Trushin, M. V., et al. (2014). Extracellular membrane vesicles secreted by mycoplasma *Acholeplasma laidlawii* PG8 are enriched in virulence proteins. *J. Proteomics* 110, 117–128. doi: 10.1016/j.jprot.2014.07.020
- Coelho, C., and Casadevall, A. (2019). Answers to naysayers regarding microbial extracellular vesicles. *Biochem. Soc. Trans.* 47, 1005–1012. doi: 10.1042/BST20180252
- Coutte, L., Alonso, S., Reveneau, N., Willery, E., Quatannens, B., Loch, C., et al. (2003). Role of adhesin release for mucosal colonization by a bacterial pathogen. *J. Exp. Med.* 197, 735–742. doi: 10.1084/jem.20021153
- Daubenspeck, J. M., Bolland, J. R., Luo, W., Simmons, W. L., and Dybvig, K. (2009). Identification of exopolysaccharide-deficient mutants of *Mycoplasma pulmonis*. *Mol. Microbiol.* 72, 1235–1245. doi: 10.1111/j.1365-2958.2009.06720.x
- Daubenspeck, J. M., Totten, A. H., Needham, J., Feng, M., Balish, M. F., Atkinson, T. P., et al. (2020). *Mycoplasma genitalium* biofilms contain poly-GlcNAc and contribute to antibiotic resistance. *Front. Microbiol.* 11:585524. doi: 10.3389/fmicb.2020.585524
- Deatherage, B. L., Lara, J. C., Bergsbaken, T., Rassouljan Barrett, S. L., Lara, S., and Cookson, B. T. (2009). Biogenesis of bacterial membrane vesicles. *Mol. Microbiol.* 72, 1395–1407. doi: 10.1111/j.1365-2958.2009.06731.x
- Delekta, P. C., Shook, J. C., Lydic, T. A., Mulks, M. H., and Hammer, N. D. (2018). *Staphylococcus aureus* utilizes host-derived lipoprotein particles as sources of fatty acids. *J. Bacteriol.* 200:e00728-17. doi: 10.1128/JB.00728-17
- Desvaux, M., Hebraud, M., Talon, R., and Henderson, I. R. (2009). Secretion and subcellular localizations of bacterial proteins: a semantic awareness issue. *Trends Microbiol.* 17, 139–145. doi: 10.1016/j.tim.2009.01.004
- Deutscher, J., Ake, F. M., Derkaoui, M., Zebre, A. C., Cao, T. N., Bouraoui, H., et al. (2014). The bacterial phosphoenolpyruvate:carbohydrate phosphotransferase system: regulation by protein phosphorylation and phosphorylation-dependent protein-protein interactions. *Microbiol. Mol. Biol. Rev.* 78, 231–256. doi: 10.1128/MMBR.00001-14
- Diedershausen, M., Overbeck, S., Arlt, S., Plumakers, B., Lintges, M., and Rink, L. (2007). *Mycoplasma arthritidis*-derived superantigen (MAM) displays DNase activity. *FEMS Immunol. Med. Microbiol.* 49, 266–271. doi: 10.1111/j.1574-695X.2006.00189.x
- Djordjevic, S. P., Cordwell, S. J., Djordjevic, M. A., Wilton, J., and Minion, F. C. (2004). Proteolytic processing of the *Mycoplasma hyopneumoniae* cilium adhesin. *Infect. Immun.* 72, 2791–2802. doi: 10.1128/iai.72.5.2791-2802.2004
- Domermuth, C. H., Nielsen, M. H., Freundt, E. A., and Birch-Andersen, A. (1964). Ultrastructure of *Mycoplasma* species. *J. Bacteriol.* 88, 727–744. doi: 10.1128/JB.88.3.727-744.1964
- Dwivedi, P., Alam, S. I., and Tomar, R. S. (2016). Secretome, surfome and immunome: emerging approaches for the discovery of new vaccine candidates against bacterial infections. *World J. Microbiol. Biotechnol.* 32:155. doi: 10.1007/s11274-016-2107-3
- Eng, J., and Froholm, O. (1971). Immune electron microscopy of not cell-bound antigen of *Mycoplasma pneumoniae*. *Acta Pathol. Microbiol. Scand. B Microbiol. Immunol.* 79, 759–763. doi: 10.1111/j.1699-0463.1971.tb00108.x
- Ganter, S., Miotello, G., Manso-Silvan, L., Armengaud, J., Tardy, F., Gaurivaud, P., et al. (2019). Proteases as secreted exoproteins in mycoplasmas from ruminant lungs and their impact on surface-exposed proteins. *Appl. Environ. Microbiol.* 85:e01439-19. doi: 10.1128/AEM.01439-19
- Gaurivaud, P., Baranowski, E., Pau-Roblot, C., Sagne, E., Citti, C., and Tardy, F. (2016). *Mycoplasma agalactiae* secretion of beta-(1→6)-glucan, a rare polysaccharide in prokaryotes, is governed by high-frequency phase variation. *Appl. Environ. Microbiol.* 82, 3370–3383. doi: 10.1128/AEM.00274-16
- Gaurivaud, P., Ganter, S., Villard, A., Manso-Silvan, L., Chevreton, D., Boule, C., et al. (2018). Mycoplasmas are no exception to extracellular vesicles release: revisiting old concepts. *PLoS One* 13:e0208160. doi: 10.1371/journal.pone.0208160
- Gaurivaud, P., Lakhdar, L., Le Grand, D., Poumarat, F., and Tardy, F. (2014). Comparison of *in vivo* and *in vitro* properties of capsulated and noncapsulated variants of *Mycoplasma mycoides* subsp. *mycoides* strain Afade: a potential new insight into the biology of contagious bovine pleuropneumonia. *FEMS Microbiol. Lett.* 359, 42–49. doi: 10.1111/1574-6968.12579
- Gaurivaud, P., Persson, A., Grand, D. L., Westberg, J., Solsona, M., Johansson, K. E., et al. (2004). Variability of a glucose phosphotransferase system permease in *Mycoplasma mycoides* subsp. *mycoides* Small Colony. *Microbiology (Reading)* 150(Pt. 12), 4009–4022. doi: 10.1099/mic.0.27247-0
- Gonzales, J., Chakraborty, T., Romero, M., Mraheil, M. A., Kutlar, A., Pace, B., et al. (2021). *Streptococcus pneumoniae* and its virulence factors H2O2 and pneumolysin are potent mediators of the acute chest syndrome in sickle cell disease. *Toxins (Basel)* 13:157. doi: 10.3390/toxins13020157
- Gourlay, R. N. (1965). Antigenicity of *Mycoplasma mycoides*. II. Further studies on the precipitating antigens in the body fluids from cases of contagious bovine pleuropneumonia. *Res. Vet. Sci.* 6, 1–8.
- Grosshennig, S., Ischebeck, T., Gibhardt, J., Busse, J., Feussner, I., and Stulke, J. (2016). Hydrogen sulfide is a novel potential virulence factor of *Mycoplasma pneumoniae*: characterization of the unusual cysteine desulfurase/desulfhydrase HapE. *Mol. Microbiol.* 100, 42–54. doi: 10.1111/mmi.13300
- Grundel, A., Jacobs, E., and Dumke, R. (2016). Interactions of surface-displayed glycolytic enzymes of *Mycoplasma pneumoniae* with components of the human extracellular matrix. *Int. J. Med. Microbiol.* 306, 675–685. doi: 10.1016/j.ijmm.2016.09.001
- Hagemann, L., Grundel, A., Jacobs, E., and Dumke, R. (2017). The surface-displayed chaperones GroEL and DnaK of *Mycoplasma pneumoniae* interact with human plasminogen and components of the extracellular matrix. *Pathog. Dis.* 75:ftx017. doi: 10.1093/femspd/ftx017
- Hames, C., Halbedel, S., Hoppert, M., Frey, J., and Stulke, J. (2009). Glycerol metabolism is important for cytotoxicity of *Mycoplasma pneumoniae*. *J. Bacteriol.* 191, 747–753. doi: 10.1128/JB.01103-08

- Hernandez, R. E., Gallegos-Monterrosa, R., and Coulthurst, S. J. (2020). Type VI secretion system effector proteins: effective weapons for bacterial competitiveness. *Cell. Microbiol.* 22:e13241. doi: 10.1111/cmi.13241
- Herrero, E. R., Slomka, V., Bernaerts, K., Boon, N., Hernandez-Sanabria, E., Passoni, B. B., et al. (2016). Antimicrobial effects of commensal oral species are regulated by environmental factors. *J. Dent.* 47, 23–33. doi: 10.1016/j.jdent.2016.02.007
- Hopfe, M., Hoffmann, R., and Henrich, B. (2004). P80, the HinT interacting membrane protein, is a secreted antigen of *Mycoplasma hominis*. *BMC Microbiol.* 4:46. doi: 10.1186/1471-2180-4-46
- Houot, L., Chang, S., Pickering, B. S., Absalon, C., and Watnick, P. I. (2010). The phosphoenolpyruvate phosphotransferase system regulates *Vibrio cholerae* biofilm formation through multiple independent pathways. *J. Bacteriol.* 192, 3055–3067. doi: 10.1128/JB.00213-10
- Hudson, J. R., Buttery, S., and Cottew, G. S. (1967). Investigations into the influence of the galactan of *Mycoplasma mycoides* on experimental infection with that organism. *J. Pathol. Bacteriol.* 94, 257–273. doi: 10.1002/path.1700940204
- Hummeler, K., Tomassini, N., and Hayflick, L. (1965). Ultrastructure of a *Mycoplasma (negroni)* isolated from human leukemia. *J. Bacteriol.* 90, 517–523. doi: 10.1128/JB.90.2.517-523.1965
- Hwang, M. H., Damte, D., Cho, M. H., Kim, Y. H., and Park, S. C. (2010). Optimization of culture media of pathogenic *Mycoplasma hyopneumoniae* by a response surface methodology. *J. Vet. Sci.* 11, 327–332. doi: 10.4142/jvs.2010.11.4.327
- Jarocki, V. M., Raymond, B. B. A., Tacchi, J. L., Padula, M. P., and Djordjevic, S. P. (2019). *Mycoplasma hyopneumoniae* surface-associated proteases cleave bradykinin, substance P, neurokinin A and neuropeptide Y. *Sci. Rep.* 9:14585. doi: 10.1038/s41598-019-51116-w
- Jarocki, V. M., Santos, J., Tacchi, J. L., Raymond, B. B., Deutscher, A. T., Jenkins, C., et al. (2015). MJH_0461 is a multifunctional leucine aminopeptidase on the surface of *Mycoplasma hyopneumoniae*. *Open Biol.* 5:140175. doi: 10.1098/rsob.140175
- Jiang, L., Schinkel, M., van Essen, M., and Schiffelers, R. M. (2019). Bacterial membrane vesicles as promising vaccine candidates. *Eur. J. Pharm. Biopharm.* 145, 1–6. doi: 10.1016/j.ejpb.2019.09.021
- Jiang, Z., Li, S., Zhu, C., Zhou, R., and Leung, P. H. M. (2021). *Mycoplasma pneumoniae* infections: pathogenesis and vaccine development. *Pathogens* 10:119. doi: 10.3390/pathogens10020119
- Jordan, D. S., Daubenspeck, J. M., and Dybvig, K. (2013). Rhamnose biosynthesis in mycoplasmas requires precursor glycans larger than monosaccharide. *Mol. Microbiol.* 89, 918–928. doi: 10.1111/mmi.12320
- Josi, C., Burki, S., Vidal, S., Dordet-Frisoni, E., Citti, C., Falquet, L., et al. (2019). Large-scale analysis of the *Mycoplasma bovis* genome identified non-essential, adhesion- and virulence-related genes. *Front. Microbiol.* 10:2085. doi: 10.3389/fmicb.2019.02085
- Khan, L. A., Miles, R. J., and Nicholas, R. A. (2005). Hydrogen peroxide production by *Mycoplasma bovis* and *Mycoplasma agalactiae* and effect of *in vitro* passage on a *Mycoplasma bovis* strain producing high levels of H₂O₂. *Vet. Res. Commun.* 29, 181–188. doi: 10.1023/b:verc.0000047506.04096.06
- Kim, J. H., Lee, J., Park, J., and Ghoo, Y. S. (2015). Gram-negative and Gram-positive bacterial extracellular vesicles. *Semin. Cell Dev. Biol.* 40, 97–104. doi: 10.1016/j.semcdb.2015.02.006
- Klimentova, J., and Stulik, J. (2015). Methods of isolation and purification of outer membrane vesicles from gram-negative bacteria. *Microbiol. Res.* 170, 1–9. doi: 10.1016/j.micres.2014.09.006
- Konoshenko, M. Y., Lekhnov, E. A., Vlassov, A. V., and Laktionov, P. P. (2018). Isolation of extracellular vesicles: general methodologies and latest trends. *Biomed Res. Int.* 2018:8545347. doi: 10.1155/2018/8545347
- Kornilov, R., Puhka, M., Mannerstrom, B., Hiidenmaa, H., Peltoniemi, H., Siljander, P., et al. (2018). Efficient ultrafiltration-based protocol to deplete extracellular vesicles from fetal bovine serum. *J. Extracell. Vesicles* 7:1422674. doi: 10.1080/20013078.2017.1422674
- Kurotchkin, T. J. (1937). Specific carbohydrate from *Asterococcus mycoides* for serologic tests of bovine pleuropneumonia. *Proc. Soc. Exp. Biol. Med.* 37, 21–22.
- Kurotchkin, T. J., and Benaradsky, C. V. (1938). Serological diagnosis of bovine pleuropneumonia through the use of the specific carbohydrate of *Asterococcus mycoides*. *Chin. Med. J. Suppl.* 2, 269–278.
- Lahteenmaki, K., Edelman, S., and Korhonen, T. K. (2005). Bacterial metastasis: the host plasminogen system in bacterial invasion. *Trends Microbiol.* 13, 79–85. doi: 10.1016/j.tim.2004.12.003
- Le Carrou, J., Laurentie, M., Kobisch, M., and Gautier-Bouchardon, A. V. (2006). Persistence of *Mycoplasma hyopneumoniae* in experimentally infected pigs after marbofloxacin treatment and detection of mutations in the parC gene. *Antimicrob. Agents Chemother.* 50, 1959–1966. doi: 10.1128/AAC.01527-05
- Leal Zimmer, F. M. A., Paes, J. A., Zaha, A., and Ferreira, H. B. (2020). Pathogenicity and virulence of *Mycoplasma hyopneumoniae*. *Virulence* 11, 1600–1622. doi: 10.1080/21505594.2020.1842659
- Leal Zimmer, F., Paludo, G. P., Moura, H., Barr, J. R., and Ferreira, H. B. (2019). Differential secretome profiling of a swine tracheal cell line infected with mycoplasmas of the swine respiratory tract. *J. Proteomics* 192, 147–159. doi: 10.1016/j.jpro.2018.08.018
- Li, P., Zhang, Y., Li, X., Zhou, W., Li, X., Jiang, F., et al. (2019). *Mycoplasma hyopneumoniae* Mhp597 is a cytotoxicity, inflammation and immunosuppression associated nuclease. *Vet. Microbiol.* 235, 53–62. doi: 10.1016/j.vetmic.2019.05.011
- Limoli, D. H., Jones, C. J., and Wozniak, D. J. (2015). Bacterial extracellular polysaccharides in biofilm formation and function. *Microbiol. Spectr.* 3. doi: 10.1128/microbiolspec.MB-0011-2014
- Lin, J., Zhang, W., Cheng, J., Yang, X., Zhu, K., Wang, Y., et al. (2017). A *Pseudomonas* T6SS effector recruits PQS-containing outer membrane vesicles for iron acquisition. *Nat. Commun.* 8:14888. doi: 10.1038/ncomms14888
- Llobet, E., Tomas, J. M., and Bengoechea, J. A. (2008). Capsule polysaccharide is a bacterial decoy for antimicrobial peptides. *Microbiology (Reading)* 154(Pt. 12), 3877–3886. doi: 10.1099/mic.0.2008/022301-0
- Lloyd, L. C. (1966). Tissue necrosis produced by *Mycoplasma mycoides* in intraperitoneal diffusion chambers. *Pathol. Bacteriol.* 92, 225–229. doi: 10.1002/path.1700920125
- Machado, L., Paes, J. A., Souza Dos Santos, P., and Ferreira, H. B. (2020). Evidences of differential endoproteolytic processing on the surfaces of *Mycoplasma hyopneumoniae* and *Mycoplasma flocculare*. *Microb. Pathog.* 140:103958. doi: 10.1016/j.micpath.2019.103958
- Madsen, M. L., Nettleton, D., Thacker, E. L., and Minion, F. C. (2006). Transcriptional profiling of *Mycoplasma hyopneumoniae* during iron depletion using microarrays. *Microbiology (Reading)* 152(Pt. 4), 937–944. doi: 10.1099/mic.0.28674-0
- Marois, C., Le Carrou, J., Kobisch, M., and Gautier-Bouchardon, A. V. (2007). Isolation of *Mycoplasma hyopneumoniae* from different sampling sites in experimentally infected and contact SPF piglets. *Vet. Microbiol.* 120, 96–104. doi: 10.1016/j.vetmic.2006.10.015
- Martinez-Torres, C., Torres-Puig, S., Monge, M., Sanchez-Alba, L., Gonzalez-Martin, M., Marcos-Silva, M., et al. (2020). Transcriptional response to metal starvation in the emerging pathogen *Mycoplasma genitalium* is mediated by Fur-dependent and -independent regulatory pathways. *Emerg. Microbes Infect.* 9, 5–19. doi: 10.1080/22221751.2019.1700762
- McGowan, C. L., Popov, V. L., and Pyles, R. B. (2009). Intracellular *Mycoplasma genitalium* infection of human vaginal and cervical epithelial cells elicits distinct patterns of inflammatory cytokine secretion and provides a possible survival niche against macrophage-mediated killing. *BMC Microbiol.* 9:139. doi: 10.1186/1471-2180-9-139
- McMillan, H. M., and Kuehn, M. J. (2021). The extracellular vesicle generation paradox: a bacterial point of view. *EMBO J.* 40:e108174. doi: 10.15252/embj.2021108174
- Minion, F. C., Jarvill-Taylor, K. J., Billings, D. E., and Tigges, E. (1993). Membrane-associated nuclease activities in mycoplasmas. *J. Bacteriol.* 175, 7842–7847. doi: 10.1128/jb.175.24.7842-7847.1993
- Monteiro, R., Chafsey, I., Ageorges, V., Leroy, S., Chambon, C., Hebraud, M., et al. (2021). The Secretome landscape of *Escherichia coli* O157:H7: deciphering the cell-surface, outer membrane vesicle and extracellular subproteomes. *J. Proteomics* 232:104025. doi: 10.1016/j.jpro.2020.104025
- Mu, H. H., Sawitzke, A. D., and Cole, B. C. (2000). Modulation of cytokine profiles by the *Mycoplasma* superantigen *Mycoplasma arthritis* mitogen parallels susceptibility to arthritis induced by *M. arthritis*. *Infect. Immun.* 68, 1142–1149. doi: 10.1128/iai.68.3.1142-1149.2000
- Nguyen, M. T., Peisl, L., Barletta, F., Lugman, A., and Gotz, F. (2018). Toll-like receptor 2 and lipoprotein-like lipoproteins enhance *Staphylococcus aureus*

- invasion in epithelial cells. *Infect. Immun.* 86:e00343-18. doi: 10.1128/IAI.00343-18
- Nocard, and Roux (1898). The microbe of pleuropneumonia. *Rev. Infect. Dis.* 12, 354–358. doi: 10.1093/clinids/12.2.354
- Olaya-Abril, A., Gonzalez-Reyes, J. A., and Rodriguez-Ortega, M. J. (2021). Approaching *in vivo* models of pneumococcus-host interaction: insights into surface proteins, capsule production, and extracellular vesicles. *Pathogens* 10:1098. doi: 10.3390/pathogens10091098
- Orench-Rivera, N., and Kuehn, M. J. (2021). Differential packaging into outer membrane vesicles upon oxidative stress reveals a general mechanism for cargo selectivity. *Front. Microbiol.* 12:561863. doi: 10.3389/fmicb.2021.561863
- Paes, J. A., Lorenzatto, K. R., de Moraes, S. N., Moura, H., Barr, J. R., and Ferreira, H. B. (2017). Secretomes of *Mycoplasma hyopneumoniae* and *Mycoplasma flocculare* reveal differences associated to pathogenesis. *J. Proteomics* 154, 69–77. doi: 10.1016/j.jprot.2016.12.002
- Pilo, P., Vilei, E. M., Peterhans, E., Bonvin-Klotz, L., Stoffel, M. H., Dobbelaere, D., et al. (2005). A metabolic enzyme as a primary virulence factor of *Mycoplasma mycoides* subsp. *mycoides* small colony. *J. Bacteriol.* 187, 6824–6831. doi: 10.1128/JB.187.19.6824-6831.2005
- Plackett, P., and Buttery, S. H. (1958). A galactan from *Mycoplasma mycoides*. *Nature* 182, 1236–1237. doi: 10.1038/1821236a0
- Plackett, P., and Buttery, S. H. (1964). A galactofuranose disaccharide from the galactan of *Mycoplasma mycoides*. *Biochem. J.* 90, 201–205. doi: 10.1042/bj0900201
- Plackett, P., Buttery, S., and Cottew, G. (1963). “Carbohydrates of some *Mycoplasma* strains,” in *Recent Progress in Microbiology VIII*, ed. N. E. Gibbons (Toronto, ON: University of Toronto Press), 533.
- Prados-Rosales, R., Weinrick, B. C., Pique, D. G., Jacobs, W. R. Jr., Casadevall, A., and Rodriguez, G. M. (2014). Role for *Mycobacterium tuberculosis* membrane vesicles in iron acquisition. *J. Bacteriol.* 196, 1250–1256. doi: 10.1128/JB.01090-13
- Raymond, B. B. A., Turnbull, L., Jenkins, C., Madhkoor, R., Schleicher, I., Uphoff, C. C., et al. (2018b). *Mycoplasma hyopneumoniae* resides intracellularly within porcine epithelial cells. *Sci. Rep.* 8:17697. doi: 10.1038/s41598-018-36054-3
- Raymond, B. B. A., Jenkins, C., Turnbull, L., Whitchurch, C. B., and Djordjevic, S. P. (2018a). Extracellular DNA release from the genome-reduced pathogen *Mycoplasma hyopneumoniae* is essential for biofilm formation on abiotic surfaces. *Sci. Rep.* 8:10373. doi: 10.1038/s41598-018-28678-2
- Raymond, B. B., Tacchi, J. L., Jarocki, V. M., Minion, F. C., Padula, M. P., and Djordjevic, S. P. (2013). P159 from *Mycoplasma hyopneumoniae* binds porcine cilia and heparin and is cleaved in a manner akin to ectodomain shedding. *J. Proteome Res.* 12, 5891–5903. doi: 10.1021/pr400903s
- Razin, S., Hasin, M., Ne’eman, Z., and Rottem, S. (1973). Isolation, chemical composition, and ultrastructural features of the cell membrane of the mycoplasma-like organism *Spiroplasma citri*. *J. Bacteriol.* 116, 1421–1435. doi: 10.1128/jb.116.3.1421-1435.1973
- Razin, S., Yoge, D., and Naot, Y. (1998). Molecular biology and pathogenicity of mycoplasmas. *Microbiol. Mol. Biol. Rev.* 62, 1094–1156. doi: 10.1128/MMBR.62.4.1094-1156.1998
- Rebollo Couto, M. S., Klein, C. S., Voss-Rech, D., and Terenzi, H. (2012). Extracellular proteins of *Mycoplasma synoviae*. *ISRN Vet. Sci.* 2012:802308. doi: 10.5402/2012/802308
- Robinson, M. W., Buchtmann, K. A., Jenkins, C., Tacchi, J. L., Raymond, B. B., To, J., et al. (2013). MHJ_0125 is an M42 glutamyl aminopeptidase that moonlights as a multifunctional adhesin on the surface of *Mycoplasma hyopneumoniae*. *Open Biol.* 3:130017. doi: 10.1098/rsob.130017
- Rojas, E. R., and Huang, K. C. (2018). Regulation of microbial growth by turgor pressure. *Curr. Opin. Microbiol.* 42, 62–70. doi: 10.1016/j.mib.2017.10.015
- Sacchini, F., Luciani, M., Salini, R., Scaccia, M., Pini, A., Lelli, R., et al. (2012). Plasma levels of TNF-alpha, IFN-gamma, IL-4 and IL-10 during a course of experimental contagious bovine pleuropneumonia. *BMC Vet. Res.* 8:44. doi: 10.1186/1746-6148-8-44
- Schieck, E., Lartigue, C., Frey, J., Vozza, N., Hegemann, J., Miller, R. A., et al. (2016). Galactofuranose in *Mycoplasma mycoides* is important for membrane integrity and conceals Adhesins but does not contribute to serum resistance. *Mol. Microbiol.* 99, 55–70. doi: 10.1111/mmi.13213
- Schmid, J. (2018). Recent insights in microbial exopolysaccharide biosynthesis and engineering strategies. *Curr. Opin. Biotechnol.* 53, 130–136. doi: 10.1016/j.copbio.2018.01.005
- Schmidt, J. A., Browning, G. F., and Markham, P. F. (2004). *Mycoplasma hyopneumoniae* p65 surface lipoprotein is a lipolytic enzyme with a preference for shorter-chain fatty acids. *J. Bacteriol.* 186, 5790–5798. doi: 10.1128/JB.186.17.5790-5798.2004
- Seymour, L. M., Jenkins, C., Deutscher, A. T., Raymond, B. B., Padula, M. P., Tacchi, J. L., et al. (2012). Mhp182 (P102) binds fibronectin and contributes to the recruitment of plasmin(ogen) to the *Mycoplasma hyopneumoniae* cell surface. *Cell. Microbiol.* 14, 81–94. doi: 10.1111/j.1462-5822.2011.01702.x
- Sharma, A. K., Dhasmana, N., Dubey, N., Kumar, N., Gangwal, A., Gupta, M., et al. (2017). Bacterial virulence factors: secreted for survival. *Indian J. Microbiol.* 57, 1–10. doi: 10.1007/s12088-016-0625-1
- Sharma, S., Markham, P. F., and Browning, G. F. (2014). Genes found essential in other mycoplasmas are dispensable in *Mycoplasma bovis*. *PLoS One* 9:e97100. doi: 10.1371/journal.pone.0097100
- Sharma, S., Tivendale, K. A., Markham, P. F., and Browning, G. F. (2015). Disruption of the membrane nuclease gene (MBOVPG45_0215) of *Mycoplasma bovis* greatly reduces cellular nuclease activity. *J. Bacteriol.* 197, 1549–1558. doi: 10.1128/JB.00034-15
- Shaw, B. M., Daubenspeck, J. M., Simmons, W. L., and Dybvig, K. (2013). EPS-I polysaccharide protects *Mycoplasma pulmonis* from phagocytosis. *FEMS Microbiol. Lett.* 338, 155–160. doi: 10.1111/1574-6968.12048
- Shin, J., Rhim, J., Kwon, Y., Choi, S. Y., Shin, S., Ha, C. W., et al. (2019). Comparative analysis of differentially secreted proteins in serum-free and serum-containing media by using BONCAT and pulsed SILAC. *Sci. Rep.* 9:3096. doi: 10.1038/s41598-019-39650-z
- Siegl, C., and Rudel, T. (2015). Modulation of p53 during bacterial infections. *Nat. Rev. Microbiol.* 13, 741–748. doi: 10.1038/nrmicro3537
- Simmons, W. L., Daubenspeck, J. M., Osborne, J. D., Balish, M. F., Waites, K. B., and Dybvig, K. (2013). Type 1 and type 2 strains of *Mycoplasma pneumoniae* form different biofilms. *Microbiology (Reading)* 159(Pt. 4), 737–747. doi: 10.1099/mic.0.064782-0
- Song, Z., Li, Y., Liu, Y., Xin, J., Zou, X., and Sun, W. (2012). alpha-Enolase, an adhesion-related factor of *Mycoplasma bovis*. *PLoS One* 7:e38836. doi: 10.1371/journal.pone.0038836
- Staats, C. C., Boldo, J. T., Broetto, L., Vainstein, M. H., and Schrank, A. (2007). Comparative genome analysis of proteases, oligopeptide uptake and secretion systems in *Mycoplasma* spp. *Genet. Mol. Biol.* 30, 225–229.
- Stentz, R., Carvalho, A. L., Jones, E. J., and Carding, S. R. (2018). Fantastic voyage: the journey of intestinal microbiota-derived microvesicles through the body. *Biochem. Soc. Trans.* 46, 1021–1027. doi: 10.1042/BST20180114
- Stentz, R., Miquel-Clopes, A., and Carding, S. R. (2022). Production, isolation, and characterization of bioengineered bacterial extracellular membrane vesicles derived from *Bacteroides thetaiotaomicron* and their use in vaccine development. *Methods Mol. Biol.* 2414, 171–190. doi: 10.1007/978-1-0716-1900-1_11
- Sukumaran, A., Woroszchuk, E., Ross, T., and Geddes-McAlister, J. (2021). Proteomics of host-bacterial interactions: new insights from dual perspectives. *Can. J. Microbiol.* 67, 213–225. doi: 10.1139/cjm-2020-0324
- Sutherland, I. W. (1972). Bacterial exopolysaccharides. *Adv. Microb. Physiol.* 8, 143–213. doi: 10.1016/s0065-2911(08)60190-3
- Sutherland, I. W. (1985). Biosynthesis and composition of Gram-negative bacterial extracellular and wall polysaccharides. *Annu. Rev. Microbiol.* 39, 243–270. doi: 10.1146/annurev.mi.39.100185.001331
- Tacchi, J. L., Raymond, B. B., Haynes, P. A., Berry, I. J., Widjaja, M., Bogema, D. R., et al. (2016). Post-translational processing targets functionally diverse proteins in *Mycoplasma hyopneumoniae*. *Open Biol.* 6:150210. doi: 10.1098/rsob.150210
- Tam, K., and Torres, V. J. (2019). *Staphylococcus aureus* secreted toxins and extracellular enzymes. *Microbiol. Spectr.* 7. doi: 10.1128/microbiolspec.GPP3-0039-2018
- Thery, C., Witwer, K. W., Aikawa, E., Alcaraz, M. J., Anderson, J. D., Andriantsitohaina, R., et al. (2018). Minimal information for studies of extracellular vesicles 2018 (MISEV2018): a position statement of the International Society for Extracellular Vesicles and update of the MISEV2014 guidelines. *J. Extracell. Vesicles* 7:1535750. doi: 10.1080/20013078.2018.1535750

- Tjalsma, H., Bolhuis, A., Jongbloed, J. D., Bron, S., and van Dijk, J. M. (2000). Signal peptide-dependent protein transport in *Bacillus subtilis*: a genome-based survey of the secretome. *Microbiol. Mol. Biol. Rev.* 64, 515–547. doi: 10.1128/MMBR.64.3.515-547.2000
- Tomassen, J., and Arenas, J. (2017). Biological functions of the secretome of *Neisseria meningitidis*. *Front. Cell. Infect. Microbiol.* 7:256. doi: 10.3389/fcimb.2017.00256
- Totte, P., Puech, C., Rodrigues, V., Bertin, C., Manso-Silvan, L., and Thiaucourt, F. (2015). Free exopolysaccharide from *Mycoplasma mycoides* subsp. *mycoides* possesses anti-inflammatory properties. *Vet. Res.* 46:122. doi: 10.1186/s13567-015-0252-6
- Tourtellotte, M. E., Morowitz, H. J., and Kasimer, P. (1964). Defined medium for *Mycoplasma laidlawii*. *J. Bacteriol.* 88, 11–15. doi: 10.1128/JB.88.1.11-15.1964
- Toyofuku, M., Nomura, N., and Eberl, L. (2019). Types and origins of bacterial membrane vesicles. *Nat. Rev. Microbiol.* 17, 13–24. doi: 10.1038/s41579-018-0112-2
- Turnbull, L., Toyofuku, M., Hynen, A. L., Kurosawa, M., Pessi, G., Petty, N. K., et al. (2016). Explosive cell lysis as a mechanism for the biogenesis of bacterial membrane vesicles and biofilms. *Nat. Commun.* 7:11220. doi: 10.1038/ncomms11220
- Voros, A., DeLongchamp, J., and Saleh, M. T. (2015). The secretome of *Mycoplasma capricolum* subsp. *capricolum* in neutral and acidic media. *J. Proteomics Bioinformatics* 8, 155–163.
- Voros, A., Dunnett, A., Leduc, L. G., and Saleh, M. T. (2009). Depleting proteins from the growth medium of *Mycoplasma capricolum* unmasks bacterium-derived enzymatic activities. *Vet. Microbiol.* 138, 384–389. doi: 10.1016/j.vetmic.2009.04.012
- Wang, G., Chen, H., Xia, Y., Cui, J., Gu, Z., Song, Y., et al. (2013). How are the non-classically secreted bacterial proteins released into the extracellular milieu? *Curr. Microbiol.* 67, 688–695. doi: 10.1007/s00284-013-0422-6
- Wang, J., Li, Y., Pan, L., Li, J., Yu, Y., Liu, B., et al. (2021). Glyceraldehyde-3-phosphate dehydrogenase (GAPDH) moonlights as an adhesin in *Mycoplasma hyorhinis* adhesion to epithelial cells as well as a plasminogen receptor mediating extracellular matrix degradation. *Vet. Res.* 52:80. doi: 10.1186/s13567-021-00952-8
- Wawegama, N. K., Browning, G. F., Kanci, A., Marenda, M. S., and Markham, P. F. (2014). Development of a recombinant protein-based enzyme-linked immunosorbent assay for diagnosis of *Mycoplasma bovis* infection in cattle. *Clin. Vaccine Immunol.* 21, 196–202. doi: 10.1128/CI.00670-13
- Whitney, J. C., and Howell, P. L. (2013). Synthase-dependent exopolysaccharide secretion in Gram-negative bacteria. *Trends Microbiol.* 21, 63–72. doi: 10.1016/j.tim.2012.10.001
- Widjaja, M., Harvey, K. L., Hagemann, L., Berry, I. J., Jarocki, V. M., Raymond, B. B. A., et al. (2017). Elongation factor Tu is a multifunctional and processed moonlighting protein. *Sci. Rep.* 7:11227. doi: 10.1038/s41598-017-10644-z
- Woodward, L., and Naismith, J. H. (2016). Bacterial polysaccharide synthesis and export. *Curr. Opin. Struct. Biol.* 40, 81–88. doi: 10.1016/j.sbi.2016.07.016
- Woolley, L. K., Fell, S., Gonsalves, J. R., Walker, M. J., Djordjevic, S. P., Jenkins, C., et al. (2012). Evaluation of clinical, histological and immunological changes and qPCR detection of *Mycoplasma hyopneumoniae* in tissues during the early stages of mycoplasmal pneumonia in pigs after experimental challenge with two field isolates. *Vet. Microbiol.* 161, 186–195. doi: 10.1016/j.vetmic.2012.07.025
- Yamamoto, T., Kida, Y., Sakamoto, Y., and Kuwano, K. (2017). Mpn491, a secreted nuclease of *Mycoplasma pneumoniae*, plays a critical role in evading killing by neutrophil extracellular traps. *Cell. Microbiol.* 19:e12666. doi: 10.1111/cmi.12666
- Yavlovich, A., Katzenell, A., Tarshis, M., Higazi, A. A., and Rottem, S. (2004a). *Mycoplasma fermentans* binds to and invades HeLa cells: involvement of plasminogen and urokinase. *Infect. Immun.* 72, 5004–5011. doi: 10.1128/IAI.72.9.5004-5011.2004
- Yavlovich, A., Tarshis, M., and Rottem, S. (2004b). Internalization and intracellular survival of *Mycoplasma pneumoniae* by non-phagocytic cells. *FEMS Microbiol. Lett.* 233, 241–246. doi: 10.1016/j.femsle.2004.02.016
- Yiwen, C., Yueyue, W., Lianmei, Q., Cuiming, Z., and Xiaoxing, Y. (2021). Infection strategies of mycoplasmas: unraveling the panoply of virulence factors. *Virulence* 12, 788–817. doi: 10.1080/21505594.2021.1889813
- Yus, E., Maier, T., Michalodimitrakis, K., van Noort, V., Yamada, T., Chen, W. H., et al. (2009). Impact of genome reduction on bacterial metabolism and its regulation. *Science* 326, 1263–1268. doi: 10.1126/science.1177263
- Zella, D., Curreli, S., Benedetti, F., Krishnan, S., Cocchi, F., Latinovic, O. S., et al. (2018). Mycoplasma promotes malignant transformation in vivo, and its DnaK, a bacterial chaperone protein, has broad oncogenic properties. *Proc. Natl. Acad. Sci. U.S.A.* 115, E12005–E12014. doi: 10.1073/pnas.1815660115
- Zhang, H., Hu, G., Lu, D., Zhao, G., Zhang, Y., Zubair, M., et al. (2021). Comparative secretome analyses of *Mycoplasma bovis* virulent and attenuated strains revealed MbovP0145 as a promising diagnostic biomarker. *Front. Vet. Sci.* 8:666769. doi: 10.3389/fvets.2021.666769
- Zhang, H., Zhao, G., Guo, Y., Menghwar, H., Chen, Y., Chen, H., et al. (2016). *Mycoplasma bovis* MBOV_RS02825 encodes a secretory nuclease associated with cytotoxicity. *Int. J. Mol. Sci.* 17:628. doi: 10.3390/ijms17050628
- Zhao, G., Zhang, H., Chen, X., Zhu, X., Guo, Y., He, C., et al. (2017). *Mycoplasma bovis* NADH oxidase functions as both a NADH oxidizing and O₂ reducing enzyme and an adhesin. *Sci. Rep.* 7:44. doi: 10.1038/s41598-017-00121-y
- Zhao, G., Zhu, X., Zhang, H., Chen, Y., Schieck, E., Hu, C., et al. (2021). Novel secreted protein of *Mycoplasma bovis* MbovP280 induces macrophage apoptosis through CRYAB. *Front. Immunol.* 12:619362. doi: 10.3389/fimmu.2021.619362
- Zhu, X., Dordet-Frisoni, E., Gillard, L., Ba, A., Hygonenq, M. C., Sagne, E., et al. (2019). Extracellular DNA: a nutritional trigger of *Mycoplasma bovis* cytotoxicity. *Front. Microbiol.* 10:2753. doi: 10.3389/fmicb.2019.02753
- Zubair, M., Khan, F. A., Menghwar, H., Faisal, M., Ashraf, M., Rasheed, M. A., et al. (2020a). Progresses on bacterial secretomes enlighten research on *Mycoplasma* secretome. *Microb. Pathog.* 144:104160. doi: 10.1016/j.micpath.2020.104160
- Zubair, M., Muhamed, S. A., Khan, F. A., Zhao, G., Menghwar, H., Faisal, M., et al. (2020b). Identification of 60 secreted proteins for *Mycoplasma bovis* with secretome assay. *Microb. Pathog.* 143:104135. doi: 10.1016/j.micpath.2020.104135

Conflict of Interest: The authors declare that the research was conducted in the absence of any commercial or financial relationships that could be construed as a potential conflict of interest.

The reviewer GB is currently organizing a Research Topic with the author FT.

Publisher's Note: All claims expressed in this article are solely those of the authors and do not necessarily represent those of their affiliated organizations, or those of the publisher, the editors and the reviewers. Any product that may be evaluated in this article, or claim that may be made by its manufacturer, is not guaranteed or endorsed by the publisher.

Copyright © 2022 Gaurivaud and Tardy. This is an open-access article distributed under the terms of the Creative Commons Attribution License (CC BY). The use, distribution or reproduction in other forums is permitted, provided the original author(s) and the copyright owner(s) are credited and that the original publication in this journal is cited, in accordance with accepted academic practice. No use, distribution or reproduction is permitted which does not comply with these terms.



Molecular Tools for Typing *Mycoplasma pneumoniae* and *Mycoplasma genitalium*

Roger Dumke*

TU Dresden, Institute of Medical Microbiology and Virology, Dresden, Germany

OPEN ACCESS

Edited by:

Meghan May,
University of New England,
United States

Reviewed by:

Li Xiao,
University of Alabama at Birmingham,
United States
Oscar Q. Pich,
Parc Taulí Foundation, Spain
Mateu Espasa,
Instituto de Investigación e
Innovación Parc Taulí (I3PT), Spain

*Correspondence:

Roger Dumke
roger.dumke@tu-dresden.de

Specialty section:

This article was submitted to
Infectious Agents and Disease,
a section of the journal
Frontiers in Microbiology

Received: 25 March 2022

Accepted: 16 May 2022

Published: 02 June 2022

Citation:

Dumke R (2022) Molecular Tools for
Typing *Mycoplasma pneumoniae* and
Mycoplasma genitalium.
Front. Microbiol. 13:904494.
doi: 10.3389/fmicb.2022.904494

Mycoplasma pneumoniae and *Mycoplasma genitalium* are cell wall-less bacteria with strongly reduced genome content and close phylogenetic relatedness. In humans, the only known natural host, the microorganisms colonize the respiratory or genitourinary mucosa and may cause a broad range of clinical presentations. Besides fundamental differences in their tissue specificity, transmission route, and ability to cause prevalence peaks, both species share similarities such as the occurrence of asymptomatic carriers, preferred populations for infection, and problems with high rates of antimicrobial resistance. To further understand the epidemiology of these practically challenging bacteria, typing of strains is necessary. Since the cultivation of both pathogens is difficult and not performed outside of specialized laboratories, molecular typing methods with adequate discriminatory power, stability, and reproducibility have been developed. These include the characterization of genes containing repetitive sequences, of variable genome regions without the presence of repetitive sequences, determination of single and multi-locus variable-number tandem repeats, and detection of single nucleotide polymorphisms in different genes, respectively. The current repertoire of procedures allows reliable differentiation of strains circulating in different populations and in different time periods as well as comparison of strains occurring subsequently in individual patients. In this review, the methods for typing *M. pneumoniae* and *M. genitalium*, including the results of their application in different studies, are summarized and current knowledge regarding the association of typing data with the clinical characteristics of infections is presented.

Keywords: *Mycoplasma pneumoniae*, *Mycoplasma genitalium*, molecular typing, epidemiology, SNP, MLST, tandem repeats

INTRODUCTION

During the evolutionary interplay with their hosts, the genomes of species of the class Mollicutes (“mycoplasma”) have been greatly reduced. Besides limited metabolic capabilities, the lack of a classical bacterial cell wall is the most striking result of this interaction. In humans, different species can be found as commensals whereas the most clinically relevant *Mycoplasma pneumoniae* and *Mycoplasma genitalium* are host-specific pathogens that infect the respiratory and genitourinary mucosa. *Mycoplasma pneumoniae* is transmitted via contaminated aerosols and is a frequent cause of community-acquired respiratory tract infections including severe cases of interstitial

pneumonia (Khoury et al., 2016). Infections can occur in all age groups but school-aged children are the preferred population. Besides small-scale outbreaks in settings with close person-to-person contacts, such as military camps or schools (Waite et al., 2017), epidemic peaks are registered every 3–7 years (Brown et al., 2016; Kenri et al., 2020). During these periods, which sometimes can be registered worldwide, *M. pneumoniae* may cause up to 50% of all community-acquired respiratory infections (Ho et al., 2015; Kogoj et al., 2015). In addition, a broad spectrum of extrapulmonary manifestations is described, mainly affecting the central nervous system and the skin (Narita, 2016). In contrast, *M. genitalium* is a sexually transmitted pathogen that causes non-gonococcal urethritis in men and is associated with urethritis, cervicitis, endometritis, and pelvic inflammatory disease in women (Jensen et al., 2022). The prevalence of infection ranges between 1.3 and 3.9% in the general population (Baumann et al., 2018) but can be significantly higher in risk groups such as men who have sex with men (MSM) and HIV-positive patients (Jansen et al., 2020; Latimer et al., 2020).

Treatment of infections with both species is challenging as mycoplasmas are intrinsically resistant to betalactams. Generally, tetracyclines and quinolones are effective but have side effects for relevant patient groups (treatment of *M. pneumoniae* in pediatrics) or are of limited clinical efficacy (*M. genitalium* and doxycycline). Hence, macrolides are the antibiotics recommended primarily for treatment of adults and children with severe clinical disease and in attempts at eradication in symptomatic or asymptomatic patients. Unfortunately, high rates of acquired resistance to macrolides (*M. pneumoniae*) and to macrolides and quinolones (*M. genitalium*) are described (Fernandez-Huerta et al., 2020a; Machalek et al., 2020; Pereyre and Tardy, 2021). Despite strong epidemiological differences, such as the location of colonized tissues and consequently the transmission route of infections, there are similarities in epidemiological characteristics. Besides the high rates of resistance, these include the occurrence of asymptomatic carriers probably able to transmit the pathogens (Spuesens et al., 2013; Gnanadurai and Fifer, 2020; de Groot et al., 2021).

As is typical for mycoplasmas, genomes of species are small but closely related phylogenetically, with around 580 kbp (*M. genitalium*) and 816 kbp (*M. pneumoniae*). Many orthologous proteins (~480) can be found in both pathogens and identity between them has been calculated as around 67% (Himmelreich et al., 1997). In the last few years, whole genome sequencing of isolates of different geographic origin and from varying time periods resulted in strong similarities between compared strains (>99%) and classification into two main lineages. Within these main genotypes, the genomes of both species were identical in >99.5%, which is remarkably high (Lluch-Senar et al., 2015; Xiao et al., 2015; Diaz et al., 2017; Fookes et al., 2017; Lee et al., 2019). Moreover, construction of phylogenetic trees of *M. pneumoniae* genomes resulted in different clades within the main types showing differences in the frequency of *in vivo* occurrence and in the number of recombination events (Kenri et al., 2020; Hsieh et al., 2022). Despite the overall conserved genomes, regions with higher heterogeneity were

shown to be associated in most cases with the occurrence of repetitive elements distributed in similar but non-identical copies in the genomes. Four repetitive elements (RepMp1, 2/3, 4, and 5) were found in *M. pneumoniae*, whereas repeated sequences from *M. genitalium* cluster in nine discrete regions are known as MgPar. Genome parts with copies of repetitive elements can be exchanged by homologous recombination (Musatovova et al., 2008; Spuesens et al., 2009; Hakim et al., 2021). This also applies to genes coding for surface-localized and antigenic proteins with special importance for the infection process such as the adhesins P1 and P40/P90 from *M. pneumoniae*, and MgpB and MgpC from *M. genitalium* (also known as P140 and P110). Resulting modifications of these proteins has been postulated as immune escape mechanism of the bacteria (Rocha and Blanchard, 2002; Hakim et al., 2021).

To further understand the epidemiology of infections by *M. pneumoniae* and *M. genitalium*, typing of strains is important. Unfortunately, cultivation of both species is difficult and only realized in few specialized centers. Therefore, molecular detection is common in routine laboratories and positive DNA from clinical material is the most frequent specimen available for typing in practice.

DEVELOPMENT OF TYPING METHODS

The first molecular method for typing *M. pneumoniae* isolates was PCR-mediated DNA fingerprinting, which confirmed that there were two main strain types (Su et al., 1990; Ursi et al., 1994). Supported by data from early whole genome sequencing of *M. pneumoniae* (type 1 strain M129; Himmelreich et al., 1996), more targeted methods were introduced in the following years. These included the restriction fragment length polymorphism procedure, which uses primers that amplify both regions of the *p1* gene (MPN141) containing copies of the repetitive elements RepMP2/3 and RepMP4 (Sasaki et al., 1996). This approach distinguished the two main *p1* types and a limited number of additional genotypes (Kenri et al., 2020). To detect all sequence variations, the more laborious amplification of RepMp copies in the *p1* gene followed by Sanger sequencing has been used (Dumke et al., 2006, 2015).

In 2009, multi-locus variable-number tandem-repeat analysis (MLVA) was introduced using five loci [HsdS (MPN089), intergenic, and hypothetical proteins (MPN501, MPN524, and MPN613)] to determine the number of repeats (Degrange et al., 2009). The results of typing of isolates showed an excellent discriminatory index (DI) of 0.92. The method was adapted for investigation of *M. pneumoniae*-positive DNA (Dumke and Jacobs, 2011). Unfortunately, the locus with the highest DI (Mpn1, coding for a subunit of type I restriction-modification enzyme, MPN089) was found to be instable (Benitez et al., 2012; Sun et al., 2013) and must be removed from the list of repeats. For the remaining four repeats, interpretation guidelines for use of MLVA were established to allow reliable interlaboratory comparison of results (Chalker et al., 2015). In some strains, differences in the length of distinct tandem repeat loci must be considered (Xue et al., 2018; Kenri et al., 2020). Further

tandem repeats were tested and might be an alternative to *Mpn1* to increase the discrimination of the method (Zhang et al., 2017). In addition, AGT repeats can be found in the region between the repetitive elements in the *p1* gene. Using this single locus of tandem repeats, strains with identical MLV type were differentiated and the number of *p1* repeats is associated with the main *p1* types (Zhao et al., 2011; Tian et al., 2013; Xiao et al., 2020). Unfortunately, there is evidence that this marker is unstable and this needs further analysis (Spuesens et al., 2016; Dumke, unpubl.). Recently, a new target of VNTR analysis was reported using the tandem repeats in subunit S of the type I restriction-modification system (MPN085) of *M. pneumoniae* for differentiation of strains (Lee et al., 2022).

Based on comprehensive comparison of the increasing number of whole genome data, two methods that use determination of single nucleotide polymorphisms (SNPs) for typing were developed. SNPs in eight genes (MPN003, MPN185, MPN246, MPN307, MPN528, MPN576, MPN600, and MPN628) coding for house-keeping proteins (Brown et al., 2015; here called MLS typing) or for house-keeping proteins (MPN004, MPN050, MPN168, MPN246, and MPN516), hypothetical lipoproteins (MPN442, MPN582), and the P1 adhesin [(MPN141); Touati et al., 2015; SNP typing] were selected. Both methods can be used not only for characterization of isolates but also for investigation of strains in DNA-positive clinical samples (Dumke and Rodriguez, 2021) and result in a numerical code or a SNP profile, which can be easily exchanged between laboratories. For a high discriminatory power of differentiation if MLS and SNP typing is performed in parallel, use of same loci [gmk (MPN246)] is disadvantageous. In addition, SNP measured in the *p1* gene (SNP typing) is located in the repetitive element RepMp2/3 and homologous recombination of this locus cannot be excluded. For the method of Brown et al., a database was established that comprises listing, consecutive numbering, and comparison of detected MLS types.¹

In addition to the aforementioned methods, various other typing methods were developed but are not widely used. Real-time PCR with high-resolution melting point analysis is able to differentiate *p1* type 1 and 2 strains (Schwartz et al., 2009). Moreover, pyrosequencing of two targets (MPN141 and MPN528a) resulted in correct classification of both main *p1* types (Spuesens et al., 2010). The MPN142 gene (historically named ORF6) contains a copy of the repetitive element RepMp5 and amplification/sequencing can be used to distinguish the main types 1 and 2 as well as some, but not all, other *p1* types (Ruland et al., 1994; Kenri et al., 2020). Investigation of the protein composition of bacteria by MALDI-ToF is not only suitable for reliable characterization of mycoplasmas on the species level but also for differentiation of the two main types of *M. pneumoniae* (Pereyre et al., 2013; Xiao et al., 2014). Of note, the procedure is described for investigation of isolates. Finally, nanorod array surface-enhanced Raman spectroscopy was used for detection of *M. pneumoniae* and typing of isolates and strains in clinical throat swabs (Hennigan et al., 2010; Henderson et al., 2015). Special equipment and experienced

staff are required for this typing method which is, therefore, reserved for specialized laboratories.

In comparison with *M. pneumoniae*, the number of procedures for typing *M. genitalium* strains is relatively small. The first method was investigation of a variable part of the MG_191 gene, which codes for the adhesin MgpB (Hjorth et al., 2006). This gene contains repetitive elements but the typing region near the 5' end (nt 180–460 in type strain G37) was found to be stable during *in vivo* and *in vitro* passage of isolates and is not influenced by homologous recombination. The results of the study by Hjorth et al. (2006) confirmed not only the sexual transmission of *M. genitalium* between couples but also the usefulness of culture-independent *mgpB* typing to investigate the circulation of genotypes in different populations and to characterize strains in cases of treatment failure. Furthermore, analysis of different short tandem repeats in the gene MG_309, which codes for a surface-localized lipoprotein, is suitable for typing (Ma and Martin, 2004; Ma et al., 2008; McGowin et al., 2009). Combining the number of these repeats (AGT/AAT) with *mgpB* typing increases the discriminatory power. Further targets of strain discrimination as well as MLVA testing were found to be not stable, not discriminatory enough, too discriminatory (Cazanave et al., 2012) or were used in a very limited number of studies (Ma and Martin, 2004; Pineiro et al., 2019) to date.

EVALUATION OF COMMON TYPING METHODS

A sufficiently large number of data for comparison of the results of different methods are available for *p1*, MLV, MLS, and SNP typing in *M. pneumoniae* and for *mgpB* and MG_309 typing in *M. genitalium* (Table 1). Using *p1* typing, calculated DI's (Hunter and Gaston, 1988) from selected studies ranged between 0.42 and 0.68. To date, 15 *p1* types have been described (Kenri et al., 2020; Xiao et al., 2020). The main types 1 and 2 contain specific repetitive sequences in their genomes, suggesting early differentiation of *M. pneumoniae* strains into these two lineages (Spuesens et al., 2009; Diaz and Winchell, 2016). In contrast, the 13 known variants can be assigned to the main genotypes but differ in one or both repetitive copies in the *p1* gene. Criteria for recognizing a strain as variant should be set in the future (e.g., length of sequence which must be different from known *p1* types to define a new type, deposition of full-length sequences of both RepMP2/3, and four elements of *p1* gene of the strain in databases). Interestingly, by contrast with *p1* type 1, more variant strains have been characterized among type 2. This might be attributed to type-specific differences in the functionality of proteins putatively involved in DNA recombination and repair in *M. pneumoniae* and *M. genitalium* (Sluijter et al., 2010; Hakim et al., 2021).

As an example for the occurrence of MLV types in various populations, the results of selected studies (characterization of >50 strains) in different countries are summarized in Table 1 and Figure 1A. With at least 24 known types, MLVA demonstrated a greater number of genotypes in comparison with *p1* typing.

¹<http://pubmlst.org/mpneumoniae>

TABLE 1 | Characteristics of frequently used molecular approaches for typing *Mycoplasma pneumoniae* and *Mycoplasma genitalium* (results of studies with >25 patients are included; if not presented in the study, HGDI's are calculated according to the data).

Species	Typing method	Number of known types	HGDI	References
<i>M. pneumoniae</i>	<i>p1</i>	15	0.42–0.68	Brown et al., 2015; Dumke et al., 2015; Touati et al., 2015; Kenri et al., 2020; Xiao et al., 2020; Dumke and Rodriguez, 2021; Meyer Sauter et al., 2021
	MLVA	24	0.58–0.68	Benitez et al., 2012; Brown et al., 2015; Dumke et al., 2015; Touati et al., 2015; Kogoj et al., 2018; Zhao et al., 2019; Kenri et al., 2020; Xiao et al., 2020; Dumke and Rodriguez, 2021; Meyer Sauter et al., 2021
	MLST	46	0.66–0.78	http://pubmlst.org/mpneumoniae ; Brown et al., 2015; Kenri et al., 2020; Dumke and Rodriguez, 2021; Meyer Sauter et al., 2021
	SNP	15	0.80–0.84	Touati et al., 2015; Kenri et al., 2020; Dumke and Rodriguez, 2021
	<i>p1</i> + MLVA; <i>p1</i> + MLST; <i>p1</i> + SNP; MLVA + SNP; and MLST + SNP	n.d.	0.60–0.88	Brown et al., 2015; Dumke et al., 2015; Touati et al., 2015; Kenri et al., 2020; Xiao et al., 2020; Dumke and Rodriguez, 2021; Meyer Sauter et al., 2021
	<i>p1</i> + MLVA + MLST; <i>p1</i> + MLVA + SNP	n.d.	0.75–0.91	Brown et al., 2015; Touati et al., 2015; Kenri et al., 2020; Dumke and Rodriguez, 2021; Meyer Sauter et al., 2021
	<i>p1</i> + MLVA + MLST + SNP	n.d.	0.88–0.90	Kenri et al., 2020; Dumke and Rodriguez, 2021
<i>M. genitalium</i>	<i>mgbB</i>	246	0.82–0.99	Hjorth et al., 2006; Ma et al., 2008; Cazanave et al., 2012; Olsen et al., 2012; Dumke et al., 2020; Fernandez-Huerta et al., 2020b; Plummer et al., 2020; Sweeney et al., 2020; Chua et al., 2021; Dumke and Spornraft-Ragaller, 2021; Guiraud et al., 2021
	VNTR MG_309	12	0.84–0.95	Ma et al., 2008; Cazanave et al., 2012; Dumke and Spornraft-Ragaller, 2021; Guiraud et al., 2021; Laumen et al., 2021
	<i>mgbB</i> + VNTR MG_309	n.d.	0.95–0.99	Ma et al., 2008; Cazanave et al., 2012; Dumke and Spornraft-Ragaller, 2021; Guiraud et al., 2021

p1, sequence differences in *p1* gene (MPN141); MLVA, multilocus variable number of tandem-repeat analysis; MLST, multilocus sequence typing; SNP, determination of single polynucleotide polymorphisms; *mgbB*, sequence differences in *mgbB* gene (MG_191); VNTR MG_309, variable number of tandem repeat in gene MG_309; HGDI, discriminatory index (Hunter and Gaston, 1988); and n.d., not determined.

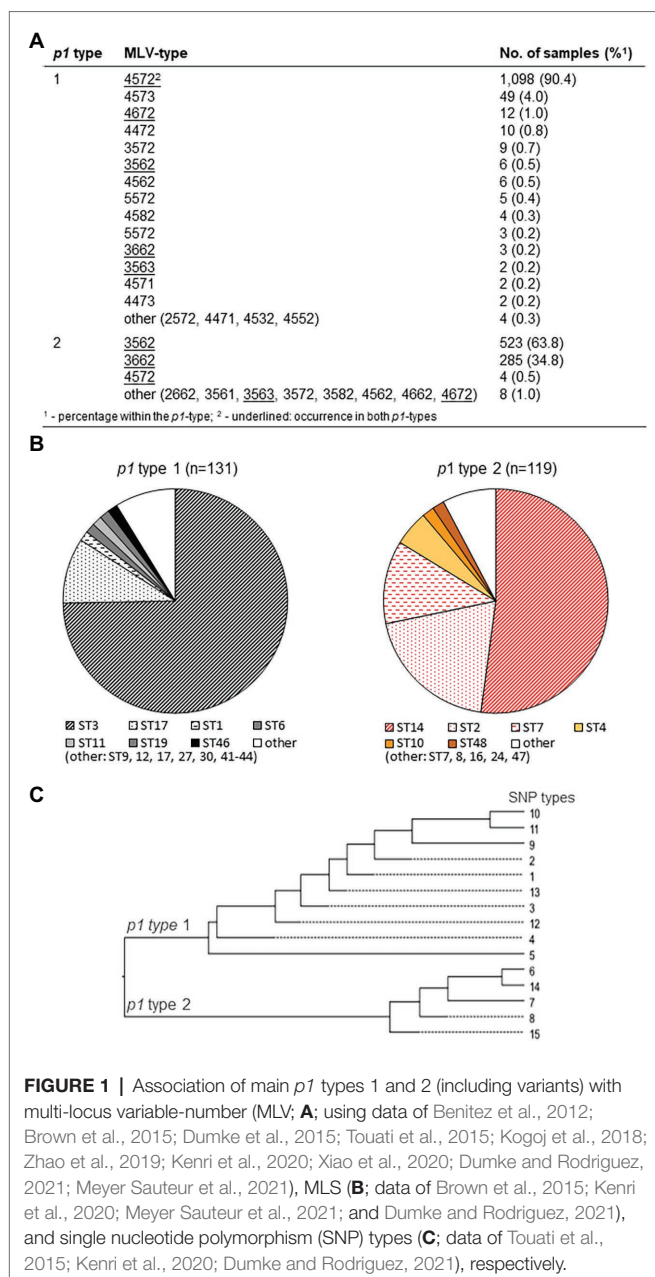
However, calculated DI's in these reports are not substantially higher due to the strong dominance (94%) of the three MLV types 4,572, 3,562, and 3,662, respectively. After review of further studies, additional MLV types were found in a small number of strains, underlining the need to summarize the typing results in an appropriate manner (preferably in a database). In contrast, 46 MLS types have been registered in the corresponding database and recent studies using MLST resulted in DI's between 0.66 and 0.78, respectively. Higher DI's up to 0.84 were calculated for SNP typing despite the fact that the overall number of SNP types is relatively low. However, it should be mentioned that this method was used to a lesser extent in comparison with the other typing methods up to now. Hence, data on the discriminatory power of this method might be preliminary.

According to the calculated DI's, adequate discrimination of *M. pneumoniae* strains ($DI \geq 0.9$) can only be achieved if different typing methods are used. For selected examples (reports in which typing results for all strains are listed), the discrimination power of method combinations was calculated in Table 1. In practice, such an approach is laborious and the volume of DNA obtained after use of automated systems for DNA preparation from clinical specimens could be too low to perform three or four typing procedures in parallel.

As the genomes of strains belonging to one of the two main lineages of *M. pneumoniae* are strongly related, an association of *p1* types 1 and 2 with genotypes identified by other typing methods is probable. As summarized in Figure 1A, many MLV types (79%) can be assigned exclusively to one of the main genotypes. In contrast, five MLV types occurred in both main lineages but in most cases (like 4,572, 3,562, and

3,662) with a clear numerical preference for a *p1* type. As errors in counting the tandem repeats cannot be excluded, consideration of guide line for VNTR typing of *M. pneumoniae* (Chalker et al., 2015) is strongly recommended. Although the number of strains with a MLV type not belonging to the preferred *p1* type is low (0.9%), MLV typing cannot be used to replace *p1* typing. In contrast, the known MLS and SNP types are in complete agreement with *p1* types (Figures 1B,C).

Regarding *M. genitalium*, *mgbB* typing has resulted in a large number of types, confirming the variability of the region of *mgbB* gene used. Nearly 250 *mgbB* types have now been described (Table 1). To answer epidemiological questions regarding the distribution of strains in different human populations, the stability and strong heterogeneity of the typing region allow reliable characterization of isolates. The corresponding DI's for *mgbB* sequencing in different studies varied between 0.82 and 0.99 whereas MG_309 typing resulted in discrimination between 0.84 and 0.95. Lower DI's seem to be associated with the investigation of more local than national populations (Dumke et al., 2020; Dumke and Spornraft-Ragaller, 2021), indicating a lower number of circulating genotypes. DI's of ≥ 0.95 were obtained after the *mgbB* and MG_309 methods were combined. With these values, further optimization of typing for *M. genitalium* does not seem necessary. For standardized comparison of *mgbB* sequences, the defined part of the gene (position 221,749–222,029 in the genome of strain G37, GenBank no. NC_000908.2) should be fully sequenced. For example, when analyzing several deposited sequences, differentiation between type 2 and 74 is not possible due to their short lengths. Additionally, determination of the number



of tandem repeats at locus MG_309 can be complicated in practice by the presence of mixed sequences in some samples. Careful inspection of the results after sequencing in both directions can help to solve this problem (Ma et al., 2008).

ASSOCIATION OF TYPING RESULTS WITH EPIDEMIOLOGICAL AND CLINICAL PARAMETERS OF INFECTIONS

Besides the use of typing to elucidate the epidemiological correlations of infections due to *M. pneumoniae* and

M. genitalium, relating typing results to clinically relevant aspects is of practical importance for clinicians. These include associations between genotypes and severity of clinical disease, distinct symptoms of infection, site of infection, or antibiotic resistance. Regarding *M. pneumoniae*, the association between typing results and clinical aspects has been investigated in only a few studies. In comparison with other MLVA types, a statistically significantly higher pneumonia severity index, longer duration of cough, and older age of patients were demonstrated after infection with the mainly p1 1-specific type 4/5/7/2 (Qu et al., 2013). In a further study, a higher rate of severe pneumonia was demonstrated if children were infected with p1 type 1 vs. type 2 (Fan et al., 2017). In contrast, Yan et al. (2019) reported a higher rate of pediatric patients with pleural effusion as a severe complication of *M. pneumoniae* pneumonia after infection with MLVA type 3/5/6/2 (mainly p1 type 2) vs. infection with type 4/5/7/2. In a study among Slovenian children, infection with p1 type 2 strains resulted in an elevated C-reactive protein level and a higher rate of hospital admissions in comparison with p1 type 1 infections (Rodman Berlot et al., 2021). Regarding extrapulmonary manifestations of infections, only very few reports have dealt with the possible influence of the genotype on this complex of diseases. In the case of *M. pneumoniae*-induced mucocutaneous disease (Steven-Johnson syndrome), a rare but severe complication of infection, genotype does not seem to be a determinant of clinical symptoms (Olson et al., 2015; Watkins et al., 2017; Meyer Sauter et al., 2021). In conclusion, the limited and partly heterogeneous results underline the need for further clinical studies with well-characterized patient populations of different age to confirm or exclude correlations of genotypes with clinical manifestations and outcomes of *M. pneumoniae* infections. This should include investigation of the pathogen in the lower and upper respiratory tract of patients, which might influence the ratio of p1 genotypes (Xiao et al., 2020). Furthermore, typing studies among symptomatic patients and asymptomatic carriers would be helpful to clarify if genotypes play a role in the differences in the clinical manifestation of *M. pneumoniae* infections between the groups (Spuesens et al., 2013; de Groot et al., 2021). In addition, further genetic, proteomic, and phenotypic investigations will help to understand differences between genotypes, which might explain clinical aspects of infections. To date, the main p1 types vary with regard to the development of biofilms (Simmons et al., 2013) and expression of the CARDS toxin (Lluch-Senar et al., 2015), which is a virulence factor with special relevance in pathogenesis (Su et al., 2021).

Circulation of different p1 types in the human population has been suggested to explain the typical epidemiology of infections as the immunodominant P1 protein is crucial for adhesion of bacteria to the cells of the respiratory epithelium as the first and essential stage in clinical manifestation. Regions of this adhesin, which contains repetitive sequences, were characterized as surface-located and it can be assumed that type-specific antibodies will be produced during host colonization (Dumke et al., 2008; Schurwanz et al., 2009; Nakane et al., 2011; Vizarraga et al., 2020). If these antibodies play a role in the adherence process, their quantitative occurrence in a host population could

influence the distribution of type 1 or 2 strains (**Figure 2**). Based on the time-dependent level of herd immunity, the reported type shifts of *p1* types in combination with an increase in the prevalence of infection might be explained by the presence of and change in type-specific antibodies. Studies have confirmed the polyclonality of strains in nation-wide investigations as a precondition for changes of genotypes and a varying dominance of type 1 or 2 in different regions (Kogoj et al., 2018; Lee et al., 2018) as well as a time period of 5–10 years for type change in Japan (Kenri et al., 2020). In some cases, the temporary dominance of a *p1* type reaches more than 90% (Sun et al., 2017; Kenri et al., 2020). In contrast, if levels of type-specific antibodies do not differ greatly, the occurrence of both *p1* types without dominance of one lineage is demonstrated (Jacobs et al., 2015; Xiao et al., 2020; Guo et al., 2022). Further studies are needed to confirm the association between type and type-specific antibodies experimentally (Dumke et al., 2010). However, results of mathematical models support the hypothesis of co-circulation of both *p1* types and the importance of herd immunity for the ratio of genotypes (Omori et al., 2015; Zhang et al., 2019). This pattern seems primarily independent of the rate of resistance in the corresponding population. Despite the regional emergence of types with high rates of macrolide resistance (Ho et al., 2015; Lee et al., 2018; Hung et al., 2021), a clear association of resistance with distinct genotypes of *M. pneumoniae* was not found. Recently, an association between the number of tandem repeats in subunit

S of the type I restriction-modification system (MPN085) and macrolide resistance in MLST-3 strains was reported (Lee et al., 2022). This interesting aspect should be investigated in future studies including further types. It can be assumed that the regional/national use of macrolides and the treatment regime in particular patients will be crucial for the development of resistant strains. Up to now, there is no *in vivo* or *in vitro* evidence for a greater rate of resistance among the described genotypes. Thus, antibiotic pressure in a population will lead to an increasing rate of resistance in the dominating type(s), which is primarily determined by the circulation of *p1* types and, due to the association with the main *p1* types, secondarily by the regional occurrence of MLV, MLS, or SNP types (**Figure 1**). Consequently, unsubstantiated use of macrolides in combination with the lack of resistance-guided therapy regimes in many settings worldwide will result in the selection of resistant strains. This hypothesis is supported by the results of studies reporting a decrease in the resistance rate after genotype change (Nakamura et al., 2021), followed by a subsequent increase among strains of the previously nondominant genotype (Wang et al., 2021). In small-scale outbreaks, time-dependent emergence of resistance among strains of the same genotype can be found (Hubert et al., 2021), emphasizing the need for mutation analysis in cases of treatment failure.

As regard *M. genitalium*, data about an association between genotypes and clinical aspects of infection are not currently available. After establishing appropriate and comparable methods, more than 20 typing studies have been published and have found many interesting aspects of the epidemiology of the pathogen (**Table 2**). This aggregation of data includes not only aspects of the transmission of infections among patients with different sexual preferences but also investigated treatment approaches in individual patients that are of great importance for comprehensive evaluation of the clinical management of infections. Overall, these reports confirmed the remarkable genetic diversity of the typing region of the *mgpB* gene among patients of different populations. However, great differences in type frequency have been found. Especially in the risk group of MSM, a striking dominance of type 4 strains in different geographic regions was noted (**Figure 3A**). It remains unclear whether this is a result of the widespread occurrence of this type in a relatively self-contained sexual network (Fernandez-Huerta et al., 2020b) and/or of a selection advantage in the rectal microenvironment (Guiraud et al., 2021). Despite the high discriminatory power of *mgpB* typing, future spread of distinct types in particular populations might require an increased use of the MG_309 method for successful differentiation (e.g., for comparison of first samples and a positive test of cure; Pineiro et al., 2019; Dumke et al., 2020; Dumke and Spornraft-Ragaller, 2021). In addition, type 4 strains have been found to be macrolide resistant in many cases. However, high rates of macrolide resistance are also observed in other genotypes that occur frequently among the different MSM populations but appear to be lower in rarer types (**Figure 3B**). In contrast, a clear distribution pattern of quinolone resistance among these genotypes is lacking. Independent mutation events can be assumed,

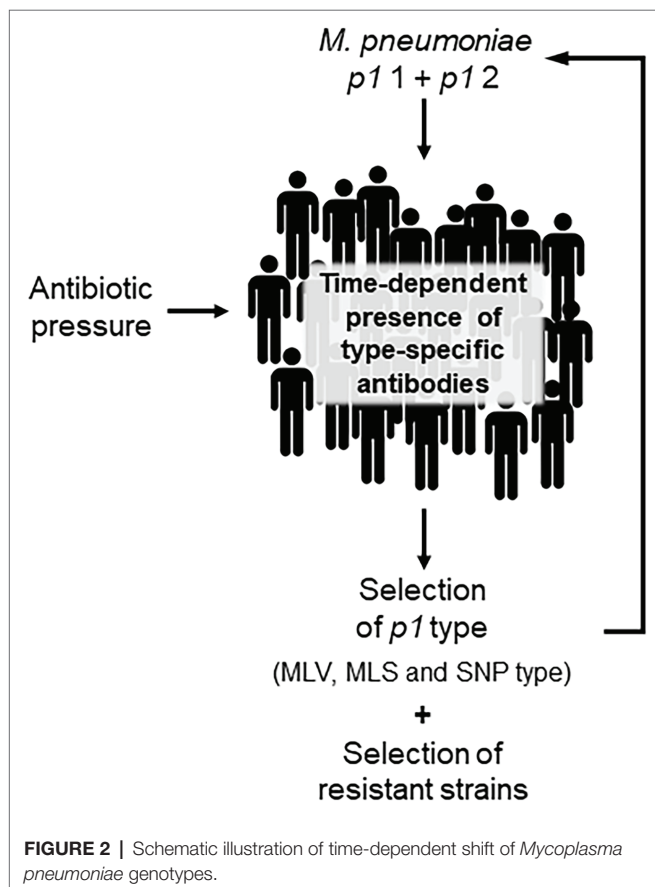


TABLE 2 | Results of *Mycoplasma genitalium* typing studies.

Main aspect	Typing method	Patients/country	No. of patients or samples	Main result(s) of the study	Reference
Methology/epidemiology	<i>mgpB</i>	Not specified + couples/worldwide	267	First description of <i>mgpB</i> typing; usefulness for investigation of sexual networks and treatment failures	Hjorth et al., 2006
<i>MgpB</i> recombination	<i>mgpB</i>	Women/Kenya	9	Intrastrain <i>mgpB</i> heterogeneity due to recombination	Iverson-Cabral et al., 2006
Methology/epidemiology	<i>mgpB</i> + VNTR MG_309	Not specified + couples/worldwide	105	Description of MG_309 typing; usefulness of <i>mgpB</i> + VNTR MG_309 typing for general epidemiological studies	Ma et al., 2008
Methology/epidemiology	<i>mgpB</i> + VNTR MG_309	Men + women with and without symptoms/France + Tunisia	76	Comparison of methods; <i>mgpB</i> typing for general epidemiological studies; <i>mgpB</i> + VNTR MG_309 typing for sexual-network studies; and MLVA not suitable	Cazanave et al., 2012
Epidemiology	<i>mgpB</i>	Women with previous STD and partners/United States	80	Evaluation of sequence variability between strains from partners and occurrence of reinfections	Musatovova and Baseman, 2009
Resistance	<i>mgpB</i>	Not specified/France	136	Evaluation of sequence variability, selection for mutation during treatment; and polyclonality of macrolide resistance	Chrisment et al., 2012
Epidemiology	<i>mgpB</i>	Women in sexual health and family planning clinics/Guinea-Bissau	30	Diversity of circulating strains	Olsen et al., 2012
Methology	<i>mgpB</i> + VNTR MG_309	Not specified/Cuba	12	Importance of typing for documentation of absence of cross-contamination	Mondeja et al., 2013
Resistance/epidemiology	<i>mgpB</i> + VNTR MG_309	Men with and without urethritis/United Kingdom	22	Two major clusters of genotypes with macrolide resistance in both clusters	Pond et al., 2014
Resistance/epidemiology	<i>mgpB</i> + VNTR MG_309	Men with NGU/Japan	20	Evaluation of genotype variability	Kikuchi et al., 2014
Resistance/epidemiology	<i>mgpB</i> + VNTR MG_309	MSM/Germany	19	Evaluation of genotype variability; comparison of first and follow-up samples	Dumke et al., 2016
Resistance/follow-up	<i>mgpB</i> + VNTR MG_309	Men (mainly MSM)/Germany	163	Evaluation of genotype variability; comparison of first and follow-up samples	Dumke et al., 2020
Resistance/epidemiology	<i>mgpB</i> + VNTR MG_309	Women in antenatal clinics/Solomon Islands	41	Two major clusters of genotypes, strain replacement after mass drug administration for trachoma elimination	Harrison et al., 2019
Resistance/follow-up	<i>mgpB</i> + VNTR MG_309	Patients with suspected STD/Spain	79	Differentiation of persistent and recurrent infections	Pineiro et al., 2019
Resistance/epidemiology	<i>mgpB</i> + VNTR MG_309	Heterosexual couples/US	33	Concordance of strains in couples	Xiao et al., 2019
Resistance/epidemiology	<i>mgpB</i> + VNTR MG_309	Mainly MSM/Spain	54	Two major clusters of genotypes with correlation to sexual networks and to macrolide resistance	Fernandez-Huerta et al., 2020b
Methology/epidemiology	<i>mgpB</i>	Patients of a sexual health center/Australia	52	Establishment of a custom amplicon sequencing approach for <i>mgpB</i> typing	Plummer et al., 2020
Resistance/epidemiology	<i>mgpB</i>	Not specified/Australia	89	Genotype variability correlated with <i>de novo</i> acquisition of resistance	Sweeney et al., 2020
Resistance/epidemiology	<i>mgpB</i>	Men in STD clinics/France	78	Lower diversity of types among macrolide-resistant strains	Guiraud et al., 2021
Epidemiology	<i>mgpB</i> + VNTR MG_309	Men and women with and without symptoms/South Africa	38	Circulation of different genotypes without geographic clustering	Laumen et al., 2021
Resistance/follow-up	<i>mgpB</i> + VNTR MG_309	Mainly MSM/Germany	54	Evaluation of first and follow-up samples during a resistance-guided treatment regime; two major clusters of genotypes with correlation to MSM and macrolide resistance	Dumke and Spornraft-Ragaller, 2021
Resistance/epidemiology	<i>mgpB</i>	Asymptomatic MSM/Australia	94	Resistance not restricted to specific genotypes	Chua et al., 2021

STD, sexually transmitted disease; VNTR MG_309, variable number of tandem repeat in gene MG_309; NGU, non-gonococcal urethritis; and MSM, men who have sex with men.

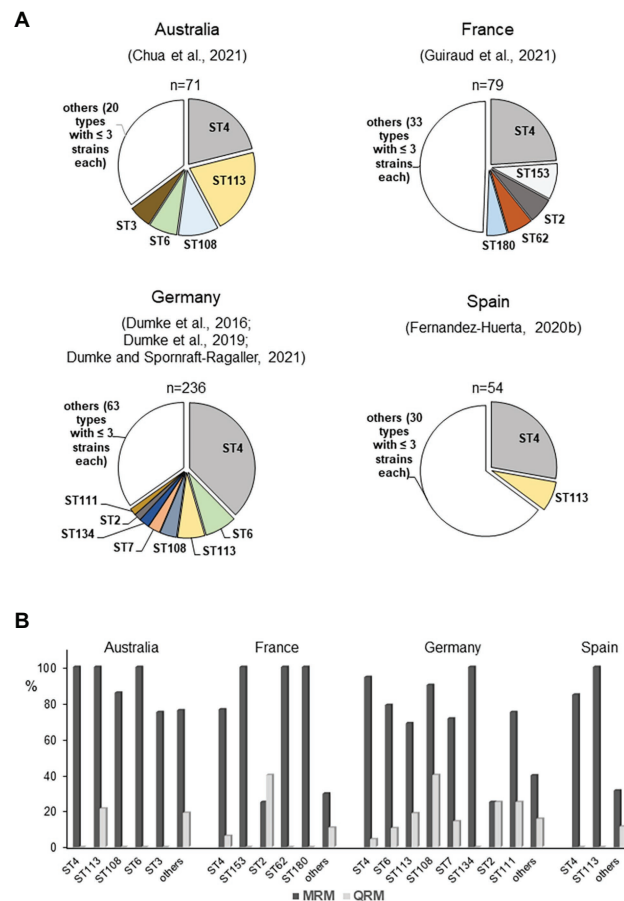



FIGURE 3 | Regional distribution of *mgbB* types (A) and association between *mgbB* type and resistance (B) among strains in selected studies included mainly men who have sex with men (MSM; Dumke et al., 2016, 2020; Fernandez-Huerta et al., 2020b; Chua et al., 2021; Dumke and Spornraft-Ragaller, 2021; Guiraud et al., 2021). Strains with S83N change of ParC are not included. ST, *mgbB* type; MRM, macrolide resistance-associated mutation; and QRM, quinolone resistance-associated mutation.

suggesting that the development of resistance is multiclonal, which might explain the lack of a correlation between genotypes and resistance. Besides transmission of resistant strains, acquired resistance after drug exposure is important for the spread of unsusceptible types (Pineiro et al., 2019). As discussed for *M. pneumoniae*, acquisition of resistance can be expected for any genotype of *M. genitalium*, and regional differences in prescriptions and consumption of macrolides and quinolones might play an important role in the resistance rate among circulating strains (Kenyon et al., 2021). This is especially the case in risk groups for sexually transmitted infections, who often receive antibiotic therapy against infections with pathogens other than *M. genitalium*. Currently, little is known about the consequences for the fitness of mycoplasma strains of acquisition of antibiotic resistance and this might be an object for future studies (Guiraud et al., 2021). In practice, clinicians should be aware that types with high rates of resistance commonly circulate in risk populations. Analogously to the P1 adhesin of *M. pneumoniae*, MgpB of *M. genitalium* contains repetitive elements and is an immunodominant protein. Different studies

have confirmed changes of the gene sequence in the course of infection, which are related to distinct regions of the gene (Iverson-Cabral et al., 2006; Ma et al., 2010; Burgos et al., 2018; Wood et al., 2020). These recombination processes are of importance for the interaction with the host immune system but do not involve the typing region. This part of the protein was found to be antigenic as well as surface-localized but corresponding antibodies were not associated with the inhibition of hemadsorption (Iverson-Cabral et al., 2015; Aparicio et al., 2020). Nevertheless, sequence differences between *mgbB* types result in amino acid changes (Musatovova and Baseman, 2009; Ma et al., 2010; Dumke et al., 2020; Fernandez-Huerta et al., 2020b). Further studies should analyze if these differences or potential conformation changes of MgpB after recombination events in strains with constant *mgbB* type will have an influence on pathogenesis (Wood et al., 2020). Examples of long-term colonization of patients with the same type (Hjorth et al., 2006; Dumke et al., 2020; Dumke and Spornraft-Ragaller, 2021) and the non-reactivity of the conserved N-terminus with antibodies from infected animals (Iverson-Cabral et al., 2015) may suggest that the

M. pneumoniae genotyping

DI		Remarks
	<i>p1</i> typing	important for host immune response
	MLV or MLS or SNP typing	higher discriminatory power
	<i>p1</i> + MLV + MLS + SNP typing	laborious

M. genitalium genotyping


DI		Remarks
	<i>mgpB</i> typing	investigation of patient groups
	<i>mgpB</i> + VNTR MG_309 typing	investigation of individual patients (e.g., follow-up samples) and of distinct patient groups (e.g., with high percentage of identical <i>mgpB</i> types)

FIGURE 4 | Use of different approaches for *Mycoplasma pneumoniae* and *Mycoplasma genitalium* typing. DI, discriminatory index.

typing region of *MgpB* is of limited importance for interaction with the host immune system.

CONCLUSION

Although whole-genome sequencing (WGS) is likely to replace current methods for molecular typing of *M. pneumoniae* and *M. genitalium*, the simplicity of these assays suggests that they may still have considerable value for epidemiological investigations. This is especially the case if isolates are not available as expected outside of reference laboratories. Whereas the discriminatory power of *mgpB*/MG_309 characterization of *M. genitalium* is high enough for successful differentiation of strains in sexual networks as well as in individual patients, several methods must be combined to reach a $DI \geq 0.9$ for typing of *M. pneumoniae* strains (Figure 4). In contrast to the variability of the typing region in the *MgpB* adhesin of *M. genitalium*, the occurrence

of *p1* types in *M. pneumoniae* seems naturally limited by the formation of a functional adhesion complex. For this pathogen, optimization of alternative typing approaches, such as an increase of loci for MLVA, has the potential to enhance their actual discriminatory power. Further studies are needed to evaluate the potential of combinations of current approaches to set internationally accepted recommendations for DI requirement of *M. pneumoniae* typing. At present, only limited knowledge is available regarding the correlation of genotypes with clinical aspects of infections caused by *M. pneumoniae* and *M. genitalium*. These include an association with high regional or population-specific rates of resistance.

AUTHOR CONTRIBUTIONS

The author confirms being the sole contributor of this work and has approved it for publication.

REFERENCES

- Aparicio, D., Scheffer, M. P., Marcos-Silva, M., Vizarraga, D., Sprankel, L., Ratera, M., et al. (2020). Structure and mechanism of the nap adhesion complex from the human pathogen *Mycoplasma genitalium*. *Nat. Commun.* 11:2877. doi: 10.1038/s41467-020-16511-2
- Baumann, L., Cina, M., Egli-Gany, D., Goutaki, M., Halbeisen, F. S., Lohrer, G. R., et al. (2018). Prevalence of *Mycoplasma genitalium* in different population groups: systematic review and meta-analysis. *Sex. Transm. Infect.* 94, 255–262. doi: 10.1136/sextrans-2017-053384
- Benitez, A. J., Diaz, M. H., Wolff, B. J., Pimentel, G., Njenga, M. K., Estevez, A., et al. (2012). Multilocus variable-number tandem-repeat analysis of *Mycoplasma pneumoniae* clinical isolates from 1962 to the present: a retrospective study. *J. Clin. Microbiol.* 50, 3620–3626. doi: 10.1128/JCM.01755-12
- Brown, R. J., Holden, M. T., Spiller, O. B., and Chalker, V. J. (2015). Development of a multilocus sequence typing scheme for molecular

- typing of *Mycoplasma pneumoniae*. *J. Clin. Microbiol.* 53, 3195–3203. doi: 10.1128/JCM.01301-15
- Brown, R. J., Nguipod-Djomo, P., Zhao, H., Stanford, E., Spiller, O. B., and Chalker, V. J. (2016). *Mycoplasma pneumoniae* epidemiology in England and Wales: a national perspective. *Front. Microbiol.* 7:157. doi: 10.3389/fmicb.2016.00157
- Burgos, R., Wood, G. E., Iverson-Cabral, S. L., and Totten, P. A. (2018). *Mycoplasma genitalium* nonadherent phase variants arise by multiple mechanisms and escape antibody-dependent growth inhibition. *Infect. Immun.* 86, e00866–e00817. doi: 10.1128/IAI.00866-17
- Cazanave, C., Charron, A., Renaudin, H., and Bebear, C. (2012). Method comparison for molecular typing of French and Tunisian *Mycoplasma genitalium*-positive specimens. *J. Med. Microbiol.* 61, 500–506. doi: 10.1099/jmm.0.037721-0
- Chalker, V. J., Pereyre, S., Dumke, R., Winchell, J., Khosla, P., Sun, H., et al. (2015). International *Mycoplasma pneumoniae* typing study: interpretation of *M. pneumoniae* multilocus variable-number tandem-repeat analysis. *New Microb. New Infect.* 7, 37–40. doi: 10.1016/j.nmni.2015.05.005
- Chrismont, D., Charron, A., Cazanave, C., Pereyre, S., and Bebear, C. (2012). Detection of macrolide resistance in *Mycoplasma genitalium* in France. *J. Antimicrob. Chemother.* 67, 2598–2601. doi: 10.1093/jac/dks263
- Chua, T. P., Bodiyaadu, K., Machalek, D. A., Garland, S. M., Bradshaw, C. S., Plummer, E. L., et al. (2021). Prevalence of *Mycoplasma genitalium* fluoroquinolone-resistance markers, and dual-class-resistance markers, in asymptomatic men who have sex with men. *J. Med. Microbiol.* 70:001429. doi: 10.1099/jmm.0.001429
- de Groot, R. C. A., Cristina Estevão, S., Meyer Sauter, P. M., Perkasa, A., Hoogenboezem, T., Spuesens, E. B. M., et al. (2021). *Mycoplasma pneumoniae* carriage evades induction of protective mucosal antibodies. *Eur. Respir. J.* 59:2100129. doi: 10.1183/13993003.00129-2021
- Degrange, S., Cazanave, C., Charron, A., Renaudin, H., Bebear, C., and Bebear, C. M. (2009). Development of multiple-locus variable-number tandem-repeat analysis for molecular typing of *Mycoplasma pneumoniae*. *J. Clin. Microbiol.* 47, 914–923. doi: 10.1128/JCM.01935-08
- Diaz, M. H., Desai, H. P., Morrison, S. S., Benitez, A. J., Wolff, B. J., Caravas, J., et al. (2017). Comprehensive bioinformatics analysis of *Mycoplasma pneumoniae* genomes to investigate underlying population structure and type-specific determinants. *PLoS One* 12:e0174701. doi: 10.1371/journal.pone.0174701
- Diaz, M. H., and Winchell, J. M. (2016). The evolution of advanced molecular diagnostics for the detection and characterization of *Mycoplasma pneumoniae*. *Front. Microbiol.* 7:232. doi: 10.3389/fmicb.2016.00232
- Dumke, R., and Jacobs, E. (2011). Culture-independent multi-locus variable-number tandem-repeat analysis (MLVA) of *Mycoplasma pneumoniae*. *J. Microbiol. Methods* 86, 393–396. doi: 10.1016/j.mimet.2011.06.008
- Dumke, R., Lück, P. C., Noppen, C., Schaefer, C., von Baum, H., Marre, R., et al. (2006). Culture-independent molecular subtyping of *Mycoplasma pneumoniae* in clinical samples. *J. Clin. Microbiol.* 44, 2567–2570. doi: 10.1128/JCM.00495-06
- Dumke, R., and Rodriguez, N. (2021). Use of different approaches for the culture-independent typing of *Mycoplasma pneumoniae* from two geographically distinct regions. *J. Microbiol. Methods* 186:106239. doi: 10.1016/j.mimet.2021.106239
- Dumke, R., Rust, M., and Glaunsinger, T. (2020). *MgpB* types among *Mycoplasma genitalium* strains from men who have sex with men in Berlin, Germany, 2016–2018. *Pathogens* 9:12. doi: 10.3390/pathogens9010012
- Dumke, R., Schnee, C., Pletz, M. W., Rupp, J., Jacobs, E., Sachse, K., et al. (2015). *Mycoplasma pneumoniae* and *Chlamydia* spp. infection in community-acquired pneumonia, Germany, 2011–2012. *Emerg. Infect. Dis.* 21, 426–434. doi: 10.3201/eid2103.140927
- Dumke, R., Schurwanz, N., and Jacobs, E. (2008). Characterisation of subtype- and variant-specific antigen regions of the P1 adhesin of *Mycoplasma pneumoniae*. *Int. J. Med. Microbiol.* 298, 483–491. doi: 10.1016/j.ijmm.2007.06.002
- Dumke, R., and Spornraft-Ragaller, P. (2021). Antibiotic resistance and genotypes of *Mycoplasma genitalium* during a resistance-guided treatment regime in a German university hospital. *Antibiotics* 10:962. doi: 10.3390/antibiotics10080962
- Dumke, R., Thürmer, A., and Jacobs, E. (2016). Emergence of *Mycoplasma genitalium* strains showing mutations associated with macrolide and fluoroquinolone resistance in the region Dresden, Germany. *Diagn. Microbiol. Infect. Dis.* 86, 221–223. doi: 10.1016/j.diagmicrobio.2016.07.005
- Dumke, R., von Baum, H., Lück, P. C., and Jacobs, E. (2010). Subtypes and variants of *Mycoplasma pneumoniae*: local and temporal changes in Germany 2003–2006 and absence of a correlation between the genotype in the respiratory tract and the occurrence of genotype-specific antibodies in the sera of infected patients. *Epidemiol. Infect.* 138, 1829–1837. doi: 10.1017/S0950268810000622
- Fan, L., Li, D., Zhang, L., Hao, C., Sun, H., Shao, X., et al. (2017). Pediatric clinical features of *Mycoplasma pneumoniae* infection are associated with bacterial P1 genotype. *Exp. Ther. Med.* 14, 1892–1898. doi: 10.3892/etm.2017.4721
- Fernandez-Huerta, M., Barbera, M. J., Serra-Pladevall, J., Esperalba, J., Martinez-Gomez, X., Centeno, C., et al. (2020a). *Mycoplasma genitalium* and antimicrobial resistance in Europe: a comprehensive review. *Int. J. STD AIDS* 31, 190–197. doi: 10.1177/0956462419890737
- Fernandez-Huerta, M., Serra-Pladevall, J., Esperalba, J., Moreno-Mingorance, A., Fernandez-Naval, C., Barbera, M. J., et al. (2020b). Single-locus-sequence-based typing of the *mgpB* gene reveals transmission dynamics in *Mycoplasma genitalium*. *J. Clin. Microbiol.* 58, e01886–e01819. doi: 10.1128/JCM.01886-19
- Fookes, M. C., Hadfield, J., Harris, S., Parmar, S., Unemo, M., Jensen, J. S., et al. (2017). *Mycoplasma genitalium*: whole genome sequence analysis, recombination and population structure. *BMC Genomics* 18:993. doi: 10.1186/s12864-017-4399-6
- Gnanadurai, R., and Fifer, H. (2020). *Mycoplasma genitalium*: A review. *Microbiology* 166, 21–29. doi: 10.1099/mic.0.000830
- Guiraud, J., Lounnas, M., Boissiere, A., Le Roy, C., Elguero, E., Banuls, A. L., et al. (2021). Lower *mgpB* diversity in macrolide-resistant *Mycoplasma genitalium* infecting men visiting two sexually transmitted infection clinics in Montpellier, France. *J. Antimicrob. Chemother.* 76, 43–47. doi: 10.1093/jac/dkaa410
- Guo, Z., Liu, L., Gong, J., Han, N., He, L., Wang, W., et al. (2022). Molecular features and antimicrobial susceptibility of *Mycoplasma pneumoniae* isolates from pediatric inpatients in Weihai, China. *J. Glob. Antimicrob. Resist.* 28, 180–184. doi: 10.1016/j.jgar.2022.01.002
- Hakim, M. S., Annisa, L., Jariah, R. O. A., and Vink, C. (2021). The mechanisms underlying antigenic variation and maintenance of genomic integrity in *Mycoplasma pneumoniae* and *Mycoplasma genitalium*. *Arch. Microbiol.* 203, 413–429. doi: 10.1007/s00203-020-02041-4
- Harrison, M. A., Harding-Esch, E. M., Marks, M., Pond, M. J., Butcher, R., Solomon, A. W., et al. (2019). Impact of mass drug administration of azithromycin for trachoma elimination on prevalence and azithromycin resistance of genital *Mycoplasma genitalium* infection. *Sex. Transm. Infect.* 95, 522–528. doi: 10.1136/sextrans-2018-053938
- Henderson, K. C., Benitez, A. J., Ratliff, A. E., Crabb, D. M., Sheppard, E. S., Winchell, J. M., et al. (2015). Specificity and strain-typing capabilities of nanorod array-surface enhanced Raman spectroscopy for *Mycoplasma pneumoniae* detection. *PLoS One* 10:e0131831. doi: 10.1371/journal.pone.0131831
- Hennigan, S. L., Driskell, J. D., Dluhy, R. A., Zhao, Y., Tripp, R. A., Waites, K. B., et al. (2010). Detection of *Mycoplasma pneumoniae* in simulated and true clinical throat swab specimens by nanorod array-surface-enhanced Raman spectroscopy. *PLoS One* 5:e13633. doi: 10.1371/journal.pone.0013633
- Himmelreich, R., Hilbert, H., Plagens, H., Pirkle, E., Li, B. C., and Herrmann, R. (1996). Complete sequence analysis of the genome of the bacterium *Mycoplasma pneumoniae*. *Nucleic Acids Res.* 24, 4420–4449. doi: 10.1093/nar/24.22.4420
- Himmelreich, R., Plagens, H., Hilbert, H., Reiner, B., and Herrmann, R. (1997). Comparative analysis of the genomes of the bacteria *Mycoplasma pneumoniae* and *Mycoplasma genitalium*. *Nucleic Acids Res.* 25, 701–712. doi: 10.1093/nar/25.4.701
- Hjorth, S. V., Björnelius, E., Lidbrink, P., Falk, L., Dohn, B., Berthelsen, L., et al. (2006). Sequence-based typing of *Mycoplasma genitalium* reveals sexual transmission. *J. Clin. Microbiol.* 44, 2078–2083. doi: 10.1128/JCM.00003-06
- Ho, P. L., Law, P. Y., Chan, B. W., Wong, C. W., To, K. K., Chiu, S. S., et al. (2015). Emergence of macrolide-resistant *Mycoplasma pneumoniae* in Hong Kong is linked to increasing macrolide resistance in multilocus variable-number tandem-repeat analysis type 4-5-7-2. *J. Clin. Microbiol.* 53, 3560–3564. doi: 10.1128/JCM.01983-15
- Hsieh, Y. C., Li, S. W., Chen, Y. Y., Kuo, C. C., Chen, Y. C., Chang, I., et al. (2022). Global genome diversity and recombination in *Mycoplasma pneumoniae*. *Emerg. Infect. Dis.* 28, 111–117. doi: 10.3201/eid2801.210497

- Hubert, D., Dumke, R., Weichert, S., Welker, S., Tenenbaum, T., and Schrotten, H. (2021). Emergence of macrolide-resistant *Mycoplasma pneumoniae* during an outbreak in a primary school: clinical characterization of hospitalized children. *Pathogens* 10:328. doi: 10.3390/pathogens10030328
- Hung, H. M., Chuang, C. H., Chen, Y. Y., Liao, W. C., Li, S. W., Chang, I. Y., et al. (2021). Clonal spread of macrolide-resistant *Mycoplasma pneumoniae* sequence type-3 and type-17 with recombination on non-P1 adhesin among children in Taiwan. *Clin. Microbiol. Infect.* 27, 1169.e1–1169.e6. doi: 10.1016/j.cmi.2020.09.035
- Hunter, P. R., and Gaston, M. A. (1988). Numerical index of the discriminatory ability of typing systems: an application of Simpson's index of diversity. *J. Clin. Microbiol.* 26, 2465–2466. doi: 10.1128/jcm.26.11.2465-2466.1988
- Iverson-Cabral, S. L., Astete, S. G., Cohen, C. R., Rocha, E. P., and Totten, P. A. (2006). Intrastrain heterogeneity of the *mgpB* gene in *Mycoplasma genitalium* is extensive in vitro and in vivo and suggests that variation is generated via recombination with repetitive chromosomal sequences. *Infect. Immun.* 74, 3715–3726. doi: 10.1128/IAI.00239-06
- Iverson-Cabral, S. L., Wood, G. E., and Totten, P. A. (2015). Analysis of the *Mycoplasma genitalium* *MgpB* adhesin to predict membrane topology, investigate antibody accessibility, characterize amino acid diversity, and identify functional and immunogenic epitopes. *PLoS One* 10:e0138244. doi: 10.1371/journal.pone.0138244
- Jacobs, E., Ehrhardt, I., and Dumke, R. (2015). New insights in the outbreak pattern of *Mycoplasma pneumoniae*. *Int. J. Med. Microbiol.* 305, 705–708. doi: 10.1016/j.ijmm.2015.08.021
- Jansen, K., Steffen, G., Potthoff, A., Schuppe, A. K., Beer, D., Jessen, H., et al. (2020). STI in times of PrEP: high prevalence of chlamydia, gonorrhea, and mycoplasma at different anatomic sites in men who have sex with men in Germany. *BMC Infect. Dis.* 20:110. doi: 10.1186/s12879-020-4831-4
- Jensen, J. S., Cusini, M., Gomberg, M., Moi, H., Wilson, J., and Unemo, M. (2022). 2021 European guideline on the management of *Mycoplasma genitalium* infections. *J. Eur. Acad. Dermatol. Venereol.* 36, 641–650. doi: 10.1111/jdv.17972
- Kenri, T., Suzuki, M., Sekizuka, T., Ohya, H., Oda, Y., Yamazaki, T., et al. (2020). Periodic genotype shifts in clinically prevalent *Mycoplasma pneumoniae* strains in Japan. *Front. Cell. Infect. Microbiol.* 10:385. doi: 10.3389/fcimb.2020.00385
- Kenyon, C., Manoharan-Basil, S. S., and van Dijck, C. (2021). Is there a resistance threshold for macrolide consumption? Positive evidence from an ecological analysis of resistance data from *Streptococcus pneumoniae*, *Treponema pallidum*, and *Mycoplasma genitalium*. *Microb. Drug Resist.* 27, 1079–1086. doi: 10.1089/mdr.2020.0490
- Khoury, T., Sviri, S., Rmeileh, A. A., Nubani, A., Abutbul, A., Hoss, S., et al. (2016). Increased rates of intensive care unit admission in patients with *Mycoplasma pneumoniae*: a retrospective study. *Clin. Microbiol. Infect.* 22, 711–714. doi: 10.1016/j.cmi.2016.05.028
- Kikuchi, M., Ito, S., Yasuda, M., Tsuchiya, T., Hatazaki, K., Takanashi, M., et al. (2014). Remarkable increase in fluoroquinolone-resistant *Mycoplasma genitalium* in Japan. *J. Antimicrob. Chemother.* 69, 2376–2382. doi: 10.1093/jac/dku164
- Kogoj, R., Mrvic, T., Praprotnik, M., and Kese, D. (2015). Prevalence, genotyping and macrolide resistance of *Mycoplasma pneumoniae* among isolates of patients with respiratory tract infections, Central Slovenia, 2006 to 2014. *Euro Surveill.* 20. doi: 10.2807/1560-7917.ES.2015.20.37.30018
- Kogoj, R., Praprotnik, M., Mrvic, T., Korva, M., and Kese, D. (2018). Genetic diversity and macrolide resistance of *Mycoplasma pneumoniae* isolates from two consecutive epidemics in Slovenia. *Eur. J. Clin. Microbiol. Infect. Dis.* 37, 99–107. doi: 10.1007/s10096-017-3106-5
- Latimer, R. L., Shilling, H. S., Vodstrcil, L. A., Machalek, D. A., Fairley, C. K., Chow, E. P. F., et al. (2020). Prevalence of *Mycoplasma genitalium* by anatomical site in men who have sex with men: a systematic review and meta-analysis. *Sex. Transm. Infect.* 96, 563–570. doi: 10.1136/sextrans-2019-054310
- Laumen, J. G. E., van Alphen, L. B., Maduna, L. D., Hoffman, C. M., Klausner, J. D., Medina-Marino, A., et al. (2021). Molecular epidemiological analysis of *Mycoplasma genitalium* shows low prevalence of azithromycin resistance and a well-established epidemic in South Africa. *Sex. Transm. Infect.* 97, 152–156. doi: 10.1136/sextrans-2019-054371
- Lee, J. K., Lee, J. H., Lee, H., Ahn, Y. M., Eun, B. W., Cho, E. Y., et al. (2018). Clonal expansion of macrolide-resistant sequence type 3 *Mycoplasma pneumoniae*, South Korea. *Emerg. Infect. Dis.* 24, 1465–1471. doi: 10.3201/eid2408.180081
- Lee, J. K., Seong, M. W., Shin, D., Kim, J. I., Han, M. S., Yeon, Y., et al. (2019). Comparative genomics of *Mycoplasma pneumoniae* isolated from children with pneumonia: South Korea, 2010–2016. *BMC Genomics* 20:910. doi: 10.1186/s12864-019-6306-9
- Lee, J. K., Seong, M. W., Yun, K. W., and Choi, E. H. (2022). Association of tandem repeat number variabilities in subunit S of the type I restriction-modification system with macrolide resistance in *Mycoplasma pneumoniae*. *J. Clin. Med.* 11:715. doi: 10.3390/jcm11030715
- Luch-Senar, M., Cozzuto, L., Cano, J., Delgado, J., Llòrens-Rico, V., Pereyre, S., et al. (2015). Comparative “-omics” in *Mycoplasma pneumoniae* clinical isolates reveals key virulence factors. *PLoS One* 10:e0137354. doi: 10.1371/journal.pone.0137354
- Ma, L., Jensen, J. S., Mancuso, M., Hamasuna, R., Jia, Q., McGowin, C. L., et al. (2010). Genetic variation in the complete *MgPa* operon and its repetitive chromosomal elements in clinical strains of *Mycoplasma genitalium*. *PLoS One* 5:e15660. doi: 10.1371/journal.pone.0015660
- Ma, L., and Martin, D. H. (2004). Single-nucleotide polymorphisms in the rRNA operon and variable numbers of tandem repeats in the lipoprotein gene among *Mycoplasma genitalium* strains from clinical specimens. *J. Clin. Microbiol.* 42, 4876–4878. doi: 10.1128/JCM.42.10.4876-4878.2004
- Ma, L., Taylor, S., Jensen, J. S., Myers, L., Lillis, R., and Martin, D. H. (2008). Short tandem repeat sequences in the *Mycoplasma genitalium* genome and their use in a multilocus genotyping system. *BMC Microbiol.* 8:130. doi: 10.1186/1471-2180-8-130
- Machalek, D. A., Tao, Y., Shilling, H., Jensen, J. S., Unemo, M., Murray, G., et al. (2020). Prevalence of mutations associated with resistance to macrolides and fluoroquinolones in *Mycoplasma genitalium*: a systematic review and meta-analysis. *Lancet Infect. Dis.* 20, 1302–1314. doi: 10.1016/S1473-3099(20)30154-7
- McGowin, C. L., Ma, L., Martin, D. H., and Pyles, R. B. (2009). *Mycoplasma genitalium*-encoded MG309 activates NF-kappaB via toll-like receptors 2 and 6 to elicit proinflammatory cytokine secretion from human genital epithelial cells. *Infect. Immun.* 77, 1175–1181. doi: 10.1128/IAI.00845-08
- Meyer Sauter, P. M., Panisova, E., Seiler, M., Theiler, M., Berger, C., and Dumke, R. (2021). *Mycoplasma pneumoniae* genotypes and clinical outcome in children. *J. Clin. Microbiol.* 59:e0074821. doi: 10.1128/JCM.00748-21
- Mondeja, B. A., Jensen, J. S., Rodríguez, I., Morier, L. F., Kouri, V., Rodríguez, N. M., et al. (2013). Isolation of *Mycoplasma genitalium* from patients with urogenital infections: first report from the Latin-American region. *New Microb. New Infect.* 1, 22–26. doi: 10.1002/2052-2975.20
- Musatovova, O., and Baseman, J. B. (2009). Analysis identifying common and distinct sequences among Texas clinical strains of *Mycoplasma genitalium*. *J. Clin. Microbiol.* 47, 1469–1475. doi: 10.1128/JCM.01602-08
- Musatovova, O., Kannan, T. R., and Baseman, J. B. (2008). Genomic analysis reveals *Mycoplasma pneumoniae* repetitive element 1-mediated recombination in a clinical isolate. *Infect. Immun.* 76, 1639–1648. doi: 10.1128/IAI.01621-07
- Nakamura, Y., Oishi, T., Kaneko, K., Kenri, T., Tanaka, T., Wakabayashi, S., et al. (2021). Recent acute reduction in macrolide-resistant *Mycoplasma pneumoniae* infections among Japanese children. *J. Infect. Chemother.* 27, 271–276. doi: 10.1016/j.jiac.2020.10.007
- Nakane, D., Adan-Kubo, J., Kenri, T., and Miyata, M. (2011). Isolation and characterization of P1 adhesin, a leg protein of the gliding bacterium *Mycoplasma pneumoniae*. *J. Bacteriol.* 193, 715–722. doi: 10.1128/JB.00796-10
- Narita, M. (2016). Classification of extrapulmonary manifestations due to *Mycoplasma pneumoniae* infection on the basis of possible pathogenesis. *Front. Microbiol.* 7:23. doi: 10.3389/fmicb.2016.00023
- Olsen, B., Mansson, F., Camara, C., Monteiro, M., Biai, A., Alves, A., et al. (2012). Phenotypic and genetic characterisation of bacterial sexually transmitted infections in Bissau, Guinea-Bissau, West Africa: a prospective cohort study. *BMJ Open* 2:e000636. doi: 10.1136/bmjopen-2011-000636
- Olson, D., Watkins, L. K. F., Demirjian, A., Lin, X., Robinson, C. C., Pretty, K., et al. (2015). Outbreak of *Mycoplasma pneumoniae*-associated Stevens-Johnson syndrome. *Pediatrics* 136, e386–e394. doi: 10.1542/peds.2015-0278
- Omori, R., Nakata, Y., Tessmer, H. L., Suzuki, S., and Shibayama, K. (2015). The determinant of periodicity in *Mycoplasma pneumoniae* incidence: an insight from mathematical modelling. *Sci. Rep.* 5:14473. doi: 10.1038/srep14473

- Pereyre, S., and Tardy, F. (2021). Integrating the human and animal sides of mycoplasmas resistance to antimicrobials. *Antibiotics* 10:1216. doi: 10.3390/antibiotics10101216
- Pereyre, S., Tardy, F., Renaudin, H., Cauvin, E., Del Pra Netto Machado, L., Tricot, A., et al. (2013). Identification and subtyping of clinically relevant human and ruminant mycoplasmas by use of matrix-assisted laser desorption ionization-time of flight mass spectrometry. *J. Clin. Microbiol.* 51, 3314–3323. doi: 10.1128/JCM.01573-13
- Pineiro, L., Idigoras, P., and Cilla, G. (2019). Molecular typing of *Mycoplasma genitalium*-positive specimens discriminates between persistent and recurrent infections in cases of treatment failure and supports contact tracing. *Microorganisms* 7:609. doi: 10.3390/microorganisms7120609
- Plummer, E. L., Murray, G. L., Bodiya, K., Su, J., Garland, S. M., Bradshaw, C. S., et al. (2020). A custom amplicon sequencing approach to detect resistance associated mutations and sequence types in *Mycoplasma genitalium*. *J. Microbiol. Methods* 179:106089. doi: 10.1016/j.mimet.2020.106089
- Pond, M. J., Nori, A. V., Witney, A. A., Lopeman, R. C., Butcher, P. D., and Sadiq, S. T. (2014). High prevalence of antibiotic-resistant *Mycoplasma genitalium* in nongonococcal urethritis: the need for routine testing and the inadequacy of current treatment options. *Clin. Infect. Dis.* 58, 631–637. doi: 10.1093/cid/cit752
- Qu, J., Yu, X., Liu, Y., Yin, Y., Gu, L., Cao, B., et al. (2013). Specific multilocus variable-number tandem-repeat analysis genotypes of *Mycoplasma pneumoniae* are associated with diseases severity and macrolide susceptibility. *PLoS One* 8:e82174. doi: 10.1371/journal.pone.0082174
- Rocha, E. P., and Blanchard, A. (2002). Genomic repeats, genome plasticity and the dynamics of *Mycoplasma* evolution. *Nucleic Acids Res.* 30, 2031–2042. doi: 10.1093/nar/30.9.2031
- Rodman Berlot, J., Krivec, U., Mrvic, T., Kogoj, R., and Kese, D. (2021). *Mycoplasma pneumoniae* p1 genotype indicates severity of lower respiratory tract infections in children. *J. Clin. Microbiol.* 59:e0022021. doi: 10.1128/JCM.00220-21
- Ruland, K., Himmelreich, R., and Herrmann, R. (1994). Sequence divergence in the ORF6 gene of *Mycoplasma pneumoniae*. *J. Bacteriol.* 176, 5202–5209. doi: 10.1128/jb.176.17.5202-5209.1994
- Sasaki, T., Kenri, T., Okazaki, N., Iseki, M., Yamashita, R., Shintani, M., et al. (1996). Epidemiological study of *Mycoplasma pneumoniae* infections in Japan based on PCR-restriction fragment length polymorphism of the P1 cytoadhesin gene. *J. Clin. Microbiol.* 34, 447–449. doi: 10.1128/jcm.34.2.447-449.1996
- Schurwanz, N., Jacobs, E., and Dumke, R. (2009). Strategy to create chimeric proteins derived from functional adhesin regions of *Mycoplasma pneumoniae* for vaccine development. *Infect. Immun.* 77, 5007–5015. doi: 10.1128/IAI.00268-09
- Schwartz, S. B., Mitchell, S. L., Thurman, K. A., Wolff, B. J., and Winchell, J. M. (2009). Identification of P1 variants of *Mycoplasma pneumoniae* by use of high-resolution melt analysis. *J. Clin. Microbiol.* 47, 4117–4120. doi: 10.1128/JCM.01696-09
- Simmons, W. L., Daubenspeck, J. M., Osborne, J. D., Balish, M. F., Waites, K. B., and Dybvig, K. (2013). Type 1 and type 2 strains of *Mycoplasma pneumoniae* form different biofilms. *Biochemistry* 159, 737–747. doi: 10.1099/mic.0.064782-0
- Sluijter, M., Kaptein, E., Spuesens, E. B., Hoogenboezem, T., Hartwig, N. G., van Rossum, A. M., et al. (2010). The *Mycoplasma genitalium* MG352-encoded protein is a Holliday junction resolvase that has a non-functional orthologue in *Mycoplasma pneumoniae*. *Mol. Microbiol.* 77, 1261–1277. doi: 10.1111/j.1365-2958.2010.07288.x
- Spuesens, E. B., Brouwer, R. W., Mol, K. H., Hoogenboezem, T., Kockx, C. E., Jansen, R., et al. (2016). Comparison of *Mycoplasma pneumoniae* genome sequences from strains isolated from symptomatic and asymptomatic patients. *Front. Microbiol.* 7:1701. doi: 10.3389/fmicb.2016.01701
- Spuesens, E. B., Fraaij, P. L., Visser, E. G., Hoogenboezem, T., Hop, W. C., van Adrichem, L. N., et al. (2013). Carriage of *Mycoplasma pneumoniae* in the upper respiratory tract of symptomatic and asymptomatic children: an observational study. *PLoS Med.* 10:e1001444. doi: 10.1371/journal.pmed.1001444
- Spuesens, E. B., Hoogenboezem, T., Sluijter, M., Hartwig, N. G., van Rossum, A. M., and Vink, C. (2010). Macrolide resistance determination and molecular typing of *Mycoplasma pneumoniae* by pyrosequencing. *J. Microbiol. Methods* 82, 214–222. doi: 10.1016/j.mimet.2010.06.004
- Spuesens, E. B., Oduber, M., Hoogenboezem, T., Sluijter, M., Hartwig, N. G., van Rossum, A. M. C., et al. (2009). Sequence variations in RepMP2/3 and RepMP4 elements reveal intragenomic homologous DNA recombination events in *Mycoplasma pneumoniae*. *Microbiology* 155, 2182–2196. doi: 10.1099/mic.0.028506-0
- Su, C. J., Dallo, S. F., and Baseman, J. B. (1990). Molecular distinctions among clinical isolates of *Mycoplasma pneumoniae*. *J. Clin. Microbiol.* 28, 1538–1540. doi: 10.1128/jcm.28.7.1538-1540.1990
- Su, X., You, X., Luo, H., Liang, K., Chen, L., Tian, W., et al. (2021). Community-acquired respiratory distress syndrome toxin: unique exotoxin for *M. pneumoniae*. *Front. Microbiol.* 12:766591. doi: 10.3389/fmicb.2021.766591
- Sun, H., Xue, G., Yan, C., Li, S., Cao, L., Yuan, Y., et al. (2013). Multiple-locus variable-number tandem-repeat analysis of *Mycoplasma pneumoniae* clinical specimens and proposal for amendment of MLVA nomenclature. *PLoS One* 8:e64607. doi: 10.1371/journal.pone.0064607
- Sun, H., Xue, G., Yan, C., Li, S., Zhao, H., Feng, Y., et al. (2017). Changes in molecular characteristics of *Mycoplasma pneumoniae* in clinical specimens from children in Beijing between 2003 and 2015. *PLoS One* 12:e0170253. doi: 10.1371/journal.pone.0170253
- Sweeney, E. L., Tickner, J., Bletchly, C., Nimmo, G. R., and Whitley, D. M. (2020). Genotyping of *Mycoplasma genitalium* suggests *de novo* acquisition of antimicrobial resistance in Queensland. *Aust. J. Clin. Microbiol.* 58, e00641–e00620. doi: 10.1128/JCM.00641-20
- Tian, X. J., Dong, Y. Q., Dong, X. P., Li, J. Y., Li, D., Jiang, Y., et al. (2013). P1 gene of *Mycoplasma pneumoniae* in clinical isolates collected in Beijing in 2010 and relationship between genotyping and macrolide resistance. *Chin. Med. J.* 126, 3944–3948. doi: 10.3760/cma.j.issn.0366-6999.20131643
- Touati, A., Blouin, Y., Sirand-Pugnet, P., Renaudin, H., Oishi, T., Vergnaud, G., et al. (2015). Molecular epidemiology of *Mycoplasma pneumoniae*: genotyping using single nucleotide polymorphisms and SNaPshot technology. *J. Clin. Microbiol.* 53, 3182–3194. doi: 10.1128/JCM.01156-15
- Ursi, D., Ieven, M., van Bever, H., Quint, W., Niesters, H. G., and Goossens, H. (1994). Typing of *Mycoplasma pneumoniae* by PCR-mediated DNA fingerprinting. *J. Clin. Microbiol.* 32, 2873–2875. doi: 10.1128/jcm.32.11.2873-2875.1994
- Vizarraga, D., Kawamoto, A., Matsumoto, U., Illanes, R., Perez-Luque, R., Martin, J., et al. (2020). Immunodominant proteins P1 and P40/P90 from human pathogen *Mycoplasma pneumoniae*. *Nat. Commun.* 11:5188. doi: 10.1038/s41467-020-18777-y
- Waites, K. B., Xiao, L., Liu, Y., Balish, M. F., and Atkinson, T. P. (2017). *Mycoplasma pneumoniae* from the respiratory tract and beyond. *Clin. Microbiol. Rev.* 30, 747–809. doi: 10.1128/CMR.00114-16
- Wang, Y., Xu, B., Wu, X., Yin, Q., Wang, Y., Li, J., et al. (2021). Increased macrolide resistance rate of M3562 *Mycoplasma pneumoniae* correlated with macrolide usage and genotype shifting. *Front. Cell. Infect. Microbiol.* 11:675466. doi: 10.3389/fcimb.2021.675466
- Watkins, L. K. F., Olson, D., Diaz, M. H., Lin, X., Demirjian, A., Benitez, A. J., et al. (2017). Epidemiology and molecular characteristics of *Mycoplasma pneumoniae* during an outbreak of *M. pneumoniae*-associated Stevens-Johnson syndrome. *Pediatr. Infect. Dis. J.* 36, 564–571. doi: 10.1097/INF.0000000000001476
- Wood, G. E., Iverson-Cabral, S. L., Gillespie, C. W., Lowens, M. S., Manhart, L. E., and Totten, P. A. (2020). Sequence variation and immunogenicity of the *Mycoplasma genitalium* MgpB and MgpC adherence proteins during persistent infection of men with non-gonococcal urethritis. *PLoS One* 15:e0240626. doi: 10.1371/journal.pone.0240626
- Xiao, L., Ptacek, T., Osborne, J. D., Crabb, D. M., Simmons, W. L., Lefkowitz, E. J., et al. (2015). Comparative genome analysis of *Mycoplasma pneumoniae*. *BMC Genomics* 16:610. doi: 10.1186/s12864-015-1801-0
- Xiao, L., Ratliff, A. E., Crabb, D. M., Mixon, E., Qin, X., Selvarangan, R., et al. (2020). Molecular characterization of *Mycoplasma pneumoniae* isolates in the United States from 2012 to 2018. *J. Clin. Microbiol.* 58, e00710–e00720. doi: 10.1128/JCM.00710-20
- Xiao, L., Waites, K. B., van der Pol, B., Aaron, K. J., Hook, E. W. 3rd, and Geisler, W. M. (2019). *Mycoplasma genitalium* infections with macrolide and fluoroquinolone resistance-associated mutations in heterosexual African American couples in Alabama. *Sex. Transm. Dis.* 46, 18–24. doi: 10.1097/OLQ.0000000000000891
- Xiao, D., Zhao, F., Zhang, H., Meng, F., and Zhang, J. (2014). Novel strategy for typing *Mycoplasma pneumoniae* isolates by use of matrix-assisted laser desorption ionization-time of flight mass spectrometry coupled with ClinProTools. *J. Clin. Microbiol.* 52, 3038–3043. doi: 10.1128/JCM.01265-14
- Xue, G., Li, M., Wang, N., Zhao, J., Wang, B., Ren, Z., et al. (2018). Comparison of the molecular characteristics of *Mycoplasma pneumoniae* from children

- across different regions of China. *PLoS One* 13:e0198557. doi: 10.1371/journal.pone.0198557
- Yan, C., Xue, G., Zhao, H., Feng, Y., Li, S., Cui, J., et al. (2019). Molecular and clinical characteristics of severe *Mycoplasma pneumoniae* pneumonia in children. *Pediatr. Pulmonol.* 54, 1012–1021. doi: 10.1002/ppul.24327
- Zhang, J., Song, X., Ma, M. J., Xiao, L., Kenri, T., Sun, H., et al. (2017). Inter- and intra-strain variability of tandem repeats in *Mycoplasma pneumoniae* based on next-generation sequencing data. *Future Microbiol.* 12, 119–129. doi: 10.2217/fmb-2016-0111
- Zhang, X. S., Zhao, H., Vynnycky, E., and Chalker, V. (2019). Positively interacting strains that co-circulate within a network structured population induce cycling epidemics of *Mycoplasma pneumoniae*. *Sci. Rep.* 9:541. doi: 10.1038/s41598-018-36325-z
- Zhao, F., Cao, B., Li, J., Song, S., Tao, X., Yin, Y., et al. (2011). Sequence analysis of the p1 adhesin gene of *Mycoplasma pneumoniae* in clinical isolates collected in Beijing in 2008 to 2009. *J. Clin. Microbiol.* 49, 3000–3003. doi: 10.1128/JCM.00105-11
- Zhao, F., Li, J., Liu, J., Guan, X., Gong, J., Liu, L., et al. (2019). Antimicrobial susceptibility and molecular characteristics of *Mycoplasma pneumoniae* isolates across different regions of China. *Antimicrob. Resist. Infect. Control* 8:143. doi: 10.1186/s13756-019-0576-5
- Conflict of Interest:** The author declares that the research was conducted in the absence of any commercial or financial relationships that could be construed as a potential conflict of interest.
- Publisher's Note:** All claims expressed in this article are solely those of the authors and do not necessarily represent those of their affiliated organizations, or those of the publisher, the editors and the reviewers. Any product that may be evaluated in this article, or claim that may be made by its manufacturer, is not guaranteed or endorsed by the publisher.

Copyright © 2022 Dumke. This is an open-access article distributed under the terms of the Creative Commons Attribution License (CC BY). The use, distribution or reproduction in other forums is permitted, provided the original author(s) and the copyright owner(s) are credited and that the original publication in this journal is cited, in accordance with accepted academic practice. No use, distribution or reproduction is permitted which does not comply with these terms.



High Prevalence of *Mycoplasma penetrans* in *Chlamydia trachomatis* Positive Rectal Samples From Men: A Brief Report

Inmaculada Pérez-Prieto^{1,2,3}, Axel Skafte-Holm³ and Jørgen Skov Jensen^{3*}

¹ Department of Biochemistry and Molecular Biology, Faculty of Sciences, University of Granada, Granada, Spain, ² Instituto de Investigación Biosanitaria ibs.GRANADA, Granada, Spain, ³ Department of Bacteria, Parasites and Fungi, Research Unit for Reproductive Microbiology, Statens Serum Institut, Copenhagen, Denmark

Mycoplasma penetrans has gained increased attention in relation to sexually transmitted infections, however, its pathogenic potential and prevalence in different populations remains to be elucidated. Among 293 *Chlamydia trachomatis* positive rectal samples submitted for lymphogranuloma venereum typing, *M. penetrans* was detected by PCR in 13.4% of 231 male samples.

Keywords: *Mycoplasma penetrans*, *Chlamydia trachomatis*, coinfection, sexually transmitted infections, rectum

OPEN ACCESS

Edited by:

Meghan May,
University of New England,
United States

Reviewed by:

Ellen Kersh,
Centers for Disease Control
and Prevention (CDC), United States
Luis Piñeiro,
Donostia University Hospital, Spain

*Correspondence:

Jørgen Skov Jensen
jsj@ssi.dk

Specialty section:

This article was submitted to
Infectious Agents and Disease,
a section of the journal
Frontiers in Microbiology

Received: 16 March 2022

Accepted: 23 May 2022

Published: 13 June 2022

Citation:

Pérez-Prieto I, Skafte-Holm A and
Jensen JS (2022) High Prevalence
of *Mycoplasma penetrans*
in *Chlamydia trachomatis* Positive
Rectal Samples From Men: A Brief
Report. *Front. Microbiol.* 13:914874.
doi: 10.3389/fmicb.2022.914874

INTRODUCTION

Sexually transmitted infections (STIs) are caused by a wide range of bacteria, viruses and parasites. According to WHO estimates, more than 1 million STIs occur every day, emerging as an increasing reproductive and sexual health concern worldwide (World Health Organization, 2019). In this context, a high prevalence of STIs among men who have sex with men (MSM) is reported, with *Chlamydia trachomatis* and *Neisseria gonorrhoeae* being the most important (Workowski et al., 2021). Serotype L1-L3 of *C. trachomatis* causes lymphogranuloma venereum (LGV), a destructive and aggressive sexually transmitted infection affecting tissue and lymph nodes, predominantly associated with rectal infection in MSM in developed countries (Stoner and Cohen, 2015). Thus, genotyping of *C. trachomatis* positive rectal samples has been recommended since these infections require extended duration of therapy (De Vries et al., 2019).

A significant proportion of patients with STI symptoms have no identified etiological agents detected. Advances in molecular methods have allowed the search for unidentified pathogens by non-culture-dependent techniques. In this regard, several studies have reported the presence of *Mycoplasma* spp., primarily *M. genitalium*, in conditions such as non-gonococcal urethritis (NGU) (Jensen et al., 1993; Taylor-Robinson et al., 2003). In addition, a recent publication found *M. penetrans* to be associated with NGU primarily in MSM (Srinivasan et al., 2021). Since anal sex increases the risk for extra-genital infections, we assessed the prevalence of *M. penetrans* in *C. trachomatis* positive rectal samples submitted for LGV typing.

MATERIALS AND METHODS

Study Setting

Chlamydia trachomatis positive samples from diagnostic laboratories throughout Denmark between March and October 2021 were submitted for molecular LGV typing in the reference laboratory at Statens Serum Institut. Of the 837 original samples, remnants of 293 rectal

samples were available and anonymized to gender and age, and analyzed for *M. penetrans*. According to Danish law, an ethical committee approval was not required due to the anonymized nature of the dataset.

Sample Preparation

DNA was extracted from the samples submitted in the nucleic acid amplification test transport medium by processing 1 ml of sample using the Large Volume Universal Pathogen Extraction protocol in a MagNA Pure 96 instrument (Roche Diagnostics, Hvidovre, Denmark) and was eluted into 100 μ l.

Real-Time PCR (qPCR)

Mycoplasma penetrans was detected by qPCR as previously described (Srinivasan et al., 2021), except that an internal process control (IPC) was constructed in order to detect Taq DNA polymerase inhibitors or suboptimal reaction conditions (Jensen et al., 2003). Each assay was performed in a 50 μ l final reaction volume in a 7,500 Real-Time PCR System instrument (Thermo Fisher Scientific, Waltham, MA, United States), programmed for 95°C for 2 min and 50 cycles of 95°C for 15 s and annealing and extension at 60°C for 1 min. Standard curves were prepared with serial dilutions of *M. penetrans* DNA containing 50,000 to 5 copies.

RESULTS

Results of *M. penetrans* detection are summarized in **Table 1**. A total of 293 rectal samples (231 of male and 62 of female origin) were included in this study. The median age was 30 years ranging from 16 to 69. Overall, *M. penetrans* was detected more frequently in male *C. trachomatis* positive samples with a prevalence of 13.4% (95%CI 9.30–18.5) compared to 1.6% (95%CI 0.00–8.66), in female samples ($p = 0.005$, Fisher's exact test). *M. penetrans* DNA concentrations ranged from 2 to 31,846 genome equivalents (GEQ)/ μ l with a median of 33 GEQ/ μ l.

DISCUSSION

In this report, we describe a high prevalence of *M. penetrans* in male *C. trachomatis* positive rectal samples, in accordance to previous results (Taylor-Robinson et al., 2003). Earlier studies have mainly aimed to detect *M. penetrans* in male populations, including healthy MSM and men who have sex with women (MSW). In the 1990's, shortly after the discovery of *M. penetrans*, several publications highlighted its potential role in

the progression of HIV infection to AIDS and for development of Kaposi's sarcoma by analyzing *M. penetrans* antibodies in serum samples from healthy controls and patients of different risk groups for AIDS (Wang et al., 1992, 1993). In our study, lack of clinical information prevented us to evaluate the association between *M. penetrans* and HIV positivity.

Two studies have detected *M. penetrans* by PCR with a prevalence of 1.4 and 1.6%, respectively, in urine samples from HIV-infected individuals (Wang et al., 2012; Chen et al., 2015). One of these studies also included sexually transmitted clinic attendees and healthy controls, where the *M. penetrans* infection rate was < 1% (Wang et al., 2012). An earlier study of urethral swabs from Japanese men with and without NGU failed to detect *M. penetrans* in any of the patients (Deguchi et al., 1996). *M. penetrans* has been detected in rectal samples from 28 MSM with or without NGU with 10 vs. 5.6% positives, respectively. In addition, the study found a 10% prevalence of *M. penetrans* in urethral and throat samples in the men with NGU (Taylor-Robinson et al., 2003). Recent evidence has suggested a role of *M. penetrans* in NGU, a syndrome with unknown etiology in > 50% of cases. In search of an etiology for idiopathic NGU, Srinivasan et al. found an association between detection of *M. penetrans* and NGU by 16S microbiota analysis. They confirmed the findings using qPCR in urine samples from 431 men with and without NGU. *M. penetrans* was found in 8% of men diagnosed with NGU compared to 1% in men without NGU (Srinivasan et al., 2021). However, the association was found only in MSM where 13% of the NGU cases were *M. penetrans* positive compared to 3% of MSW with NGU. The present study revealed a 13% prevalence of *M. penetrans* in male *C. trachomatis* positive rectal samples. Due to the anonymization, we are not able to determine the proportion of MSM in our population, but it is probably nearly 100%, as rectal swabs are rarely obtained from MSW. Among MSM, bacterial STIs are common in the rectal site, and some studies have found a much higher positive rate in rectal swabs as compared to urine (Munson et al., 2021).

Due to the absence of cell wall, *Mycoplasma* spp. are naturally resistant to a wide spectrum of antibiotics. The most frequently used treatment of infection are macrolides, tetracyclines and fluoroquinolones, however, in the urogenital pathogen *M. genitalium*, several mutations associated with macrolide and fluoroquinolone resistance have been identified (Machalek et al., 2020). Only few isolates of *M. penetrans* are available and the literature is sparse on its antimicrobial susceptibility, however, early studies suggested that most isolates of *M. penetrans* were susceptible to all three antimicrobial classes (Hayes et al., 1995). In a more recent study, one *M. penetrans* strain showed evidence of macrolide resistance (Duffy et al., 2000). Similarly, a recent communication found complete resistance to azithromycin on four urogenital isolates from immunocompetent men suffering idiopathic NGU (Schwab et al., 2021). This development suggests that macrolide resistance in *M. penetrans* may be increasing over time, just as it has been shown for *M. genitalium* (Machalek et al., 2020). Altogether, these results emphasize the need for collection of contemporary *M. penetrans* isolates with antimicrobial susceptibility testing and

TABLE 1 | Distribution of *M. penetrans* among *C. trachomatis* positive rectal samples.

Gender	Rectal samples, n	<i>M. penetrans</i> detected, n	Percentage (95% CI)
Male	231	31	13.4 (9.3–18.5)
Female	62	1	1.6 (0.0–8.7)

molecular studies to determine the basis for the resistance in this emerging etiologic agent of NGU.

There are several limitations to our study. Due to the anonymized nature of the samples, important clinical, demographic and behavioral data are missing. Furthermore, it was not possible to evaluate whether multiple samples from the same subject were included, which could affect numbers. The high prevalence of *M. penetrans* in male rectal swabs supports the findings from previous studies of a strong link between MSM behavioral factors and *M. penetrans* detection. Future research should evaluate the role of *M. penetrans* as a pathogen potentially implicated in different STIs but should emphasize differences in sexual behavior.

CONCLUSION

The prevalence of *M. penetrans* in *C. trachomatis* positive male rectal swabs was surprisingly high at 13%. Although clinical data were missing because of anonymization, the presence of *M. penetrans* appears to be strongly associated with MSM behavior as suggested also in previous studies. Our findings indicate that *M. penetrans* may cause coinfection with *C. trachomatis*, however, the implications for symptoms and treatment outcomes require further research.

DATA AVAILABILITY STATEMENT

The original contributions presented in the study are included in the article/supplementary material, further inquiries can be directed to the corresponding author.

REFERENCES

- Chen, L. S., Wu, J. R., Wang, B., Yang, T., Yuan, R., Zhao, Y. Y., et al. (2015). Epidemiology of *Mycoplasma acquisition* in male HIV-1 infected patients: a multistage cross-sectional survey in Jiangsu, China. *Epidemiol. Infect.* 143, 3327–3334. doi: 10.1017/S0950268815000461
- De Vries, H. J. C., De Barbeyrac, B., De Vrieze, N. H. N., Viset, J. D., White, J. A., Vall-Mayans, M., et al. (2019). 2019 European guideline on the management of lymphogranuloma venereum. *J. Eur. Acad. Dermatol. Venereol.* 33, 1821–1828. doi: 10.1111/jdv.15729
- Deguchi, T., Gilroy, C. B., and Taylor-Robinson, D. (1996). Failure to detect *Mycoplasma fermentans*, *Mycoplasma penetrans*, or *Mycoplasma pirum* in the urethra of patients with acute nongonococcal urethritis. *Eur. J. Clin. Microbiol. Infect. Dis.* 15, 169–171. doi: 10.1007/BF01591493
- Duffy, L. B., Crabb, D., Searcey, K., and Kempf, M. C. (2000). Comparative potency of gemifloxacin, new quinolones, macrolides, tetracycline and clindamycin against *Mycoplasma* spp. *J. Antimicrob. Chemother.* 45 (Suppl 1), 29–33. doi: 10.1093/jac/45.suppl_3.29
- Hayes, M. M., Foo, H. H., Timenetsky, J., and Lo, S. C. (1995). *In vitro* antibiotic susceptibility testing of clinical isolates of *Mycoplasma penetrans* from patients with AIDS. *Antimicrob. Agents Chemother.* 39, 1386–1387.
- Jensen, J. S., Borre, M. B., and Dohn, B. (2003). Detection of *Mycoplasma genitalium* by PCR amplification of the 16S rRNA gene. *J. Clin. Microbiol.* 41, 261–266. doi: 10.1128/JCM.41.1.261-266.2003
- Jensen, J. S., Orsum, R., Dohn, B., Uldum, S., Worm, A. M., and Lind, K. (1993). *Mycoplasma genitalium*: a cause of male urethritis? *Genitourin Med.* 69, 265–269. doi: 10.1136/sti.69.4.265
- Machalek, D. A., Tao, Y., Shilling, H., Jensen, J. S., Unemo, M., Murray, G., et al. (2020). Prevalence of mutations associated with resistance to macrolides and fluoroquinolones in *Mycoplasma genitalium*: a systematic review and meta-analysis. *Lancet Infect. Dis.* 20, 1302–1314. doi: 10.1016/S1473-3099(20)30154-7
- Munson, E., Morgan, E., Sienkiewicz, L., Thomas, Y., Buehler, K., Ryan, D., et al. (2021). Molecular screening in a longitudinal cohort of young men who have sex with men and young transgender women: associations with focus on the emerging sexually transmitted pathogen *Mycoplasma genitalium*. *Sex Transm. Infect.* 97, 434–440. doi: 10.1136/sextrans-2020-054463
- Schwab, N., Toh, E., Nzenwata, D., Mikulin, J., Timothy, W., Nelson, D., et al. (2021). “Characterization of *Mycoplasma penetrans* isolates acting as possible etiologic agents of idiopathic urethritis in immunocompetent men,” in *Proceeding of the XXIII Biennial Congress of the International Organization for Mycoplasmaology (IOM)* (Tel Aviv), 81–82.
- Srinivasan, S., Chambers, L. C., Tapia, K. A., Hoffman, N. G., Munch, M. M., Morgan, J. L., et al. (2021). Urethral microbiota in men: association of *Haemophilus influenzae* and *Mycoplasma penetrans* With Nongonococcal Urethritis. *Clin Infect Dis* 73, e1684–e1693. doi: 10.1093/cid/ciaa1123
- Stoner, B. P., and Cohen, S. E. (2015). Lymphogranuloma venereum 2015: clinical presentation, diagnosis, and treatment. *Clin. Infect. Dis.* 61 (Suppl 8), S865–S873. doi: 10.1093/cid/civ756

ETHICS STATEMENT

Ethical review and approval was not required for the study on human participants in accordance with the Local Legislation and Institutional Requirements. Written informed consent for participation was not required for this study in accordance with the National Legislation and the Institutional Requirements.

AUTHOR CONTRIBUTIONS

IP-P performed the experimental assays and wrote the manuscript. AS-H participated in writing phase and statistical analysis, elaborated the table, and reviewed the initial manuscript draft for important intellectual content. JSJ conceptualized and designed the study, supervised the manuscript, and reviewed the manuscript for important intellectual content. All authors contributed to the article and approved the submitted version.

FUNDING

This work was supported by the Spanish Ministry of Science, Innovation and Universities (FPU19/05561) and the European Society of Human Reproduction and Embryology Traveling Fellowship to IP-P.

ACKNOWLEDGMENTS

This study was part of a Ph.D. thesis conducted at the Biomedicine Doctoral Studies of the University of Granada, Spain.

- Taylor-Robinson, D., Gilroy, C. B., and Keane, F. E. (2003). Detection of several *Mycoplasma* species at various anatomical sites of homosexual men. *Eur. J. Clin. Microbiol. Infect. Dis.* 22, 291–293. doi: 10.1007/s10096-003-0910-x
- Wang, B., Wu, J. R., Guo, H. J., Yang, H. T., Ai, J., Hui, M., et al. (2012). The prevalence of six species of *Mycoplasmataceae* in an HIV/AIDS population in Jiangsu Province, China. *Int. J. STD AIDS* 23, e7–e10. doi: 10.1258/ijsa.2009.009396
- Wang, R. Y., Shih, J. W., Grandinetti, T., Pierce, P. F., Hayes, M. M., Wear, D. J., et al. (1992). High frequency of antibodies to *Mycoplasma penetrans* in HIV-infected patients. *Lancet* 340, 1312–1316.
- Wang, R. Y., Shih, J. W., Weiss, S. H., Grandinetti, T., Pierce, P. F., Lange, M., et al. (1993). *Mycoplasma penetrans* infection in male homosexuals with AIDS: high seroprevalence and association with Kaposi's sarcoma. *Clin. Infect. Dis.* 17, 724–729. doi: 10.1093/clinids/17.4.724
- Workowski, K. A., Bachmann, L. H., Chan, P. A., Johnston, C. M., Muzny, C. A., Park, I., et al. (2021). Sexually transmitted infections treatment guidelines, 2021. *MMWR Recomm. Rep.* 70, 1–187.
- World Health Organization (2019). *Sexually Transmitted Infections: Evidence Brief*. Geneva: World Health Organization.
- Conflict of Interest:** JSJ reports grants, personal fees, and non-financial support from Hologic, personal fees from Roche, grants and personal fees from SpeeDx, grants and personal fees from Nabriva, grants and personal fees from Cepheid, grants and personal fees from Abbott, and grants and personal fees from GSK all outside the submitted work.
- The remaining authors declare that the research was conducted in the absence of any commercial or financial relationships that could be construed as a potential conflict of interest.
- Publisher's Note:** All claims expressed in this article are solely those of the authors and do not necessarily represent those of their affiliated organizations, or those of the publisher, the editors and the reviewers. Any product that may be evaluated in this article, or claim that may be made by its manufacturer, is not guaranteed or endorsed by the publisher.

Copyright © 2022 Pérez-Prieto, Skafte-Holm and Jensen. This is an open-access article distributed under the terms of the Creative Commons Attribution License (CC BY). The use, distribution or reproduction in other forums is permitted, provided the original author(s) and the copyright owner(s) are credited and that the original publication in this journal is cited, in accordance with accepted academic practice. No use, distribution or reproduction is permitted which does not comply with these terms.



OPEN ACCESS

EDITED BY

Meghan May,
University of New England,
United States

REVIEWED BY

Lei Shi,
Chalmers University of Technology,
Sweden
Wiep Klaas Smits,
Leiden University, Netherlands

*CORRESPONDENCE

Jörg Stülke
jstuelk@gwdg.de

†These authors have contributed
equally to this work

SPECIALTY SECTION

This article was submitted to
Evolutionary and Genomic
Microbiology,
a section of the journal
Frontiers in Microbiology

RECEIVED 03 May 2022

ACCEPTED 01 July 2022

PUBLISHED 25 July 2022

CITATION

Elfmann C, Zhu B, Pedreira T,
Hoßbach B, Lluch-Senar M, Serrano L
and Stülke J (2022) MycoWiki:
Functional annotation of the minimal
model organism *Mycoplasma
pneumoniae*.
Front. Microbiol. 13:935066.
doi: 10.3389/fmicb.2022.935066

COPYRIGHT

© 2022 Elfmann, Zhu, Pedreira,
Hoßbach, Lluch-Senar, Serrano and
Stülke. This is an open-access article
distributed under the terms of the
[Creative Commons Attribution License
\(CC BY\)](https://creativecommons.org/licenses/by/4.0/). The use, distribution or
reproduction in other forums is
permitted, provided the original
author(s) and the copyright owner(s)
are credited and that the original
publication in this journal is cited, in
accordance with accepted academic
practice. No use, distribution or
reproduction is permitted which does
not comply with these terms.

MycoWiki: Functional annotation of the minimal model organism *Mycoplasma pneumoniae*

Christoph Elfmann ^{1†}, Bingyao Zhu^{1†}, Tiago Pedreira ^{1†},
Ben Hoßbach¹, Maria Lluch-Senar², Luis Serrano² and
Jörg Stülke ^{1*}

¹Department of General Microbiology, Göttingen Center for Molecular Biosciences, Georg-August
University Göttingen, Göttingen, Germany, ²EMBL/CRG Systems Biology Research Unit, Centre
for Genomic Regulation (CRG), Universitat Pompeu Fabra (UPF), Barcelona, Spain

The human pathogen *Mycoplasma pneumoniae* is viable independently from host cells or organisms, despite its strongly reduced genome with only about 700 protein-coding genes. The investigation of *M. pneumoniae* can therefore help to obtain general insights concerning the basic requirements for cellular life. Accordingly, *M. pneumoniae* has become a model organism for systems biology in the past decade. To support the investigation of the components of this minimal bacterium, we have generated the database MycoWiki. (<http://mycowiki.uni-goettingen.de>) MycoWiki organizes data under a relational database and provides access to curated and state-of-the-art information on the genes and proteins of *M. pneumoniae*. Interestingly, *M. pneumoniae* has undergone an evolution that resulted in the limited similarity of many proteins to proteins of model organisms. To facilitate the analysis of the functions of *M. pneumoniae* proteins, we have integrated structure predictions from the AlphaFold Protein Structure Database for most proteins, structural information resulting from *in vivo* cross-linking, and protein-protein interactions based on a global *in vivo* study. MycoWiki is an important tool for the systems and synthetic biology community that will support the comprehensive understanding of a minimal organism and the functional annotation of so far uncharacterized proteins.

KEYWORDS

MycoWiki, genome annotation, essential genes, systems biology, database

Introduction

Bacteria of the genus *Mycoplasma* are characterized by their strongly reduced genomes that still encode all the functions required for autonomous growth. Bacteria such as *Mycoplasma genitalium* and *Mycoplasma pneumoniae* have genomes of only 480 and 816 kb and encode about 480 and 700 proteins, respectively. These small

genomes have put these bacteria into the spotlight of systems and synthetic biology, two recent disciplines in biology that aim for a complete understanding of all processes in a living cell up to mathematic modeling and for the creation of artificial forms of life, respectively.

Starting with global analyses of the metabolism, gene expression, and protein-protein interactions in 2009 (Güell et al., 2009; Kühner et al., 2009; Yus et al., 2009), *M. pneumoniae* has become one of the model organisms of systems biology. Many aspects of its biology such as metabolism, DNA and protein modifications, the micro-proteome, protein degradation, regulatory networks, and gene essentiality have been studied at the global level as well (Schmidl et al., 2010; van Noort et al., 2012; Lluch-Senar et al., 2013, 2015; Wodke et al., 2013; Miravet-Verde et al., 2019; Yus et al., 2019; Burgos et al., 2020; Montero-Blay et al., 2020). The small proteome of *M. pneumoniae* facilitates the investigation of protein function at the global scale as revealed by the first large-scale global *in vivo* study of protein-protein interactions. This analysis resulted in the visualization of important protein complexes and in the identification of functions of so far unknown proteins (O'Reilly et al., 2020).

In addition to its role in systems biology, *M. pneumoniae* is also intensively studied due to its role as a lung pathogen (Meyer Sauter et al., 2014; Waites et al., 2017; Esposito et al., 2021). Its main virulence determinants are a specific ADP-ribosylating and vacuolating cytotoxin (CARDS, MPN372) (Kannan and Baseman, 2006; Becker et al., 2015), hydrogen peroxide which is produced by glycerol phosphate oxidase (GlpO) as a product of phospholipid and glycerol utilization (Schmidl et al., 2011; Blötz and Stülke, 2017), hydrogen sulfide is produced by the cysteine desulfurase HapE during cysteine degradation (Großhennig et al., 2016), and the immunoglobulin binding protein IbpM helps the bacteria to escape the human immune system (Blötz et al., 2020).

As a minimal pathogen, *M. pneumoniae* might also be useful in fighting disease by delivering therapeutics to the human host or by directly combatting other bacteria (Piñero-Lambea et al., 2015; Garrido et al., 2021). Such applications are favored by the fact that the genetic code used by *M. pneumoniae* is unique, thus preventing horizontal gene transfer, and by the development of methods that allow the construction of attenuated strains by deleting the genes that encode virulence factors. Indeed, this strategy has recently been employed to eliminate biofilms of the harmful and often multiresistant human pathogen *Staphylococcus aureus* (Garrido et al., 2021).

The importance of *M. pneumoniae* as a human pathogen, as a potential therapeutic agent, and its role in systems and synthetic biology suggests that this bacterium will remain the focus of intense research. This requires tools that allow easy access to all available information on the genes and

proteins of *M. pneumoniae* and their functional and regulatory interactions. To facilitate the investigation of *M. pneumoniae*, we have developed MycoWiki, a database centered around the genes and proteins of this bacterium. This database shares its framework with the established databases SubtiWiki and SynWiki, which provide functional annotation of *Bacillus subtilis* and the artificial minimal organism *Mycoplasma mycoides* JCVI-syn3A, respectively (Pedreira et al., 2022a,b). MycoWiki presents the available information on the genes and proteins of *M. pneumoniae* in a highly intuitive manner. A particular focus on MycoWiki is the presentation of links and interactions between different genes and proteins, which allows the scientific community to develop novel hypotheses. The information provided in MycoWiki is derived from earlier annotations of the *M. pneumoniae* genome (Dandekar et al., 2000; Wodke et al., 2015) and the published body of knowledge.

Description of the database

MycoWiki (<http://mycowiki.uni-goettingen.de>) is built upon the same framework as the aforementioned databases SubtiWiki and SynWiki (Pedreira et al., 2022a,b). As a result, the general organization of data entities and their relations to each other, and the layout of the web pages, are the same. However, some features are exclusive to MycoWiki, such as the representation of cross-linking data combined with protein structures.

The structure of MycoWiki is centered around genes and their products. Most of the information represented in this database is associated with a specific gene/protein, and thus the *Gene* pages are the core part of MycoWiki. They integrate the most data relating to a particular gene, but also connect to separate web pages, for example, pages on certain groups of genes, such as specific functional categories. The *Gene* page also links to *browsers*, which allow exploring some aspects of a gene or the gene product and possible interactions of the encoded protein (such as the *Expression*, *Interaction*, and *Pathway Browsers*).

The front page

The front page of MycoWiki gives access to the *Gene* pages via a search bar, which can be used to query genes by unique identifiers (Figure 1). One option is to use a gene's name, usually a mnemonic of three or four letters as it is commonly the case for bacterial genes (such as *eno* for enolase). Genes can also be identified via their locus tags, which are largely based on genome re-annotations (Dandekar et al., 2000; Lluch-Senar et al., 2015). For example, MPN606 is the locus tag for *eno*, and it is guaranteed to never change, even if the mnemonic designation

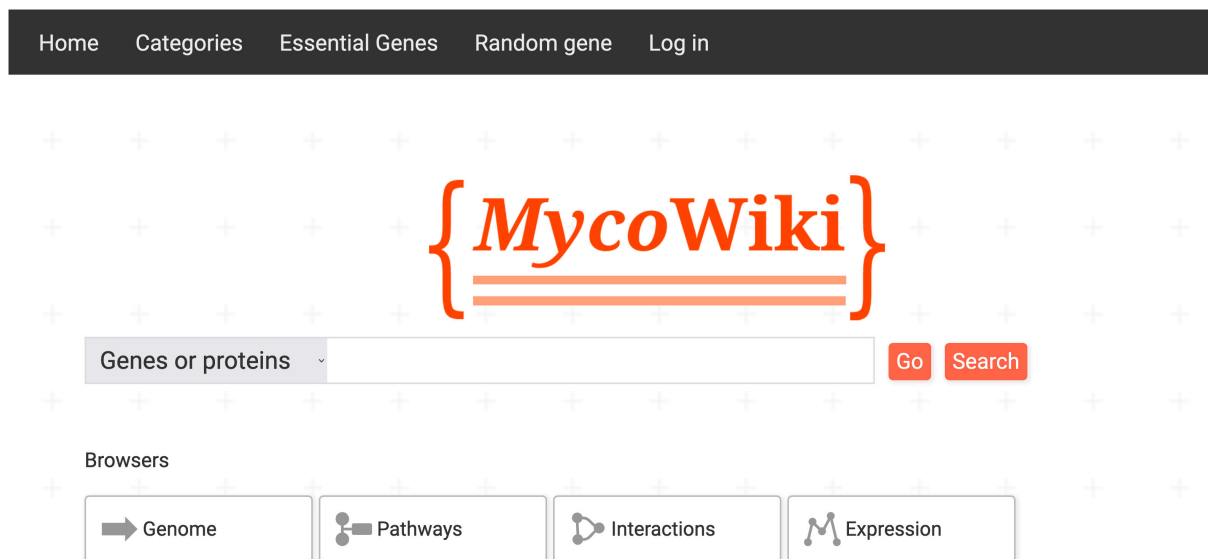


FIGURE 1

Front page of *MycoWiki*. The central search bar allows to query genes by name or locus tag, but also facilitates full-text searches. Below, the data browsers are linked for quick access. In the top bar, direct access to an overview of categories and a list of essential genes is provided, and utility links for jumping to a random gene page and for logging in.

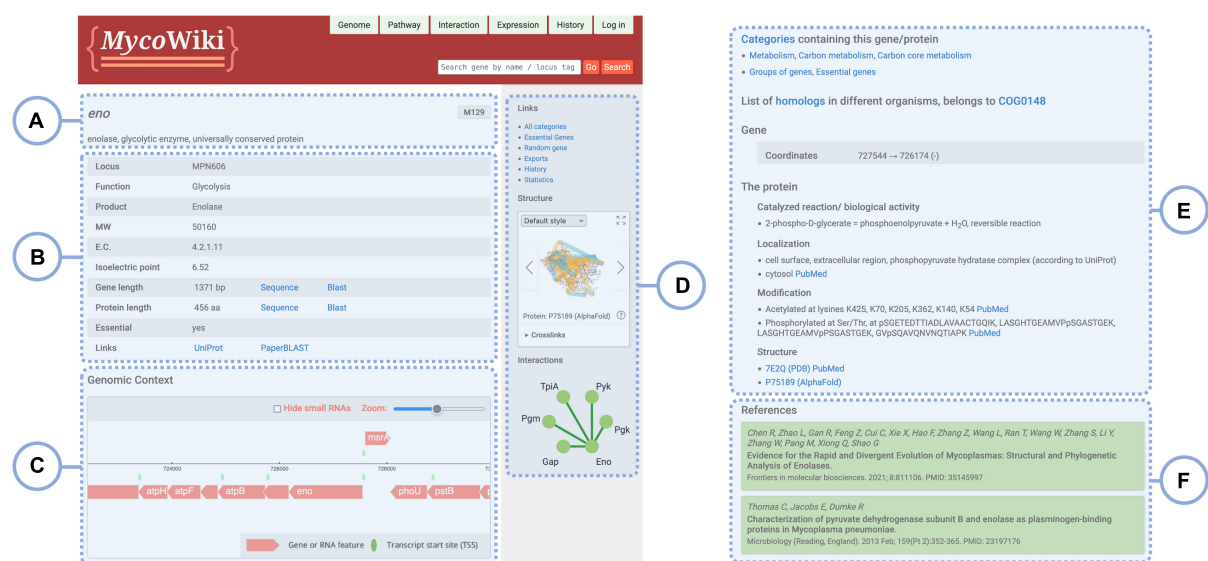


FIGURE 2

The gene page for *eno*. The general structure of gene pages is the same for all genes, but individual sections and interactive elements may vary due to different information being available. (A) Gene name, strain, and description; (B) table summarizing basic information on the gene and its product; (C) embedded genomic region display; (D) sidebar containing helpful links and additional tools, such as the *Structure Viewer*; (E) further sections describing various aspects of the gene; and (F) list of publications as sources of information.

of the gene should be changed. In some cases, a name has not been assigned to a gene yet, so the locus tag is the primary identifier. Aside from these two identifiers, a full-text search of a gene's data is possible *via* the "Search" button.

Moreover, the top bar of the front page gives access to an overview of the functional categories each gene/protein

was assigned to, a list of essential genes, and to a random gene page. Finally, it allows the user to log into the database. These links also appear on all gene pages in the right-side bar (Figure 2D, see below). Below the search bar, links to the interactive *MycoWiki* browsers (see below) are provided.

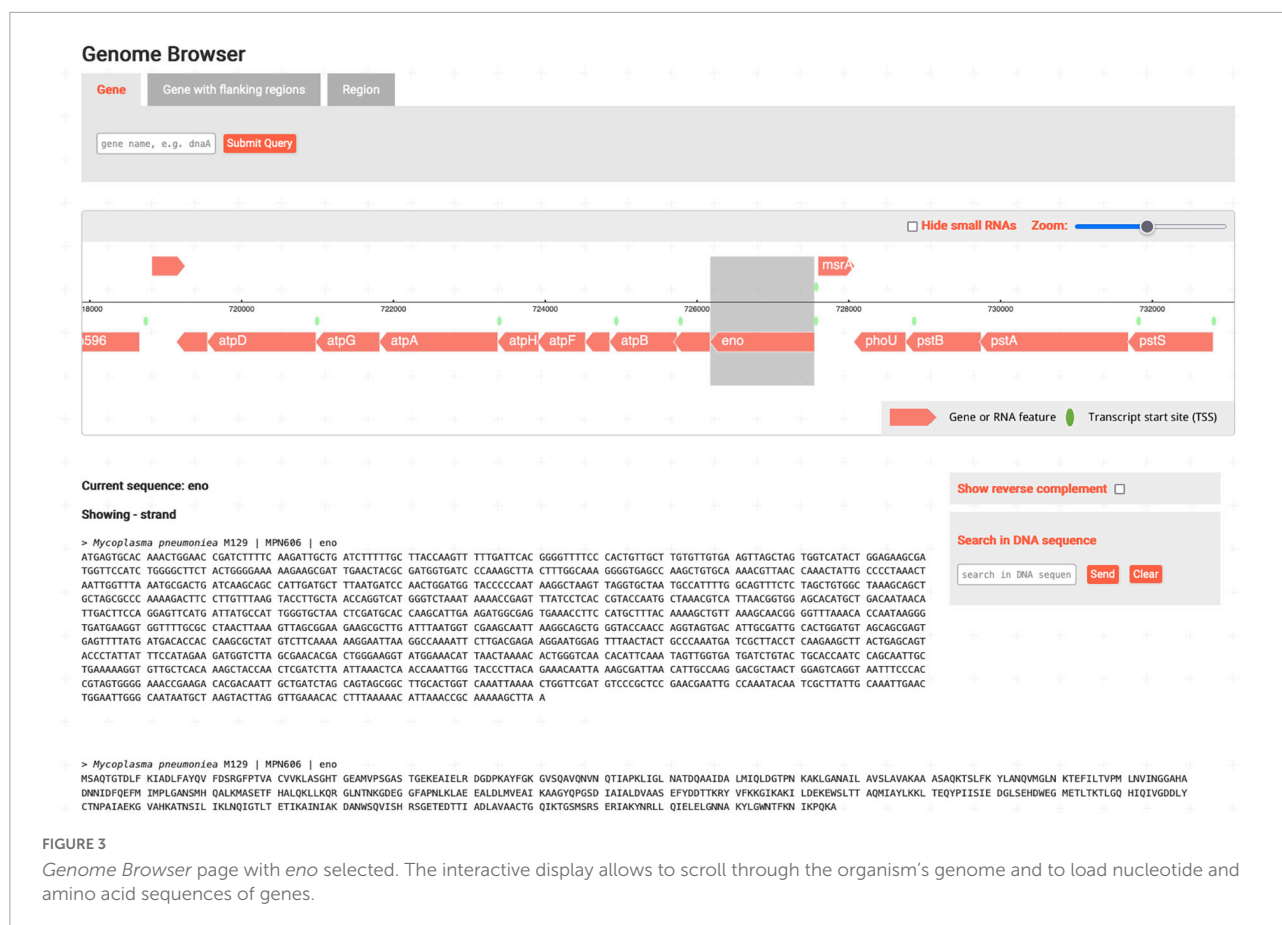


FIGURE 3

Genome Browser page with *eno* selected. The interactive display allows to scroll through the organism's genome and to load nucleotide and amino acid sequences of genes.

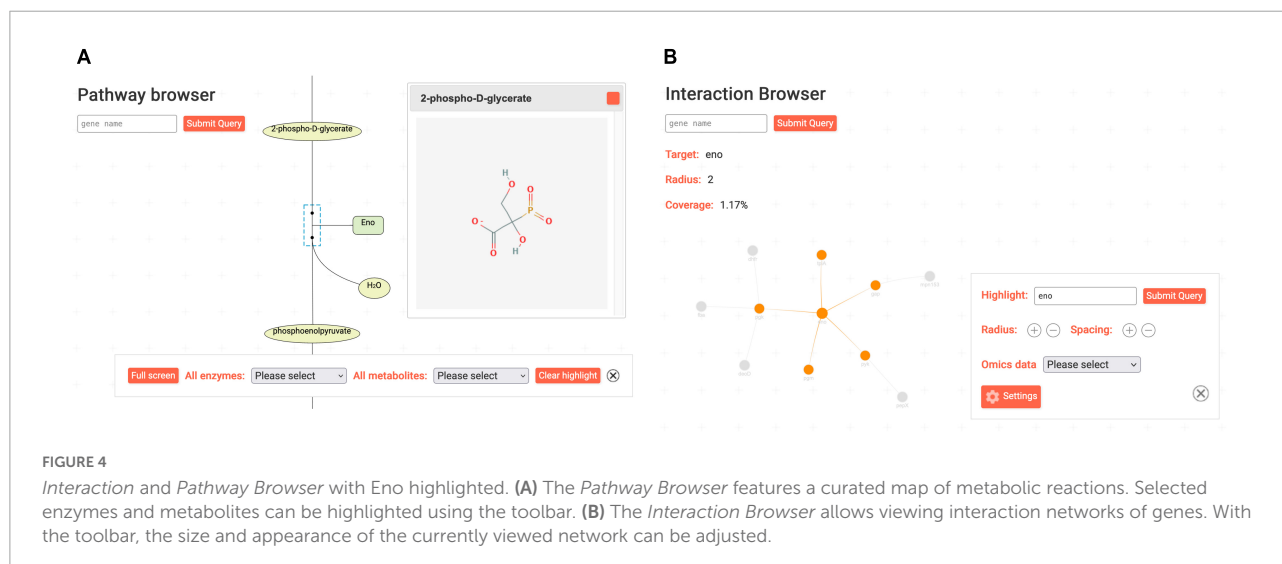


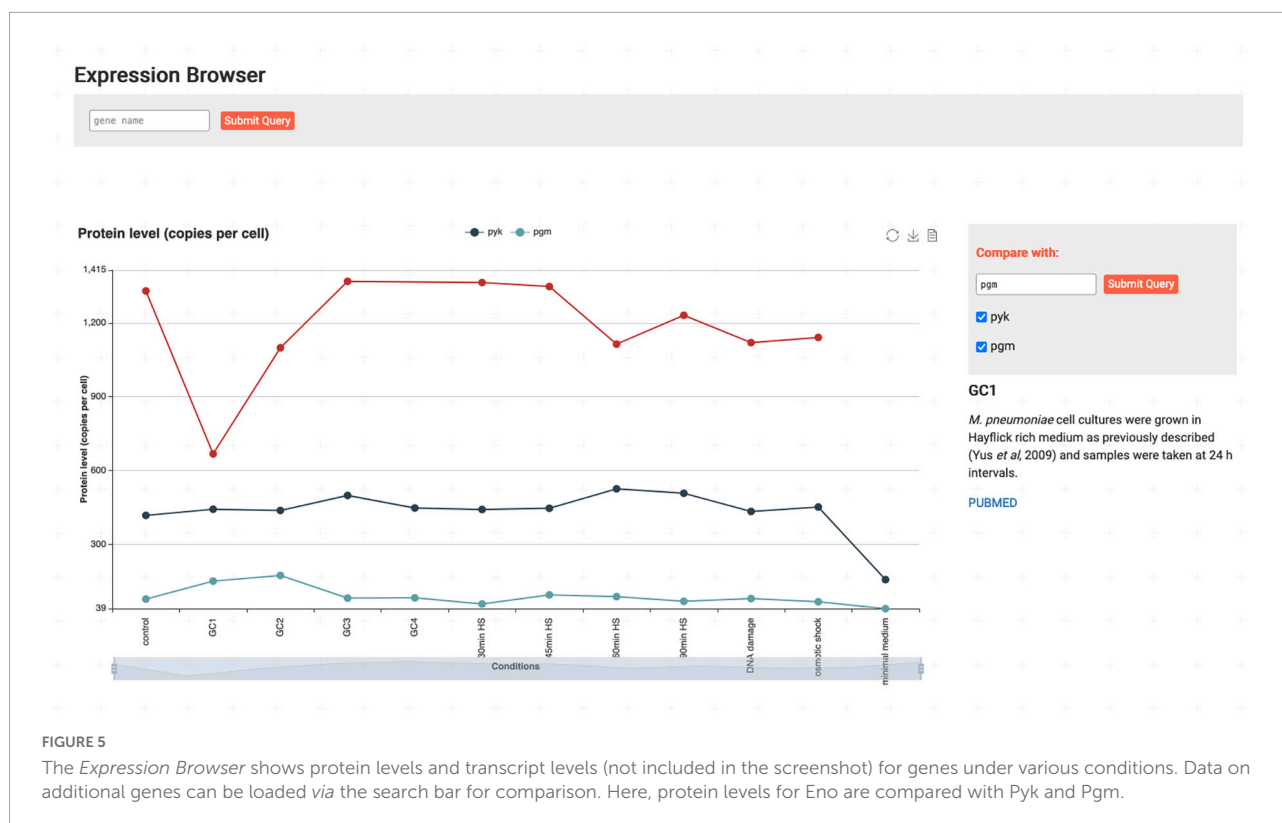
FIGURE 4

Interaction and Pathway Browser with *Eno* highlighted. (A) The Pathway Browser features a curated map of metabolic reactions. Selected enzymes and metabolites can be highlighted using the toolbar. (B) The Interaction Browser allows viewing interaction networks of genes. With the toolbar, the size and appearance of the currently viewed network can be adjusted.

The gene pages

In *MycoWiki*, the *Gene* pages provide access to all data relating to a particular gene. Most of the annotation can be directly viewed on the page, and links to browsers are provided which investigate certain aspects of the gene in more detail.

All gene pages share the same basic structure. Figure 2 shows the page for *eno*. The top bar (Figure 2A) contains links to the data browsers, the change history of the page, and a log-in pop-up. It also features the search bar, which has the same functionality as the one presented on the front page. At the top of the main view (Figure 2B), the gene name is



indicated as the page title. Below, a short general description is displayed, and the name of the *M. pneumoniae* strain M129 is shown on the side. Next, a table summarizes some basic information about the gene such as the locus tag, function, and sequence information. The latter is accompanied by utility links used to directly BLAST (Sayers et al., 2022) the nucleotide or translated amino acid sequence. This table also features data on the gene's product, for example, the molecular weight and enzyme commission number of the encoded protein. Further down, an interactive presentation of the genomic region is embedded in the page (Figure 2C), which allows viewing the genomic neighborhood of the gene. It does not feature all of the functionality of the full *Genome Browser*, which can be accessed *via* the top bar, and which will be explained below. On the sidebar (Figure 2D), a group of links provides access to helpful pages. Depending on the gene and the available data, additional interactive elements follow: the *Structure Viewer* shows 3D visualizations of the protein structure and cross-linking data, if available (see below). The *Interaction overview* displays a graph of the protein-protein interactions between the protein and its interaction partners. Proteins are represented by nodes that can be clicked to open the corresponding gene pages. In addition, the edges, which depict interactions, link to relevant publications.

Further down below on the page (Figure 2E), additional sections shed light on various aspects of the gene/protein, such as assigned categories, genomic coordinates, details about the

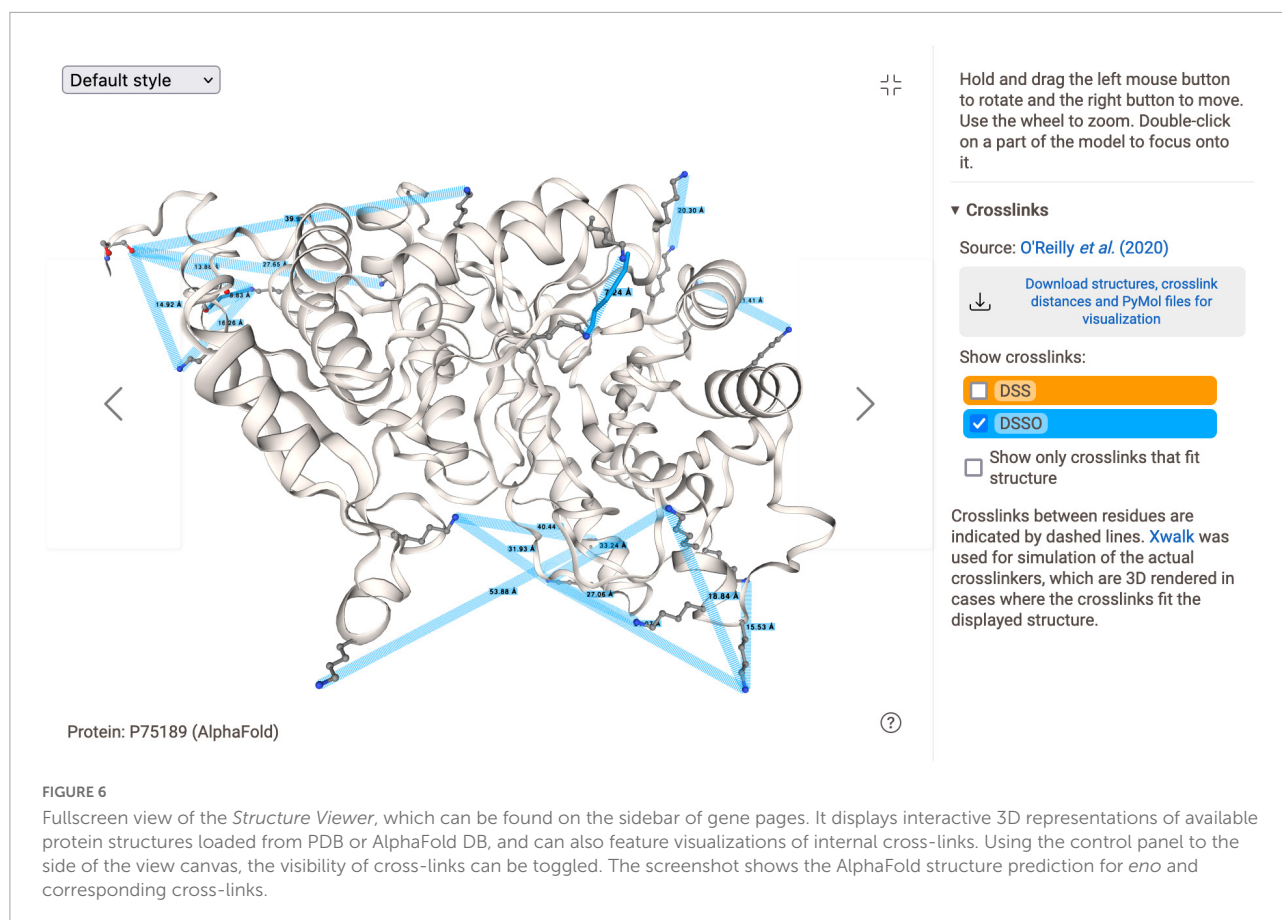
gene product, and other data. At the end of the page, a list of relevant publications is featured (Figure 2F).

Browsers

MycoWiki and its siblings *SubtiWiki* and *SynWiki* feature various *browsers*, which are interactive, graphical displays that allow users to explore certain types of data in an intuitive manner. When they are accessed *via* a gene page's top bar, the data corresponding to that gene are highlighted. However, data on other genes can be easily loaded in the browsers by the use of search bars, which allows the user to compare and contrast information on multiple genes effortlessly. These search bars are located in the top left corner of any browser. *MycoWiki* currently features four different browsers.

The *Genome Browser* (Figure 3) allows the user to see the immediate neighborhood of the gene and the orientations and lengths of genes, scroll through the genome, and adjust the zoom level. In addition, it includes the display of DNA and protein sequences. Clicking on a gene displays the corresponding sequences below the interactive genome display, where the user can search for substrings and toggle the reverse complement sequence. Flanking regions of genes or freely defined substrings of the genome can be loaded *via* the search bar.

The *Pathway Browser* visualizes a curated map of metabolic pathways and related metabolites and enzymes



for *M. pneumoniae*. In **Figure 4A**, the reaction catalyzed by Eno as part of the glycolytic pathway is shown. Clicking on enzymes in the map opens a small pop-up window featuring a basic summary for the corresponding gene/protein. Using the collapsible toolbar, the user can enter a full-screen mode and select enzymes or metabolites to be highlighted.

Protein-protein interactions are important clues to characterize proteins of unknown function. *M. pneumoniae* is the first organism for which a global analysis of the *in vivo* interactome was performed (O'Reilly et al., 2020). The results and the outcome of other more protein-specific studies are displayed in the *Interaction Browser*. In this browser, networks of interacting proteins can be visualized in a dynamic and interactive manner (**Figure 4B**). Similar to the corresponding interactive element on the gene page sidebar, proteins and their interactions are represented by nodes and edges of a graph. However, the browser display is more flexible: the user can rearrange nodes by dragging them with the cursor, and other visualization options can be adjusted *via* the toolbar. More proteins can be included in the display by increasing the *radius*, and the distance between nodes on the screen is controlled by the *spacing* setting. In addition, specific proteins can be highlighted, and the color scheme can be adjusted *via* the “Settings” button. Left-clicking nodes open a summary

pop-up window, while right-clicking somewhere on the screen triggers a context menu. The latter features options to export the displayed interaction network as an image or to download the corresponding list of interactions. In the top left corner, an info box displays the currently viewed gene, the radius of the network, and the proportion of proteins contained in the network.

With the *Expression Browser* (**Figure 5**), the user can investigate protein and transcript levels (not shown) of genes/proteins under different conditions (Yus et al., 2009; Maier et al., 2011). Additional genes can be dynamically loaded for comparison using the search bar, and descriptions of the individual conditions are available by clicking on the corresponding data points. Options for data export are provided as well.

Structure viewer

MycoWiki introduces a new 3D protein structure viewer (**Figure 6**), which is not yet present in either *SubtiWiki* or *SynWiki*. It is able to load and display structures from the Protein Data Bank (PDB) (Burley et al., 2019) and structure predictions from the AlphaFold Protein Structure Database

TABLE 1 List of top-level categories and their subcategories used in MycoWiki, and the number of genes assigned to each of them.

	Subcategory	Number of genes
Cellular processes	Cell envelope and cell division	2
	Homeostasis	14
	Transporters	64
	Movement and adhesion	31
Metabolism	Amino acid acquisition and metabolism	18
	ATP synthesis	11
	Carbon metabolism	47
	Cofactor acquisition	14
	Sulfur metabolism	2
	Lipid metabolism	18
	Nucleotide metabolism	21
	Phosphate metabolism	5
	Detoxification reactions	6
Information processing	Genetics	60
	RNA synthesis and degradation	23
	Protein synthesis, modification and degradation	188
	Regulation	11
Virulence and pathogenicity	Virulence and pathogenicity	4
Groups of genes	Membrane proteins	188
	Secreted proteins	1
	Essential genes	332
	Conditional essential genes	58
	Universally conserved proteins	1
	Poorly characterized enzymes	44
	Proteins of unknown function	195

(Varadi et al., 2022). In addition, it features the visualization of internal cross-links based on data from a global *in vivo* study of protein-protein interactions (O'Reilly et al., 2020).

A minimized form of the *Structure Viewer* can be found on the gene page sidebar. While it features full functionality, a full-screen view is also available (shown in the figure), which includes information on how to control the viewer. By using the arrow icons, the user can cycle through the available structures of a protein, which are also found in the main body of the gene page in the section “The protein > Structure.” An info text in the bottom left corner indicates the currently viewed structure, and also links to the respective PDB or AlphaFold DB page. The user can choose different molecular representation styles from the drop-down selection in the upper left corner, such as renderings of the protein surface indicating hydrophobicity or electrostatic values. The visualization of structures and cross-links is performed with NGL Viewer, a web-based tool for molecular 3D graphics (Rose and Hildebrand, 2015). To the

side of the viewer, additional information is displayed, including instructions about how to control the viewer and further details about the structure, if available.

As shown in the figure, visualization of cross-linking data is also available in MycoWiki. The data result from a large-scale *in vivo* study (O'Reilly et al., 2020), in which whole-cell cross-linking mass spectrometry with two different cross-linkers (DSS and DSSO) was performed. For the *Structure Viewer*, only internal (intraprotein) cross-links were extracted and mapped to the AlphaFold structure predictions of the corresponding proteins. Of the 686 predictions assigned to MycoWiki genes, internal cross-links were available for 441 structures. Cross-linked residues of a protein are highlighted in the viewer by dashed lines indicating the Euclidean distance between them. Furthermore, if the distance between the cross-linked residues is smaller than the spacer arms of the respective cross-linker, a molecular 3D representation of the linker is fitted to the structure. This representation was calculated and rendered using the program Xwalk, which determines the *Solvent Accessible Surface Distance* (SASD) between cross-linked amino acids (Kahraman et al., 2011). It corresponds to the shortest path between them only using solvent-occupied space, without passing through the protein surface. For DSS and DSSO, distances of 11.4 and 10.1 Å, respectively, plus a 1.5 Å tolerance were chosen as the maximum distance for which they could be fitted to the structure. In the *Structure Viewer*, the visibility of the different distance representations can be toggled *via* controls at the side of the viewer panel. In addition, a download link for an archive file of all structures and cross-link data is provided.

Implementation and data

The MycoWiki platform shares its framework with its predecessor *SubtiWiki* (Pedreira et al., 2022b). Accordingly, it is implemented using the same custom PHP backend framework and frontend functionality, and uses MySQL for its relational database. The application is hosted with Apache HTTP Server. Some differences *SubtiWiki* and *SynWiki* exist in presentation due to differing availability of data for the corresponding organisms, and some frontend features slightly vary in design.

MycoWiki contains a mixture of manually curated information, which is gathered from recent publications and evaluated by experts, and individual bulk data imports from existing data sources, such as other databases or published experimental data. The platform received a lot of its original annotation from the database MyMpn (Wodke et al., 2015), which was discontinued in 2020. With its structure similar to the one of MycoWiki, many parts of MyMpn could be directly adopted, such as genomic coordinates, enzyme commission numbers, and post-translational modifications. The main body

Organism	Protein name	Identity	Similarity	Bidirectional best hit
<i>Mycoplasma genitalium</i>	Eno	79.7%	94.6%	Yes
<i>Mycoplasma mycoides spp mycoides</i>	Eno	59.2%	77.5%	Yes
JCVI Syn3A	JCVISYN3A_0213	59.1%	77.5%	Yes
<i>Mesoplasma florum</i>	Eno	56.2%	76.6%	Yes
<i>Acholeplasma laidlawii</i>	Eno	54.9%	79.8%	Yes
<i>Bacillus subtilis</i>	Eno	54.3%	80.2%	Yes
<i>Listeria monocytogenes</i>	Eno	54.3%	80.5%	Yes
<i>Streptococcus pneumoniae</i>	Eno	53.7%	80.0%	Yes
<i>Clostridium acetobutylicum</i>	Eno	53.6%	79.6%	Yes
<i>Corynebacterium glutamicum</i>	Eno	53.7%	77.4%	No
<i>Streptomyces coelicolor</i>	Eno1	52.8%	77.3%	Yes
<i>Escherichia coli</i>	Eno	55.3%	79.8%	Yes
<i>Prochlorococcus marinus</i>	Eno	53.1%	79.0%	Yes
<i>Synechococcus elongatus</i>	Eno	57.1%	78.1%	Yes
<i>Synechocystis sp</i>	Eno	55.6%	77.5%	Yes
<i>Borrelia burgdorferi</i>	Eno	56.4%	80.6%	Yes

FIGURE 7

Protein homology table for Eno. Best BLAST hits for 16 representative related organisms are featured, and scores on identity and similarity are provided.

of information on protein-protein interactions comes from a global *in vivo* study (O'Reilly et al., 2020).

Similar to *SubtiWiki* and *SynWiki*, a specialized set of categories was conceived for *MycoWiki*. They are represented by a tree-like structure that classifies genes by their functions, but also groups them according to their localization, essentiality, or quality of characterization, among others. **Table 1** shows the five top-level categories and their immediate subcategories, while lower-level subcategories are omitted. The main part of the categories has been adapted from *SynWiki*, however, “Virulence and pathogenicity” has been added as a top-level category to help characterization of the organism as a pathogen.

As in *SubtiWiki* and *SynWiki*, a list of precomputed best-hit protein homologs in selected related bacteria based on a FASTA pipeline (Pedreira et al., 2022b) has been added to each protein. A specialized page with a corresponding table (**Figure 7**) can be accessed from the “Homologs” section on any gene page. In total, 16 species were deemed representative of protein homologies, among them *Mycoplasma genitalium*, *Mycoplasma mycoides subsp. mycoides*, the artificial synthetic

organism *M. mycoides* JCVI Syn3A, *Escherichia coli*, and *Bacillus subtilis*. Identity and similarity scores are given for each potential homolog, and an indication as to whether the homolog in question is also the best hit for the protein in the other direction.

To keep functional genome annotation up to date, joint efforts of the corresponding scientific community are required. Therefore, *MycoWiki* is open to contributions from all scientists in the field of *Mycoplasma* research. This is a major distinctive feature as compared to other databases that include information on *M. pneumoniae*. In addition, MyMpn, as mentioned above, has not received updates in the past years. BioCyc, a large suite of databases for many species including *M. pneumoniae* (Karp et al., 2019), is only available behind a paywall after very few pages access whereas *MycoWiki* is freely accessible to the scientific community. Finally, PATRIC, the Pathosystems Resource Integration Center (Davis et al., 2020), has a strong focus on genes rather than proteins. Thus, we are confident that *MycoWiki* will become a valuable tool for the *Mycoplasma* research community.

Curation and community

To further enhance the information provided in MycoWiki, the *Mycoplasma* research community is invited to register and participate in the curation of the database. While access to the complete contents is free for everyone, only registered users are able to log in and contribute. The entries will be curated by the team behind MycoWiki to ensure continuous high quality of the information provided.

Future perspectives

With MycoWiki, we have released a new comprehensive model organism database for the minimal bacterium *M. pneumoniae*. It utilizes the popular framework of SubtiWiki to facilitate intuitive exploration of the available annotation. Particular focus is put on the interactions between different genes and proteins, which may support the scientific community in the development of novel research hypotheses. Customized categories are used to classify the functions and other qualities of genes and their products concisely. In addition, the inclusion of a homology analysis could help to infer the functional annotation of genes. AlphaFold structure predictions have been assigned for the proteins, allowing a visual representation even in cases where no experimentally determined structure exists. While the rendering of internal cross-links for these structures can give an idea about the quality of the prediction, interprotein cross-links could be integrated in the future to explore the interaction between proteins in more detail. We hope that MycoWiki will become a valuable tool for the *M. pneumoniae* research community, and in turn an asset to the ongoing systems and synthetic biology research. Moreover, the wealth of information provided in MycoWiki and the easy access to classes of proteins based on the categories will help in the further development of *M. pneumoniae* as a chassis to target therapeutical compounds.

For the family of databases that includes MycoWiki, SubtiWiki, and SynWiki, we will develop novel features including protein-RNA, RNA-RNA, and protein-metabolite interactions that will certainly enhance the value of the databases.

References

- Becker, A., Kannan, T. R., Taylor, A. B., Pakhomova, O. N., Zhang, Y., Somarajan, S. R., et al. (2015). Structure of CARDS toxin, a unique ADP-ribosylating and vacuolating cytotoxin from *Mycoplasma pneumoniae*. *Proc. Natl. Acad. Sci. U.S.A.* 112, 5165–5170. doi: 10.1073/pnas.1420308112
- Blötz, C., and Stülke, J. (2017). Glycerol metabolism and its implication in virulence in *Mycoplasma*. *FEMS Microbiol. Rev.* 41, 640–652.

Data availability statement

The original contributions presented in this study are included in the article/supplementary material, further inquiries can be directed to the corresponding author.

Author contributions

CE, BZ, and TP developed the framework of the database and integrated the data. BH performed initial work for the development of the structure viewer and integration of cross-link data. ML-S and LS provided data for the database. JS provided funding and supervised the development of the database. CE and JS wrote the manuscript. All authors read and approved the current submission.

Acknowledgments

We are grateful to Cedric Blötz and Ole Hinrichs for their help with the initial work on MycoWiki and to Marc Weber for the help with data collection.

Conflict of interest

ML-S was employed by Pulmobiotics Ltd., Spain.

The remaining authors declare that the research was conducted in the absence of any commercial or financial relationships that could be construed as a potential conflict of interest.

Publisher's note

All claims expressed in this article are solely those of the authors and do not necessarily represent those of their affiliated organizations, or those of the publisher, the editors and the reviewers. Any product that may be evaluated in this article, or claim that may be made by its manufacturer, is not guaranteed or endorsed by the publisher.

- Blötz, C., Singh, N., Dumke, R., and Stülke, J. (2020). Characterization of an immunoglobulin binding protein (IbpM) from *Mycoplasma pneumoniae*. *Front. Microbiol.* 11:685. doi: 10.3389/fmicb.2020.00685

- Burgos, R., Weber, M., Martinez, S., Lluch-Senar, M., and Serrano, L. (2020). Protein quality control and regulated proteolysis in the genome-reduced organism *Mycoplasma pneumoniae*. *Mol. Syst. Biol.* 16:e9530. doi: 10.15252/msb.20209530

- Burley, S. K., Berman, H. M., Bhikadiya, C., Bi, C., Chen, L., Costanzo, L. D., et al. (2019). Protein Data Bank: the single global archive for 3D macromolecular structure data. *Nucleic Acids Res.* 47, D520–D528.
- Dandekar, T., Huynen, M., Regula, J. T., Ueberle, B., Zimmermann, C. U., Andrade, M. A., et al. (2000). Re-annotating the *Mycoplasma pneumoniae* genome sequence: adding value, function and reading frames. *Nucleic Acids Res.* 28, 3278–3288. doi: 10.1093/nar/28.17.3278
- Davis, J. J., Wattam, A. R., Aziz, R. K., Brettin, T., Butler, R., Butler, R. M., et al. (2020). The PATRIC bioinformatics resource center: expanding data and analysis capabilities. *Nucleic Acids Res.* 48, D606–D612.
- Esposito, S., Argentiero, A., Gramegna, A., and Principi, N. (2021). *Mycoplasma pneumoniae*: a pathogen with unsolved therapeutic problems. *Expert. Opin. Pharmacother.* 22, 1193–1202. doi: 10.1080/14656566.2021.1882420
- Garrido, V., Piñero-Lambeck, C., Rodríguez-Arce, I., Paetzold, B., Ferrar, T., Weber, M., et al. (2021). Engineering a genome-reduced bacterium to eliminate *Staphylococcus aureus* biofilms *in vivo*. *Mol. Syst. Biol.* 17:e10145.
- Großhennig, S., Ischebeck, T., Gihardt, J., Busse, J., Feussner, I., and Stülke, J. (2016). Hydrogen sulfide is a novel potential virulence factor of *Mycoplasma pneumoniae*: characterization of the unusual cysteine desulfurase/desulphydrase HapE. *Mol. Microbiol.* 100, 42–54. doi: 10.1111/mmi.13300
- Güell, M., van Noort, V., Yus, E., Chen, W. H., Leigh-Bell, J., Michalodimitrak, K., et al. (2009). Transcriptome complexity in a genome-reduced bacterium. *Science* 326, 1268–1271. doi: 10.1126/science.1176951
- Kahraman, A., Malmström, L., and Aebersold, R. (2011). Xwalk: computing and visualizing distances in cross-linking experiments. *Bioinformatics* 27, 2163–2164. doi: 10.1093/bioinformatics/btr348
- Kannan, T. R., and Baseman, J. B. (2006). ADP-ribosylating and vacuolating cytotoxin of *Mycoplasma pneumoniae* represents unique virulence determinant among bacterial pathogens. *Proc. Natl. Acad. Sci. U.S.A.* 103, 6724–6729. doi: 10.1073/pnas.0510644103
- Karp, P. D., Billington, R., Caspi, R., Fulcher, C. A., Latendresse, M., Kothari, A., et al. (2019). The BioCyc collection of microbial genomes and metabolic pathways. *Brief Bioinf.* 20, 1085–1093.
- Kühner, S., van Noort, V., Betts, M. J., Leo-Macias, A., Batisse, C., Rode, M., et al. (2009). Proteome organization in a genome-reduced bacterium. *Science* 326, 1235–1240. doi: 10.1126/science.1176343
- Lluch-Senar, M., Delgado, J., Chen, W. H., Lloréns-Rico, V., O'Reilly, F. J., Wodke, J. A., et al. (2015). Unraveling the hidden universe of small proteins in bacterial genomes. *Mol. Syst. Biol.* 11:780. doi: 10.15252/msb.20188290
- Lluch-Senar, M., Luong, K., Lloréns-Rico, V., Delgado, J., Fang, G., Spittle, K., et al. (2013). Comprehensive methylome characterization of *Mycoplasma genitalium* and *Mycoplasma pneumoniae* at single-base resolution. *PLoS Genet.* 9:e1003191. doi: 10.1371/journal.pgen.1003191
- Maier, T., Schmidt, A., Güell, M., Kühner, S., Gavin, A. C., Aebersold, R., et al. (2011). Quantification of mRNA and protein and integration with protein turnover in a bacterium. *Mol. Syst. Biol.* 7:511. doi: 10.1038/msb.2011.38
- Meyer Sauteur, P. M., van Rossum, A. M., and Vink, C. (2014). *Mycoplasma pneumoniae* in children: carriage, pathogenesis, and antibiotic resistance. *Curr. Opin. Infect. Dis.* 27, 220–227. doi: 10.1097/QCO.0000000000000063
- Miravet-Verde, S., Ferrar, T., Espadas-García, G., Mazzolini, R., Gharrah, A., Sabido, E., et al. (2019). Defining a minimal cell: essentiality of small ORFs and ncRNAs in a genome-reduced bacterium. *Mol. Syst. Biol.* 15:e8290. doi: 10.15252/msb.20145558
- Montero-Blay, A., Piñero-Lambeck, C., Miravet-Verde, S., Lluch-Senar, M., and Serrano, L. (2020). Inferring active metabolic pathways from proteomics and essentiality data. *Cell Rep.* 31:107722. doi: 10.1016/j.celrep.2020.107722
- O'Reilly, F. J., Xue, L., Graziadei, A., Sinn, L., Lenz, S., Tegunov, D., et al. (2020). In-cell architecture of an actively transcribing-translating expressome. *Science* 369, 554–557. doi: 10.1126/science.abb3758
- Pedreira, T., Elfmann, C., and Stülke, J. (2022b). The current state of SubtiWiki, the database for the model organism *Bacillus subtilis*. *Nucleic Acids Res.* 50, D875–D882.
- Pedreira, T., Elfmann, C., Singh, N., and Stülke, J. (2022a). SynWiki: functional annotation of the first artificial organism *Mycoplasma mycoides* JCVI-syn3A. *Protein Sci.* 31, 54–62. doi: 10.1002/pro.4179
- Piñero-Lambeck, C., Ruano-Gallego, D., and Fernández, L. Á. (2015). Engineered bacteria as therapeutic agents. *Curr. Opin. Biotechnol.* 35, 94–102.
- Rose, A. S., and Hildebrand, P. W. (2015). NGL viewer: a web application for molecular visualization. *Nucleic Acids Res.* 43, W576–W579.
- Sayers, E. W., Bolton, E. E., Brister, J. R., Canese, K., Chan, J., Comeau, D. C., et al. (2022). Database resources of the national center for biotechnology information. *Nucleic Acids Res.* 50, D20–D26.
- Schmidl, S. R., Gronau, K., Pietack, N., Hecker, M., Becher, D., and Stülke, J. (2010). The phosphoproteome of the minimal bacterium *Mycoplasma pneumoniae*: analysis of the complete known Ser/Thr kinome suggests the existence of novel kinases. *Mol. Cell. Proteomics* 9, 1228–1242. doi: 10.1074/mcp.M900267-MCP200
- Schmidl, S. R., Otto, A., Lluch-Senar, M., Piñol, J., Busse, J., Becher, D., et al. (2011). A trigger enzyme in *Mycoplasma pneumoniae*: impact of the glycerophosphodiesterase GlpQ on virulence and gene expression. *PLoS Pathog.* 7:e1002263. doi: 10.1371/journal.ppat.1002263
- van Noort, V., Seebacher, J., Bader, S., Mohammed, S., Vonkova, I., Betts, M. J., et al. (2011). Cross-talk between phosphorylation and lysine acetylation in a genome-reduced bacterium. *Mol. Syst. Biol.* 8:571. doi: 10.1038/msb.2012.4
- Varadi, M., Anyango, S., Deshpande, M., Nair, S., Natassia, C., Yordanova, G., et al. (2022). AlphaFold protein structure database: massively expanding the structural coverage of protein-sequence space with high-accuracy models. *Nucleic Acids Res.* 50, D439–D444. doi: 10.1093/nar/gkab1061
- Waites, K. B., Xiao, L., Liu, Y., Balish, M. F., and Atkinson, T. P. (2017). *Mycoplasma pneumoniae* from the respiratory tract and beyond. *Clin. Microbiol. Rev.* 30, 747–809.
- Wodke, J. A., Alibés, A., Cozzuto, L., Hermoso, A., Yus, E., Lluch-Senar, M., et al. (2015). MyMpn: a database for the systems biology model organism *Mycoplasma pneumoniae*. *Nucleic Acids Res.* 43, D618–D623. doi: 10.1093/nar/gku1105
- Wodke, J. A., Puchalka, J., Lluch-Senar, M., Marcos, J., Yus, E., Godinho, M., et al. (2013). Dissecting the energy metabolism in *Mycoplasma pneumoniae* through genome-scale metabolic modeling. *Mol. Syst. Biol.* 9:653. doi: 10.1038/msb.2013.6
- Yus, E., Lloréns-Rico, V., Martínez, S., Gallo, C., Eilers, H., Blötz, C., et al. (2019). Determination of the gene regulatory network of a genome-reduced bacterium highlights alternative regulation independent of transcription factors. *Cell Syst.* 9, 143–158. doi: 10.1016/j.cels.2019.07.001
- Yus, E., Maier, T., Michalodimitrak, K., van Noort, V., Yamada, T., Chen, W. H., et al. (2009). Impact of genome reduction on metabolism and its regulation. *Science* 326, 1235–1240.



OPEN ACCESS

EDITED BY

Glenn Francis Browning,
The University of Melbourne, Australia

REVIEWED BY

Muhammad Suleman,
University of Veterinary and Animal
Sciences, Pakistan
Damián Lobato-Márquez,
University of London,
United Kingdom
Satoshi Gondaira,
Rakuno Gakuen University,
Japan

*CORRESPONDENCE

Bo Han
hanbo@cau.edu.cn

SPECIALTY SECTION

This article was submitted to
Infectious Agents and Disease,
a section of the journal
Frontiers in Microbiology

RECEIVED 04 May 2022

ACCEPTED 05 July 2022

PUBLISHED 26 July 2022

CITATION

Xu M, Liu Y, Mayinuer T, Lin Y, Wang Y,
Gao J, Wang D, Kastelic JP and
Han B (2022) *Mycoplasma bovis* inhibits
autophagy in bovine mammary epithelial
cells via a PTEN/PI3K-Akt-mTOR-
dependent pathway.
Front. Microbiol. 13:935547.
doi: 10.3389/fmicb.2022.935547

COPYRIGHT

© 2022 Xu, Liu, Mayinuer, Lin, Wang, Gao,
Wang, Kastelic and Han. This is an open-
access article distributed under the terms
of the [Creative Commons Attribution
License \(CC BY\)](https://creativecommons.org/licenses/by/4.0/). The use, distribution or
reproduction in other forums is permitted,
provided the original author(s) and the
copyright owner(s) are credited and that
the original publication in this journal is
cited, in accordance with accepted
academic practice. No use, distribution or
reproduction is permitted which does not
comply with these terms.

Mycoplasma bovis inhibits autophagy in bovine mammary epithelial cells via a PTEN/PI3K-Akt-mTOR-dependent pathway

Maolin Xu¹, Yang Liu¹, Tuerdi Mayinuer¹, Yushan Lin¹,
Yue Wang¹, Jian Gao¹, Dong Wang², John P. Kastelic³ and
Bo Han^{1*}

¹Department of Clinical Veterinary Medicine, College of Veterinary Medicine, China Agricultural University, Beijing, China, ²College of Life Science, Ningxia University, Yinchuan, China,

³Department of Production Animal Health, Faculty of Veterinary Medicine, University of Calgary, Calgary, AB, Canada

Although autophagy can eliminate some intracellular pathogens, others, e.g., *Staphylococcus aureus*, *Salmonella*, *Mycoplasma bovis*, can evade it. The phosphoinositide 3-kinase (PI3K)/protein kinase B (Akt)/mammalian target of rapamycin (mTOR) pathway, a key regulator of autophagy, is involved in initiation and promotion of a range of pathological diseases. As the effects of *M. bovis* on the autophagic pathway are not well documented, our objective was to elucidate the effects of *M. bovis* infection on the PI3K-Akt-mTOR cellular autophagic pathway in bovine mammary epithelial cells (bMECs). Ultrastructure of bMECs infected with *M. bovis* was assessed with transmission electron microscopy, co-localization of LC3 puncta with *M. bovis* was confirmed by laser confocal microscopy, and autophagy-related indicators were quantified with Western blotting and RT-PCR. In *M. bovis*-infected bMECs, intracellular *M. bovis* was encapsulated by membrane-like structures, the expression level of LC3-II and Beclin1 protein decreased at the middle stage of infection, degradation of SQSTM1/P62 was blocked, autophagy of bMECs was inhibited, and PI3K-Akt-mTOR protein was activated by phosphorylation. Furthermore, the tumor suppressor PTEN can inhibit the PI3K-Akt signaling pathway through dephosphorylation of phosphatidylinositol 3,4,5-trisphosphate and may be important for cellular resistance to infection. In the present study, the number of intracellular *M. bovis* was inversely related to the change in the level of autophagy markers (e.g., LC3-II, SQSTM1/P62) within host cells induced by the low knockdown of Akt or PTEN. We concluded that *M. bovis*-infected bMECs alleviated cellular autophagy through a PI3K-Akt-mTOR pathway, and that PTEN acted as a protective gene regulating autophagy, a key step in controlling infection.

KEYWORDS

Mycoplasma bovis, bovine mammary epithelial cells, autophagy, PI3K-Akt-mTOR pathway, PTEN

Introduction

Mycoplasma bovis is a devastating pathogen in dairy cows worldwide, causing pneumonia, arthritis, mastitis, and keratoconjunctivitis (Maunsell and Chase, 2019). Its control is complicated by increasing antimicrobial resistance and a lack of effective vaccines (Gautier-Bouchardon et al., 2014; Perez-Casal, 2020). Therefore, better understanding of *M. bovis* pathogenesis and immune evasion are needed for evidence-based control.

Autophagy is a lysosome-dependent and ubiquitous self-digestion process in eukaryotic cells (Kim et al., 2018). In addition, intracellular pathogens can be targets of selective autophagy (xenophagy) that recognizes, captures, and transports heterologous components to lysosomes for degradation to control infection (Mostowy, 2013). Microtubule-associated protein light chain 3 (Atg8/LC3) is the most widely monitored autophagy-related protein, the protein diffusely distributed in the cytoplasm, is linked to target substrates (Mizushima and Yoshimori, 2007). The SQSTM1/P62 protein serves as a link between LC3 and ubiquitinated substrates. SQSTM1 and SQSTM1-bound polyubiquitinated proteins become incorporated into the completed autophagosome and are degraded in autolysosomes, thus serving as a readout of autophagic degradation (Bjørkøy et al., 2005). BECN1/Atg6 and PIK3C3/VPS34 are essential partners in the autophagy interactome that signals the onset of autophagy, and many researchers use BECN1 as a way to monitor autophagy (Yang and Klionsky, 2010). However, some pathogens can evade degradation by autophagy or even inhibit autophagy (Choy and Roy, 2013; Huang and Brummell, 2014). For example, *M. bovis* can invade various host cells, including epithelial or immune cells (Josi et al., 2018; Liu et al., 2020). In addition, *Mycoplasma hyopneumoniae* infection can induce incomplete autophagy in host cells, which enhances its ability to multiply in host cells (Wang et al., 2021b). Furthermore, we reported *M. bovis* promoted replication by blocking its delivery to autophagosomes and lysosomes (Liu et al., 2021).

Several cell signaling pathways are linked to regulation of autophagy, including the phosphoinositide 3-kinase/protein kinase B (Akt)/mammalian target of rapamycin (PI3K-Akt-mTOR) signaling pathway. Furthermore, the first class of PI3Ks (PI3K-I) activates Akt and mTOR activity to inhibit cellular autophagy by triggering phosphorylation of Akt and mTOR (Farrell et al., 2013). Inhibition of the PI3K-Akt-mTOR signaling pathway can affect post-infection inflammatory, apoptotic, and autophagic responses, protecting host cells from various pathogens, including *Mycobacterium tuberculosis* (Lachmandas et al., 2016), *Legionella pneumophila* (Abshire et al., 2016), and *Listeria monocytogenes* (Gessain et al., 2015). In addition, *M. bovis* infection of dairy mammary tissue up-regulated the mRNA expression level of PI3K-Akt signaling pathway (Özdemir and Altun, 2020).

The phosphatase and tensin homolog deleted on chromosome ten (PTEN), a lipid phosphatase, inhibits the PI3K-Akt-mTOR signaling pathway, mainly through dephosphorylation of

phosphatidylinositol 3,4,5-trisphosphate; furthermore, expression of exogenous PTEN in PTEN mutant cells restores the normal pattern of PKB/Akt phosphorylation (Dempsey et al., 2021; He et al., 2021). A deficiency of PTEN hypersensitizes multiple cell types to *Mycoplasma* and *Mycobacterium bovis* infections and the lipid phosphatase activity of PTEN is required to attenuate infection (Huang et al., 2012). Thus, influencing cellular autophagy by modulating key autophagic signaling pathways is an important novel clearance strategy against intracellular pathogen invasion. However, effects of *Mycoplasma* infection on autophagy signaling pathways are not well understood.

The objective was to determine the role of PTEN/PI3K-Akt-mTOR signaling pathway in *M. bovis* infection, using an *in vitro* model with bovine mammary epithelial cells (bMECs). This is apparently the first report showing that *M. bovis* regulates cellular autophagy through the PTEN/PI3K-Akt-mTOR pathway.

Materials and methods

Statement of ethics

This study was conducted in accordance with ethical guidelines and standard biosecurity and institutional safety procedures of China Agricultural University (CAU; Beijing, China). Prior to the start of the study, ethical approval was granted by the Departmental Committee of the College of Veterinary Medicine, CAU.

Antibodies and reagents

Enhanced Cell Counting Kit-8 (CCK-8), Ad-GFP-LC3B, DiI (1,1'-dioctadecyl-3,3,3',3'-tetramethylindocarbocyanine perchlorate), Bicinchoninic acid (BCA) protein assay kit, and radioimmunoprecipitation assay (RIPA) lysis buffer (Beyotime Biotechnology) were all purchased from Beyotime (Shanghai, China). The pleuropneumonia-like organism (PPLO) broth was from BD Biosciences (San Jose, CA, United States), whereas Fetal Bovine Serum (FBS), Dulbecco's modification of Eagle's medium (DMEM) with high glucose and Opti-MEM were from Gibco (Grand Island, NY, United States). Horse serum was purchased from Hyclone (Logan, UT, United States). Penicillin G, amphotericin and bovine serum albumin (BSA) were from Coolaber (Beijing, China). Dimethyl sulfoxide (DMSO) was acquired from Sigma-Aldrich Chemical (Sigma, St. Louis, MO, United States). The pan-ErbB inhibitor CI-1033 was purchased from MedChemExpress (Monmouth Junction, NJ, United States). TransScriptFirst-Strand complementary DNA (cDNA) Synthesis SuperMix and SYBRGreen PCR Core Reagents were purchased from TransGenBiotech (Beijing, China). Trizol Reagent was bought from Invitrogen (Carlsbad, CA, United States). Small interfering RNA (siRNA) against the Akt, PTEN, negative-control siRNA, and siRNA-mate transfection reagent were all purchased from GenePharma (Shanghai, China). Polyvinylidene

difluoride membrane was from Millipore (Bedford, MA, United States). Glutaraldehyde, 2.5% (EM Grade), coverslips, and 4',6-Diamidino-2'-phenylindole dihydrochloride (DAPI) were all purchased from Solarbio (Beijing, China). An enhanced chemiluminescence (ECL) kit was obtained from Thermo Fisher Scientific Pierce (Rockford, IL, United States). Anti-PTEN antibody (Catalogue number: 22034-1-AP), anti-mTOR antibody (Catalogue number: 28273-1-AP), anti-Becn1 antibody (11306-1-AP), anti-Sequestosome 1 (SQSTM1/p62) antibody (Catalogue number: 18420-1-AP), anti- β -actin antibody (Catalogue number: 66009-1-Ig), anti-glyceraldehyde 3-phosphate dehydrogenase (GAPDH) antibody (Catalogue number: 60004-1-Ig), anti-mouse Ig G-horseradish peroxidase (HRP; Catalogue number: SA00001-1), and Goat anti-rabbit IgG (Catalogue number: SA00001-2) were all purchased from Proteintech (Chicago, IL, United States). Anti-LC3B antibody (#3868), anti-Akt antibody (#9272), Anti-p-PI3 Kinase p85 (Tyr458)/p55 (Tyr199; #17366), Anti-p-Akt (Ser473; #4060), Anti-p-mTOR (Ser2448; #5536) were from Cell Signaling Technology (Danvers, MA, United States).

Mycoplasma bovis strain and cell culture

M. bovis strain PG45 (ATCC 25523) was purchased from the ATCC. For infection experiments, *M. bovis* was cultured in PPLO broth with 20% horse serum and penicillin (100 IU/l) in 5% CO₂ at 37°C for 72 h. The PPLO broth was prepared by dissolving 10.5 g of Difco PPLO medium (BD Biosciences) and 1 g of yeast extract (BD Biosciences) in 400 ml ultrapure water, then autoclaving it at 121°C for 30 min. *M. bovis* was collected by centrifugation (6000 \times g for 15 min) and then washing with phosphate-buffered saline (PBS). The number of colony forming units was determined by performing 10-fold serial dilutions in PBS and subsequently spotting on PPLOA plates (Bürki et al., 2015), prepared by supplementing PPLO broth with 20% horse serum and 0.75% agar. Bacteria were suspended in PBS to a cell density of 10⁸ colony-forming units per milliliter (CFU/mL), and the suspension was stored at -70°C until use (Gondaira et al., 2021). A line of bovine mammary epithelial cells (bMECs; MAC-T; Shanghai Jingma Biological Technology Co., Ltd., Shanghai, China) was cultured in cell culture plates (Corning Inc., Corning, NY, United States) in DMEM supplemented with 10% FBS at 37°C with 5% CO₂. In all experiments, bMECs were allowed to grow and adhere for 24 h in culture medium prior to being infected with *M. bovis*. The bMECs were seeded at a concentration of 1 \times 10⁵ cells/mL in 6-well plates (2 ml per well) 24 h prior to experiments.

Cell infection and gentamicin protection assay

When bMECs cultured in a 6-well plate reached 60–70% confluence, the bMECs were inoculated (time = 0 h) with

M. bovis PG45 strain at a multiplicity of infection (MOI) of 1:30. After infection at 37°C for 1 h, the inoculum was removed and cells were washed twice with autoclaved PBS, 2 ml/well, to remove non-adherent *M. bovis*. Thereafter, all extracellular *M. bovis* was killed by adding 2 ml/well DMEM with 400 μ g/ml gentamicin for 2 h at 37°C (time = 2 h). Cells were again washed as described above. Finally, fresh DMEM with 10% fetal bovine serum (FBS) and 10 μ g/ml gentamicin was added to the infected cells, 2 ml/well (time = 1 h).

Enumerating intracellular *Mycoplasma bovis*

At designated time points, cells were washed 3 times with PBS after treatment, as described above, and CFU enumerated as described (Bürki et al., 2015). Cells were detached from plates with a 23-gauge needle and syringe, and bacterial concentrations confirmed by plating 10-fold serial dilutions (Bürki et al., 2015). To enumerate CFU, *M. bovis* in each cell well were counted, with six repeats on plates.

Transfection

Transfection with GFP-LC3B has been widely used to monitor autophagy or co-localization with cargo (Klionsky et al., 2021). Ad-GFP-LC3B, an adenovirus expressing GFP-LC3B fusion protein (Klionsky et al., 2021), was used, in accordance with manufacturer's instructions, to transfect bMECs. Briefly, bMECs were seeded on 6-well plates with coverslips, followed by incubation in 5% CO₂ at 37°C for 12 h. When bMECs density was 40–50% confluence, cells were infected with Ad-GFP-LC3B at MOI of 1:10 in DMEM containing 10% FBS. Then, cells were incubated in 5% CO₂ at 37°C for 24 h.

To knock down Akt and PTEN, specific small interfering RNA (siRNA) duplexes targeting the bovine Akt and PTEN gene and 2 siRNA negative controls were purchased from GenePharma (Shanghai, China). First, 2.5 nmol Akt and PTEN siRNA and control siRNA were dissolved in 125 μ l of DEPC water and stored at -70°C. Then, Akt and PTEN siRNA and control siRNA stock solution were diluted in Opti-MEM medium and diluted siRNA was added to siRNA-mate reagent and incubated for 10 min in Opti-MEM (2 μ l of Akt and PTEN siRNA and control siRNA, 200 μ l of Opti-MEM medium, and 4 μ l of siRNA-mate reagent). Cells were treated with an siRNA directed against Akt, PTEN and the scrambled control siRNA (final concentrations, 25 nM) using siRNA-mate reagent in Opti-MEM without serum, according to manufacturer's instructions. After 6 h, transfection medium was removed and 2 ml of DMEM supplemented with 10% FBS at 37°C with 5% CO₂ was added to recover cell growth for 48 h. Subsequently, cells were infected with *M. bovis*.

Induction of autophagy

Epidermal growth factor receptor (EGFR) is located on the cell surface and induces PI3K activation. To reduce PI3K signaling in bMECs without completely inhibiting intracellular PI3K function, we selected the pan-ErbB inhibitor Canertinib (CI-1033), a potent EGFR inhibitor, to treat cells prior to infection. The bMECs were inoculated into 6-well plates for 24 h. CI-1033 (1 μ M) was added to the culture medium and co-cultured for 1 h. Moreover, effects of CI-1033 on *M. bovis* viability were determined. Specifically, 1×10^6 CFU/ml *M. bovis* was incubated in PPLO medium with 20% horse serum, with or without CI-1033. The CFU of *M. bovis* was determined as described above, after incubation in 5% CO₂ at 37°C for 24 h. Effects of CI-1033 on viability of bMECs were evaluated with CCK-8 assays (Geng et al., 2020). Briefly, bMECs were seeded in 96-well plates (1×10^4 cells/well) in 100 μ l DMEM with 10% FBS. After incubation in 5% CO₂ at 37°C for 24 h, cells reached 60–70% confluence. Cells were treated with CI-1033 (1 μ M in DMEM with 10% FBS) or nothing (Control), followed by 24 h incubation in 5% CO₂ at 37°C. Then, fresh DMEM containing 10% CCK-8 was placed in the well, cells were incubated in 5% CO₂ at 37°C for 2 h and optical density was determined with a microplate reader (Bio-Rad, Hercules, CA, United States) at 450 nm. The density of treated cells relative to control cells was calculated.

Western blotting

At designated time points, cells were washed 3 times with PBS and total protein extracted with RIPA lysis buffer on ice. The liquid was centrifuged at $12,000 \times g$ for 20 min. Protein concentrations were determined with a BCA protein assay kit, according to manufacturer's instructions. For each sample, equal amounts of protein were separated by electrophoresis on 8 and 12% sodium dodecyl sulfate-polyacrylamide gels (SDS-PAGE). Subsequently, proteins were transferred onto a PolyVinylidene Fluoride (PVDF) using a semi-dry blotting system. Blots were first blocked with 5% skim milk in 0.1% Tris buffered saline-Tween-20 (TBST), pH 7.4 at room temperature for 2 h, followed by 3 washes in TBST for 10 min each. After blocking, membranes were incubated with specific primary antibodies overnight at 4°C. After 3 washes in TBST for 10 min each, membranes were probed with HRP-conjugated secondary antibody for 1 h at room temperature. Signals were detected using an ECL-Plus Western blot detection system and band density analyzed with ImageJ (National Institutes of Health, Bethesda, MD, United States).

RNA extraction, cDNA synthesis and real-time PCR

At the various time points indicated, bMECs were harvested with 1 ml TransZol Up lysis solution and total RNA was

extracted with a total RNA extraction kit (TransGen Biotech), according to manufacturer's instructions. The cDNA was synthesized using TransScript® II All-in-One First-Strand cDNA Synthesis SuperMix for qPCR (One-Step gDNA Removal; TransGen Biotech). To verify that the extracted RNA was free of DNA contamination, a control group without reverse transcriptase was set up while reverse transcribing the RNA samples into cDNA, which was detected by PCR amplification and 1% agarose gel electrophoresis to ensure the absence of DNA contamination. Both RNA and cDNA were quantified with a NanoDrop One spectrophotometer (Thermo Fisher Scientific, Waltham, MA, United States). For autophagy-associated genes, mRNA expression levels were verified with real time PCR, as follows: pre-denaturation at 94°C for 2 min, followed by 40 cycles of denaturation at 95°C for 5 s, and annealing at 60°C for 60 s using the Applied Biosystems StepOnePlus Real Time PCR system (Thermo Fisher Scientific). For melt curve analysis, PCR products were heated from 55 to 95°C, with the fluorescence signal assessed every 0.5°C to verify primer specificity. Cycle threshold (Ct) values were determined with StepOne™ Software version 2.3 (Thermo Fisher Scientific). In this study, $\Delta C_t = C_t \text{ target gene} - C_t \text{ endogenous control}$ (arithmetic mean of the reference gene), whereas $\Delta\Delta C_t = \Delta C_t \text{ sample} - \Delta C_t \text{ control}$ (uninfected cells). To visualize impacts of *M. bovis* on responses of target genes in bMECs, relative mRNA expression data were presented as $2^{-\Delta\Delta C_t}$. Real-time quantitative PCR was used to amplify 100 ng of cDNA using the following pairs of primers: cattle Akt upstream primer 5'-ggcacatcaagatcaccgac-3' and down-stream primer 5'-tcctggttgtagaaggcag-3' (NCBI Reference Sequence: NM_173986.2); cattle SQSTM1/P62 upstream primer 5'-tctgccctgactacgaccta-3' and down-stream primer 5'-cccaaagtgcctatgttca-3' (NCBI Reference Sequence: NM_176641.1); cattle LC3B upstream primer 5'-gtccgactatccgagagca-3' and down-stream primer 5'-tggacacactcaccatgcta-3' (NCBI Reference Sequence: NM_001001169.1); cattle Beclin1 upstream primer 5'-actggacacgagcttcaaga-3' and down-stream primer 5'-agatgcctccccaatcagag-3' (NCBI Reference Sequence: NM_001033627.2); cattle GAPDH upstream primer 5'-aaggccatcaccattctcca-3' and down-stream primer 5'-tcacgcccatcacaacatg-3' (NCBI Reference Sequence: NM_001034034.2). For these studies, GAPDH was the reference gene.

Transmission electron microscopy

The bMECs were removed with a cell scraper and centrifuged at $1000 \times g$ for 5 min. Cells were washed twice with PBS, fixed with 2.5% glutaraldehyde for ≥ 2 h, then fixed in 1% osmium tetroxide for 2 h at 4°C. After dehydration in a graded ethanol series, samples were embedded in epoxy resin-acetone mixtures for 2 h, followed by immersion in a pure resin solution overnight at 37°C. After polymerization, ultrathin sections (50 ~ 70 nm) were cut, stained with saturated uranyl

acetate in 50% ethanol and lead citrate, and examined with a transmission electron microscope (JEM-1400, JEOL, Tokyo, Japan).

Confocal laser microscopy inspection

To assess co-localization of autophagy-associated genes with intracellular *M. bovis*, LC3B and *M. bovis* were detected by confocal laser microscopy (Liu et al., 2021). *M. bovis* was collected by centrifugation ($6,000 \times g$, 15 min) washed with PBS, pre-stained with DiI cell membrane red fluorescent probe ($10 \mu\text{M}$) for 20 min, protected from light, centrifuged again at $6000 \times g$ for 15 min, washed 3 times with PBS, resuspended in DMEM, and then used to infect bMECs that had been pre-seeded in 6-well plates containing coverslips. Cells on coverslips were fixed with 4% paraformaldehyde for 15 min at room temperature, then washed 3 times with PBS. Finally, coverslips were stained with fluorescence mounting medium containing DAPI and mounted on glass slides. Images were captured with a Nikon A1 LFOV confocal microscope at laser wavelengths of 405, 561 and 488 nm. Pixel co-localization analysis of specific regions within cells was performed using Pearson's correlation coefficient using Image J software with JaCoP plug-in. Representative cells were selected and photographed. There were 20 cells per sample and at least 60 cells per group for statistical analysis.

Statistical analyses

All assays were repeated 3 times independently, unless otherwise stated. To calculate the p values, a one-way analysis of variance (ANOVA) with Dunnett's *post-hoc* test was used for Figures 1D–F, 2C–F, 3B, whereas a two-way ANOVA with Bonferroni posttest was used for Figures 4C,D, 5C,D, 6C,D. All statistical analyses were done with SPSS 26.0 software (IBM Corp., Armonk, NY, United States) and histograms produced with GraphPad Prism 8.0 (GraphPad Software, Inc., San Diego, CA, United States). Data were expressed as mean \pm standard deviation (SD) and $p < 0.05$ was considered significant. Significant differences were designated as follows: $^*p > 0.05$; $^*p < 0.05$; $^{**}p < 0.01$; and $^{***}p < 0.001$.

Results

Mycoplasma bovis infection increases the levels of autophagic markers in bMECs

To determine whether *M. bovis* infection affects cellular autophagy, transmission electron microscopy (TEM) was used to assess ultrastructure of bMECs infected with the *M. bovis* strain PG45. Numbers of autophagosome-like membrane vesicles were increased in the cytoplasm of *M. bovis*-infected bMECs (Figures 1Aa–c), with some *M. bovis* sequestered in these membrane vesicles (Figure 1Ad). In contrast, similar

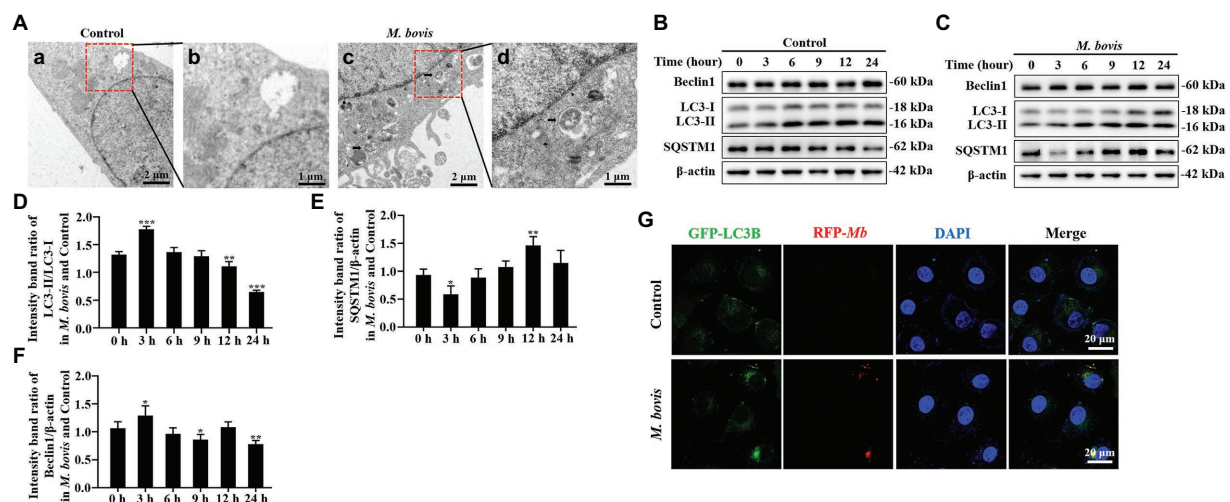


FIGURE 1

M. bovis infection induced autophagy in bMECs. (A) Ultra-microstructure observations of intracellular *M. bovis*, bMECs control (a) or *M. bovis* strain PG45 infected at an MOI of 30 for 3 h (c); the black arrow is an autophagosome-like membrane vesicle. Control and *M. bovis*-infected cells were fixed and processed for electron microscopy. Scale bars, 2 μm (a,c) and 1 μm (b,d). (B,C) bMECs were control or infected with *M. bovis* (MOI=30) for 0, 3, 6, 9, 12, and 24 h. At the end of the infection, expression levels of LC3, SQSTM1, Beclin1, ATG5, and β -actin (loading control) were analyzed by Western blotting with specific antibodies. (D–G) Relative quantification of LC3-II, SQSTM1, Beclin1, ATG5 protein levels compared to LC3-I or β -actin protein levels was determined by densitometry, and the ratio of *M. bovis* infected group to control group protein levels was calculated. (H) Ad-GFP-LC3B transfected bMECs for 24 h and then cells were infected with *M. bovis* (stained red with DiI, MOI=30). Cells were fixed and nuclei counterstained with DAPI prior to confocal laser microscopy. Scale bars: 20 μm . Data represent mean \pm SD of 3 independent experiments. $^*p < 0.05$; $^{**}p < 0.01$; $^{***}p < 0.001$.

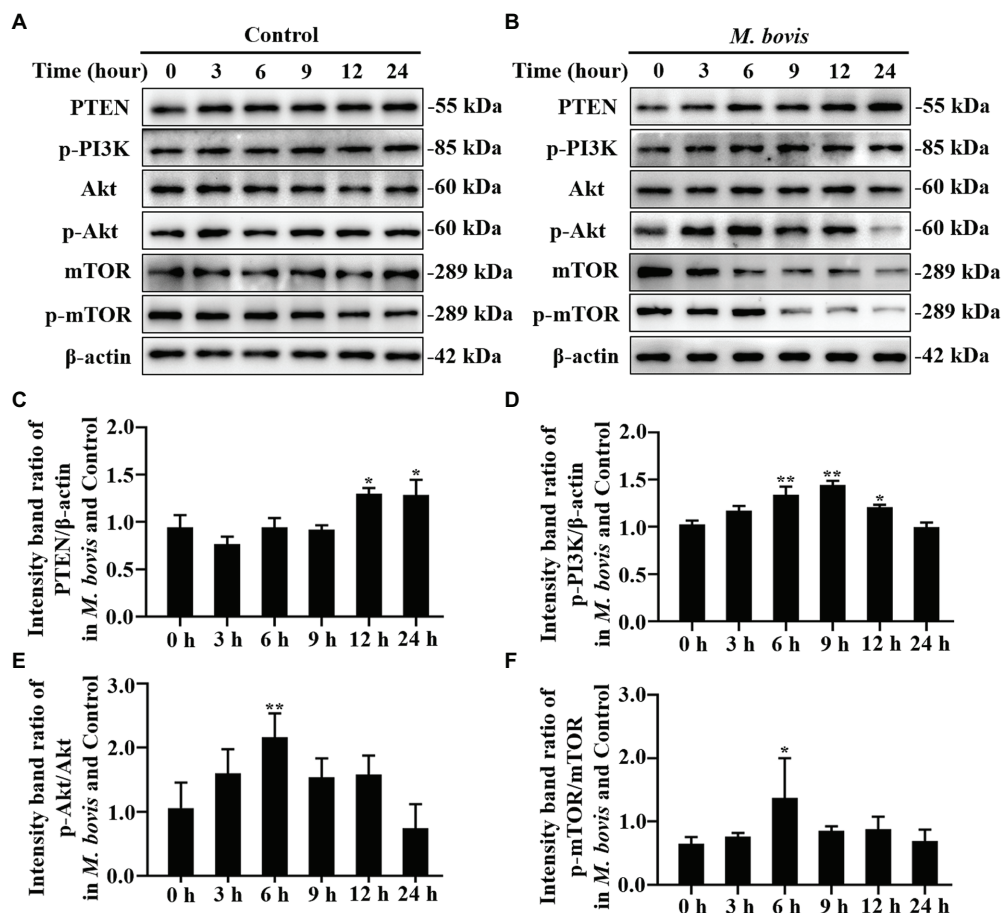


FIGURE 2

The role of PTEN/PI3K-Akt-mTOR pathway in *M. bovis* affecting autophagy in bMECs. (A,B) bMECs were control or infected with *M. bovis* (MOI=30). Cells were harvested at 0, 3, 6, 9, 12, and 24 h and then Western blotted with anti-PTEN, anti-p-PI3K, anti-p-mTOR, anti-mTOR, anti-p-Akt, anti-Akt, and anti- β -actin (loading control) antibodies. (C) PTEN protein levels relative to β -actin were determined by densitometry. (D) p-PI3K protein levels relative to β -actin were determined by densitometry. (E) p-mTOR levels relative to mTOR were determined by densitometry. (F) p-Akt levels relative to Akt were determined by densitometry. The ratio of *M. bovis* infected group to control group protein levels was calculated. Data represent the mean \pm SD of 3 independent experiments. * $p < 0.05$; ** $p < 0.01$.

vesicles were rarely seen in uninfected cells (Figure 1Aa). To further determine whether autophagy can be triggered by *M. bovis* infection, we next examined bMECs autophagy-associated protein LC3, SQSTM1/P62, Beclin1, ATG5 levels, important hallmarks of autophagy, using Western blotting analyses. LC3-II protein levels were increased at 3 h of *M. bovis* infection (Figures 1B–D). Levels of SQSTM1 protein were decreased in infected cells at 3 h (Figures 1B,C,E). Furthermore, Beclin1 was higher at 3 h (Figures 1B,C,F).

In addition, we further determined the localization relationship between the autophagosomal marker LC3B and *M. bovis* in bMECs by confocal laser microscopy. *M. bovis* infection significantly enhanced LC3B (green) punctate staining signals distributed throughout the entire cytoplasm (Figure 1G), whereas control bMECs exhibited a faint diffuse staining pattern and limited LC3B punctate accumulation. Moreover, *M. bovis* (stained red with DiI) signals in infected bMECs displayed punctate accumulation, and the *M. bovis* red

fluorescent punctate staining was highly co-localized with LC3B green fluorescent punctate staining. Thus, *M. bovis* infection was capable of causing autophagy in bMECs.

The role of PTEN/PI3K-Akt-mTOR pathway in *Mycoplasma bovis* inhibiting autophagy in bMECs

The PI3K, Akt and mTOR kinase-dependent signaling pathway controls autophagy. The PTEN protein, a phosphatase for the second messenger phosphatidylinositol 3,4,5-triphosphate, is required for activation of the Akt kinase in the PI3K-Akt pathway. Decreased SQSTM1 protein at 3 h was attributed to autophagic degradation, whereas gradually restored levels of SQSTM1 implied that the autophagy flux was blocked at 6 to 12 h (Figure 1E). Meanwhile, LC3-II and Beclin1 protein expression levels returned to normal at 6 h of infection (Figures 1D,F). To

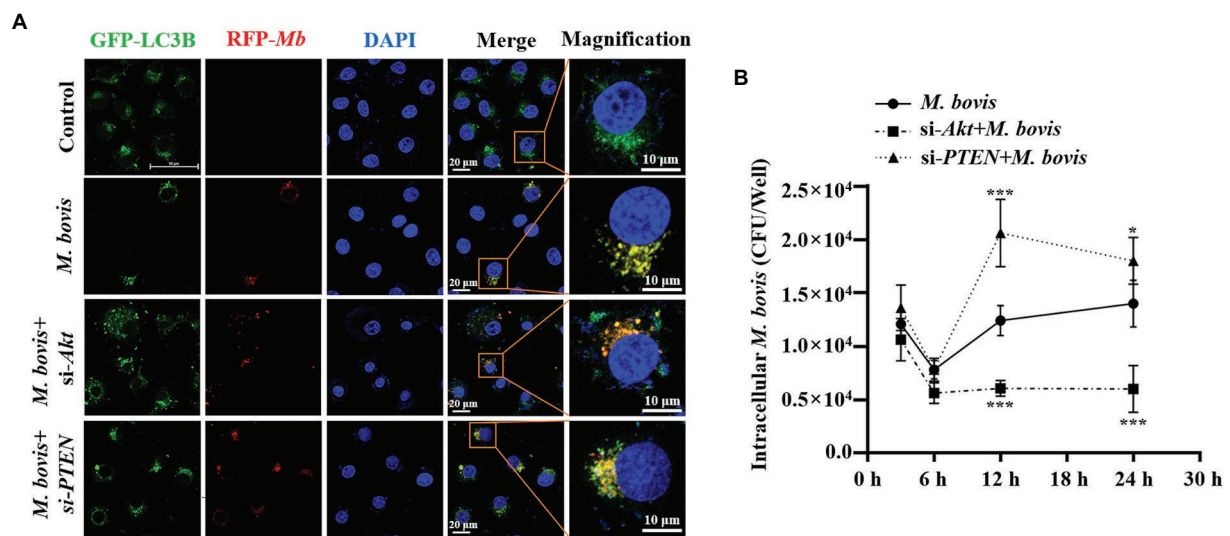


FIGURE 3

PTEN promoted autophagy of bMECs by inhibiting PI3K-Akt-mTOR pathway to suppress replication of *M. bovis*. (A) bMECs were transfected with siRNA-Akt (25 nM) and siRNA-PTEN (25 nM) for 48 h and then infected with *M. bovis* (MOI=30). Co-localization of LC3B (green) with *M. bovis* (red) was detected by confocal microscopy at 6 h post-infection. Cell nuclei were counterstained with DAPI. Scale bar: 10 and 20 μ m. (B) Comparison of intracellular replication of *M. bovis* in bMECs with downregulated Akt or PTEN status. bMECs were transfected with siRNA-Akt (25 nM) and siRNA-PTEN (25 nM) for 48 h and then infected with *M. bovis* (MOI=30); the intracellular *M. bovis* load was measured at 3, 6, 12, and 24 h postinfection. Data represent mean \pm SD of 3 independent experiments. * p <0.05; *** p <0.001.

determine whether PTEN/PI3K-Akt-mTOR modulated autophagy upon *M. bovis* infection, the PTEN, PI3K, Akt and mTOR activity in host cells were determined. Compared to control bMECs, PI3K, Akt and mTOR phosphorylation in *M. bovis*-infected bMECs was increased at 6 h (Figures 2A,B,D-F). However, PTEN did not remain increased at 0 to 9 h (Figures 2A-C). Therefore, *M. bovis* inhibited autophagy in bMECs by activating the PI3K-Akt-mTOR signaling pathway.

Phosphorylation of Akt is positively related to the inhibition of autophagy by *Mycoplasma bovis*

The association between PI3K basal activity and *M. bovis* inhibition of autophagy by modulating PI3K-dependent signaling in bMECs and effects of *M. bovis* infection of bMECs on autophagy were investigated. To decrease PI3K signaling in bMECs without irreversibly inhibiting Akt phosphorylation, before infection, cells were treated with the pan-ErbB inhibitor CI-1033. Based on the CCK-8 assay, CI-1033 did not reduce bMECs viability (Figure 4A). Furthermore, CI-1033 decreased the amount of p-Akt without significantly affecting the total amount of Akt, indicating that CI-1033 specifically inhibited Akt phosphorylation and thereby PI3K signaling in bMECs. In CI-1033 pretreated bMECs, LC3-II protein expression was significantly increased, SQSTM1 protein expression was significantly decreased, and cellular autophagy was activated (Figures 4B,C). When protein expression levels of bMECs pretreated with *M. bovis* infection CI-1033 were measured, p-Akt protein expression was re-elevated and p-Akt was

re-activated, whereas LC3-II protein expression levels were significantly decreased and SQSTM1 protein expression levels were significantly increased (Figures 4B,C). The relative mRNA expression levels of Akt and autophagy-related genes were detected by real-time PCR; there was no significant difference between groups in the mRNA expression levels of Akt. In addition, SQSTM1 mRNA levels were significantly lower in the *M. bovis* infection CI-1033 pretreatment group compared to the CI-1033 alone treatment group (Figure 4D). Therefore, after reducing PI3K signaling without completely inhibiting PI3K function, *M. bovis* infection activated phosphorylation of Akt and inhibited autophagy of bMECs.

Inhibition of Akt with specific siRNAs targeting Akt reverses the inhibition of autophagy in bMECs by *Mycoplasma bovis*

To further verify impacts of Akt on *M. bovis*-inhibit bMECs autophagy, bMECs were transfected for 48 h with small interfering (siRNA)-control (NC) or siRNA-Akt. After transfection with siRNA-Akt-1, siRNA-Akt-2 and siRNA-Akt-3, protein levels of Akt were significantly decreased compared to control and NC-transfected cells, indicating that expression of the Akt proteins was successfully inhibited. Furthermore, as siRNA-Akt-1 had the highest inhibitory efficiency for Akt among the 3 siRNA-Akt groups (Figure 5A), it was used to inhibit Akt expression (designated siRNA-Akt).

Based on Western blotting, in bMECs infected with *M. bovis* after siRNA-Akt transfection, downregulation of Akt by siRNA markedly suppressed *M. bovis*-induced activation of

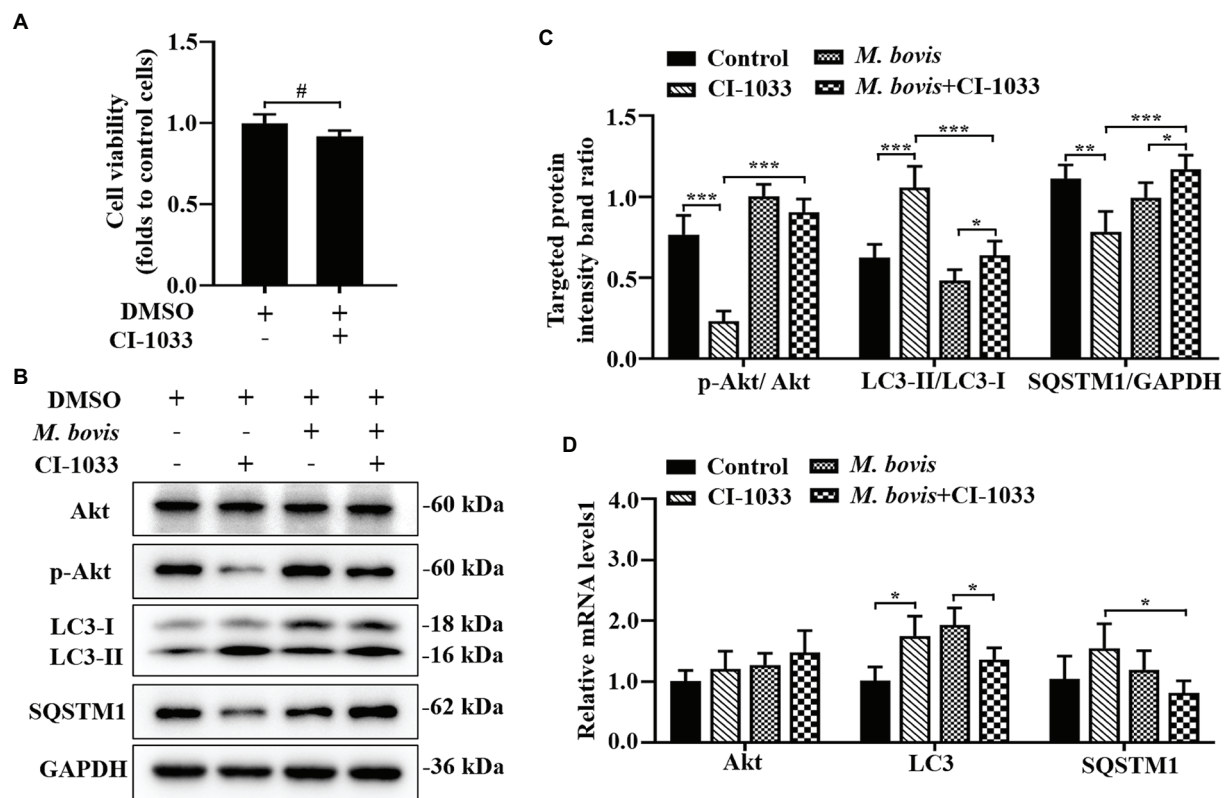


FIGURE 4

Phosphorylation of Akt was positively related to inhibition of autophagy by *M. bovis*. (A) Effects of CI-1033 on viability of bMECs in DMEM medium containing 10% FBS based on CCK-8 assays. (B) Cells were pre-treated with CI-1033 (1 μ M) for 1 h and then control with DMSO, and cells infected with *M. bovis* (MOI=30) were further cultured for 6 h. Thereafter, cell samples were analyzed by Western blotting with anti-Akt, anti-p-Akt, anti-LC3, anti-SQSTM1, and anti-GAPDH (loading control) antibodies. (C) Relative quantification of p-Akt protein levels compared to Akt protein, LC3-II protein levels compared to LC3-I protein, and SQSTM1 protein levels compared to GAPDH protein was determined by densitometry in *M. bovis*-infected bMECs in the absence or presence of CI-1033. (D) Transcriptional levels of PI3K-Akt-mTOR signaling pathway and autophagy-related genes including Akt, LC3-II and SQSTM1, were detected by real-time PCR in bMECs. The data represent the mean \pm SD of 3 independent experiments. * p <0.05; ** p <0.01; *** p <0.001.

p-Akt. Meanwhile, expression levels of Beclin1 and LC3-II proteins were elevated, and the expression level of SQSTM1 protein was decreased (Figures 5B,C). The relative mRNA expression levels of Akt and autophagy-related genes were detected by real-time PCR; siRNA-Akt transfection down-regulated the mRNA expression level of Akt. Meanwhile, bMECs after *M. bovis* infection with siRNA-Akt knockdown had LC3, Beclin1 and SQSTM1 mRNA levels significantly upregulated compared to the *M. bovis*-infected group. (Figure 5D). Therefore, downregulation of Akt expression with siRNA targeting activated autophagy in bMECs and this activation was not reversed by bovine mycoplasma infection.

Absence of PTEN expression exacerbates the inhibition of autophagy of bMECs by *Mycoplasma bovis*

To determine effects of activation of the PI3K-Akt-mTOR signaling pathway on autophagy in *M. bovis*-infected bMECs,

we knocked down PTEN, a phosphatase that dephosphorylates PIP3 into PIP2, to ensure steady PI3K signaling. The bMECs were transfected for 48 h with small interfering (siRNA)-control (NC), siRNA-PTEN-1, siRNA-PTEN-2 and siRNA-PTEN-3, and PTEN depletion assessed by Western blotting. As siRNA-PTEN-1 had the highest inhibitory efficiency for PTEN (Figure 6A), it was used to inhibit PTEN (designated siRNA-PTEN). Based on Western blotting, siRNA-PTEN strongly increased p-Akt, indicating that PI3K signaling is activated under conditions of PTEN knocked down. After downregulation of PTEN with siRNA, *M. bovis* infection significantly increased *M. bovis*-induced activation of p-Akt. Furthermore, expression of Beclin1 and LC3-II proteins decreased, but expression of SQSTM1 protein also decreased compared to the control group (Figures 6B,C). Based on real-time PCR, loss of PTEN inhibited transcription of autophagy-related genes (e.g., Beclin1, LC3-II) to varying degrees. However, only Beclin1 mRNA levels were down-regulated, whereas LC3 mRNA levels were up-regulated and SQSTM1 mRNA levels were not significantly changed after *M. bovis* infection with bMECs knockdown by siRNA-PTEN compared to the *M. bovis*-infected

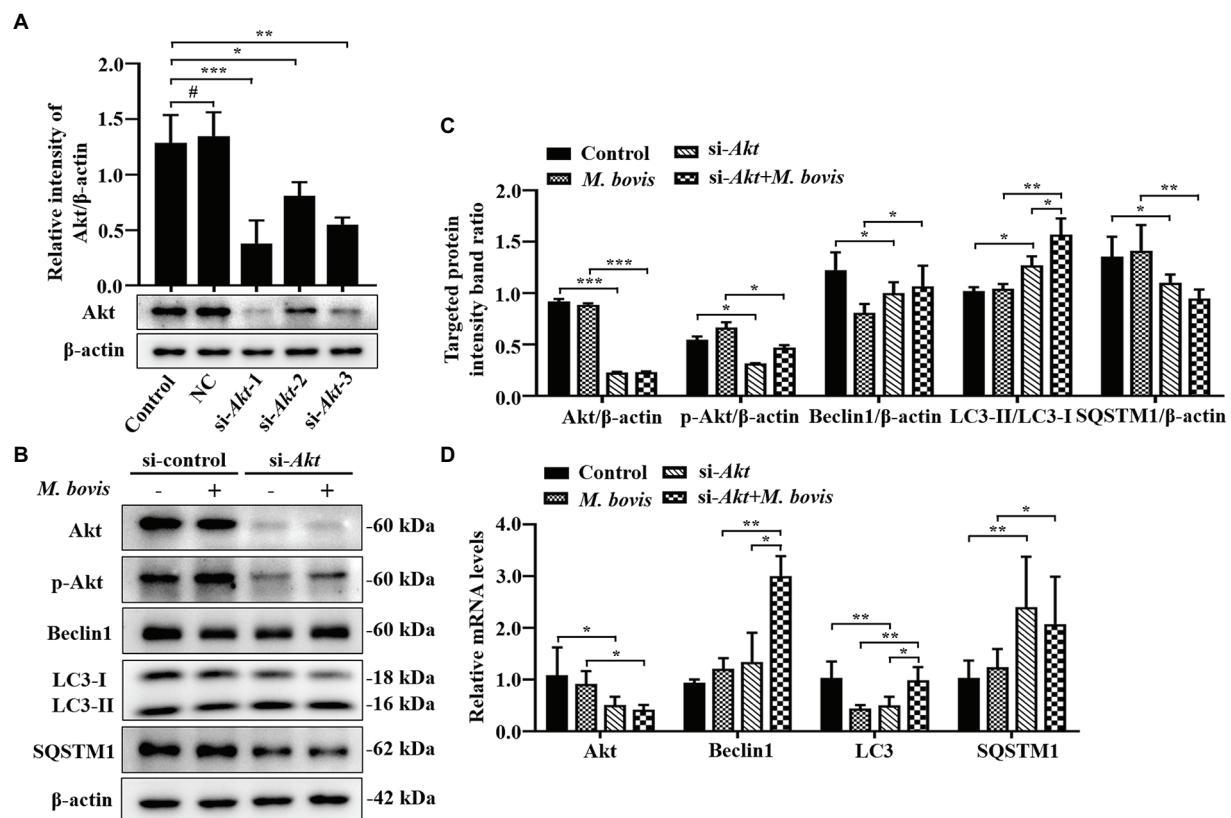


FIGURE 5

Inhibition of Akt with specific siRNAs targeting Akt reversed inhibition of autophagy in bMECs by *M. bovis*. (A) bMECs were transfected with siRNA-control (NC; 25 nM) and siRNA-Akt-1/2/3 (25 nM) for 48 h. Akt protein expression were analyzed by Western blotting. (B) bMECs were transfected with siRNA-Akt-1 targeting Akt for 48 h; then, cells were infected with *M. bovis* (MOI=30) for 6 h. Thereafter, cell samples were analyzed by Western blotting with anti-Akt, anti-p-Akt, anti-LC3, anti-SQSTM1, and anti-β-actin (loading control) antibodies. (C) Relative quantification of target protein levels compared to β-actin protein was determined by densitometry in transfected siRNA-Akt-1 cells. (D) Transcriptional levels of PI3K-Akt-mTOR signaling pathway and autophagy-related genes including Akt, LC3-II and SQSTM1, were detected by real-time PCR in bMECs. Data represent mean±SD of 3 independent experiments. * $p > 0.05$; * $p < 0.05$; ** $p < 0.01$; *** $p < 0.001$.

group (Figure 6D). Therefore, downregulation of PTEN expression exacerbated the inhibition of autophagy in bMECs by bovine mycoplasma infection.

PTEN promotes autophagy of bMECs by inhibiting PI3K-Akt-mTOR pathway to suppress replication of *Mycoplasma bovis*

To explore effects of PI3K-Akt-mTOR signaling pathway activation on *M. bovis* survival in bMECs, co-localization of LC3 and *M. bovis* were assessed by confocal laser microscopy and intracellular *M. bovis* enumerated. We used siRNA-Akt and siRNA-PTEN to knock down expression of Akt and PTEN in bMECs. After transfection with siRNA-Akt and siRNA-PTEN for 48 h, bMECs were infected with *M. bovis*, there was co-localization of LC3B and *M. bovis* in bMECs; furthermore, co-localization of LC3B and *M. bovis* increased after downregulating Akt expression (Figure 3A). In contrast, co-localization of LC3B and *M. bovis* was decreased after downregulating PTEN expression (Figure 3A).

Subsequently, intracellular proliferation of *M. bovis* was detected at 3, 6, 12, and 24 h post-infection. Intracellular *M. bovis* was significantly decreased at 12 and 24 h post-infection in the siRNA-Akt group relative to the *M. bovis* infection group (Figure 3B). However, there were considerably more *M. bovis* in the siRNA-PTEN group at 12 and 24 h post-infection (Figure 3B). Taken together, our results indicated a causal relationship between the Akt and PTEN status of bMECs and their permissiveness to intracellular pathogens.

Discussion

Autophagy, a common non-selective self-digestion process in cells (Riebischt et al., 2021), is also a highly selective defense against intracellular pathogens (Mostoway, 2013). However, various pathogenic microorganisms have evolved to evade and utilize cellular autophagy (Choy and Roy, 2013; Huang and Brumell, 2014). For example, *M. bovis* inhibited phagosomal-lysosomal maturation to evade cellular autophagy (Liu et al., 2021). In the present study,

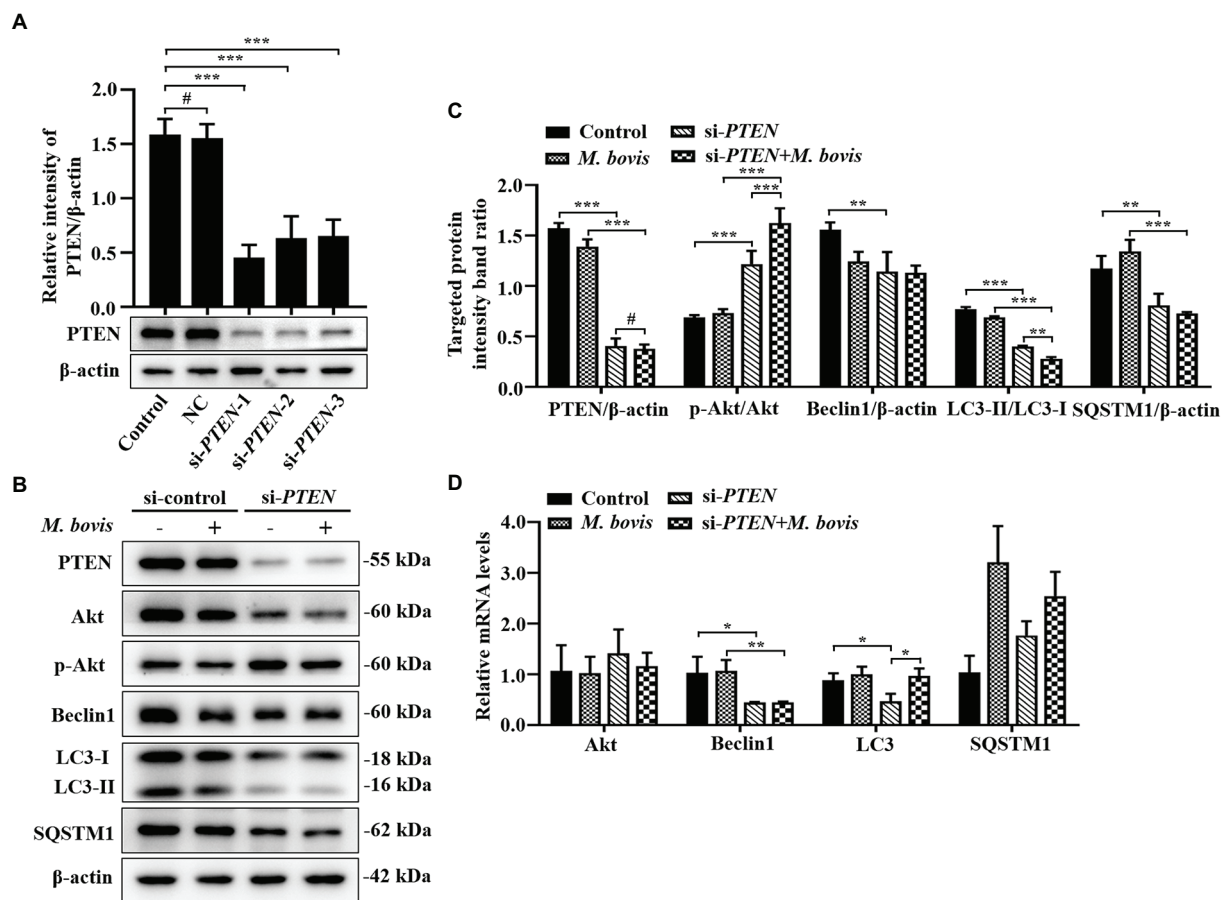


FIGURE 6

Absence of PTEN expression exacerbated inhibition of autophagy of bMECs by *M. bovis*. (A) bMECs were transfected with siRNA-control (NC; 25 nM) and siRNA-PTEN-1/2/3 (25 nM) for 48 h. PTEN protein expression was analyzed by Western blotting. (B) bMECs were transfected with siRNA-PTEN-1 targeting PTEN for 48 h; then, cells were infected with *M. bovis* (MOI=30) for 6 h. Thereafter, cell samples were analyzed by Western blotting with anti-PTEN, anti-Akt, anti-p-Akt, anti-Beclin1, anti-LC3, and anti-β-actin (loading control) antibodies. (C) Relative quantification of target protein levels compared to β-actin protein was determined by densitometry in transfected siRNA-PTEN-1 cells. (D) Transcriptional levels of PI3K-Akt-mTOR signaling pathway and autophagy-related genes including Akt, Beclin1 and LC3-II, were detected by real-time PCR in bMECs. Data represent the mean±SD of 3 independent experiments. * $p > 0.05$; * $p < 0.05$; ** $p < 0.01$; *** $p < 0.001$.

M. bovis activated the early autophagic response in bMECs and inhibited autophagy by activating the PI3K-Akt-mTOR signaling pathway at later stages of infection, whereas downregulation of PTEN gene expression promoted replication of *M. bovis* in bMECs.

We established an *in vitro* autophagy model of *M. bovis* infection with bMECs, based on the ability of *M. bovis* to invade a variety of cells, including lymphocytes and epithelial cells (van der Merwe et al., 2010; Liu et al., 2021). It is noteworthy that *M. bovis* invades cells, evades cellular immunity and the killing effect of some antibiotics, promoting persistent infections and transmission (Bürki et al., 2015). There is accumulating evidence that *Mycoplasma* infection is closely associated with autophagy (Lu et al., 2017; Luo et al., 2020; Liu et al., 2021). In the present study, membrane-like material was wrapped around *M. bovis*, perhaps due to fusion of *M. bovis* with autophagic vesicles, consistent with previous findings of autophagy targeting *M. bovis* (Liu et al., 2021). In addition, upregulated expression of LC3-II,

Beclin1 proteins and reduced expression of SQSTM1 protein (LC3-II, Beclin1, and SQSTM1 are the most widely recognized molecular indicators of autophagy) during the early stages of *M. bovis* infection with bMECs. Our findings were consistent with a report that both *Mycoplasma ovipneumoniae* and *Mycoplasma bovis* infections altered expression levels of proteins critical for cellular autophagy (Luo et al., 2020; Liu et al., 2021). *Staphylococcus aureus* infection upregulated LC3-II expression and GFP-LC3B clustered around intracellular bacteria (Geng et al., 2020). In this study, GFP-LC3B was co-localized with *M. bovis* and LC3-II expression was upregulated. Autophagy is an important player in cellular protection against pathogenic infection (Deretic, 2021). Therefore, in the present study, *M. bovis*-invading cells successfully induced autophagy in bMECs at an early stage. However, from 6 h of *M. bovis* infection, LC3-II and Beclin1 protein expression in bMECs was reduced. Thereafter, SQSTM1 protein levels gradually recovered, indicating

that degradation of SQSTM1 protein was inhibited. Under normal circumstances, SQSTM1 is a link between LC3 and substrates, with SQSTM1 and SQSTM1-bound substrates incorporated into the completed autophagosome during the initial stage and subsequently degraded in autolysosomes (Hua et al., 2015). Therefore, autophagy was inhibited in mid and late stages of *M. bovis* infection, consistent with inhibition of cellular autophagy by *M. bovis* (Liu et al., 2021).

Despite the key role of autophagy to control pathogens, the latter have also adopted many defense mechanisms to defend against and exploit cellular autophagy (Choy and Roy, 2013; Huang and Brumell, 2014; Li et al., 2015; Sudhakar et al., 2019). However, molecular mechanisms by which *M. bovis* evades cellular autophagy are largely unknown. Phosphatidylinositol 3-kinases (PI3Ks) have key roles in regulation of autophagy. PtdIns (3,4,5) P₃, the product of class I PI3Ks, trigger the mTOR signalling pathway, which inhibits autophagy (Farrell et al., 2013). In addition, mTOR, a highly conserved kinase in the phosphatidylinositol 3-kinase family with serine/threonine activity, responds rapidly to various environmental cues and regulates cellular metabolism and immune responses by modulating the kinase Akt (Cobbold, 2013). Activation of the PI3K-Akt-mTOR signaling pathway inhibits the autophagy required for development and survival of nutrient deprivation (Zhao et al., 2019). In the present study, PI3K-Akt-mTOR was activated by phosphorylation in the middle phase of *M. bovis* infection. Invasion of *M. tuberculosis* also initiated the PI3K-Akt-mTOR signaling pathway (Lachmandas et al., 2016). Furthermore, inhibition of autophagy by *M. bovis* in bMECs requires phosphorylation activation of Akt. Treatment of bMECs with pan-ErbB inhibitor CI-1033 inhibited Akt phosphorylation and also inhibited the autophagic activity of bMECs. It was surprising that Akt was activated by rephosphorylation and autophagy was subsequently inhibited when *M. bovis* infected bMECs. Furthermore, following downregulation of Akt expression by small interfering RNA, the autophagic flux of bMECs was increased and cellular autophagy was activated, and this activation of autophagy was not inhibited by *M. bovis* infection. *Streptococcus agalactiae* infection may inhibit PI3K-Akt-mTOR signaling, thereby affecting the autophagic response (Qi et al., 2022). Furthermore, Akt also has an important role in mediating infection of epithelial cells and macrophages by *Salmonella* (Reggio et al., 2020). Several hypotheses have been proposed to explain the mechanism by which Akt promotes bacterial intracellular proliferation or survival, including the idea that by accelerating the recycling of the RAB14 small G protein, Akt delays phagosome-lysosome fusion and thus may enhance bacterial intracellular survival (Kehl et al., 2020). Therefore, we inferred that *M. bovis* inhibited bMECs autophagy and promoted intracellular survival of bMECs through activation of the PI3K-Akt-mTOR signaling pathway.

Activation of PI3K-Akt-mTOR phosphorylation was regulated by multiple upstream proteins, with the tumor suppressor PTEN protein required for activation of Akt/PKB

kinase in the PI3K-Akt pathway (Dempsey et al., 2021; He et al., 2021). PTEN is a second messenger phosphatidylinositol 3,4,5-trisphosphate phosphatase that catalyzed conversion of PIP₃ to PIP₂ through its acidase activity, thereby regulating activity of Akt and mTOR (Chia et al., 2015). Competent PTEN protein is apparently not only critical for tumor suppression but also for resisting infection of mammalian cells by *Mycobacterium bovis* Bacillus Calmette-Guérin (BCG) and *Mycoplasma*, 2 pathogens with distinct pathogenic strategies (Huang et al., 2012). However, whether the presence of PTEN genes affects the regulation of PI3K-Akt-mTOR by *M. bovis* and thus alters the autophagic state of bMECs, is unclear. In the present study, small interfering RNAs downregulated PTEN expression and Akt phosphorylation was maintained, which in turn inhibited autophagy of bMECs, whereas the co-localization between GFP-LC3B and *M. bovis* was reduced, consistent with the findings of Wang et al. (2021a). However, the decreased SQSTM1 protein may be attributed to inhibition of SQSTM1 protein production by Akt phosphorylation. To confirm effects of downregulation of PTEN and inhibition of PI3K-Akt-mTOR signaling pathway on intracellular *M. bovis*, bMECs were treated with small interfering RNA PTEN or small interfering RNA Akt; the intracellular number of *M. bovis* was related to the level of autophagy in the host cells induced by downregulation of PTEN or disruption of Akt signaling was inversely related to changes in the level of autophagy in host cells caused by downregulation of PTEN or disruption of Akt signaling, consistent with previous reports for *Mycoplasma bovis* (Liu et al., 2021). Furthermore, downregulation of the PTEN gene increased intracellular *M. bovis* replication, consistent with previous reports that downregulation of PTEN gene exacerbated *Mycobacterium bovis* Bacillus Calmette-Guérin (BCG) and *Mycoplasma* infection and proliferation (Huang et al., 2012). Therefore, we inferred that PTEN promoted autophagy during *M. bovis* infection of bMECs by inhibiting the PI3K-Akt-mTOR pathway to suppress survival and replication of *M. bovis*.

Although important discoveries were revealed by these studies, there are still limitations. In this study, only *in vitro* models were used to assess effects of intracellular *M. bovis* on autophagy and autophagic signaling pathways. However, it is well known that various cellular interactions *in vivo* give rise to more complex mechanisms.

Conclusion

M. bovis infection activated the PI3K-Akt-mTOR signaling pathway, inhibited autophagy of bMECs, and promoted their survival and replication, whereas PTEN has an important role in cellular autophagy caused by *M. bovis* infection (Figure 7). These findings provided new insights into molecular mechanisms enabling *M. bovis* to evade cellular autophagy. Perhaps targeted regulators of autophagy will be developed to better understand intracellular pathogens, with potential to increase vaccine efficacy.

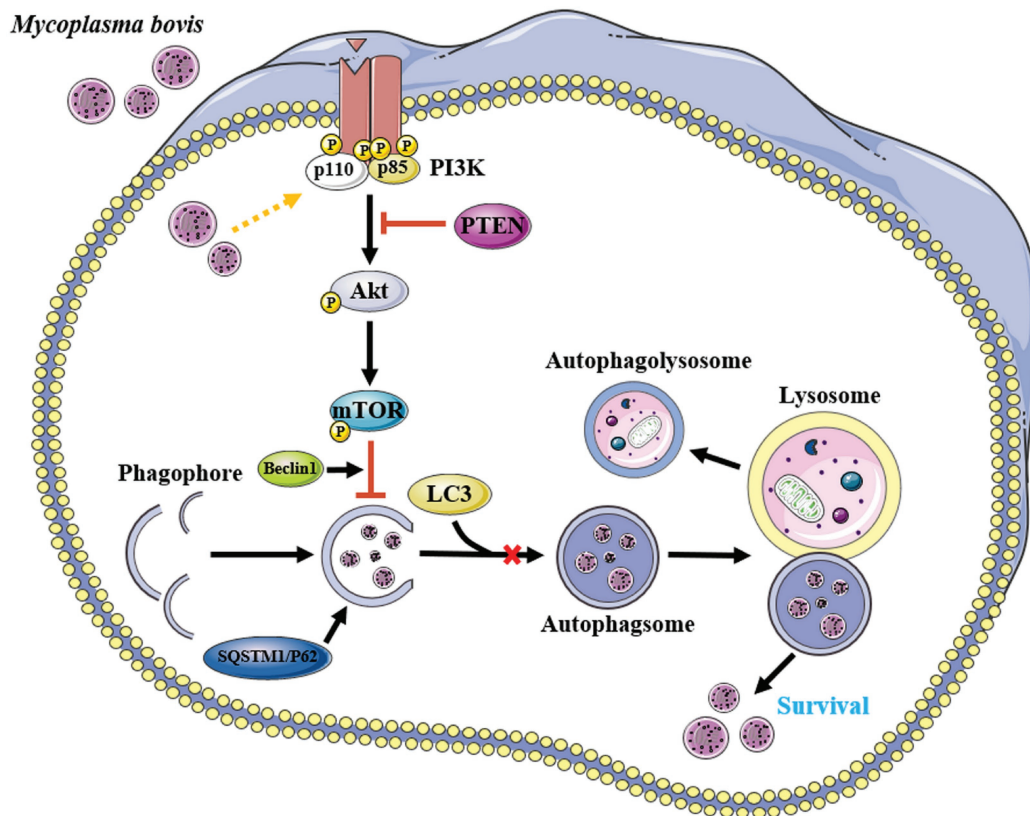


FIGURE 7

Proposed model for inhibition of autophagy by *M. bovis* via the PTEN/PI3K-Akt-mTOR pathway. Infection of invading bMECs by *M. bovis* activated phosphorylation of Akt and inhibited the onset of downstream autophagic activity, preventing autophagosomes from delivering engulfed *M. bovis* to lysosomes for degradation, thereby enabling *M. bovis* to survive. Yellow arrow and red bar indicate stimulation and inhibition, respectively. This figure was partially made using Servier Medical Art (smart.servier.com).

Data availability statement

The original contributions presented in the study are included in the article/supplementary material, further inquiries can be directed to the corresponding author.

Author contributions

BH and MX conceived and designed the experiment. MX, YLu, TM, YLn, YW, JG, and DW performed the research and wrote the manuscript. JK and TM assisted in the analyses and re-edited the manuscript. JK and BH revised the manuscript. All authors contributed to the article and approved the submitted version.

Funding

This study was supported financially by the National Natural Science Foundation of China (Nos. 32172928 and

31760751), Ningxia Key R&D Project (No. 2019BBF02027), the High-End Foreign Experts Recruitment Program (No. GDT20171100013), and the Natural Science Foundation of Ningxia (No. 2022AAC02022).

Conflict of interest

The authors declare that the research was conducted in the absence of any commercial or financial relationships that could be construed as a potential conflict of interest.

Publisher's note

All claims expressed in this article are solely those of the authors and do not necessarily represent those of their affiliated organizations, or those of the publisher, the editors and the reviewers. Any product that may be evaluated in this article, or claim that may be made by its manufacturer, is not guaranteed or endorsed by the publisher.

References

- Abshire, C. F., Dragoi, A. M., Roy, C. R., and Ivanov, S. S. (2016). mTOR-driven metabolic reprogramming regulates *Legionella pneumophila* intracellular niche homeostasis. *PLoS Pathog.* 12:e1006088. doi: 10.1371/journal.ppat.1006088
- Bjorkøy, G., Lamark, T., Brech, A., Outzen, H., Perander, M., Overvatn, A., et al. (2005). p62/SQSTM1 forms protein aggregates degraded by autophagy and has a protective effect on huntingtin-induced cell death. *The J Cell Biol.* 171, 603–614. doi: 10.1083/jcb.200507002
- Bürki, S., Gaschen, V., Stoffel, M. H., Stojilkovic, A., Frey, J., Kuehni-Boghenbor, K., et al. (2015). Invasion and persistence of *Mycoplasma bovis* in embryonic calf turbinates. *Vet. Res.* 46:53. doi: 10.1186/s13567-015-0194-z
- Chia, Y. C., Catimel, B., Lio, D. S., Ang, C. S., Peng, B., Wu, H., et al. (2015). The C-terminal tail inhibitory phosphorylation sites of PTEN regulate its intrinsic catalytic activity and the kinetics of its binding to phosphatidylinositol-4,5-bisphosphate. *Arch. Biochem. Biophys.* 587, 48–60. doi: 10.1016/j.abb.2015.10.004
- Choy, A., and Roy, C. R. (2013). Autophagy and bacterial infection: an evolving arms race. *Trends Microbiol.* 21, 451–456. doi: 10.1016/j.tim.2013.06.009
- Cobbold, S. P. (2013). The mTOR pathway and integrating immune regulation. *Immunology* 140, 391–398. doi: 10.1111/imm.12162
- Dempsey, D. R., Viennet, T., Iwase, R., Park, E., Henriquez, S., Chen, Z., et al. (2021). The structural basis of PTEN regulation by multi-site phosphorylation. *Nat. Struct. Mol. Biol.* 28, 858–868. doi: 10.1038/s41594-021-00668-5
- Deretic, V. (2021). Autophagy in inflammation, infection, and immunometabolism. *Immunity* 54, 437–453. doi: 10.1016/j.immuni.2021.01.018
- Farrell, F. O., Rusten, T. E., and Stenmark, H. (2013). Phosphoinositide 3-kinases as accelerators and brakes of autophagy. *FEBS J.* 280, 6322–6337. doi: 10.1111/febs.12486
- Gautier-Bouchardon, A. V., Ferré, S., Le Grand, D., Paoli, A., Gay, E., and Poumarat, F. (2014). Overall decrease in the susceptibility of *Mycoplasma bovis* to antimicrobials over the past 30 years in France. *PLoS One* 9:e87672. doi: 10.1371/journal.pone.0087672
- Geng, N., Wang, X., Yu, X., Wang, R., Zhu, Y., Zhang, M., et al. (2020). *Staphylococcus aureus* avoids autophagy clearance of bovine mammary epithelial cells by impairing lysosomal function. *Front. Immunol.* 11:746. doi: 10.3389/fimmu.2020.00746
- Gessain, G., Tsai, Y. H., Travier, L., Bonazzi, M., Grayo, S., Cossart, P., et al. (2015). PI3-kinase activation is critical for host barrier permissiveness to *Listeria monocytogenes*. *J. Exp. Med.* 212, 165–183. doi: 10.1084/jem.20141406
- Gondaira, S., Nishi, K., Fujiki, J., Iwano, H., Watanabe, R., Eguchi, A., et al. (2021). Innate immune response in bovine neutrophils stimulated with *Mycoplasma bovis*. *Vet. Res.* 52:58. doi: 10.1186/s13567-021-00920-2
- He, Y., Sun, M. M., Zhang, G. G., Yang, J., Chen, K. S., Xu, W. W., et al. (2021). Targeting PI3K/Akt signal transduction for cancer therapy. *Signal Transduct. Target. Ther.* 6:425. doi: 10.1038/s41392-021-00828-5
- Hua, F., Li, K., Yu, J. J., Lv, X. X., Yan, J., Zhang, X. W., et al. (2015). TRB3 links insulin/IGF to tumour promotion by interacting with p62 and impeding autophagic/ proteasomal degradations. *Nat. Commun.* 6:7951. doi: 10.1038/ncomms8951
- Huang, J., and Brumell, J. H. (2014). Bacteria-autophagy interplay: a battle for survival. *Nat. Rev. Microbiol.* 12, 101–114. doi: 10.1038/nrmicro3160
- Huang, G., Redelman-Sidi, G., Rosen, N., Glickman, M. S., and Jiang, X. (2012). Inhibition of mycobacterial infection by the tumor suppressor PTEN. *J. Biol. Chem.* 287, 23196–23202. doi: 10.1074/jbc.M112.351940
- Josi, C., Bürki, S., Stojilkovic, A., Wellnitz, O., Stoffel, M. H., and Pilo, P. (2018). Bovine epithelial in vitro infection models for *Mycoplasma bovis*. *Front. Cell. Infect. Microbiol.* 8:329. doi: 10.3389/fcimb.2018.00329
- Kehl, A., Göser, V., Reuter, T., Liss, V., Franke, M., John, C., et al. (2020). A trafficome-wide RNAi screen reveals deployment of early and late secretory host proteins and the entire late endo-lysosomal vesicle fusion machinery by intracellular *Salmonella*. *PLoS Pathog.* 16:e1008220. doi: 10.1371/journal.ppat.1008220
- Kim, J., Choi, S., Kim, J. O., and Kim, K. K. (2018). Autophagy-mediated upregulation of cytoplasmic claudin 1 stimulates the degradation of SQSTM1/p62 under starvation. *Biochem. Biophys. Res. Commun.* 496, 159–166. doi: 10.1016/j.bbr.2018.01.017
- Klionsky, D. J., Abdel-Aziz, A. K., Abdelfatah, S., Abdellatif, M., Abdoli, A., Abel, S., et al. (2021). Guidelines for the use and interpretation of assays for monitoring autophagy (4th edition). *Autophagy* 17, 1–382. doi: 10.1080/15548627.2020.1797280
- Lachmandas, E., Beigier-Bompadre, M., Cheng, S. C., Kumar, V., van Laarhoven, A., Wang, X., et al. (2016). Rewiring cellular metabolism via the Akt/mTOR pathway contributes to host defence against *Mycobacterium tuberculosis* in human and murine cells. *Eur. J. Immunol.* 46, 2574–2586. doi: 10.1002/eji.201546259
- Li, P., Shi, J., He, Q., Hu, Q., Wang, Y. Y., Zhang, L. J., et al. (2015). *Streptococcus pneumoniae* induces autophagy through the inhibition of the PI3K-I/Akt/mTOR pathway and ROS hypergeneration in A549 cells. *PLoS One* 10:e0122753. doi: 10.1371/journal.pone.0146071
- Liu, Y., Deng, Z., Xu, S., Liu, G., Lin, Y., Khan, S., et al. (2021). *Mycoplasma bovis* subverts autophagy to promote intracellular replication in bovine mammary epithelial cells cultured in vitro. *Vet. Res.* 52:130. doi: 10.1186/s13567-021-01002-z
- Liu, Y., Zhou, M., Xu, S., Khan, M. A., Shi, Y., Qu, W., et al. (2020). *Mycoplasma bovis*-generated reactive oxygen species and induced apoptosis in bovine mammary epithelial cell cultures. *J. Dairy Sci.* 103, 10429–10445. doi: 10.3168/jds.2020-18599
- Lu, Z., Xie, D., Chen, Y., Tian, E., Muhammad, I., Chen, X., et al. (2017). TLR2 mediates autophagy through ERK signaling pathway in *Mycoplasma gallisepticum*-infected RAW264.7 cells. *Mol. Immunol.* 87, 161–170.
- Luo, H., Wu, X., Xu, Z., Hao, X., Wang, Y., and Li, M. (2020). NOD2/c-jun NH(2)-terminal kinase triggers *Mycoplasma ovipneumoniae*-induced macrophage autophagy. *J. Bacteriol.* 202:e00689-19.
- Maunsell, F. P., and Chase, C. (2019). *Mycoplasma bovis*: Interactions with the immune system and failure to generate an effective immune response. *Vet. Clin. North Am. Food Anim. Pract.* 35, 471–483. doi: 10.1016/j.cvfa.2019.08.003
- Mizushima, N., and Yoshimori, T. (2007). How to interpret LC3 immunoblotting. *Autophagy* 3, 542–545. doi: 10.4161/auto.4600
- Mostowy, S. (2013). Autophagy and bacterial clearance: a not so clear picture. *Cell. Microbiol.* 15, 395–402. doi: 10.1111/cmi.12063
- Özdemir, S., and Altun, S. (2020). Genome-wide analysis of mRNAs and lncRNAs in *Mycoplasma bovis* infected and non-infected bovine mammary gland tissues. *Mol. Cell. Probes* 50:101512. doi: 10.1016/j.mcp.2020.101512
- Perez-Casal, J. (2020). Pathogenesis and virulence of *Mycoplasma bovis*. *Vet. Clin. North Am. Food Anim. Pract.* 36, 269–278. doi: 10.1016/j.cvfa.2020.02.002
- Qi, M., Geng, H., Geng, N., Cui, Y., Qi, C., Cheng, G., et al. (2022). *Streptococcus agalactiae*-induced autophagy of bovine mammary epithelial cell via PI3K/Akt/mTOR pathway. *J. Dairy Res.* 89, 178–184. doi: 10.1017/S0022029922000243
- Reggio, A., Buonomo, V., and Grumati, P. (2020). Eating the unknown: Xenophagy and ER-phagy are cytoprotective defenses against pathogens. *Exp. Cell Res.* 396:112276. doi: 10.1016/j.yexcr.2020.112276
- Riebisich, A. K., Mühlen, S., Beer, Y. Y., and Schmitz, I. (2021). Autophagy-A story of bacteria interfering with the host cell degradation machinery. *Pathogens* 10:110. doi: 10.3390/pathogens10020110
- Sudhakar, P., Jacomin, A. C., Hautefort, I., Samavedam, S., Fatemian, K., Ari, E., et al. (2019). Targeted interplay between bacterial pathogens and host autophagy. *Autophagy* 15, 1620–1633. doi: 10.1080/15548627.2019.1590519
- van der Merwe, J., Prysliak, T., and Perez-Casal, J. (2010). Invasion of bovine peripheral blood mononuclear cells and erythrocytes by *Mycoplasma bovis*. *Infect. Immun.* 78, 4570–4578. doi: 10.1128/IAI.00707-10
- Wang, Z., Lan, R., Xu, Y., Zuo, J., Han, X., Phouthapane, V., et al. (2021a). Taurine alleviates *Streptococcus uberis*-induced inflammation by activating autophagy in mammary epithelial cells. *Front. Immunol.* 12:631113. doi: 10.3389/fimmu.2021.631113
- Wang, Z., Wen, Y., Zhou, B., Tian, Y., Ning, Y., and Ding, H. (2021b). Incomplete autophagy promotes the replication of *Mycoplasma hyopneumoniae*. *J. Microbiol.* 59, 782–791. doi: 10.1007/s12275-021-1232-3
- Yang, Z., and Klionsky, D. J. (2010). Mammalian autophagy: core molecular machinery and signaling regulation. *Curr. Opin. Cell Biol.* 22, 124–131. doi: 10.1016/j.ccb.2009.11.014
- Zhao, X., Feng, W., Zhu, X., Li, C., Ma, X., Li, X., et al. (2019). Conserved autophagy pathway contributes to stress tolerance and virulence and differentially controls autophagic flux upon nutrient starvation in *Cryptococcus neoformans*. *Front. Microbiol.* 10:2690. doi: 10.3389/fmicb.2019.02690



OPEN ACCESS

EDITED BY

Meghan May,
University of New England, United States

REVIEWED BY

Owen Brad Spiller,
Cardiff University,
United Kingdom
Marissa Valentine-King,
Baylor College of Medicine, United States
Laurent Xavier Nouvel,
Ecole Nationale Vétérinaire de Toulouse,
France

*CORRESPONDENCE

Li Xiao
lixiao@uabmc.edu

†PRESENT ADDRESS

Arthur H. Totten,
Department of Laboratory Medicine,
Clinical Center, National Institutes of
Health, Bethesda, MD, United States

SPECIALTY SECTION

This article was submitted to
Infectious Agents and Disease,
a section of the journal
Frontiers in Microbiology

RECEIVED 06 April 2022

ACCEPTED 27 June 2022

PUBLISHED 01 August 2022

CITATION

Xiao L, Totten AH, Crabb DM,
Atkinson TP and Waites KB (2022)
Antimicrobial susceptibilities and
mechanisms of resistance of commensal
and invasive *Mycoplasma salivarium*
isolates.
Front. Microbiol. 13:914464.
doi: 10.3389/fmicb.2022.914464

COPYRIGHT

© 2022 Xiao, Totten, Crabb, Atkinson and
Waites. This is an open-access article
distributed under the terms of the [Creative
Commons Attribution License \(CC BY\)](#). The
use, distribution or reproduction in other
forums is permitted, provided the original
author(s) and the copyright owner(s) are
credited and that the original publication in
this journal is cited, in accordance with
accepted academic practice. No use,
distribution or reproduction is permitted
which does not comply with these terms.

Antimicrobial susceptibilities and mechanisms of resistance of commensal and invasive *Mycoplasma salivarium* isolates

Li Xiao^{1*}, Arthur H. Totten^{2†}, Donna M. Crabb³,
Thomas Prescott Atkinson² and Ken B. Waites³

¹Department of Medicine, University of Alabama at Birmingham, Birmingham, AL, United States, ²Department of Pediatrics, University of Alabama at Birmingham, Birmingham, AL, United States, ³Department of Pathology, University of Alabama at Birmingham, Birmingham, AL, United States

Mycoplasma salivarium, an oral commensal organism, can cause severe invasive infections in immunocompromised individuals. Currently there is no treatment guidance for such infections. We performed antimicrobial susceptibility tests on 39 commensal and invasive *M. salivarium* isolates and investigated the mechanisms of antimicrobial resistance. Clindamycin was the most active agent [minimum inhibition concentration (MIC) range: 0.004–128mg/L, MIC₅₀=0.031mg/L, MIC₉₀=0.125mg/ml], followed by tetracycline and levofloxacin. All isolates were resistant to erythromycin (MIC ≥4mg/L) due to the presence of 2057A (*Escherichia coli* numbering) in 23S rRNA. Three isolates with elevated clindamycin MICs (≥8mg/L) harbored A2058T/G mutations in 23S rRNA gene; four sequential isolates from one patient developed C2611T and A2059G mutations accompanying the increase of clindamycin MICs. Five isolates with elevated tetracycline MICs (≥4mg/L) had mutations in 16S rRNA gene (A965G/T, G966T, or A967C/T) and one of them harbored *TetM*. Nine isolates with elevated levofloxacin MICs (≥4mg/L) had one or more mutations in *gyrA*, *gyrB*, *parC*, or *parE*. Susceptibility breakpoints for clindamycin, tetracycline and levofloxacin were suggested to be ≤0.125, ≤2, and ≤2mg/L, respectively. Antimicrobial resistance to any of the three agents (clindamycin, tetracycline, or levofloxacin) was documented in 12 (34.3%) non-duplicate isolates, of which 10 were invasive. Levofloxacin resistance was most frequent (25.7%). Multi-drug resistance was also observed (14.3%). This study demonstrates the frequent occurrence of antimicrobial resistance in *M. salivarium*, emphasizing the need for culture and susceptibility testing to guide antimicrobial therapy.

KEYWORDS

Mycoplasma salivarium, susceptibility, antimicrobial resistance, mutation, minimum inhibition concentration, quinolone resistance determining region, Clinical and Laboratory Standards Institute, single nucleotide polymorphisms

Introduction

Mycoplasma salivarium is one of several mycoplasmal species that are endogenous within the human oropharynx, usually as commensals. This organism commonly resides in dental plaque and gingival sulci and has been associated with periodontal disease (Uchida et al., 1981; Watanabe et al., 1986; Lamster et al., 1997). It is also reported to be heavily associated with oral leukoplakia (Mizuki et al., 2017) and oral carcinoma in patients with Fanconi anemia (Henrich et al., 2014). Extra-oropharyngeal infections are uncommon, but this organism has been detected in synovial fluid in persons with acute or chronic arthritis, prosthetic joint infections, empyemas, abscesses in the brain, and infections in other body sites (So et al., 1983; Johnson et al., 2007; Grisold et al., 2008; Orsted et al., 2011; Baracaldo et al., 2012; Buchsel et al., 2016; Thoendel et al., 2017; Totten et al., 2021). A recent study showed that lower airway enrichment of *M. salivarium* is associated with poor clinical outcome in mechanically ventilated COVID-19 patients (Sulaiman et al., 2021). Invasive infections in a normally sterile body site most often occurs in association with humoral immune deficiency or other immunosuppressed states (So et al., 1983; Buchsel et al., 2016; Thoendel et al., 2017; Totten et al., 2021). Currently there is no *M. salivarium* infection prevalence data among immunocompromised populations.

Besides a few case reports, very little data regarding what constitutes the most effective treatments or *in vitro* antimicrobial susceptibility profiles of *M. salivarium* are available in published literature (Grisold et al., 2008; Buchsel et al., 2016; Totten et al., 2021). Treatment alternatives are somewhat limited, as all *Mycoplasma* spp. are intrinsically resistant to β -lactams due to their lack of a cell wall, but they are generally susceptible to fluoroquinolones and tetracyclines, as well as macrolides and/or lincosamides (Waites et al., 2014). There are only three case reports performed *in vitro* susceptibility testing for *M. salivarium* and the main drugs showing *in vitro* susceptibility are clindamycin, tetracycline, and moxifloxacin (Grisold et al., 2008; Buchsel et al., 2016; Totten et al., 2021). Acquired resistance to macrolides, lincosamides, fluoroquinolones, and/or tetracyclines has been documented in all of the *Mycoplasma* spp. known to be pathogenic in humans (Waites et al., 2014). There are two reports described fluoroquinolone resistance in invasive *M. salivarium* isolates causing septic arthritis and another report detected a mutation possibly related to macrolide resistance in *M. salivarium* that caused prosthetic joint infection (Buchsel et al., 2016; Thoendel et al., 2017; Totten et al., 2021). In this study, we determined the minimum inhibition concentrations (MICs) for four classes of antimicrobial agents against clinical isolates and reference strains of *M. salivarium* and investigated the genetic mechanisms associated with antimicrobial resistance. This study provides guidance for empiric

treatment of invasive *M. salivarium* infections and determines the extent that acquired antimicrobial resistance occurs.

Materials and methods

Microorganisms

A total of 39 *M. salivarium* isolates were evaluated (Supplementary Table S1). Among them, two were ATCC strains, 33 were clinical isolates from non-duplicate patients collected from 13 facilities in 12 states (AL, CO, CT, IL, KS, MA, MN, OH, PA, TN, UT, and WA) between 2002 and 2021, and four were additional isolates obtained sequentially from synovial fluid of one of the above non-duplicate patients between 2018 and 2021. Among the 33 non-duplicated clinical isolates, 13 were commensals from throats of healthy adults in 2013 in a previous study (Centor et al., 2015), 20 were invasive isolates from synovial fluid (5), lower respiratory tract (5), chest wall/sternum (3), pleural fluid (2), or miscellaneous tissues/fluid (5). All clinical isolates were obtained by culture in SP4 broth incubated at 37°C for 3–5 days, and their species identities were confirmed by sequencing of the full length 16S rRNA gene using primer pair fD1 and rP1 (Weisburg et al., 1991; La Scola et al., 1997).

Antimicrobial susceptibility test

Antimicrobial susceptibility of the 39 isolates against levofloxacin, clindamycin, erythromycin, and tetracycline were determined by broth microdilution using SP4 broth in accordance with methods established for human mycoplasmas by the Clinical and Laboratory Standards Institute (2011). Considering the close phylogenetic relationship, *Mycoplasma hominis* strain ATCC 23114 was used for quality control. The MIC plates were sealed with Parafilm and incubated at 37°C for 72–120 h until the color of growth controls changed which indicating the time point to read the MICs. MICs for levofloxacin, clindamycin, and tetracycline were initially interpreted using susceptibility breakpoints published for *M. hominis* (Clinical and Laboratory Standards Institute, 2011). Erythromycin MICs were initially interpreted using the breakpoint for *Mycoplasma pneumoniae* as there is no erythromycin breakpoint established by the Clinical and Laboratory Standards Institute (CLSI) for *M. hominis* (Clinical and Laboratory Standards Institute, 2011).

Genetic analyses

PCR and sequencing primers were designed or obtained from published literature for designated targets (Supplementary Table S2). According to the genome sequence of ATCC strain 23064 (GenBank number NZ_LR214938), *M. salivarium* has a single copy of 16S rRNA and 23S rRNA genes. Erythromycin and clindamycin resistance mechanisms were investigated by sequencing the full length of the 23S rRNA gene and ribosomal protein genes *rplD* (L4) and *rplV* (L22). Quinolone resistance mechanisms were investigated

Abbreviations: MIC, Minimum inhibition concentration; QRDR, Quinolone resistance determining region; CLSI, Clinical and Laboratory Standards Institute; SNPs, Single nucleotide polymorphisms.

by sequencing the quinolone resistance determining region (QRDR) of DNA gyrase genes *gyrA* and *gyrB* and DNA topoisomerase IV genes *parC* and *parE*. Genetic mechanisms associated with tetracycline resistance were assessed by 16S *rRNA* gene sequencing and testing for the presence of the *tetM* gene (Blanchard et al., 1992). Genomic DNA of *Ureaplasma urealyticum* serovar 9 that is known to contain the *tetM* sequence was used as *tetM* PCR positive control. A no template negative control was included in every PCR run. PCRs were performed on a Veriti 96-well thermal cycler (Applied Biosystems, Foster City, CA, United States) with a 25 µl PCR reaction volume containing 0.4 µmol/L of each primer, 2.5 µl of 10X AccuPrime Pfx reaction mix (Thermo Fisher, Fremont, CA, United States), 0.5 U of AccuPrime Pfx DNA polymerase and 2 µl of template DNA. Amplicons were sequenced by Sanger technique at the UAB Heflin Genomics Center and analyzed using CLC Genomics Workbench 21 (Qiagen, Redwood City, CA, United States). *Mycoplasma salivarium* reference sequences were obtained from the genome sequence of *M. salivarium* strain NCTC 10113 (alternative strain name: ATCC 23064, GenBank number NZ_LR214938). Reference sequences for *Escherichia coli* were obtained from the genome sequence of strain K-12, substr. MG1655 (GenBank number U00096.3). Reference sequence for *tetM* was GenBank U08812.1. The assembled sequences were submitted to GenBank and the accession numbers are: OM864597 to OM864634 for 16S *rRNA* gene, ON023780 to ON023817 for 23S *rRNA* gene, ON036345 to ON036382 for *rplD*, ON036383 to ON036420 for *rplV*, ON036193 to ON036230 for *gyrA*, ON036231 to ON036268 for *gyrB*, ON036269 to ON036306 for *parC* and ON036307 to ON036344 for *parE*.

Statistical analysis

Chi-square analysis or Fisher's exact test was performed to compare the antimicrobial resistance rates between invasive and non-invasive isolates using IBM SPSS 27 (IBM Corp., Armonk, NY, United States). A resistant isolate is defined as an isolate is resistant to any of the three drugs excluding erythromycin. If an isolate is resistant to two or more drugs, it is considered multi-drug resistant. A value of $p < 0.05$ was considered statistically significant.

Results

Erythromycin MICs and resistance associated mutations

A summary of MIC data on 35 non-duplicated isolates (two ATCC strains and 33 non-duplicated clinical strains) is provided in Table 1, and a complete tabulation of MICs and genotypic analyses for the 35 *M. salivarium* isolates tested is provided in Supplementary Table S1. The distribution of MIC data is shown in Figure 1.

Similar to *M. hominis* (Waites et al., 2014), elevated MICs to erythromycin ranging from 4 to ≥ 256 mg/L were observed in all

TABLE 1 Minimum inhibition concentration summary for 35 *M. salivarium* isolates.

Reagent	Suggested susceptibility breakpoint (mg/L)	MIC Range (mg/L)			MIC ₅₀ (mg/L)			MIC ₉₀ (mg/L)			No. and percentage resistant ^a		
		Overall (n = 35)	Non-invasive (n = 15)	Invasive (n = 20)	Overall (n = 35)	Non-invasive (n = 15)	Invasive (n = 20)	Overall (n = 35)	Non-invasive (n = 15)	Invasive (n = 20)	Overall (n = 35)	Non-invasive (n = 15)	Invasive (n = 20)
Levofloxacin	≤ 2	0.5–32	0.5–2	0.5–32	1	1	2	8	2	16	9 (25.7)	0 (0.0)	9 (45.0)
Tetracycline	≤ 2	0.016–32	0.25–32	0.016–16	0.5	1	0.25	8	2	8	5 (14.3)	1 (6.7)	4 (20.0)
Clindamycin	≤ 0.125	0.004–128	0.016–32	0.004–128	0.031	0.031	0.031	0.125	0.125	0.063	3 (8.6)	1 (6.7)	2 (10.0)
Erythromycin	≤ 0.5 (Mpn)	4 to ≥ 256	8 to ≥ 256	4 to ≥ 256	32	32	32	≥ 256	128	≥ 256	35 (100.0)	15 (100.0)	20 (100.0)
Total ^b					32	32	32	≥ 256	128	≥ 256	12 (34.3)	2 (13.3)	10 (50.0)
													0.034

^aSusceptibility was designated using suggested MIC breakpoints determined by this study for levofloxacin (≤ 2 mg/L), tetracycline (≤ 2 mg/L), and clindamycin (≤ 0.125 mg/L). The breakpoint for erythromycin was adopted from the Clinical and Laboratory

Standards Institute reference for *M. pneumoniae* (Mpn, $S \leq 0.5$ mg/L).

^bErythromycin was excluded in overall resistance rate calculation.

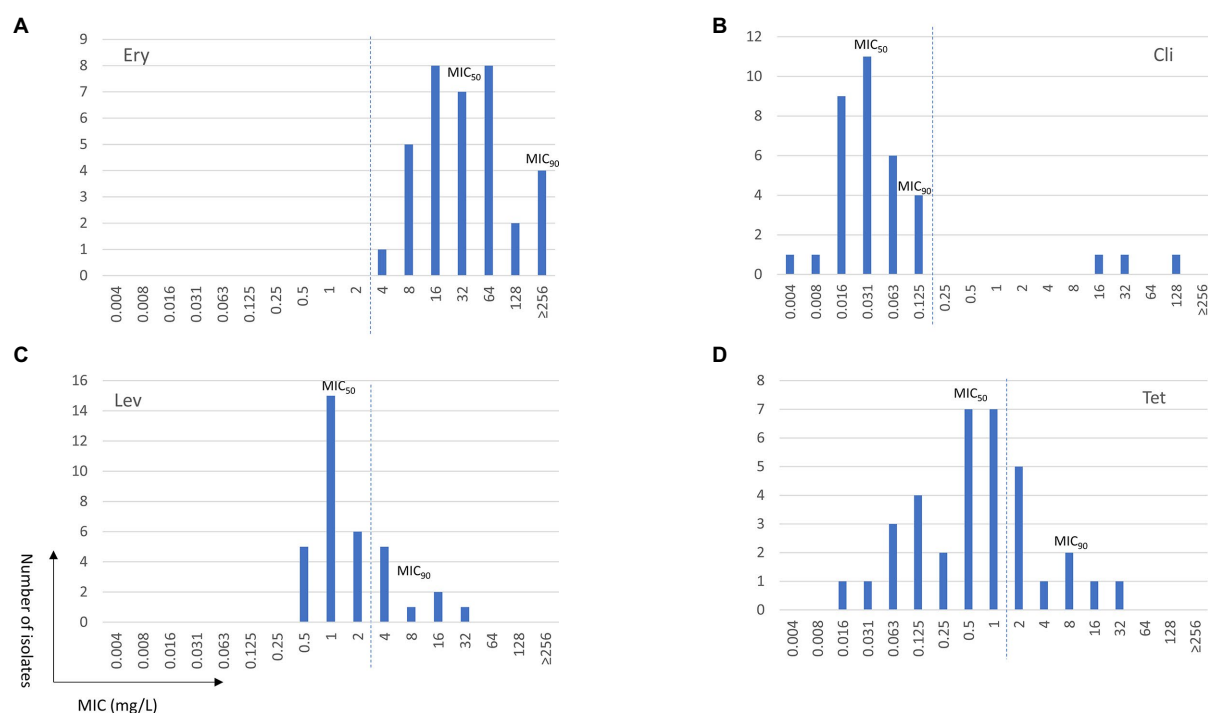


FIGURE 1
Minimum inhibition concentration (MIC) distributions of erythromycin (Ery, A), clindamycin (Cli, B), levofloxacin (Lev, C), and tetracycline (Tet, D) for *Mycoplasma salivarium* isolates. The dashed line divides the cutoff values for wild type (left) and mutant (right) strains.

M. salivarium isolates tested (Figure 1A). Four isolates showed highly elevated MICs to erythromycin (≥ 256 mg/L). Mutations in domain V in 23S rRNA are known to be associated with erythromycin resistance in mycoplasmas (Waite et al., 2014). Using *E. coli* 23S rRNA gene as reference, a G to A transition at position 2057 (*E. coli* numbering) in the central loop of domain V was identified in all isolates. This alteration is reported to be associated with intrinsic resistance to the 14- and 15-membered macrolides in *M. hominis* and several *Mycoplasma* spp. of animal origin (Whithear et al., 1983; Furneri et al., 2000; Pereyre et al., 2002; Stakenborg et al., 2005; Lysnyansky et al., 2015). In the 4 isolates with erythromycin MIC ≥ 256 mg/L, three harbored mutations at position 2058 (A to T/G) and one had a 9-amino acid deletion at position 139 ($\Delta 139$ EAKKEAKAT) in ribosomal protein L22 (Table 2). A2058T mutation was also reported in a case report of *M. salivarium* caused prosthetic joint infection without *in vitro* susceptibility data (Thoendel et al., 2017).

Clindamycin MICs and resistance associated mutations

The MIC range for clindamycin in the 35 non-duplicated isolates was 0.004–128 mg/L. The MIC distribution showed a bimodal format (Table 1; Figure 1B). Using the CLSI susceptibility breakpoint for *M. hominis*, 32 out of 35 (91.4%) isolates were susceptible with MICs ≤ 0.125 mg/L, while the other 3 isolates had elevated MICs ranging from 16 to 128 mg/L. The three

isolates were obtained between 2013 and 2018 from throat swab of a healthy volunteer and synovial fluid and sputum of two other patients. These isolates were also highly resistant to erythromycin (MIC ≥ 256 mg/L). Overall, clindamycin was the most potent drug tested with MIC₅₀ and MIC₉₀ values of 0.031 and 0.125 mg/L, respectively.

Clindamycin resistance in *M. hominis* has been shown to be related to mutations in 23S rRNA at positions 2059 and 2611 (*E. coli* numbering; Pereyre et al., 2002). In this study, the 23S rRNA mutations were at position 2058 (A to T/G) in all 3 *M. salivarium* isolates with elevated MICs for clindamycin (Table 2). These mutations were not observed in the remaining isolates with MICs ≤ 0.125 mg/L. Interestingly, the isolate with a 9-amino acid deletion in ribosomal protein L22 that was highly resistant to erythromycin was susceptible to clindamycin. In the sequential isolates collected from one patient between 2018 and 2021, mutations emerging with the development of clindamycin resistance were observed (Supplementary Table S1). The initial isolate (72114) was susceptible to clindamycin (MIC=0.031 mg/L). Emergence of a C2611T mutation in the second isolate (72094) caused a slight increase of MIC (0.125 mg/L); then the presence of mutation A2059G caused further elevation of MICs to clindamycin (MICs ≥ 8 mg/L) in all subsequent isolates. There were many other single nucleotide polymorphisms (SNPs) identified in 23S rRNA, *rplD* (L4) and *rplV* (L22) genes in the clinical strains compared to the two ATCC strains which did not exhibit elevated clindamycin MICs (Table 2; Supplementary Tables S3 and S4).

TABLE 2 Clindamycin MIC and alterations in *23S rRNA* gene and ribosomal proteins.

Isolate	MIC (mg/L)		Alterations		
	Cli	Ery	23S rRNA (<i>Escherichia coli</i> numbering)	L4 (Amino acid)	L22 (Amino acid)
ATCC 23064	0.031	16	-	-	-
ATCC 14277	0.031	16	-	-	-
48759	0.004	8	T391C (343); G426A (375); C1260T (1222)	V228I	A202V
73363	0.008	64	T391C (343); G676A (625); C2223T (2207)	-	-
49906	0.016	32	C385T (337); T391C (343);	-	A136T; A144T; A146T; P158S; T186A; T195A; A202V; P213T
59228	0.016	16	T391C (343)	-	-
59258	0.016	32	T391C (343); G2685A (2668)	P21S	V204I
59260	0.016	64	T391C (343)	-	R35T (mixed); A136T; A144T; A146T; P158S; T186A; T195A; A202V
59838	0.016	8	T391C (343); C945T (893)	-	A136T; A144T; A146T; P158S; T186A; T195A; A202V
62771	0.016	128	T391C (343); G1364A (1328)	-	-
83426	0.016	32	T391C (343); G1130A (1080); C1890T (1874)	-	T195A; A202V; D224N
83735	0.016	16	T391C (343); G775A (723)	-	P158S
84893	0.016	64	T391C (343); T2027C (2011)	P21S	E143G
59229	0.031	16	T391C (343)	P21S	-
59262	0.031	16	T391C (343); G2388A (2371)	-	-
59263	0.031	32	T391C (343); G428A (377)	N134D	K199T; E200K
59266	0.031	128	T391C (343); G650A (602)	-	-
59272	0.031	16	T391C (343); G1165A (1115); G1354A (1318)	-	-
72114	0.031	8	T391C (343); C1277T (1239)	-	-
82217	0.031	4	T391C (343); G428A (377)	A233T	A155V; T186A
84726	0.031	64	T391C (343)	-	-
84850	0.031	32	T391C (343); A500G (449); G650A (602); T1318C (1282); T1753C (1712)	-	A136T; A144T; A146T; P158S; T186A; T195A; A202V
63019	0.063	16	-	-	D123N
72036	0.063	64	T391C (343); C1277T (1239)	-	F93L
78192	0.063	32	T391C (343)	A32V	S150T
81314	0.063	64	T391C (343)	H164Y	-
82746	0.063	256	T391C (343)	-	Δ139EAKKEAKAT; A202T
84114	0.063	8	C140T (139); T391C (343); G606A (558); G650A (602); G2172A (2156)	-	-
59240	0.125	8	C385T (337); T391C (343); G1614A (1573)	N134D	-
59243	0.125	64	A340G (insertion 293); T391C (343)	P21S	A136T; A202T
59247	0.125	64	C140T (139); T391C (343); C2841T (2841)	-	-
59271	0.125	32	C590T (540)	-	-
72904*	0.125	8	T391C (343); C1277T (1239); C2628T (2611)	-	-
85051*	4	128	T391C (343); C1277T (1239); A2075G (2059); C2628T (2611)	-	-
80422*	8	32	T391C (343); C1277T (1239); A2075G (2059); C2628T (2611)	-	-
82061*	8	256	T391C (343); C1277T (1239); A2075G (2059); C2628T (2611)	-	-
69499	16	256	T391C (343); G1186A (1136); C1351T (1315); G1373A (1337); A2074G (2058)	P21S	-
59283	32	256	T391C (343); G1471A (1436); A2074G (2058)	T5I; A32V	P158S; T186A; T195A; A202V; D224N
73273	128	256	T391C (343); G650A (602); C776T (724); A2074T (2058) ; C2423T (2406)	-	-

1. Both ATCC strains 23064 and 14277 were used as reference.

2. All isolates have G2057A transition compared to *E. coli*.

3. * Sequential isolates from the same patient after isolate 72114.

4. Mutations associated with resistance were bolded. Cli, clindamycin and Ery, erythromycin.

Considering the MIC distribution and the genetic alterations identified in these isolates, a clindamycin susceptibility breakpoint for *M. salivarium* of 0.125 mg/L, one dilution below to that of *M. hominis* (0.25 mg/L; [Clinical and Laboratory Standards Institute, 2011](#)), can be suggested.

Levofloxacin MICs and resistance associated mutations

The MIC range for levofloxacin was 0.5–32 mg/L and MIC₅₀ and MIC₉₀ values were 1 and 8 mg/L, respectively, in the 35 non-duplicated isolates ([Table 1](#); [Figure 1C](#)). There were 26 out of 35 (74.3%) isolates having MICs ≤ 2 mg/L, while the remaining nine isolates had elevated MICs ranging from 4 to 32 mg/L ([Table 3](#)). These nine isolates were obtained between 2014 and 2021 from synovial fluid, lower respiratory tract, chest wounds, or pelvic aspirate, and all were invasive ([Supplementary Table S1](#)).

Fluoroquinolone resistance in *M. hominis* is associated with mutations in the QRDR of *gyrA*, *gyrB*, *parC*, or *parE* genes ([Waites et al., 2014](#)). The nine isolates with elevated MICs had one or more mutations in these genes ([Table 3](#)). Among them, three had mutations in *ParC* (S80I and E84K, *E. coli* numbering) and 4 had mutation in *ParE* (D420N, *E. coli* numbering). These mutations have been reported to be associated with fluoroquinolone resistance in *M. hominis*, *M. genitalium*, and/or *U. urealyticum* ([Bebear et al., 2000](#); [Tagg et al., 2013](#)). Six isolates had multiple mutations. *GyrA* mutation S84P appeared together with *ParC* mutations S80I/E84K in one non-duplicate isolate and the five isolates from one patient that had a higher levofloxacin MIC (≥ 8 mg/ml). In the 26 isolates with levofloxacin MIC ≤ 2 mg/L, 21 had no mutations and four had single mutation (A411V in *ParE*) outside the QRDR, which is unlikely to be associated with quinolone resistance. The complete list of SNPs identified are summarized in [Supplementary Table S5](#). Thus, the cutoff of levofloxacin susceptibility breakpoint could tentatively be set at ≤ 2 mg/L, similar to other human *Mycoplasma* spp. ([Clinical and Laboratory Standards Institute, 2011](#)).

Tetracycline MICs and resistance associated mechanisms

The MIC range for tetracycline was 0.016–32 mg/L in the 35 non-duplicated isolates ([Table 1](#); [Figure 1D](#)). There were five isolates (four invasive and one commensal) having elevated tetracycline MICs of 4–32 mg/L, while others were ≤ 2 mg/L ([Table 4](#); [Supplementary Table S1](#)).

All five isolates with elevated tetracycline MICs had mutations at position 965, 966, or/and 967 in *16S rRNA* gene ([Table 4](#)), which have been reported to be associated with tetracycline resistance in *M. hominis* induced by *in vitro* selection ([Waites et al., 2014](#)) and in *M. genitalium* clinical specimens with unknown tetracycline exposure history ([Le Roy et al., 2021](#)). There were 2 (out of 5) other commensal isolates with MIC of 2 mg/L harboring A965G mutation in *16S rRNA* gene, and one of them was a mix with wild type. Other SNPs identified in the *16S rRNA* gene not associated with

tetracycline resistance are listed in [Supplementary Table S6](#). A *tetM* element was detected in 13 isolates (37.1%) and 12 of them had MIC ≤ 2 mg/L ([Table 4](#); [Supplementary Table S1](#)). The majority (10) of the *tetM*-positive isolates were commensals. Sequencing was successful for 12 isolates and derived partial amino acid sequences of TetM can be divided into two major groups and eight different types ([Figure 2](#)). BLASTP analysis revealed that group 1 (containing six sequences) was 99%–100% identical to the sequences of TetM of *E. faecium*, *Streptococcus suis*, *Clostridioides difficile* and others, while group 2 (containing another six sequences) was 98%–100% identical to the TetM sequences of *S. pneumoniae*, *E. coli* and others. Expanded comparison with TetM sequences from *Ureaplasma* spp. obtained by [Dumke \(2021\)](#) showed a clear cluster of *M. salivarium* group (containing eight sequences) and an *Ureaplasma* group (containing five sequences from *Ureaplasma* spp. and four sequences from *M. salivarium*), suggesting that these *M. salivarium* isolates had acquired *tetM* element from two major different sources.

We suggest tetracycline susceptibility breakpoint for *M. salivarium* could be tentatively set at ≤ 2 mg/L, one dilution below that of *M. hominis* (4 mg/L). Having a lower cutoff of ≤ 1 mg/L for *M. salivarium* may be appropriate, but additional isolates would need to be investigated and treatment outcomes assessed in order to make such a decision with confidence.

Antimicrobial resistance frequencies

Using the above suggested antimicrobial susceptibility breakpoints for *M. salivarium*, the occurrence of acquired resistance, besides intrinsic erythromycin resistance, to one or more antimicrobial classes was observed in 12 (34.3%) non-duplicate isolates. Among them, nine were resistant to levofloxacin (25.7%), five to tetracycline (14.3%) and three to clindamycin (8.6%; [Table 1](#)). Half of the invasive isolates (10/20) were resistant, compared to only two resistant ones in non-invasive isolates (2/15, 13.3%, $p=0.034$; [Table 1](#)). Specifically, for levofloxacin, all non-invasive isolates were susceptible, while 45.0% of invasive isolates (9/20) were resistant ($p=0.004$, [Table 1](#)). Multi-drug resistance was also observed. There were five invasive isolates (5/35, 14.3%) from non-duplicated patients showing resistance to two classes of antimicrobials ([Supplementary Table S1](#)). Among those, one was resistant to levofloxacin and clindamycin and four were resistant to levofloxacin and tetracycline. For the sequential isolates, the first two isolates from 2018 were resistant to levofloxacin and tetracycline; the three subsequent isolates from 2019 to 2021 were resistant to all antimicrobials tested. There were no obvious changes of MICs or resistance to clindamycin, levofloxacin and tetracycline among invasive isolates over time.

Discussion

We have determined the MICs of commensal and invasive *M. salivarium* isolates and suggested the susceptibility breakpoints for clindamycin, tetracycline and levofloxacin. Mutations associated with antimicrobial resistance were identified. To our knowledge, this

TABLE 3 Levofloxacin MIC and alterations in GyrA, GyrB, ParC, and ParE proteins.

Isolate	MIC (mg/L)	Amino acid alterations (<i>E. coli</i> numbering)			
	Lev	GyrA	GyrB	ParC	ParE
ATCC 23064	0.5	-	-	-	-
ATCC 14277	2	-	-	-	-
49906	0.5	-	-	-	-
59240	0.5	-	-	-	-
59266	0.5	-	-	-	-
73363	0.5	-	-	-	-
48759	1	-	-	-	-
59247	1	-	-	-	-
59258	1	-	-	-	-
59260	1	-	-	-	-
59262	1	-	-	-	A411V
59263	1	-	-	-	-
59271	1	-	-	-	-
59272	1	-	-	-	-
59283	1	-	-	-	-
59838	1	-	-	-	-
62771	1	-	-	-	-
72036	1	-	-	-	A411V
81314	1	-	-	-	-
82217	1	-	-	-	-
83735	1	-	-	-	-
59229	2	-	-	-	-
59243	2	-	-	-	-
59228	2	-	-	-	A411V
69499	2	-	-	-	-
84726	2	-	-	-	A411V
63019	4	S132A	-	-	A411V; D420N
78192	4	-	-	-	D420N
82746	4	-	-	E84K	-
83426	4	-	-	P59S; A144T	A411V
84114	4	-	D409N	E151K	-
84893	8	-	-	-	A411V; D420N
85051*	8	S84P	-	E84K	A411V
72904*	16	S84P	-	E84K	A411V
73273	16	-	-	-	D420N
80422*	16	S84P	-	E84K	A411V
82061*	16	S84P	-	E84K	A411V
84850	16	S84P	-	S80I	-
72114	32	S84P	-	E84K	A411V

Both ATCC strains 23064 and 14277 are used as reference. Mutations previously reported to be associated with resistance are bolded. Lev, levofloxacin.

*Sequencial isolates from the same patient after isolate 72114.

is the first *in vitro* survey of invasive *M. salivarium* isolates collected over two decades from a broad geographic area of US, comparing reference type strains and throat isolates from healthy volunteers to examine the *in vitro* antimicrobial susceptibilities of this organism.

Mycoplasma salivarium is now becoming a recognized cause of opportunistic infections in immunocompromised hosts (So et al., 1983; Buchsel et al., 2016; Thoendel et al., 2017; Totten et al., 2021). Our results have important implications for diagnosis and

management of *M. salivarium* infections. Macrolides such as erythromycin are to be avoided since there was universal resistance in all isolates tested. Clinical failure or *in vitro* resistance has already been observed on erythromycin and clarithromycin in previous reports (So et al., 1983; Buchsel et al., 2016; Totten et al., 2021). Acquired resistance to one or more classes of antimicrobials, presumably driven by selective antimicrobial pressure, occurred in half of the invasive isolates tested, and most commonly affected

TABLE 4 Tetracycline MIC and genetic alterations.

Isolate	Tet MIC (mg/L)	TetM	16S rRNA gene alteration (<i>E. coli</i> numbering)
ATCC 23064	0.5	-	-
ATCC 14277	1	-	-
63019	0.016	-	G974T (1023)
49906	0.031	-	C936T (986); A1355G (1408)
73273	0.063	Pos	C223T (264); C368T (409)
73363	0.063	Pos	-
83735	0.063	-	G985A (1039)
62771	0.125	-	-
69499	0.125	-	-
78192	0.125	-	-
81314	0.125	-	-
59240	0.25	Pos	-
72036	0.25	-	-
48759	0.5	-	C585T (625)
59228	0.5	Pos	-
59262	0.5	-	-
59263	0.5	Pos	G984A (1038); G1213T (1267)
59272	0.5	Pos	-
59838	0.5	-	-
59229	1	Pos	-
59247	1	Pos	-
59266	1	Pos	-
59271	1	-	-
82217	1	-	C1396T (1449)
84893	1	-	-
59258	2	Pos	G224A (265)
59260	2	Pos	C304T (345); A915G (mixed, 965) ; G923A (973)
59283	2	Pos	A915G (965)
82746	2	-	-
84726	2	-	-
72904*	4	-	A915T (965) ; C1141T (1195)
80422*	4	-	A915T (965) ; C1141T (1195)
82061*	4	-	A915T (965) ; C1141T (1195)
83426	4	-	G376A (417); A915G (965)
85051*	4	-	A915T (965) ; C1141T (1195)
72114	8	-	A915T (965) ; A919C (969); C1141T (1195)
84850	8	-	T6C (41); A915G (965) ; A917T (967) ; A1406G (1462)
84114	16	-	G659A (519); G916T (966) ; A917C (967)
59243	32	Pos	A915G (965) ; G1213T (1267)

Both ATCC strains 23064 and 14277 are used as reference. Mutations known to be associated with resistance are bolded. Tet, tetracycline.

*Sequential isolates from the same patient after isolate 72114.

fluoroquinolones, possibly because they are among the most commonly prescribed antimicrobials. Our findings also support the need for attempting isolation of *M. salivarium* by culture whenever a clinically significant infection is suspected and obtaining *in vitro* antimicrobial susceptibilities through a reference laboratory whenever possible for guidance of antimicrobial choices. Based on

our data, first line treatments should include clindamycin and tetracycline since the occurrence of resistance was lowest in these agents. It is known that the two drugs are distributed widely to tissues and body fluids, including the invasive infection sites (Baird et al., 1978; Beauduy and Winston, 2017). Previous case reports have shown clinical cure by treatment using clindamycin, doxycycline or minocycline in joint and brain infections (So et al., 1983; Orsted et al., 2011; Baracaldo et al., 2012; Buchsel et al., 2016). Moxifloxacin can be successful if the sensitivity is approved by *in vitro* susceptibility testing (Grisold et al., 2008), even the isolate was resistant to levofloxacin (Totten et al., 2021). New synthetic tetracycline derivatives such as omadacycline and the pleuromutilin lefamulin, both of which have activity *in vitro* against other human mycoplasmas that are resistant to other drug classes (Waites et al., 2016, 2017), may also be useful for treatment of *M. salivarium* infections, but thus far they have not been evaluated against this species.

This study also determined the molecular mechanisms of antimicrobial resistance in *M. salivarium*. The intrinsic erythromycin resistance in *M. salivarium* was due to the presence of 2057A in 23S rRNA, similar in several other *Mycoplasma* species (Whithear et al., 1983; Furneri et al., 2000; Pereyre et al., 2002; Stakenborg et al., 2005; Lysnyansky et al., 2015). In the sequential isolates from the same patient, a gradual increase of erythromycin and clindamycin MICs along with the development of C2611T and A2059G point mutations in 23S rRNA was observed, indicating a rapid evolution/adaptation of this organism. Although no treatment information was available for this patient, macrolide/clindamycin antibiotic pressure might be present during the study period. We also noticed that isolate 80422 collected in 2019 had a lower erythromycin MIC (32 mg/ml) compared to the two later isolates 82061 and 85051 collected in 2020 and 2021 (MIC = 256 and 128 mg/ml), while all three isolates had the same sequences in 23S rRNA, *rplD* and *rplV*. Other mechanisms of resistance might be involved and worth further investigation. We identified a 9-amino acid deletion at position 139 in ribosomal protein L22 that caused a high MIC for erythromycin (≥ 256 mg/ml) but not for clindamycin. The amino acid sequence around position 139 is unique for *M. salivarium* and may provide an interacting site specific for erythromycin but not for clindamycin.

We noticed there were 12 (out of 13) isolates harboring *tetM* sequence that were not resistant to tetracycline. Since all isolates were grown directly from original clinical specimens and no filter-clone procedure was performed to purify the organisms, there could be contaminations of *tetM* elements from other organisms carried in the original specimens. On the other hand, *tetM*-positive isolates susceptible to tetracyclines have been observed in *M. hominis* and *Ureaplasma* spp. (Degrange et al., 2008; Beeton et al., 2009). A recent study on *Ureaplasma* isolates showed that less than 10% of strains harboring *tetM* sequences were phenotypically resistant to tetracycline (Dumke, 2021). The diversity of the *TetM* sequences identified in this study suggests multiple acquisition sources, which means it is unlikely that the majority of the isolates acquired dysfunctional *tetM* genes. Other mechanisms of *tetM* regulation, such as transcriptional attenuation, or regulation mediated by small

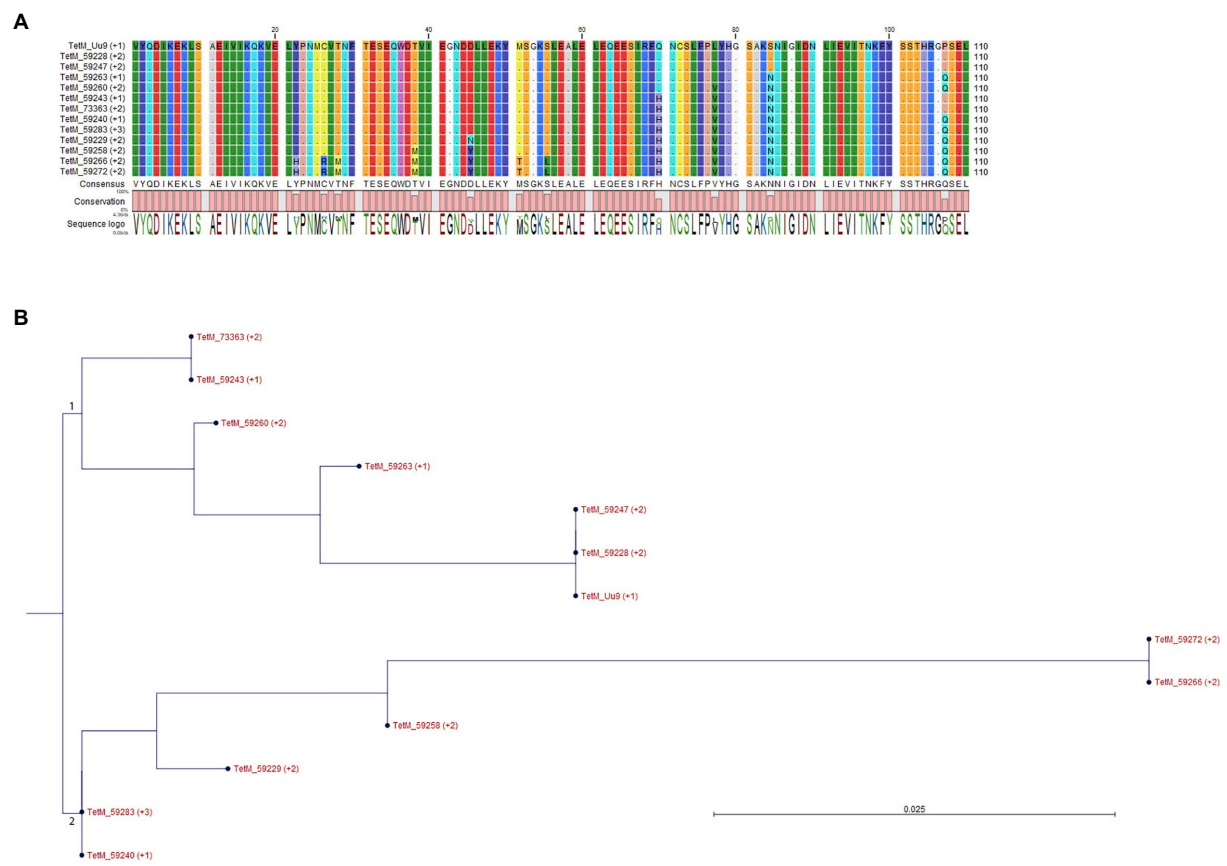


FIGURE 2
Alignment and grouping of the derived partial amino acid sequences of TetM. **(A)** Sequence alignment. Residues identical to that of TetM from *Ureaplasma urealyticum* serovar 9 (TetM_Uu9) were shown as dot. **(B)** Phylogenetic tree was constructed based on the alignment of **(A)** by Neighbor Joining method using Jukes–Cantor protein distance measurement and bootstrap of 100 replicates. The major groups 1 and 2 were indicated.

RNA (Su et al., 1992; Le Neindre et al., 2022), need further investigation. It is possible that tetracycline resistance could be induced through subculture of these isolates with low levels of tetracycline which activates *tetM* expression as reported in other organisms (Su et al., 1992; Degrange et al., 2008). Contrasting to the *tetM* sequences, mutations in 16S *rRNA* gene showed a better correlation with the observed tetracycline resistance in the *M. salivarium* isolates in this study. We believe this is the first complete documentation of a naturally occurring tetracycline resistance mechanism supported by phenotypic MIC data in a human mycoplasmal species other than the *tetM* transposon, which is fairly widespread among *M. hominis* and *Ureaplasma* spp. (Waites et al., 2014).

There are some limitations of this study. First, the number of isolates tested is small. Second, the susceptibility testing methods and MIC breakpoints have not been standardized specifically for *M. salivarium*, meaning that methods and interpretive criteria for other human mycoplasmas were utilized for reference. Third, the detailed clinical information on antimicrobial history of the patients from whom invasive isolates were obtained were not available, while the occurrence of acquired resistance could be related to their medical and antimicrobial exposure histories. Fourth, mechanisms of *tetM* regulation were not investigated in

this study, e.g., no attempt to induce tetracycline resistance in susceptible isolates with *tetM* was performed.

In a summary, our study demonstrates the frequent occurrence of acquired antimicrobial resistance in *M. salivarium*, which can involve multiple drug classes, and underscores the need for culture, susceptibility testing, or a molecular testing approach to guide effective treatment.

Data availability statement

The data presented in the study are deposited in the GenBank repository, accession numbers are: OM864597 to OM864634 for *16S rRNA* gene, ON023780 to ON023817 for *23S rRNA* gene, ON036345 to ON036382 for *rplD*, ON036383 to ON036420 for *rplV*, ON036193 to ON036230 for *gyrA*, ON036231 to ON036268 for *gyrB*, ON036269 to ON036306 for *parC* and ON036307 to ON036344 for *parE*.

Author contributions

LX, AT, TA, and KW conceived and designed the study. DC performed antimicrobial susceptibility testing. LX performed

genetic and statistical analysis. LX, AT, and KW wrote the main manuscript draft. All authors contributed to the article and approved the submitted version.

Acknowledgments

We thank Melanie Fecanin and Amy Ratliff for their technical support.

Conflict of interest

The authors declare that the research was conducted in the absence of any commercial or financial relationships that could be construed as a potential conflict of interest.

References

- Baird, P., Hughes, S., Sullivan, M., and Willmot, I. (1978). Penetration into bone and tissues of clindamycin phosphate. *Postgrad. Med. J.* 54, 65–67. doi: 10.1136/pgmj.54.628.65
- Baracaldo, R., Foltz, M., Patel, R., and Bourbeau, P. (2012). Empyema caused by *Mycoplasma salivarium*. *J. Clin. Microbiol.* 50, 1805–1806. doi: 10.1128/JCM.06839-11
- Bauduy, C. E., and Winston, L. G. (2017). “Tetracyclines, macrolides, clindamycin, chloramphenicol, streptogramins, and oxazolidinones,” in *Basic and clinical pharmacology*, 14e. ed. B. G. Katzung (New York, NY: McGraw-Hill Education)
- Bebear, C. M., Renaudin, H., Charron, A., Gruson, D., Lefrançois, M., and Bebear, C. (2000). In vitro activity of trovafloxacin compared to those of five antimicrobials against mycoplasmas including *Mycoplasma hominis* and *Ureaplasma urealyticum* fluoroquinolone-resistant isolates that have been genetically characterized. *Antimicrob. Agents Chemother.* 44, 2557–2560. doi: 10.1128/AAC.44.9.2557-2560.2000
- Beeton, M. L., Chalker, V. J., Maxwell, N. C., Kotecha, S., and Spiller, O. B. (2009). Concurrent titration and determination of antibiotic resistance in ureaplasma species with identification of novel point mutations in genes associated with resistance. *Antimicrob. Agents Chemother.* 53, 2020–2027. doi: 10.1128/AAC.01349-08
- Blanchard, A., Crabb, D. M., Dybvig, K., Duffy, L. B., and Cassell, G. H. (1992). Rapid detection of tetM in *Mycoplasma hominis* and *Ureaplasma urealyticum* by PCR: tetM confers resistance to tetracycline but not necessarily to doxycycline. *FEMS Microbiol. Lett.* 74, 277–281. doi: 10.1111/j.1574-6968.1992.tb05379.x
- Buchsel, M., Pletschen, L., Fleiner, M., Hacker, G., and Serr, A. (2016). A case of septic arthritis caused by a *Mycoplasma salivarium* strain resistant towards ciprofloxacin and clarithromycin in a patient with chronic lymphatic leukemia. *Diagn. Microbiol. Infect. Dis.* 86, 115–117. doi: 10.1016/j.diagmicrobio.2016.05.018
- Centor, R. M., Atkinson, T. P., Ratliff, A. E., Xiao, L., Crabb, D. M., Estrada, C. A., et al. (2015). The clinical presentation of *Fusobacterium*-positive and streptococcal-positive pharyngitis in a university health clinic: a cross-sectional study. *Ann. Intern. Med.* 162, 241–247. doi: 10.7326/M14-1305
- Clinical and Laboratory Standards Institute (2011). *Methods for antimicrobial susceptibility testing of human mycoplasmas. approved guideline*. Wayne, PA: Clinical and Laboratory Standards Institute.
- Degrange, S., Renaudin, H., Charron, A., Bebear, C., and Bebear, C. M. (2008). Tetracycline resistance in *Ureaplasma* spp. and *Mycoplasma hominis*: prevalence in Bordeaux, France, from 1999 to 2002 and description of two tet(M)-positive isolates of *M. hominis* susceptible to tetracyclines. *Antimicrob. Agents Chemother.* 52, 742–744. doi: 10.1128/AAC.00960-07
- Dumke, R. (2021). Antimicrobial resistance in clinical isolates of *Ureaplasma* spp. from samples in Germany. *Antimicrob. Agents Chemother.* 65:e02342-20. doi: 10.1128/AAC.02342-20
- Furneri, P. M., Rappazzo, G., Musumarra, M. P., Tempera, G., and Roccasalva, L. S. (2000). Genetic basis of natural resistance to erythromycin in *Mycoplasma hominis*. *J. Antimicrob. Chemother.* 45, 547–548. doi: 10.1093/jac/45.4.547
- Grisold, A. J., Hoenigl, M., Leitner, E., Jakse, K., Feierl, G., Raggam, R. B., et al. (2008). Submasseteric abscess caused by *Mycoplasma salivarium* infection. *J. Clin. Microbiol.* 46, 3860–3862. doi: 10.1128/JCM.00807-08
- Henrich, B., Rummig, M., Sczyrba, A., Velleuer, E., Dietrich, R., Gerlach, W., et al. (2014). *Mycoplasma salivarium* as a dominant coloniser of Fanconi anaemia associated oral carcinoma. *PLoS One* 9:e92297. doi: 10.1371/journal.pone.0092297
- Johnson, S. M., Bruckner, F., and Collins, D. (2007). Distribution of *Mycoplasma pneumoniae* and *Mycoplasma salivarium* in the synovial fluid of arthritis patients. *J. Clin. Microbiol.* 45, 953–957. doi: 10.1128/JCM.01973-06
- La Scola, B., Michel, G., and Raoult, D. (1997). Use of amplification and sequencing of 16S rRNA gene to diagnose *Mycoplasma pneumoniae* osteomyelitis in a patient with hypogammaglobulinemia. *Clin. Infect. Dis.* 24, 1161–1163. doi: 10.1086/513631
- Lamster, I. B., Grbic, J. T., Bucklan, R. S., Mitchell-Lewis, D., Reynolds, H. S., and Zambon, J. J. (1997). Epidemiology and diagnosis of HIV-associated periodontal diseases. *Oral Dis.* 3, S141–S148. doi: 10.1111/j.1601-0825.1997.tb00348.x
- Le Neindre, K., Dejoies, L., Reissier, S., Guerin, F., Felden, B., and Cattoir, V. (2022). Small RNA-mediated regulation of the tet(M) resistance gene expression in *Enterococcus faecium*. *Res. Microbiol.* 173:103941. doi: 10.1016/j.resmic.2022.103941
- Le Roy, C., Touati, A., Balcon, C., Garraud, J., Molina, J. M., Bercot, B., et al. (2021). Identification of 16S rRNA mutations in *Mycoplasma genitalium* potentially associated with tetracycline resistance in vivo but not selected in vitro in *M. genitalium* and *Chlamydia trachomatis*. *J. Antimicrob. Chemother.* 76, 1150–1154. doi: 10.1093/jac/dkab016
- Lysnyansky, I., Gerchman, I., Flaminio, B., and Catania, S. (2015). Decreased susceptibility to macrolide-Lincosamide in *Mycoplasma synoviae* is associated with mutations in 23S ribosomal RNA. *Microb. Drug Resist.* 21, 581–589. doi: 10.1089/mdr.2014.0290
- Mizuki, H., Abe, R., Kogi, S., and Mikami, T. (2017). Immunohistochemical detection of *Mycoplasma salivarium* in oral lichen planus tissue. *J. Oral Pathol. Med.* 46, 649–656. doi: 10.1111/jop.12568
- Orsted, I., Gertsen, J. B., Schonheyder, H. C., Jensen, J. S., and Nielsen, H. (2011). *Mycoplasma salivarium* isolated from brain abscesses. *Clin. Microbiol. Infect.* 17, 1047–1049. doi: 10.1111/j.1469-0691.2011.03462.x
- Pereyre, S., Gonzalez, P., De Barbeyrac, B., Darnige, A., Renaudin, H., Charron, A., et al. (2002). Mutations in 23S rRNA account for intrinsic resistance to macrolides in *Mycoplasma hominis* and *Mycoplasma fermentans* and for acquired resistance to macrolides in *M. hominis*. *Antimicrob. Agents Chemother.* 46, 3142–3150. doi: 10.1128/AAC.46.10.3142-3150.2002
- So, A. K., Furr, P. M., Taylor-Robinson, D., and Webster, A. D. (1983). Arthritis caused by *Mycoplasma salivarium* in hypogammaglobulinemia. *Br. Med. J. (Clin. Res. Ed.)* 286, 762–763. doi: 10.1136/bmj.286.6367.762
- Stakenborg, T., Vicca, J., Butaye, P., Maes, D., Minion, F. C., Peeters, J., et al. (2005). Characterization of In vivo acquired resistance of *Mycoplasma hyopneumoniae* to macrolides and lincosamides. *Microb. Drug Resist.* 11, 290–294. doi: 10.1089/mdr.2005.11.290

Publisher's note

All claims expressed in this article are solely those of the authors and do not necessarily represent those of their affiliated organizations, or those of the publisher, the editors and the reviewers. Any product that may be evaluated in this article, or claim that may be made by its manufacturer, is not guaranteed or endorsed by the publisher.

Supplementary material

The Supplementary material for this article can be found online at: <https://www.frontiersin.org/articles/10.3389/fmicb.2022.914464/full#supplementary-material>

- Su, Y. A., He, P., and Clewell, D. B. (1992). Characterization of the tet(M) determinant of Tn916: evidence for regulation by transcription attenuation. *Antimicrob. Agents Chemother.* 36, 769–778. doi: 10.1128/AAC.36.4.769
- Sulaiman, I., Chung, M., Angel, L., Tsay, J. J., Wu, B. G., Yeung, S. T., et al. (2021). Microbial signatures in the lower airways of mechanically ventilated COVID-19 patients associated with poor clinical outcome. *Nat. Microbiol.* 6, 1245–1258. doi: 10.1038/s41564-021-00961-5
- Tagg, K. A., Jeoffreys, N. J., Couldwell, D. L., Donald, J. A., and Gilbert, G. L. (2013). Fluoroquinolone and macrolide resistance-associated mutations in *Mycoplasma genitalium*. *J. Clin. Microbiol.* 51, 2245–2249. doi: 10.1128/JCM.00495-13
- Thoendel, M., Jeraldo, P., Greenwood-Quaintance, K. E., Chia, N., Abdel, M. P., Steckelberg, J. M., et al. (2017). A novel prosthetic joint infection pathogen, *Mycoplasma salivarium*, identified by metagenomic shotgun sequencing. *Clin. Infect. Dis.* 65, 332–335. doi: 10.1093/cid/cix296
- Totten, A. H., Xiao, L., Crabb, D. M., Ratliff, A. E., Waites, K. B., Hwangpo, T., et al. (2021). Septic polyarthrititis with *Mycoplasma salivarium* in a patient with common variable immunodeficiency: case report and review of the literature. *Access Microbiol.* 3:221. doi: 10.1099/acmi.0.000221
- Uchida, A., Horikawa, T., Matsuura, M., and Watanabe, T. (1981). A preliminary study on isolation and enumeration of mycoplasmas in dental plaques: the effect of sonication on viability of oral mycoplasmas. *Bull. Tokyo Med. Dent. Univ.* 28, 111–116. PMID: 6947863
- Waites, K. B., Crabb, D. M., Duffy, L. B., Jensen, J. S., Liu, Y., and Paukner, S. (2017). In vitro activities of lefamulin and other antimicrobial agents against macrolide-susceptible and macrolide-resistant *Mycoplasma pneumoniae* from the United States, Europe, and China. *Antimicrob. Agents Chemother.* 61, 302008–302016. doi: 10.1128/AAC.02008-16
- Waites, K. B., Crabb, D. M., Liu, Y., and Duffy, L. B. (2016). In vitro activities of omadacycline (PTK 0796) and other antimicrobial agents against human mycoplasmas and ureaplasmas. *Antimicrob. Agents Chemother.* 60, 7502–7504. doi: 10.1128/AAC.01734-16
- Waites, K. B., Lysnyansky, I., and Bebear, C. M. (2014). “Antibiotic susceptibility testing and resistance in mycoplasmas of humans and animals,” in *Mollicutes molecular biology and pathogenesis*. eds. G. Browning and C. Citti (Norfolk, UK: Caister Academic Press), 289–322.
- Watanabe, T., Matsuura, M., and Seto, K. (1986). Enumeration, isolation, and species identification of mycoplasmas in saliva sampled from the normal and pathological human oral cavity and antibody response to an oral mycoplasma (*Mycoplasma salivarium*). *J. Clin. Microbiol.* 23, 1034–1038. doi: 10.1128/jcm.23.6.1034-1038.1986
- Weisburg, W. G., Barns, S. M., Pelletier, D. A., and Lane, D. J. (1991). 16S ribosomal DNA amplification for phylogenetic study. *J. Bacteriol.* 173, 697–703. doi: 10.1128/jb.173.2.697-703.1991
- Whithear, K. G., Bowtell, D. D., Ghiocas, E., and Hughes, K. L. (1983). Evaluation and use of a micro-broth dilution procedure for testing sensitivity of fermentative avian mycoplasmas to antibiotics. *Avian Dis.* 27, 937–949. doi: 10.2307/1590195



OPEN ACCESS

EDITED BY

Glenn Francis Browning,
The University of Melbourne, Australia

REVIEWED BY

Katarzyna Dudek,
National Veterinary Research Institute
(NVR), Poland
Ewelina Szacawa,
National Veterinary Research Institute
(NVR), Poland
Nadeeka Wawegama,
The University of Melbourne, Australia

*CORRESPONDENCE

Changmin Hu
hcm@mail.hzau.edu.cn
Aizhen Guo
aizhen@mail.hzau.edu.cn

SPECIALTY SECTION

This article was submitted to
Infectious Agents and Disease,
a section of the journal
Frontiers in Microbiology

RECEIVED 21 April 2022

ACCEPTED 08 July 2022

PUBLISHED 03 August 2022

CITATION

Zhang H, Lu S, Chao J, Lu D, Zhao G,
Chen Y, Chen H, Faisal M, Yang L, Hu C
and Guo A (2022) The attenuated
Mycoplasma bovis strain promotes
apoptosis of bovine macrophages by
upregulation of CHOP expression.
Front. Microbiol. 13:925209.
doi: 10.3389/fmicb.2022.925209

COPYRIGHT

© 2022 Zhang, Lu, Chao, Lu, Zhao,
Chen, Chen, Faisal, Yang, Hu and Guo.
This is an open-access article
distributed under the terms of the
[Creative Commons Attribution License
\(CC BY\)](https://creativecommons.org/licenses/by/4.0/). The use, distribution or
reproduction in other forums is
permitted, provided the original
author(s) and the copyright owner(s)
are credited and that the original
publication in this journal is cited, in
accordance with accepted academic
practice. No use, distribution or
reproduction is permitted which does
not comply with these terms.

The attenuated *Mycoplasma bovis* strain promotes apoptosis of bovine macrophages by upregulation of CHOP expression

Hui Zhang^{1,2}, Siyi Lu¹, Jin Chao¹, Doukun Lu¹, Gang Zhao¹,
Yingyu Chen¹, Huanchun Chen¹, Muhammad Faisal¹,
Liguo Yang³, Changmin Hu^{1*} and Aizhen Guo^{1,4,5*}

¹State Key Laboratory of Agricultural Microbiology, College of Veterinary Medicine, Huazhong Agricultural University, Wuhan, China, ²College of Animal Husbandry and Veterinary Medicine, Southwest Minzu University, Chengdu, China, ³College of Animal Science and Technology, Huazhong Agricultural University, Wuhan, China, ⁴Key Laboratory of Development of Veterinary Diagnostic Products, Huazhong Agricultural University, Wuhan, China, ⁵Hubei Hongshan Laboratory, Huazhong Agricultural University, Wuhan, China

Mycoplasma bovis (*M. bovis*) is one of the major pathogens in the bovine respiratory disease complex, which includes pneumonia, mastitis, and arthritis and causes a great economic loss in the cattle industry. In China, a live-attenuated vaccine strain *M. bovis* P150 was obtained by a continuous culture of the wild-type strain *M. bovis* HB0801 (P1) *in vitro* for 150 passages. Using the infected bovine macrophage cell line BoMac, this work attempted to investigate the mechanism of P150 attenuation and protective immune response. To begin, we show that *M. bovis* P150 effectively triggered cytotoxicity and apoptosis in BoMac, although with lower intracellular survival than P1. The transcriptomes of BoMac after infection with *M. bovis* strains P1 and P150 were sequenced, and bioinformatic analysis identified 233 differentially expressed genes (DEGs), with 185 upregulated and 48 downregulated. Further Gene Ontology (GO) and Kyoto encyclopedia of genes and genomes (KEGG) pathway enrichment analyses revealed that the majority of the DEGs were linked to CHOP complex, MAP kinase phosphatase activity and were involved in the IL-17 signaling pathway in immune response, MAPK signaling pathway in signal transduction, and p53 signaling pathway in cell growth and death. Among them, the level of C/EBP homologous protein (CHOP) was significantly upregulated in P150-infected BoMac compared to P1-infected cells at different time points, along with its upstream and downstream genes phosphorylated-PERK, phosphorylated-EIF2 α , ATF4, and GADD45A increased in the PERK-dependent ER stress response. The role of CHOP in apoptosis was further verified by *M. bovis*-induced siCHOP knockdown in BoMac cells. The results showed that CHOP knockdown enhanced P150-induced apoptosis and dramatically increased the *M. bovis* P1

and P150 intracellular survival, particularly for P150. These data suggest that P150 infection upregulates CHOP expression, which can increase apoptosis and mediate a crosstalk between ER stress and apoptosis during infection, and hence, contribute to high cytotoxicity and low intracellular survival.

KEYWORDS

Mycoplasma bovis, CHOP, attenuation, apoptosis, transcriptome, endoplasmic reticulum stress, intracellular survival

Introduction

Mycoplasmas are the most basic self-replicating prokaryotes that are found in both humans and animals. They colonize the mucous surface of the respiratory, urogenital tracts, mammary glands, eyes and joints, exhibiting organ and tissue specificity (Citti and Blanchard, 2013). *Mycoplasma bovis* (*M. bovis*) is a common pathogen in cattle causing bovine mycoplasmosis, which can cause pneumonia, mastitis, genital disorders, arthritis, otitis, keratoconjunctivitis, or meningitis (Pfützner and Sachse, 1996; Alberti et al., 2006; Maunsell et al., 2012; Suwanruengsri et al., 2021). These illnesses have significant economic consequences, resulting in losses in the beef and dairy industries around the world (Calcutt et al., 2018). Due to the lack of effective vaccine, a restricted drug repertoire for disease treatment and increased development of antimicrobial resistance of *M. bovis*, management of bovine mycoplasmosis has remained difficult (Dudek et al., 2021).

Inactivated vaccines elicited a modest immunological response, which was insufficient to create antibodies against reinfection. For example, inactivated *Brucella* vaccines have been found to have issues such as inadequate protection, local responses caused by adjuvants, and serological issues (Lalsiamthara and Lee, 2017). Bacille Calmette-Guerin (BCG) is the only licensed vaccination against *Mycobacterium tuberculosis*, and it is more effective than inactivated vaccine (Fatima et al., 2020). It was observed that inactivated vaccines for enzootic pneumonia in mycoplasma species have improved, but illness decrease has been minimal (Nicholas et al., 2009). So far, a recent study shows that live-attenuated vaccines for several mycoplasmosis have already been created and have a higher effectiveness, such as *Mycoplasma gallisepticum* strain ts-304 (Kanci Condello et al., 2020) and *Mycoplasma synoviae* strain MS-H (Zhu et al., 2019) through chemical mutagenesis, and *Mycoplasma hyopneumoniae* strain 168 through *in vitro* continuous passaging (Xiong et al., 2014). After continuous development, *in vitro* for 150 passages, we generated an attenuated vaccine *M. bovis* strain P150 from the wild-type *M. bovis* HB0801 strain (designated as P1) after continuous culture *in vitro* for 150 passages (Zhang et al., 2014).

The P150 strain has low virulence but remains a critical protection against a virulent challenge from the P1 strain (Chao et al., 2019). Further genome sequencing indicated that P150 genome was missing one 14.2-kb section and that the strain has 46 non-sense single-nucleotide polymorphisms and indels (Rasheed et al., 2017). The P1 infection tended to induce a pro-inflammatory pathogenic Th17 response in bovine peripheral blood mononuclear cells, whereas P150 infection induced a Th1 response (Chao et al., 2019). However, the mechanism of the P150 strain's attenuation and protective immune response in comparison to the P1 strain is unknown.

Through successful recognition, clearance of germs, cytokine generation, and antigen presentation, macrophages play a crucial role in the early management of bacterial infections. Variation in surface antigens, production of biofilms and cleavage of the IgG heavy chains are only a few of the ways *M. bovis* uses to avoid opsonization and phagocytosis by the macrophages, allowing it to avoid the activation of an effective immune response (Maunsell and Chase, 2019). To limit bacterial infection, host macrophages also send out an apoptotic signal (Borchsenius et al., 2020). *M. bovis* has been shown to delay apoptosis in bovine monocytes *in vitro*, extending bacterial viability and facilitating bacterial dissemination (Mulongo et al., 2014). *M. bovis* may also suppress the intrinsic apoptotic pathway in bovine macrophage BoMac cells (Maina et al., 2019). However, *M. bovis* of varying virulence has been observed to modulate PBMC proliferation, apoptosis, and survival in distinct ways (Suleman et al., 2016). Understanding how *M. bovis* infection causes apoptosis would aid in identifying host immune responses that could be used to limit infection.

This study aimed to investigate the mechanism by which P150 was attenuated by comparing the transcriptome sequences of BoMac cells infected with *M. bovis* P1 and P150, and revealing the function of critical genes associated with the viability of infected BoMac cells and mycoplasma survival after infection. The findings suggest that elevation of CHOP expression may be responsible for the increased apoptosis produced by P150. The findings add to our understanding of *M. bovis* P150 attenuation and likely explain the protective immune response.

Materials and methods

Strains, cells, and reagents

Mycoplasma bovis HB0801 wild-type strain (P1) (GenBank accession no. NC_018077.1) was isolated from the lung of a diseased cattle with pneumonia in Hubei Province, China (Qi et al., 2012), and its attenuated strain *M. bovis* P150 strain (P150) (GenBank accession no. CP007590.1) was produced from P1 following continuous passaging *in vitro* 150 times and maintained in our laboratory (Zhang et al., 2014). Both strains were cultivated at 37°C in 5% CO₂ for 36 h in pleuropneumonia-like organisms (PPLO) medium (BD Company, MD, United States) supplemented with 10% horse serum (Hyclone, UT, United States). A 0.1 ml of culture with serial dilutions was plated on the PPLO medium containing 1.5% agarose (BD Difco™, San Diego, United States) and incubated at 37°C in 5% CO₂ for 72 h to count the quantity of mycoplasma (CFU/ml).

BoMac, a bovine peritoneal macrophage cell line donated by Judith R. Stabel of the United States Department of Agriculture's Johnes's disease Research Project in Ames, Iowa, was grown in Roswell Park Memorial Institute (RPMI) medium supplemented with 10% heat-inactivated fetal bovine serum (FBS) (Gibco, NY, United States).

The Cell Signaling Technology company (Danvers, MA, United States) provided antibodies against PERK Rabbit mAb (5683), Phospho-PERK Rabbit mAb (3179), phospho-eIF2α Rabbit mAb (3398), CHOP Mouse mAb (2895), GADD45A Rabbit mAb (4632). Proteintech (Wuhan, China) supplied the β-actin Mouse mAb (60008-1). All these prime antibodies have species cross-reactivity with bovine cells according to the product manual. The secondary antibodies used HRP-conjugated goat anti-mouse or anti-rabbit IgG (SouthernBiotech Company, Birmingham, United Kingdom).

Cell viability assay

The MTT assay was used to investigate the *M. bovis* P1 and P150 on the viability of BoMac cells. BoMac cells (1×10^4 cells/100 μl) were plated overnight in a 96-well plate and infected with *M. bovis* P1 and P150 at different multiplicities of infection (MOI) of 0.1, 1, 10, 100, 500, 1000 for another 12 h at 37°C. Each well received a 10 μl MTT solution (Beyotime Biotechnology, Shanghai, China) and was incubated for additional 4 h. Then, on a shaker at a low speed for 10 min, 110 μl of formazan solution was added to each well to fully dissolve the crystals. The absorbance at 490 nm was measured using a microplate reader (Victor NIVO, PerkinElmer Inc., United States). The cell viability was determined using the formula: cell viability (%) = $(OD_{\text{sample}} - OD_{\text{blank}}) / (OD_{\text{nc}} - OD_{\text{blank}}) \times 100\%$.

Cell apoptosis assay

Mycoplasma bovis P1 and P150 strains were infected into BoMac cells (1×10^6 cells/ml) at various MOIs of 10, 100, 500, 1,000, and 2,000 for 12 h, or at an MOI of 1,000 for 3, 6, 12, and 24 h. The cells were collected and stained with the Annexin V-FITC/PI detection kit (Vazyme, Nanjing, China) according to the manufacturer's protocol for flow cytometry detection, and the apoptotic cells were detected using a flow cytometer (Cytoflex, Beckman Coulter, Inc., United States) and analyzed using the FlowJo VX software.

Mycoplasma bovis survival in BoMac by gentamicin protection assay

The gentamicin assay was used to assess mycoplasma survival in BoMac cells, as previously described (Burgi et al., 2018). *M. bovis* P1 and P150 were infected into BoMac cells at MOI of 50. The cells were rinsed twice with PBS after 3 h of infection, then given the DMEM medium supplemented with 400 μg/ml gentamicin. The plates were incubated for another 3 h before being washed three times with PBS to remove gentamicin and replaced with fresh DMEM medium. The cells were then collected at 0, 3, 12, 24, 36, and 50 h, lysed with sterile water, and the amount of mycoplasma (CFU/ml) was determined by plating the 10-fold serially diluted lysate on PPLO agar plates.

Observation of cell morphology and ultrastructure with transmission electronic microscopy

Mycoplasma bovis and the infected cells were seen using transmission electron microscopy (TEM) (HITACHI, Tokyo, Japan). BoMac cells were seeded in 6-well plates, infected at an MOI of 1,000 with *M. bovis* P1 and P150, and incubated for 12 h. The cells were then rinsed in PBS and fixed with 1.5% glutaraldehyde in 0.1 M cacodylate buffer, then postfixed for 2 h at 4°C in 2% osmium tetroxide, dehydrated in a graded series of ethanol, embedded in Epon 812, and cut into ultrathin section (75 nm). Before being examined with a HITACHI H-600 electron microscope at 80 kV, the slices were stained with uranyl acetate and lead citrate.

RNA extraction, RNA sequencing, and bioinformatic analysis

BoMac cells (1×10^6 cells/ml) were seeded into 6-well cell plates and inoculated with *M. bovis* P1 and P150 at an MOI of 1,000 for 12 h. The entire RNA extraction, cDNA library construction, and RNA-seq method were carried out as previously described (Ouyang et al., 2016). Total RNA was

isolated using TRIzol® Reagent (Invitrogen, United States), quality-verified using agarose gel electrophoresis, and quantified using an Agilent 2100 bioanalyzer (Agilent Technologies, CA, United States). The RNA integrity numbers (RIN) greater than eight were further processed for sequencing.

The mRNA was extracted using magnetic oligo (dT) beads and cleaved into short fragments after total RNA samples were treated with DNase I. Then, using the mRNA fragments as templates, cDNA was generated and appropriate fragments purified by agarose gel electrophoresis were chosen as PCR templates. Finally, the Illumina HiSeq high-throughput sequencing platform was used to sequence six samples from each of the three groups. After filtering the adapters, clean reads were recovered and mapped to reference sequences using HISAT2. The DESeq2 program was then used to find differentially expressed genes (DEGs) in P1 and P150 infected cells. The significance of gene expression differences was judged using the $p < 0.05$ and the fold change ($\log_2\text{ratio} > 1$) thresholds. The Clustering software was used to do hierarchical cluster analysis of DEGs.

Functional categorization

The generated list of DEGs was analyzed using DAVID¹ and KOBAS² online tools to perform Gene Ontology (GO) enrichment analysis and KEGG pathway enrichment analysis, respectively.

Validation of sequencing data by qRT-PCR assay

A total of fourteen DEGs with substantial fold changes at a false discovery rate of $p < 0.01$ were chosen for qRT-PCR validation of expression diversity to validate the RNA-seq results. As previously stated, the total RNA was isolated from BoMac cells using TRIzol (Invitrogen, Carlsbad, California, United States). cDNA was synthesized using 1 µg of total RNA and a reverse transcription (RT) kit (Vazyme, Nanjing, China). Further, qRT-PCR was performed using the SYBR Green master mix (Vazyme). Each target gene's expression was compared to that of GAPDH. **Table 1** lists the primer sequences designed by us that were used in this study.

Western blot assay

Mycoplasma bovis P1 and P150 were infected into BoMac cells at an MOI of 1000 and harvested at 6, 12,

TABLE 1 The primers used for qRT-PCR in this study.

Primers	Sequences (5'-3')	Amplicon size (bp)
CXCR4-F	GCAGGTAGCAAAGTGACCCT	162
CXCR4-R	CGGAAGCAGGGTTCCCTTCAT	
CHAC1-F	CAACCACTCAAGGCATTGGC	130
CHAC1-R	AGTACTCAAGGTTGTGCCCG	
CXCL8-F	ATTCCACACCTTTCCACCCC	126
CXCL8-R	CCTTGGGGTTTAGGCAGACC	
GADD45A-F	CTCGGCTGGAGAGCAAAAGA	235
GADD45A-R	CTCACAGCAGAATGCCTGGA	
DDIT4-F	GCAAAGAACTACTGCGCCTG	206
DDIT4-R	GGCAGAGCTAAACAACCCCT	
PPP1R15A-F	CAACCAGGAGACACAGAGGA	222
PPP1R15A-R	ACTCTGGGTCTGAAGGGAGG	
CHOP-F	CCTGAGGAGAGAGTGTCCAG	219
CHOP-R	CTCCTTGTTCAGGGGGTG	
TCIM-F	GTAAGACCCTGACACGCACA	206
TCIM-R	TGACATCAGCGCCAGTCTTT	
TRIB3-F	ACTTTTAAGGAAGCCCGCGT	94
TRIB3-R	ATTTGCTGGAACGCCAGGG	
DUSP6-F	GGGTGGATTGTAGGTGCAGT	227
DUSP6-R	GCAGGCGAGACCGAAGTAAA	
IL1β-F	TCCACGTGGGCTGAATAACC	93
IL1β-R	TCGGGCATGGATCAGACAAC	
PTGS2-F	TGATCCCCAGGGCACAAATC	275
PTGS2-R	CAGGAACATGAGGCGGGTAG	
MYC-F	GAAGGGAGATCCGGAGTCAAA	300
MYC-R	CTGCAAGCCCGTATTTCAC	
ATF4-F	GCACCAAAACCTCGCAACAT	143
ATF4-R	AAGCATCCTCCTGTGTGTGT	
GAPDH-F	ACCCAGAAGACTGTGGATGG	129
GAPDH-R	CAACAGACACGTTGGGAGTG	

and 24 h post-infection (pi). Equal numbers of cells were lysed with RIPA lysis buffer with protease inhibitor cocktail and phosphatase inhibitors (Sigma-Aldrich, St. Louis, MO, United States). A BCA protein assay kit (Beyotime) was used to quantify protein concentrations, and 20 µg of total proteins were separated by 12% SDS-PAGE. The proteins in the gel were transferred onto polyvinylidene fluoride membranes (Millipore, Billerica, MA, United States), which were blocked for 1 h at room temperature with 5% (w/v) skim milk in Tris-buffered saline with 0.05% Tween 20 (TBST), and then incubated with different primary antibodies (1:1000 in dilution) overnight at 4°C. The membranes were then incubated and treated with goat anti-mouse IgG or anti-rabbit IgG (1:5000 in dilution, SouthernBiotech) for 1 h after being rinsed three times with TBST. Enhanced chemiluminescence (ECL) reagents (Thermo Fisher, Waltham, MA, United States) were utilized to detect the tagged proteins, with β-actin serving as an

¹ <https://david.ncifcrf.gov/>

² <http://kobas.cbi.pku.edu.cn/kobas3/>

internal control. ImageJ software was used to determine the intensity of each band.

C/EBP homologous protein-specific interference in BoMac cells

Table 2 lists the exact sequences of CHOP gene small interfering RNA (siRNA) oligos and non-target control siRNA (siCtrl) designed and manufactured by Gene Pharma Co., Ltd. (Suzhou, China), which were used to interfere with CHOP gene expression as follows. Then 55 μ mol siCHOP was transfected into BoMac cells using jetPRIMER[®] transfection reagent (Polyplus transfection, French) according to the manufacturer's manual. The cells were next treated with *M. bovis* P1 and P150 at an MOI of 1,000 for an additional 12 h at 37°C, as described above. After that, the cells were collected for the qRT-PCR and Western blot assay.

Statistical analysis

The statistical analysis was performed with GraphPad Prism 8.0 software (San Diego, CA, United States). The data were expressed as means \pm standard deviation (SD) of at least three independent experiments. The significance of the differences in each group was determined with either a two-tailed student's *t*-test for one comparison or a one-way analysis of variance (ANOVA) for over one comparison. The *p*-values less than 0.05 were regarded as statistically significant difference and denoted in the figures as follows: ns, not significant; **p* < 0.05, ***p* < 0.01, ****p* < 0.001, *****p* < 0.0001.

Data availability statement

Our SRA records were deposited in the NCBI database and will be accessible with the following link: <https://www.ncbi.nlm.nih.gov/bioproject/PRJNA769187>.

TABLE 2 Small interfering RNA (siRNA) sequences used in this study.

Name	Sense sequences (5'-3')	Antisense sequences (5'-3')
siCHOP-170	GCAGCUGAGUCACUGC CUUTT	AAGGCAGUGACUCAGC UGCTT
siCHOP-514	GCAACGCAUGAAGGAG AAATT	UUUCUCCUUAUGCGU UGCTT
siCHOP-649	GAUGGUUAAUCUGCAC CAATT	UUGGUGCAGAUUAACC AUCTT
siCtrl	UUCUCCGAACGUGUCA CGUTT	ACGUGACACGUUCGGA GAATT

Results

P150 induced higher levels of cytotoxicity and apoptosis, but lower intracellular survival

An MTT test was used to analyze the cytotoxic effect of *M. bovis* virulent P1 and attenuated P150 strains on BoMac cells. The P150 infection dramatically reduced cell viability at higher MOIs of 500 and 1,000, as seen in **Figure 1A**. The apoptosis levels of infected BoMac cells were detected using Annexin FITC/PI staining using flow cytometry to further study the reason underlying the lower cell viability. Infection of both strains caused increased levels of apoptosis in a dose- and time-dependent manner when compared to the control group (**Figures 1B,C**). At high MOIs of 500, 1,000, and 2,000, P150 triggered considerably more apoptosis than P1 (*p* < 0.01) (**Figure 1B**). The findings showed that both the two *M. bovis* strains increased the proportions of apoptotic cells from 6 h post-infection (pi) onward, compared to the blank control, but the apoptosis levels in the P150-infected cells were significantly higher than those in the P1-infected cells (*p* < 0.01) at 6, 12, and 24 h post-infection (pi) (**Figure 1C**).

The intracellular survival of mycoplasma was also tested. Although both strains' intracellular mycoplasma increased with time from 24 h pi onward, more viable bacteria were recovered from P1-infected BoMac cells than P150 (**Figure 1D**), showing that P1 has a better intracellular survival ability than P150.

After infection for 12 h, the ultrastructure of P1- and P150-infected BoMac cells was investigated under TEM. The typical morphological traits of apoptotic cells were frequently detected in P150-infected cells, including multiple cytoplasmic vacuoles, chromatin condensation and margination, and the formation of a crescent under the nuclear membrane (**Figure 1E**). In addition, after *M. bovis* P150 infection, the ER compartment was enlarged—a morphological sign of ER stress. The above morphological change was difficult to discern in P1-infected cells (**Figure 1E**).

Differentially expressed genes in BoMac cells induced by P1 and P150

Mycoplasma bovis P1- and P150- infected with BoMac cells were collected 12 h to determine the gene expression profile, and six transcript RNA libraries were created, with six samples called P1_1, P1_2, P1_3, P150_1, P150_2, and P150_3. **Supplementary Table 1** contains all information on the quality of transcriptomic sequencing. About filtering out the adapter and the value of Q30, around 27.4–33.6 million clean reads were recovered, and the comparison between the GC content of sequencing results was about 50.08–50.97%, indicating that

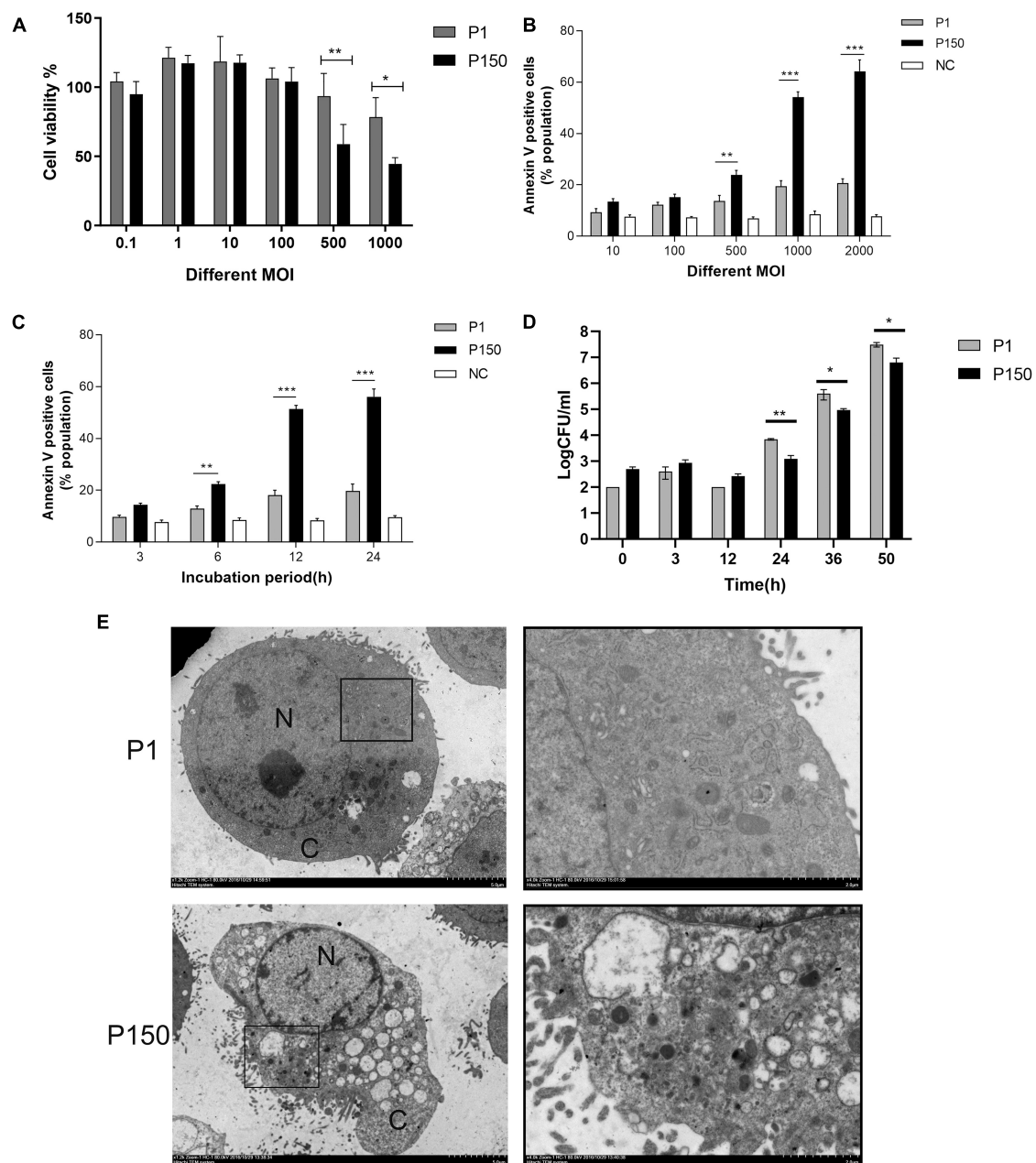


FIGURE 1

The differential viability and apoptosis of BoMac cells infected by *M. bovis* P1 and P150 and intracellular survival of both strains. (A) MTT assay demonstrated that infection decreased cell viability in dose-dependent manner with the high multiplicities of infection (MOI) of 500 and 1000, but P150 showed stronger ability to reduce cell viability than P1. (B) Flow cytometry assay on apoptosis of the infected BoMac cells at various MOIs after being stained with Annexin V-FITC and propidium iodide (PI) showed that P150 induced significantly higher levels of apoptosis at high MOIs. (C) Flow cytometry assay on apoptosis of infected BoMac cells at various times post-infection at an MOI of 1000 showed that P150 induced significantly higher levels of apoptosis from 6 h onward. (D) Intracellular survival and growth of *M. bovis* P1 and P150 in BoMac cells. The data represent the mean \pm SD of 3 independent experiments. *, **, and *** represent $p < 0.05$, $p < 0.01$, and $p < 0.001$, respectively. (E) TEM micrographs of BoMac cells infected with P1 and P150 where the P150 infected cells are characterized by typical morphology of apoptotic cells including cytoplasmic vacuolation, chromatin condensation and margination, and formation of a crescent. The perinuclear rough ER regions on the images in the left panel are magnified on the right panels. Asterisk indicates ER lamellae infection by P1 and P150. N, nucleus; C, cytoplasm.

the sequencing data are suitable for further study. Using TopHat v2.0.12, we mapped the high quantity clean to the cow genome (*Bos taurus*). Total cleaning reads were 95.40–95.67% mapped to

the cattle genome, with 93.14–93.44% of them uniquely mapped to a specific location within the cattle genome. Furthermore, the percentage of multi-mapped reads in each sample was less than

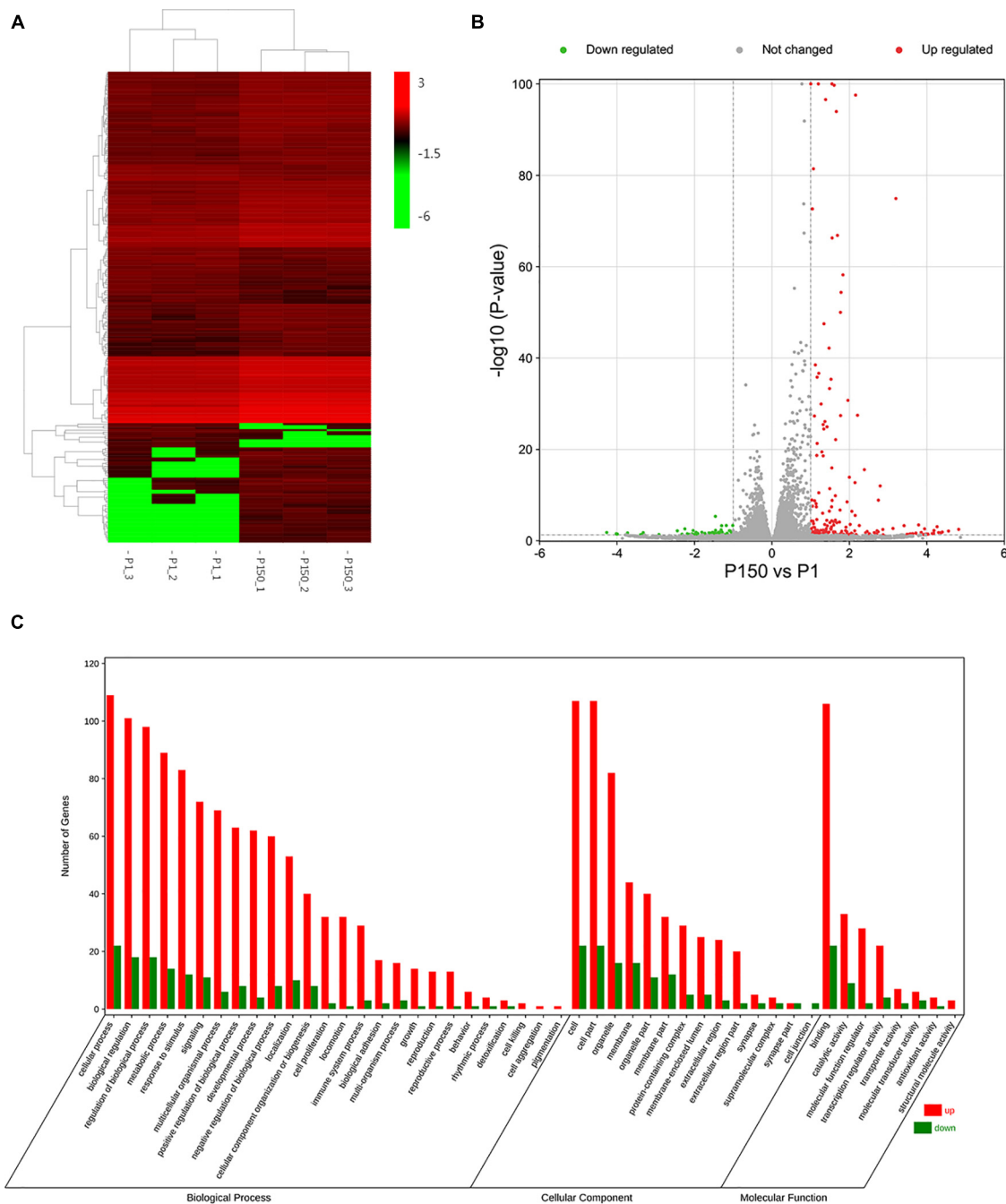


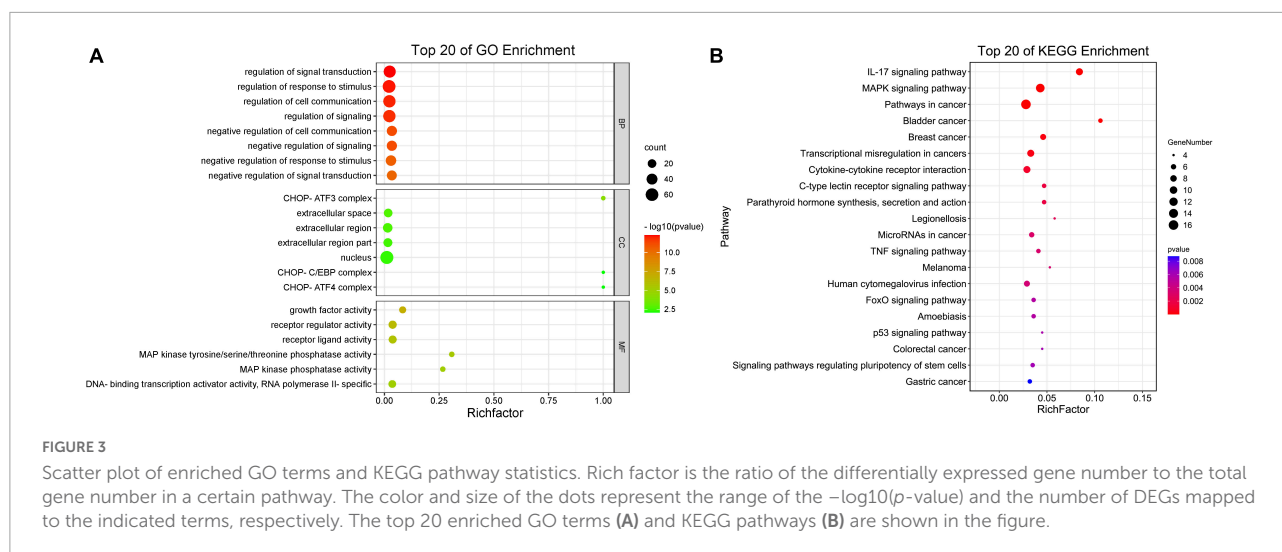
FIGURE 2

DEGs analysis of BoMac cell after the P1 and P150 infection. **(A)** The heat map showed the expression levels of DEGs in the pair of P150 vs. P1. The red color represents the upregulated expression of genes, while the green color represents a downregulated expression of genes. The gradient color barcode at the right top indicates $\log_2(\text{FPKM})$ value. Each row represents a gene and each column represents a sample. **(B)** Volcano map showed the differential mRNA expression between P150 and P1 ($\log_2(\text{Fold Change}) > 1$, $p\text{-value} < 0.05$). **(C)** Gene ontology (GO) functional classification of upregulated (Red) and downregulated (Green) DEGs. Genes were annotated in three categories: biological process, molecular function, and cellular component. The X-axis means the number of DEGs, while Y-axis represents GO terms.

5%, which is within industry standards and indicates that these data were available for DEGs analysis.

Heat maps were created based on $\log_2(\text{Fold change}) > 1$ and $p < 0.05$ values to display the findings of clustering analysis

using Cluster 3.0 software, in which one little square represents one gene and its color represents the gene's expression level, as shown in Figure 2A. Each column shows the expression level of all genes in each sample, whereas each row represents the



expression level of each gene in a distinct sample. **Figure 2B** and **Supplementary Table 2** show that out of the 16,329 genes in the annotated bovine genome, the clustering analysis revealed 233 DEGs in the P150-infected cells vs. the P1-infected cells, with 185 DEGs upregulated and only 48 DEGs downregulated ($\log_2\text{FoldChange} > 1$, $p\text{-value} < 0.05$).

Gene ontology and Kyoto encyclopedia of genes and genomes pathway enrichment analysis of differentially expressed genes

We used a web-based DAVID database to do GO analysis to learn more about the biological activities of the DEGs. A total of 162 out of 233 profiled DEGs were ascribed to 26 biological processes, 14 cellular components, and 8 molecular function terms. The GO terms of molecular function category were binding, catalytic activity, and molecular function regulator. The top five GO terms in biological functions were mostly related to cellular process, biological regulation, regulation of biological process, metabolic process, and response to stimulus. The top five GO terms in cellular component function included cell, cell part, organelle, membrane, and organelle part. **Figure 2C** depicts typical GO terms with full data in **Supplementary Table 3**.

The top 20 enriched GO terms were further examined using the Rich Factor, with the “CHOP-ATF3 complex,” “CHOP-C/EBP complex,” and “CHOP-ATF4 complex” in cellular component function and “MAP kinase phosphatase activity” in the molecular function being the most significantly enriched GO terms (**Figure 3A** and **Supplementary Table 3**). Two of the top 20 KEGG enrichment pathways were linked to the immune system, including the IL-17 signaling pathway and C-type lectin receptor signaling pathway. Three pathways were involved in signal transduction, such as

MAPK signaling pathway, TNF signaling pathway, and FoxO signaling pathway. The p53 signaling pathway, for example, was implicated in cell growth and death. Three pathways were associated with infectious diseases, such as legionellosis, human cytomegalovirus infection, and amebiasis (**Figure 3B** and **Supplementary Table 4**). Based on the p -values and GO enrichment score, 20 genes were most significantly upregulated after the P150 infection. **Table 3** has further information on these genes. These DEGs potential targets could be important mediators in the *M. bovis* infection.

Validation of differentially expressed genes involved in inflammatory response and apoptosis

For the qRT-PCR validation, 14 upregulated DEGs implicated in the inflammatory response and CHOP complex were chosen. When compared to P1, the expression of CHOP (DDIT3, DNA damage-inducible transcript 3) and ATF4 (activating transcription factor 4) genes, which are involved in the PERK signaling pathway and the intrinsic apoptotic signaling pathway in response to ER stress, was confirmed to be upregulated in the P150-infected cells. Furthermore, the expression of proapoptotic genes such as CHAC1 (glutathione specific gamma-glutamylcyclotransferase 1), TRIB3 (tribbles pseudokinase 3), GADD45A (growth arrest and DNA damage-inducible alpha), and DUSP6 (dual specificity phosphatase 6) was also upregulated. Furthermore, in P150-infected cells, expression of numerous positive apoptotic genes such as TCIM (transcriptional and immune response regulator), MYC (MYC proto-oncogene), PPP1R15 (protein phosphatase 1 regulatory subunit 15A) was elevated. CXCL8, CXCR4, and IL1B, all of which contribute to the inflammatory response, were also elevated. The relative expression levels of all 14 DEGs were consistent with the RNA-seq results in general (**Figure 4**).

TABLE 3 Mostly upregulated enriched 20 DEGs in *M. bovis* P150 infected BoMac compared to P1 strain.

Gene names	Description	GO terms	log2Fold change	P-values
TCIM	transcriptional and immune response regulator	GO:0006915 apoptotic process GO:0045746 negative regulation of Notch signaling pathway	3.20	1.20E-75
HMOX1	heme oxygenase 1	GO:0006915 apoptotic process GO:0043065 positive regulation of apoptotic process GO:0006979 response to oxidative stress	1.21	2.17E-37
CHOP	DDIT3, C/EBP homologous protein	GO:0006915 apoptotic process GO:0070059 intrinsic apoptotic signaling pathway in response to endoplasmic reticulum stress GO:0034976 response to endoplasmic reticulum stress GO:1990622 CHOP-ATF3 complex	1.78	4.22E-55
BNIP1	BCL2 interacting protein like	GO:0006915 apoptotic process GO:0008285 negative regulation of cell proliferation	1.12	0
PPP1R15A	protein phosphatase 1 regulatory subunit 15A	GO:0006915 apoptotic process	1.12	3.16E-39
INHBE	inhibin subunit beta E	GO:0042981 regulation of apoptotic process	1.20	0.01
GDF15	growth differentiation factor 15	GO:0042981 regulation of apoptotic process	1.83	6.26E-59
MYC	MYC proto-oncogene, bHLH transcription factor	GO:0008284 positive regulation of cell proliferation GO:0060070 canonical Wnt signaling pathway GO:0042981 regulation of apoptotic process	1.61	1.89E-100
DUSP1	dual specificity phosphatase 1	GO:0042981 regulation of apoptotic process	1.07	3.70E-82
DUSP6	dual specificity phosphatase 6	GO:0043065 positive regulation of apoptotic process	1.04	2.31E-73
GADD45A	growth arrest and DNA-damage-inducible alpha	GO:0043065 positive regulation of apoptotic process	1.55	1.60E-113
OSGIN1	oxidative stress induced growth inhibitor 1	GO:0043065 positive regulation of apoptotic process	1.27	1.10E-30
TRIB3	tribbles pseudokinase 3	GO:0070059 intrinsic apoptotic signaling pathway in response to endoplasmic reticulum stress GO:0034976 response to endoplasmic reticulum stress	1.77	9.84E-51
CHAC1	ChaC glutathione specific gamma-glutamylcyclotransferase 1	GO:0045746 negative regulation of Notch signaling pathway GO:0070059 intrinsic apoptotic signaling pathway in response to endoplasmic reticulum stress	1.96	1.79E-31
CXCL8	C-X-C motif chemokine ligand 8	GO:0006955 immune response GO:0006954 inflammatory response GO:0070098 chemokine-mediated signaling pathway GO:0034976 response to endoplasmic reticulum stress	2.21	3.24E-28
KLF4	Kruppel like factor 4	GO:0008285 negative regulation of cell proliferation GO:0060070 canonical Wnt signaling pathway	1.10	4.71E-28
SPRY2	sprouty RTK signaling antagonist 2	GO:0008285 negative regulation of cell proliferation GO:0010628 positive regulation of gene expression	1.16	0.000022
CYP27B1	cytochrome P450 family 27 subfamily B member 1	GO:0008285 negative regulation of cell proliferation	1.18	0.004959799
SRXN1	sulfiredoxin 1	GO:0006979 response to oxidative stress	1.49	4.67E-34
PTGS2	prostaglandin-endoperoxide synthase 2	GO:0006979 response to oxidative stress	1.63	0.0000465

log2Fold changes (P150/P1) display the mean value of 3 replicate samples obtained per group. Genes were ranked according to the expression changes detected by RNA-seq.

Overall, this verification revealed that infection of BoMac with P150 activated the proapoptotic signaling pathway more than the infection with P1.

Increased expression of endoplasmic reticulum-stress-associated genes during P150 infection

As shown above, three out of fourteen genes (ATF4, CHOP, and GADD45A) involved in the activation of the PERK pathway during ER stress were upregulated after P150 infection

compared to P1. The phosphorylation of the eukaryotic initiation factor 2 alpha subunit (eIF2 α) and expression of ATF4, an ER-stress-inducible transcription factor, could be activated by activating the proapoptotic genes CHOP and GADD45A when the PERK pathway is activated (Rozpedek et al., 2016). The P150-infected cells had considerably higher ATF4 mRNA expression at 8, 12, and 16 h pi than P1 and negative control cells, as expected (Figure 5A). In addition, its two downstream genes CHOP and GADD45A were shown to be considerably elevated in P150 (Figures 5B,C). Furthermore, whole-cell lysates were produced and analyzed for 6, 12, and 24 h pi by western blotting. The target protein's relative levels were

normalized to β -actin as an internal loading control protein, and densitometry measurement was determined using ImageJ software. We found that the CHOP protein levels were much greater in the P150-infected cells than in the P1-infected cells at 12 and 24 h, as seen in **Figures 5D,E**, showing that P150 infection could potentially boost the CHOP expression. We also looked at the expression of PERK, phosphorylated-PERK (P-PERK), phosphorylated EIF2 α (P-EIF2 α), and GADD45A to see whether the *M. bovis* P150 infection affected the PERK signal pathway. As shown in **Figures 5F,G**, the levels of P-PERK/PERK were significantly higher in the P150-infected cells than in the P1-infected at 4 and 8 h. The levels of P-EIF2 α were both higher in the P1- and P150-infected cells than in the negative control at 8, 12, and 24 h (**Figures 5F,H**). Interestingly, the levels of GADD45A were much higher in the P150-infected than in P1-infected or negative control cells (**Figures 5F,I**).

C/EBP homologous protein knockdown suppressed *M. bovis*-induced apoptosis

Three synthetic siRNAs against CHOP, including siCHOP-170, siCHOP-514, and siCHOP-649, were used to interfere with endogenous CHOP expression to further indicate that CHOP played a critical role during *M. bovis*-induced apoptosis. When compared to the non-targeting siCtrl, all three siCHOP had a significant inhibitory impact ($p < 0.0001$), however, siCHOP-514 and siCHOP-649 primarily decreased the CHOP expression (**Figure 6A**). Furthermore, the western blot assay confirmed that transfection of BoMac cells with siCHOP-649 almost eliminated the CHOP expression compared to non-targeting siCtrl control (**Figures 6B,C**). The siCHOP-649 was also used to investigate the effect of CHOP knockdown in apoptosis regulation. Flow cytometry was used to detect apoptosis, and the results revealed that the apoptotic cell percentage (right upper quadrant and right lower quadrant represent the late-stage apoptosis rate and early stage apoptosis rate, respectively) after CHOP knockdown dramatically reduced in the P150-infected cells at 12 h after infection ($p < 0.001$), but did not affect P1-induced cell death (**Figures 6D,E**).

Effect of C/EBP homologous protein-mediated apoptosis on intracellular survival of P150

Based on the findings, it is fair to believe that P150-induced apoptosis in ER stress response *via* CHOP could affect intracellular bacteria survival. Before infection with *M. bovis* P1 and P150, BoMac cells were transfected with

siCHOP. At 24 h PI. The total number of intracellular bacteria were considerably higher with siCHOP treatment than with siCtrl, and significantly higher than P1 with siCHOP treatment (**Figure 6F**).

Discussion

Mycoplasma bovis is a significant contributor to the global burden of bovine respiratory illness. In a recent work, an attenuated *M. bovis* strain P150 derived from several *in vitro* passages of the virulent strain P1 elicited a strong innate immune response, suggesting that it could protect calves from infection with the virulent strain P1 (Zhang et al., 2014). However, the pathogenicity of the two *M. bovis* strains to calves differs (Chao et al., 2019). In this investigation, we discovered that the *M. bovis*-attenuated-strain P150 could cause more apoptosis in BoMac cells than strain P1, and we investigated the transcriptional profile of BoMac cells at 12 h during *M. bovis* P1 and P150 infections, respectively. Our findings led to several intriguing conclusions. Validation of 14 elevated genes related to inflammatory response and apoptosis was found by comparing 233 DEGs. CHOP-mediated ER stress was surprisingly enriched as the most notable GO category. We also discovered that the CHOP gene is a key regulator of apoptosis in a PERK-dependent signal pathway and that it may be responsible for the ER-stress-induced apoptosis differences between P1 and P150.

Many studies have been done to develop various types of *M. bovis* vaccines to control its infections, including inactivated vaccines, subunit vaccines, and live-attenuated vaccines. Inactivated vaccines are the most commonly used in studies to prevent infections with *M. bovis* and there are two licensed vaccines for the prevention of *M. bovis* infections in the United States. However, the authors found that the two vaccines were not efficacious in reducing the number of *M. bovis* colonizing and the number of *M. bovis*-specific lesions (Soehnlen et al., 2011). Another attempt was made to develop an effective subunit vaccine against *M. bovis* associated with several immunogenic proteins, such as GAPDH, PdhA, PepA, Tuf, P48, P81, OppA, LppA, PepQ, O256, and DeoB (Pryslak and Perez-Casal, 2016). Unfortunately, there was an insufficient cell-mediated response to the *M. bovis* recall antigens and no protection against the *M. bovis* challenge, although a strong humoral immune response was observed based on the IgG1 and IgG2 serum responses (Pryslak et al., 2013). Whereas live-attenuated vaccines are relatively safe and effective, which have been licensed and accepted by swine, poultry, and cattle producers in many countries (Feng et al., 2013; Zhang et al., 2014; Kanci Condello et al., 2020). However, we still lack information about its mechanism of attenuation and protective immune response. In recent years, apoptosis inhibition by different bacteria has been suggested as a mechanism of survival by allowing the pathogen to replicate and disseminate in the

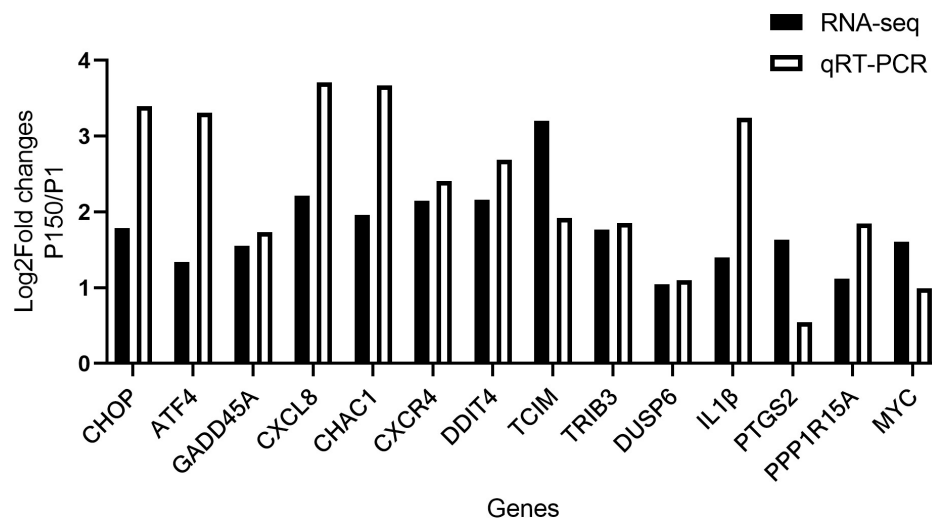


FIGURE 4

Validation of RNA-seq results by qRT-PCR. Log2Fold changes (P150 vs. P1) obtained by qRT-PCR were compared with the sequencing results for 14 DEGs.

host (Maina et al., 2019). Here, we show the difference in the modulation of apoptosis and survival in BoMac cells by *M. bovis* P1 and P150. The cell viability was dramatically reduced at a high MOI of 1,000. The findings are in partial agreement with previous work that *M. bovis*-induced apoptosis in epithelial cells (MAC-T and EBL cells) via a mitochondria-dependent pathway and ER-stress-dependent signaling pathway, respectively (Liu et al., 2020; Wu et al., 2021). Consistent with our previous study, live *M. bovis* P1 induced around 14–15% apoptosis in BoMac cells (Zhao et al., 2021). However, we found that the attenuated strain P150 induced significantly more apoptosis than the wild-type strain P1-infected BoMac cells. Furthermore, we used TEM to examine the morphology of BoMac after infection with *M. bovis* P1 and P150, and discovered obvious vacuolation and enlargement of the ER compartment in P150 infection, indicating that *M. bovis*-attenuated strain exactly induces cell damage and is more serious than P1-infected. Comparative genomics previously showed that one 14.2 kb deleted region covering 14 genes was missing in P150 (Rasheed et al., 2017), but the functions of most deleted genes (9/14) are unknown, and therefore, it is hard to suppose their role in the deleted genes in P150-induced apoptosis. In addition, there are many other kinds of mutations such as 46 SNPs and indels at the nucleic acid level between the P150 and P1, which would be possible to induce cell apoptosis. However, it remains to be verified in the future.

The fact that *M. bovis* P150 infection causes more apoptosis in BoMac cells than *M. bovis* P1 infection could have many ramifications. To begin with, a high amount of apoptosis would help to inhibit bacterial growth in phagocytes by killing pathogens. We also discovered that P150 recovered 24 h after infection and had much fewer intracellular bacteria than P1 after gentamicin treatment, indicating *M. bovis* P150 lacks

the ability to survive in BoMac cells compared to strain P1. The findings are in agreement with a study that attenuated *Mycobacterium tuberculosis* H37Ra and *Mycobacterium bovis* BCG strongly induce THP-1 apoptosis than virulent wild-type *M. tuberculosis* H37Rv, which is associated with its reduced intracellular viability (Riendeau and Kornfeld, 2003). Second, apoptosis was previously recognized to destroy germs, avoiding severe host tissue damage and allowing for fast immune system clearance. Furthermore, the higher level of apoptosis generated by P150 could be linked to its increased antigen presentation and immune protection as an attenuated vaccine. *Salmonella enterica* serovar Typhimurium strain VNP 20009 is an attenuated strain with the ability of anti-tumor effects by inducing higher apoptosis and then boosting the innate and adaptive anti-tumor immunity (Li et al., 2020).

The secretory pathway's key intracellular organelle, the endoplasmic reticulum (ER), is responsible for protein translocation, folding, and post-translational modifications, which allow proteins to be transported to the Golgi and then to vesicles for secretion. Disorder in ER function, often known as "ER stress," causes death in diverse host cells by initiating the unfolded protein response (UPR) (Jing et al., 2012). There are three branches of UPR that are initiated by distinct ER stress: PKR-like endoplasmic reticulum kinase (PERK), inositol-requiring enzyme 1 (IRE1), and activating transcription factor 6 (ATF6) (Jing et al., 2012). In our research, we discovered that the genes of CHOP, ATF4, and GADD45A in the PERK signal pathway, as well as other proapoptotic genes such as CHAC1, TRIB3, DUSP6, TCIM, MYC, and PPP1R15, were increased in P150-infected BoMac cells compared with P1-infected cells. Various intracellular bacteria, such as *Mycobacterium tuberculosis* (Sharma et al., 2021), *Brucella*

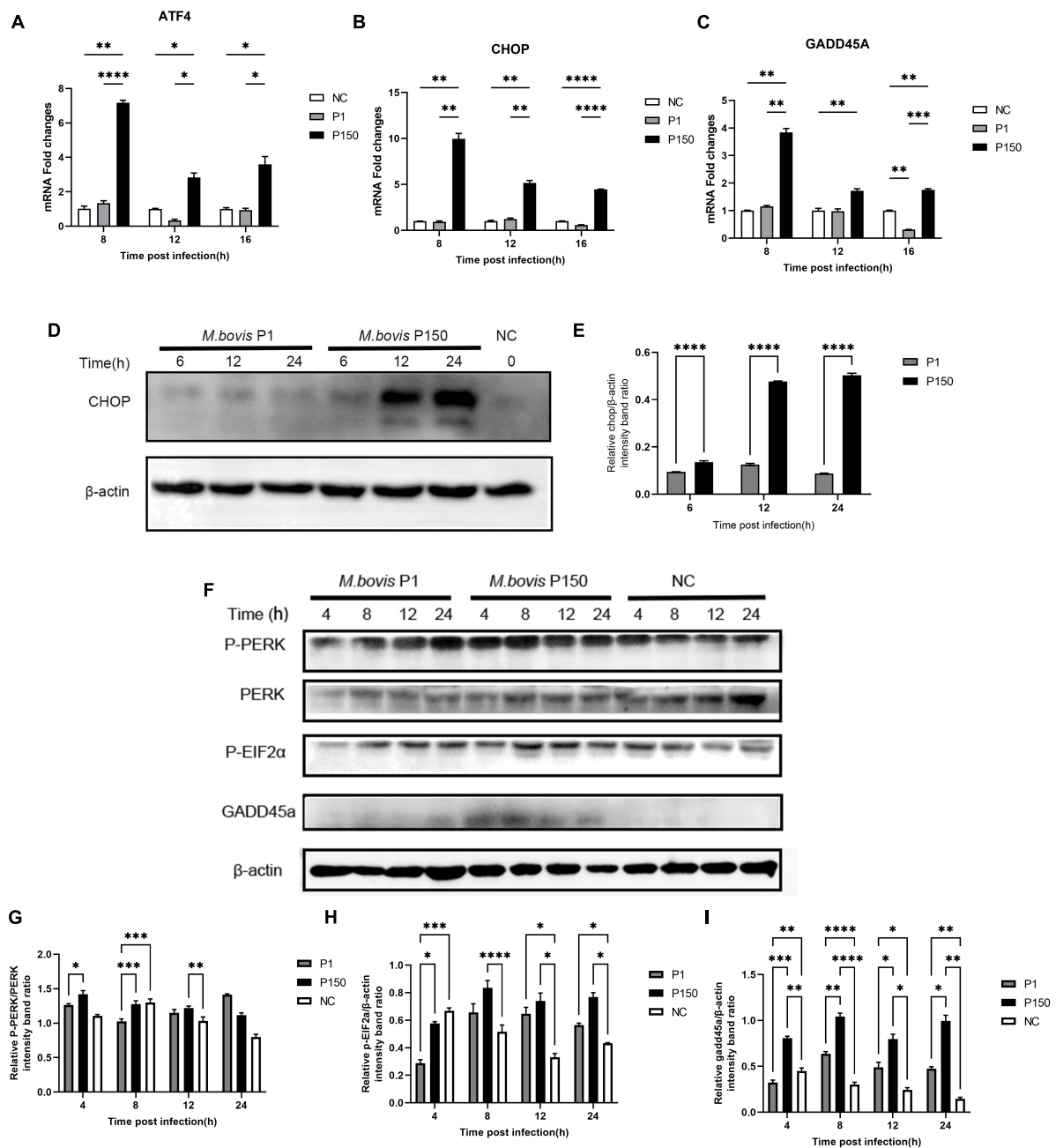


FIGURE 5

Different expression of ER-stress responsive genes and proteins critical to PERK signal pathway in BoMac cells induced by *M. bovis* P1 and P150 strains. (A–C) The mRNA expression of ATF4, CHOP, and GADD45A, respectively, in PERK signal pathway at 8, 12, and 16 h post-infection by *M. bovis* P1 and P150 in BoMac cells using the qRT-PCR assay. Data are presented as the means \pm SD of the results from three independent experiments. (D) Western blot assay indicated that CHOP was significantly increased in P150-infected cells at 6, 12, and 24 h post-infection compared to P1-infected. (E) Represents the relative intensity of western blot bands of panel D for expression of CHOP evaluated with ImageJ and normalized to β -actin. (F) The effect of *M. bovis* on target proteins in the PERK signal pathway was analyzed by western blot probed with specific antibodies. (G–I) Densitometry quantification of P-PERK, P-EIF2 α , and GADD45A was calculated by ImageJ analysis. Statistically significant difference was assessed by one-way ANOVA with Dunnett's multiple-comparison test between P1 and P150 and annotated as follows: * $p < 0.05$; ** $p < 0.01$; *** $p < 0.001$; and **** $p < 0.0001$.

melitensis (Smith et al., 2013), and *Listeria monocytogenes* (Pillich et al., 2012), have been documented to activate the UPR to control intracellular bacterial number during infection.

These findings show that the *M. bovis* P150 infection increases the expression of ER-stress-associated genes in the PERK signal pathway compared to P1 infection, resulting in higher

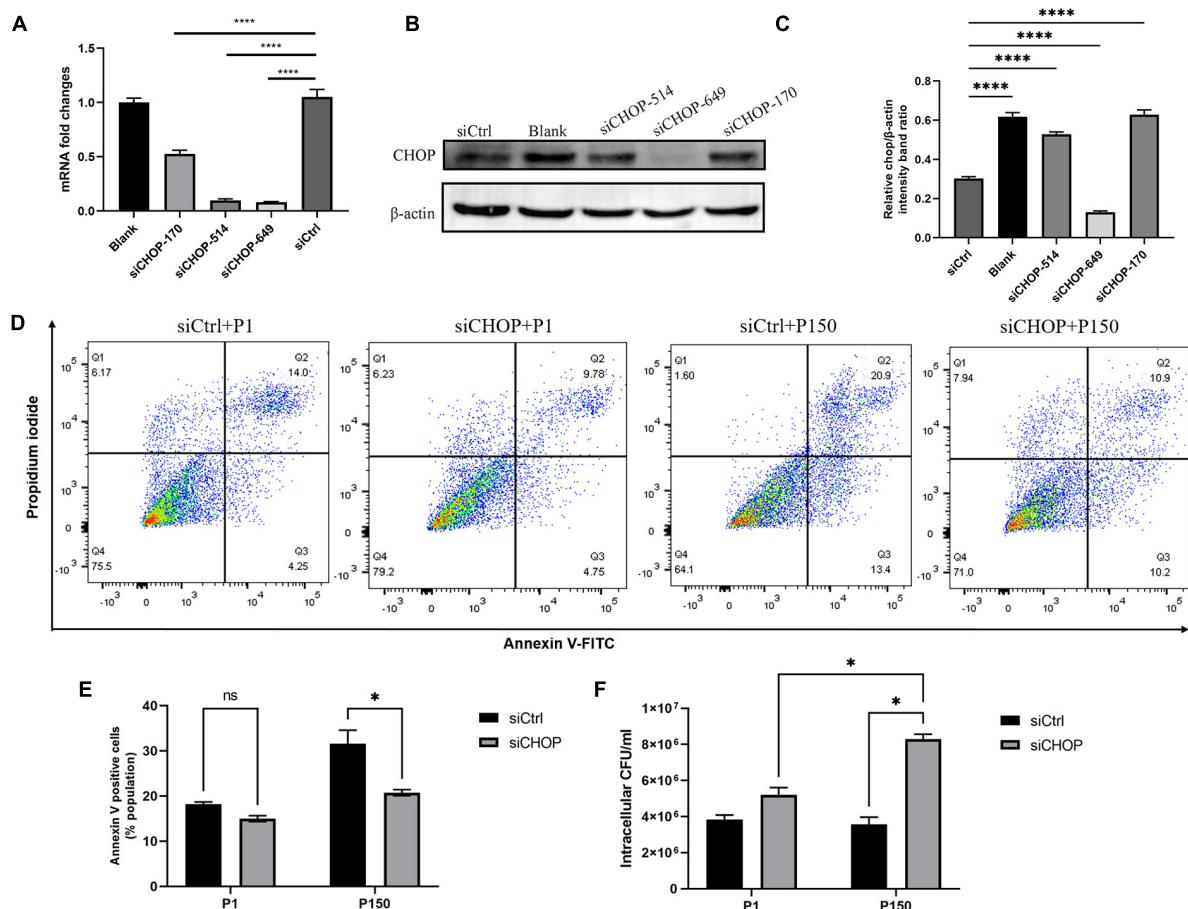


FIGURE 6

Effect of CHOP knockdown with siRNA interference on apoptosis and intracellular survival of *M. bovis* P1 and P150. qRT-PCR (A) and western blot analysis (B,C) were performed to evaluate the expression of CHOP in transfected BoMac cells. (D,E) Apoptosis assay by flow cytometry showed that CHOP knockdown significantly decreased the apoptosis of BoMac cells induced by P150 infection, but not by P1 infection. (F) Quantification of intracellular survival of *M. bovis* P1 and P150 in BoMac cells. Cells were harvested at 24-h post-infection with *M. bovis* and bacteria number was determined by gentamicin invasion assay. Data are presented as the means \pm SD of the results from three independent experiments. A significant difference was assessed by one-way ANOVA relative to the control. * $p < 0.05$ and **** $p < 0.0001$.

apoptosis than P1 infection. We speculate that the wild-type strain might inhibit apoptosis *via* ER stress. Earlier research has reported that *M. hyopneumoniae* infection inhibited the host UPR by inhibition of all three pathways controlled by PERK, IRE1, and ATF6 (Pan et al., 2020). Although the UPR plays an important function in microbial infectivity, its significance in *M. bovis* pathogenesis is uncertain and requires more research.

C/EBP homologous protein is an important component in ER-stress-induced cell death. By modulating the expression of BCL-2, TRB3, death receptor 5, ERO1 α , and PPP1R15A, and perturbing the cellular redox state, CHOP synthesis may trigger cell apoptosis (McCullough et al., 2001; Wang et al., 2009). Furthermore, CHOP increases the expression of GADD45 (growth arrest and DNA-damage-inducible protein), which causes cell apoptosis by stopping protein synthesis altogether (Saha et al., 2010). CHOP is ubiquitously expressed

at relatively low levels in typical cells but is substantially expressed in most cells when they are stressed (Chikka et al., 2013). This study looked at CHOP expression during *M. bovis* P1 and P150 infections and found that while *M. bovis* P1 infection reduces CHOP expression, P150 infection might boost it. We anticipated that *M. bovis* virulent strain P1 might interfere with the expression of CHOP protein during the pathogen-induced ER stress because CHOP is the major proapoptotic transcription factor activated by UPR. This could be one of the reasons for the *M. bovis*-infected cells' delayed apoptosis (Maina et al., 2019). To learn more about the role of CHOP in apoptosis in *M. bovis* P150 infection, we used siRNA against the CHOP gene to reduce apoptosis while also decreasing intracellular survival. These findings imply that *M. bovis* P150-induced apoptosis is mediated by CHOP, a protein that has the ability to effectively govern intracellular survival.

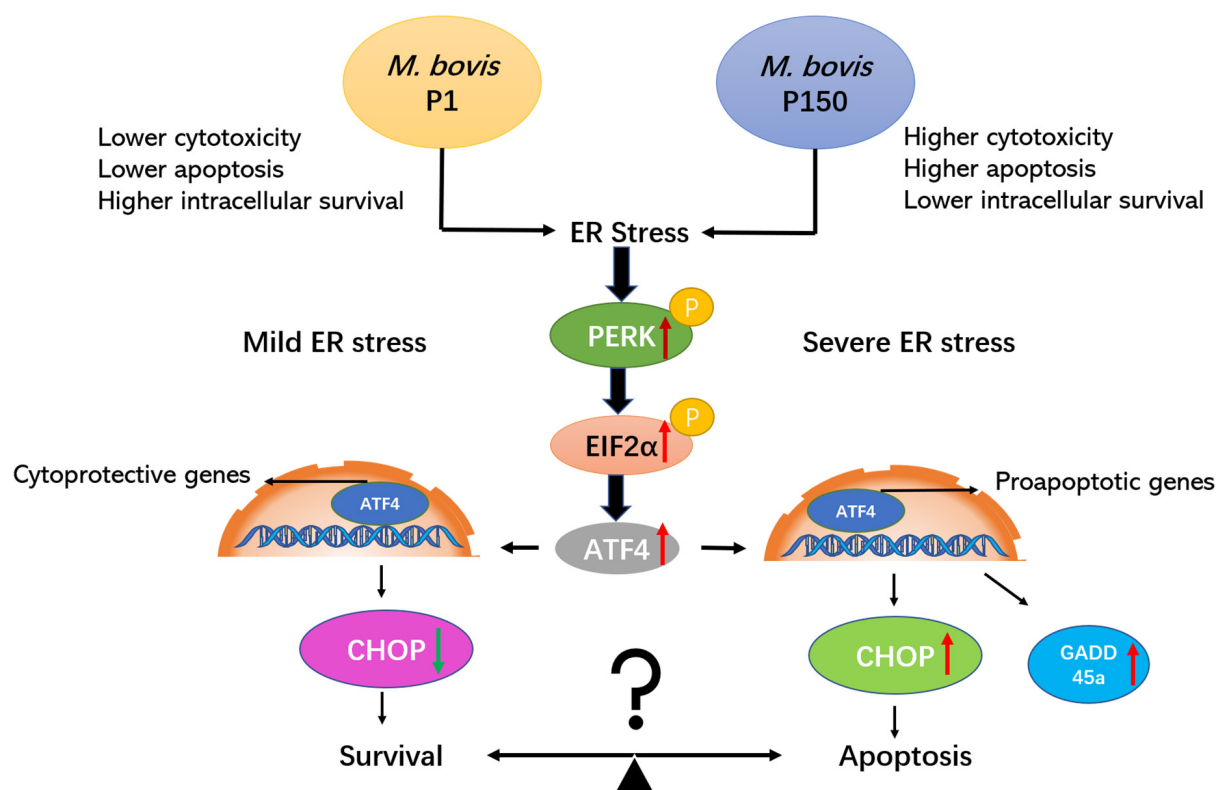


FIGURE 7

The attenuated *M. bovis* strain P150 induces higher apoptosis of BoMac through a CHOP-upregulated mechanism via the protein kinase R-like endoplasmic reticulum kinase (PERK)-dependent signal pathway activation. After *M. bovis* P150 is infected, it induces an ER stress and activates phosphorylation of PERK and subsequently with the ability to phosphorylate EIF2α. The result is the induction of ATF4 mRNA expression, which upregulates the expression of proapoptotic genes, e.g., CHOP and GADD45A. CHOP, the key downstream target of ATF4, as well as GADD45A, are upregulated and subsequently promoted apoptosis. Finally, the apoptosis of cell was increased that might be associated with a lower level of mycoplasma intracellular survival. The PERK/EIF2α/ATF4/CHOP/GADD45A axis is certainly involved in both survival and apoptotic signaling pathways.

As a result of these studies, we propose a possible mechanism in which *M. bovis*-attenuated strain P150 shortens the life of infected bovine alveolar macrophages during ER stress by upregulating the expression of phosphorylated-PERK, phosphorylated-EIF2α, ATF4, CHOP, and GADD45A signaling cascade, thus mediating crosstalk between ER stress and apoptosis signaling (Figure 7). As a result, the balance between apoptosis and survival may be controlled by ER stress caused by *M. bovis* P1 and P150. These findings reveal a variety of possible intervening targets, primarily the apoptotic pathway, and lay the groundwork for more research into the whole or partial apoptosis signaling cascades.

This research has certain drawbacks. First, because this is a transcriptome comparison between *M. bovis* and BoMac, changes in gene expression may not correspond to changes in protein expression as a result of posttranscriptional alteration. Second, increased CHOP was discovered in P150-infected cells, which played a critical role in apoptotic pathway cell fate decisions, however, which key protein

prevents CHOP expression from *M. bovis* wild-type strain P1 and whether those missing genes encoded in the 14.2-kb-deleted region affect apoptosis have not been determined. Furthermore, we found that there was no obviously different expression in P-PERK and P-EIF2α during P1 and P150 infection at 12 and 24 h, indicating that the two signal factors were both activated. However, the downstream proteins of CHOP and GADD45A were only upregulated in P150-infected cells. It is still unknown which factor directly induced CHOP expressed via the PERK/P-EIF2α/ATF4 axis. Further research is needed to see if there are any additional controlled parameters that can cause host cell survival following infection with the wild-type strain.

Data availability statement

The data presented in this study are deposited in the NCBI BioProject repository, accession number: PRJNA769187.

Author contributions

HZ contributed to conceptualization and writing—original draft preparation. HZ and SL contributed to methodology and software. MF, CH, and AG contributed to writing—review and editing. SL and DL contributed to validation. JC and GZ contributed to data curation. MF, YC, and CH contributed to formal analysis. HC, LY, and AG contributed to supervision. AG contributed to project administration and funding acquisition. All authors have read and agreed to the published version of the manuscript.

Funding

This research was supported by the Youth Program of National Natural Science Foundation of China (No. 32002290), National Key Research and Development Program of the Ningxia Hui Autonomous Region in China (No. 2021BEF02028), Special Fund for Chinese Agricultural Research System (Beef/Yaks) (CARS-37), and the Special Fund for National Distinguished Scholars in Agricultural Research and Technical Innovative Team.

Acknowledgments

The authors thank Judith R. Stabel for kindly offering, and Ganwu Li for shipping, the BoMac cell line from

USDA-ARS-NADC. The authors also thank Shengsong Xie and Xiongwei Nie from the College of Animal Science, Huazhong Agricultural University, for their critical comments and guidance.

Conflict of interest

The authors declare that the research was conducted in the absence of any commercial or financial relationships that could be construed as a potential conflict of interest.

Publisher's note

All claims expressed in this article are solely those of the authors and do not necessarily represent those of their affiliated organizations, or those of the publisher, the editors and the reviewers. Any product that may be evaluated in this article, or claim that may be made by its manufacturer, is not guaranteed or endorsed by the publisher.

Supplementary material

The Supplementary Material for this article can be found online at: <https://www.frontiersin.org/articles/10.3389/fmicb.2022.925209/full#supplementary-material>

References

- Alberti, A., Addis, M. F., Chessa, B., Cubeddu, T., Profiti, M., Rosati, S., et al. (2006). Molecular and antigenic characterization of a *Mycoplasma bovis* strain causing an outbreak of infectious keratoconjunctivitis. *J. Vet. Diagn. Invest.* 18, 41–51. doi: 10.1177/104063870601800106
- Borchsenius, S. N., Vishnyakov, I. E., Chernova, O. A., Chernov, V. M., and Barlev, N. A. (2020). Effects of *Mycoplasmas* on the Host Cell Signaling Pathways. *Pathogens* 9:308. doi: 10.3390/pathogens9040308
- Burgi, N., Josi, C., Burki, S., Schweizer, M., and Pilo, P. (2018). *Mycoplasma bovis* co-infection with bovine viral diarrhea virus in bovine macrophages. *Vet. Res.* 49:2. doi: 10.1186/s13567-017-0499-1
- Calcutt, M. J., Lysnyansky, I., Sachse, K., Fox, L. K., Nicholas, R. A. J., and Ayling, R. D. (2018). Gap analysis of *Mycoplasma bovis* disease, diagnosis and control: an aid to identify future development requirements. *Transbound. Emerg. Dis.* 65, 91–109. doi: 10.1111/tbed.12860
- Chao, J., Han, X., Liu, K., Li, Q., Peng, Q., Lu, S., et al. (2019). Calves Infected with Virulent and Attenuated *Mycoplasma bovis* Strains Have Upregulated Th17 Inflammatory and Th1 Protective Responses. *Respectively Genes*. 10:656. doi: 10.3390/genes10090656
- Chikka, M. R., McCabe, D. D., Tyra, H. M., and Rutkowski, D. T. (2013). C/EBP homologous protein (CHOP) contributes to suppression of metabolic genes during endoplasmic reticulum stress in the liver. *J. Biol. Chem.* 288, 4405–4415. doi: 10.1074/jbc.M112.432344
- Citti, C., and Blanchard, A. (2013). *Mycoplasmas* and their host: emerging and re-emerging minimal pathogens. *Trends Microbiol.* 21, 196–203. doi: 10.1016/j.tim.2013.01.003
- Dudek, K., Szacawa, E., and Nicholas, R. A. J. (2021). Recent Developments in Vaccines for Bovine Mycoplasmoses Caused by *Mycoplasma bovis* and *Mycoplasma mycoides* subsp. *mycoides*. *Vaccines* 9:549. doi: 10.3390/vaccines9060549
- Fatima, S., Kumari, A., Das, G., and Dwivedi, V. P. (2020). Tuberculosis vaccine: a journey from BCG to present. *Life Sci.* 252:117594. doi: 10.1016/j.lfs.2020.117594
- Feng, Z. X., Wei, Y. N., Li, G. L., Lu, X. M., Wan, X. F., Pharr, G. T., et al. (2013). Development and validation of an attenuated *Mycoplasma hyopneumoniae* aerosol vaccine. *Vet. Microbiol.* 167, 417–424. doi: 10.1016/j.vetmic.2013.08.012
- Jing, G., Wang, J. J., and Zhang, S. X. (2012). ER stress and apoptosis: a new mechanism for retinal cell death. *Exp. Diabetes Res.* 2012:589589. doi: 10.1155/2012/589589
- Kanci Condello, A., Underwood, G. J., Shil, P. K., Noormohammadi, A. H., Markham, P. F., Wawegama, N. K., et al. (2020). *Mycoplasma gallisepticum* strain ts-304 is a safe and effective live attenuated vaccine for use in chickens. *Vet. Microbiol.* 244:108654. doi: 10.1016/j.vetmic.2020.108654
- Lalsiamthara, J., and Lee, J. H. (2017). Development and trial of vaccines against *Brucella*. *J. Vet. Sci.* 18, 281–290. doi: 10.4142/jvs.2017.18.S1.281
- Li, M., Lu, M., Lai, Y., Zhang, X., Li, Y., Mao, P., et al. (2020). Inhibition of acute leukemia with attenuated *Salmonella typhimurium* strain VNP20009. *Biomed. Pharmacother.* 129:110425. doi: 10.1016/j.biopha.2020.110425
- Liu, Y., Zhou, M., Xu, S., Khan, M. A., Shi, Y., Qu, W., et al. (2020). *Mycoplasma bovis*-generated reactive oxygen species and induced apoptosis in bovine mammary epithelial cell cultures. *J. Dairy Sci.* 103, 10429–10445. doi: 10.3168/jds.2020-18599

- Maina, T., Prysliak, T., and Perez-Casal, J. (2019). Mycoplasma bovis delay in apoptosis of macrophages is accompanied by increased expression of anti-apoptotic genes, reduced cytochrome C translocation and inhibition of DNA fragmentation. *Vet. Immunol. Immunopathol.* 208, 16–24. doi: 10.1016/j.vetimm.2018.12.004
- Maunsell, F., Brown, M. B., Powe, J., Ivey, J., Woolard, M., Love, W., et al. (2012). Oral inoculation of young dairy calves with Mycoplasma bovis results in colonization of tonsils, development of otitis media and local immunity. *PLoS One* 7:e44523. doi: 10.1371/journal.pone.0044523
- Maunsell, F. P., and Chase, C. (2019). Mycoplasma bovis: interactions with the Immune System and Failure to Generate an Effective Immune Response. *Vet. Clin. North Am. Food Anim. Pract.* 35, 471–483. doi: 10.1016/j.cvfa.2019.08.003
- McCullough, K. D., Martindale, J. L., Klotz, L. O., Aw, T. Y., and Holbrook, N. J. (2001). Gadd153 sensitizes cells to endoplasmic reticulum stress by down-regulating Bcl2 and perturbing the cellular redox state. *Mol. Cell Biol.* 21, 1249–1259. doi: 10.1128/MCB.21.4.1249-1259.2001
- Mulongo, M., Prysliak, T., Scruten, E., Napper, S., and Perez-Casal, J. (2014). In vitro infection of bovine monocytes with Mycoplasma bovis delays apoptosis and suppresses production of gamma interferon and tumor necrosis factor alpha but not interleukin-10. *Infect. Immun.* 82, 62–71. doi: 10.1128/IAI.00961-13
- Nicholas, R. A., Ayling, R. D., and McAuliffe, L. (2009). Vaccines for Mycoplasma diseases in animals and man. *J. Comp. Pathol.* 140, 85–96. doi: 10.1016/j.jcpa.2008.08.004
- Ouyang, Y., Pan, J., Tai, Q., Ju, J., and Wang, H. (2016). Transcriptomic changes associated with DKK4 overexpression in pancreatic cancer cells detected by RNA-Seq. *Tumour. Biol.* 37, 10827–10838. doi: 10.1007/s13277-015-4379-x
- Pan, Q., Wang, X., Liu, T., Yu, Y., Li, L., Zhou, R., et al. (2020). Mycoplasma hyopneumoniae Inhibits Porcine Beta-Defensin 2 Production by Blocking the Unfolded Protein Response To Facilitate Epithelial Adhesion and Infection. *Infect. Immun.* 88:e164–e120. doi: 10.1128/IAI.00164-20
- Pfützner, H., and Sachse, K. (1996). Mycoplasma bovis as an agent of mastitis, pneumonia, arthritis and genital disorders in cattle. *Rev. Sci. Tech.* 15, 1477–1494. doi: 10.20506/rst.15.4.987
- Pillich, H., Loose, M., Zimmer, K. P., and Chakraborty, T. (2012). Activation of the unfolded protein response by Listeria monocytogenes. *Cell Microbiol.* 14, 949–964. doi: 10.1111/j.1462-5822.2012.01769.x
- Prysliak, T., and Perez-Casal, J. (2016). Immune responses to Mycoplasma bovis proteins formulated with different adjuvants. *Can. J. Microbiol.* 62, 492–504. doi: 10.1139/cjm-2015-0762
- Prysliak, T., Van Der Merwe, J., and Perez-Casal, J. (2013). Vaccination with recombinant Mycoplasma bovis GAPDH results in a strong humoral immune response but does not protect feedlot cattle from an experimental challenge with M. bovis. *Microb. Pathog.* 55, 1–8. doi: 10.1016/j.micpath.2012.12.001
- Qi, J., Guo, A., Cui, P., Chen, Y., Mustafa, R., Ba, X., et al. (2012). Comparative geno-plasticity analysis of Mycoplasma bovis HB0801 (Chinese isolate). *PLoS One* 7:e38239. doi: 10.1371/journal.pone.0038239
- Rasheed, M. A., Qi, J., Zhu, X., Chenfei, H., Menghwar, H., Khan, F. A., et al. (2017). Comparative Genomics of Mycoplasma bovis Strains Reveals That Decreased Virulence with Increasing Passages Might Correlate with Potential Virulence-Related Factors. *Front. Cell Infect. Microbiol.* 7:177. doi: 10.3389/fcimb.2017.00177
- Riendeau, C. J., and Kornfeld, H. (2003). THP-1 cell apoptosis in response to Mycobacterial infection. *Infect. Immun.* 71, 254–259. doi: 10.1128/IAI.71.1.254-259.2003
- Rozpedek, W., Pytel, D., Mucha, B., Leszczynska, H., Diehl, J. A., and Majsterek, I. (2016). The Role of the PERK/eIF2alpha/ATF4/CHOP Signaling Pathway in Tumor Progression During Endoplasmic Reticulum Stress. *Curr. Mol. Med.* 16, 533–544. doi: 10.2174/1566524016666160523143937
- Saha, A., Kuzuhara, T., Echigo, N., Fujii, A., Suganuma, M., and Fujiki, H. (2010). Apoptosis of human lung cancer cells by curcumin mediated through up-regulation of "growth arrest and DNA damage inducible genes 45 and 153". *Biol. Pharm. Bull.* 33, 1291–1299. doi: 10.1248/bpb.33.1291
- Sharma, N., Shariq, M., Quadir, N., Singh, J., Sheikh, J. A., Hasnain, S. E., et al. (2021). Mycobacterium tuberculosis Protein PE6 (Rv0335c), a Novel TLR4 Agonist, Evokes an Inflammatory Response and Modulates the Cell Death Pathways in Macrophages to Enhance Intracellular Survival. *Front. Immunol.* 12:696491. doi: 10.3389/fimmu.2021.696491
- Smith, J. A., Khan, M., Magnani, D. D., Harms, J. S., Durward, M., Radhakrishnan, G. K., et al. (2013). Brucella induces an unfolded protein response via TcpB that supports intracellular replication in macrophages. *PLoS Pathog.* 9:e1003785. doi: 10.1371/journal.ppat.1003785
- Soehnlen, M. K., Aydin, A., Lengerich, E. J., Houser, B. A., Fenton, G. D., Lysczek, H. R., et al. (2011). Blinded, controlled field trial of two commercially available Mycoplasma bovis bacterin vaccines in veal calves. *Vaccine* 29, 5347–5354. doi: 10.1016/j.vaccine.2011.05.092
- Suleman, M., Prysliak, T., Clarke, K., Burrage, P., Windeyer, C., and Perez-Casal, J. (2016). Mycoplasma bovis isolates recovered from cattle and bison (*Bison bison*) show differential in vitro effects on PBMC proliferation, alveolar macrophage apoptosis and invasion of epithelial and immune cells. *Vet. Microbiol.* 186, 28–36. doi: 10.1016/j.vetmic.2016.02.016
- Suwanruangsri, M., Uemura, R., Izzati, U. Z., Kanda, T., Fuke, N., Yasuda, M., et al. (2021). Mycoplasma bovis May Travel Along the Eustachian Tube to Cause Meningitis in Japanese Black Cattle. *J. Comp. Pathol.* 188, 13–20. doi: 10.1016/j.jcpa.2021.08.001
- Wang, X., Liao, Y., Yap, P. L., Png, K. J., Tam, J. P., and Liu, D. X. (2009). Inhibition of protein kinase R activation and upregulation of GADD34 expression play a synergistic role in facilitating coronavirus replication by maintaining de novo protein synthesis in virus-infected cells. *J. Virol.* 83, 12462–12472. doi: 10.1128/JVI.01546-09
- Wu, X., Zhang, S., Long, C., An, Z., Xing, X., Wen, F., et al. (2021). Mycoplasmas bovis P48 induces apoptosis in EBL cells via an endoplasmic reticulum stress-dependent signaling pathway. *Vet. Microbiol.* 255:109013. doi: 10.1016/j.vetmic.2021.109013
- Xiong, Q., Wei, Y., Xie, H., Feng, Z., Gan, Y., Wang, C., et al. (2014). Effect of different adjuvant formulations on the immunogenicity and protective effect of a live Mycoplasma hyopneumoniae vaccine after intramuscular inoculation. *Vaccine* 32, 3445–3451. doi: 10.1016/j.vaccine.2014.03.071
- Zhang, R., Han, X., Chen, Y., Mustafa, R., Qi, J., Chen, X., et al. (2014). Attenuated Mycoplasma bovis strains provide protection against virulent infection in calves. *Vaccine* 32, 3107–3114. doi: 10.1016/j.vaccine.2013.12.004
- Zhao, G., Zhu, X., Zhang, H., Chen, Y., Schieck, E., Hu, C., et al. (2021). Novel Secreted Protein of Mycoplasma bovis MbovP280 Induces Macrophage Apoptosis Through CRYAB. *Front. Immunol.* 12:619362. doi: 10.3389/fimmu.2021.619362
- Zhu, L., Shahid, M. A., Markham, J., Browning, G. F., Noormohammadi, A. H., and Marends, M. S. (2019). Comparative genomic analyses of Mycoplasma synoviae vaccine strain MS-H and its wild-type parent strain 86079/7NS: implications for the identification of virulence factors and applications in diagnosis of M. synoviae. *Avian Pathol.* 48, 537–548. doi: 10.1080/03079457.2019.1637514



OPEN ACCESS

EDITED BY

Chih-Horng Kuo,
Academia Sinica, Taiwan

REVIEWED BY

Jun-Yi Yang,
National Chung Hsing University,
Taiwan
Amit Yadav,
National Centre for Cell Science, India
Kenro Oshima,
Hosei University, Japan

*CORRESPONDENCE

Bianca Rodrigues Jardim
20171100@students.latrobe.edu.au

SPECIALTY SECTION

This article was submitted to
Evolutionary and Genomic
Microbiology,
a section of the journal
Frontiers in Microbiology

RECEIVED 06 May 2022

ACCEPTED 29 June 2022

PUBLISHED 12 August 2022

CITATION

Rodrigues Jardim B, Tran-Nguyen LTT,
Gambley C, Rodoni B and
Constable FE (2022) Iodixanol density
gradients as an effective phytoplasma
enrichment approach to improve
genome sequencing.
Front. Microbiol. 13:937648.
doi: 10.3389/fmicb.2022.937648

COPYRIGHT

© 2022 Rodrigues Jardim,
Tran-Nguyen, Gambley, Rodoni and
Constable. This is an open-access
article distributed under the terms of
the [Creative Commons Attribution
License \(CC BY\)](https://creativecommons.org/licenses/by/4.0/). The use, distribution
or reproduction in other forums is
permitted, provided the original
author(s) and the copyright owner(s)
are credited and that the original
publication in this journal is cited, in
accordance with accepted academic
practice. No use, distribution or
reproduction is permitted which does
not comply with these terms.

Iodixanol density gradients as an effective phytoplasma enrichment approach to improve genome sequencing

Bianca Rodrigues Jardim^{1,2*}, Lucy T. T. Tran-Nguyen³,
Cherie Gambley⁴, Brendan Rodoni^{1,2} and
Fiona E. Constable^{1,2}

¹School of Applied Systems Biology, La Trobe University, Bundoora, VIC, Australia, ²Agriculture Victoria Research, Department of Jobs, Precincts and Regions, AgriBio Centre, Bundoora, VIC, Australia, ³Plant Health Australia, Deakin, ACT, Australia, ⁴Horticulture and Forestry Science, Department of Agriculture and Fisheries, Maroochy Research Facility, Nambour, QLD, Australia

Obtaining complete phytoplasma genomes is difficult due to the lack of a culture system for these bacteria. To improve genome assembly, a non-ionic, low- and iso-osmotic iodixanol (Optiprep™) density gradient centrifugation method was developed to enrich for phytoplasma cells and deplete plant host tissues prior to deoxyribonucleic acid (DNA) extraction and high-throughput sequencing (HTS). After density gradient enrichment, potato infected with a '*Candidatus* Phytoplasma australasia'-related strain showed a ~14-fold increase in phytoplasma HTS reads, with a ~1.7-fold decrease in host genomic reads compared to the DNA extracted from the same sample without density gradient centrifugation enrichment. Additionally, phytoplasma genome assemblies from libraries equalized to 5 million reads were, on average, ~15,000 bp larger and more contiguous (N50 ~14,800 bp larger) than assemblies from the DNA extracted from the infected potato without enrichment. The method was repeated on capsicum infected with Sweet Potato Little Leaf phytoplasma ('Ca. Phytoplasma australasia'-related strain) with a lower phytoplasma titer than the potato. In capsicum, ~threefold more phytoplasma reads and ~twofold less host genomic reads were obtained, with the genome assembly size and N50 values from libraries equalized to 3.4 million reads ~137,000 and ~4,000 bp larger, respectively, compared to the DNA extracted from infected capsicum without enrichment. Phytoplasmas from potato and capsicum were both enriched at a density of 1.049–1.058 g/ml. Finally, we present two highly contiguous 'Ca. Phytoplasma australasia' phytoplasma reference genomes sequenced from naturally infected *Solanaceae* hosts in Australia. Obtaining high-quality phytoplasma genomes from naturally infected hosts will improve insights into phytoplasma taxonomy, which will improve their detection and disease management.

KEYWORDS

host DNA contamination, unculturable bacteria, phytopathogen, natural host, Optiprep™, density gradient centrifugation, high-throughput sequencing, 16S rII phytoplasma

Introduction

Phytoplasmas (class Mollicutes) are unculturable, insect-vectored phytopathogens of more than 700 economically important plants (Trivellone and Dietrich, 2021). They lack cell walls and reside intracellularly in their insect and plant hosts (phloem limited). Phytoplasmas are associated with disrupted development of stem, leaf, or fruiting tissues and, thereby, reduce the yield or survival of the infected plant. Whole genome sequences are central to our understanding of phytoplasma symptomatology and metabolic properties, their evolution and taxonomy, epidemiology, and can improve diagnosis (Oshima et al., 2004; Sugio et al., 2011; Chung et al., 2013; Orlovskis et al., 2017; Cho et al., 2020; Zhao et al., 2021). However, obtaining complete phytoplasma genomes is difficult because they are yet to be cultured and their low titer in most plant hosts limits the amount of phytoplasma chromosomes obtained from total deoxyribonucleic acid (DNA) extractions. Additionally, phytoplasma genomes are AT-rich (generally over 70% AT) and contain many duplicated genes, which makes assembly from widely used short-read sequencing data a further challenge (Oyola et al., 2012).

Recovering phytoplasma genomes directly from an infected host remains a major technical challenge due to the high proportion of “contaminating” host genomic and organellar DNA (mitochondrial DNA, plastid DNA) compared to phytoplasma DNA (Tran-Nguyen and Gibb, 2007). Phytoplasma genomes are also many magnitudes smaller than the host genome and direct sequencing of these samples reduces the depth to which phytoplasma-derived DNA is sequenced. It is therefore inefficient and costly to close sequence gaps in the target phytoplasma genomes when a high proportion of host DNA is present in the DNA extract. While genome assembly algorithms are improving to recover complete or draft metagenomic-assembled genomes of a high accuracy and quality, there is still a need to use and develop procedures to deplete host DNA and/or enrich for microbial DNA (Pereira-Marques et al., 2019), especially for unculturable phytopathogens such as phytoplasmas.

To date, only three complete phytoplasma genomes have been obtained without enrichment procedures (Orlovskis et al., 2017; Coetzee et al., 2019; Huang et al., 2022), and most others were obtained using the post-DNA extraction enrichment approaches, such as cesium chloride (CsCl) density gradient centrifugation and/or pulsed-field gel electrophoresis (PFGE) (Oshima et al., 2004; Bai et al., 2006; Kube et al., 2008; Tran-Nguyen et al., 2008; Andersen et al., 2013; Wang et al., 2018). Many draft genomes have been assembled from DNA extractions from original phytoplasma-infected hosts or artificially infected high-titer hosts with (Chen et al., 2014; Kakizawa et al., 2014; Fischer et al., 2016; Music et al., 2019) or without enrichment procedures (Chung et al., 2013). However, some of these methods require several days of

wet lab processing, multiple sets of specialized equipment, the use of harsh chemicals, and are only effective when the phytoplasma titer in the host plant is high; for example, the method implementing CsCl density gradient centrifugation followed by PFGE.

A phytoplasma enrichment method that is cost-effective, requires minimal specialized equipment, shorter processing times, and that does not rely on transmission of the phytoplasma to high-titer hosts for the method to be effective will advance our current understanding of phytoplasma genomics. Ideally, the enrichment method should be applied either prior to or after nucleic acid extraction but before sequencing to reduce the sequencing cost and to improve the accuracy of assembled genomes from metagenomic datasets. Recently, a kit-based post-DNA extraction method was used to deplete methylated host DNA directly from greenhouse-maintained (Nijo et al., 2021) or field-collected (Kirdat et al., 2021) plants infected with phytoplasmas. A more phytoplasma-targeted enrichment method was also developed based on the immunodominant membrane proteins (IMPs) in phytoplasma membranes (Tan et al., 2021). Here, we report the development of an approach using iodixanol (Optiprep™, Sigma-Aldrich, Missouri, MI, United States), a clinical-grade, non-ionic, and iso-osmotic density gradient medium, to enrich for phytoplasma cells directly from two naturally infected hosts prior to the DNA extraction. Using quantitative polymerase chain reaction (qPCR) and reference mapping of metagenomic reads, we demonstrate that the method reduces the proportion of host-derived sequences and increases phytoplasma sequences in the DNA extract; thus, improving the quality and completeness of the metagenomic-assembled phytoplasma genomes, particularly for ‘Ca. Phytoplasma australasiae’-related phytoplasmas infecting *Solanaceae* species. The resultant draft phytoplasma genome assemblies of the infected potato and capsicum were used in comparative genomic analyses to illustrate that the method produces genomes with a suitable completeness to infer taxonomic relationships between taxa.

Materials and methods

Plant material

The plant samples used in this study are listed in Table 1. The potato sample was propagated and maintained under natural daylight and day length conditions at ambient temperature in a greenhouse, with a regular watering and in an insect-proof cage. The potato was maintained in the greenhouse for approximately 15 months from initial propagation to sampling. The capsicum field sample was processed directly without propagation.

TABLE 1 Sample name, host information, collection location in Australia of samples positive for phytoplasma used in the study as well as the phytoplasma identity based on the top BLASTn hit of the R16F2n/m23sr amplicon and species assignment.

Sample name	Host common name (species name)	Host family	Sampling location in Australia	Highest percent identity (accession number)	BLASTn top hit description
o4P	Potato (<i>Solanum tuberosum</i> cv Nadine)	Solanaceae	Melbourne, VIC	99.94% (Y10096)	'Ca. Phytoplasma australasia'
o7C	Capsicum (<i>Capsicum annuum</i>)	Solanaceae	Stanthorpe, QLD	99.87% (JQ868446)	Sweet Potato Little Leaf phytoplasma

Polymerase chain reaction-based phytoplasma detection and identification

To confirm infection and determine the phytoplasma species present in the samples, total DNA was extracted, PCR amplified, and Sanger sequenced (Macrogen Korea) as stated in Rodrigues Jardim et al. (2021). The identity of the sequenced amplicon was confirmed by BLASTn analysis (Altschul et al., 1997) of the approximately 1,600 base pair (bp) sequence.

Estimation of phytoplasma titer and concentration using quantitative polymerase chain reaction

To estimate the efficiency of the qPCR reaction and, hence, accurately monitor the presence of phytoplasma, qualitatively and quantitatively, in the DNA extracts of samples collected prior to enrichment, after the differential centrifugation, and after the density gradient centrifugation, a standard curve was produced using a plasmid ligated with the R16F2n/m23sr-nested PCR amplicon of the phytoplasma-infected potato sample used in this study. The amplicon was cloned, purified, and Sanger sequenced as previously described (Rodrigues Jardim et al., 2021) to confirm the identity of the insert DNA. Plasmids ligated with the R16F2n/m23sr amplicon were extracted using the QIAprep Spin Miniprep Kit (Qiagen) following the manufacturer's specifications. The extracted plasmid DNA concentration was measured using a NanoDropTM spectrophotometer. To produce a qPCR standard curve with the phytoplasma 16S rRNA gene sequence as the target, the ligated plasmids were serially diluted 10-fold with UltraPureTM DNase/RNase-Free Distilled Water (Thermo Fisher Scientific, Massachusetts, MA, United States) for a total of eight dilution points.

The GoTaq[®] Probe 1-Step qPCR System (Promega Wisconsin, WI, United States) was used for qPCR according to the manufacturer's instructions for a total reaction volume of 20 μ l. The phytoplasma 16S rRNA gene specific primers and TaqMan probes described by Christensen et al. (2004) were used at published concentrations. Four microliters of template DNA from each sample or each plasmid dilution were used per

qPCR reaction. Four replicates of each plasmid serial dilution were included in every qPCR 96- or 384-well plate for absolute quantification of phytoplasma DNA, as well as four replicates of a template-free control to monitor for contamination, and three replicates from each sample were included. All qPCRs were set up and run on a QuantStudioTM 3 Real-Time PCR System (Thermo Fisher Scientific, Massachusetts, MA, United States) with analysis performed using the QuantStudioTM Design and Analysis Software (Thermo Fisher Scientific, Massachusetts, MA, United States). The qPCR efficiencies and R^2 values per run were estimated using the QuantStudioTM Design and Analysis Software (Thermo Fisher Scientific, Massachusetts, MA, United States).

Sample preparation for iodixanol density gradient centrifugation

Supplementary Appendix 1 contains a detailed step-by-step protocol for sample preparation, differential centrifugation, and iodixanol density gradient centrifugation with specifications for three technical replicates per host and one negative control per run (see also Supplementary Appendix Figure 1), iodixanol fraction sampling (Supplementary Appendix Figure 2), and a DNA extraction protocol for all sample types. The details of Supplementary Appendix 1 are summarized with the appropriate references.

Tissue sampling

Potato tissues with typical phytoplasma symptoms were collected from the greenhouse and processed on the day of collection. The symptomatic capsicum sample was transported at ambient temperature for approximately 3 days from the sampling location (Table 1) to the laboratory and then stored at 4°C upon arrival and until use. The capsicum sample was processed within 5 days of sampling to minimize the impact of degradation on the intactness of phytoplasma cells. Whole leaves, petioles, and stems of the potato and capsicum samples were used.

Sample preparation and homogenization

To homogenize the samples, 16 g of plant material was added to an extraction bag (BIOREBA Kanton Reinach, Switzerland) with 210-ml ice-cold Phytoplasma Grinding Buffer

(pH 7.6 at 4°C; [Palmano, 2001](#)). All samples were then gently homogenized using the semi-automated HOMEX 6 (BIOREBA Kanton Reinach, Switzerland) set at a low speed (10% of the maximum speed). The homogenates were refrigerated at 4°C for 20 min to allow all cells to plasmolyze.

Differential centrifugation

After plasmolysis, the tissue homogenates were split into two 48 ml aliquots in ice-cold 50-ml conical screw cap tubes and centrifuged at a low speed (1,500 rcf) for 10 min at 4°C in a fixed-angle rotor (F-3-6-38 rotor; Eppendorf) to remove cellular and environmental debris from the sample. The resultant supernatants were then transferred to new ice-cold 50-ml conical screw cap tubes and centrifuged at a high speed (10,000 rcf) for 30 min at 4°C in the same fixed-angle rotor to pellet intact cells. The resultant pellets from the first high-speed centrifugation were gently resuspended in 40 ml Tris-Sucrose-EDTA buffer (TSE, pH 8 at 4°C; [Quan et al., 2013](#)) and differentially centrifuged as above, with the exception that the resultant high-speed centrifugation pellets were each resuspended in 800-μl TSE, pooled into a single 50-ml conical screw cap tube (referred to as “differentially centrifuged pellet” or abbreviated with the suffix “TSE” in tables and figures), and kept at 4°C until use. The samples collected for DNA extraction and subsequent phytoplasma quantification by qPCR and high-throughput sequencing (HTS) included approximately 400 μl each of unprocessed tissue homogenate (no differential centrifugation) and the final pellet after differential centrifugation (resuspended in 4 ml of CTAB extraction buffer). Each sample was reserved in a separate 2-ml capped centrifuge tube and stored at –20°C until required.

Iodixanol density gradient centrifugation

A 40% (v/v) iodixanol (Optiprep™, Sigma–Aldrich, Missouri, MI, United States) working solution was prepared by diluting the 60% iodixanol stock solution with the diluent solution (0.15-M NaCl, 1-mM EDTA, 15-mM Tris; pH 7.6 at 4°C; [Frampton et al., 2018](#)). Three subsequent iodixanol solutions [14, 22, and 30% (v/v)] were prepared by diluting the 40% (v/v) iodixanol working solution in a NaCl-EDTA-Tris buffer (0.15-M NaCl, 0.5-mM EDTA, 5-mM Tris; pH 7.6 at 4°C; [Frampton et al., 2018](#)). The density gradient was prepared on ice and by first adding 3 ml 30% (v/v) iodixanol to a 13.2-ml open-top thin wall polypropylene centrifuge tube (Beckman Coulter Life Sciences, California, CA, United States) using a 20 gauge needle (Terumo Medical Corporation, Tokyo, Japan) and a 20-ml syringe, followed by gently adding 4 ml of the 22% (v/v) iodixanol solution, and 4 ml of the 14% (v/v) iodixanol. Three technical replicates were prepared and each gradient was overlaid with 400 μl of the final TSE cell suspension immediately after they were prepared. An additional gradient was used as a negative

iodixanol control in every run and was overlaid with 400-μl TSE buffer (cell-free). All tubes were balanced prior to centrifugation with cell-free TSE buffer. After the addition of the samples or control, the gradients were centrifuged in a pre-cooled Beckman Coulter Optima L-100 XP ultracentrifuge (SW 41 Ti rotor; 80,000 rcf, Beckman Coulter Life Sciences, California, CA, United States) for 3 h at 4°C. Seven 1.4-ml fractions (Fractions 1–7) and one approximately 2-ml fraction (Fraction 8) of the gradients were consecutively sampled from the top to the bottom of the centrifuge tube, resulting in eight fractions per replicate. The fractions were frozen at –20°C until needed for the DNA extraction. The density in g/ml of each fraction ([Supplementary Table 1](#)) was estimated prior to the DNA extraction by weighing the sampled fraction to three decimal places using a Pioneer™ Plus analytical balance (Model PA214C, Ohaus®).

Deoxyribonucleic acid extraction, quantification, and quality measures of unprocessed, differentially centrifuged, and density gradient samples

Total DNA was extracted from 400 μl of unprocessed homogenate or resuspended pellet that resulted after two rounds of differential centrifugation, and 1.4–2 ml of the density gradient fractions using a modified CTAB and chloroform:isoamyl alcohol (24:1) method ([Zhang et al., 1998](#)). The modifications to the DNA extraction method included using 5 ml each of CTAB and chloroform:isoamyl alcohol (24:1) (Sigma–Aldrich, Missouri, MI, United States) per sample, and incubation with isopropanol was done overnight at –20°C to precipitate the DNA. All DNA extractions were performed in 15-ml conical screw cap tubes and were centrifuged in a swinging bucket rotor (A-4-44 rotor, Eppendorf). During the chloroform:isoamyl alcohol (24:1) partitioning step, the samples were centrifuged at 3,500 rcf for 5 min at room temperature. This partitioning step was repeated 2–3 times per sample by adding 5 ml of chloroform:isoamyl alcohol (24:1) until the white interface was absent. The samples were centrifuged at 4,500 rcf for 20 min at 4°C after overnight precipitation in isopropanol (same volume as sample) and the pelleted DNA washed twice with 5 ml of 75% ethanol by centrifugation at 3,500 rcf for 15 min at 4°C. The DNA was resuspended in 60-μl UltraPure™ DNase/RNase-Free Distilled Water (Thermo Fisher Scientific, Massachusetts, MA, United States). A non-template (negative) DNA extraction control was performed alongside extractions to monitor for contamination during the DNA extraction and within the reagents. All DNA extractions were stored at –20°C until use. The DNA quantity ([Supplementary Table 2](#)) was estimated using the Qubit™ 1X dsDNA HS Assay Kit (Thermo Fisher Scientific, Massachusetts, MA, United States) on a Qubit™ 2.0 fluorometer (Thermo Fisher Scientific, Massachusetts, MA, United States).

Deoxyribonucleic acid sequencing library preparation and Illumina high-throughput sequencing

Library preparation was performed on DNA of the unprocessed plant homogenates, differentially centrifuged pellets, and density gradient samples using the NEXTFLEX® Rapid XP DNA-Seq Kit (PerkinElmer, Massachusetts, MA, United States) with the NEXTFLEX 384 Unique Dual Index Barcodes version 19.06 (PerkinElmer, Massachusetts, MA, United States). The protocol for library preparation without size selection and for inputs of 1 ng specified by the NEXTFLEX Rapid XP DNA-Seq Kit was followed for all samples. All replicates were sequenced for iodixanol fractions that showed the highest concentration of phytoplasma DNA as determined by qPCR screening, while only one replicate was sequenced for the remaining iodixanol fractions to determine their phytoplasma enrichment profiles (**Supplementary Table 2**). Since the DNA extractions from iodixanol fractions generally had a low DNA concentration (<0.005–1.05 ng/μl based on the Qubit™ fluorometer; **Supplementary Table 2**), the same volumes of the extracted DNA (34 μl) were used as inputs for library preparation to maximize the data output for each. The input DNA of the unprocessed homogenates and the differentially centrifuged pellets were diluted to 1-ng input DNA to apply the same library preparation protocol as the low DNA concentration iodixanol samples. The input DNA was fragmented according to the manufacturer's protocol to generate libraries with fragment sizes between 300 and 400 bp. The concentration and fragment sizes of the final libraries were estimated using an Agilent 2200 TapeStation System with the HSD1000 ScreenTape assay (Agilent Technologies, California, CA, United States). The resultant libraries were size-selected using ProNex® Size Selective Purification System (Promega Wisconsin, WI, United States), pooled together in equimolar concentrations, and sequenced on an Illumina NovaSeq 6000 System with an SP Reagent Kit v1.5 (2 × 250 bp).

Bioinformatic analyses

Illumina reads quality control

FastP (Chen et al., 2018), with the specified parameters -3 -5 -q 20 -l 50, was used to trim adapters and low-quality sequences, and to discard reads shorter than 50 bp from the sequence data. To enable a fair comparison between all sequenced samples, the number of trimmed reads per library were randomly down-sampled using Seqtk-1.3 (r106)¹ to achieve equal sequencing depths. All libraries of interest for the potato and capsicum samples were down-sampled to contain 5,000,000 and 3,400,000 reads/library,

respectively. The negative control libraries were not randomly down-sampled to enable the effective detection of any contamination but also due to their low total read numbers after sequencing.

Metagenome assemblies and assembly assessments

To obtain a high-quality reference genome and plasmid assemblies of the phytoplasma infecting the potato and capsicum samples investigated in the study, all trimmed reads without down-sampling were *de novo* assembled using SPAdes 3.15.2 (Prjibelski et al., 2020) with the following parameters: -meta, -k 21,33,55,77,99,127 (Nurk et al., 2017). Putative phytoplasma-derived genome and plasmid contigs were identified by BLASTn searches against the NCBI non-redundant database (acquired on January 1, 2022) using BLAST + v2.11.0 (Altschul et al., 1997). Genome sizes and GC content were estimated using Geneious prime 2022.1.1.² The genome N50 values of these draft genome assemblies were evaluated using metaQUAST (Mikheenko et al., 2016). Phytoplasma-derived protein-coding, tRNA, and rRNA genes were annotated and counted using Prodigal (Hyatt et al., 2010), ARAGORN (Laslett and Canback, 2004), and RNAmmer (Lagesen et al., 2007), respectively, implemented in Prokka 1.14.5 (Seemann, 2014). The coverage of the assembled phytoplasma genomes was estimated using BBSplit implemented in the BBMap v.38.61b software suite (Bushnell, 2014) using the assembled phytoplasma as its reference to which the corresponding reads were mapped. Of all these assemblies, one phytoplasma genome per host was selected as the reference phytoplasma genome for the potato and capsicum samples when the genome (i) had the largest N50 value of all assemblies, (ii) encoded a similar number tRNA genes as other publicly available phytoplasma genomes from closely related phytoplasma taxa, (iii) had the highest read coverage, and (iv) had less than 50 phytoplasma-specific contigs above 1,000 bp in size. The *secA* and *tufB* genes were extracted from each chosen reference genome and used in gene alignments with those of 'Ca. Phytoplasma australasia' (GenBank accession numbers EU168728 and JQ824250, respectively) and 'Ca. Phytoplasma aurantifolia' (GenBank accession numbers EU168731 and JQ824276, respectively) to determine the phytoplasma species from which the genome arises according to guidelines by Bertaccini et al. (2022).

For the fair assessments on the completeness and contiguity of phytoplasma genomes assembled from samples that underwent iodixanol-based density gradient centrifugation and those that did not, the down-sampled reads were also used in *de novo* assemblies (referred to as down-sampled assemblies) using the same SPAdes and BLASTn parameters discussed above. Additionally, the same genome annotation and quality assessments were performed for the down-sampled

¹ <https://github.com/lh3/seqtk>

² www.geneious.com

genome assemblies as those performed for assemblies without read down-sampling.

Read mapping pipeline and taxonomic classification of unmapped reads

Trimmed reads and the randomly down-sampled trimmed reads were mapped to reference genomes (publicly available and assembled in this study, [Table 2](#)) using BBSplit 38.61 from the BBMap v.38.61b software suite ([Bushnell, 2014](#)) to estimate the relative proportion of phytoplasma DNA, host genomic DNA (gDNA), host mitochondrial DNA (mtDNA), and host chloroplast DNA (cpDNA) per library. The default parameters were used and “ambig2=best” specified to assign the reads to the best-mapped site. The reference genomes specified for BBSplit 38.61 were downloaded from the NCBI (last accessed May 2022) and included, where available, host genomic DNA (potato: GCF_000226075.1; capsicum: GCF_000710875.1), host chloroplast genome (potato: NC_008096.2; capsicum: NC_018552.1), host mitochondrial genome (potato: NC_059127.1; capsicum: NC_024624.1), and two phytoplasma genomes of closely related phytoplasma taxa, as well as the reference genomes assembled in this study ([Table 2](#)).

Unmapped reads from the libraries (not down-sampled) were taxonomically classified using k-mer-based classification with Kraken2 using the abfvhp (archaea, bacteria, fungi, virus, human, and plasmid) genome database ([Wood et al., 2019](#)). Kraken2 reports were visualized in Pavian ([Breitwieser and Salzberg, 2020](#)).

Whole genome comparisons

Publicly available phytoplasma genomes and the phytoplasma reference genomes assembled in this study from potato and capsicum hosts were compared with phytoplasma genomes assembled from down-sampled reads from the unprocessed tissue homogenates, differentially centrifuged pellets, and iodixanol fraction with the highest proportion of phytoplasma HTS reads for the infected potato and capsicum hosts ([Table 2](#)). The average nucleotide identities (ANIs) between the genomes were calculated using FastANI version 1.33 ([Jain et al., 2018](#)), and the proportion of mapped genomic segments were calculated according to [Cho et al. \(2020\)](#) per sample.

Results

Phytoplasma screening and identification by polymerase chain reaction and Sanger sequencing

BLASTn analysis of the directly Sanger sequenced R16F2n/m23sr nested PCR amplicon confirmed the infection

of a ‘*Candidatus* Phytoplasma australasiae’ phytoplasma in the potato sample and a Sweet Potato Little Leaf (SPLL) phytoplasma in the capsicum sample ([Table 1](#)).

Iodixanol fraction densities after centrifugation

After centrifugation, the density of the sampled fractions ranged between 1.049 (Fraction 1) and 1.196 g/ml (Fraction 8) for the potato replicates, and from 1.058 (Fraction 1) to 1.157 g/ml (Fraction 8) for the capsicum replicates ([Supplementary Table 1](#)).

Deoxyribonucleic acid concentration estimates before density gradient centrifugation, and across all fractions after density gradient centrifugation

DNA concentrations of unprocessed homogenates for each sample were all above 20 ng/μl ([Table 3](#) and [Supplementary Table 2](#)). When compared to the DNA extracted from the same volume of the differentially centrifuged pellets, the unprocessed homogenates showed a 20-fold higher concentration in the case of the potato samples, and an almost fourfold higher DNA concentration for the capsicum sample.

After performing density gradient centrifugation, the average DNA concentrations for all fractions were below 1 ng/μl regardless of the host and were often below the detectable range of the Qubit™ 1X dsDNA HS Assay Kit ([Table 3](#) and [Supplementary Table 2](#)). The average DNA concentrations were highest in Fractions 1 and 4 for the potato replicates (0.67 and 0.21 ng/μl, respectively). For the capsicum replicates, Fraction 4 had the highest average DNA concentration at 0.86 ng/μl, followed by Fraction 5 (0.20 ng/μl) and then Fraction 1 (0.15 ng/μl).

Evaluations of phytoplasma genome reference assemblies

The draft phytoplasma reference genome assembled from the potato host (Fraction 2 from replicate 2) is 555,927 bp in size (N50 = 41,668 bp) and consists of 30 contigs ([Table 2](#)). The average GC content of this genome is 23.9%. The annotation includes 1 16S rRNA gene, 25 tRNA genes, and 463 protein-coding genes. Similarly, the draft phytoplasma reference genome assembled from the capsicum host (Fraction 7 from replicate 1) is 555,321 bp (N50 = 41,719 bp), consists of 29 contigs, with an average GC content of 23.7%. The annotation includes 1 16S rRNA gene, 25 tRNA genes, and 458 protein-coding genes ([Table 2](#)). Alignments of the *secA* and *tufB* genes extracted

TABLE 2 Assembly details and statistics for phytoplasma genomes used as references in this study, including GenBank accession numbers, closest phytoplasma relative, sequencing details where available (tissue sampled, enrichment method, sequencing platforms, and sequencing depths), genome properties, plasmid accession number/name.

Sample name (accession number)	NCHU2014 (GCA_001307505.2)	PR08 (GCA_015239935.3)	o4P (JALQCT000000000) ^A	o7C (JALQCV000000000) ^A
Putative phytoplasma species	' <i>Ca. Phytoplasma aurantifolia</i> '-related strain	' <i>Ca. Phytoplasma australasia</i> '-related strain	' <i>Ca. Phytoplasma australasia</i> '-related strain	SPLL ' <i>Ca. Phytoplasma australasia</i> '-related strain
Host tissue sampled	<i>Catharanthus roseus</i> (periwinkle) mature leaves	<i>Parthenium hysterophorus</i> leaves	<i>Solanum tuberosum</i> (potato) leaves, petioles, and stems	<i>Capsicum annuum</i> (capsicum) leaves, petioles, and stems
Enrichment method	Transmission to periwinkle by dodder, and immunoprecipitation	NA	Differential centrifugation and iodixanol density gradient centrifugation, iodixanol Fraction 2 from replicate 2	Differential centrifugation and iodixanol density gradient centrifugation, iodixanol Fraction 7 from replicate 1
Sequencing platform(s)	Illumina and Oxford Nanopore Technology	Illumina and Oxford Nanopore Technology	Illumina	Illumina
Amount of HTS data used (bp)	Approx. 0.67×10^9 (Oxford Nanopore Technology) with approx. 17.16×10^9 (Illumina)	NA	5.94×10^9	19.14×10^9
No. of contigs	1	1	30	29
Est. genome size (bp)	635,584	588,746	555,927	555,321
N50 value (bp)	635,584	588,746	41,668	41,719
Est. genome coverage (×)	2117	2757.98	1372	117
GC (%)	24.5	24.3	23.9	23.7
No. protein coding genes	471	468	463	458
No. tRNAs	24	27	25	25
No. 16S rRNAs	2	2	1	1
Plasmid recovered? (accession number)	Yes (CP040926.1)	No	Putative plasmid: po4P16SrIID	Putative plasmid: po7C16SrIID
References	Chang et al., 2015; Tan et al., 2021	NA	This study	This study

NA, not available.

^A*secA* and *tuB* gene regions extracted from the genome assemblies of strain o4 and strain o7 share 100% nucleotide sequence identity to those of '*Ca. Phytoplasma australasia*' (GenBank accession numbers EU168728 and JQ824250, respectively) and only 91–94% with the genes of '*Ca. Phytoplasma aurantifolia*' (GenBank accession numbers EU168731 and JQ824276, respectively). This places both strains as '*Ca. Phytoplasma australasia*'-related species based on recommendations by Bertaccini et al. (2022).

from the reference genomes of strains o4P and o7C with those available for '*Ca. Phytoplasma aurantifolia*' and '*Ca. Phytoplasma australasia*' (Table 2) showed that the phytoplasma strains investigated here were more closely related to '*Ca. Phytoplasma australasia*' (100% nucleotide sequence identity for both genes) than to '*Ca. Phytoplasma aurantifolia*' (91–94% nucleotide sequence identity).

Evaluations of putative phytoplasma plasmids from reference assemblies

A contig with BLASTn hits to publicly available phytoplasma plasmids were identified for the potato and capsicum hosts investigated in this study. The putative plasmid-derived contigs varied in size for the different hosts, at 4,370 bp for the potato sample with two open reading frames encoded, and 2,913 bp for the capsicum sample encoding three open reading frames. Both putative

plasmid contigs contained an approximately 230 bp region bearing >97% sequence identity with the Tomato big bud phytoplasma plasmid (pTBBperi, DQ119297, 3319 bp total length).

Phytoplasma enrichment evaluations using quantitative polymerase chain reaction and down-sampled high-throughput sequencing sequence data

All negative control samples did not show amplification in the phytoplasma qPCR assays (Supplementary Table 2) and over 98% of their HTS reads remained unmapped after reference-based mapping using the phytoplasma and host genomes as references (Supplementary Table 3). Additionally, the percentages of unmapped, phytoplasma- and host-derived reads of the down-sampled trimmed reads

TABLE 3 Summary of iodixanol fraction densities after gradient centrifugation of phytoplasma infected potato (o4P) and capsicum (o7C) tissues, based on three (x) technical replicates of density gradient centrifugation for each sample; DNA concentrations of all samples; mean qPCR standard curve-based estimates of phytoplasma titer for all samples; HTS read mapping results after read down-sampling; and phytoplasma genome assembly quality metrics of down-sampled libraries.

Sample ^a	Mean fraction density (g/ml)	DNA concentration (ng/μl)	qPCR Ct values	Total reads retained in down-sampling (Million reads)	Mean phytoplasma reads mapped (%)	Mean host gDNA reads mapped (%)	Mean host cpDNA reads mapped (%)	Mean host mtDNA reads mapped (%)	Mean unmapped reads (%)	Phytoplasma genome assembly size (bp)	Largest phytoplasma contig mean (bp)	Phytoplasma genome mean N50 (bp)	Mean reference genome fold coverage
o4P-Homogenate	NA	34.000	16.65	5.0	1.67	85.44	6.48	1.46	4.95	565,143	92,921	37,285	29
o4P-TSE pellet	NA	1.630	12.30	5.0	9.39	69.37	7.57	4.58	9.10	569,323	71,194	28,898	132
o4P_x-Fraction1	1.049	0.668	11.87	5.0	23.37	50.80	14.48	4.04	7.31	580,942	107,718	49,236	362
o4P_x-Fraction2	1.063	0.085	14.83	5.0	16.56	60.19	9.46	5.24	8.54	568,242	107,652	37,285	255
o4P _x -Fraction3	1.063	<0.064	16.09	5.0	12.36	61.31	9.05	7.92	9.37	565,250	107,678	37,285	200
o4P_x-Fraction4	1.078	0.214	14.50	5.0	5.69	70.08	6.99	7.81	9.43	564,351	66,839	30,110	92
o4P _x -Fraction5	1.095	<0.094	17.73	5.0	5.00	72.66	5.68	5.87	10.79	566,373	69,878	26,752	92
o4P _x -Fraction6	1.104	<0.005	19.07	ND	5.74	50.51	2.26	1.29	40.20	565,998	71,194	33,168	60
o4P _x -Fraction7	1.133	<0.005	19.35	ND	4.06	69.12	2.68	1.44	22.70	565,113	107,877	37,285	57
o4P _x -Fraction8	1.196	<0.005	21.66	ND	4.24	51.38	2.78	1.90	39.71	566,077	71,194	38,094	54
o7C-Homogenate	NA	61.900	23.80	3.4	0.27	79.33	2.60	2.75	15.05	385,814	3,547	0,936	6
o7C-TSE pellet	NA	17.300	16.58	3.4	0.21	62.42	3.27	3.53	30.57	279,439	3,420	0,723	5
o7C_x-Fraction1	1.058	0.147	22.76	3.4	0.75	38.65	5.67	14.38	40.55	495,819	15,341	4,892	19
o7C_x-Fraction2	1.072	<0.005	26.46	3.4	0.57	28.53	3.96	7.52	59.43	514,099	7,684	1,943	13
o7C_x-Fraction3	1.073	<0.059	26.05	3.4	0.59	31.23	2.79	7.07	58.33	507,400	7,285	1,622	12
o7C_x-Fraction4	1.083	0.860	19.38	3.4	0.43	30.40	1.25	6.75	61.18	361,156	4,497	0,981	9
o7C _x -Fraction5	1.108	<0.198	22.79	3.4	0.24	14.58	1.44	6.36	77.38	341,085	4,040	0,932	7
o7C _x -Fraction6	1.109	0.057	24.70	3.4	0.41	17.16	1.81	8.39	72.23	463,744	5,106	1,224	9
o7C _x -Fraction7	1.119	<0.060	23.31	3.4	0.61	30.16	2.03	14.23	52.98	545,833	13,829	2,542	12
o7C _x -Fraction8	1.157	<0.082	26.23	3.4	0.37	23.31	1.95	8.83	65.54	397,225	5,341	1,008	9

N50 refers to the contig length such that contigs of equal or greater lengths produce 50% of the genome's length. Note that not all technical replicates were sequenced for all fractions derived from density gradient centrifugation (see Section "Results").

^aSample naming convention: the suffix "-Homogenate" refers to the unprocessed tissue homogenate, "-TSE pellet" refers to the pellet, resuspended in TSE buffer that results after two rounds of differential centrifugation and is loaded to the top of the iodixanol density gradient, "-F1 to -F8" indicates the iodixanol fraction sampled per host.

Bold indicates averages taken from replicates submitted for HTS, values not in bold font indicates a single replicate submitted for HTS.

NA, not available; ND, not done; UD, undetermined.

were almost identical to the percentages in corresponding libraries that were not down-sampled ([Supplementary Table 3](#)).

Potato sample

The qPCR assay for the potato sample plate met the MIQE guidelines ([Bustin et al., 2009](#)) with an R^2 value of 0.997 and an efficiency of 99.993%. The starting relative phytoplasma concentration in the DNA extracted from the unprocessed potato homogenate indicated a high phytoplasma titer with a cycle threshold (C_t) of 16.65 ([Table 3](#) and [Supplementary Table 2](#)). The estimated phytoplasma concentration increased after the differential centrifugation, with a C_t value of 12.30, for this sample. The phytoplasma concentration was also higher than the unprocessed homogenate in Fraction 1 (mean C_t of 11.87, range 11.62–12.29), Fraction 2 (mean C_t of 14.83; range, 14.42–15.23), Fraction 3 (mean C_t of 16.09; range, 15.39–16.79), and Fraction 4 (mean C_t of 14.50; range, 14.20–14.90). Therefore, all three technical replicates were prepared and submitted for Illumina sequencing for potato Fraction 1, Fraction 2, and Fraction 4, and only one replicate of the remaining fractions were sequenced.

Mapping results from the total DNA extract from the potato tissue homogenate indicated that the library was composed of 85.44% gDNA, 6.48% cpDNA, and 1.46% mtDNA (a total host-derived DNA of 93.38%, [Table 3](#)). Additionally, 1.67% of the reads from the unprocessed tissue homogenate were phytoplasma-derived, and approximately 5.0% of reads remained unmapped ([Table 3](#)). After differential centrifugation, the percent of the host-derived reads were reduced to 81.51% (69.37% gDNA, 7.57% cpDNA, and 4.58% mtDNA) of the total library, while the phytoplasma-derived and the unmapped reads increased to 9.39 and 9.10% of the library, respectively. Fraction 1 consistently showed the highest proportion of phytoplasma reads across all three technical replicates (mean, 23.37%; range, 19.12–29.58%). The replicates of Fraction 2 showed the second highest level of phytoplasma reads (mean, 16.56%; range, 14.89–19.04%). The reads mapping to potato gDNA were reduced to an average of 69.32% for Fraction 1, and 74.90% for Fraction 2 ([Table 3](#)) compared to the unprocessed tissue homogenate (85.44%). The percent of the cpDNA-derived reads was higher for Fraction 1 (mean, 14.48%; range, 13.09–16.09%), Fraction 2 (mean, 9.46%; range, 9.29–9.51%), and Fraction 3 (7.92%) than in the unprocessed homogenate and differentially centrifuged pellet.

Taxonomic profiling of all unmapped reads indicated that bacteria were enriched for after the differential centrifugation and in the iodixanol fractions showing phytoplasma enrichment when compared to the unprocessed homogenate (e.g., ~90% bacteria and ~9% Eukaryota in unprocessed homogenate vs. ~96% bacteria and ~3% Eukaryota in Fraction 1; [Supplementary Figure 1](#)).

When the percent of phytoplasma reads were high as in Fraction 1 after gradient enrichment, the reads spanned the entire potato phytoplasma reference genome ([Supplementary Figure 2A](#)) with an average of 362-fold coverage after mapping ([Table 3](#) and [Supplementary Table 2](#)) when down-sampled to 5 million reads/library. Libraries with a low percentage of phytoplasma reads left a few regions of the reference genome unmapped and with a lower percentage of overall coverage (e.g., 29-fold coverage for the unprocessed potato homogenate, and 132-fold coverage for the differentially centrifuged pellet; [Supplementary Figure 2A](#)).

Capsicum sample

The qPCR assay for the capsicum 96-well qPCR plate met the MIQE guidelines ([Bustin et al., 2009](#)) with an R^2 value of 0.990 and an efficiency of 101.049%. The C_t value for the capsicum unprocessed homogenate was 23.80 based on the qPCR assay ([Table 3](#) and [Supplementary Table 2](#)). The phytoplasma concentration increased after differential centrifugation, with a C_t value of 16.58 ([Table 3](#) and [Supplementary Table 2](#)). Phytoplasma cells were also enriched compared to the unprocessed homogenate after density gradient centrifugation in Fraction 1 (mean C_t 22.76; range, 22.25–23.12), Fraction 4 (mean C_t 19.38; range, 18.62–19.83). Since phytoplasma cells seemed to be enriched in Fraction 1 and Fraction 4 for the capsicum sample, all three technical replicates for those fractions were prepared and submitted for Illumina sequencing. All three technical replicates for Fraction 2 and Fraction 3 were also sequenced to obtain mapping profiles for all fractions between Fraction 1 and Fraction 4. One technical replicate was sequenced for the remaining fractions.

The mapping results from the total DNA extract from the capsicum tissue homogenate indicated that the library was composed of 84.68% host-derived reads (79.33% gDNA, 2.60% cpDNA, and 2.75% mtDNA), 0.27% phytoplasma-derived reads, with 15.05% of reads remaining unmapped ([Table 3](#) and [Supplementary Table 2](#)). After differential centrifugation, the percent of host-derived reads were reduced to 69.22% (62.42% gDNA, 3.27% cpDNA, and 3.53% mtDNA), and phytoplasma-derived reads reduced slightly to 0.21%, while unmapped reads approximately doubled to 30.57% of the library. Fraction 1 showed the highest average enrichment of phytoplasma DNA (mean, 0.75%; range, 0.47–1.04%), followed by the single replicate of Fraction 7 (0.61%) and Fraction 3 (mean, 0.59%; range, 0.37–0.90%). The total percent of capsicum gDNA-derived reads were reduced to below an average of 45% in all iodixanol fractions. The reads derived from the capsicum cpDNA were enriched in the differentially centrifuged pellet, Fraction 1 and Fraction 2 compared to the unprocessed homogenate, but the percent of cpDNA was reduced for the remainder of the iodixanol fractions. Capsicum mtDNA appeared to be enriched with the phytoplasmas, however, and

increased from 2.7% in the unprocessed homogenate to over 14.0% in Fraction 1 and Fraction 7.

Taxonomic profiling indicated that the unmapped reads of the capsicum sample were mostly of bacterial origin regardless of the enrichment procedure, at over 99.5%, with differential centrifugation increasing this percentage the most to 99.95% ([Supplementary Figure 1](#)).

When the phytoplasma reads were high as in Fraction 1 after iodixanol gradient enrichment, the reads spanned more regions of the capsicum phytoplasma reference genome ([Supplementary Figure 2B](#)) with a higher coverage (average of 19-fold coverage after mapping with 3.4 million reads/library, [Table 3](#) and [Supplementary Table 2](#)) than those without iodixanol-based enrichment. The samples for which the phytoplasma enrichment was not achieved showed a lower fold-coverage of the reference genome and mapping to fewer regions of the phytoplasma reference genome of the capsicum sample (e.g., five and sixfold coverage of the reference genome from 3.4 million reads for the unprocessed capsicum homogenate and differentially centrifuged pellet samples, respectively, [Table 3](#), [Supplementary Figure 2B](#), and [Supplementary Table 2](#)).

Effect of enrichment on phytoplasma genome assembly quality (down-sampled assemblies)

Potato sample

For the potato-derived phytoplasma genomes assembled from 5 million reads, genomes obtained from Fraction 1 were approximately 15,800 bp larger than the assembly from the unprocessed potato homogenate and 11,600 bp larger than the differentially centrifuged pellet. Phytoplasma genomes from Fraction 1 had the highest N50 values (mean, 49,236 bp; range, 28,898–59,408 bp), while the genome N50 values of the unprocessed potato homogenate and the differentially centrifuged pellet genomes were smaller at 37,285 and 28,898 bp, respectively, with the differentially centrifuged pellet showing one of the smallest genome N50 values for all the samples analyzed ([Table 3](#) and [Supplementary Table 2](#)). On average, the largest assembled contig was approximately 107,700 bp for Fraction 1, Fraction 2, and Fraction 3, while the largest assembled contig for the unprocessed pellet and differentially centrifuged pellet was 92,900 and 71,200 bp, respectively ([Table 3](#) and [Supplementary Table 2](#)).

A putative phytoplasma plasmid was only recovered in one replicate of Fraction 4 for the potato in the down-sampled genome assemblies (data not shown). The putative plasmid was 3,832 bp in size and encoded two open reading frames.

Capsicum sample

For phytoplasma genomes assembled from the infected capsicum sample (down-sampled to 3.4 million reads), the

largest genomes were assembled for Fraction 7 (545,833 bp), Fraction 2 (mean, 514,099 bp), Fraction 3 (mean, 507,400 bp), and Fraction 1 (mean, 495,819 bp). The phytoplasma genomes assembled from the unprocessed capsicum homogenate and differentially centrifuged pellet were two of the smallest assemblies at 385,814 and 279,439 bp, respectively. Fraction 1 produced a genome assembly with the highest average genome N50 value (mean, 4,892 bp), followed by Fraction 7 (mean, 2,542 bp), and Fraction 2 and Fraction 3 with average genome N50 values of 1,943 and 1,622 bp, respectively ([Table 3](#) and [Supplementary Table 2](#)). The genome assemblies from the unprocessed homogenate and differentially centrifuged pellet had similar N50 values, which were below 1,000 bp on average. The largest phytoplasma contig assembled on average was produced for Fraction 1 (mean, 15,341 bp), followed by Fraction 7 (mean, 13,829 bp), Fraction 2 (mean, 7,684 bp), and Fraction 3 (mean, 7,285 bp). The largest contig assembled in the unprocessed homogenate and the differentially centrifuged sample were similar in size at 3,547 and 3,420 bp, respectively.

The putative phytoplasma plasmids were recovered from all replicates of Fraction 1, Fraction 3, Fraction 5, and Fraction 7, as well as from two replicates of Fraction 2. A putative plasmid most similar in size to that recovered for the reference genome assembly was identified from Fraction 3 (technical replicate 2) and was 3,396 bp in size (data not shown).

Whole genome comparisons

As an additional estimate of the genetic divergence of the reference genomes (publicly available and those assembled in this study), we calculated the ANI and the proportion of mapped genomic segments between these genomes in a reciprocal manner ([Figure 1](#)). The lowest ANI values between two different genomes were between the publicly available reference genomes of strain NCHU2014 and strain PR08 at 98.2%; while the highest ANI was 99.8% between strain NCHU2014 and the ‘*Ca. Phytoplasma australasiae*’-related strain o4P. The reference genome of strain o7C shared 94.1% of its genomic segments with the reference genome of strain o4P. The reference genomes of strains o4P and o7C shared 87.1–87.7% of mapped genomic segments with strain NCHU2014, and over 91.8% mapped reads with the publicly available genome of strain PR08.

To evaluate whether genome sequencing of phytoplasma genomes after iodixanol-based enrichment is suitable for comparative genomic analyses, we analyzed the ANIs of genomes from the down-sampled assemblies of the unprocessed homogenate, the differentially centrifuged pellet, and the iodixanol fraction with the highest proportion of phytoplasma-mapped HTS reads of the infected potato and capsicum hosts against the four reference genomes of the closely related taxa used in this study ([Figure 2](#)). The ANI values for the phytoplasma genomes assembled from 5 million reads for the

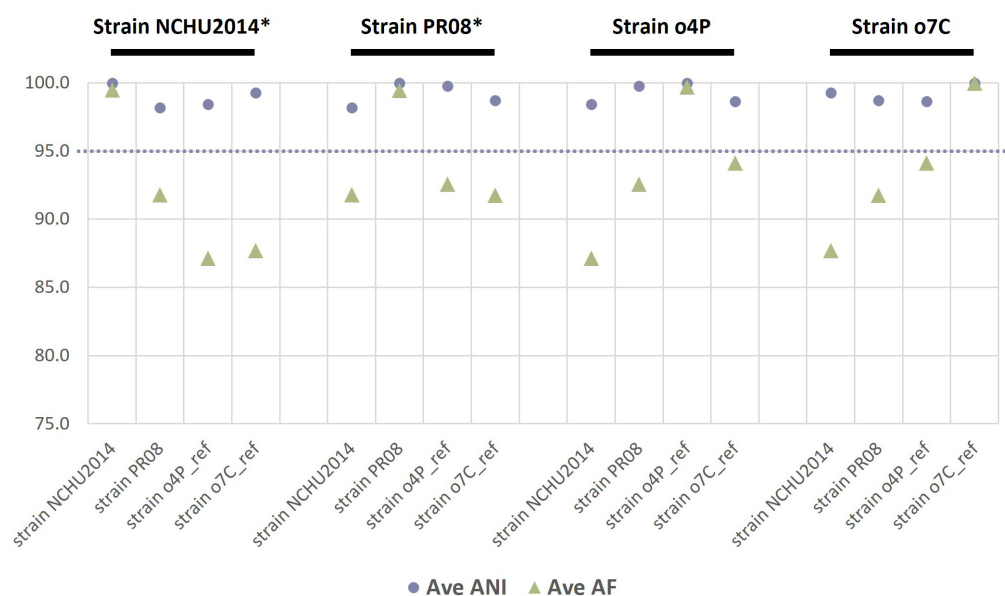


FIGURE 1

Reciprocal mean average nucleotide identities (ANI, %) and proportion of aligned genomic segments (AF, %) for the two phytoplasma reference genomes assembled in this study and two publicly available phytoplasma reference genomes (strain NCHU2014 and strain PR08). The phytoplasma genome used as a reference in each case is indicated above the graph in black font, with an asterisk indicating a complete genome. The dashed line indicates the proposed 95% ANI species delimitation threshold value.

unprocessed homogenate (o4P-IB), differentially centrifuged pellet (o4P-TSE), and three replicates of iodixanol Fraction 1 (o4P1-F1 to o4P3-F1) from potato differed by less than 1% in comparisons with all reference genomes used in this study (Figure 2A). The proportion of mapped genomic segments between these genomes ranged between 86.0 and 98.8% (Figure 2A). Iodixanol density gradient centrifugation resulted in a higher proportion of mapped genomic segments compared to the homogenate and differentially centrifuged pellet, but the difference was less than 1% in the case of the infected potato. The ANI values from the capsicum phytoplasma down-sampled assemblies for the unprocessed homogenate (o7C-IB), differentially centrifuged pellet (o7C-TSE), and two replicates of the iodixanol Fraction 1 (o7C1-F1 and o7C2-F1) differed by less than 3% in comparisons with all reference genomes (Figure 2B). The capsicum phytoplasma genomes assembled from iodixanol Fraction 1 consistently had a much greater proportion of mapped genomic segments (52.7–85.5%) with the reference genomes compared to the unprocessed capsicum homogenate and the differentially centrifuged pellet (50.2–50.6%; Figure 2B).

Discussion

Both qPCR and mapping of HTS reads showed phytoplasma enrichment using the iodixanol density gradient centrifugation method developed in this study. This enrichment, in turn, significantly improved the contiguity and coverage

of phytoplasma genome assemblies obtained from the metagenomic data for the two naturally infected phytoplasma hosts investigated here, irrespective of the relative starting titer (Table 3 and Supplementary Figure 2). The highest levels of phytoplasma enrichment were observed in the lower density iodixanol fractions, between an average density of 1.049 and 1.058 g/ml (Fraction 1) and a maximum average density of 1.078–1.083 g/mL (Fraction 4). Host gDNA was also consistently depleted in these iodixanol fractions, shown by at least 30% less HTS reads mapping to the host gDNA reference in the chosen iodixanol fraction than the unprocessed homogenate for both hosts (Table 3). Additionally, we obtained high-quality draft phytoplasma genome sequences from both *Solanaceae* hosts investigated in this study from fractions that had undergone iodixanol density gradient centrifugation (Table 3).

The study demonstrates that iodixanol is ideal to enrich for delicate, wall-less phytoplasma cells due to the non-ionic, non-toxic, and metabolically inert nature of the substance, which help keep cells intact (Ford et al., 1994). Other factors that reduce the risk of cell lysis include the fact that iodixanol is iso-osmotic and maintains a low osmolarity throughout the gradient; thus, preventing pressure-sensitive phytoplasma cells from experiencing large pressure changes during centrifugation. Moreover, iodixanol has a low viscosity allowing for cells to separate based on their buoyant densities during a relatively short centrifugation time, further reducing the risk of lysing phytoplasma cells. Additional precautions to

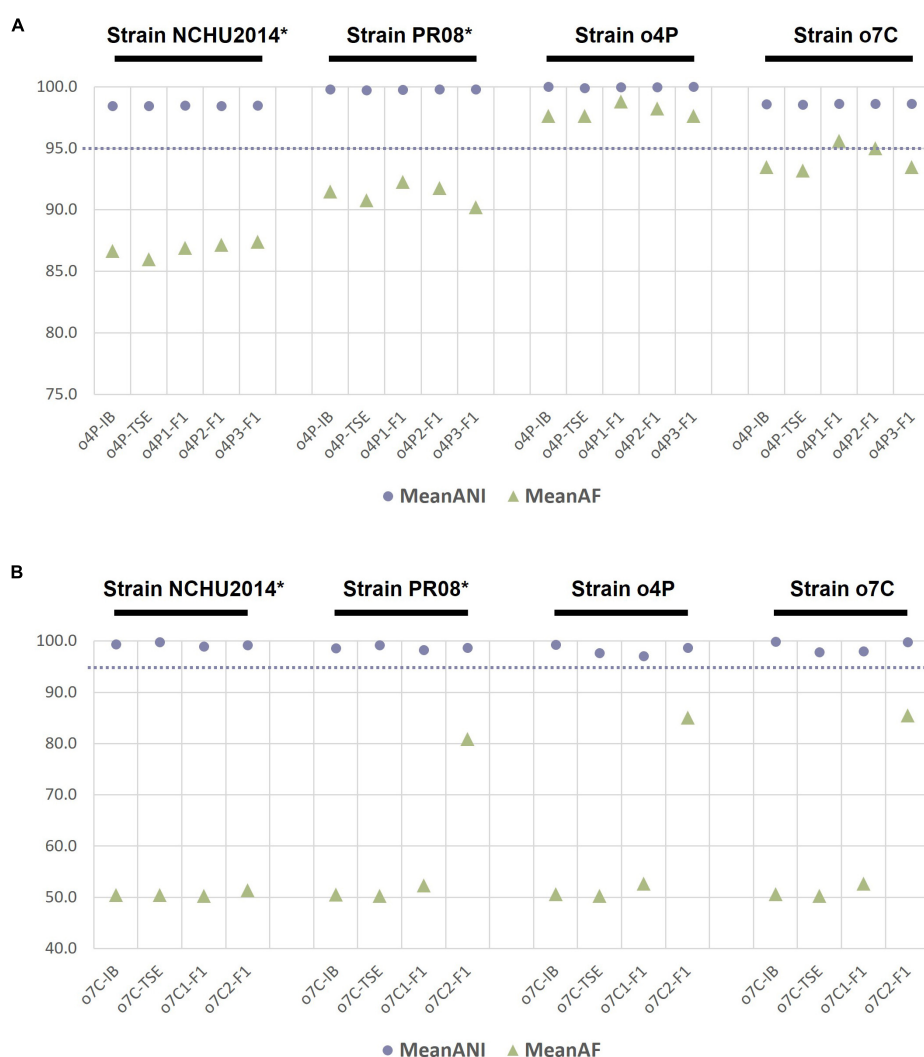


FIGURE 2

Average nucleotide identity (ANI, %) and proportion of aligned genomic segments (AF,%) for down-sampled assemblies compared to the phytoplasma reference genomes assembled in this study and two publicly available phytoplasma reference genomes for (A) the infected potato host and (B) the infected capsicum host. The samples analyzed for each host included the unprocessed tissue homogenate (suffix "-IB"), differentially centrifuged pellet (suffix "-TSE"), and the iodixanol fraction with the highest percent of phytoplasma reads (suffix "-F1"). The phytoplasma genome used as the reference in each case is indicated above the graph in black font, with an asterisk indicating a complete genome. The dashed line indicates the proposed 95% ANI species delimitation threshold value.

keep the phytoplasma cells intact for their improved recovery included the use of the Phytoplasma Grinding Buffer for cell plasmolysis (Kirkpatrick et al., 1987) which may stabilize phytoplasma cells by reducing their turgor pressure, as well as gentle tissue homogenization and by maintaining all buffers, reagents, tubes, and centrifuges at 4°C throughout the method.

Phytoplasma-derived DNA was detected throughout the density gradient at various proportions for both hosts investigated (Table 3). This may be due to several factors that could affect phytoplasma cell sizes and densities, including their stage in reproduction (parent cell vs. budding cell), their extracellular components (plasmid present or absent,

number of plasmids per cell), and the pleiomorphic nature of phytoplasma cells. Cell-free phytoplasma DNA may also separate throughout the iodixanol gradient during centrifugation. These factors and their effect on the efficiency of phytoplasma enrichment by iodixanol density centrifugation, however, remain to be determined.

Phytoplasma genome quality improved significantly with host gDNA depletion using the iodixanol density gradient centrifugation method developed here. We adjusted and tested the effect of the number of differential centrifugation rounds (work by Shrestha, 2021) and the iodixanol gradient set up (data not shown) while developing the method described here,

and chose the best of these conditions for this study. However, improvements could be made to further reduce contaminating host gDNA which, based on HTS mapping, was still present at different concentrations throughout the iodixanol gradient after centrifugation (Table 3). This would be particularly important for extremely low-titer hosts. Additional adjustments could be applied to further reduce host gDNA to improve sequencing outputs and phytoplasma genome assembly, including applying additional rounds of differential centrifugation, altering the times and speeds of differential and/or density gradient centrifugation, or even adjusting the concentrations of the isotonic buffer or iodixanol density gradient solutions. Coupling the differential centrifugation step with filtration methods applied in other studies (Palmano, 2001; Tan et al., 2021) could further deplete host cells, and therefore gDNA. However, there is the risk of reducing the phytoplasma yield due to their cell lysis by filtration and/or due to the longer processing time prior to density gradient centrifugation. Another, possibly better-suited approach, involves combining iodixanol density gradient centrifugation with chemical depletion of methylated host gDNA using a commercial kit to the DNA extractions from iodixanol fractions prior to Illumina sequencing. In previous studies, this kit was effective for phytoplasma enrichment by host gDNA reduction with Kirdat et al. (2021) stating a fivefold host gDNA reduction based on host-specific qPCR quantification; and close to 60% less host gDNA reads as identified by their taxonomic classification in Nijo et al. (2021). An issue to applying the kit is the low DNA concentration obtained from the fractions. This could be addressed by resuspending the DNA in a lower volume of eluate (at the expense of their volumes used in the qPCR assay) or by pooling corresponding fractions from multiple replicates. An increase in total DNA would have an additional advantage as it would permit the use of Oxford Nanopore sequencing for long-read sequencing, which has proven useful for improving the contiguity and completeness of phytoplasma genomes (e.g., ‘*Ca. Phytoplasma aurantifolia*’-related strain NCHU2014, Tan et al., 2021; Table 2).

The reduction of host gDNA was consistently observed between Fraction 1 and Fraction 4 of the iodixanol density gradient and greatly improved the quality of phytoplasma genome assemblies (phytoplasma genome assembly sizes up to 137,000 bp larger than without enrichment, N50 values up to 12,000 bp larger, Table 3; and higher read coverage, Supplementary Figure 2). The host-associated non-phytoplasma bacterial DNA, mtDNA, and cpDNA were almost always enriched in these fractions, however, and therefore remain as competitors for HTS sequencing reads (Table 3). This was expected as the plant organelles and bacterial cells are smaller and have a lower density than nuclei (Graham et al., 1994). Additionally, similar iodixanol-based density gradient centrifugation methods have been used to enrich for various subcellular components, such as mitochondria

(Choi et al., 2021), as well as Gram-negative bacteria from human and animal cells (Henríquez et al., 2003; Beder et al., 2016) and from insect vectors (Frampton et al., 2018). Similar patterns of host-associated organismal and organellar enrichment was also observed for two phytoplasma enrichment methods recently investigated, one involving methylated DNA depletion (Nijo et al., 2021) and the other developed for phytoplasma-specific enrichment by immunoprecipitation (Tan et al., 2021). Plant organellar DNA “contamination” of phytoplasma-enriched DNA has also been observed for the CsCl density gradient centrifugation method (Malembic-Maher et al., 2008) as these organelles contain AT-rich genomes similar to phytoplasmas (Tran-Nguyen and Schneider, 2012). Improving the specificity of current phytoplasma enrichment methods, combining multiple phytoplasma enrichment and/or host depletion methods, or developing host organellar DNA depletion methods would further enhance the efficiency and therefore the cost of phytoplasma whole genome sequencing in the absence of a phytoplasma culture system. Nevertheless, non-phytoplasma bacterial enrichment by the iodixanol density gradient method developed here is broadly useful, serving as a method that is suitable for genome sequencing of other unculturable and intracellular phytopathogenic bacteria, such as ‘*Candidatus Liberibacter*’ species (Frampton et al., 2018).

The iodixanol density gradient method described here is a significant improvement over some other methods used to enrich for phytoplasmas because it is cost- and time-efficient, and offers increased safety for researchers. For example, during phytoplasma enrichment with CsCl density gradient centrifugation, there are multiple centrifugation steps amounting to over 200 h (Tran-Nguyen and Gibb, 2007), while centrifugation through the iodixanol density gradient in this study only took 3 h. Additionally, the iodixanol density medium is an inert and clinical-grade reagent, making it a much safer to handle compared to those associated with CsCl-based enrichment (Andersen and Liefing, 2013). The iodixanol-based method only made use of (ultra)centrifuges and the appropriate tubes, without the requirement for additional and less frequently used equipment or consumables, making the method more widely feasible and cost-effective for many users to set up. Using the method described here also allowed for direct sequencing from the natural host. This ensures that the most biologically relevant phytoplasma is sequenced and a high-quality genome obtained (Table 2), without requiring transmission to a high-titer experimental host such as periwinkle, which is not always feasible or practical.

The reference genomes of two ‘*Ca. Phytoplasma australasia*’-related strains were assembled from the naturally infected potato and capsicum hosts used in this study, which were all comprised of 30 or fewer contigs and with high contiguity (N50 values of approximately 40,000 bp) (Table 2). This was due to the high sequencing depth achieved for some of the samples coupled with phytoplasma enrichment by iodixanol

density gradient centrifugation (see o4P2-F2 and o7C1-F7 in [Supplementary Table 2](#)). Since the genomes represent moderately contiguous assemblies, these genomes could be useful in comparisons of whole genome structure and synteny. Their sizes are similar to previous PFGE-based size estimates of closely related phytoplasma genomes, which range between 605,000 and 790,000 bp ([Marcone et al., 1999](#); [Padovan et al., 2000](#)). However, it is difficult to estimate true phytoplasma genome sizes and, therefore, the level of completeness of the reference genomes assembled in this study. This is not only due to the tendency of PFGE-based estimates representing an overestimate of genome size by 10–15% ([Tsai et al., 2018](#); [Music et al., 2019](#)) but also because natural genome size variations exist even between closely related phytoplasma strains attributed to the high genomic plasticity reported for phytoplasma genomes ([Andersen et al., 2013](#); [Music et al., 2019](#); [Huang et al., 2022](#)). Although a high sequencing depth of Illumina reads was achieved, short-read technologies and their associated assembly programs are often unable to resolve the repeat-rich regions of phytoplasma genomes, indicating that there is an opportunity to resolve the gaps in these reference genomes using Sanger and/or long-read sequencing technologies in the future. Moreover, contigs representing putative phytoplasma plasmids were consistently identified from assemblies of both hosts, but require further validation.

This study illustrates the importance of producing high-quality phytoplasma genomes to make accurate comparative genomic and taxonomic inferences. In our comparative genomic analyses, we show that ANI estimates are only slightly affected by the completeness of the phytoplasma genome. For example, the ANI values between all genomes assembled from the potato or capsicum hosts did not differ more than 3%, irrespective of the level of phytoplasma enrichment ([Figure 2](#)). This relatively small error in ANI estimation could pose problems for taxa sitting at the borderline of the 95% ANI threshold which was recently recommended to distinguish two separate phytoplasma species ([Cho et al., 2020](#); [Bertaccini et al., 2022](#)). However, the proportion of mapped genomic segments implemented with ANI estimates is more severely affected by the completeness of the genomes under consideration, with a lower proportion mapping with more incomplete genomes ([Figure 2](#)). The combination of ANI and the proportion of mapped genomic segments are being recognized as important algorithms for robust estimations of taxonomic boundaries of prokaryotes ([Barco et al., 2020](#)). In the ANI analysis presented here, phytoplasma genomes assembled from the iodixanol fraction where the highest level of phytoplasma enrichment was observed performed most similarly to the reference genome assembled from the same host, despite read down-sampling prior to assembly, highlighting the benefits of phytoplasma enrichment and the effectiveness of our iodixanol density gradient method on genomic analyses of phytoplasmas ([Figures 1, 2](#)). These results are important to consider as

phytoplasma research increasingly embraces high-throughput sequencing to delineate species boundaries of these yet-to-be-cultured phytopathogens ([Firrao et al., 2013](#); [Cho et al., 2020](#); [Bertaccini et al., 2022](#)).

Data availability statement

The data presented in this study are deposited in the NCBI repository (<https://www.ncbi.nlm.nih.gov/>), accession numbers: JALQCT000000000 and JALQCV000000000.

Author contributions

BRJ participated in the design of the study and carried out the laboratory work, data analysis, interpretation, and drafting the manuscript. CG participated in the collection of samples. FC, BR, CG, and LT-N participated in design of the study and data interpretation and contributed to reviewing and editing the manuscript. All authors read and approved the final manuscript.

Funding

This project was funded by Hort Innovation using vegetable industry levies with co-investment from the Queensland Department of Agriculture and Fisheries; Victorian Department of Jobs, Precincts and Regions; the Northern Territory Department of Industry, Tourism and Trade; the Western Australia Department of Primary Industries and Regional Development, and the University of Tasmania. Hort Innovation was the grower-owned, not-for-profit research, and development corporation for Australian horticulture. We would also like to acknowledge Agriculture Victoria Research and La Trobe University for financial support of BRJ through their provision of a Living Allowance Scholarship and the La Trobe Full Fee Research Scholarship (LTUFFRS), respectively. This research was conducted using the facilities of Agriculture Victoria.

Acknowledgments

We thank the growers and CSIRO for allowing the sample collection on their properties, and colleagues who assisted in collecting or sending samples for the present study. Thanks to Elisse Nogarotto (Agriculture Victoria Research) for technical

assistance, especially at the early stages of method development, as well as Wycliff M. Kinoti (Agriculture Victoria Research) and Conrad Trollip (Agriculture Victoria Research) for input regarding bioinformatic analyses. We are grateful to Rebekah A. Frampton and Sarah M. Thompson (both at The New Zealand Institute for Plant and Food Research Limited) for sharing details of their iodixanol density gradient enrichment approach.

Conflict of interest

The authors declare that the research was conducted in the absence of any commercial or financial relationships that could be construed as a potential conflict of interest.

References

- Altschul, S. F., Madden, T. L., Schäffer, A. A., Zhang, J., Zhang, Z., Miller, W., et al. (1997). Gapped BLAST and PSI-BLAST: a new generation of protein database search programs. *Nucleic Acids Res.* 25, 3389–3402. doi: 10.1111/j.1365-3059.1995.tb02715.x
- Andersen, M. T., and Liewing, L. W. (2013). “Phytoplasma Plasmid DNA Extraction,” in *Phytoplasma: Methods and Protocols, Methods in Molecular Biology*, ed. M. D. Hodgetts (Berlin: Springer Science+Business Media), 371–379. doi: 10.1007/978-1-62703-089-2
- Andersen, M. T., Liewing, L. W., Havukkala, I., and Beever, R. E. (2013). Comparison of the complete genome sequence of two closely related isolates of “*Candidatus Phytoplasma australiense*” reveals genome plasticity. *BMC Genomics* 14:52. doi: 10.1186/1471-2164-14-529
- Bai, X., Zhang, J., Ewing, A., Miller, S. A., Jancso Radek, A., Shevchenko, D. V., et al. (2006). Living with genome instability: the adaptation of phytoplasmas to diverse environments of their insect and plant hosts. *J. Bacteriol.* 188, 3682–3696. doi: 10.1128/JB.188.10.3682-3696.2006
- Barco, R. A., Garrity, G. M., Scott, J. J., Amend, J. P., Nealson, K. H., Emerson, D., et al. (2020). A genus definition for bacteria and archaea based on a standard genome relatedness index. *mBio* 11:e02475-19. doi: 10.1128/MBIO.02475-19
- Beder, T., Scheven, M. T., Praetzel, D., Westermann, M., and Saluz, H. P. (2016). Purification of infectious and non-infectious chlamydial particles using iodixanol for density gradient preparation. *J. Microbiol. Methods* 128, 20–23. doi: 10.1016/j.mimet.2016.06.029
- Bertaccini, A., Arocha-Rosete, Y., Contaldo, N., Duduk, B., Fiore, N., Montano, H. G., et al. (2022). Revision of the “*Candidatus Phytoplasma*” species description guidelines. *Int. J. Syst. Evol. Microbiol.* 72:005353. doi: 10.1099/ijsem.0.005353
- Breitwieser, F. P., and Salzberg, S. L. (2020). Pavian: interactive analysis of metagenomics data for microbiome studies and pathogen identification. *Bioinformatics* 36, 1303–1304. doi: 10.1093/bioinformatics/btz715
- Bushnell, B. (2014). *BBMap: A Fast, Accurate, Splice-Aware Aligner*. Berkeley, CA: Lawrence Berkeley National Lab.(LBNL). doi: 10.1186/1471-2105-13-238
- Bustin, S. A., Benes, V., Garson, J. A., Hellemans, J., Huggett, J., Kubista, M., et al. (2009). The MIQE guidelines: minimum information for publication of quantitative real-time PCR experiments. *Clin. Chem.* 55, 611–622. doi: 10.1373/clinchem.2008.112797
- Chang, S. H., Cho, S. T., Chen, C. L., Yang, J. Y., and Kuo, C. H. (2015). Draft genome sequence of a 16SrII-A subgroup phytoplasma associated with purple coneflower (*Echinacea purpurea*) witches’ broom disease in Taiwan. *Genome Announce* 3, 6–7. doi: 10.1128/genomeA.01398-15
- Chen, S., Zhou, Y., Chen, Y., and Gu, J. (2018). Fastp: an ultra-fast all-in-one FASTQ preprocessor. *Bioinformatics* 34, i884–i890. doi: 10.1093/bioinformatics/bty560
- Chen, W., Li, Y., Wang, Q., Wang, N., and Wu, Y. (2014). Comparative genome analysis of wheat blue dwarf phytoplasma, an obligate pathogen that causes wheat blue dwarf disease in China. *PLoS ONE* 9:96436. doi: 10.1371/journal.pone.0096436
- Cho, S. T., Kung, H. J., Huang, W., Hogenhout, S. A., and Kuo, C. H. (2020). Species Boundaries and Molecular Markers for the Classification of 16SrI Phytoplasmas Inferred by Genome Analysis. *Front. Microbiol.* 11:1531. doi: 10.3389/fmicb.2020.01531
- Choi, C. Y., Vo, M. T., Nicholas, J., and Choi, Y. B. (2021). Autophagy-competent mitochondrial translation elongation factor TUFM inhibits caspase-8-mediated apoptosis. *Cell Death Differ.* 29, 451–464. doi: 10.1038/s41418-021-00868-y
- Christensen, N. M., Nicolaisen, M., Hansen, M., and Schulz, A. (2004). Distribution of phytoplasmas in infected plants as revealed by real-time PCR and bioimaging. *Mol. Plant Microbe Interact.* 17, 1175–1184. doi: 10.1094/MPMI.2004.17.11.1175
- Chung, W. C., Chen, L. L., Lo, W. S., Lin, C. P., and Kuo, C. H. (2013). Comparative Analysis of the Peanut Witches’-Broom Phytoplasma Genome Reveals Horizontal Transfer of Potential Mobile Units and Effectors. *PLoS ONE* 8:62770. doi: 10.1371/journal.pone.0062770
- Coetzee, B., Douglas-Smit, N., Maree, H. J., Burger, J. T., Krüger, K., and Pieterse, G. (2019). Draft Genome Sequence of a “*Candidatus Phytoplasma asteris*”-Related Strain (Aster Yellow, Subgroup 16SrI-B) from South Africa. *Microbiol. Resour. Announce* 8:e00148-19. doi: 10.1128/mra.00148-19
- Firrao, G., Martini, M., Ermacor, P., Loi, N., Torelli, E., Foissac, X., et al. (2013). Genome wide sequence analysis grants unbiased definition of species boundaries in “*Candidatus Phytoplasma*”. *Syst. Appl. Microbiol.* 36, 539–548. doi: 10.1016/j.syapm.2013.07.003
- Fischer, A., Santana-Cruz, I., Wambua, L., Olds, C., Midega, C., Dickinson, M., et al. (2016). Draft genome sequence of “*Candidatus Phytoplasma oryzae*” strain Mbital, the causative agent of Napier grass stunt disease in Kenya. *Genome Announce* 4:e00297-16. doi: 10.1128/genomeA.00297-16
- Ford, T., Graham, J., and Rickwood, D. (1994). Iodixanol: a nonionic iso-osmotic centrifugation medium for the formation of self-generated gradients. *Anal. Biochem.* 220, 360–366.
- Frampton, R. A., Thompson, S. M., Kalamorz, F., David, C., Addison, S. M., and Smith, G. R. (2018). Draft genome sequence of a “*Candidatus Liberibacter europaeus*” strain assembled from broom psyllids (*Arytainilla spartiophila*) from New Zealand. *Genome Announce* 6:e00430-18. doi: 10.1128/genomeA.00430-18
- Graham, J., Ford, T., and Rickwood, D. (1994). The preparation of subcellular organelles from mouse liver in self-generated gradients of iodixanol. *Anal. Biochem.* 220, 367–373.
- Henriquez, V., Rojas, M. V., and Marshall, S. H. (2003). An alternative efficient procedure for purification of the obligate intracellular fish bacterial pathogen *Piscirickettsia salmonis*. *Appl. Environ. Microbiol.* 69, 6268–6271. doi: 10.1128/AEM.69.10.6268-6271.2003

Publisher’s note

All claims expressed in this article are solely those of the authors and do not necessarily represent those of their affiliated organizations, or those of the publisher, the editors and the reviewers. Any product that may be evaluated in this article, or claim that may be made by its manufacturer, is not guaranteed or endorsed by the publisher.

Supplementary material

The Supplementary Material for this article can be found online at: <https://www.frontiersin.org/articles/10.3389/fmicb.2022.937648/full#supplementary-material>

- Huang, C.-T., Cho, S. T., Lin, Y. C., Tan, C. M., Chiu, Y. C., Yang, J. Y., et al. (2022). Comparative genome analysis of “*Candidatus* Phytoplasma luffae” reveals the influential roles of potential mobile units in phytoplasma evolution. *Front. Microbiol.* 13:773608. doi: 10.3389/fmicb.2022.773608
- Hyatt, D., Chen, G. L., LoCascio, P. F., Land, M. L., Larimer, F. W., Hauser, L. J., et al. (2010). Prodigal: prokaryotic gene recognition and translation initiation site identification. *BMC Bioinformatics* 11:119. doi: 10.1186/1471-2105-11-119
- Jain, C., Rodriguez-R, L. M., Phillippy, A. M., Konstantinidis, K. T., and Aluru, S. (2018). High throughput ANI analysis of 90K prokaryotic genomes reveals clear species boundaries. *Nat. Commun.* 9:5114. doi: 10.1038/s41467-018-07641-9
- Kakizawa, S., Makino, A., Ishii, Y., Tamaki, H., and Kamagata, Y. (2014). Draft Genome Sequence of “*Candidatus* Phytoplasma asteris” Strain OY-V, an Unculturable Plant-Pathogenic Bacterium. *Genome Announce*. 2:e00944-14. doi: 10.1128/genomeA.00944-14. Copyright
- Kirdat, K., Tiwarekar, B., Thorat, V., Sathe, S., Shouche, Y., and Yadav, A. (2021). ‘*Candidatus* Phytoplasma sacchari. a novel taxon-associated with sugarcane grassy shoot (SCGS) disease. *Int. J. Syst. Evol. Microbiol.* 71, 1–7. doi: 10.1099/ijsem.0.004591
- Kirkpatrick, B. C., Stenger, D. C., Morris, T. J., and Purcell, A. H. (1987). Cloning and Detection of DNA from a Nonculturable Plant Pathogenic Mycoplasma-like organism. *Science* 238, 197–200.
- Kube, M., Schneider, B., Kuhl, H., Dandekar, T., Heitmann, K., Migdoll, A. M., et al. (2008). The linear chromosome of the plant-pathogenic mycoplasma “*Candidatus* Phytoplasma mali”. *BMC Genomics* 9:306. doi: 10.1186/1471-2164-9-306
- Lagesen, K., Hallin, P., Rødland, E. A., Staerfeldt, H. H., Rognes, T., Ussery, D. W., et al. (2007). RNAmmer: consistent and rapid annotation of ribosomal RNA genes. *Nucleic Acids Res.* 35, 3100–3108. doi: 10.1093/nar/gkm160
- Laslett, D., and Canback, B. (2004). ARAGORN, a program to detect tRNA genes and tmRNA genes in nucleotide sequences. *Nucleic Acids Res.* 32, 11–16. doi: 10.1093/nar/gkh152
- Malembic-Maher, S., Constable, F., Cimerman, A., Arnaud, G., Carle, P., Foissac, X., et al. (2008). A chromosome map of the Flavescence dorée phytoplasma. *Microbiology* 154, 1454–1463. doi: 10.1099/mic.0.2007/013888-0
- Marcone, C., Neimark, H., Ragozzino, A., Lauer, U., and Seemüller, E. (1999). Chromosome sizes of phytoplasmas composing major phylogenetic groups and subgroups. *Phytopathology* 89, 805–810. doi: 10.1094/PHYTO.1999.89.9.805
- Mikheenko, A., Saveliev, V., and Gurevich, A. (2016). MetaQUAST: evaluation of metagenome assemblies. *Bioinformatics* 32, 1088–1090. doi: 10.1093/bioinformatics/btv697
- Music, M. S., Samarzija, I., Hogenhout, S. A., Haryono, M., Cho, S. T., and Kuo, C. H. (2019). The genome of “*Candidatus* Phytoplasma solani” strain SA-1 is highly dynamic and prone to adopting foreign sequences. *Syst. Appl. Microbiol.* 42, 117–127. doi: 10.1016/j.syapm.2018.10.008
- Nijo, T., Iwabuchi, N., Tokuda, R., Suzuki, T., Matsumoto, O., Miyazaki, A., et al. (2021). Enrichment of phytoplasma genome DNA through a methyl-CpG binding domain-mediated method for efficient genome sequencing. *J. Gen. Plant Pathol.* 87, 154–163. doi: 10.1007/s10327-021-00993-z
- Nurk, S., Meleshko, D., Korobeynikov, A., and Pevzner, P. A. (2017). MetaSPAdes: a new versatile metagenomic assembler. *Genome Res.* 27, 824–834. doi: 10.1101/gr.213959.116
- Orlovskis, Z., Canale, M. C., Haryono, M., Lopes, J. R. S., Kuo, C. H., and Hogenhout, S. A. (2017). A few sequence polymorphisms among isolates of Maize bushy stunt phytoplasma associate with organ proliferation symptoms of infected maize plants. *Ann. Bot.* 119, 869–884. doi: 10.1093/aob/mcw213
- Oshima, K., Kakizawa, S., Nishigawa, H., Jung, H. Y., Wei, W., Suzuki, S., et al. (2004). Reductive evolution suggested from the complete genome sequence of a plant-pathogenic phytoplasma. *Nat. Genetics* 36, 27–29. doi: 10.1038/ng1277
- Oyola, S. O., Otto, T. D., Gu, Y., Maslen, G., Manske, M., Campino, S., et al. (2012). Optimizing Illumina next-generation sequencing library preparation for extremely at-biased genomes. *BMC Genomics* 13:1. doi: 10.1186/1471-2164-13-1
- Padovan, A. C., Firrao, G., Schneider, B., and Gibb, K. S. (2000). Chromosome mapping of the sweet potato little leaf phytoplasma reveals genome heterogeneity within the phytoplasmas. *Microbiology* 146, 893–902. doi: 10.1099/00221287-146-4-893
- Palmano, S. (2001). A comparison of different phytoplasma DNA extraction methods using competitive PCR. *Phytopathol. Mediterr.* 40, 99–107.
- Pereira-Marques, J., Hout, A., Ferreira, R. M., Weber, M., Pinto-Ribeiro, I., van Doorn, L. J., et al. (2019). Impact of host DNA and sequencing depth on the taxonomic resolution of whole metagenome sequencing for microbiome analysis. *Front. Microbiol.* 10:01277. doi: 10.3389/fmicb.2019.01277
- Prijbelski, A., Antipov, D., Meleshko, D., Lapidus, A., and Korobeynikov, A. (2020). Using SPAdes De Novo Assembler. *Curr. Protoc. Bioinf.* 70, 1–29. doi: 10.1002/cpbi.102
- Quan, S., Hiniker, A., Collet, J. F., and Bardwell, J. C. (2013). Isolation of bacteria envelope proteins. *Methods Mol. Biol.* 966, 359–366. doi: 10.1007/978-1-62703-245-2_22
- Rodrigues Jardim, B., Kinoti, W. M., Tran-Nguyen, L. T. T., Gambley, C., Rodoni, B., and Constable, F. E. (2021). “*Candidatus* Phytoplasma stylosanthi”, a novel taxon with a diverse host range in Australia, characterised using multilocus sequence analysis of 16S rRNA, *secA*, *tuf*, and *rp* genes. *Int. J. Syst. Evol. Microbiol.* 71:ijsem004589. doi: 10.1099/ijsem.0.004589
- Seemann, T. (2014). Prokka: rapid prokaryotic genome annotation. *Bioinformatics* 30, 2068–2069. doi: 10.1093/bioinformatics/btu153
- Shrestha, S. (2021). *Optimization of an enrichment technique to facilitate whole genome sequencing of phytoplasmas*. M.Sc. thesis. Bundoora, VIC: La Trobe University.
- Sugio, A., MacLean, A. M., Kingdom, H. N., Grieve, V. M., Manimekalai, R., and Hogenhout, S. A. (2011). Diverse targets of phytoplasma effectors: from plant development to defense against insects. *Annu. Rev. Phytopathol.* 49, 175–195. doi: 10.1146/annurev-phyto-072910-095323
- Tan, C. M., Lin, Y. C., Li, J. R., Chien, Y. Y., Wang, C. J., Chou, L., et al. (2021). Accelerating complete phytoplasma genome assembly by immunoprecipitation-based enrichment and MinION-Based DNA sequencing for comparative analyses. *Front. Microbiol.* 12:766221. doi: 10.3389/fmicb.2021.766221
- Tran-Nguyen, L. T. T., and Gibb, K. S. (2007). Optimizing phytoplasma DNA purification for genome analysis. *J. Biomol. Techniq.* 18, 104–112.
- Tran-Nguyen, L. T. T., Kube, M., Schneider, B., Reinhardt, R., and Gibb, K. S. (2008). Comparative genome analysis of “*Candidatus* Phytoplasma australiense” (subgroup tuf-Australia I; rp-A) and “*Ca. phytoplasma asteris*” strains OY-M and AY-WB. *J. Bacteriol.* 190, 3979–3991. doi: 10.1128/JB.01301-07
- Tran-Nguyen, L. T. T., and Schneider, B. (2012). Cesium Chloride-Bisbenzimidazole Gradients for Separation of Phytoplasma and Plant DNA. *Methods Mol. Biol.* 381–393.
- Trivellone, V., and Dietrich, C. H. (2021). Evolutionary Diversification in Insect Vector-Phytoplasma-Plant Associations. *Ann. Entomol. Soc. Am.* 114, 137–150. doi: 10.1093/aesa/saaa048
- Tsai, Y. M., Chang, A., and Kuo, C. H. (2018). Horizontal gene acquisitions contributed to genome expansion in insect-symbiotic *Spiroplasma clarkii*. *Genome Biol. Evol.* 10, 1526–1532. doi: 10.1093/gbe/evy113
- Wang, J., Song, L., Jiao, Q., Yang, S., Gao, R., Lu, X., et al. (2018). Comparative genome analysis of jujube witches’-broom phytoplasma, an obligate pathogen that causes jujube witches’-broom disease. *BMC Genomics* 19:1. doi: 10.1186/s12864-018-5075-1
- Wood, D. E., Lu, J., and Langmead, B. (2019). Improved metagenomic analysis with Kraken 2. *Genome Biol.* 20:257. doi: 10.1186/s13059-019-1891-0
- Zhang, Y. P., Uyemoto, J. K., and Kirkpatrick, B. C. (1998). A small-scale procedure for extracting nucleic acids from woody plants infected with various phytopathogens for PCR assay. *J. Virol. Methods* 71, 45–50. doi: 10.1016/S0166-0934(97)00190-0
- Zhao, Y., Wei, W., Davis, R. E., Lee, I. M., and Bottner-Parker, K. D. (2021). The agent associated with blue dwarf disease in wheat represents a new phytoplasma taxon, “*Candidatus* phytoplasma tritici”. *Int. J. Syst. Evol. Microbiol.* 71, 1–11. doi: 10.1099/ijsem.0.004604



OPEN ACCESS

EDITED BY

Florence Tardy,
Agence Nationale de Sécurité Sanitaire de
l'Alimentation, de l'Environnement et du
Travail (ANSES), France

REVIEWED BY

Jun-Yi Yang,
National Chung Hsing University, Taiwan
Xavier Foissac,
Institut National de Recherche pour
l'Agriculture, l'Alimentation et
l'Environnement (INRAE), France

*CORRESPONDENCE

Tim J. Dumonceaux
tim.dumonceaux@agr.gc.ca

SPECIALTY SECTION

This article was submitted to
Infectious Agents and Disease,
a section of the journal
Frontiers in Microbiology

RECEIVED 01 June 2022

ACCEPTED 05 September 2022

PUBLISHED 29 September 2022

CITATION

Pusz-Bochenska K, Perez-Lopez E, Wist TJ,
Bennypaul H, Sanderson D, Green M and
Dumonceaux TJ (2022) Multilocus
sequence typing of diverse phytoplasmas
using hybridization probe-based sequence
capture provides high resolution strain
differentiation.
Front. Microbiol. 13:959562.
doi: 10.3389/fmicb.2022.959562

COPYRIGHT

© 2022 Pusz-Bochenska, Perez-Lopez,
Wist, Bennypaul, Sanderson, Green and
Dumonceaux. This is an open-access
article distributed under the terms of the
[Creative Commons Attribution License \(CC
BY\)](https://creativecommons.org/licenses/by/4.0/). The use, distribution or reproduction in
other forums is permitted, provided the
original author(s) and the copyright
owner(s) are credited and that the original
publication in this journal is cited, in
accordance with accepted academic
practice. No use, distribution or
reproduction is permitted which does not
comply with these terms.

Multilocus sequence typing of diverse phytoplasmas using hybridization probe-based sequence capture provides high resolution strain differentiation

Karolina Pusz-Bochenska^{1,2}, Edel Perez-Lopez^{3,4},
Tyler J. Wist^{1,2}, Harvinder Bennypaul⁵, Daniel Sanderson⁵,
Margaret Green⁵ and Tim J. Dumonceaux^{1,6*}

¹Agriculture and Agri-Food Canada Saskatoon Research and Development Centre, Saskatoon, SK, Canada, ²Department of Biology, University of Saskatchewan, Saskatoon, SK, Canada, ³Centre de Recherche et d'innovation sur les Végétaux (CRIV), Faculté des Sciences de l'Agriculture et de l'Alimentation, Département de Phytologie, Université Laval, Québec, QC, Canada, ⁴Institut de Biologie Intégrative et des Systèmes, Université Laval, Québec, QC, Canada, ⁵Canadian Food Inspection Agency (CFIA), Sidney Laboratory, Centre for Plant Health, North Saanich, BC, Canada, ⁶Department of Veterinary Microbiology, University of Saskatchewan, Saskatoon, SK, Canada

Phytoplasmas are insect-vectored, difficult-to-culture bacterial pathogens that infect a wide variety of crop and non-crop plants, and are associated with diseases that can lead to significant yield losses in agricultural production worldwide. Phytoplasmas are currently grouped in the provisional genus '*Candidatus* Phytoplasma', which includes 49 '*Candidatus*' species. Further differentiation of phytoplasmas into ribosomal groups is based on the restriction fragment length polymorphism (RFLP) pattern of the 16S rRNA-encoding operon, with more than 36 ribosomal groups (16Sr) and over 100 subgroups reported. Since disease symptoms on plants are not associated with phytoplasma identity, accurate diagnostics is of critical importance to manage disease associated with these microorganisms. Phytoplasmas are typically detected from plant and insect tissue using PCR-based methods targeting universal taxonomic markers. Although these methods are relatively sensitive, specific and are widely used, they have limitations, since they provide limited resolution of phytoplasma strains, thus necessitating further assessment of biological properties and delaying implementation of mitigation measures. Moreover, the design of PCR primers that can target multiple loci from phytoplasmas that differ at the sequence level can be a significant challenge. To overcome these limitations, a PCR-independent, multilocus sequence typing (MLST) assay to characterize an array of phytoplasmas was developed. Hybridization probe s targeting *cpn60*, *tuf*, *secA*, *secY*, and *nusA* genes, as well as 16S and *rp* operons, were designed and used to enrich DNA extracts from phytoplasma-infected samples for DNA fragments corresponding to these markers prior to Illumina sequencing. This method was tested using different phytoplasmas including '*Ca. P. asteris*' (16SrI-B), '*Ca. P. pruni*' (16SrIII-A), '*Ca. P. prunorum*' (16SrX-B), '*Ca. P. pyri*' (16SrX-C), '*Ca. P. mali*' (16SrX-A), and '*Ca. P. solani*' (16SrXII-A). Thousands of reads were obtained for each gene with multiple overlapping fragments,

which were assembled to generate full-length (typically >2kb), high-quality sequences. Phytoplasma groups and subgroups were accurately determined based on 16S ribosomal RNA and *cpn60* gene sequences. Hybridization-based MLST facilitates the enrichment of target genes of phytoplasmas and allows the simultaneous determination of sequences corresponding to seven different markers. In this proof-of-concept study, hybridization-based MLST was demonstrated to be an efficient way to generate data regarding ‘*Ca. Phytoplasma*’ species/strain differentiation.

KEYWORDS

‘*Candidatus Phytoplasma*’, phytoplasma taxonomy, hybridization probes, aster yellows, apple proliferation, pear decline, bois noir, X-disease

Introduction

Phytoplasmas are phytopathogenic bacteria that are grouped into the provisional genus ‘*Candidatus Phytoplasma*’, which includes 49 known species (Bertaccini et al., 2022). These pathogens infect a wide variety of plant species including both crops and weedy species, and can cause agricultural production losses in all production areas of the world. Phytoplasmas are mainly transmitted by hemipteran insects (Weintraub and Beanland, 2006), but they can also be spread through vegetative propagation, grafting, or seeds (Satta et al., 2020; Ranebennur et al., 2022). Phytoplasma-infected plants usually show symptoms such as yellowing, virescence, witches’ broom, phyllody, leaf roll, and generalized decline (Bertaccini, 2022). Symptoms of phytoplasma infection are often overlooked or confused with the response of plants to viral diseases and abiotic stressors; therefore, accurate diagnosis is required for choosing appropriate management strategies. Moreover, like other plant pathogens such as viruses, phytoplasmas are grouped in a variety of groups and subgroups, and genetically distinguishable phytoplasmas can infect the same plant species. Additionally, in many cases, the insect vectors are unknown. Therefore, detecting, monitoring, and controlling diseases associated with these pathogens is very challenging.

Species boundaries for phytoplasmas have been defined by sequence analysis of 16S rRNA-encoding genes, with a sequence identity of the full-length 16S rRNA gene of 98.65% as a cutoff for determining species (Bertaccini et al., 2022). In addition to the ‘*Candidatus*’ species designations, phytoplasmas have been classified into ribosomal groups and subgroups based on RFLP analysis of a fragment of the 16S rRNA gene (Gundersen and Lee, 1996; Zhao et al., 2009). This classification has resulted in the designation of more than 37 ribosomal groups (16Sr) and over 150 subgroups (Wei and Zhao, 2022). Differentiation of phytoplasma strains based on the sequences of 16S rRNA genes is complicated by the relatively low inter-taxon sequence differences observed, and by the fact that the two copies of the 16S rRNA gene within a single genome are in some cases distinct from one another (16S rRNA-encoding gene heterogeneity) (Liefting et al., 1996;

Jomantiene et al., 2002; Davis et al., 2003; Perez-Lopez et al., 2019). Therefore, supplementary sequence information from single-copy, protein-coding gene markers is recommended for resolution of phytoplasma strains. There are 49 recognized ‘*Candidatus Phytoplasma*’ species, and while whole-genome draft sequence analysis is becoming available for some phytoplasmas (Firrao et al., 2013; Cho et al., 2020), many of them still do not have genome sequences available.

Multilocus sequence typing (MLST) is well recognized as an improvement over single-marker sequencing for differentiation of bacterial strains in general, and particularly for difficult-to-culture bacteria such as phytoplasmas. Accordingly, MLST has been extensively and recently applied to the differentiation of various groups of phytoplasmas. For example, in defining the taxon ‘*Ca. P. pruni*’, Davis et al. suggested that the strains should best be differentiated by including not only 16S rRNA gene sequences, but also additional sequence information from *secY* and *rp* genes (Davis et al., 2013). Moreover, closely related, but distinct, phytoplasmas belonging to ribosomal group 16SrV (“flavescence dorée”) were successfully differentiated using 16S, *map*, *uvrB-degV*, and *secY* sequences (Arnaud et al., 2007). Strains within group 16SrI associated with azalea little leaf disease were discerned using another set of markers, which included 16S, *rpsS*, *rplIV*, *rpsC*, and *secY* genes (Wei et al., 2011). Phytoplasmas classified within ribosomal groups XI and XIV associated with sugarcane white leaf disease, Napier grass stunt, and Bermuda grass white leaf are difficult to differentiate based only on 16S genes, but a MLST scheme using group-specific primers generating a 1 kb fragment of *leuS* (leucyl tRNA synthetase), in combination with *secA* and 16S sequences, provided clarity to their differentiation (Abeyasinghe et al., 2016). More recently, MLST has been applied for the differentiation of phytoplasmas within ribosomal group 16SrIV, associated with palm lethal decline. Sequences of the 16S rRNA gene, 16S-23S intergenic spacer region, *secA*, and *groEL* (*cpn60*) demonstrated that three palm lethal decline phytoplasmas could be observed (‘*Ca. P. palmae*’, ‘*Ca. P. aculeata*’, and ‘*Ca. P. hispanola*’), which were distinct from a Tanzanian strain (‘*Ca. P. cocotanzaniae*’). Furthermore, the sequence identity

TABLE 1 Phytoplasma-infected and uninfected samples used for hybridization-based MLST.

Phytoplasma	Host	Identifier	Group/subgroup	Source location
'Ca. P. asteris'	<i>Brassica napus</i>	BnAY-high	16SrI-B	Saskatoon, SK Canada
'Ca. P. asteris'	<i>Brassica napus</i>	BnAY-medium	16SrI-B	Saskatoon, SK Canada
'Ca. P. asteris'	<i>Brassica napus</i>	BnAY-low	16SrI-B	Saskatoon, SK Canada
'Ca. P. asteris'	<i>Brassica napus</i>	BnAY-vlow	16SrI-B	Saskatoon, SK Canada
none	<i>Brassica napus</i>	Uninfected	–	Saskatoon, SK Canada
'Ca. P. asteris'	<i>Brassica napus</i>	BnAY-BR1	16SrI-B	Saskatoon, SK Canada
'Ca. P. asteris'	<i>Fragaria × ananassa</i>	STRAW4	16SrI-R	Quebec, Canada
'Ca. P. asteris'	<i>Fragaria × ananassa</i>	Sb7	16SrXIII	Jalisco, Mexico
'Ca. P. asteris'	<i>Fragaria × ananassa</i>	Sb41	16SrXIII/16SrI	Jalisco, Mexico
'Ca. P. prunorum' (ESFY)	<i>Prunus marianna</i>	2813-1C1	16SrX-B	Sidney, BC, Canada
'Ca. P. mali' (AP)	<i>Malus domestica</i>	3516-1A1	16SrX-A	Sidney, BC, Canada
'Ca. P. pyri' (PD)	<i>Pyrus communis</i>	1847-2C1	16SrX-C	Sidney, BC, Canada
'Ca. P. pyri' (PYLR)	<i>Prunus persica</i>	1847-4C3	16SrX-C	Sidney, BC, Canada
'Ca. P. pruni'	<i>Syringa 'Charisma'</i>	3194-2A1	16SrIII-A	Sidney, BC, Canada
'Ca. P. pruni'	<i>Prunus avium</i>	1847-6A1	16SrIII-A	Sidney, BC, Canada
'Ca. P. solani'	<i>Vitis vinifera</i> ^d	NA18-199	16SrXII-A	Sidney, BC, Canada
none	<i>Vitis vinifera</i>	Uninfected	–	Sidney, BC, Canada

of multiple genes within ribosomal group IV confirmed that distinct ribosomal RNA gene subgroups are properly considered to be the same species, '*Ca. P. aculeata*' (Soto et al., 2021). All of these studies confirm and support the utility of determining the sequences of multiple genetic markers for accurate differentiation of phytoplasma strains.

The objective of the current study was to develop and validate a rapid, convenient, and accurate method of determining the sequences of multiple taxonomic markers for diverse phytoplasma strains. A hybridization-based MLST assay using a set of capture probes corresponding to seven taxonomic markers from a variety of phytoplasmas was developed. Hybridization probes were designed targeting the 16S ribosomal RNA-encoding gene as well as six other protein-coding genes. The protein-coding, single-copy genes selected to develop a multilocus panel were *cpn60* (also known as *groEL* or *hsp60*) (Mitrović et al., 2011; Pérez-López et al., 2016), *tuf* (Marcone et al., 2000), *secA* (Hodgetts et al., 2008), *secY* (Lee et al., 2010), and *nusA* (Shao et al., 2006). In addition, this MLST sequencing panel includes the ribosomal protein (*rp*) operon, which consists of several short genes including *rplV-rpsC* and intergenic regions (Martini et al., 2007).

Moreover, to provide a proof-of-concept that the method can detect and type these sequences accurately from a variety of phytoplasmas, six distinct phytoplasmas were examined: '*Ca. P. asteris*' (16SrI), '*Ca. P. pruni*' (16SrIII-A), '*Ca. P. prunorum*' (16SrX-B), '*Ca. P. pyri*' (16SrX-C), '*Ca. P. mali*' (16SrX-A), and '*Ca. P. solani*' (16SrXII-A). The hybridization-based MLST was used to determine the sequences of these markers from each of these phytoplasmas, and in samples with a wide range of phytoplasma concentrations in infected tissues.

Materials and methods

Infected plant samples

Plant material indicated in Table 1 that was infected with '*Ca. P. mali*', '*Ca. P. prunorum*', '*Ca. P. pyri*', '*Ca. P. solani*', and '*Ca. P. pruni*' were maintained in appropriate hosts (Table 1) at the Centre for Plant Health, Canadian Food Inspection Agency, North Saanich, BC. Infected canola was collected at the research farm of Agriculture and Agri-Food Canada in Saskatoon, SK. Strain TW1 was collected in 2018 as previously described (Town et al., 2018), and was used to prepare a dilution series of known phytoplasma concentrations in a background of DNA extracted from healthy *B. napus*. Uninfected canola DNA was prepared by germinating phytoplasma-free *B. napus* seeds (Plant Gene Resources of Canada, accession no. CN42942) on filter paper soaked with sterile water, and shoots were collected after 7–10 days of germination in the dark at room temperature. Strain BR1 was collected at the same site as strain TW1, but in 2021. Samples from infected strawberries were collected from fields in Quebec in the summer of 2021 as previously described (Plante et al., 2021). Samples from infected strawberries in Mexican production fields have been described previously (Pérez-López et al., 2017).

DNA extraction and quality control

Midribs were excised from the leaves of infected plants for all samples except TW1 (inflorescence) and healthy canola (shoots from germinated seeds). The tissue (~0.1 g) was cut into ~5 mm pieces, placed into a 2 ml tube with 2 sterile steel beads (3.2 mm, BioSpec Products), and immediately frozen in liquid nitrogen.

Frozen tissue was pulverized using a homogenizer (Retsch, model no. MM 400) using 2 pulses of 30 s of shaking at 30 Hz. Powdered samples were then briefly centrifuged, and DNA was extracted using a Qiagen Plant DNA mini kit. DNA was eluted into 100 µl of 10 mM Tris-Cl pH 8.0 (kit elution buffer). DNA concentration was measured using a Qubit Broad Range kit (Invitrogen).

Quantitative PCR (qPCR) was used to determine the level of phytoplasma in each of the DNA extracts from infected tissue samples prior to hybridization and sequencing. Primers and probes were purchased from IDT (Coralville, IA). Their sequences, along with amplification conditions, are provided as supplementary information (Supplementary Table S1). For all samples except '*Ca. P. pruni*', qPCR used 1x SsoFast Universal Probes Supermix (Bio-Rad), 0.3 µM each primer, and 0.2 µM probe in a final volume of 20 µl. For '*Ca. P. pruni*', qPCR used 1x SsoFast Universal Probes Supermix, 0.4 µM primer 16SF, 1.2 µM primer 16SR, 0.2 µM probe 16S72, and 1x SsoFast Universal Probes Supermix. qPCR standards were prepared from plasmid DNA containing the *cpn60* universal target sequence from the respective phytoplasma (Muirhead et al., 2019a). qPCR standards for '*Ca. P. pruni*' were prepared using infected cherry DNA calibrated to 200,000 copies/µl, and infected plum DNA at 200 copies/µl. Amplifications used a C1000 thermocycler base with a CFX96 qPCR module and results were analyzed using Bio-Rad CFX Manager v3.1.1517.0823. Statistical correlations between *cpn60* input DNA copies measured by qPCR and *cpn60* read numbers post-hybridization were calculated using SigmaPlot v14.5.

To prepare a dilution series of '*Ca. P. asteris*', DNA extracted from infected *B. napus* inflorescence (strain TW1) was mixed with DNA extracted from uninfected *B. napus* shoots. Briefly, AY *cpn60* copies were measured in the TW1 inflorescence extract using qPCR, then the sample was adjusted to approximately 5×10^5 *cpn60* copies/ul in 10 mM Tris-Cl, pH 8.0. This sample is referred to as BnAY-high. Three serial 10-fold dilutions of BnAY-high were then prepared, with 50 µl of DNA from uninfected canola (Bn-H) added to each dilution and the volume adjusted to 110 µl using 10 mM Tris-Cl, pH 8.0. These "spiked-in" samples are labeled BnAY-medium, BnAY-low, and BnAY-vlow (very low). The DNA concentration and number of AY *cpn60* copies/µl were measured in each final pool as described.

PCR amplification and cloning of target gene sequences

The 16S rRNA-encoding gene locus was amplified from DNA extracts using a nested PCR strategy consisting of primers P1 (Deng and Hiruki, 1991) and P7 (Schneider et al., 1995) in a first round, generating a product of >1.8 kb. This PCR product was diluted 1:30, then 2 µl was used as template in a secondary PCR step using primers R16F2n and R16R2 (Gundersen and Lee, 1996), which generated the ~1.2 kb F2nR2 amplicon that is commonly used for phytoplasma detection and typing (Zhao et al., 2009). Both rounds of PCR for 16S used 1x PCR buffer (Invitrogen), 2.5 mM

MgCl₂, 500 nM dNTPs, and 400 nM each primer using previously described methodologies (Pérez-López et al., 2017). Thermal cycling conditions were 95°C, 10 min (1x), 95°C, 1 min; 55°C, 1 min; 72°C, 1.75 min (35X), 72°C, 10 min (1x). The universal target region from the *cpn60* gene (Dumonceaux et al., 2014) was amplified using a primer cocktail as described at cpnclassifyr.ca (Muirhead et al., 2019a). Amplicons were generated from the *rp* operon of AY infected samples using nested PCR with primers rpF1 and rpR1 (Lim and Sears, 1992) in the first round, and rp(I) F1A/rp(I)R1A in the second round as described (Lee et al., 2004).

Amplicons were cloned into the vector pGEM-T Easy (Promega, Madison, WI) according to the instructions provided, then plasmids were transformed into chemically competent *E. coli* TOP10 cells (Life Technologies). 5–6 individual clones were sequenced from each amplicon using a commercial sequencing service (Eurofins Genomics, Toronto, ON).

Hybridization probe design

Gene targets for probe design were selected from publicly available sequences at GenBank (Table 2). 27 genes were selected from genome sequences and individual gene sequences, with 7 targets from each of '*Ca. P. asteris*' (16SrI-B); '*Ca. P. mali*' (16SrX-A); '*Ca. P. solani*' (16SrXII-A), and 6 genes from '*Ca. P. pruni*' (16SrIII-A). A total of 351 probes were designed with a length of 120 nucleotides and 1x tiling density using the IDT X-gen design tool found.¹ Probe sequences are provided as Supplementary File S1.

Hybridization and sequencing

Detailed protocols for DNA preparation for hybridization and sequencing have been published elsewhere (Dumonceaux et al., 2017), and these were generally followed. Wherever possible, DNA was diluted to 2.5 ng/ul in a total volume of 100 µl of 10 mM Tris-Cl pH 8.0. If the DNA concentration was below this level, it was used at its extracted concentration, with the volume adjusted to 100 µl for shearing. Shearing proceeded using a Bioruptor 300 (Diagenode # B01020001) in 0.2 ml shearing tubes (Diagenode #C30010015) on a setting of "high" with 30 cycles of 30 s on, 45 s off, and cooling to 4°C. Sheared DNA was concentrated using Amicon YM-30 filter membranes to a volume of 60 µl. DNA concentration was determined using a Qubit Broad Range kit (1 µl). Illumina adaptors and indices were added using a NEBNext Ultra DNA library prep kit for Illumina (NEB, cat no E7370) according to the manufacturer's instructions. Prior to index addition, size selection was used to isolate fragments of 400–500 bp by using 35 µl of SPRI beads (Cytiva) in the first bead selection and 25 µl in the second bead selection. Index addition proceeded using 8 cycles of PCR under the conditions recommended by the

¹ <https://www.idtdna.com/site/order/designtool/index/XGENDESIGN>

TABLE 2 GenBank accession numbers of gene sequences used for probe design.

Gene target	16Sr group/subgroup			
	16SrI-B	16SrIII-A	16SrX-A	16SrXII-A
<i>cpn60</i>	QGKT01000000	NA ¹	NC_011047	FO393427
<i>tuf</i>	QGKT01000000	NZ_LHCF01000000	NC_011047	FO393427
<i>secY</i>	KP796188 ²	NZ_LHCF01000000	NC_011047	FO393427
<i>secA</i>	QGKT01000000	NZ_LHCF01000000	NC_011047	FO393427
<i>nusA</i>	QGKT01000000	NZ_LHCF01000000	NC_011047	FO393427
16S-23S	KX551964	HQ589202	X68375	JQ730740
<i>rp</i>	QGKT01000000	JQ360955 ³	EF193367	KC481241
Total nucleotides	10687	9162	10518	10546
Total number of probes	92	78	90	91
Probe length	120	120	120	120
Tiling density	1x	1x	1x	1x

¹'*Ca. P. pruni*' (16SrIII) lacks a *cpn60* gene (Saccardo et al., 2012).

²*secY* annotated in TW1 genome appears to have a premature stop codon.

³GenBank entry for strain CX *rp* locus had N's – therefore changed to a clean sequence from related strain CX-95.

manufacturer, and indexed fragments were purified using a 1:1 volume ratio of SPRI beads (Cytiva) and eluted in a volume of 30 µl. Results were examined using a TapeStation (Agilent) and DNA concentration was determined using a Qubit High Sensitivity (HS) kit.

Hybridization was performed using an xGen hybridization and wash kit (IDT) and the recommended protocols (IDT xGen hybridization capture of DNA libraries manual version 4, 2019). Up to 500 ng of indexed DNA was added to each hybridization reaction along with xGen universal blockers (TS mix, IDT). All samples were hybridized with the same set of capture probes containing sequences from all seven markers from all of the targeted phytoplasmas (Table 1). Hybridizations proceeded at 65°C for 16 h. After washing, libraries were purified using a 1:1 volume ratio of SPRI beads (Cytiva) and amplified for 14 cycles using the x-Gen library amplification primer (IDT) and KAPA HiFi HotStart ReadyMix (Roche) under cycling conditions recommended by the manufacturer. After another SPRI purification, DNA concentration was determined using a Qubit HS kit. If the DNA yield was insufficient (under approx. 1 ng/µl), a second amplification reaction was performed using 1 µl of the first amplification reaction with 19 µl water and the same primer; products were then re-purified using SPRI beads. Samples were pooled to 4 nM and sequenced using an Illumina nano kit v2 (500 cycles) using a MiSeq instrument according to the manufacturer's recommendations.

Data analysis

Illumina reads were processed with trimmomatic (v0.39) to remove adapters and low quality bases (<Q15) and R1/R2 reads were merged using flash2 (v2.2.00). Merged reads were mapped to the sequences of the genes used for hybridization probe design using bowtie2 --local (v2.4.4). The reference sequences used for mapping are included as Supplementary File S2. Reads mapped to

each target sequence were extracted using samtools (v1.9), and the corresponding fastq files were then assembled as individual bins using transabyss (v2.0.1). Assemblies were filtered to include only contigs >500 nucleotides.

To remove off-target reads that mapped to undesired 16S sequences (16S genes from other bacteria, along with host chloroplast and mitochondrial genes), assembled contigs that were not phytoplasma 16S sequences were identified using BLAST. These contigs were then added as reference sequences for a second round of mapping for 16S-mapped reads only using bowtie2 --local to remove these non-target sequences from the assembly dataset. This was done only in cases where the initial assembly using the mapped 16S genes generated short or only nonspecific contigs. The code used for mapping and assembly is provided as Supplementary File S3.

Phylogenetic analysis

Sequences assembled from the post-hybridization sequencing and mapping data were oriented manually by BLAST to determine sequence orientation (coding, or reverse-complement), then reverse-complementing as necessary. Oriented sequences were aligned using clustalw, then trimmed manually to the length of the shortest sequence in the alignment. Phylogenetic relationships among the sequences were inferred by using the Neighbor Joining algorithm (Saitou and Nei, 1987) in MEGA X (Kumar et al., 2018). Trees were bootstrapped using 1,000 replications, and consensus trees were reported with percentages of trees in which the associated taxa clustered together indicated next to each branch. The evolutionary distances were computed using the Maximum Composite Likelihood method (Tamura et al., 2004).

A schematic representation of the methodology used in this study is presented in Figure 1.

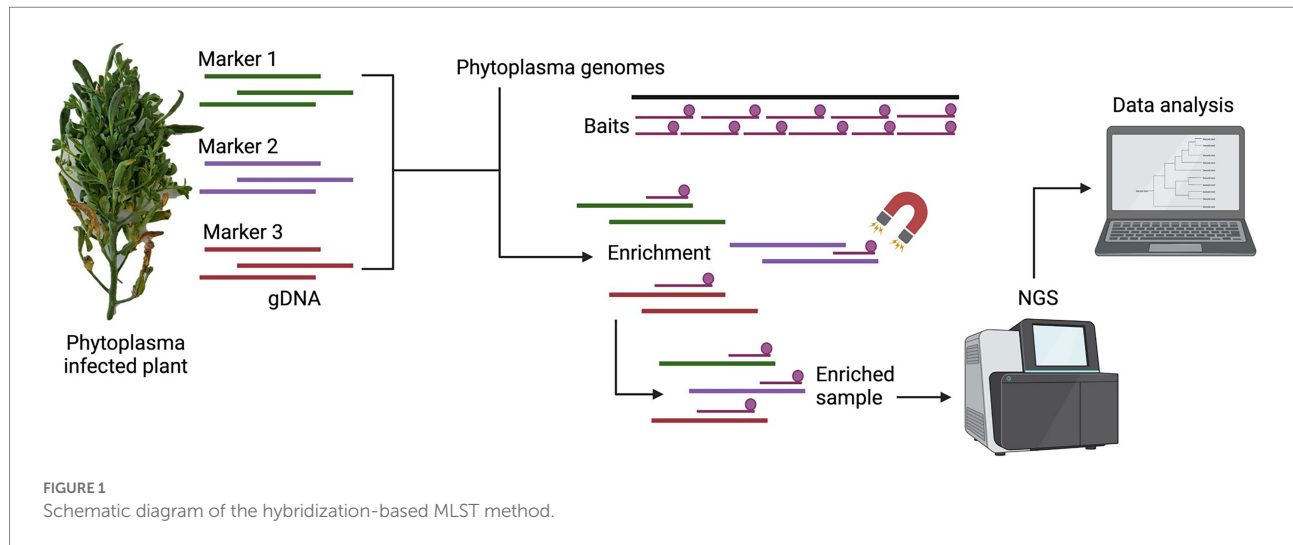


TABLE 3 DNA yield and phytoplasma levels in each sample.

Phytoplasma	Host	strain ID/CPH no	Group/subgroup	(DNA), ng/μl	qPCR C _q mean	qPCR copies/μl
BnAY-high	<i>Brassica napus</i>	TW1	16SrI-B	16.1	17.62	566875
BnAY-medium	<i>Brassica napus</i>	TW1	16SrI-B	9.76	20.29	88627
BnAY-low	<i>Brassica napus</i>	TW1	16SrI-B	9.53	23.66	8524
BnAY-vlow	<i>Brassica napus</i>	TW1	16SrI-B	9.45	27.12	765
None	<i>Brassica napus</i>	uninfected	–	18.8	0	0
' <i>Ca. P. asteris</i> '	<i>Brassica napus</i>	BR1	16SrI-B	4.7	14.03	8395731
' <i>Ca. P. asteris</i> '	<i>Fragaria × ananassa</i>	STRAW4	16SrI-R	3.77	26.79	531
' <i>Ca. P. asteris</i> '; ' <i>Ca. P. hispanicum</i> '	<i>Fragaria × ananassa</i>	Sb7 ¹	16SrXIII	1.99	21.68 (XIII)/ND ³ (I)	34836 (XIII)/ND (I)
' <i>Ca. P. asteris</i> '; ' <i>Ca. P. hispanicum</i> '	<i>Fragaria × ananassa</i>	Sb41 ²	16SrXIII/16SrI	too low	32.49 (XIII)/ 28.62 (I)	8.7 (XIII)/1,024 (I)
' <i>Ca. P. prunorum</i> ' (ESFY)	<i>Prunus marianna</i>	2813-1C1	16SrX-B	6.8	27.05	1740
' <i>Ca. P. mali</i> ' (AP)	<i>Malus domestica</i>	3516-1A1	16SrX-A	12.3	25.22	4292
' <i>Ca. P. pyri</i> ' (PD)	<i>Pyrus communis</i>	1847-2C1	16SrX-C	12.4	27.04	500
' <i>Ca. P. pyri</i> ' (PYLR)	<i>Prunus persica</i>	1847-4C3	16SrX-C	7.9	22.53	9531
' <i>Ca. P. pruni</i> '	<i>Syringa 'Charisma'</i>	3194-2A1	16SrIII-A	14.9	19.66	216177
' <i>Ca. P. pruni</i> '	<i>Prunus avium</i>	1847-6A1	16SrIII-A	9.6	19.29	256025
' <i>Ca. P. solani</i> '	<i>Vitis vinifera</i> ⁴	NA18-199	16SrXII-A	0.756	20.46	558826
None	<i>Vitis vinifera</i>	uninfected	–	1.13	0	0

¹Sample was previously determined to be infected with '*Ca. P. hispanicum*' (16SrXIII) – (Pérez-López et al., 2017), and was not previously known to be co-infected with '*Ca. P. asteris*'.

²Sample was previously determined to be co-infected with '*Ca. P. hispanicum*' (16SrIII) and 16SrI ('*Ca. P. asteris*') – (Pérez-López et al., 2017).

³ND, not determined.

Results

DNA extraction and qPCR

DNA yield from infected leaf midribs was somewhat variable, ranging from under 1 ng/ul ('*Ca. P. solani*', Sb41) to approximately 15 ng/ul in lilac infected with '*Ca. P. pruni*' (Table 3). The mean DNA concentration for all samples was 8.74 ng/ul. Similarly, samples displayed a wide range of phytoplasma levels in the infected plant tissue; C_q values were quite high in some samples

(25–27 for ESFY, AP, and PD) but lower in other samples approximately 20 in the '*Ca. P. pruni*' and '*Ca. P. solani*'-infected samples (Table 3). The sample from the canola plant infected with '*Ca. P. asteris*' strain BR1 had the lowest C_q (14) of the samples examined, reflecting the highest phytoplasma concentration. Samples of canola DNA that were purposefully constructed to contain various levels of phytoplasma DNA had C_q values ranging from 17.62 (BnAY-TW1) ('*Ca. P. asteris*'-high) to 27.12 (BnAY-TW1-vlow). All samples were successfully sheared and indexed, regardless of the DNA input amounts.

TABLE 4 Number of sequencing reads mapping to each gene after hybridization.

Phytoplasma ¹	strain ID/CPH no	<i>cpn60</i>	16S-23S	<i>tuf</i>	<i>secY</i>	<i>secA</i>	<i>nusA</i>	<i>rp</i>
BnAY-high	TW1	4732	8402	3482	3298	6873	2970	3208
BnAY-medium	TW1	6299	11399	4334	4358	9034	3935	4097
BnAY-low	TW1	293	1134	309	163	449	172	203
BnAY-vlow	TW1	71	285	53	53	86	37	55
None	uninfected	0	192	2	0	1	2	0
'Ca. P. asteris'	BR1	13214	23511	9714	9075	18126	8113	9099
'Ca. P. asteris'	STRAW4	12090	19426	8011	6821	10024	6003	7780
'Ca. P. asteris'	Sb7	250	233716	1341	149	285	128	183
'Ca. P. asteris'	Sb41	25891	90732	22429	18064	34831	16452	22576
'Ca. P. prunorum' (ESFY)	2813-1C1	840	5000	986	755	1094	113	1704
'Ca. P. mali' (AP)	3516-1A1	13714	9917	8302	4767	12750	6900	8314
'Ca. P. pyri' (PD)	1847-2C1	460	729	389	53	253	107	412
'Ca. P. pyri' (PYLR)	1847-4C3	5671	10033	4320	188	3028	1579	5015
'Ca. P. pruni'	3194-2A1	–	6225	3532	3888	7381	3384	4384
'Ca. P. pruni'	1847-6A1	–	6150	5534	8692	19253	8184	8935
'Ca. P. solani'	NA18-199	11281	23101	7006	10328	20863	8109	11152
None	uninfected	86	3784	46	41	76	57	14

¹The same set of 351 hybridization probes, containing capture probes for all genes from all of the targeted phytoplasmas, was used in each hybridization.

Hybridization and Illumina sequencing

Post-hybridization read numbers mapping to each gene are shown in Table 4. Depending on the amount of phytoplasma DNA in the sample, the configuration of the sequencing run, and other technical variables, hundreds to thousands of reads typically mapped to each gene. Fewer reads were observed in the lower concentration samples such as ESYF and PD, with the latter showing one of the lowest proportions of reads mapping at ~3% (Table 4). In most cases, the 16S ribosomal gene had the highest number of mapped reads. Samples from uninfected canola and grape showed lower numbers of mapped reads compared to the corresponding infected plants, especially for the protein-coding genes (Table 4). Without hybridization, samples from the canola phytoplasma mixtures produced very few reads mapping to the target genes (Table 5).

The qPCR assays targeting the *cpn60* gene (Supplementary Table S1) provided input concentrations of phytoplasma. Examining the relationship between the initial phytoplasma levels in each sample and the number of reads mapping to *cpn60* generated revealed a significant correlation (Pearson $r^2 = 0.696$, $p < 0.05$; Spearman's $\rho = 0.770$, $p < 0.05$), suggesting that the number of reads mapping was related to the starting concentration of phytoplasma in the sample, at least within the same Illumina run. Such a determination could not be made for the other protein-coding genes due to the lack of gene-targeted qPCR assays, but this correlation was not evident in the 16S ribosomal gene datasets (Table 4). The actual number of reads mapping to each target was variable across samples and was quite high in some samples, even those that had relatively low concentration of phytoplasma such as STRAW4 (Table 4).

A large number of reads typically mapped to the 16S ribosomal gene target in all samples, including uninfected tissue. In fact, the

TABLE 5 Number of reads mapping to each gene in non-hybridized, spiked samples.

Phytoplasma	<i>cpn60</i>	16S-23S	<i>tuf</i>	<i>secY</i>	<i>secA</i>	<i>nusA</i>	<i>rp</i>
BnAY-high	4	17	3	0	3	4	2
BnAY-medium	3	45	2	1	2	0	3
BnAY-low	0	122	0	1	1	0	1
BnAY-vlow	26	268	14	15	27	12	23

large number of reads mapping to the 16S ribosomal gene in each sample were found to include many reads that did not correspond to the target gene, including host chloroplast and mitochondrial genes, 16S ribosomal genes from non-phytoplasma bacteria, and other nonspecific DNA sequences. Examination of the nucleotide identities of the post-hybridization reads that mapped to the 16S ribosomal gene compared to the probe sequences using BLAST revealed that the lower spike levels contained a substantial proportion of reads with <95% nucleotide identity to any of the probes (Supplementary Figure S1A). These non-target reads interfered in some samples with the assembly process, to the extent that the 'Ca. P. asteris' samples spiked at low and very low levels assembled only nonspecific host chloroplast sequences (Supplementary Table S2). Other samples, such as PYLR, assembled only 16S contigs that were too short for classification using the iPhyClassifier (Supplementary Table S2). Incorporating a second mapping step that included these nonspecific assembled sequences as mapping targets provided a much higher proportion of reads (average read length 274 bp) with >98% identity to a probe sequence (Supplementary Figure S1B), and greatly improved most of the 16S assemblies (Supplementary Table S2). This was most pronounced with the 'Ca. P. asteris' mixtures, with the medium and low titer samples yielding 16S assemblies that were > 2 kb after this step, and

TABLE 6 Longest assembled contig lengths (in base pairs) and RFLP-based typing results (16S and *cpn60* only) for each gene in each sample.

Sample	<i>cpn60</i>	<i>cpn60</i> RFLP type ¹	16S-23S	16Sr RFLP subgroup ²	<i>tuf</i>	<i>secY</i>	<i>secA</i>	<i>nusA</i>	<i>rp</i>
BnAY-high	2367	I-IB (1.0)	2654	I-B (1.0)	1855	1963	3173	1813	1993
BnAY-medium	2306	I-IB (1.0)	2557	I-B (1.0)	1878	1867	3177	1784	1899
BnAY-low	1906	I-IB (1.0)	2230	I-B (0.97)	1494	1561	2650	1255	1628
BnAY-vlow	1926	I-IB (1.0)	925	Not typeable ³	1494	1490	2781	1217	1714
BnAY-BR1	2131	I-IB (1.0)	2396	I-B (1.0)	1697	1853	2903	1572	1763
'Ca. P. asteris' – STRAW4	2216	I-IC (1.0)	2561	I-R (0.98)	1843	1879	3056	1649	1801
'Ca. P. asteris' – Sb7	1258	I-IIIB (1.0)	2631	XIII-H (0.98)	1007	1432	2732	1189	1411
'Ca. P. asteris' – Sb41	2200	I-IIIB (1.0)	2463	I-B (0.97)	1793	1808	2970	1611	1787
'Ca. P. prunorum' (ESFY)	1749	X-IF (1.0)	2184	X-B (0.98)	1299	945	2130	620	1638
'Ca. P. mali' (AP)	2330	X-IA (1.0)	2287	X-A (1.0)	1943	1805	2975	1836	1854
'Ca. P. pyri' (PD)	1876	X-IC (1.0)	2085	X-C (1.0)	1496	687	1970	752	1622
'Ca. P. pyri' (PYLR)	1972	X-IC (1.0)	2218	X-C (0.99)	1766	599	2143	1125	1736
'Ca. P. pruni' – 2A1	No data ⁴	No data	2435	III-A (1.0)	1861	1915	3214	1755	2028
'Ca. P. pruni' – 6A1	No data ⁴	No data	2400	III-A (1.0)	1912	1917	3225	1785	2046
'Ca. P. solani' – NA18-199	2147	XII-IA (1.0)	1950	XII-A (1.0)	1638	994	3082	1611	1767

¹*cpn60* RFLP typing results determined using the CpnClassiPhyr (Muirhead et al., 2019a). *F*-value is provided in parentheses.

²16S RFLP typing results determined using the iPhyClassifier (Zhao et al., 2013). *F*-value is provided in parentheses.

³Assembled 16S rRNA-encoding gene was too short for iPhyClassifier (<1,200bp).

⁴'Ca. P. pruni' (16SrIII) does not contain *cpn60* (Saccardo et al., 2012).

the very low sample yielding a 925 nucleotide 16S assembly compared to no detectable 16S sequence after the initial mapping (Supplementary Table S2). This two-step mapping strategy for 16S rRNA sequences was not required for other samples. In particular, the 16SrIII samples generated 16S assemblies >2.4 kb by mapping only to the target 16S gene sequence, so in this case a two-step mapping strategy was not necessary (Supplementary Table S2). In contrast, the initially mapped reads from the spiked canola samples corresponding to a protein-coding gene (*cpn60*) had >98% sequence identity to a probe sequence at all spike levels, and therefore represented high-quality sequence reads that were used in the assemblies (Supplementary Figure S1C).

Assembly of the mapped reads for each gene generated sequences that ranged from 599 nucleotides (PYLR *secY*) to 3,225 nucleotides ('Ca. P. pruni' 6A1 *secA*) (Table 6). Most of the sequences were at least 1,500 nucleotides, with an average contig length of 1927 nucleotides and a median of 1867 nucleotides. The *secA* assemblies were the longest (average of 2,812 nucleotides), while the *nusA* assemblies tended to be shorter (average of 1,438 nucleotides). This is consistent with the target gene lengths (*secA* is the longest target gene at ~2,500 nucleotides, and *nusA* the shortest at ~1,075 nucleotides).

Sequence typing and phylogenetic analysis

16S ribosomal RNA gene and *cpn60* sequence types

All samples yielded 16S ribosomal RNA gene and *cpn60* sequences that typed correctly using the corresponding

RFLP-based classifiers (Table 6). In all cases except Sb7 (Strawberry – Mexico) and STRAW4 (Strawberry-Quebec), the *cpn60* and 16S sequence types were in agreement. For Sb7, the *cpn60* sequence generated typed as *cpn60* I-IIIB: maize bushy stunt (MBS), while the 16S sequence corresponded to the group 16SrXIII-H. For STRAW4, the *cpn60* typed as I-IC while the 16S sequence typed as 16SrI-R (Table 6).

Phylogenetic analysis of target gene assemblies

16S rRNA gene sequences

16S rRNA-encoding gene sequences generated from the samples that were infected with group 16SrX phytoplasmas (AP, ESFY, PYLR, PD) clustered with their respective reference sequences (Figure 2A), in most cases with nearly zero branch length, indicating sequence identity. Although the hybridization probes were designed using the 16S rRNA-encoding gene sequence of 16SrX-A (strain AT; Table 1), hybridization of other subgroups 16SrX-C (PYLR/PD) and 16SrX-B (ESFY) was also successful. Similarly, the 16S ribosomal RNA gene sequences generated from samples infected with 16SrIII clustered with their respective reference sequences with near sequence identity (Figure 2A). The grape sample infected with 16SrXII was slightly different from the strain used for hybridization probe design, and clustered with a "stolbur" phytoplasma strain within the same subgroup 16SrXII-A.

The samples that were infected with various 16SrI subgroups generated 16S rRNA gene sequences that were generally consistent with the expected groupings. The AY-infected strawberry from Quebec (STRAW4) yielded a sequence that

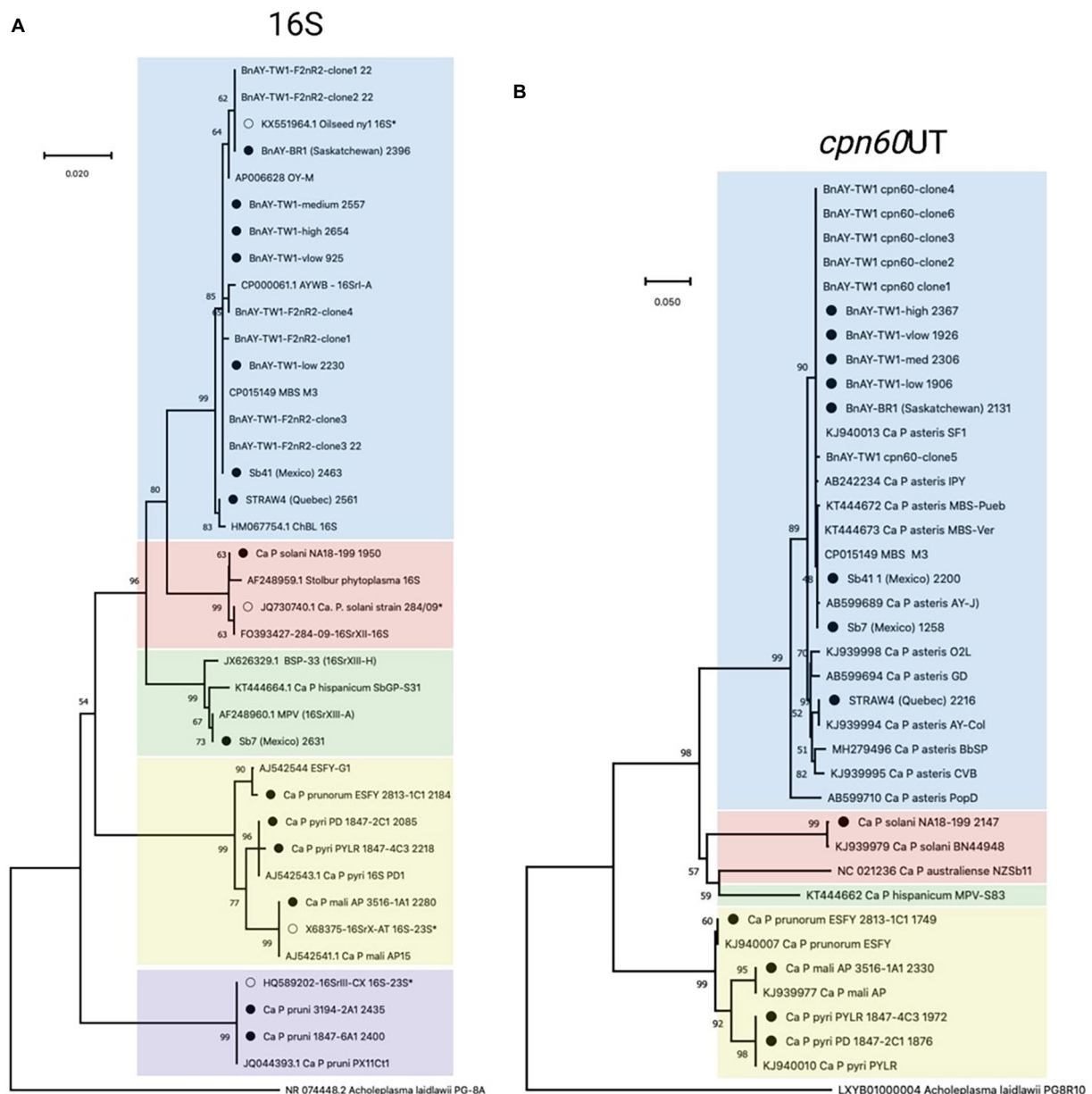


FIGURE 2
Phylogenetic analysis of 16S (A) and *cpn60* UT (B) sequences generated in this study. 16S sequences corresponded to the F2nR2 fragment (~1.2kb), and *cpn60* sequences were trimmed to the universal target length (~550bp) using the CpnClassiPhyR (Muirhead et al., 2019a). Phylogenetic analysis was performed using the Neighbor Joining algorithm using 1000 replicates, as described in Methods. Sequences corresponding to the samples analyzed in this study (Table 1) are indicated with a filled circle, while samples with an open circle represent the sequences used for hybridization probe design (Table 2). Samples are color-coded according to the 16Sr groups represented within the samples and the probes described in this study – 16SrI (blue); 16SrII (pink); 16SrXIII (green); 16SrX (yellow); 16SrIII (purple); 16S only (grey).

clustered with a strain of 16SrI-R (Figure 2A), consistent with the RFLP-based typing results (Table 6). The AY-infected canola samples from Saskatchewan provided 16S gene sequences that mostly clustered with strains from subgroup 16SrI-B, as expected from the RFLP typing results. This included strain BnAY-BR1, which was collected in 2021 from the same field as strain BnAY-TW1 (collected in 2017). Examination of F2nR2 clone sequences generated from strain BnAY-TW1 revealed that 5/6

clones clustered with 16SrI-B, while one (clone 4) was more closely related to 16SrI-A. The clones that clustered within 16SrI-B were therefore differentiated into two types, consistent with the RFLP typing results for these clones. The sequences that were assembled from the hybridization, however, all appeared to cluster with the 16SrI-B sequences. These sequences were slightly distinct from the sequence used for the design of hybridization probes (Figure 2A).

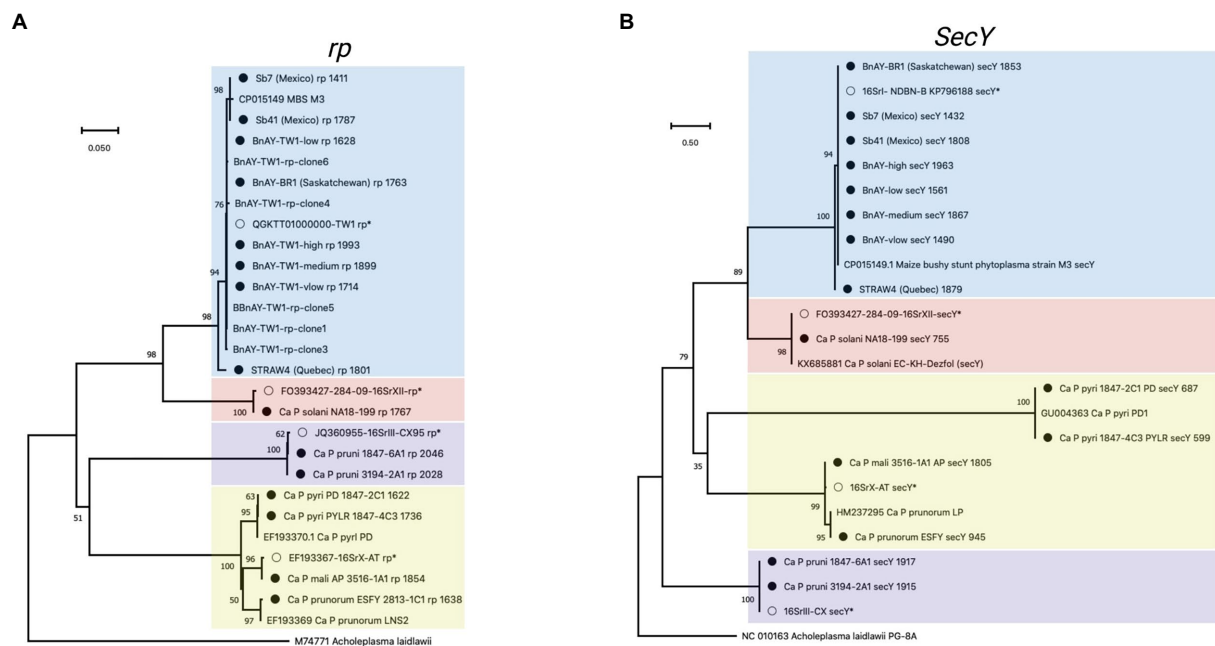


FIGURE 3
Phylogenetic analysis of *rp* (A), and (B) *secY* sequences generated in this study. Sequences were trimmed manually to the length of the shortest sequence analyzed (see Methods). Samples are indicated as described for Figure 2, and the length of the original assembly prior to trimming (Table 6) is indicated for each sample (filled circles).

Strawberry samples Sb41 and Sb7, which were collected in Jalisco, Mexico (Pérez-López et al., 2017), provided 16S gene sequences that clustered with 16SrI-B (Sb41) and 16SrXIII-A (Sb7) (Figure 2A). Despite the previously reported double infection of sample Sb41 with 16SrXIII and 16SrI (Pérez-López et al., 2017), no evidence of 16S rRNA gene sequences from 16SrXIII was found in sample Sb41.

cpn60

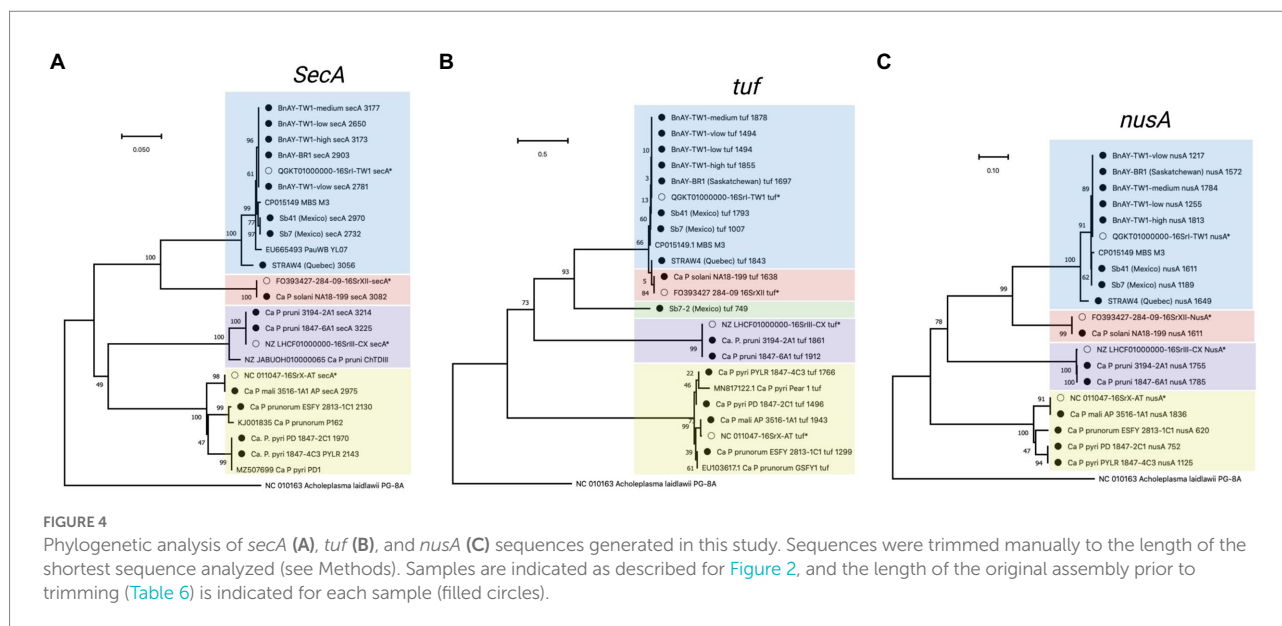
The length of the *cpn60* assemblies (Table 6) allowed the use of more than the ~550bp universal target region (Muirhead et al., 2019b) for phylogenetic analysis. The sample infected with 16SrX-A generated a *cpn60* sequence that was identical to that of the strain that was used for hybridization probe design (Supplementary Figure S2). There is no full-length *cpn60* sequence available for ESYF (16SrX-B), but the PYLR/PD (16SrX-C) *cpn60* sequences were identical to a strain from the GenBank database (Supplementary Figure S2), indicating that the assemblies were correct for the 16SrX-C samples. In addition, the *cpn60* sequence from the 16SrXII-infected sample clustered with the corresponding sequence used for hybridization probe design (Supplementary Figure S2).

Sequences generated from infected canola plants in Saskatchewan, including BnAY-TW1 and BnAY-BR1, clustered with the sequence used to generate the hybridization probes with zero branch length (Supplementary Figure S2). However, the sequences from infected strawberries clustered independently with no reference sequence (STRAW4, Quebec), or with subgroup 16SrI-B detected in samples Sb7 and Sb41 from Mexico.

Trimming the sequences to the universal target using the CpnClassiPhyr (Muirhead et al., 2019a) permitted the use of an expanded set of reference sequences, along with RFLP analysis. This trimming provided results that were consistent with the longer sequences (Figure 3A), and further showed that the 16SrX samples corresponding to ESYF, PYLR, and PD clustered with their respective reference sequences, and that the sample from infected strawberries in Quebec (STRAW4) clustered with the *cpn60* UT I-IC sample (AY-Col). Moreover, all six *cpn60* UT amplicon clones generated from strain BnAY-TW1 were identical to the assembled sequence and to the reference sequence used to design the hybridization probes (Figure 2B).

rp

Results of phylogenetic analysis using the *rp* sequences assembled from hybridized infected samples are shown in Figure 3A. A similar theme was observed; sequences obtained from infected 'Ca. P. mali' clustered with the sequence used to generate the probes, while the sequences from the other 16SrX subgroups represented by strains ESYF, PYLR, and PD clustered separately, and were identical to their respective reference sequences. The samples infected with 16SrIII and 16SrXII also generated sequences that were identical to the sequence used for hybridization probe design. The AY infected canola samples were all virtually identical to one another and to the probe sequence, along with 5 PCR-amplified *rp* clones from BnAY-TW1. The infected strawberry from Quebec



generated a distinct sequence, while the sequences from infected strawberries in Mexico clustered with the aster yellows *rp* sequences.

secY

Despite the fact that the *secY* reads generated assemblies that were, on average across all strains analyzed, longer (average length 1,514 bp – Table 6) than those of the shorter target gene *nusA* (average length 1,438 bp – Table 6), the alignment and trimming of the *secY* sequences to a common fragment resulted in the shortest sequence comparison among the genes analyzed; phylogenetic analysis was based on a fragment of only ~530 nucleotides. This was mostly due to the shorter assemblies that were generated for ‘*Ca. P. prunorum*’ (ESFY) and ‘*Ca. P. pyri*’ (PD and PYLR) – see Table 6. The *secY* sequences assembled from infected samples showed that this gene is highly discriminatory for 16SrX strains (Figure 3B). The >1,800 nucleotide sequence that was assembled from the ‘*Ca. P. mali*’-infected sample, as expected, was almost identical to the sequence used for probe design, while the ESFY (16SrX-B) sequence was identical to its reference sequence and distinct from the ‘*Ca. P. mali*’ (16SrX-A) sequence. However, the *secY* sequences that were assembled from ‘*Ca. P. pyri*’ (16SrX-C) displayed a long branch length compared to the other 16SrX samples, consistent with their lower nucleotide sequence identity (~90%). As with other genes, the *secY* sequences generated from 16SrIII samples were identical to the target sequence, and the sequence assembled from the ‘*Ca. P. solani*’-infected sample was nearly identical to its target sequence. *secY* sequences were less discriminatory with the 16SrI samples, as all sequences except STRAW4 were identical, including the closely related samples generated from the infected strawberries in Mexico that were also identical to MBS *secY* (Figure 3B).

secA

The longest target gene in the MLST scheme was *secA*, which was approximately 2,500 nucleotides. Phylogenetic analysis was therefore based on a relatively long fragment of approximately 1,970 nucleotides, corresponding to the length of the shortest sequence generated (‘*Ca. P. pyri*’ PD). The sequence generated for ‘*Ca. P. mali*’ was identical to the sequence used for group 16SrX probe design, while the sequences obtained from the other 16SrX-infected samples clustered separately (Figure 4A). While there was no reference sequence available for ESFY, the PYLR and PD sequences were identical to a reference sequence from ‘*Ca. P. pyri*’ (isolate PD1; Figure 4A). Similarly, the 16SrXII- and 16SrIII-infected samples generated *secA* sequences that were identical to the sequence used for probe design (Figure 4). The *secA* sequences of the infected strawberries from Mexico clustered with MBS phytoplasma (16SrI-B) *secA* sequence, although the sequence differences were not as great as those observed with other markers. The infected strawberry sample from Quebec (STRAW4) provided a *secA* sequence that clustered separately from the other AY-infected samples. Finally, the sequences assembled from infected canola in Saskatchewan were all identical to the sequence used for probe design, corresponding to the BnAY-TW1 *secA* sequence (Figure 4A).

Tuf

The *tuf* gene sequences also provided results that were consistent with expectations. The 16SrX samples yielded sequences that clustered together more tightly than the *secY* sequences, but the different subgroups were readily differentiated (Figure 4B). Again, the ‘*Ca. P. mali*’ sequence was nearly identical to the hybridization target sequence, while the other 16SrX infected samples yielded sequences that were somewhat distinct. The sample infected with ‘*Ca. P. prunorum*’ (ESFY) provided a

sequence that was nearly identical to a reference sequence from ESFY. The ‘*Ca. P. pyri*’ samples were identical to one another, and clustered with a short reference sequence for this taxon with a sequence identity of >95%. The 16SrIII and 16SrXII-infected samples also generated sequences that were identical to the respective hybridization target sequence. Unlike *secY*, *tuf* gene sequences were able to differentiate the MBS phytoplasma sequences (Sb7 and Sb41) from the canola samples that were also infected with 16SrI-B, all of which yielded identical sequences. The infected strawberry sample from Quebec (STRAW4) provided a distinct *tuf* sequence from the other 16SrI infected samples. The infected strawberry sample from Mexico, Sb7, generated a second, shorter *tuf* sequence (749 nucleotides) that was unlike any previously reported *tuf* sequence, but shared ~88% sequence identity with 16SrXII-B and 16SrXII-A 284/09 strain.

nusA

The *nusA* assemblies tended to be the shortest across all samples analyzed, consistent with the length of the *nusA* gene (1,074 nucleotides, the shortest gene analyzed). These sequences were trimmed to 620 bp, which was the length of the shortest *nusA* assembly (from ESFY). Like *secY* and *tuf*, *nusA* sequences from 16SrX phytoplasmas placed ‘*Ca. P. pyri*’ (PYLR/PD) in a clade with ‘*Ca. P. prunorum*’ (ESFY), with ‘*Ca. P. mali*’ (AP) forming a distinct but related group (Figure 4C). No *nusA* reference sequences are available for ESFY and PYLR/PD. Sequences assembled from 16SrIII and 16SrXII were identical to the hybridization target sequences, as observed with other genes. The *nusA* sequences could differentiate weakly the AY sequences assembled from the infected Mexican strawberries, and all *nusA* sequences assembled from the infected canola were identical to one another and to the target sequence (Figure 4C). STRAW4 clustered separately but within the AY group, as with the other genes (Figure 4C).

Discussion

The detection, identification, and classification of phytoplasma strains has typically relied upon PCR amplification and sequencing of the 16S rRNA-encoding gene (Zhao et al., 2013). Due to the well-recognized limitations of this approach for various phytoplasma groups, a wide variety of MLST schemes has been described, nearly all of which use PCR amplification and sequencing of specific protein-coding marker genes to improve strain differentiation. An alternative approach to PCR-based MLST was developed and applied to a variety of phytoplasma ribosomal groups, which produces the sequences of seven molecular markers simultaneously and with high accuracy. An important feature of this hybridization-based MLST approach is that it is independent of the design of “universal” primers targeting a subset of phytoplasmas, which overcomes a limitation of some MLST schemes that have been described. In this MLST scheme, hybridization-based gene enrichment was demonstrated to

be advantageous. For example, the number of sequencing reads for the BnAY-high sample that mapped to all genes before hybridization was 33, compared to 32,965 reads post-hybridization. These numbers of reads resulted in the assembly of rather long sequences for most of the gene targets (global average of 1929 nucleotides) that are commonly supported by at least hundreds or thousands of reads, providing confidence in the results that are obtained. Reliable reads of this length would be very difficult to obtain using Sanger sequencing from the ends of a clone or amplicon. The assembly of longer protein-coding sequences containing both coding and flanking non-coding regions greatly improves phylogenetic resolution (Gardner et al., 2020). Unlike PCR-based methods, hybridization and assembly does not provide reads with ends that are defined by primer binding locations; therefore, the phylogenetic analysis used fragments that were trimmed manually to the length of the shortest assembly. The ends of the assembled sequence are roughly defined by the sequences of the hybridization probes and are affected by the number of reads mapping to that gene in a given sample. This, in turn, is related to the amount of phytoplasma in the analyzed sample.

Hybridization probe-based detection, differentiation, and classification of difficult-to-culture phytopathogenic bacteria has been previously investigated. For example, in a pioneering study of phytoplasmas, dot and Southern hybridization were used to differentiate phytoplasma strains (Lee et al., 1990, 1992). More recently, enrichment approaches for determining whole-genome sequences of phytoplasmas have been described, using an antibody-based protocol that depletes a sample of eukaryotic DNA (Nijo et al., 2021). An alternative protocol using hybridization probes, similar to that described here, was used to enrich samples infected with the phloem-limited citrus pathogen, ‘*Candidatus Liberibacter asiaticus*’ for target bacterial DNA. This facilitated the assembly of the complete genome of the pathogen, including from samples with low levels (Cq ~30) of the target DNA (Cai et al., 2019).

The results presented here demonstrate that, similar to the observations of (Cai et al., 2019), phytoplasma-infected samples with a low concentration can still generate very long, phylogenetically informative assemblies. Ultimately, a standard fragment length for MLST analysis could be implemented bioinformatically using a tool such as *cutadapt*, which can trim sequences between two specified, degenerate sequences- this tool is used to trim *cpn60* sequences to the universal target by the CpnClassPhyr (Muirhead et al., 2019a). In almost all cases, for 16S ribosomal and *cpn60* sequences, the hybridization-based MLST approach provided sequences that were of sufficient length and quality for typing using the relevant RFLP-based classifiers, providing additional data that was useful for accurate classification of the samples.

While the hybridization-based approach obviates the need for the design of PCR primers, clearly the phytoplasmas that are targeted are limited to those that possess sequences that are closely related to those of the hybridization probes. The capture of

phytoplasma-derived DNA fragments that do not quite match the sequences of the hybridization probes (“off-target” hybridization) is desirable because it can increase the number of distinct phytoplasmas that can be profiled (Ranwez et al., 2011). Some amount of off-target hybridization was observed, consistent with other hybridization-based approaches for determining molecular marker sequences (Gasc and Peyret, 2018). For example, the ribosomal group X-infected samples examined in this work included 16SrX-A, which exactly matches the hybridization target sequence, along with other group X subgroups (16SrX-C and 16SrX-B), which did not exactly match the hybridization probe sequences. In most cases, the lack of a perfect match to the capture probes did not prevent the appearance of the off-target reads in the assembly dataset, since relatively long, robust assemblies were observed for even low concentration samples such as PD. However, *secY* generated off-target assemblies of lesser quality, which is presumably related to the fact that these sequences are more distinct among 16SrX strains. Off-target hybridization was also observed in samples that were infected by phytoplasmas from 16Sr groups that were not represented at all in the hybridization panel, such as Sb7 and Sb41. For example, we observed evidence of a novel *tuf* sequence most likely corresponding to that of 16SrXIII (*‘Ca. P. hispanicum’*), which was found in the Sb7 *tuf* assembly and had no match to anything known at the GenBank database. In a previous study (Pérez-López et al., 2017), sample Sb41 showed evidence of double infection with an on-target (16SrI) and off-target (16SrXIII) phytoplasma. Sample Sb41 had low levels of 16SrXIII and slightly higher levels of 16SrI (Table 3), but only assemblies corresponding to 16SrI (which typed as closely related to MBS phytoplasma, consistent with their geographic origin in Mexico) were observed. Sample Sb7, however, had much higher levels of 16SrXIII, and was demonstrated to be additionally infected with 16SrI (Table 3), although the levels of the latter were not measured. Nevertheless, assemblies generated from Sb7 mostly corresponded to 16SrI, except for the 16S rRNA gene, which was from 16SrXIII (Table 6). It appears therefore that off-target hybridization does occur, but inefficiently in the case of sequences from phytoplasmas from distinct ribosomal groups (as opposed to subgroups). The protein-coding genes from 16SrXIII also lacked reference genes to use for mapping, which may have resulted in these reads not being represented in the assembly dataset even if they had hybridized to the probes.

Conversely, the capture of non-phytoplasma DNA targets (nonspecific hybridization) is potentially less desirable and can interfere with the assembly of the correct DNA sequences. The number of reads mapping to the different taxonomic marker genes was quite variable across samples and in some cases was quite high, even for samples with relatively low phytoplasma levels (Table 4). This is explained at least in part by variability in read numbers generated in each Illumina run, and variation in the number of samples that were simultaneously processed on a single flowcell (which affects the number of reads allocated to each sample). There may also be technical variability in hybridization stringency and washing efficacy between repeats, which affects the

number of reads that are observed in each mapped dataset. The actual number of reads mapping to a given target gene is less important than the quality and length of the assemblies that are produced from these reads. For protein-coding genes such as *cpn60*, virtually all of the mapped reads had very high sequence identity to a probe sequence (Supplementary Figure S1C), representing high-quality sequences that enabled the assembly of long target sequences that were supported by tens to thousands of reads. This contrasts with PCR-based MLST, which typically has two slightly overlapping Sanger reads to support the relatively short contigs that are produced.

In the case of the 16S rRNA gene, many reads were observed in the initial mapping datasets for all phytoplasma-infected samples that corresponded to non-phytoplasma bacteria, along with host chloroplast and mitochondrial genes. In some cases, these reads interfered with the assembly of the correct taxonomic markers, and resulted in samples from uninfected plants showing post-hybridization reads (uninfected grape and canola). The most likely explanation for the preponderance of nonspecific reads in the 16S datasets is that the 16S gene is insufficiently distinct between different bacterial taxa to provide selectivity at both the hybridization and mapping steps. In the case of 16S rRNA genes, many of these “bleed-through” reads corresponded to 16S genes from non-phytoplasma bacteria, as well as 16S-like genes from host chloroplast and mitochondrial genomes. For 16S rRNA target genes only, a second mapping step was required that incorporated these reads; once so cleansed of the nonspecific reads, the assemblies improved considerably. In the case of the small number of protein-coding gene reads that appeared in the uninfected datasets, some amount of nonspecific hybridization and/or mapping can be expected, but these reads did not assemble into the target genes and so may be considered background noise. Therefore, this method is not suited to differentiating phytoplasma positive from negative samples, but that is not its intended use. In most cases, the MLST method will be applied to known positive samples. In addition, the non-hybridized samples showed higher read numbers mapping to all markers, including 16S rRNA, in the samples with lower amounts of phytoplasma (Table 5). While the explanation for this is not obvious, it is worth noting that these relatively small number of reads did not permit the assembly of the complete taxonomic markers in these non-hybridized samples, which demonstrates that necessity of the hybridization step.

This MLST scheme is effective for ribosomal groups 16SrI, 16SrIII, 16SrX, 16SrXII, and various subgroups within each. In addition, this relatively small panel of 351 probes could easily be expanded to design probes to include other phytoplasma groups and subgroups. This process would be straightforward, as it would use already available sequences and software for probe design and follows the hybridization procedures, protocols, and manufacturer guidelines that are well-tested and proven. Another advantage of this method is its potential to analyze a higher number of samples at the same time. For example, by including multiple samples (up to 12) in each hybridization and utilizing a plate format for simultaneous processing of 32 samples, up to 32

$\times 12 = 384$ samples could be processed simultaneously, making high throughput MLST for phytoplasma strains a possibility. Inclusion of other distinct phytoplasmas in the MLST panel is limited only by the availability of reference sequences, as demonstrated by '*Ca. P. hispanicum*' (16SrXIII), which would be impossible to represent due to the lack of reference sequences for several genes included in the MLST scheme.

A challenge faced by all molecular methods for differentiating phytoplasmas, including PCR-based methods, is dealing with samples containing either two distinct strains representing a mixed infection, or heterogeneous phytoplasma strains that feature two distinct but closely related phytoplasma 16S rRNA genes. For example, BnAY-TW1 from canola (Town et al., 2018) was found, by PCR and cloning, to contain 2 distinct 16S rRNA-encoding genes, which typed as 16SrI-A and 16SrI-B. Clone sequences generated from the more divergent genes *cpn60* and *rp* were identical to one another, consistent with the presence of a single strain that contains two 16S rRNA genes that type distinctly using RFLP analysis. The genome sequence of strain TW1 was identified as a possible chimeric artifact resulting from the combination of a long-read genome containing 16SrI-A scaffolds, polished with Illumina reads from a 16SrI-B phytoplasma strain (Cho et al., 2020). The hybridization results presented here are inconsistent with this hypothesis, since all the assembled protein-coding genes, and the clone sequences generated, clustered with 16SrI-B sequences. Moreover, the sequences that were assembled were identical or very nearly identical in all cases to the genes identified within the reported TW-1 genome sequence that were used to design the hybridization probes. In addition, the AY-infected strawberry sample from Quebec, STRAW4, provided distinct typing results using the assembled *cpn60* and 16S rRNA genes (Table 6). This sample has also been shown through cloning to contain two distinct 16S genes, which type as 16SrI-R and 16SrI-S along with a single *cpn60* sequence type (Brochu, AS et al., manuscript submitted). In cases of strains with heterogeneous 16S rRNA genes, the hybridization-based method described here would presumably produce a composite sequence from the two distinct loci, much like direct sequencing of PCR-generated amplicon would. Therefore, caution must be used in applying this method to strains that are known to feature 16S rRNA gene heterogeneity, and this should be investigated in each case using PCR amplification, cloning, and sequencing.

In conclusion, this hybridization-based MLST scheme is a method for phytoplasma characterization and provides a proof-of-concept for molecular characterization of other bacterial pathogens that are difficult to culture, despite the limitations listed above. All single-locus classification systems will suffer from a lack of taxonomic resolution due to the limited amount of sequencing information that can be generated from a single marker. This MLST scheme is based on gene targets of proven utility and generates high-quality sequences corresponding to seven different molecular markers. High resolution molecular marker sequences can be determined in this way for phytoplasmas within host plant

tissue, even those with low concentrations of this pathogen. Given how straightforward the probe design process is and its high throughput potential, this hybridization-based MLST scheme can be a very efficient molecular tool that provides resolution of closely related phytoplasmas.

The use of DNA sequencing for classification and typing of phytoplasmas will continue to be essential for understanding and monitoring the detrimental effects of phytoplasma infections on crop production. Implementation of a novel, universal, standardized approach for MLST could benefit these efforts and will result in an increased understanding of the spread and effects of these organisms on crop plants worldwide.

Data availability statement

The datasets generated for this study can be found in GenBank under BioProject accession number 642 PRJNA837572. <https://www.ncbi.nlm.nih.gov/bioproject/PRJNA837572>.

Author contributions

HB, TD, DS, and MG were responsible for experimental design. TD, KP-B, DS, and MG performed the experiments. TD and EL analyzed the data. TW and HB provided intellectual input. EL and TD prepared the figures and Supplementary material. TD and KP-B wrote the initial draft of the manuscript. HB, DS, MG, EL, TW, TD, and HB edited the manuscript. TD, TW, and HB acquired the funding, and supervised the project. All authors contributed to the article and approved the submitted version.

Funding

This work was funded by Canadian Food Inspection Agency grant # SID-P-1802, "Evaluation of Next generation Sequencing (NGS) for the detection and identification of Phytoplasmas." Graduate stipends for KP-B were provided through two projects funded by Western Grains Research Foundation (Project 1 and 2) and SaskCanola (Project 2), to TW and TD, "An early warning system to predict aster yellows outbreaks in Western Canada: origin and arrival of migrant leafhoppers (AAFC AGR-14988; WGRF # AGR1817), and "Continuing to watch the winds: the origin and arrival of migrant aster leafhoppers and diamondback moths" (AAFC AGR-17913; SaskCanola Ref: CARP ADF2020.409; WGRF Ref: AGR2105).

Acknowledgments

We thank Jennifer Town for advice and assistance on the data analysis code, and Christine Hammond for DNA sequencing support and commentary on the manuscript.

Conflict of interest

The authors declare that the research was conducted in the absence of any commercial or financial relationships that could be construed as a potential conflict of interest.

Publisher's note

All claims expressed in this article are solely those of the authors and do not necessarily represent those of their affiliated

organizations, or those of the publisher, the editors and the reviewers. Any product that may be evaluated in this article, or claim that may be made by its manufacturer, is not guaranteed or endorsed by the publisher.

Supplementary material

The supplementary material for this article can be found online at: <https://www.frontiersin.org/articles/10.3389/fmicb.2022.959562/full#supplementary-material>

References

- Abeyasinghe, S., Abeyasinghe, P. D., Kanatiwela-De Silva, C., Udagama, P., Warawichanee, K., Aljafar, N., et al. (2016). Refinement of the taxonomic structure of 16SrXI and 16SrXIV phytoplasmas of gramineous plants using multilocus sequence typing. *Plant Dis.* 100, 2001–2010. doi: 10.1094/PDIS-02-16-0244-RE
- Arnaud, G., Malembic-Maher, S., Salar, P., Bonnet, P., Maixner, M., Marcone, C., et al. (2007). Multilocus sequence typing confirms the close genetic interrelatedness of three distinct flavescence doree phytoplasma strain clusters and group 16SrV phytoplasmas infecting grapevine and alder in Europe. *Appl. Environ. Microbiol.* 73, 4001–4010. doi: 10.1128/AEM.02323-06
- Bertaccini, A. (2022). Plants and Phytoplasmas: when bacteria modify plants. *Plan. Theory* 11:11. doi: 10.3390/plants11111425
- Bertaccini, A., Arocha-Rosete, Y., Contaldo, N., Duduk, B., Fiore, N., Montano, H. G., et al. (2022). Revision of the 'Candidatus Phytoplasma' species description guidelines. *Int. J. Syst. Evol. Microbiol.* 72:72. doi: 10.1099/ijsem.0.005353
- Cai, W., Nunziata, S., Rascoe, J., and Stulberg, M. J. (2019). SureSelect targeted enrichment, a new cost effective method for the whole genome sequencing of *Candidatus Liberibacter asiaticus*. *Sci. Rep.* 9:18962. doi: 10.1038/s41598-019-55144-4
- Cho, S.-T., Kung, H.-J., Huang, W., Hogenhout, S. A., and Kuo, C.-H. (2020). Species boundaries and molecular markers for the classification of 16SrI phytoplasmas inferred by genome analysis. *Front. Microbiol.* 11. doi: 10.3389/fmicb.2020.01531
- Davis, R. E., Jomantiene, R., Kalvelyte, A., and Dally, E. L. (2003). Differential amplification of sequence heterogeneous ribosomal RNA genes and classification of the 'Fragaria multiplicata' phytoplasma. *Microbiol. Res.* 158, 229–236. doi: 10.1078/0944-5013-00201
- Davis, R. E., Zhao, Y., Dally, E. L., Lee, I. M., Jomantiene, R., and Douglas, S. M. (2013). 'Candidatus Phytoplasma pruni', a novel taxon associated with X-disease of stone fruits, *Prunus* spp.: multilocus characterization based on 16S rRNA, secY, and ribosomal protein genes. *Int. J. Syst. Evol. Microbiol.* 63, 766–776. doi: 10.1099/ijms.0.041202-0
- Deng, S., and Hiruki, C. (1991). Amplification of 16S rRNA genes from culturable and nonculturable Mollicutes. *J. Microbiol. Meth.* 14, 53–61. doi: 10.1016/0167-7012(91)90007-D
- Dumoncaux, T. J., Green, M., Hammond, C., Perez, E., and Olivier, C. (2014). Molecular diagnostic tools for detection and differentiation of phytoplasmas based on chaperonin-60 reveal differences in host plant infection patterns. *PLoS One* 9:e116039. doi: 10.1371/journal.pone.0116039
- Dumoncaux, T. J., Links, M. G., Town, J. R., Hill, J. E., and Hemmingsen, S. M. (2017). Targeted capture of cpn60 gene fragments for PCR-independent microbial community profiling. *Nat. Protoc. Exch.* doi: 10.1038/protex.2017.100
- Firrao, G., Martini, M., Ermacor, P., Loi, N., Torelli, E., Foissac, X., et al. (2013). Genome wide sequence analysis grants unbiased definition of species boundaries in 'Candidatus Phytoplasma'. *Syst. Appl. Microbiol.* 36, 539–548. doi: 10.1016/j.syapm.2013.07.003
- Gardner, E. M., Johnson, M. G., Pereira, J. T., Puad, A. S. A., Arifiani, D., Sahromi, W., et al. (2020). Paralogs and off-target sequences improve phylogenetic resolution in a densely sampled study of the breadfruit genus (*Artocarpus*, Moraceae). *Syst. Biol.* 70, 558–575. doi: 10.1093/sysbio/syaa073
- Gasc, C., and Peyret, P. (2018). Hybridization capture reveals microbial diversity missed using current profiling methods. *Microbiome* 6:61. doi: 10.1186/s40168-018-0442-3
- Gundersen, D. E., and Lee, I. M. (1996). Ultrasensitive detection of phytoplasmas by nested-PCR assays using two universal primer pairs. *Phytopathol. Mediterr.* 35, 144–151.
- Hodgett, J., Boonham, N., Mumford, R., Harrison, N., and Dickinson, M. (2008). Phytoplasma phylogenetics based on analysis of *secA* and 23S rRNA gene sequences for improved resolution of candidate species of 'Candidatus Phytoplasma'. *Int. J. Syst. Evol. Microbiol.* 58, 1826–1837. doi: 10.1099/ijms.0.05668-0
- Jomantiene, R., Davis, R. E., Valiunas, D., and Alminaitė, A. (2002). New group 16SrIII phytoplasma lineages in Lithuania exhibit rRNA interperon sequence heterogeneity. *Eur. J. Plant Pathol.* 108, 507–517. doi: 10.1023/A:1019982418063
- Kumar, S., Stecher, G., Li, M., Knyaz, C., and Tamura, K. (2018). MEGA X: molecular evolutionary genetics analysis across computing platforms. *Molec. Biol. Evol.* 35, 1547–1549. doi: 10.1093/molbev/msy096
- Lee, I. M., Bottner-Parker, K. D., Zhao, Y., Davis, R. E., and Harrison, N. A. (2010). Phylogenetic analysis and delineation of phytoplasmas based on *secY* gene sequences. *Int. J. Syst. Evol. Microbiol.* 60, 2887–2897. doi: 10.1099/ijms.0.019695-0
- Lee, I. M., Davis, R. E., Chen, T. A., Chiykowski, L. N., Fletcher, J., Hiruki, C., et al. (1992). A genotype-based system for identification and classification of mycoplasma-like organisms (MLOs) in the aster yellows MLO strain cluster. *Phytopathology* 82, 977–986. doi: 10.1094/Phyto-82-977
- Lee, I. M., Davis, R. E., and Dewitt, N. D. (1990). Nonradioactive screening method for isolation of disease-specific probes to diagnose plant diseases caused by mycoplasma-like organisms. *Appl. Environ. Microbiol.* 56, 1471–1475. doi: 10.1128/aem.56.5.1471-1475.1990
- Lee, I. M., Gundersen-Rindal, D. E., Davis, R. E., Bottner, K. D., Marcone, C., and Seemüller, E. (2004). 'Candidatus Phytoplasma asteris', a novel phytoplasma taxon associated with aster yellows and related diseases. *Int. J. Syst. Evol. Microbiol.* 54, 1037–1048. doi: 10.1099/ijms.0.02843-0
- Liefting, L. W., Andersen, M. T., Beever, R. E., Gardner, R. C., and Forster, R. L. (1996). Sequence heterogeneity in the two 16S rRNA genes of Phormium yellow leaf phytoplasma. *Appl. Environ. Microbiol.* 62, 3133–3139. doi: 10.1128/aem.62.9.3133-3139.1996
- Lim, P. O., and Sears, B. B. (1992). Evolutionary relationships of a plant-pathogenic mycoplasma-like organism and *Acholeplasma laidlawii* deduced from two ribosomal protein gene sequences. *J. Bacteriol.* 174, 2606–2611. doi: 10.1128/jb.174.8.2606-2611.1992
- Marcone, C., Lee, I. M., Davis, R. E., Ragazzino, A., and Seemüller, E. (2000). Classification of aster yellows-group phytoplasmas based on combined analyses of rRNA and *tuf* gene sequences. *Int. J. Syst. Evol. Microbiol.* 50, 1703–1713. doi: 10.1099/00207713-50-5-1703
- Martini, M., Lee, I. M., Bottner, K. D., Zhao, Y., Botti, S., Bertaccini, A., et al. (2007). Ribosomal protein gene-based phylogeny for finer differentiation and classification of phytoplasmas. *Int. J. Syst. Evol. Microbiol.* 57, 2037–2051. doi: 10.1099/ijms.0.05013-0
- Mitrović, J., Kakizawa, S., Duduk, B., Oshima, K., Namba, S., and Bertaccini, A. (2011). The *gro EL* gene as an additional marker for finer differentiation of 'Candidatus Phytoplasma asteris'-related strains. *Ann. Appl. Biol.* 159, 41–48. doi: 10.1111/j.1744-7348.2011.00472.x
- Muirhead, K., Pérez-López, E., Bahder, B. W., Hill, J. E., and Dumoncaux, T. (2019a). The Cpn Classi PhyR is a resource for *cpn60* universal target-based classification of phytoplasmas. *Plant Dis.* 103, 2494–2497. doi: 10.1094/PDIS-03-19-0454-A
- Muirhead, K., Pérez-López, E., Bahder, B. W., Hill, J. E., and Dumoncaux, T. J. (2019b). "The Cpn Classi PhyR facilitates phytoplasma classification and taxonomy using *cpn60* universal target sequences" in *Sustainable Management of Phytoplasma Diseases in Crops Grown in the Tropical Belt: Biology and Detection*. eds. C. Y.

- Olivier, T. J. Dumonceaux and E. Pérez-López (Cham: Springer International Publishing), 1–27.
- Nijo, T., Iwabuchi, N., Tokuda, R., Suzuki, T., Matsumoto, O., Miyazaki, A., et al. (2021). Enrichment of phytoplasma genome DNA through a methyl-CpG binding domain-mediated method for efficient genome sequencing. *J. Gen. Plant Pathol.* 87, 154–163. doi: 10.1007/s10327-021-00993-z
- Pérez-López, E., Olivier, C. Y., Luna-Rodríguez, M., and Dumonceaux, T. J. (2016). Phytoplasma classification and phylogeny based on *in silico* and *in vitro* RFLP analysis of *cpn60* universal target sequences. *Int. J. Syst. Evol. Microbiol.* 66, 5600–5613. doi: 10.1099/ijsem.0.001501
- Pérez-López, E., Rodríguez-Martínez, D., Olivier, C. Y., Luna-Rodríguez, M., and Dumonceaux, T. J. (2017). Molecular diagnostic assays based on *cpn60* UT sequences reveal the geographic distribution of subgroup 16SrXIII-(a/I) I phytoplasma in Mexico. *Sci. Rep.* 7:950. doi: 10.1038/s41598-017-00895-1
- Perez-Lopez, E., Vincent, C., Moreau, D., Hammond, C., Town, J., and Dumonceaux, T. J. (2019). A novel '*Candidatus* Phytoplasma asteris' subgroup 16SrI-(E/AI) AI associated with blueberry stunt disease in eastern Canada. *Int. J. Syst. Evol. Microbiol.* 69, 322–332. doi: 10.1099/ijsem.0.003100
- Plante, N., Brochu, A.-S., Goulet, C., Thibault, P., Fournier, V., and Pérez-López, E. (2021). First evidence of the occurrence of a putative new subgroup of '*Candidatus* Phytoplasma asteris' (16SrI) associated with strawberry green petal disease in Quebec, Canada. *New Dis. Rep.* 44:e12038. doi: 10.1002/ndr2.12038
- Ranebennur, H., Rawat, K., Rao, A., Kumari, P., Chalam, V. C., Meshram, N., et al. (2022). Transmission efficiency of a '*Candidatus* Phytoplasma australasia' (16SrII-D) related strain associated with sesame phyllody by dodder, grafting and leafhoppers. *Eur. J. Plant Pathol.* doi: 10.1007/s10658-022-02550-6
- Ranwez, V., Harispe, S., Delsuc, F., and Douzery, E. J. P. (2011). MACSE: multiple alignment of coding SEquences accounting for frameshifts and stop codons. *PLoS One* 6:e22594. doi: 10.1371/journal.pone.0022594
- Saccardo, F., Martini, M., Palmano, S., Ermacora, P., Scortichini, M., Loi, N., et al. (2012). Genome drafts of four phytoplasma strains of the ribosomal group 16SrIII. *Microbiology* 158, 2805–2814. doi: 10.1099/mic.0.061432-0
- Saitou, N., and Nei, M. (1987). The neighbor-joining method: a new method for reconstructing phylogenetic trees. *Mol. Biol. Evol.* 4, 406–425. doi: 10.1093/oxfordjournals.molbev.a040454
- Satta, E., Carminati, G., and Bertaccini, A. (2020). Phytoplasma presence in carrot seedlings. *Aust. Plant. Dis. Notes* 15:11. doi: 10.1007/s13314-020-0377-y
- Schneider, B., Seemuller, E., Smart, C. D., and Kirkpatrick, B. C. (1995). "Phylogenetic classification of plant pathogenic mycoplasma-like organisms or phytoplasmas" in *Molecular and Diagnostic Procedures in Mycoplasma*. eds. R. Razin and J. G. Tully (San Diego: Academic Press), 369–380.
- Shao, J. Y., Jomantiene, R., Dally, E. L., Zhao, Y., Lee, I.-M., Nuss, D. L., et al. (2006). Phylogeny and characterization of phytoplasmal nus a and use of the nus a gene in detection of group 16SrI strains. *J. Plant Pathol.* 88, 193–201.
- Soto, N., Helmick, E. E., Harrison, N. A., and Bahder, B. W. (2021). Genetic variability of palm lethal decline phytoplasmas in the Caribbean basin and Florida, U.S.A., based on a multilocus analysis. *Phytopathology* 111, 2203–2212. doi: 10.1094/PHYTO-04-21-0130-R
- Tamura, K., Nei, M., and Kumar, S. (2004). Prospects for inferring very large phylogenies by using the neighbor-joining method. *Proc. Natl. Acad. Sci. U. S. A.* 101, 11030–11035. doi: 10.1073/pnas.0404206101
- Town, J. R., Wist, T., Perez-Lopez, E., Olivier, C. Y., and Dumonceaux, T. J. (2018). Genome sequence of a plant-pathogenic bacterium, '*Candidatus* Phytoplasma asteris' strain TW1. *Microbiol. Resour. Announc.* 7:e01109-18. doi: 10.1128/MRA.01109-18
- Wei, W., Cai, H., Jiang, Y., Lee, I.-M., Davis, R. E., Ding, Y., et al. (2011). A new phytoplasma associated with little leaf disease in azalea: multilocus sequence characterization reveals a distinct lineage within the aster yellows phytoplasma group. *Ann. Appl. Biol.* 158, 318–330. doi: 10.1111/j.1744-7348.2011.00468.x
- Wei, W., and Zhao, Y. (2022). Phytoplasma taxonomy: nomenclature, classification, and identification. *Biology (Basel)* 11:11. doi: 10.3390/biology11081119
- Weintraub, P. G., and Beanland, L. (2006). Insect vectors of phytoplasmas. *Annu. Rev. Entomol.* 51, 91–111. doi: 10.1146/annurev.ento.51.110104.151039
- Zhao, Y., Wei, W., Lee, I.-M., Shao, J., Suo, X., and Davis, R. E. (2009). Construction of an interactive online phytoplasma classification tool, iPhyClassifier, and its application in analysis of the peach X-disease phytoplasma group (16SrIII). *Int. J. Syst. Evol. Microbiol.* 59, 2582–2593. doi: 10.1099/ijms.0.010249-0
- Zhao, Y., Wei, W., Lee, I. M., Shao, J., Suo, X., and Davis, R. E. (2013). The iPhyClassifier, an interactive online tool for phytoplasma classification and taxonomic assignment. *Methods Mol. Biol.* 938, 329–338. doi: 10.1007/978-1-62703-089-2_28



OPEN ACCESS

EDITED BY

Christine Citti,
Institut National de recherche pour
l'agriculture, l'alimentation et
l'environnement (INRAE), France

REVIEWED BY

Mitchell F. Balish,
Miami University,
United States
Miaomiao Shi,
The University of Chicago, United States

*CORRESPONDENCE

Makoto Miyata
miyata@omu.ac.jp

SPECIALTY SECTION

This article was submitted to
Microbial Physiology and Metabolism,
a section of the journal
Frontiers in Microbiology

RECEIVED 27 July 2022

ACCEPTED 01 September 2022

PUBLISHED 06 October 2022

CITATION

Sasajima Y, Kato T, Miyata T, Kawamoto A,
Namba K and Miyata M (2022) Isolation and
structure of the fibril protein, a major
component of the internal ribbon for
Spiroplasma swimming.
Front. Microbiol. 13:1004601.
doi: 10.3389/fmicb.2022.1004601

COPYRIGHT

© 2022 Sasajima, Kato, Miyata, Kawamoto,
Namba and Miyata. This is an open-access
article distributed under the terms of the
[Creative Commons Attribution License \(CC
BY\)](https://creativecommons.org/licenses/by/4.0/). The use, distribution or reproduction in
other forums is permitted, provided the
original author(s) and the copyright
owner(s) are credited and that the original
publication in this journal is cited, in
accordance with accepted academic
practice. No use, distribution or
reproduction is permitted which does not
comply with these terms.

Isolation and structure of the fibril protein, a major component of the internal ribbon for *Spiroplasma* swimming

Yuya Sasajima¹, Takayuki Kato², Tomoko Miyata³,
Akihiro Kawamoto², Keiichi Namba^{3,4,5} and Makoto Miyata^{1,6*}

¹Graduate School of Science, Osaka Metropolitan University, Osaka, Japan, ²Institute for Protein Research, Osaka University, Suita, Osaka, Japan, ³Graduate School of Frontier Biosciences, Osaka University, Suita, Osaka, Japan, ⁴RIKEN Center for Biosystems Dynamics Research and Spring-8 Center, Suita, Osaka, Japan, ⁵JEOL YOKOGUSHI Research Alliance Laboratories, Osaka University, Suita, Osaka, Japan, ⁶The OCU Advanced Research Institute for Natural Science and Technology (OCARINA), Osaka Metropolitan University, Osaka, Japan

Spiroplasma, which are known pathogens and commensals of arthropods and plants, are helical-shaped bacteria that lack a peptidoglycan layer. *Spiroplasma* swim by alternating between left- and right-handed helicity. Of note, this system is not related to flagellar motility, which is widespread in bacteria. A helical ribbon running along the inner side of the helical cell should be responsible for cell helicity and comprises the bacterial actin homolog, MreB, and a protein specific to *Spiroplasma*, fibril. Here, we isolated the ribbon and its major component, fibril filament, for electron microscopy (EM) analysis. Single-particle analysis of the fibril filaments using the negative-staining EM revealed a three-dimensional chain structure composed of rings with a size of 11nm wide and 6nm long, connected by a backbone cylinder with an 8.7nm interval with a twist along the filament axis. This structure was verified through EM tomography of quick-freeze deep-etch replica sample, with a focus on its handedness. The handedness and pitch of the helix for the isolated ribbon and fibril filament agreed with those of the cell in the resting state. Structures corresponding to the alternative state were not identified. These results suggest that the helical cell structure is supported by fibril filaments; however, the helical switch is caused by the force generated by the MreB proteins. The isolation and structural outline of the fibril filaments provide crucial information for an in-depth clarification of the unique swimming mechanism of *Spiroplasma*.

KEYWORDS

helical shape, motility, cytoskeleton, filament, single particle analysis, quick freeze replica electron microscopy, electron tomography

Introduction

Mollicutes, which are parasitic or commensal bacteria, evolved from the phylum, Firmicutes, including *Bacillus* and *Clostridium* by reducing their genome size (Razin et al., 1998; Razin and Hayflick, 2010; Grosjean et al., 2014; Miyata et al., 2020). During the course of evolution, the cells became softer and smaller owing to the loss of the peptidoglycan layer. These changes may have allowed some species to transmit the movements of their internal housekeeping proteins to the outside, resulting in the acquisition of at least three unique motility mechanisms (Relich et al., 2009; Miyata and Hamaguchi, 2016a,b; Distelhorst et al., 2017; Miyata et al., 2020; Kiyama et al., 2021; Toyonaga et al., 2021). Two of the three well studied mechanisms are exerted by *Mycoplasma mobile* and *Mycoplasma pneumoniae*. These species exhibit gliding motilities on solid surfaces, in which leg structures repeatedly catch sialylated oligosaccharides on host

cells based on two mechanisms (Miyata, 2010; Miyata and Hamaguchi, 2016a,b). Another motility system is the helicity-switching swimming of *Spiroplasma*, which is the subject of the present study (Supplementary Movie_S1; Shaevitz et al., 2005; Wada and Netz, 2009; Harne et al., 2020b; Sasajima and Miyata, 2021). *Spiroplasma* species are parasitic to plants and arthropods and are characterized as polarized helical-shaped cells with one tapered end (Gasparich, 2002; Harumoto and Lemaitre, 2018; Harne et al., 2020b). These species exhibit obvious chemotaxis despite the absence of genes for the two-component regulatory system in the genome, which is generally responsible for bacterial chemotaxis (Liu et al., 2017). In general, swimming bacteria, including spirochetes, can migrate through the rotational motion of the flagellar motor fixed to the peptidoglycan layer, whereas *Spiroplasma* has a unique swimming system in which kinks propagate along the cell body with a switch between left- and right-handed cell helicity (Figure 1A). The outline of this

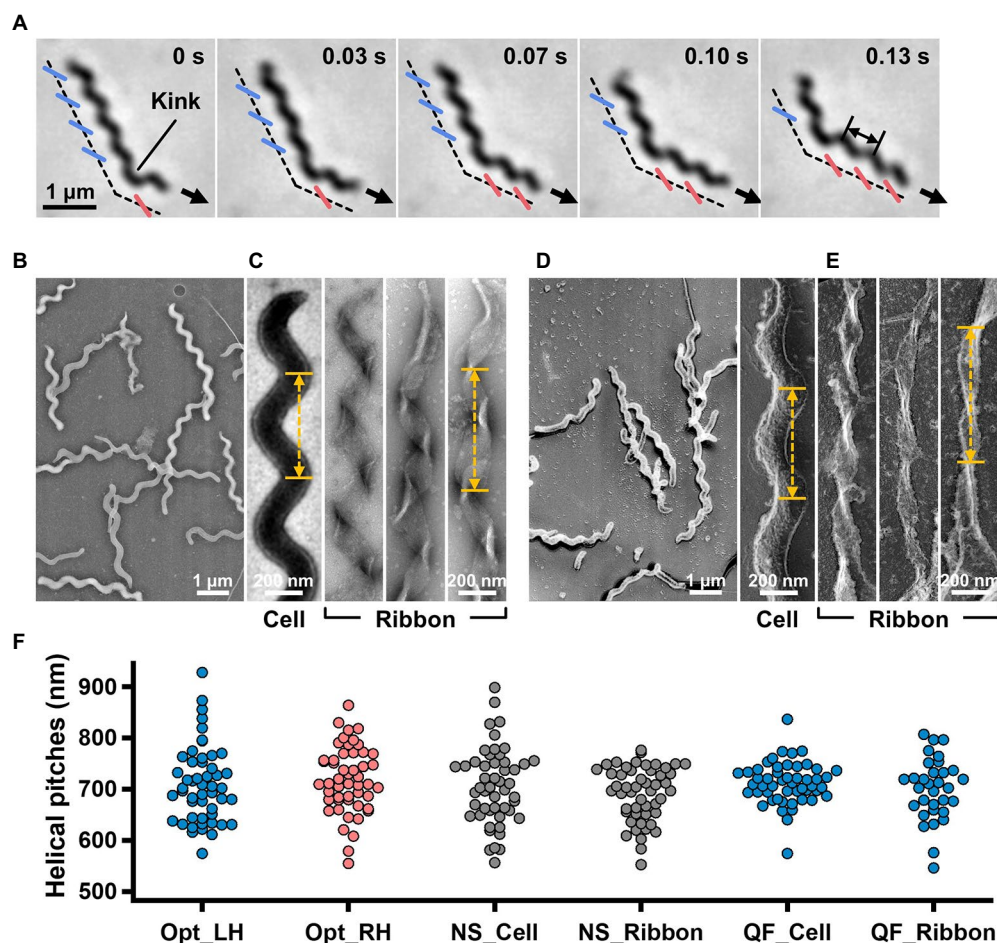


FIGURE 1

Helicity of the cell and ribbon structure. (A) Phase-contrast microscopy of swimming cell. The blue and red segments, and broken line indicate the left- and right-handed helicity, and cell axes, respectively. The pitch was measured as indicated by a double headed arrow. (B,C) Cell and ribbon images acquired by negative-staining EM. (D,E) Cell and ribbon images acquired by QFDE EM. (F) Helical pitches of cells and ribbon measured by optical microscopy, negative-staining EM, and QFDE-EM. Handedness was judged by optical microscopy and QFDE-EM. All cells analyzed by QFDE-EM were left-handed as they were grown under a starved condition.

mechanism has been clarified as follows. The rotation of helical cells linked to the helicity switch pushes the water back (Trachtenberg and Gilad, 2001; Trachtenberg et al., 2003b; Kürner et al., 2005; Shaevitz et al., 2005; Wada and Netz, 2009; Sasajima and Miyata, 2021). The helicity might be dominated by an intracellular structure called the “ribbon,” which localizes along the innermost line of the helical cell structure and is composed of protofilaments. Based on structural studies, ribbons may switch their helicity through changes in the protofilament length (Trachtenberg and Gilad, 2001; Kürner et al., 2005; Cohen-Krausz et al., 2011). Ribbons are known to be composed of fibril proteins specific for *Spiroplasma* species and some *Spiroplasma* MreB (SMreB) proteins related to MreB that are common in rod-shaped bacteria. Although fibril filaments are featured by repetitive ring structures, nanometer-order three-dimensional structure has not been clarified (Trachtenberg and Gilad, 2001; Trachtenberg et al., 2003a, 2008; Kürner et al., 2005; Cohen-Krausz et al., 2011; Liu et al., 2017).

In the present study, we isolated the filament of fibrils, the major component protein of ribbons and clarified its nanometer-order three-dimensional structure using electron microscopy (EM) and image analyses. The fibril filament has a repetitive structure featuring a ring and a cylinder with a helical pitch similar to those of the ribbon and cell.

Materials and methods

Bacterial strains and culture conditions

The type strain, TDA-040725-5^T, of *Spiroplasma eriocheiris* was cultured in R2 medium (2.5% [wt/vol] heart infusion broth, 8% sucrose, and 10% horse serum) at 30°C until an optical density of 0.06 to 0.1 was achieved at 600 nm (Liu et al., 2017; Terahara et al., 2017).

Optical microscopy

Cultured cells were centrifuged at 11,000 × g, 10°C for 10 min and suspended in PBS consisting of 75 mM sodium phosphate [pH 7.3], 100 mM NaCl containing 20 mM glucose, and 0.6% methylcellulose, to achieve a cell density 10-fold higher than that of the original (Liu et al., 2017; Terahara et al., 2017). Cells were inserted into a tunnel chamber assembled by taping coverslips, as previously described, and observed under an IX71 microscope (Olympus, Tokyo, Japan; Uenoyama et al., 2004). A video was captured using a DMK33UX174 complementary metal–oxide–semiconductor (CMOS) camera (The Imaging Source, Taipei, Taiwan) and analyzed using ImageJ v1.53a.¹

Electron microscopy

To observe the intact cells, the cell suspension was placed on a hydrophilized grid, fixed using 2% glutaraldehyde, washed with water, and stained with 2% uranyl acetate. To observe the internal structure, the cell suspension on a grid was treated with PBS containing 0.1 mg/ml DNase and 1 mM MgCl₂ for 20 s, washed, and stained with 2% uranyl acetate. QFDE-EM was performed as previously reported for specimens suspended in a solution, 10 mM HEPES (pH 7.6), and 150 mM NaCl containing mica flakes (Tulum et al., 2019). The Triton X-100 treatment was done on glass surface before freezing, to observe the internal structure. Images were acquired using a JEM1010 EM (JEOL, Akishima, Japan) equipped with a FastScan-F214(T) charge-coupled device (CCD) camera (TVIPS, Gauting, Germany) and analyzed using ImageJ v1.53a. For tomography, images were captured using a Talos F200C EM (FEI, Eindhoven, Netherlands) equipped with a Ceta 16M CMOS camera (FEI). Single-axis tilt series were collected covering an angular range from −50° to +50° with 1.5° steps and analyzed using IMOD (ver 4.11) and PEET (ver 1.15.0).

Isolation of the ribbon and fibril

To isolate the internal structure, 10 ml of cell suspension in PBS was treated with 1% Triton X-100, 0.1 mg/ml DNase, 1 mM MgCl₂, and 0.1 mM PMSE, with shaking for 10 min at 4°C. The insoluble fraction was recovered *via* centrifugation at 20,000 × g for 30 min at 4°C, and suspended in PBS to obtain a final volume of 0.2 ml. The sample was placed at the top of sucrose solution layers of 0, 20, 30, 40, 50, and 60%, and centrifuged at 20,000 × g for 20 min at 4°C in a 1.5 ml tube at a fixed angle. To isolate the fibril filament, the insoluble fraction was additionally treated with a solution consisting of 2% cholic acid, 20 mM Tris-Cl pH 8.0, 150 mM NaCl at 4°C for 8 h, and subjected to stepwise density gradient centrifugation. SDS-PAGE and peptide mass fingerprinting were performed as described previously (Nakane and Miyata, 2007; Kawakita et al., 2016; Liu et al., 2017). Band intensities were calculated using ImageJ, from scanned gel images.

Preparation of the single-stranded fibril filament

The isolated fibril was adjusted to 1 mg/ml in 20 mM Tris-Cl pH 8.0 and 150 mM NaCl. The fibril suspension (1 ml in a 1.5-ml test tube) was treated on ice for 5 s using a sonicator (UR-21P, TOMY, Tokyo, Japan). The condition of the fibril filament was checked *via* negative-staining electron microscopy (EM). The processes of sonication and observation were repeated with the fibril suspension until more than 90% of the filaments became single-stranded.

¹ <https://imagej.nih.gov/ij/> (accessed September 6, 2022).

Reconstitution of the 3D structure

The contrast transfer function (CTF) parameters for negative-staining EM images were estimated using the Gctf25 software (Zhang, 2016). The images of fibril filaments were selected automatically using RELION 3.0 (Zivanov et al., 2018) as helical objects and segmented as squares of 200×200 pixels with a 90% overlap. These 14,543 images were 2D-classified and 11,867 images were selected for further analyses. *Ab-initio* reconstitution was performed using cisTEM (Grant et al., 2018) based on segmented images from 12 classes. The selected 11,867 particle images were 3D-classified using the 3D map in RELION 3.0 (Zivanov et al., 2018).

Results

Cell helicity is derived from the internal ribbon structure

To clarify the relationship between the helical cell morphology and the internal ribbon structure, we first measured the helical pitches of the swimming cells using optical microscopy. Under phase-contrast microscopy, the helical shape of the cells can be observed as a series of dense segments in the defocused image plane relative to the cell axis (Figure 1A). We measured the pitches along the cell axis for the segments of left and right handedness (Figure 1F). The helical pitches were 709 ± 74 ($n=50$) and 718 ± 65 nm ($n=50$) for the left- and right-handed segments, respectively.

EM was subsequently employed to analyze the internal ribbon structure and compare the helical pitches of the cells and ribbons. Negative-staining EM revealed images of helical-shaped cells with a narrow tip on one side (Figure 1B).

The internal ribbon structure was exposed by treating the cells with 0.1% Triton X-100 on the grid (Figure 1C). The ribbon had a “helical” flat structure. These observations are consistent with those of previous studies (Trachtenberg and Gilad, 2001). Thereafter, the pitches of the cell and the exposed ribbon were measured (Figure 1F). Generally, the specimens for negative-staining EM are placed in vacuum and dried, which can result in distortions and is disadvantageous for evaluating the helicity. We therefore applied quick-freeze, deep-etch (QFDE) EM to visualize the structure in a state as closely as possible to the

original (Heuser, 2011). In QFDE, a sample is frozen in milliseconds and exposed by fracturing and etching. Thereafter, a platinum replica was created by shadowing. The observation of the replica by transmission EM provides images with high contrast and resolution, which is markedly better than that provided by conventional scanning electron microscopy (SEM; Heuser, 2011; Tulum et al., 2019). Replicas were then prepared by fracturing and platinum coating. QFDE-EM revealed cell morphology consistent with that obtained using negative-staining EM (Figure 1D). Using QFDE-EM, we observed the ribbons exposed to 0.1% Triton X-100 treatment (Figure 1E). The ribbon had a structure in which the twisted positions were assembled in a line, showing that the images observed by negative-staining EM were flattened. Interestingly, all ribbons were left-handed (Figures 1D,E). When the cells were starved in phosphate-buffered saline (PBS) without glucose for 30 min, they showed a left-handed helix with the same pitch. Therefore, this structure was assumed to be the default state of the cell, and the ribbon switched to the default structure during the visualization process. The helical pitches of the cells and ribbons aligned well with each other, indicating that the ribbon has a critical role for cell helicity (Figure 1F, Table 1).

Isolation and characterization of the ribbon

For further characterization, we isolated the internal ribbon structure. The cell suspension was treated with 1% Triton X-100 and subjected to stepwise gradient centrifugation with 0, 20, 30, 40, 50, and 60% sucrose layers. After centrifugation, we found a dense layer of cell contents at the bottom of the 40% sucrose layer. The fraction was recovered and then observed by EM. Based on the observation, the ribbon was found to comprise protofilaments with a width of 66 ± 12 nm ($n=20$) and a length longer than $2 \mu\text{m}$, which may correspond to the full length of the cell (Figure 2A). To analyze the number and width of the protofilaments involved in the isolated ribbon, we traced a cross sectional image profile of the ribbon (Figure 2D(a)). Six to nine protofilaments were detected, with peak distances ranging between 4 and 16 nm (Figure 2D(b,c)), consistent with the findings of the previous studies (Trachtenberg and Gilad, 2001; Liu et al., 2017). Ribbon twists are observed as periodic frays in the ribbons. The ribbon pitches were measured from the frays as 350 ± 17 nm ($n=47$; Figure 2D(d)), which is comparable to the helical pitches of the

TABLE 1 Dimensions of the cell and ribbon.

Parameters	Negative-staining EM	QFDE-EM	Optical microscopy
Cell helical pitch	706 ± 74 nm 703 nm	711 ± 41 nm (LH) 711 nm (LH)	709 ± 74 nm (LH) 702 nm (LH) 718 ± 65 nm (RH) 711 nm (RH)
Ribbon helical pitch	691 ± 53 nm 700 nm	700 ± 60 nm (LH) 706 nm (LH)	
Isolated ribbon 1/2 helical pitch	350 ± 17 nm 352 nm		
Isolated fibril 1/2 helical pitch	341 ± 27 nm 335 nm	351 ± 34 nm (LH) 352 nm (LH)	

Handedness is represented by LH and RH.

The mean, standard deviation, and median are shown from the left.

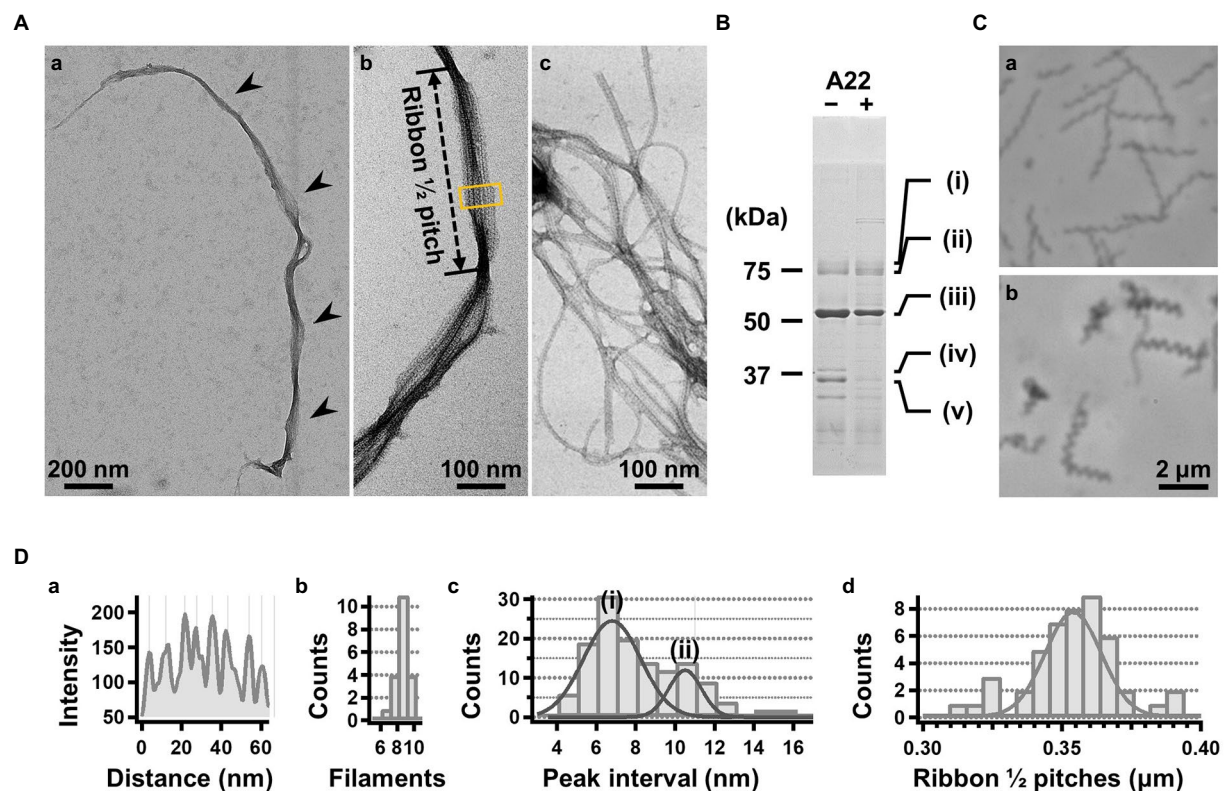


FIGURE 2

Isolation and characterization of the ribbon. (A) Isolated ribbon structure. (a) The whole structure of the isolated ribbon with helicity as shown by periodical wide positions (marked by arrows). (b) The magnified image of the isolated ribbon and the helical pitch is indicated by a bidirectional arrow. (c) Ribbon fraction isolated from cells treated with A22. (B) Protein profiles of the ribbon fraction isolated from cells untreated and treated with A22. (C) Cell images before (a) and after (b) treatment with 1mM A22 for 2min. (D) Numerical characterization. (a) Sectional image profile of the area boxed in panel (A b). The peaks correspond to the center of the protofilament. (b) Histogram for the number of protofilaments involved in a ribbon. (c) Histogram for the protofilament width in ribbons. The distribution can be fitted by two Gaussian curves marked (i) and (ii), with peaks around 7.0 and 10.5nm, respectively. (d) Histogram for the helical pitches of the isolated ribbon, fitted by a Gaussian curve with a peak at 351 ± 16 nm ($n=47$).

TABLE 2 Protein components of the ribbon isolated from original cells¹.

Protein band ¹	Gene ID	Annotation	Mascot score ²	Mass (kDa) ³	Density ratio (%)	
					Original	A22 treated
(i)	SPE-1201	Hypothetical protein	72	85.8	4	5
(ii)	SPE-0013	FtsH	84	77.0	12	17
(iii)	SPE-0666	Fibril	206	58.7	47	67
(iv)	SPE-1231	SMreB5	98	38.5	10	7
(v)	SPE-1224 SPE-1230	SMreB2 SMreB4	80	37.8 40.7	27	4

¹From A22-treated cells, the proteins common to the original cells were identified for bands (i)–(iv). For band (v) only, SMreB2 was identified.

²Mascot score is the logarithm of probability that the observed match is a random event.

³Calculated from the amino acid sequence as a monoisotopic molecule.

cells and the ribbons exposed from cells on grids (Figure 1, Table 1; $p=0.7>0.01$). SDS-PAGE and peptide mass fingerprinting analyses of this fraction revealed five protein bands, including six proteins (Figure 2B, Table 2, Supplementary Table S1). Band (v) contains SMreBs 2 and 4. The whole ribbon fraction mainly comprised the fibril protein (band iii) and a protein mixture of SMreBs 2 and 4 (band v), with an intensity ratio of 47 and 27% of

the total protein amount, respectively. Further studies are necessary to conclude physical interactions of SPE-1201 and FtsH to fibril protein, because these proteins are abundant in *S. eriocheiris* cells (Liu et al., 2017).

We intended to use A22, an inhibitor of MreB polymerization, to examine the role of SMreBs in ribbon formation (Shi et al., 2018); this is because the binding of A22 to SMreBs has been

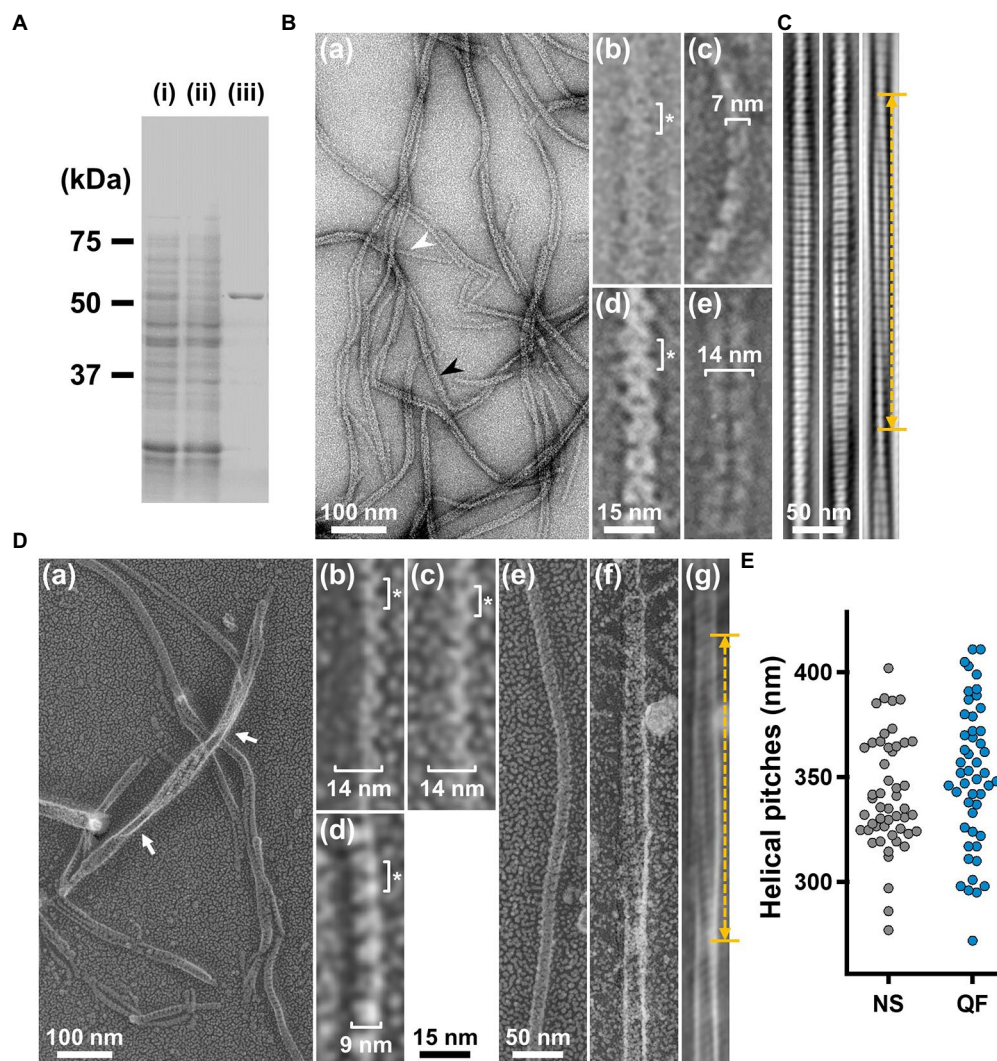


FIGURE 3

Structures of the isolated fibril filament. **(A)** Protein profiles of the fractions in the purification process for fibril protein. (i) Whole cell lysate. (ii) Supernatant. (iii) Isolated ribbon. The sample amount was adjusted to be delivered from the same cell number. **(B)** Purified fibril filaments observed by negative-staining EM. (a) Field image. White and black arrows indicate typical single and double strands, respectively. (b, c) Front and side views of the single-stranded fibril filament. (d, e) Front and side views of the double-stranded fibril filament. The ring intervals marked by an asterisk were 9 nm for both single and double strands. **(C)** Double-stranded filaments reconstituted through Fourier filtering. **(D)** Fibril filaments observed by QFDE-EM. Field (a) and single-stranded filaments (b, c, d) are presented. The back (b), front (c), and side (d) views are shown. (e) Single-stranded filament. (f, g) Double-stranded filament image. (f) was reduced for noise through Fourier filtering as shown in (g). The helical pitch was measured as depicted by a double headed broken arrow. The handedness was clearly observed at the points marked by white arrows in the panel (a), and panel (f) image.

suggested from amino acid sequences (Takahashi et al., 2020). First, the effect of 1 mM A22 on the swimming *Spiroplasma* cells was determined. The cells lost their original shape and stopped moving within 2 min (Figure 2C), suggesting that the functions of SMreBs were inhibited by A22. Thereafter, we isolated the ribbon from cells maintained in 1 mM A22 for 2.5 h at 30°C. The ribbons were found to be dispersed (Figure 2A(c)). SDS-PAGE analysis revealed contents of 67 and 11% for fibril (band iii) and SMreB2 (band v) proteins, respectively (Figure 2B), suggesting that the protofilaments comprising fibril proteins are stabilized and modified by SMreBs in the ribbon structure.

Isolation and helical pitch of the fibril filament

To analyze the detailed structure of fibril filaments, we treated the ribbon fraction with cholic acid and isolated fibril proteins using sucrose-gradient centrifugation. SDS-PAGE analysis showed that the fraction only contained fibril protein (Figure 3A). Negative-staining EM revealed that the fibril protein formed filaments that included single-, double-, and more-stranded filaments, suggesting various types of interactions between the fibril protein molecules (Figure 3B(a)). A single-stranded fibril

filament consisted of repeated ring units with approximately 9 nm intervals (Figure 3B(b,c)), consistent with previous studies (Townsend et al., 1980; Williamson et al., 1991; Trachtenberg and Gilad, 2001; Liu et al., 2017). The ring units were connected by the backbone cylinder (Figure 3B(c)). The double-stranded fibril filament appeared to be formed *via* the alignment of two single-stranded filaments contacting with each other at the ring side not the cylinder side, resulting in a thickness of 14 nm, double that of the single-stranded filament (7 nm; Figure 3B(d,e)). We analyzed the helical pitches for the double-stranded fibril filaments as the double-stranded fibril filament had a sufficient length of stable helix to cover the pitch, with a clear twist of the ring pattern along the filament axis. Images of the fibril filament cropped from the electron micrographs using the straightening selection tool of the ImageJ software were subjected to Fourier filtering to remove noise (Figure 3C). However, the handedness of the fibril filament could not be concluded as the negative-staining EM images are projections of the object, and the alignment of the filament on the EM grid was not distinguishable. Therefore, we analyzed the isolated fibril filament using QFDE-EM (Figure 3D) as the replica synthesized with platinum covers only one side of the object surface. The structures shared features with those from the negative-staining EM (Figure 3D, Supplementary Figure S1). We succeeded in determining their handedness (Figure 3D(a–f)) and concluded that the double-stranded fibril filament formed a left-handed helix. The half pitch was distributed at 351 ± 33 nm ($n = 50$), which aligns with the results of negative-staining EM (Figure 3E). The agreement of helix pitches in the cell, isolated ribbon, and fibril filament suggests that the fibril filament is a major component of ribbon formation and cell helicity (Table 1).

Three-dimensional reconstruction of the fibril filaments

To clarify the fibril filament from a three-dimensional (3D) viewpoint, a single-particle analysis was performed on negative-staining EM images. The double-stranded fibril filament was not suitable for image averaging, which might be due to the positional variation in the binding of the two filaments (Figure 3, Supplementary Figure S2). Therefore, we sonicated the purified fibril fraction to increase the proportion of single-stranded filament and successfully acquired single-stranded images (Figure 4A). From the selected 11,867 particles with good quality, the 2D-averaged images were classified into three types: (i), (ii), and (iii) (Figure 4A(b)). The initial 3D image was reconstructed using the *ab-initio* 3D function of cisTEM software (Grant et al., 2018), and used as the reference for the subsequent 3D classification (Figure 4A(c)). 3D structures of the fibril filament reconstructed from 11,867 particles using RELION 3.0 revealed three different conformations (i.e., class 1, left-handed mainly straight (49%); class 2, left-handed with curvature (24%); and class 3, right-handed with curvature (27%; Figure 4A(d), Supplementary Figure S3). The class 1 structure reconstituted with rotational symmetry (C2) was not

significantly different from that without symmetry (C1), suggesting that the fibril filament had rotational symmetry without polarity (Supplementary Figure S3). We therefore reconstructed the structures of the fibril filaments with C2 symmetry. The 2D reprojections from these three structures corresponded well with the 2D class averages, indicating the validity of the obtained 3D structures (Supplementary Figure S3). The 3D structure of the fibril filament had repeating elliptical rings with a pitch of 8.7 nm along the filament axis, and the ring size was 11 wide and 6 nm long along the filament. A short backbone cylinder tilted slightly to the right was found to connect the ring units, resulting in a positive curvature (Figure 4A(d)). These characteristics were common to all three classes.

Although the superimposition of class 1 and others showed their structural differences, the positions responsible for the differences could not be identified owing to the low resolution of the structures (Figure 4B). The fibril filaments of all classes were twisted along the filament axis, but with different rotational angles (Supplementary Figure S4). The twisting angles were estimated from the angle averages of the first and fourth units, as 5.9 (left-handed), 7.3 (left-handed), and 9.7 (right-handed) degrees for classes 1, 2, and 3, respectively. The twisting angles were estimated from the subunit numbers in the double-stranded images (Figure 3) for negative-staining and QFDE-EM as 4.9° and 4.7°, respectively. These numbers slightly differed from those obtained from the reconstituted 3D structures, suggesting conformational differences between the curved and straight filament forms. These structures can explain the peak distance observed in the density profile of the isolated ribbon (Figure 2D(c), Supplementary Figure S5).

We proceeded to examine the variation in the ring interval (Figure 4C, Supplementary Figure S6). 2D averaged images were measured for 60 ring intervals. The intervals were 8.86 ± 0.24 nm ($n = 60$) and did not show group separation, suggesting that the intervals do not have clear conformational change, despite some having an elasticity up to 2.7%.

Handedness verified based on the tomography of the QFDE replica

The 3D images reconstituted from negative-staining EM had common features, despite variations in curvature and twist. The reconstructed structures all have rings and cylinders tilted slightly to the right along the filament axis when viewed from the front and back sides, respectively (Figure 4A(d)), indicating that the three classes belong to the same side of mirror images. As the images by negative-staining EM are projections of the objects, the reconstituted structures may mirror images of the real structures. Thereafter, we intended to verify the handedness of the reconstituted structures by EM tomography of the QFDE replica sample (Figure 5); this is because the tomogram cannot be a mirror image (Briegleb et al., 2013; Jensen, 2015).

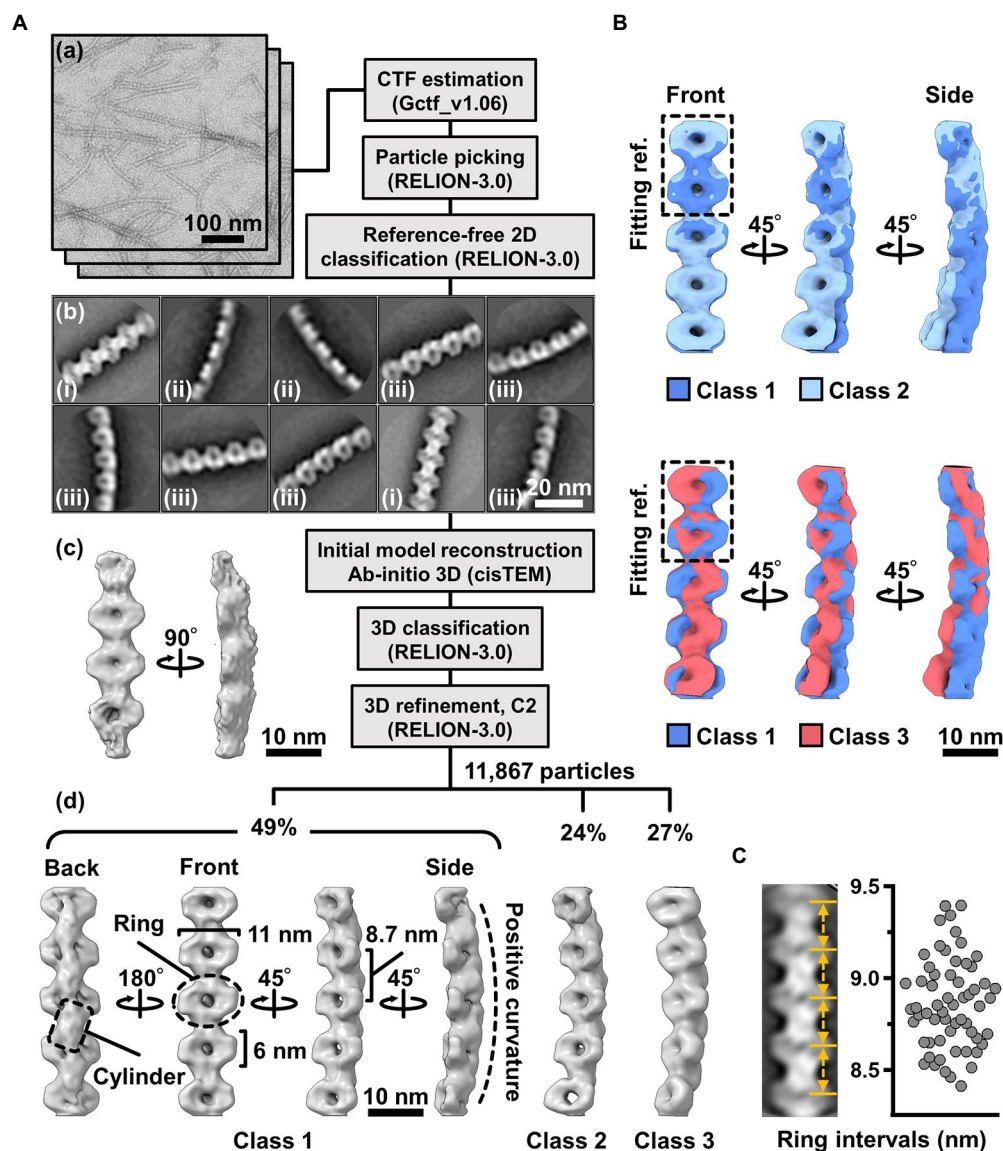


FIGURE 4

Three-dimensional reconstruction of the fibril filaments. (A) Workflow of single particle analysis by negative-staining EM. (a) Field images of single-stranded fibril filaments prepared by sonication. (b) Eight averaged images obtained by a function of 2D classification in RELION software. (c) The initial 3D model generated by a function of *ab-initio* reconstruction in cisTEM software. (d) Three different conformations of the fibril filament reconstituted by a function of 3D refinement in RELION software. (B) Superpose of class 1 (left-handed) and class 2 (left-handed) and class 3 (right-handed) structures. The fitting reference is indicated by a dashed box. (C) Distribution of the ring intervals. Left: Ring intervals in an averaged image with complete rings. Right: Plotted ring intervals.

We made QFDE replicas from the fraction containing single-stranded fibril filaments, acquired images every 1.5° to 50° specimen tilt for both directions, reconstituted tomograms (Supplementary Movie_S4; Figure 5A), and then obtained a structure by averaging 60 subtomograms (Figure 5B). As expected, the resulting filament structure had rings and cylinders. The rings and cylinders were tilted from the filament axis, rising to the right from the horizontal axis by 4–5° and 74–82° when viewed from the front and back, respectively (Figure 5C, Supplementary Figure S7), which align well with the features of structures from negative-staining EM. These

results indicate that the classes of structures from negative-staining EM had the same handedness as the real structures (Figure 5C).

Discussion

Structures of the isolated fibril

The unique swimming of *Spiroplasma* is believed to be caused by the ribbon structure (Kürner et al., 2005; Cohen-Krausz et al.,

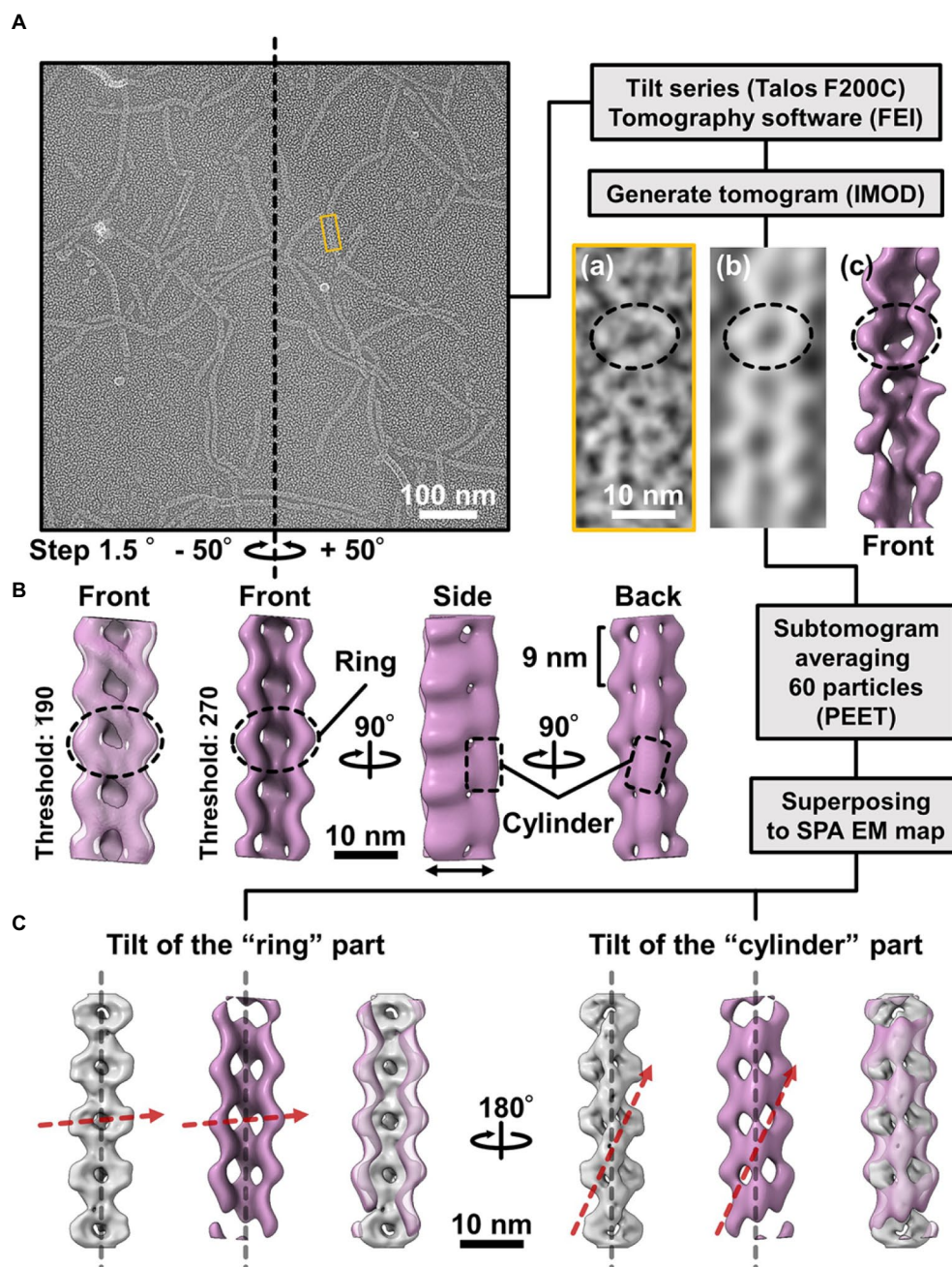


FIGURE 5

Comparison of the 3D structures of the fibril filament reconstructed from QFDE and negative-staining EM. **(A)** Replica image of mainly single-stranded fibril filaments. Left: A field image is shown from a tilt series (Supplementary Movie_S2). Right lower: Magnified images of single fibril filament are shown as a raw image (a), a slice from the tomogram (b), and a subtomogram (c). **(B)** Structure averaged from 60 subtomograms. The leftmost image is presented under different thresholds from other three images. **(C)** Superpose of the 3D structures from single-particle analysis (grey) and subtomogram averaging (magenta). Long axes of ring and cylinder are depicted by broken red arrows. The filament axes were detected by a function "relion_align_symmetry --sym d2" in RELION-3.0.

2011; Harne et al., 2020b; Sasajima and Miyata, 2021). In this study, we isolated filaments of fibrils, the major protein of the ribbon, and revealed the 3D structure of the single-stranded filament at the nanometer scale using EM. Fibril filaments have been isolated for a long time, and their EM images show a

characteristic ring repeat structure with a high contrast (Townsend et al., 1980; Williamson et al., 1991; Trachtenberg and Gilad, 2001; Trachtenberg et al., 2003a; Cohen-Krausz et al., 2011; Liu et al., 2017). However, a nanometer-order three-dimensional fibril filament structure is yet to be revealed. Sonication during the

isolation process was effective in isolating the single-stranded filament, whose uniform structure was advantageous for image averaging (Figure 3). Negative-staining EM was used to reconstruct the structure (Figure 4). However, as this method produces projection images, the handedness of the reconstructed structure may be incorrect. Therefore, we confirmed the handedness of the structure by tomographic analysis of platinum replicas prepared by QFDE-EM (Figure 5). The final structure was a repeating structure of elliptical rings connected by backbone cylinders aligned off-axis with a gentle left-handed helix, which is consistent with that of previous studies. No polarity was observed in the filament structure.

These results raise questions regarding the alignment of the 512 amino acid residues of the fibril protein with the structure and the structure formed by the 1–228 amino acid residues possessing obvious sequence similarity to methylthioadenosine/S-adenosylhomocysteine (MTA/SAH) nucleosidase (Cohen-Krausz et al., 2011; Parveen and Cornell, 2011; Sasajima and Miyata, 2021). These questions will be answered *via* cryo-EM analysis of the single-stranded fibril filaments prepared in this study.

Ribbon structure in the cell

When *Spiroplasma* cells were lysed with a detergent, the ribbon structure appeared to run along the entire length of the cell axis (Figure 1; Trachtenberg and Gilad, 2001). In this study, we isolated ribbons with a length equivalent with the entire length of the cell (Figure 2). These observations suggest that the ribbon is a relatively stable structure rather than a highly dynamic one that disappears in a short time. Furthermore, as the extraction procedure with cholic acid yielded a structure consisting only of fibril filaments (Figure 3), the stable properties of the ribbon are likely to be derived from the fibril filament. The helix of the fibril filament was directly observed in the double-stranded filament (Figure 3). The constant helical pitch of a single strand could not be detected, which may be due to its irregular attachment to the EM grid. The two strands of double-stranded filaments may stabilize the inherent helical character of the filament by combining them. The handedness and pitch observed in the duplexes were left-handed and 351 ± 34 (702 ± 68) nm, respectively, aligning with the helical character of the cells at rest (Figures 1, 3). As previous observations revealed the presence of ribbons in the innermost portion of the cell helix (Kürner et al., 2005; Trachtenberg et al., 2008), the helix of the resting cell should directly reflect the characteristics of the fibril filament.

During swimming, the cell switches its helical form into a right-handed one with a helical pitch similar to the left-handed one (Figure 1). However, we could not find the corresponding right-handed helical structures in the isolated fibril filaments or ribbons. Only class 3 3D image reconstructed from 27% of the negative-staining EM images suggested a right-handed helical structure (Figure 4);

however, a further investigation is needed to conclude that this structure is stable one as the protein can be distorted by sticking to the EM grid in this analysis. These observations suggest that the right-handed helical structure observed in cells during swimming does not originate from another stable fibril filament structure (Figure 4). The helix switch can also be explained by assuming that two types of filaments running parallel to the ribbon are alternately extended and contracted (Kürner et al., 2005; Cohen-Krausz et al., 2011). To test this notion, we examined the distribution of the fibril filament lengths and found that the length distribution had a single peak at 8.86 ± 0.24 nm (Figure 4). Such finding suggests that the fibril filament has only one stable length and does not support a helical switch caused by a length change in the fibril filament.

Role of fibril in the swimming mechanism

The fibril protein is conserved in most *Spiroplasma* species with high amino acid sequence similarity (Ku et al., 2014). However, *Spiroplasma sabaudiense* and *Spiroplasma helicoide* do not contain fibril proteins, despite exhibiting helicity-switching swimming (Harne et al., 2020b). Recently, the expression of two SMreB proteins in the non-swimming synthetic bacterium, syn3.0B, was demonstrated to reproduce cell helicity and helicity-switching swimming (Hutchison et al., 2016; Kiyama et al., 2021). Moreover, the expression of SMreB induced cell helicity and its switching in spherical Mollicutes species (Lartigue et al., 2021), implying that the helix formation of the cell and the force generation for switching are caused by SMreBs. Then, what is the role of fibril filaments in most *Spiroplasma* species? Isolated SMreB binds to fibril filaments (Harne et al., 2020a). Further, our results (Figure 2) support the binding of SMreB to the fibril filaments. These observations suggest that SMreB exerts a force on fibril filaments for swimming. SMreBs might cause helicity-switching swimming, and fibril filaments might be effective at obtaining high energy efficiency and chemotaxis; this is supported by the observation that swimming reconstructed in syn3.0B by SMreBs lacks processivity (Kiyama et al., 2021).

Data availability statement

The original contributions presented in the study are included in the article/Supplementary material, further inquiries can be directed to the corresponding author.

Author contributions

YS and MM designed the experiments. YS performed the experiments. YS, TK, TM, AK, and KN acquired and analyzed the images. YS and MM wrote the manuscript. All authors contributed to the article and approved the submitted version.

Funding

This study was supported by Grants-in-Aid for Scientific Research A (MEXT KAKENHI, Grant Number JP17H01544), JST CREST (Grant Number JPMJCR19S5), the Osaka City University (OCU) Strategic Research Grant 2017 for top priority research to MM, JSPS KAKENHI (Grant Number JP25000013), the Platform Project for Supporting Drug Discovery and Life Science Research (BINDS) from AMED (Grant Number JP19am0101117 and support number 1282), the Cyclic Innovation for Clinical Empowerment (CiCLE) from AMED (Grant Number JP17pc0101020), and JEOL YOKOGUSHI Research Alliance Laboratories of Osaka University to KN.

Acknowledgments

We thank Isil Tulum, Peng Liu, Yuhei O. Tahara, Daichi Takahashi, Hana Kiyama, and Ikuko Fujiwara at the Graduate School of Science, Osaka Metropolitan University, Japan, for their helpful discussions.

References

- Briegleb, A., Pilhofer, M., Mastroratte, D. N., and Jensen, G. J. (2013). The challenge of determining handedness in electron tomography and the use of DNA origami gold nanoparticle helices as molecular standards. *J. Struct. Biol.* 183, 95–98. doi: 10.1016/j.jsb.2013.04.008
- Cohen-Krausz, S., Cabahug, P. C., and Trachtenberg, S. (2011). The monomeric, tetrameric, and fibrillar organization of Fib: the dynamic building block of the bacterial linear motor of *Spiroplasma melliferum* BC3. *J. Mol. Biol.* 410, 194–213. doi: 10.1016/j.jmb.2011.04.067
- Distelhorst, S. L., Jurkovic, D. A., Shi, J., Jensen, G. J., and Balish, M. F. (2017). The variable internal structure of the *Mycoplasma penetrans* attachment organelle revealed by biochemical and microscopic analyses: implications for attachment organelle mechanism and evolution. *J. Bacteriol.* 199:e00069-17. doi: 10.1128/JB.00069-17
- Gasparich, G. E. (2002). *Spiroplasmas*: evolution, adaptation and diversity. *Front. Biosci.* 7, d619–d640. doi: 10.2741/A799
- Grant, T., Rohou, A., and Grigorieff, N. (2018). cisTEM, user-friendly software for single-particle image processing. *elife* 7:e35383. doi: 10.7554/eLife.35383
- Grosjean, H., Breton, M., Sirand-Pugnet, P., Tardy, F., Thiaucourt, F., Citti, C., et al. (2014). Predicting the minimal translation apparatus: lessons from the reductive evolution of mollicutes. *PLoS Genet.* 10:e1004363. doi: 10.1371/journal.pgen.1004363
- Harne, S., Duret, S., Pande, V., Bapat, M., Beven, L., and Gayathri, P. (2020a). MreB5 is a determinant of rod-to-helical transition in the cell-wall-less bacterium *Spiroplasma*. *Curr. Biol.* 30, 4753–4762.e7. doi: 10.1016/j.cub.2020.08.093
- Harne, S., Gayathri, P., and Beven, L. (2020b). Exploring *Spiroplasma* biology: opportunities and challenges. *Front. Microbiol.* 11:589279. doi: 10.3389/fmicb.2020.589279
- Harumoto, T., and Lemaitre, B. (2018). Male-killing toxin in a bacterial symbiont of *Drosophila*. *Nature* 557, 252–255. doi: 10.1038/s41586-018-0086-2
- Heuser, J. E. (2011). The origins and evolution of freeze-etch electron microscopy. *J. Electron Microsc.* 60, S3–S29. doi: 10.1093/jmicro/dfr044
- Hutchison, C. A., Chuang, R. Y., Noskov, V. N., Assad-Garcia, N., Deerinck, T. J., Ellisman, M. H., et al. (2016). Design and synthesis of a minimal bacterial genome. *Science* 351:aad6253. doi: 10.1126/science.aad6253
- Jensen, G. J. (2015). “Getting started in Cryo-EM with professor Grant Jensen.” <https://cryo-em-course.caltech.edu>
- Kawakita, Y., Kinoshita, M., Furukawa, Y., Tulum, I., Tahara, Y. O., Katayama, E., et al. (2016). Structural study of MPN387, an essential protein for gliding motility

Conflict of interest

The authors declare that the research was conducted in the absence of any commercial or financial relationships that could be construed as a potential conflict of interest.

Publisher’s note

All claims expressed in this article are solely those of the authors and do not necessarily represent those of their affiliated organizations, or those of the publisher, the editors and the reviewers. Any product that may be evaluated in this article, or claim that may be made by its manufacturer, is not guaranteed or endorsed by the publisher.

Supplementary material

The supplementary material for this article can be found online at: <https://www.frontiersin.org/articles/10.3389/fmicb.2022.1004601/full#supplementary-material>

- of a human-pathogenic bacterium, *Mycoplasma pneumoniae*. *J. Bacteriol.* 198, 2352–2359. doi: 10.1128/JB.00160-16
- Kiyama, H., Kakizawa, S., Sasajima, Y., Tahara, Y. O., and Miyata, M. (2021). Reconstitution of minimal motility system based on *Spiroplasma* swimming by expressing two bacterial actins in synthetic minimal bacterium. *bioRxiv*. doi: 10.1101/2021.11.16.468548
- Kuo, C., Lo, W. S., and Kuo, C. H. (2014). Molecular evolution of the actin-like MreB protein gene family in wall-less bacteria. *Biochem. Biophys. Res. Commun.* 446, 927–932. doi: 10.1016/j.bbrc.2014.03.039
- Kürner, J., Frangakis, A. S., and Baumeister, W. (2005). Cryo-electron tomography reveals the cytoskeletal structure of *Spiroplasma melliferum*. *Science* 307, 436–438. doi: 10.1126/science.1104031
- Lartigue, C., Lambert, B., Rideau, F., Decossas, M., Hillion, M., Doulez, J.-P., et al. (2021). Tuning spherical cells into kinking helices in wall-less bacteria. *bioRxiv*. doi: 10.1101/2021.11.16.467908
- Liu, P., Zheng, H., Meng, Q., Terahara, N., Gu, W., Wang, S., et al. (2017). Chemotaxis without conventional two-component system, based on cell polarity and aerobic conditions in helicity-switching swimming of *Spiroplasma eriocheiris*. *Front. Microbiol.* 8:58. doi: 10.3389/fmicb.2017.00058
- Miyata, M. (2010). Unique centipede mechanism of *Mycoplasma* gliding. *Annu. Rev. Microbiol.* 64, 519–537. doi: 10.1146/annurev.micro.112408.134116
- Miyata, M., and Hamaguchi, T. (2016a). Integrated information and prospects for gliding mechanism of the pathogenic bacterium *Mycoplasma pneumoniae*. *Front. Microbiol.* 7:960. doi: 10.3389/fmicb.2016.00960
- Miyata, M., and Hamaguchi, T. (2016b). Prospects for the gliding mechanism of *mycoplasma mobile*. *Curr. Opin. Microbiol.* 29, 15–21. doi: 10.1016/j.mib.2015.08.010
- Miyata, M., Robinson, R. C., Uyeda, T. Q. P., Fukumori, Y., Fukushima, S. I., Haruta, S., et al. (2020). Tree of motility: a proposed history of motility systems in the tree of life. *Genes Cells* 25, 6–21. doi: 10.1111/gtc.12737
- Nakane, D., and Miyata, M. (2007). Cytoskeletal “jellyfish” structure of *Mycoplasma mobile*. *Proc. Natl. Acad. Sci. U. S. A.* 104, 19518–19523. doi: 10.1073/pnas.0704280104
- Parveen, N., and Cornell, K. A. (2011). Methylthioadenosine/S-adenosylhomocysteine nucleosidase, a critical enzyme for bacterial metabolism. *Mol. Microbiol.* 79, 7–20. doi: 10.1111/j.1365-2958.2010.07455.x
- Razin, S., and Hayflick, L. (2010). Highlights of mycoplasma research: an historical perspective. *Biologicals* 38, 183–190. doi: 10.1016/j.biologics.2009.11.008

- Razin, S., Yogev, D., and Naot, Y. (1998). Molecular biology and pathogenicity of mycoplasmas. *Microbiol. Mol. Biol. Rev.* 62, 1094–1156. doi: 10.1128/MMBR.62.4.1094-1156.1998
- Relich, R. F., Friedberg, A. J., and Balish, M. F. (2009). Novel cellular organization in a gliding mycoplasma, *Mycoplasma insons*. *J. Bacteriol.* 191, 5312–5314. doi: 10.1128/JB.00474-09
- Sasajima, Y., and Miyata, M. (2021). Prospects for the mechanism of *Spiroplasma* swimming. *Front. Microbiol.* 12:706426. doi: 10.3389/fmicb.2021.706426
- Shaevitz, J. W., Lee, J. Y., and Fletcher, D. A. (2005). *Spiroplasma* swim by a processive change in body helicity. *Cells* 122, 941–945. doi: 10.1016/j.cell.2005.07.004
- Shi, H., Bratton, B. P., Gitai, Z., and Huang, K. C. (2018). How to build a bacterial cell: MreB as the foreman of *E. coli* construction. *Cells* 172, 1294–1305. doi: 10.1016/j.cell.2018.02.050
- Takahashi, D., Fujiwara, I., and Miyata, M. (2020). Phylogenetic origin and sequence features of MreB from the wall-less swimming bacteria *Spiroplasma*. *Biochem. Biophys. Res. Commun.* 533, 638–644. doi: 10.1016/j.bbrc.2020.09.060
- Terahara, N., Tulum, I., and Miyata, M. (2017). Transformation of crustacean pathogenic bacterium *Spiroplasma eriocheiris* and expression of yellow fluorescent protein. *Biochem. Biophys. Res. Commun.* 487, 488–493. doi: 10.1016/j.bbrc.2017.03.144
- Townsend, R., Archer, D. B., and Plaskitt, K. A. (1980). Purification and preliminary characterization of *Spiroplasma* fibrils. *J. Bacteriol.* 142, 694–700. doi: 10.1128/jb.142.2.694-700.1980
- Toyonaga, T., Kato, T., Kawamoto, A., Kadera, N., Hamaguchi, T., Tahara, Y. O., et al. (2021). Chained structure of dimeric F₁-like ATPase in *Mycoplasma mobile* gliding machinery. *MBio* 12:e0141421. doi: 10.1128/mBio.01414-21
- Trachtenberg, S., Andrews, S. B., and Leapman, R. D. (2003a). Mass distribution and spatial organization of the linear bacterial motor of *Spiroplasma citri* R8A2. *J. Bacteriol.* 185, 1987–1994. doi: 10.1128/JB.185.6.1987-1994.2003
- Trachtenberg, S., Dorward, L. M., Speransky, V. V., Jaffe, H., Andrews, S. B., and Leapman, R. D. (2008). Structure of the cytoskeleton of *Spiroplasma melliferum* BC3 and its interactions with the cell membrane. *J. Mol. Biol.* 378, 778–789. doi: 10.1016/j.jmb.2008.02.020
- Trachtenberg, S., and Gilad, R. (2001). A bacterial linear motor: cellular and molecular organization of the contractile cytoskeleton of the helical bacterium *Spiroplasma melliferum* BC3. *Mol. Microbiol.* 41, 827–848. doi: 10.1046/j.1365-2958.2001.02527.x
- Trachtenberg, S., Gilad, R., and Geffen, N. (2003b). The bacterial linear motor of *Spiroplasma melliferum* BC3: from single molecules to swimming cells. *Mol. Microbiol.* 47, 671–697. doi: 10.1046/j.1365-2958.2003.t01-1-03200.x
- Tulum, I., Tahara, Y. O., and Miyata, M. (2019). Peptidoglycan layer and disruption processes in *Bacillus subtilis* cells visualized using quick-freeze, deep-etch electron microscopy. *Microscopy (Oxf)* 68, 441–449. doi: 10.1093/jmicro/dfz033
- Uenoyama, A., Kusumoto, A., and Miyata, M. (2004). Identification of a 349-kilodalton protein (Gli349) responsible for cytoadherence and glass binding during gliding of *Mycoplasma mobile*. *J. Bacteriol.* 186, 1537–1545. doi: 10.1128/JB.186.5.1537-1545.2004
- Wada, H., and Netz, R. R. (2009). Hydrodynamics of helical-shaped bacterial motility. *Phys. Rev. E Stat. Nonlinear Soft Matter Phys.* 80:021921. doi: 10.1103/PhysRevE.80.021921
- Williamson, D. L., Renaudin, J., and Bove, J. M. (1991). Nucleotide sequence of the *Spiroplasma citri* fibril protein gene. *J. Bacteriol.* 173, 4353–4362. doi: 10.1128/jb.173.14.4353-4362.1991
- Zhang, K. (2016). Gctf: real-time CTF determination and correction. *J. Struct. Biol.* 193, 1–12. doi: 10.1016/j.jsb.2015.11.003
- Zivanov, J., Nakane, T., Forsberg, B. O., Kimanius, D., Hagen, W. J., Lindahl, E., et al. (2018). New tools for automated high-resolution cryo-EM structure determination in RELION-3. *elife* 7:e42166. doi: 10.7554/eLife.42166



OPEN ACCESS

EDITED BY

Meghan May,
University of New England, United states

REVIEWED BY

Yuefeng Chu,
Chinese Academy of Agricultural Sciences,
China
Bidyut Mohapatra,
The University of the West Indies, Barbados
Remco Dijkman,
Royal GD,
Netherlands

*CORRESPONDENCE

Sara M. Klose
sara.klose@unimelb.edu.au

SPECIALTY SECTION

This article was submitted to
Infectious Agents and Disease,
a section of the journal
Frontiers in Microbiology

RECEIVED 12 September 2022

ACCEPTED 25 October 2022

PUBLISHED 25 November 2022

CITATION

Klose SM, Omotainse OS, Zare S, Vaz PK,
Armat P, Shil P, Wawegama N, Kanci
Condello A, O'Rourke D, Disint JF,
Andrews DM, Underwood GJ, Morrow CJ,
Marenda MS and
Noormohammadi AH (2022) Virulence
factors of *Mycoplasma synoviae*: Three
genes influencing colonization,
immunogenicity, and transmissibility.
Front. Microbiol. 13:1042212.
doi: 10.3389/fmicb.2022.1042212

COPYRIGHT

© 2022 Klose, Omotainse, Zare, Vaz,
Armat, Shil, Wawegama, Kanci Condello,
O'Rourke, Disint, Andrews, Underwood,
Morrow, Marenda and Noormohammadi.
This is an open-access article distributed
under the terms of the [Creative Commons
Attribution License \(CC BY\)](https://creativecommons.org/licenses/by/4.0/). The use,
distribution or reproduction in other
forums is permitted, provided the original
author(s) and the copyright owner(s) are
credited and that the original publication in
this journal is cited, in accordance with
accepted academic practice. No use,
distribution or reproduction is permitted
which does not comply with these terms.

Virulence factors of *Mycoplasma synoviae*: Three genes influencing colonization, immunogenicity, and transmissibility

Sara M. Klose^{1*}, Oluwadamilola S. Omotainse¹, Sahar Zare¹, Paola K. Vaz², Parisa Armat², Pollob Shil¹, Nadeeka Wawegama², Anna Kanci Condello², Denise O'Rourke¹, Jillian F. Disint¹, Daniel M. Andrews³, Gregory J. Underwood³, Chris J. Morrow^{2,3}, Marc S. Marenda¹ and Amir H. Noormohammadi¹

¹Asia-Pacific Centre for Animal Health, Faculty of Veterinary and Agricultural Sciences, Melbourne Veterinary School, The University of Melbourne, Werribee, VIC, Australia, ²Asia-Pacific Centre for Animal Health, Faculty of Veterinary and Agricultural Sciences, Melbourne Veterinary School, The University of Melbourne, Parkville, VIC, Australia, ³Bioproperties Pty Ltd., Ringwood, VIC, Australia

Infections caused by *Mycoplasma synoviae* are major welfare and economic concerns in poultry industries worldwide. These infections cause chronic respiratory disease and/or synovitis in chickens and turkeys leading to reduced production and increased mortality rates. The live attenuated vaccine strain MS-H (Vaxsafe® MS), commonly used for protection against *M. synoviae* infection in many countries, contains 32 single nucleotide variations compared to its wildtype parent strain, 86079/7NS. Genomic analysis of vaccine strains reisolated from flocks following the administration of MS-H has identified reversions to the original 86079/7NS sequence in the *obgE*, *oppF* and *gapdh* genes. Here, three MS-H field reisolates containing the 86079/7NS genotype in *obgE* (AS2), *obgE* and *oppF* (AB1), and *obgE*, *oppF* and *gapdh* (TS4), as well as the vaccine MS-H and the parental strain 86079/7NS were experimentally inoculated to chickens. The strains were assessed for their ability to infect and elicit immune responses in the recipient chickens, as well as in naïve in-contact chickens. Despite the loss of temperature sensitivity phenotype and colonization of the reisolates in the lower respiratory tract, there was no significant differences detected in the microscopic mucosal thickness of the middle or lower trachea of the inoculated chickens. Concurrent reversions in ObgE, OppF and GAPDH proteins were associated with higher gross air sac lesion scores and increased microscopic upper-tracheal mucosal thickness in chickens directly inoculated with the reisolates following intratracheal administration of a virulent strain of infectious bronchitis virus. The gross air sac lesions of the chickens in-contact with those inoculated with reisolates were not significantly different to those of chickens in-contact with MS-H inoculated chickens, suggesting that horizontal transmission of the reisolates in the poultry flock will not lead to higher pathogenicity or clinical signs. These results suggest a significant role of GAPDH and/or cumulative effect

of *ObgE*, *OppF* and *GAPDH* on *M. synoviae* pathogenicity. Future experiments will be required to investigate the effect of single mutations in *gapdh* or *oppF* gene on pathogenicity of *M. synoviae*.

KEYWORDS

Mycoplasma, live vaccine, pathogenicity, immunogenicity, temperature sensitivity

Introduction

Mycoplasma synoviae is an important pathogen of commercial poultry affecting multiple organs in chickens and turkeys and imposing welfare concerns due to respiratory illness and lameness (Ferguson-Noel et al., 2020; Yadav et al., 2021). The infections caused by this bacterium are responsible for significant economic loss to the intensive poultry industry due to reduced egg production and downgrading of egg quality (Nascimento et al., 2005; Feberwee et al., 2009). The Vaxsafe® MS (MS-H) vaccine was developed by chemical mutagenesis of the *M. synoviae* field strain 86079/7NS (Morrow et al., 1998). While the virulent strain 86079/7NS, hereafter referred to as 7NS, can grow at temperatures up to 39.5°C, the MS-H strain is temperature-sensitive (*ts*⁺) and unable to grow optimally at 39.5°C (Morrow et al., 1998). This property is the basis for the phenotypic assessment of *M. synoviae* field isolates obtained from vaccinated flocks. It is hypothesized that *ts*⁺ mycoplasma vaccines colonize the upper respiratory tract, which has a lower temperature than the core body temperature, and induce an immune response without invading or causing inflammation in the lower respiratory system which is at a higher temperature (Whithear et al., 1990). However, occasional detection of *ts*⁻ MS-H reisolates from vaccinated chickens in the absence of disease suggested that attenuation of MS-H is not exclusively due to its *ts*⁺ phenotype (Morrow, 1991; Noormohammadi et al., 2003; Nicholas et al., 2009). The discovery of 32 single nucleotide polymorphisms (SNPs) between the genomes of MS-H and its parent strain (Zhu et al., 2019) has given insights on the basis of virulence attenuation in the vaccine strain. Unusually high systemic antibody responses to *M. synoviae* in vaccinated flocks have been reported, and several MS-H derivatives have been isolated from these farms. The genomes of these reisolates occasionally carry reversions to the 7NS genotype in the genes *obgE*, *oppF* and *gapdh*, along with diverse repertoires of other sequence variations (Kordafshari et al., 2020). These observations raised the question of the genetic, phenotypic, and immunogenic stability of MS-H in field conditions. In the present study, three *M. synoviae* isolates recovered from vaccinated flocks were sequenced entirely and their genomes were compared to those of strains 7NS and MS-H. This analysis identified three loci carrying reversions to the 7NS genotype, while the rest of the genome retained the MS-H sequence. One isolate contained a single reversion in the *obgE* gene, another isolate carried an additional reversion in the *oppF* gene, and the last isolate had an

additional reversion in the *gapdh* gene, resulting in three different genotypes representing a progressive accumulation of these three sequence variations. To evaluate the effect of these sequence variations *in vivo*, and to provide insight into the behavior of the live vaccine in poultry farms, specific pathogen free (SPF) chickens were experimentally infected with each of the three MS-H reisolates carrying variation(s) in these loci. The inoculated and in-contact chickens were monitored for the presence of live *M. synoviae*, lesions, and seroconversion.

Materials and methods

Culture medium

The *M. synoviae* cultures were grown in mycoplasma broth (MB) containing 10% swine serum (Sigma-Australia) and 0.01% nicotinamide adenine dinucleotide (Sigma-Australia) based on the formulation of Frey's medium with minor modification (Frey, 1968; Jones et al., 2006). The cultures were incubated at 37°C until late logarithmic phase (approximately pH 6.8; Shahid et al., 2013a).

Mycoplasma strains

The wild-type parent 7NS strain was available in our laboratory and its origin has been described previously (Morrow, 1991). The MS-H working seed used in commercial production of the Vaxsafe® MS vaccine, was provided by Bioproperties, Pty. Ltd, Melbourne, Australia. The AS2, AB1, and TS4 reisolates were collected from the choanal cleft of commercial layer chickens from different Australian poultry farms, 11, 28, and 28 weeks after vaccination with Vaxsafe® MS, respectively (Jones, 2007). For DNA extraction and whole genome sequencing, cultures were thawed and 200 µL were inoculated in 40 mL MB and incubated at 37°C until late logarithmic phase.

Illumina sequencing and variation assessment

An aliquot of each re isolate was grown in 40 mL MB and incubated at 37°C until late logarithmic phase. Cells were collected from the culture by centrifugation at 10,000 ×g for 20 min at 4°C

followed by two steps of washing with 1 mL PBS. The DNA was extracted using Qiagen's DNeasy Blood and tissue kit and the concentration and quality of the extracted DNA was determined using Qubit and Nanodrop, respectively. In the next step, 100 ng of extracted DNA was used to prepare sequencing libraries using Illumina's Nextera Flex DNA library prep kit. Sequencing was performed on the Miseq platforms using paired end 300 bp reads at the Charles River Laboratories, Victoria, Australia. The Illumina short-reads were processed using Trim Galore v0.6.6 (Krueger, 2015) to trim bases below Phred quality 25 and remove the Nextera adapter sequences, followed by confirmation of the quality of the filtered reads using FastQC v0.11.9 (Andrews, 2010). The reads were aligned to the MS-H sequence (Genbank accession number CP021129) for SNP and insertion/deletion (indel) analyses using Snippy v4.6.0 (Seemann, 2015). The key parameters of variant calling by snippy included a minimum number of 10 reads coverage to consider variant calling, and at least 5% of those reads differing from the reference to call a variation. The highly repetitive, variable, and similar regions of the genomes such as the *vlhA* gene and pseudogenes, IS1634 family transposase, and type III restriction endonuclease subunit M regions were excluded from variation assessment.

Nanopore sequencing and genome assembly

The cells were collected and washed as described above. The DNA was extracted using Promega Wizard® HMW DNA Purification Kit, the concentration and quality of the extracted DNA was determined using Qubit and Implen, respectively. In the next step, 400 ng of extracted DNA was used to prepare sequencing libraries using Oxford Nanopore Technology (ONT) Rapid Barcoding (SQK-RBK004) kit. Sequencing was performed on a MinION MK-I device fitted with a FLO-MIN106 flow cell (R9.5 chemistry) and processed using the ONT high accuracy Guppy basecaller v6.1.7. The Nanopore reads were processed using Guppy barcoder v6.1.7 to remove the barcodes and then filtered using NanoFilt v2.6.0 to include only the reads with a minimum length of 1000 bp and quality score of 12 (De Coster et al., 2018). The filtered Nanopore reads were *de novo* assembled using Flye v2.9 (Kolmogorov et al., 2019). The long-read assembly was then polished based on the Illumina short reads using Polypolish v0.5.0 (Wick and Holt, 2022). The polished long-read assembly was used alongside with the long and short reads for hybrid *de novo* assembly using Unicycler v0.4.9b (Wick et al., 2017). To confirm the accuracy of the assembly, short and long reads were mapped to the assembled genome using Geneious Mapper with medium sensitivity in Geneious Prime v2021.1.1 software.

Titration of the cultures used in chicken inoculation

The strains/reisolates were recovered from -70°C by 1:20 dilution in fresh MB medium and incubated at 37°C for 18 h,

followed by a 1:10 dilution in fresh MB medium to make a final volume of 100 mL. The cultures were incubated at 37°C until reaching the mid-logarithmic phase of growth. The starting cultures were diluted in a final volume of 100 mL so that all contained similar titres. An aliquot of each culture was removed prior to aerosolisation to estimate the viable count of the cultures using the most probable number (MPN) method by serial dilution in MB in 96-well plates (Thermo Fisher Scientific). The color change in the medium after 2 weeks of incubation, indicating growth of the bacteria, was used to determine the MPN of mycoplasmas present in each of the inocula (Meynell and Meynell, 1970).

Temperature sensitivity phenotyping

The temperature-sensitive (*ts*⁺) phenotype of cultures was determined by titration and incubation at permissive (33°C) and non-permissive (39.5°C) temperatures, as described previously (Morrow et al., 1998). Briefly, the strains/reisolates were recovered from -70°C by 1:10 dilution in fresh MB medium and incubated at 33°C for 18 h, followed by serial dilution in MB in four 96-well plates (Thermo Fisher Scientific), and incubation of duplicate trays at 33°C and 39.5°C for 2 weeks. The titres of strains/reisolates at different temperature was determined as described above. Temperature sensitive phenotype was defined by observation of decrease in titre of more than 10^3 CCU/mL when grown at 39.5°C compared to that of 33°C (Nonomura and Imada, 1982).

Inoculation and exposure of chickens

All procedures involving animals were reviewed and approved by the University of Melbourne Animal Ethics Committee under approval number 21064. A total of 120 four-week-old SPF chickens were hatched from eggs supplied by Australian SPF Services (Woodend, Victoria, Australia) at the animal experimentation facilities of the Asia-Pacific Centre for Animal Health (APCAH). They were randomly allocated into six groups of 20 chickens and housed in separate High Efficiency Particulate Air (HEPA) filtered isolator unit under negative pressure, with feed and water provided *ad libitum* (Figure 1). The *M. synoviae* cultures were grown *in vitro* to mid-logarithmic phase prior to aerosolisation as described above. A virulent Australian field strain of infectious bronchitis virus (IBV) strain V1/71 (Ignjatovic et al., 2002), was administered intratracheally ($7.9 \times 10^{3.5}$ EID₅₀/mL in a final volume of 200 μL per chicken) to chickens immediately prior to inoculation with each *M. synoviae* strains/reisolates as described previously (Markham et al., 1998). The chickens were inoculated with 32 to 36 mL of MS-H, AS2, AB1, TS4 and 7NS strain containing 1.18 to 3.66×10^7 color changing units (CCU) per milliliter (Supplementary Table S2) by aerosolisation of 100 mL cultures using compressed air into a purpose-built infection chamber for 40 min (Kanci et al., 2017). One group of chickens was inoculated with sterile MB media by

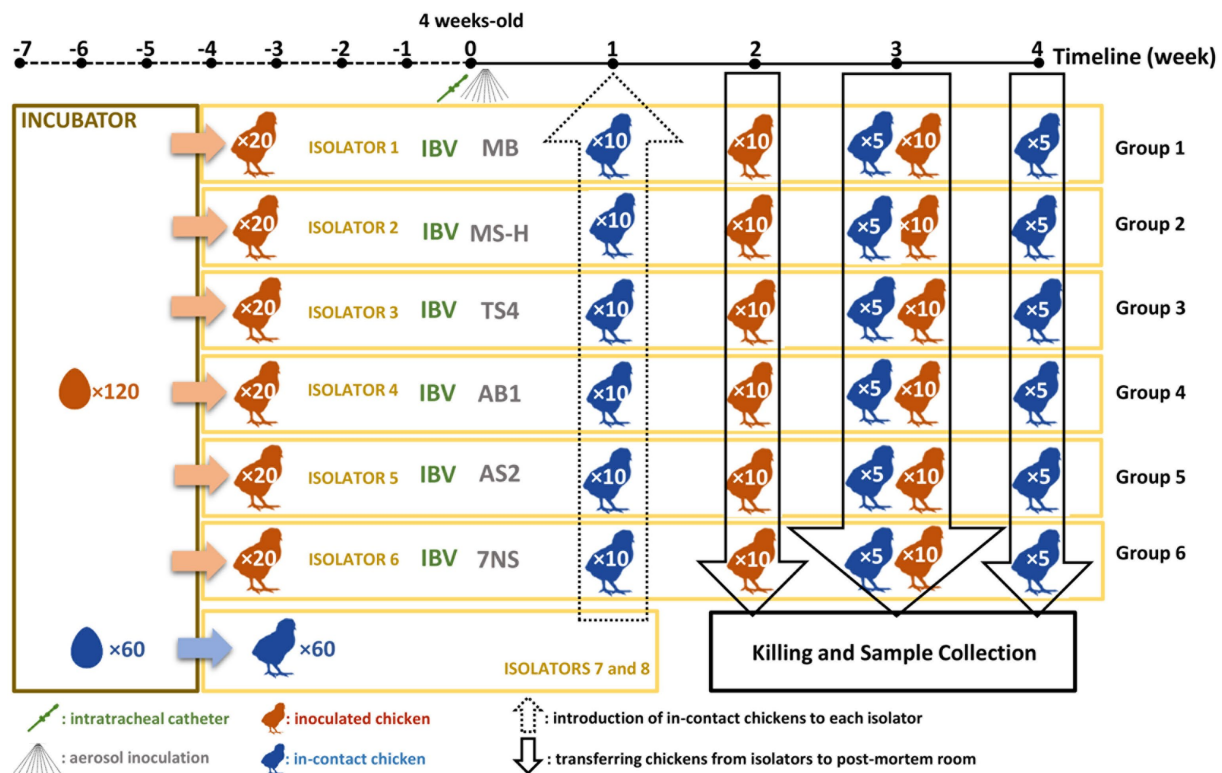


FIGURE 1

Schematic figure of the chicken experiment. A total number of 180 specific pathogen free (SPF) chickens were hatched. A total of 120 chickens (test chickens) were randomly divided into 6 isolators, while 60 in-contact chickens were randomly allocated into 3 separate isolators. At the age of 4-week, the test chickens inoculated with test substances. One week later, the in-contact chickens were moved into the test isolators (10 chickens per isolator). A total number of 60 chickens (10 from each group) will then be humanely killed 2 weeks later. After one more week, the rest of the test chickens (10 per group) as well as 5 in-contact chickens per group were humanely killed. One week later, the rest of the in-contact chickens (5 per group) were humanely killed.

aerosol and IBV by intratracheal route, as a negative *M. synoviae* control. One week after inoculation, 10 uninoculated (in-contact) 5-week-old SPF chickens were placed into each isolator (Figure 1).

Assessment of pathogenicity

Ten randomly selected inoculated chickens from each group were humanely killed and necropsied at 6 weeks of age (2 weeks post inoculation; WPI), and the remaining ten inoculated chickens were humanely killed and necropsied at 7 weeks of age (3 WPI). Five randomly selected in-contact chickens were humanely killed and necropsied at 7 weeks of age (2 weeks post exposure, WPE), and the remaining five test chickens were humanely killed and necropsied at 7 weeks of age (3 WPE). Thoracic and abdominal air sac lesions were scored grossly for severity as described previously (Noormohammadi et al., 2003). A cumulative lesion score for each chicken was determined by combining the individual scores given to each anatomically distinct air sac on a scale of 0–3 (with a maximum score of 18 for a chicken if all six air sacs were given a score of 3). The overall lesion scores were compared using the Dunn's

corrected Kruskal–Wallis test, with $P < 0.01$ considered significant. The tissues collected from upper, middle, and lower trachea were processed and stained with hematoxylin and eosin for histopathology examination as described previously (Omotainse et al., 2022). The tracheal mucosal thickness was measured at upper, middle, and lower trachea using a graticule lens at a magnification of 400X at six equidistant points. An average thickness was calculated from these three levels as well. The Tukey's corrected 2-way ANOVA test was used to compare the thickness of tracheal mucosa with $P < 0.01$ considered significant.

Serology

Serum samples were obtained from blood clot in heart chambers during post-mortem examination and stored at -20°C for future enzyme-linked immunosorbent assay (ELISA). An in-house recombinant MSPB ELISA was used to measure the systemic antibody responses against the *M. synoviae* strains/reisolates (Noormohammadi et al., 1999). The means of the absorbance obtained from duplicated serum samples were

interpolated from a standard curve using a *M. synoviae* positive serum to determine the relative antibody units. The Tukey's corrected 2-way ANOVA test was used to compare the relative antibody units with $P < 0.01$ considered significant. Three-Sigma limit (three standard deviations from mean) of relative antibody unit values in known negative group was used to calculate a cut-off value. Sera with relative antibody unit values above the cut-off value were considered positive. Two-tailed Fisher's Exact test was used to compare the seropositivity rates with $P < 0.01$ considered significant.

Reisolation of *Mycoplasma synoviae* from chickens

Swabs taken from upper trachea, lower trachea, air sacs, spleen or kidney were used to inoculate MB, which was then incubated at 37°C and examined daily for an acidic color change indicative of mycoplasma growth. Colonization rates were determined from the number of cultures showing color change compared to total number of cultures (presented as percentage). Cultures with no color change after 3 weeks incubation were considered as lack of colonization of the strain/reisolate in that anatomic region. Two-tailed Fisher's Exact test was used to compare the reisolation rates with $P < 0.01$ considered significant.

Statistical analysis

The statistical analyses for all the experiments were performed using GraphPad Prism (v9.2.0 for Windows). Specific tests used for different criteria have been described in relevant sections above.

Results

One to three loci reverted to a parental genotype in MS-H reisolates, while 29/32 sequence variations associated with the vaccine strain were conserved

The genomes of the strains AS2, AB1 and TS4, which were all reisolated from vaccinated poultry farms, were nearly identical to the sequence of the MS-H vaccine. Only three reversions into a 7NS genotype were identified in these reisolates, as follows: (1) A/G SNP at nucleotide position 193771, resulting in amino acid change from Arginine to Glycine at position 123 of the ObgE GTPase coding sequence; (2) T insertion at nucleotide position 397777, resulting in frameshift at position 156 of the OppF ATP-binding cassette (ABC) transporter coding sequence; and (3) A/G SNP at nucleotide position 296526 resulting in amino acid change from Lysine to Arginine at position 306 of the Glyceraldehyde-3-phosphate dehydrogenase (GAPDH) coding sequence. The occurrence and

distribution of these three reversions to a 7NS genotype were strain-dependent. Reisolate AS2 (GenBank accession number CP103982) contained a variation in the *obgE* gene. Reisolate AB1 (GenBank accession number CP103981) contained variations in the *obgE* and *oppF* genes. Reisolate TS4 (GenBank accession number CP103980) contained variations in the *obgE*, *oppF* and *gapdh* genes (Table 1).

All three MS-H field reisolates had *ts* phenotype consistent with that of 7NS

The viable cell counts of the cultures at permissive (33°C) and non-permissive (39.5°C) temperatures were measured (Table 2). The 7NS, AS2, AB1, TS4 titres at 39.5°C did not show any fold change above 10^1 CCU/mL when compared to the titres at 33°C, reflecting *ts*⁻ phenotype. However, MS-H showed a 2.07×10^5 CCU/mL decline in the titre at 39.5°C compared to 33°C, reflecting its *ts*⁺ phenotype.

In-contact chickens from the groups inoculated with reisolates had high humoral antibody responses

Means and standard deviations of relative antibody units against MSPB at 2- and 3-week post inoculation, and 2- and 3-week post exposure of the in-contact chickens are shown in Supplementary Table S3. All the chickens inoculated with the TS4 reisolate showed significant higher seropositivity compared to the negative control (Table 3). At 3-week post inoculation, the AB1 and 7NS inoculated chickens showed significant higher seropositivity compared to the negative control. The seropositivity of the in-contact chickens after 3-week contact with chickens inoculated with AS2 was significantly higher than the negative control (Table 3).

The MS-H reisolates colonised the trachea of most inoculated chickens

The MS-H strain could not be recovered from the upper trachea, lower trachea, air sacs, spleen or kidney of the MS-H inoculated chickens and the in-contact chickens (Table 4). None of the strains or reisolates were reisolated from kidney or spleen of any of the inoculated chickens. In comparison to MS-H, the strain AS2 was recovered significantly higher from the upper trachea of inoculated chickens. The reisolate AB1 was recovered significantly higher than MS-H from upper trachea of inoculated chickens 3-week post inoculation. At 2-week post inoculation, the TS4 reisolate was recovered significantly higher than MS-H from the upper trachea of inoculated chickens 2-week post inoculation, as well as upper and lower trachea of inoculated chickens 3-week post inoculation.

TABLE 1 Comparison of genome sequences of the MS-H reisolates to those of MS-H and 7NS (excluding the repetitive and variable regions).

Nucleotide position*	86079/7NS	UoM_MS-H	AS2	AB1	TS4	Protein/Region	Amino acid change*
14181	G	A	A	A	A	tRNA methyltransferase	-
36932	A	T	T	T	T	Non-coding region	-
61685	G	A	A	A	A	Topoisomerase IV subunit A	-
62874	G	A	A	A	A	Excinuclease ABC subunit B	-
67028	G	A	A	A	A	tRNA-Trp	-
104704	G	A	A	A	A	Non-coding region	-
107765	G	A	A	A	A	Multiple sugar ABC transporter	-
193771	G	A	G	G	G	GTP-binding protein, ObgE	Arg123Gly
201094	G	A	A	A	A	p80-related protein	-
203205	C	A	A	A	A	Non-coding region	-
242451	G	A	A	A	A	Glyceraldehyde-3-phosphate dehydrogenase, GAPDH	-
296526	G	A	A	A	G	Glyceraldehyde-3-phosphate dehydrogenase, GAPDH	Lys306Arg
352952	G	A	A	A	A	VACB-like ribonuclease II	-
389629	G	A	A	A	A	Aspartate-ammonia ligase	-
397777	T	—	—	T	T	ABC transporter, OppF	Asn156fs
433343	G	A	A	A	A	Alanyl-tRNA synthetase	-
438657	G	A	A	A	A	Triacylglycerol lipase	-
481287	G	A	A	A	A	Haemolysin C	-
498421	T	C	C	C	C	Histidyl-tRNA synthetase	-
502827	TA	—	—	—	—	Non-coding region	-
522899	G	A	A	A	A	Hypothetical protein	-
563391	G	A	A	A	A	Hexosephosphate transport protein	-
567729	C	A	A	A	A	DNA-directed RNA polymerase beta	-
584838	G	A	A	A	A	Hypothetical protein	-
615741	G	A	A	A	A	Potassium uptake protein, KtrB	-
628272	G	A	A	A	A	DNA polymerase III alpha	-
679814	G	A	A	A	A	Cation-transporting P-type ATPase	-
686265	G	A	A	A	A	Non-coding region	-
716623	G	A	A	A	A	Hypothetical protein	-
737180	G	A	A	A	A	Hypothetical protein	-
780237	AT	—	—	—	—	Non-coding region	-
794057	G	A	A	A	A	Uridylate kinase	-

*Nucleotide position and amino acid change corresponding to the UoM_MS-H genome and amino acid sequences (Genbank accession number CP021129); fs: frame shift.

Gross air sac lesion scores of the reisolate in-contact chickens were not significantly different to those of the chickens in-contact with MS-H inoculated chickens

Median and range of cumulative air sac scores for each group are shown in [Supplementary Table S1](#). While there were only minor lesions observed in the in-contact chickens from the groups that received the MS-H vaccine or the farm reisolates, the in-contact chickens exposed to 7NS-inoculated chickens contained more severe gross air sac lesions (range: 0–11) 3-week post exposure ([Figure 2](#)). At 2-week post inoculation, the chickens from the groups inoculated with AS2 and 7NS showed air sac lesions with a median score significantly ($p < 0.01$) higher than the negative control group ([Figure 2](#)). However, the median air sacs

lesion scores of chickens directly inoculated with AS2, AB1, TS4, and 7NS were not significantly different to those of MS-H inoculated chickens 3 weeks after inoculation.

No significant differences were observed in mucosal thickness of lower or middle trachea of the inoculated chickens

The tracheal mucosal thickness was measured for the chickens inoculated with different strains or reisolates. Means and standard deviations for mucosal thickness for upper, lower, and middle trachea for each group are shown in [Table 5](#). No statistically significant differences were found between groups at lower and middle trachea either 2- or 3-week post inoculation. The mucosal thickness at upper trachea of the chickens inoculated with the TS4

reisolate were significantly ($p < 0.01$) higher than all other groups at 2- and 3-week post inoculation (Supplementary Figure S1). With mucosal thicknesses from three levels of trachea (upper,

TABLE 2 Viable counts of *Mycoplasma synoviae* strains/reisolates (CCU/mL) in this study at permissive (33°C) and non-permissive (39.5°C) temperatures.

	33°C	39.5°C	Log change	Phenotype
MS-H	2.4×10^7 (1×10^7)	1.15×10^2 (1.88×10^1)	7.38	<i>ts</i> ⁺
AS2	4.93×10^7 (3.08×10^7)	3.46×10^7 (1×10^7)	0	<i>ts</i> ⁻
AB1	6.66×10^7 (0)	2.4×10^7 (1×10^7)	0	<i>ts</i> ⁻
TS4	7.99×10^7 (1.88×10^7)	2.69×10^7 (5.97×10^6)	0	<i>ts</i> ⁻
7NS	6.97×10^6 (3.96×10^7)	4.88×10^6 (2.51×10^7)	0	<i>ts</i> ⁻

Data are presented as means (standard deviation). Log change denotes the difference between the calculated viable counts measured at 33°C and the viable counts measured at 39.5°C. CCU, color changing units. *ts*⁺, temperature-sensitive. *ts*⁻, non-temperature-sensitive.

TABLE 3 Seropositivity of the *M. synoviae* cultures 2- and 3-week after aerosol inoculation of SPF chickens with various strains or reisolates of *M. synoviae* following intratracheal inoculation with a virulent strain of IBV, and 2- and 3-week after exposure of in-contact chickens with the inoculated chickens.

Inoculum	Inoculated chickens		In-contact chickens	
	2 WPI	3 WPI	2 WPI	3 WPI
MB	0/10	0/10	0/5	0/5
MS-H	2/10	0/10	2/5	2/5
AS2	6/10	3/10	4/5	5/5*
AB1	6/10	8/10**	3/5	2/5
TS4	10/10***	10/10***	2/5	1/5
7NS	3/10	8/10**	3/5	3/5

Data are presented as the numbers of seropositive chickens/the numbers of all the chickens in the same group. Sera with relative antibody unit values above the cut-off value calculated using the Three-Sigma limit (three standard deviations from mean) of relative antibody unit values in the negative control group, were considered positive. * $p < 0.01$, ** $p < 0.001$, *** $p < 0.0001$ (two-tailed Fisher's Exact test). WPI, weeks post inoculation; WPE, weeks post exposure; AS2, MS-H reisolate containing reversion in *obgE* gene; AB1, MS-H reisolate containing reversions in *obgE* and *oppF* genes; TS4, MS-H reisolate containing reversions in *obgE*, *oppF* and *gapdh* genes; MB, mycoplasma broth.

TABLE 4 Reisolation of the *M. synoviae* strains from upper trachea (UT), lower trachea (LT), or air sacs (AS), 2- and 3-week after aerosol inoculation of SPF chickens with various strains or reisolates of *M. synoviae* following intratracheal inoculation with a virulent strain of IBV, and 2- and 3-week after exposure of in-contact chickens with the inoculated chickens.

Inoculum	Inoculated chickens						In-contact chickens	
	2 WPI			3 WPI			2 WPE	3 WPE
	UT	LT	AS	UT	LT	AS	UT	UT
MB	0/10	0/10	0/10	0/10	0/10	0/10	0/5	0/5
MS-H	0/10	0/10	0/10	0/10	0/10	0/10	0/5	0/5
AS2	7/10*	0/10	0/10	8/10**	0/10	0/10	1/5	4/5
AB1	5/10	2/10	1/10	7/10*	3/10	0/10	0/5	2/5
TS4	9/10**	5/10	2/10	10/10***	7/10*	4/10	0/5	2/5
7NS	2/10	1/10	0/10	3/10	0/10	0/10	1/5	3/5

Data are presented as number of cultures showing color change/number of all the cultures in the same group. * $p < 0.01$, ** $p < 0.001$, *** $p < 0.0001$ (two-tailed Fisher's Exact test). WPI, weeks post inoculation; WPE, weeks post exposure; AS2, MS-H reisolate containing reversion in *obgE* gene; AB1, MS-H reisolate containing reversions in *obgE* and *oppF* genes; TS4, MS-H reisolate containing reversions in *obgE*, *oppF* and *gapdh* genes.

middle, and lower), an average tracheal thickness was also calculated for each group (Table 5). At 3-week post inoculation, the chickens inoculated with TS4 showed average tracheal thicknesses that were significantly greater than those inoculated with MS-H or MB ($p < 0.01$).

Discussion

In this study, we selected three MS-H reisolates containing reversions to wildtype 7NS solely in *ObgE*, *OppF*, or *GAPDH* proteins, in order to evaluate the effect of gradual combinations of these three sequence variations *in vivo*. Based on our recent observations, such genomic patterns may occur, albeit rarely, in vaccinated poultry flocks. The *in vivo* experiment in the present study was designed to examine an extreme scenario where such MS-H derivatives carrying sequence reversions may appear and circulate within a population of field chickens. Thus, the strains were administered by aerosol to the “inoculated” groups. These chickens were co-inoculated with a virulent strain of IBV to exacerbate the gross and microscopic lesions (Markham et al., 1998). In addition to this, “in-contact” chickens were added to each group to investigate pathogenicity and humoral response following horizontal transmission in chickens. It is notable that the strain of chickens used in this study (mini leghorn) may behave differently to those used in commercial production, and therefore future studies are needed to investigate the effect of these strains on the chickens used for poultry meat and/or egg production.

High seropositivity rates were observed in the TS4 and AB1 inoculated chickens 3 weeks after inoculation. More importantly, the humoral responses of the in-contact chickens in groups exposed to the MS-H reisolates were consistent with the high systemic antibody responses to *M. synoviae* occasionally observed in a vaccinated flock (Kordafshari et al., 2020). Notably, the only group of in-contact chickens which developed more severe lesions were the group in-contact with

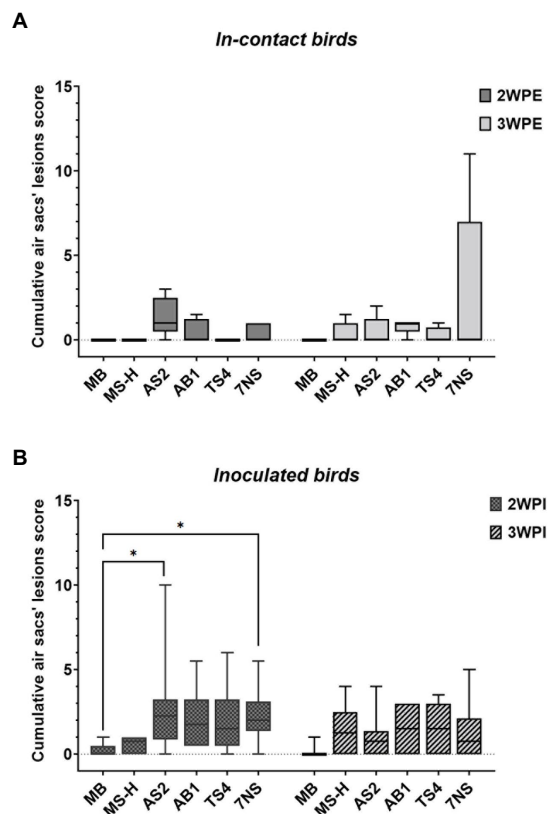


FIGURE 2
Box plots showing the data range (boxes: upper and lower quartile, whiskers: minimum and maximum) and line indicating the median value of the scores of the gross air sac lesions, 2- and 3-week after exposure of in-contact chickens to inoculated chickens (A), and 2- and 3-week after aerosol inoculation of chickens with various strains or reisolates of *M. synoviae* following intratracheal inoculation of virulent IBV (B). Air sac lesions were scored grossly for severity on a scale of 0–3, and a cumulative score was determined for each chicken by adding the scores of all air sacs. * $p < 0.01$ (Dunn's corrected Kruskal–Wallis test). WPI, weeks post inoculation; WPE, weeks post exposure; AS2, MS-H reisolates containing reversion in *obgE* gene; AB1, MS-H reisolates containing reversions in *obgE* and *oppF* genes; TS4, MS-H reisolates containing reversions in *obgE*, *oppF* and *gapdh* genes.

the 7NS inoculated chickens despite the low reisolation rate, serological response, and tracheal mucosal thickness in 7NS inoculated chickens. It is plausible that the fitness of the primary 7NS inoculum in chickens had somewhat decreased upon successive *in vitro* cultures and was regained after one passage *in vivo*. It is unclear whether this was due to sequence modifications or transient metabolic adaptations to these changing conditions. Future work to determine the whole genome sequence of the 7NS clones isolated from the in-contact chickens will be required to elucidate this question. The level of relative antibody units and the gross air sac lesions was not significantly different in the chickens in-contact with those inoculated with MS-H reisolates compared to that of chickens

in-contact with MS-H inoculated chickens. These findings suggest that such regained fitness observed in wildtype 7NS did not occur in MS-H reisolates following passage *in vivo*. This is also consistent with the usual absence of serious pathology in vaccinated flocks, even when MS-H strains with some sequence reversions are isolated from the farms. While aerosol administration is not the registered vaccination method for MS-H, it was used to inoculate the chickens for consistency in reproducing the airborne propagation of *M. synoviae* which is expected to occur in a flock. The finding that the MS-H vaccine was not reisolated from the trachea following primary aerosol administration has been reported previously (Noormohammadi et al., 2003) and is likely due to a sub-optimal inoculation and/or dose.

ObgE has a role in transmission but not in virulence

All the three reisolates assessed in this study carried the wildtype ObgE. This protein has a role in ribosome maturation, DNA replication initiation and chromosome segregation in *Caulobacter crescentus*, *Bacillus subtilis*, and *Escherichia coli* (Morimoto et al., 2002; Ulanowska et al., 2003; Datta et al., 2004; Kint et al., 2014) and is involved in the thermosensory mechanisms of *M. synoviae* (Shahid et al., 2013b). All the three reisolates containing variation in *obgE* showed a *ts* phenotype which is consistent with previous reports on association of this variation in *obgE* and loss of *ts* phenotype in MS-H reisolates (Shahid et al., 2013b). Interestingly, despite the loss of *ts* phenotype in these reisolates *in vitro*, only the TS4 reisolates was recovered significantly higher than MS-H from the lower trachea of inoculated chickens 3-week post inoculation. This finding confirms that the capacity to grow at higher temperatures *in vitro* does not always exclude colonization in lower parts of the respiratory tract *in vivo*. In the in-contact chickens 3 weeks after the exposure, the AS2 reisolates was reisolated at a higher rate compared to other reisolates, suggesting transmission of AS2 from the inoculated chickens to a greater number of in-contact chickens. However, the absence of any significant air sac lesions in the in-contact chickens exposed to the AS2 reisolates suggest that the reversion in ObgE does not have an impact on pathogenicity following horizontal transmission. The AS2 reisolates showed a significantly higher lesion scores in gross air sac examination in inoculated chickens but was not isolated from air sacs. For consistency, a particular section of the left abdominal air sac was swabbed, but air sac lesions were more commonly detected in the right abdominal air sac, which may explain the low isolation rate. The increased air sac lesions observed in the AS2 inoculated chickens but not in the in-contact chickens exposed to the AS2 might be due to a higher dose of inoculum received after artificial aerosolisation compared to natural transmission.

TABLE 5 Mucosal thicknesses of upper trachea (UT), middle trachea (MT), and lower trachea (LT) collected 2- and 3-week after inoculation of chickens with various strains or reisolates of MS following intratracheal inoculation of a virulent strain of IBV.

Inoculum	2 WPI				3 WPI			
	UT	MT	LT	Average	UT	MT	LT	Average
MB	73.5 (20.7) ^a	54.0 (9.3) ^a	43.2 (7.5) ^a	56.9 (10.4) ^a	56.3 (13.9) ^a	46.0 (9.4) ^a	43.1 (6.2) ^a	50.1 (8.5) ^a
MS-H	79.0 (24.9) ^a	63.7 (16.8) ^a	45.6 (9.4) ^a	63.5 (12.3) ^a	67.1 (9.4) ^{ab}	50.7 (11.2) ^a	44.9 (8.7) ^a	54.2 (7.8) ^a
AS2	76.1 (10.6) ^a	55.1 (6.0) ^a	52.3 (6.4) ^a	61.7 (7.0) ^a	79.6 (33.1) ^{ab}	57.7 (12.9) ^a	50.2 (21.3) ^a	62.8 (20.3) ^{ab}
AB1	82.6 (18.8) ^a	66.9 (22.4) ^a	49.7 (7.0) ^a	68.5 (18.3) ^a	110.2 (38.2) ^{ab}	63.2 (20.6) ^a	52.9 (10.6) ^a	75.4 (20.4) ^{ab}
TS4	131.5 (56.5) ^b	66.0 (10.5) ^a	58.5 (24.3) ^a	85.4 (26.0) ^a	126.0 (51.2) ^c	66.0 (13.3) ^a	58.8 (13.0) ^a	86.5 (26.4) ^b
7NS	92.8 (16.3) ^a	62.0 (16.9) ^a	56.5 (9.4) ^a	70.6 (7.6) ^a	91.3 (25.1) ^b	50.7 (10.0) ^a	58.2 (21.5) ^a	66.7 (12.8) ^{ab}

Data are presented as means (standard deviation). Statistically significant differences within each column are shown with different lowercase superscript letters, $p < 0.01$ (Tukey's corrected 2-way ANOVA). WPI, weeks post inoculation; MB: mycoplasma broth. Average denotes the average figure calculated from mucosal thicknesses measured at three distinct levels of trachea, upper, middle, and lower.

OppF is involved in humoral immune responses

The oligopeptide (Opp) permease in mycoplasmas consists of two integral membrane proteins, OppB and OppC, two nucleotide-binding proteins, OppD and OppE, and an extracellular substrate-binding protein, OppA (Zhu et al., 2019). The OppA subunit of *M. hominis* and the OppD subunit of *M. gallisepticum* have been reported to be involved in host cell attachment and colonization, respectively, suggesting the Opp permease is likely to play a role in virulence (Hopfe et al., 2011; Tseng et al., 2017). The reisolation and seropositivity rates of AB1 inoculated chickens were significantly higher than those of MS-H inoculated chickens 3 weeks after inoculation. A significant greater upper tracheal mucosal thickness was observed in the AB1 inoculated chickens compared to that of AS2 and MS-H inoculated chickens, as well as significant higher reisolation and seropositivity rates compared to those of MS-H inoculated chickens 3 weeks after inoculation. These findings lend support to the possibility of the role of OppF in the improved attachment or multiplication of *M. synoviae* onto host cells in the upper trachea and induction of the immune response. However, there was no significant difference in the lower and middle mucosal thicknesses and the air sac lesions of the AB1 inoculated chickens compared to those of MS-H and AS2 inoculated chickens. These findings imply that reisolates containing the wildtype OppF and ObgE are less likely to affect lower parts of the respiratory tract and therefore, less likely to lead to substantial clinical signs. The absence of any significant reisolation rate and air sac lesions in the in-contact chickens exposed to the AB1 inoculated chickens indicates that the concurrent reversions in ObgE and OppF do not affect pathogenicity following horizontal transmission in the poultry flocks.

GAPDH is a key player in pathogenesis

The genome of *M. synoviae* 7NS strain contains two identical copies of the 1005 bp *gapdh* gene positioned on each side of the *vlhA* locus. However, these coding regions differ from each other (and from 7NS) in MS-H genome, with G to A SNPs at positions 554 of the MSH_RS01150 (GAPDH-1150) and 917 of the MSH_RS01365

(GAPDH-1365) genes (Zhu et al., 2019). The GAPDH-1150 of TS4 isolate is identical to that of MS-H, but the GAPDH-1365 is identical to GAPDH of 7NS. The homologous GAPDH protein in many mycoplasmas has been shown to contain a surface localized fraction contributing to host cell adhesion, with the C-terminal region confirmed in the cytoadhesion of *M. pneumoniae* (Alvarez et al., 2003; Dumke et al., 2011; Gründel et al., 2016; Song et al., 2018; Grimmer and Dumke, 2019; Wang et al., 2021). Both copies of GAPDH in TS4 reisolate contain the identical C-terminal to that of 7NS. Among the reisolates, the TS4 reisolates showed the highest reisolation and seropositivity rates as well as the greatest mucosal thicknesses in upper trachea. These findings indicate the possibility of an improved attachment or multiplication of TS4 onto host cells in the upper trachea and induction of the immune response due to the presence of wildtype GAPDH-1365. While TS4 reisolate showed a superior pathogenicity in the upper trachea, the absence of any significant differences in middle and lower trachea indicates the virulence of this reisolate is less likely to be enhanced drastically. The incremental increase in pathogenicity and immunogenicity of TS4 compared to those of AB1, and of AB1 compared to those of AS2 suggest a cumulative effect of the wildtype *obgE*, *oppF* and *gapdh* genotypes. However, the probability of occurrence of concurrent reversions is likely to be negligible at a flock level. Furthermore, the developed immunity following vaccination in the majority of chickens in poultry flocks provides protection against such reisolates. Since the AS2, AB1 and TS4 reisolates emerged in vaccinated populations, a further study involving challenging vaccinated SPF chickens or field chickens with these reisolates would provide a more realistic picture of their significance in the field.

In conclusion, this study demonstrates that while the MS-H reisolates (even containing three wildtype proteins) might induce a higher systemic antibody response, they do not cause pathogenicity in lower parts of the respiratory system, and thus less likely to result in significant clinical signs. The study provides important insights into the molecular basis of attenuation of the MS-H vaccine and emphasizes the role of ObgE, GAPDH and OppF proteins in pathogenicity, immunogenicity, and transmission of *M. synoviae*. These results also have implications for Mycoplasma species affecting other animals and humans.

Data availability statement

The data presented in this study have been deposited in the NCBI GenBank repository under accession numbers CP103982 (AS2), CP103981 (AB1), and CP103980 (TS4).

Ethics statement

The animal study was reviewed and approved by the University of Melbourne Animal Ethics Committee under approval number 21064.

Author contributions

SK: substantial contributions to the design of the work, and the acquisition, analysis, interpretation of data for the work. Drafting the work OO, SZ, PA, PV, PS, NW, AC, DO, JD, and DA: substantial contributions to the acquisition of data for the work and revising the work critically for important intellectual content. GU, CM, MM, and AN: substantial contributions to the conception and design of the work and the interpretation of data for the work and revising the work critically for important intellectual content. All authors contributed to the article and approved the submitted version.

Funding

This study was funded by the Australian Research Council and Bioproperties Pty. Ltd. through the ARC Linkage Project grant LP180100762.

References

- Alvarez, R. A., Blaylock, M. W., and Baseman, J. B. (2003). Surface localized glyceraldehyde-3-phosphate dehydrogenase of *Mycoplasma genitalium* binds mucin. *Mol. Microbiol.* 48, 1417–1425. doi: 10.1046/j.1365-2958.2003.03518.x
- Andrews, S. (2010). *FastQC: A Quality Control Tool for High Throughput Sequence Data* (Babraham Bioinformatics, Babraham Institute, Cambridge, United Kingdom).
- Datta, K., Skidmore, J. M., Pu, K., and Maddock, J. R. (2004). The *Caulobacter crescentus* GTPase CgtAC is required for progression through the cell cycle and for maintaining 50S ribosomal subunit levels. *Mol. Microbiol.* 54, 1379–1392. doi: 10.1111/j.1365-2958.2004.04354.x
- De Coster, W., D'Hert, S., Schultz, D. T., Cruts, M., and Van Broeckhoven, C. (2018). NanoPack: visualizing and processing long-read sequencing data. *Bioinformatics* 34, 2666–2669. doi: 10.1093/bioinformatics/bty149
- Dumke, R., Hausner, M., and Jacobs, E. (2011). Role of *Mycoplasma pneumoniae* glyceraldehyde-3-phosphate dehydrogenase (GAPDH) in mediating interactions with the human extracellular matrix. *Microbiology* 157, 2328–2338. doi: 10.1099/mic.0.048298-0
- Ferberwee, A., de Wit, J. J., and Landman, W. J. (2009). Induction of eggshell apex abnormalities by *Mycoplasma synoviae*: field and experimental studies. *Avian Pathol.* 38, 77–85. doi: 10.1080/03079450802662772
- Ferguson-Noel, N., Armour, N. K., Noormohammadi, A. H., El-Gazzar, M., and Bradbury, J. M. (2020). "Mycoplasmosis," in *Diseases of Poultry*. eds. D. E. Swayne, M. Boulianne, C. M. Logue, L. R. McDougald, V. Nair, D. L. Suarez, et al. 907–965.
- Frey, M. (1968). A medium for the isolation of avian mycoplasmas. *Am. J. Vet. Res.* 29, 2163–2171. PMID: 5693465
- Grimmer, J., and Dumke, R. (2019). Organization of multi-binding to host proteins: The glyceraldehyde-3-phosphate dehydrogenase (GAPDH) of *Mycoplasma pneumoniae*. *Microbiol. Res.* 218, 22–31. doi: 10.1016/j.micres.2018.09.006
- Gründel, A., Pfeiffer, M., Jacobs, E., Dumke, R., and Roy, C. R. (2016). Network of surface-displayed glycolytic enzymes in *Mycoplasma pneumoniae* and their interactions with human plasminogen. *Infect. Immun.* 84, 666–676. doi: 10.1128/IAI.01071-15
- Hopfe, M., Dahlmans, T., and Henrich, B. (2011). In *Mycoplasma hominis* the OppA-mediated cytoadhesion depends on its ATPase activity. *BMC Microbiol.* 11:185. doi: 10.1186/1471-2180-11-185
- Ignjatovic, J., Ashton, D., Reece, R., Scott, P., and Hooper, P. (2002). Pathogenicity of Australian strains of avian infectious bronchitis virus. *J. Comp. Pathol.* 126, 115–123. doi: 10.1053/jcpa.2001.0528
- Jones, J.F. (2007). Investigations into *Mycoplasma synoviae* Infection. PhD Dissertation, University of Melbourne, Australia.
- Jones, J. F., Whithear, K. G., Scott, P. C., and Noormohammadi, A. H. (2006). Duration of immunity with *Mycoplasma synoviae*: comparison of the live attenuated vaccine MS-H (Vaxsafe MS) with its wild-type parent strain, 86079/7NS. *Avian Dis.* 50, 228–231. doi: 10.1637/7465-103005R.1
- Kanci, A., Wawegama, N. K., Marenda, M. S., Mansell, P. D., Browning, G. F., and Markham, P. F. (2017). Reproduction of respiratory mycoplasmosis in calves by

Acknowledgments

The authors gratefully acknowledge the assistance of Ms June Daly and Ms Angela Chircop for care of the chickens.

Conflict of interest

This study was funded by the Australian Research Council and Bioproperties Pty. Ltd. through the ARC Linkage Project grant LP180100762.

The MS-H vaccine is produced by the Bioproperties Pty. Ltd., Australia. The authors declare that this study received funding from Bioproperties Pty. Ltd. The funder had the following involvement in the study: study design, decision to publish, and reviewing the manuscript.

Publisher's note

All claims expressed in this article are solely those of the authors and do not necessarily represent those of their affiliated organizations, or those of the publisher, the editors and the reviewers. Any product that may be evaluated in this article, or claim that may be made by its manufacturer, is not guaranteed or endorsed by the publisher.

Supplementary material

The Supplementary material for this article can be found online at: <https://www.frontiersin.org/articles/10.3389/fmicb.2022.1042212/full#supplementary-material>

- exposure to an aerosolised culture of *Mycoplasma bovis*. *Vet. Microbiol.* 210, 167–173. doi: 10.1016/j.vetmic.2017.09.013
- Kint, C., Verstraeten, N., Hofkens, J., Fauvart, M., and Michiels, J. (2014). Bacterial Ogb proteins: GTPases at the nexus of protein and DNA synthesis. *Crit. Rev. Microbiol.* 40, 207–224. doi: 10.3109/1040841X.2013.776510
- Kolmogorov, M., Yuan, J., Lin, Y., and Pevzner, P. A. (2019). Assembly of long, error-prone reads using repeat graphs. *Nat. Biotechnol.* 37, 540–546. doi: 10.1038/s41587-019-0072-8
- Kordafshari, S., Shil, P., Marenda, M. S., Olaogun, O. M., Konsak-Ilievski, B., Disint, J., et al. (2020). Preliminary comparative analysis of the genomes of selected field reisolates of the *Mycoplasma synoviae* vaccine strain MS-H reveals both stable and unstable mutations after passage in vivo. *BMC Genomics* 21, 1–10. doi: 10.1186/s12864-020-07067-y
- Krueger, F. (2015). *Trim Galore: A Wrapper Tool Around Cutadapt FastQC to Consistently Apply Quality Adapter Trimming to FastQ Files* (Babraham Bioinformatics, Babraham Institute, Cambridge, United Kingdom).
- Markham, J. F., Morrow, C. J., Scott, P. C., and Whithear, K. G. (1998). Safety of a temperature-sensitive clone of *Mycoplasma synoviae* as a live vaccine. *Avian Dis.* 42, 677–681. doi: 10.2307/1592702
- Meynell, G. G., and Meynell, E. (1970). *Theory and Practice in Experimental Bacteriology*. 2nd Edn. Cambridge: Cambridge University Press Archive.
- Morimoto, T., Loh, P. C., Hirai, T., Asai, K., Kobayashi, K., Moriya, S., et al. (2002). Six GTP-binding proteins of the Era/Ogb family are essential for cell growth in *Bacillus subtilis*. *Microbiology* 148, 3539–3552. doi: 10.1099/00221287-148-11-3539
- Morrow, C. J. (1991). Pathogenicity, Immunogenicity, and Strain Identification of Australian Isolates of *Mycoplasma synoviae*. PhD Dissertation, University of Melbourne, Australia.
- Morrow, C. J., Markham, J. F., and Whithear, K. G. (1998). Production of temperature-sensitive clones of *Mycoplasma synoviae* for evaluation as live vaccines. *Avian Dis.* 42, 667–670. doi: 10.2307/1592700
- Nascimento, E. R., Pereira, V., Nascimento, M., and Barreto, M. (2005). Avian mycoplasmosis update. *Braz J. Poultry Sci.* 7, 1–9. doi: 10.1590/S1516-635X2005000100001
- Nicholas, R. A. J., Ayling, R. D., and McAuliffe, L. (2009). Vaccines for mycoplasma diseases in animals and man. *J Comp Pathol.* 140, 85–96. doi: 10.1016/j.jcpa.2008.08.004
- Nonomura, I., and Imada, Y. (1982). Temperature-sensitive mutant of *Mycoplasma synoviae*. I. production and selection of a nonpathogenic but immunogenic clone. *Avian Dis.* 26, 763–775. doi: 10.2307/1589862
- Noormohammadi, A. H., Jones, J. F., Harrigan, K. E., and Whithear, K. G. (2003). Evaluation of the non-temperature-sensitive field clonal isolates of the *Mycoplasma synoviae* vaccine strain MS-H. *Avian Dis.* 47, 355–360. doi: 10.1637/0005-2086(2003)047[0355:EOTNFC]2.0.CO;2
- Noormohammadi, A. H., Markham, P. F., Markham, J. F., Whithear, K. G., and Browning, G. F. (1999). *Mycoplasma synoviae* surface protein MSPB as a recombinant antigen in an indirect ELISA. *Microbiology* 145, 2087–2094. doi: 10.1099/13500872-145-8-2087
- Omotaïne, O. S., Wawegama, N. K., Kulappu Arachchige, S. N., Coppo, M. J., Vaz, P. K., Woodward, A. P., et al. (2022). Tracheal cellular immune response in chickens inoculated with *Mycoplasma synoviae* vaccine, MS-H or its parent strain 86079/7NS. *Vet. Immun. Immunopathol.* 251:110472. doi: 10.1016/j.vetimm.2022.110472
- Seemann, T. (2015). Snippy: fast bacterial variant calling from NGS reads. Available at: <https://github.com/tseemann/snippy>.
- Shahid, M. A., Ghorashi, S. A., Agnew-Crumpton, R., Markham, P. F., Marenda, M. S., and Noormohammadi, A. H. (2013a). Combination of differential growth at two different temperatures with a quantitative real-time polymerase chain reaction to determine temperature-sensitive phenotype of *Mycoplasma synoviae*. *Avian Pathol.* 42, 185–191. doi: 10.1080/03079457.2013.779363
- Shahid, M. A., Markham, P. F., Markham, J. F., Marenda, M. S., and Noormohammadi, A. H. (2013b). Mutations in GTP binding protein Ogb of *Mycoplasma synoviae* vaccine strain MS-H: implications in temperature-sensitivity phenotype. *PLoS One* 8:e73954. doi: 10.1371/journal.pone.0073954
- Song, Q., Song, W., Zhang, W., He, L., Fang, R., Zhou, Y., et al. (2018). Identification of erythrocyte membrane proteins interacting with *Mycoplasma suis* GAPDH and OSGEP. *Res. Vet. Sci.* 119, 85–90. doi: 10.1016/j.rvsc.2018.05.001
- Tseng, C.-W., Chiu, C.-J., Kanci, A., Citti, C., Rosengarten, R., Browning, G. F., et al. (2017). The oppD gene and putative peptidase genes may be required for virulence in *Mycoplasma gallisepticum*. *Infect. Immun.* 85:e00023-17. doi: 10.1128/IAI.00023-17
- Ulanowska, K., Sikora, A., Węgrzyn, G., and Czyż, A. (2003). Role of the cgtA gene function in DNA replication of extrachromosomal elements in *Escherichia coli*. *Plasmid* 50, 45–52. doi: 10.1016/S0147-619X(03)00021-0
- Wang, J., Li, Y., Pan, L., Li, J., Yu, Y., Liu, B., et al. (2021). Glyceraldehyde-3-phosphate dehydrogenase (GAPDH) moonlights as an adhesin in *Mycoplasma hyorhinis* adhesion to epithelial cells as well as a plasminogen receptor mediating extracellular matrix degradation. *Vet. Res.* 52:80. doi: 10.1186/s13567-021-00952-8
- Whithear, K., Harrigan, K., and Ghiocas, E. J. (1990). Safety of temperature sensitive mutant *Mycoplasma gallisepticum* vaccine. *Aus. Vet. J.* 67, 159–165. doi: 10.1111/j.1751-0813.1990.tb07745.x
- Wick, R. R., and Holt, K. E. (2022). Polypolish: short-read polishing of long-read bacterial genome assemblies. *PLOS Comput. Biol.* 18:e1009802. doi: 10.1371/journal.pcbi.1009802
- Wick, R. R., Judd, L. M., Gorrie, C. L., and Holt, K. E. (2017). Unicycler: resolving bacterial genome assemblies from short and long sequencing reads. *PLOS Comput. Biol.* 13:e1005595. doi: 10.1371/journal.pcbi.1005595
- Yadav, J. P., Tomar, P., Singh, Y., and Khurana, S. K. (2021). Insights on *Mycoplasma gallisepticum* and *Mycoplasma synoviae* infection in poultry: a systematic review. *Animal Biotechnol.* 1–10. doi: 10.1080/10495398.2021.1908316
- Zhu, L., Shahid, M. A., Markham, J., Browning, G. F., Noormohammadi, A. H., and Marenda, M. S. (2019). Comparative genomic analyses of *Mycoplasma synoviae* vaccine strain MS-H and its wild-type parent strain 86079/7NS: implications for the identification of virulence factors and applications in diagnosis of *M. synoviae*. *Avian Pathol.* 48, 537–548. doi: 10.1080/03079457.2019.1637514



OPEN ACCESS

EDITED BY

Glenn Francis Browning,
The University of Melbourne,
Australia

REVIEWED BY

Pascal Rainard,
Institut National de Recherche pour
l'Agriculture,
l'Alimentation et l'Environnement (INRAE),
France
Evelyn Meyer,
Ghent University,
Belgium
Turner H. Swartz,
Michigan State University,
United States

*CORRESPONDENCE

Nahum Y. Shpigel
✉ nahum.shpigel@mail.huji.ac.il

SPECIALTY SECTION

This article was submitted to
Infectious Agents and Disease,
a section of the journal
Frontiers in Microbiology

RECEIVED 18 December 2022

ACCEPTED 27 February 2023

PUBLISHED 24 March 2023

CITATION

Schneider P, Salamon H, Weizmann N,
Nissim-Eliraz E, Lysnyansky I and
Shpigel NY (2023) Immune profiling of
experimental murine mastitis reveals conserved
response to mammary pathogenic *Escherichia coli*,
Mycoplasma bovis, and *Streptococcus uberis*.
Front. Microbiol. 14:1126896.
doi: 10.3389/fmicb.2023.1126896

COPYRIGHT

© 2023 Schneider, Salamon, Weizmann,
Nissim-Eliraz, Lysnyansky and Shpigel. This is
an open-access article distributed under the
terms of the [Creative Commons Attribution
License \(CC BY\)](#). The use, distribution or
reproduction in other forums is permitted,
provided the original author(s) and the
copyright owner(s) are credited and that the
original publication in this journal is cited, in
accordance with accepted academic practice.
No use, distribution or reproduction is
permitted which does not comply with these
terms.

Immune profiling of experimental murine mastitis reveals conserved response to mammary pathogenic *Escherichia coli*, *Mycoplasma bovis*, and *Streptococcus uberis*

Peleg Schneider¹, Hagit Salamon¹, Nathalie Weizmann¹,
Einat Nissim-Eliraz¹, Inna Lysnyansky² and Nahum Y. Shpigel^{1*}

¹Department of Basic Sciences, The Koret School of Veterinary Medicine, The Hebrew University of Jerusalem, Rehovot, Israel, ²Mycoplasma Unit, Kimron Veterinary Institute, Beit Dagan, Israel

Mastitis is one of the most prevalent and economically important diseases of dairy animals. The disease is caused by ascending bacterial infection through the teat canal. Among the most common mastitis-causing bacteria are Gram-negative coliforms, Gram-positive streptococci and staphylococci, and mycoplasma. The most prominent cellular hallmark of acute mammary infection is a massive recruitment of blood neutrophils into the tubular and alveolar milk spaces. The complex biological processes of leukocyte recruitment, activation, adhesion, and migration in the mammary gland remain largely elusive to date. While field research of mastitis in dairy animals contributed a lot to the development of mitigation, control, and even eradication programs, little progress was made toward understanding the molecular mechanisms underlying the pathogenesis of the disease. We report here experimental mastitis model systems in lactating mice challenged with field strains of common udder pathogens in dairy cows. We used these model systems to apply recently developed multiplex gene expression technology (Nanostring nCounter), which enabled us to study the expression of over 700 immune genes. Our analysis revealed a core of 100 genes that are similarly regulated and functionally or physically interacting in *E. coli*, *M. bovis*, and *Strep uberis* murine mastitis. Common significantly enriched gene sets include TNF α signaling via NF κ B, Interferon gamma and alpha response, and IL6-JAK-STAT3 signaling. In addition, we show a significantly enriched expression of genes associated with neutrophil extracellular traps (NET) in glands challenged by the three pathogens. Ligand-receptor analysis revealed interactions shared by the three pathogens, including the interaction of the cytokines IL1 β , IL1 α , and TNF α with their receptors, and proteins involved in immune cell recruitment such as complement C3 and ICAM1 (with CD11b), chemokines CCL3 and CCL4 (with CCR1), and CSF3 (with CSF3R). Taken together, our results show that mammary infection with *E. coli*, *M. bovis*, and *Strep uberis* culminated in the activation of a conserved core of immune genes and pathways including NET formation.

KEYWORDS

mastitis, murine model, *Escherichia coli*, *Mycoplasma bovis*, *Streptococcus uberis*, immune profiling

Introduction

Mastitis, inflammation of the mammary gland, is an important disease in dairy animals and breast-feeding women. The disease is caused by ascending infection through the teat canal of pathogenic bacteria such as *Escherichia coli*, *Streptococcus uberis*, *Staphylococcus aureus*, and *Mycoplasma bovis* (Shpigel et al., 1998; Dyson et al., 2022; Gelgie et al., 2022; Kurban et al., 2022). Mastitis is a good example of an infectious disease caused by a dominant pathogen and heeding the concept of Koch's postulates. In field cases, the etiological agent is usually isolated in pure cultures of milk samples and the disease can be recapitulated by experimental infection in dairy animals or laboratory mice. The first phase of the disease requires massive growth of invading bacteria and colonization of the milk spaces in the tubular system and alveoli. Invading bacteria require to grow in milk and withstand innate antimicrobial mechanisms active in the milk such as the complement system and essential nutrients chelators. Next, inflammation is activated by microbial-associated molecular patterns (MAMPs) released by the growing bacteria leading to massive recruitment of blood neutrophils into the alveolar and milk spaces (Rainard et al., 2022). MAMPs activate a plethora of innate receptors and signaling systems in mammary epithelial cells (MEC) and alveolar macrophages which are the first line of response to the invading pathogens. These cells are known to express and release numerous inflammatory mediators such as cytokines, interleukins, chemokines, and reactive oxygen and nitrogen species (RONS). These inflammatory mediators initiate the recruitment of blood neutrophils which requires endothelial and epithelial adherence and transmigration along the trajectory from the blood vessels, across the vasculature, parenchyma, and MEC. This process involves adhesion molecules, chemoattractants, and receptors expressed on immune cell surfaces, blood vessels, and stromal mammary tissue. The complex biological processes of leukocyte recruitment, activation, adhesion, and migration in the mammary gland remain largely elusive to date. While field research of mastitis in dairy animals contributed a lot to the development of mitigation, control, and even eradication (for some pathogens) programs, little progress was made toward understanding the molecular mechanisms underlying the pathogenesis of the disease. To this end, we have used and further developed experimental mastitis model systems in lactating mice and applied recently developed multiplex gene expression technology (Nanostring nCounter) that enabled us to study the expression of over 700 immune genes in the disease (Warren, 2018). We show here that a core of activated immune genes and pathways including the formation of neutrophil extracellular traps (NETs) are all conserved in *E. coli*, *M. bovis*, and *Strep. uberis* mastitis.

Materials and methods

Bacterial strains

Escherichia coli strain P4-NR O15:H21H54, phylogroup B1 was isolated from the milk of an experimentally infected dairy cow (Shpigel et al., 1997; Leimbach et al., 2017; Mintz et al., 2019) and prepared for challenge in lactating mice as previously reported by us (Salamon et al., 2020). Briefly, bacteria from frozen stock were grown on Luria Bertani (LB) agar plates at 37°C for 24 h after which one

isolated bacteria colony was transferred to 10 mL of LB broth for overnight growth at 37°C with shaking at 110 rpm. Pre-cultured bacteria were diluted 1:100 with fresh LB broth and grew to log phase for 3 h at 37°C with shaking at 110 rpm. Next, culture was centrifuged for 10 min at 4,000 × rpm and bacteria were washed twice with sterile PBS. Bacteria were resuspended in sterile PBS and inoculum was divided to 50 µL doses in 0.3 mL insulin syringes, approximately ~10⁴ CFUs and kept on ice until the IMM challenge. Challenge was quantified and confirmed by plating the inoculum as serial 10-fold dilutions on LB agar plates.

Streptococcus uberis strain PS10 and *Staphylococcus epidermidis* strain PS20 were isolated by the National Service for Udder Health and Milk Quality (NSUHQ) laboratory from quarter milk samples originating from Israeli dairy cows affected by clinical mastitis. Bacteriological examination was performed according to National Mastitis Council guidelines (Shwimmer et al., 2007). Strains identification was further validated using 16S rRNA PCR analysis and sequencing as previously described (Wald et al., 2017). Strains were cryopreserved in 20% glycerol at −80°C until further processing. For IMM challenge, *Streptococcus uberis* and *Staphylococcus epidermidis* bacteria were grown on Heart Infusion Broth (238,400, HI, BD DIFCO) agar plates at 37°C for 24 h after which one isolated bacteria colony was transferred to 10 mL of HI broth for overnight growth at 37°C with shaking at 110 rpm. Pre-cultured bacteria were diluted 1:100 with fresh HI broth and grew to log phase for 3 h at 37°C with shaking at 110 rpm. Next, culture was centrifuged for 10 min at 4,000 × rpm and bacteria were washed twice with sterile PBS. Bacteria were resuspended in sterile PBS and inoculum was divided to 50 µL doses in 0.3 mL insulin syringes, approximately ~10⁴ CFUs and kept on ice until the IMM challenge. Challenge was quantified and confirmed by plating the inoculum as serial 10-fold dilutions on HI agar plates.

Mycoplasma bovis strain PG45 (ATCC 25523 / NCTC 10131) (Hale et al., 1962; Wise et al., 2011) was used in this study and prepared for challenge in lactating mice as previously reported by us (Schneider et al., 2022). Bacteria were propagated at 37°C in FF modified broth medium (Friis, 1975) supplemented with 0.5% (w/v) sodium pyruvate and 0.005% (w/v) phenol red. Stock cultures were grown to the titers of 10⁸–10⁹ CFUs/mL, aliquoted, and maintained at −80°C. For each stock, the number of CFUs per mL was determined by performing serial 10-fold dilutions in FF broth and by plating each dilution on agar in triplicates (Rodwell and Whitcomb, 1983); the agar plates were grown at 37°C, under an atmosphere of 5% CO₂/95% air. For challenge, mycoplasma cultures were grown until mid-log phase and then harvested by centrifugation at 10,000 × g for 10 min at 4°C. The bacterial pellets were washed twice with the same volume of sterile PBS × 1 (Gibco1by Life Technologies) and centrifuged as described above. The bacterial cultures were resuspended in 500 µL of PBS to a final concentration of ~2 × 10¹⁰ CFUs/mL. The titers of *M. bovis* were calculated by plating serial 10-fold dilutions on FF agar.

Murine mastitis model systems

Twelve to fourteen week-old female BALB/c mice were used in this project (Envigo, Israel). Intramammary challenge (IMM) was performed 8 days post-partum. Mice pups were removed before the challenge. Mice were first anesthetized (1.5–2.5% isoflurane in O₂) and

then challenged with 10^4 CFUs of *E. coli* P4-NR, *Strep. uberis*, and *S. epidermidis* or with 10^9 CFUs of *M. bovis* PG45. IMM infusion was performed through the teat canal in both L4 and R4 abdominal mammary glands (the fourth pair found from head to tail). Three mice/six glands were used in every experiment. Injections were conducted under a binocular using 0.3 mL insulin syringes with a 33-gauge blunt needle. Mice were sacrificed 24 h (*E. coli*, *Strep. uberis*, and *Staph. epidermidis*) or 48 h (*M. bovis*) post challenge, and mammary tissues were harvested for histology, total RNA extraction and total bacterial counts. Glands harvested from normal non-challenged mice were used as controls.

Bacterial counts and histological analysis

Mammary tissues were trisected for histology, total RNA extraction, and total bacterial counts as previously described (Mintz et al., 2019; Salamon et al., 2020). Harvested mammary tissues were weighed and homogenized in ice-cold PBS immediately after their removal and homogenates were plated as serial 10-fold dilutions on agar plates with and without antibiotics and bacterial colonies were counted following incubation at 37°C for 24 h to determine the output CFUs per 1 g of tissue. Specifically, *E. coli* was incubated on LB agar plates with and without chloramphenicol (25 µg/mL) for 24 h, *Streptococcus uberis* and *Staphylococcus epidermidis* were incubated on HI agar plates for 24 h, and *Mycoplasma bovis* was incubated on FF-modified broth medium agar plates for 3 to 5 days under an atmosphere of 5% CO₂/95% air to determine the number of CFUs/g of tissue.

Samples for histological analysis were fixed in neutral buffered 4% PFA and embedded in paraffin (FFPE blocks), and sections were cut at a thickness of 5 µm and stained with hematoxylin and eosin (H&E) according to standard procedures. For immunofluorescent staining, FFPE sections were first incubated in a 70°C oven for 20 min, dewaxed in xylene and rehydrated by sequentially immersing slides in 100, 95, 80, and 70% ethanol, and then in DDW. Following rehydration, slides were placed in Tris/EDTA buffer, pH 9, for antigen retrieval (S236784-2, Agilent Dako) and boiled for 40 min. After cooling to room temperature, slides were washed twice in TBS-T solution (Tris-Buffered Saline, pH 7.6; Alfa Aesar, United Kingdom) with 0.1% Tween-20 (Fisher Scientific) and blocked by incubation in blocking solution containing 5% (v/v) donkey serum (Sigma) in TBS-T. FFPE sections were stained with DAPI (Sigma, Rehovot, Israel), and rat anti-mouse S100A9 (ab105472, Abcam), rabbit anti-mouse CD31 (Clone D8V9E, Ionpath), and rabbit anti-mouse Na/K-ATPase (Clone EP1845Y, Ionpath) primary antibodies. Next, sections were incubated with the following secondary antibodies; goat anti-rat IgG conjugated with Alexa Fluor 488 (a11006, Invitrogen), donkey anti-rabbit IgG conjugated with Alexa Fluor 647 (a31573, Invitrogen), and donkey anti-rabbit IgG conjugated with Alexa Fluor 694 (a21207, Invitrogen).

Fresh mammary tissues for fluorescence staining were fixed in 4% PFA overnight at room temperature, incubated with 15% (wt/vol) sucrose for 72 h at 4°C, and frozen in optimal cutting temperature compound (Sigma-Aldrich). Serial 15 µm cryosections were stained with DAPI and phalloidin (Sigma, Rehovot, Israel) and rabbit anti-human Ly6G (EPR3094; Abcam), rat anti-mouse ICAM-1 (Alexa Fluor 488 conjugated, 116,112, Biolegend), goat anti-mouse

myeloperoxidase (AF3667, Biotest), rabbit anti-mouse Citrullinated histone H3 (ab5103, Abcam), rabbit anti-mouse ACKR1 (MBS7005916, MyBioSource), and rat anti-mouse CD90 (ab3105, Abcam) primary antibodies. Donkey anti-rabbit IgG conjugated with Alexa Fluor 546 (A10040, Sigma Thermo Fisher), and the above described secondary antibodies were used as described above. All immunofluorescence stainings were performed in blocking solution, and mounted with fluorescent mounting medium (S3023, Dako).

Pericytes were visualized in mammary tissues of transgenic mice expressing GFP under Nestin promoter (Mignone et al., 2004). Surplus tissues were kindly shared by Dr. Dalit Sela-Donenfeld, the Hebrew University. Telocytes were visualized in mammary tissues of transgenic mice expressing GFP under Foxo1 promoter (Shoshkes-Carmel et al., 2018). Surplus tissues were kindly shared by Dr. Michal Shoshkes-Carmel, the Hebrew University.

Microscopic analysis was performed using M1 Imager Axio epifluorescence microscope with an MRm Axio camera (Zeiss), and images were captured using Zen software V3.4.

Real-time PCR and multiplex gene expression analysis

Lymph node divested L4 or R4 mammary glands were dissected from unchallenged and challenged mice and RNA was extracted for quantitative real-time PCR (qPCR) and Nanostring nCounter profiling. The qPCR analysis of mammary tissues was performed as previously described by us (Salamon et al., 2020). Briefly, total RNA was isolated from mammary tissue using the GeneElute Mammalian Total RNA Miniprep Kit (Sigma-Aldrich, Rehovot, Israel) combined with on-Column DNase I Digestion Set (Sigma). Reverse transcription was performed using qScript cDNA Synthesis Kit (Quanta BioSciences, Gaithersburg, MD, United States) and cDNA was used for subsequent qPCR reactions. PCR was conducted on a StepOne Plus PCR instrument (Applied Biosystems) using the FAST qPCR Universal Master Mix (Kappa Biosystems, Boston, MA, United States). All reactions were performed in triplicates and the gene expression levels for each amplicon were calculated using the $\Delta\Delta CT$ method (Livak and Schmittgen, 2001) and normalized against Ptma mRNA. Melting curve analysis was performed on each primer set to confirm amplification of a single product and all amplicons were sequenced to ensure reaction specificity (data not shown).

Using 100 ng of RNA per sample, RNA was profiled using Nanostring nCounter Mouse Myeloid Innate Immunity V2 Panel of 754 genes, including 20 internal reference genes for data normalization.¹ Data was analyzed using nSolver™ analysis software version 4.0, GraphPad, and Excel softwares. Differential expression analysis was performed with *p*-values adjusted for multiple comparisons according to Benjamini and Hochberg, corresponding to a false discovery rate (Benjamini and Hochberg, 1995). Differentially expressed gene sets were mapped onto gene interaction networks from STRING v.11 (Szklarczyk et al., 2018).

¹ <https://www.nanostring.com/products/PanelPro>

Gene Set Enrichment Analysis (GSEA)

Gene Set Enrichment Analysis (GSEA) (Subramanian et al., 2005) was done using the java-based GSEA program and curated molecular signature database (MSigDB) both provided by the BROAD institute.² The Hallmark gene set of 50 well-defined biological states or processes (Liberzon et al., 2015), c5GOBP gene set (MSigDB; c5 Gene ontology Biological Processes), and neutrophil extracellular trap formation gene set taken from Wu et al. (2020) were used to assess the effect of bacterial challenge on murine mammary transcript expression.

Ligand-receptor analysis

Bulk gene expression data of 734 murine immune genes was produced using Nanostring nCounter technology. Ligand-receptor communication scores were calculated using the expression correlation method as previously described by Armingol et al. (2021). For comprehensive systematic analysis of putative ligand-receptor interactions, we used CellTalkDB (Shao et al., 2020) which is a manually curated database of literature-supported ligand-receptor interactions in human and mouse. The communication score (CS) was computed for every ligand-receptor pair in the gene expression data. Correlation coefficients were calculated as CS for each ligand-receptor pair across all data samples. We assumed that a communication pathway is active only when ligand and receptor were both significantly (adjusted p -value < 0.05) differentially expressed with fold change (FC) greater than 1 (see representation of data analysis using Volcano and correlation plots in Supplementary Figure 1). Ligand-receptor interactions and CS were visualized using heatmaps (GraphPad) and Sankey diagrams (SankeyMATIC).³

Results

Establishment of murine mastitis model system

Experimental mastitis model systems were established in lactating BALB/c mice using intramammary (IMM) infusion of bacterial suspension to glands L4 and R4 (Figure 1A). We have used *E. coli* strain P4-NR and the type strain *M. bovis* PG45 as previously reported by us (Salamon et al., 2020; Schneider et al., 2022). Field strains of *Strep. uberis* (strain PS10) and *Staph. epidermidis* (strain PS20), isolated from clinical mastitis in dairy cows, are reported here for the first time. The disease in lactating mice was characterized by high bacterial counts in the gland tissue homogenates (Figure 1B), massive recruitment of blood neutrophils into tubular and alveolar milk spaces (Figure 1C), which is further supported by increased expression of the neutrophil marker Ly6G (Figure 1D), and increased expression of inflammatory markers such as *Tnfa*, *Il1 β* , *Cxcl1* (KC), *Cxcl2* (Mip2), and *Ikba* (Figure 1D).

The above described murine mastitis model systems represent the most prevalent mammary pathogenic bacteria in dairy animals; Gram-negative coliforms, Gram-positive streptococci and staphylococci, and mycoplasma. The shared hallmark of the disease caused by acute mammary infection by all these pathogens is massive recruitment of blood neutrophils into the tubular and alveolar milk spaces (Figures 1C,D). Neutrophil trafficking requires transendothelial, parenchymal, and transepithelial neutrophil migration. The structural cellular elements putatively involved in this process are schematically outlined in Figure 1C. Using immunofluorescence staining for S100a9, myeloperoxidase (MPO), and Ly6G as neutrophil markers, we demonstrate here neutrophils at each of the above stages of recruitment (Figure 2 and Supplementary Figures 2, 3). The immensely arborized alveolar and tubular epithelial duct system of the lactating mammary gland is surrounded by elaborative honeycomb-like vascular system in close proximity to all epithelial elements (Supplementary Figure 2C). The site of neutrophil extravasation and the underlying molecular mechanisms involved are still unknown in the mammary gland. In mice, the capillaries branch from approximately 10 μ m lumen diameter vessels to reach an average of <6 μ m diameter, then converge into larger post-capillary venules with diameter > 6 μ m, that project to ascending venules (Fujiwara and Uehara, 1984; Kucharz et al., 2021). Based on size and the pan-endothelial cell marker, CD31, the mammary vascular system can be visualized and identified (Figures 2B, 3A and Supplementary Figure 2C). Moreover, as previously reported, we show here steady state expression of the adhesion molecule ICAM-1 by these blood vessels (Figures 3A,B), and their surrounding networks of pericytes (Nestin⁺ and CD90⁺) and telocytes (Foxl1⁺) (Figures 3C,D; Fujiwara and Uehara, 1984; Gherghiceanu and Popescu, 2005; Klein et al., 2022). Post capillary venules, which are considered a specialized site of immune cells recruitment, were demonstrated using the ACKR1 marker (Figure 3E; Thiriot et al., 2017; Girbl et al., 2018).

Immune genes response elicited by mastitis pathogens

To better understand the molecular mechanisms underlying the above described inflammatory process and neutrophil recruitment, we next performed immune profiling of mammary glands challenged with *E. coli*, *M. bovis*, and *Strep. uberis* bacteria. These strains were chosen as representatives of mammary pathogenic Gram-positive, Gram-negative, and mycoplasma species, while *Staph. epidermidis* was not further analyzed in this study. We used the Nanostring nCounter technology to profile the expression of 734 immune genes in challenged glands in comparison with normal unchallenged glands. Total and differential gene expression (log₂ fold-changes) in *E. coli*, *M. bovis*, or *Strep. uberis* challenged glands are presented and compared in Figure 4. Cluster analysis showed higher similarity in gene expression following challenge with *M. bovis* and *Strep. uberis* than following *E. coli* challenge (Figure 4A). MA (Figures 4B–D) and Volcano (Figures 4E–G) plots present normalized expression and relative expression for each challenge organism. In the *E. coli* challenged glands, 255 genes (159 upregulated and 96 downregulated) were significantly differentially expressed in comparison with the normal unchallenged glands

² <https://www.broadinstitute.org/gsea/index.jsp>

³ <https://sankeymatic.com/>

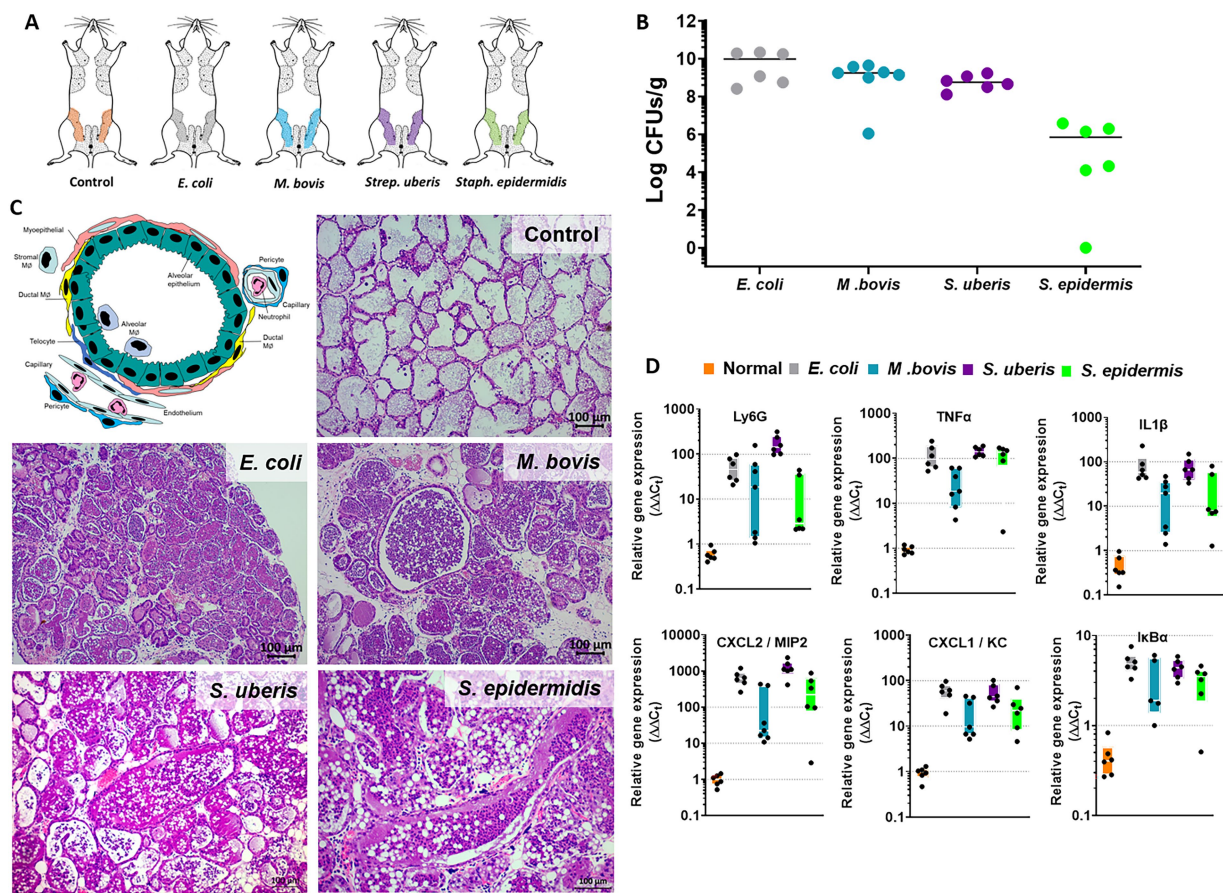


FIGURE 1

The murine mastitis model system. Lactating 6–8 weeks old BALB/c mice were infected with live *E. coli* P4-NR, *M. bovis* PG45, *Strep. uberis* PS10 and *Staph. epidermidis* PS20 bacteria by intramammary infusion through the teat canal (A). Mice were humanely sacrificed after 24 or 48 h (*M. bovis* only) and mammary tissues were processed for total bacterial counts (B), histology (H&E staining of FFPE tissue sections in C) and QPCR analysis (D). Annotated schematic diagram of mammary alveolar structural and immune cell elements is shown in C (left top panel). Diseased glands were characterized by bacterial counts (B), massive recruitment of blood neutrophils into the alveolar and ductal spaces (C) also indicated by increased relative expression of the neutrophil marker Ly6G (D). Mammary inflammation was associated with increased expression of TNFα, IL1β, CXCL1, CXCL2, and IκBα (D). Scale bars; 100 μm.

(adjusted p -value < 0.05). In the *M. bovis* challenged glands, 141 genes (107 upregulated and 34 downregulated) were significantly differentially expressed in comparison with the normal unchallenged glands (adjusted p -value < 0.05). In the *Strep. uberis* challenged glands, 167 genes (139 upregulated and 28 downregulated) were significantly differentially expressed in comparison with the normal unchallenged glands (adjusted p -value < 0.05). Next, we used correlation scatter plots (Figures 4H–J) and Venn diagram analysis (Figures 5A,B) of upregulated and downregulated differentially expressed genes to analyze the similarities and differences in mammary immune gene response to each pathogen. Scatter plots present all significantly changed genes (P_{adj} -value < 0.05; $|\log_2 \text{fold-change}| > 1$) in either challenged gland, while non-significant \log_2 fold-changes are assigned the value of 1 and are located on the x -axis or on the y -axis ($\log_2 = 0$ in Figures 4H–J). Taken together, our analysis revealed a core of 100 genes which are similarly regulated in *E. coli*, *M. bovis*, and *Strep. uberis* challenged glands (Figures 5A–D) and based on STRING analysis functionally and/or physically interacting (Figure 5C) in response to the challenge with each pathogen.

Gene Set Enrichment Analysis (GSEA)

To further explore the immune processes associated with these differentially expressed genes, we next performed Gene Set Enrichment Analysis (GSEA) of our expression data comparing bacterial infections to control samples (Figure 6). Significantly enriched gene sets common to the three pathogens are presented in Figure 6A and include TNFα signaling via NFκB, Interferon gamma and alpha response, IL1-mediated signaling, myeloid leukocyte response, and IL6-JAK-STAT3 signaling. Moreover, since neutrophil extracellular trap (NET) genes set is not available in MSigDB, we created a new gene set based on previously published data (Wu et al., 2020). GSEA revealed significant enriched expression of genes associated with NET in glands challenged by all three pathogens (Figure 6B). This finding was further validated using immunofluorescence staining for citrullinated histone 3 (CitH3; Figure 6C), MPO and DNA staining (Supplementary Figure 4) of mammary tissues infected by each of the three pathogens. CitH3, combined with MPO and DNA staining, is a specific marker of neutrophils forming NET (Radermecker et al., 2022; Sanders et al., 2022). We show here that some, albeit not all, neutrophils recruited

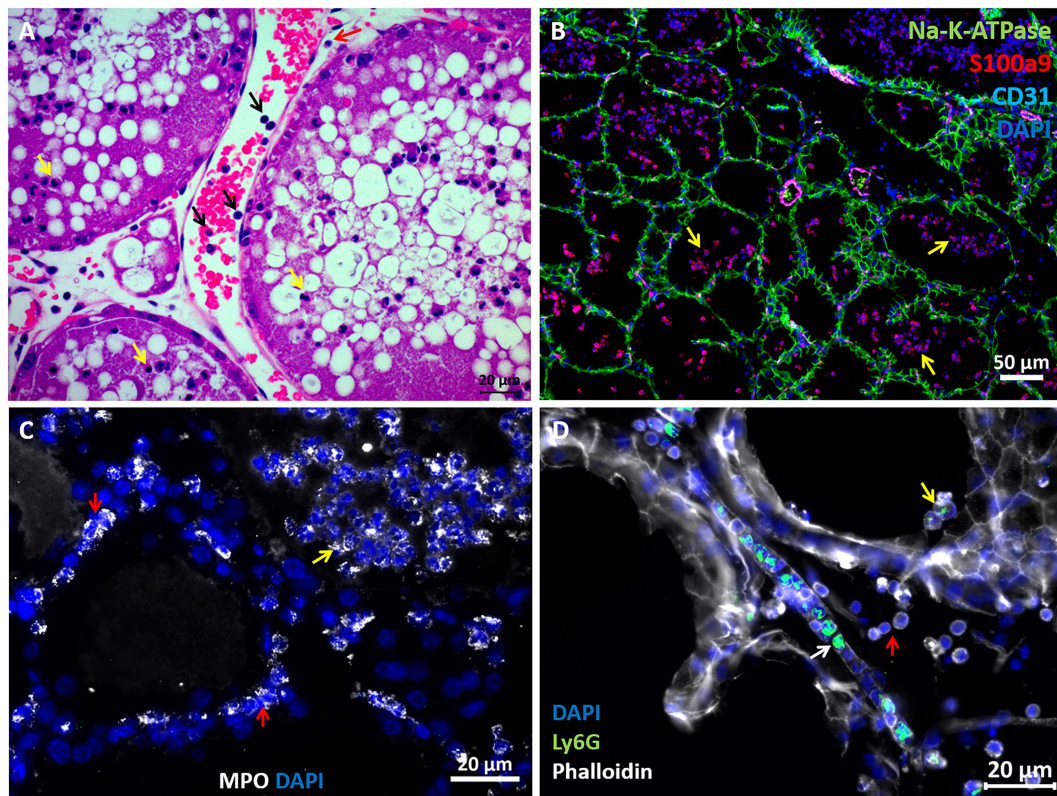


FIGURE 2

Visualization of neutrophil recruitment in infected mammary glands. H&E staining of FFPE section showing post capillary venule adjacent to the alveoli (A). Blood neutrophils are visible with RBCs and adherent to the endothelium (black arrows in A). Neutrophils are also visible in the parenchyma (red arrow in A) and alveolar space (yellow arrows in A). Fluorescence staining of cryosections from infected glands using DAPI (blue in B–D), anti Na-K-ATPase (green in B), S100a9 (red in B), CD31 (purple in B), myeloperoxidase (MPO, white in C) and Ly6G (green in D) antibodies, and phalloidin (white in D). Mammary epithelial cells are demarcated with anti Na-K-ATPase (green in B) or phalloidin (white in D). Neutrophil (S100a9⁺, MPO⁺, and Ly6G⁺) are visible in blood vessels (white arrow in D), parenchyma (red arrows in C) and alveoli (yellow arrows in B–D). Individual channels merged in B are shown in [Supplementary Figure 2](#). Scale bars; 20μm (A, C, D) and 50μm (B). Representative images from mammary glands 24h after IMM challenge with *E. coli* P4-NR bacteria.

from blood into the alveolar and tubular milk spaces form NET in response to IMM infection with *E. coli*, *M. bovis*, and *Strep. uberis*.

Receptor-ligand analysis

To better understand the molecular mechanisms unveiled by our expression data, we applied computational analysis of ligand-receptor (L-R) gene pairs ([Figure 7](#)). While many putative L-R interactions were pathogen-specific ([Figures 7A–C](#)), our analysis revealed interactions shared by the three pathogens ([Figure 7D](#)). These include interaction of the cytokines IL1β, IL1α, TNFα, and Csf3 with their receptors (Il1r2, Tnfrsf1b, and Csf3r, respectively), chemokines CCL3 and CCL4 (with CCR1), and complement C3 and ICAM1 (with Itgam). Normalized gene expressions of C3, Icam1, and Itgam (Cd11b) are presented in [Figure 7E](#). The high expression of ICAM-1 in blood vessels of infected mammary glands was further validated using immunostaining and epifluorescence microscopy ([Supplementary Figure 5](#)).

Discussion

Mastitis in dairy animals is a prevalent and economically important disease. The disease is caused by ascending bacterial

infection through the teat canal and *E. coli*, *M. bovis*, *Strep. uberis*, and *Staph. epidermidis* (coagulative-negative staphylococcus) are common etiologies. Studying the disease mechanism is difficult in dairy animals and to this end, murine mastitis models are useful experimental platforms. Although murine mastitis studies using the above-mentioned pathogens were performed for many years ([Anderson et al., 1976](#); [Anderson, 1983](#); [Sordillo and Nickerson, 1986](#); [Breyne et al., 2015](#)), current development of genetic and analytic technologies supersedes all those used in previous studies. The advantages and limitations of the murine mastitis model system were eloquently reviewed and discussed by [Ingman et al. \(2015\)](#). We present here a panel of murine mastitis models in lactating mice infected with mammary pathogenic bacteria cultured from field cases of clinical mastitis in dairy cows. Histopathological analysis of the glands shows an undistinguishable inflammatory response characterized by massive recruitment of blood neutrophils into alveolar and tubular milk spaces. As previously showed ([Breyne et al., 2015](#)), no changes were observed in control glands infused with the aqueous carrier of the bacteria and therefore not included in the current analysis. These acute pathological changes recapitulate the disease processes observed in field cases and underscore the translational utility of the murine model systems. Moreover, the transcriptional response observed in our model systems is highly similar to those reported in numerous studies in dairy animals ([Younis et al., 2016](#); [Rainard et al., 2022](#)). It is

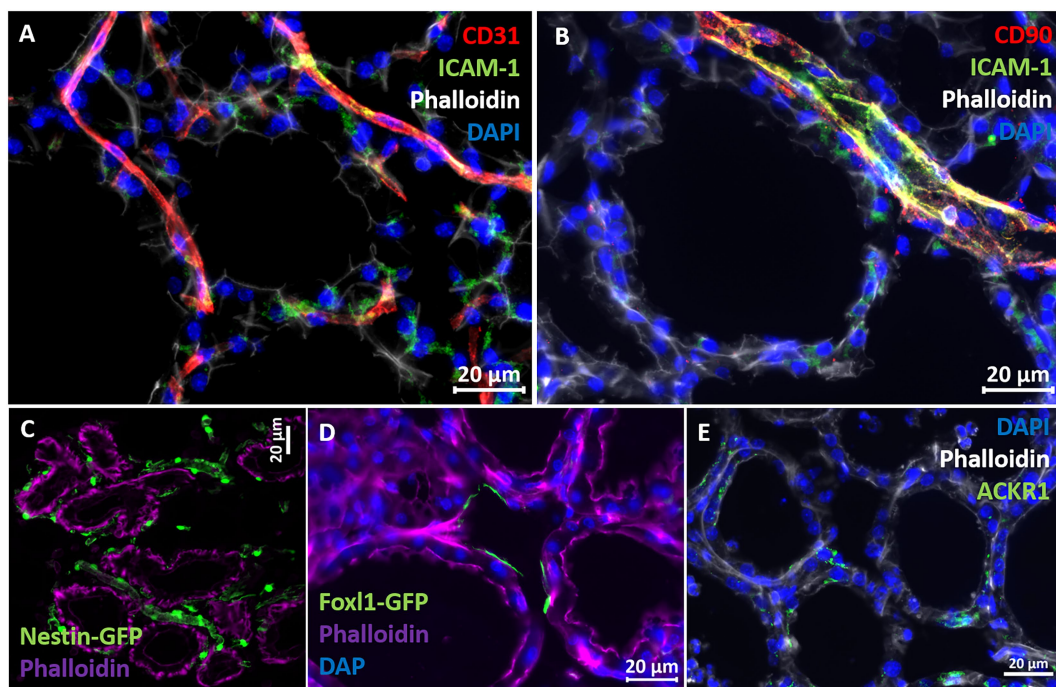


FIGURE 3

Characterization of vascular structures enveloping the alveoli in normal murine mammary gland. Capillaries (A) and post capillary venules (B) were demonstrated using the pan-endothelial marker CD31 (A) and pericyte marker CD90 (B). Cell adhesion protein ICAM-1 is expressed by endothelial cells and pericytes (A,B). Expression of the post capillary venules marker ACKR1 is visualized in C. Representative sections of cryosections stained with DAPI, phalloidin, and fluorescent anti-CD31 (A), anti-ICAM1 (A,B), anti-CD90 (B), and anti-ACKR1 antibodies (E). Pericytes were further demonstrated using normal mammary tissues obtained from Nestin-GFP transgenic mice (C), and telocytes were demonstrated using mammary tissues obtained from normal Foxp1-GFP transgenic mice (D). Scale bars; 20µm.

generally accepted that mastitis is a MAMP-mediated disease and that specialized bacterial virulence factors other than fitness factors that enable initial growth and colonization are unlikely to play a role in acute mastitis (Keane, 2019; Salamon et al., 2020). Our aim was to develop experimental platforms and research tools that will enable us to decipher the molecular mechanisms activated by MAMPs of diverse mammary pathogens yet culminating uniformly in the recruitment of blood neutrophils into milk spaces. To better understand the mechanisms of neutrophil trafficking from capillaries and post capillary venules which are surrounded by a network of pericytes and telocytes. The role pericytes and telocytes play in neutrophil recruitment to the mammary gland is currently unknown; however, transgenic mice presented in our study can expedite this avenue of research.

MAMPs released by colonizing bacteria activate MAE cells and alveolar macrophages, causing them to release inflammatory mediators, chemo attractants, and chemokines which are the enablers of neutrophil trafficking (Rainard et al., 2022). Our gene expression results are well corroborated with previous *in vitro* and *in vivo* studies showing that activation of mammary inflammation by MAMPs is mediated by TNF α , IL-1 β , and the NF κ B and IL6-JAK-STAT3 pathways (Kobayashi et al., 2013; Sharifi et al., 2018; Weller et al., 2019; Passe Pereira et al., 2021). Activation of the above pathways leads to increased production of chemokines which function as chemo attractants triggering neutrophil trafficking. In our challenge studies, the three pathogens significantly increased the expression of the

chemokines Cxcl1 (KC), Cxcl2 (Mip2), Cxcl3, Cxcl5, Ccl3, Ccl4, and Ccl7. Neutrophil recruitment occurs through an adhesion cascade, which consists of several steps. Initially, neutrophils are slowed by selectin-mediated interactions, which allows for chemokine-induced activation of integrins, firm adhesion, and transmigration across the endothelial layer. Indeed, we show here that the expression the Selp gene encoding P-selectin was significantly increased in mammary tissues infected by each of the three pathogens. The Itgam gene encodes the protein CD11b which together with CD18 (encoded by Itgb2) forms the α M β 2 integrin MAC-1. The Itgam-Icam1 pair was scored high in our L-R analysis and we also showed the expression of ICAM-1 on the mammary vasculature. These data suggest that MAC-1 which is constitutively expressed on blood neutrophils enables adherence of neutrophils to endothelial surface and transendothelial migration. Following transendothelial migration, neutrophils en route to the alveolar space need to transverse the parenchyma and epithelial cell layer. We can only speculate that the upstream of inflammatory mediators originating from the mammary epithelial cells and macrophages keep them on track. Moreover, transversing the alveolar epithelial cell layer might also involve CD11b/CD18 interactions as previously reported in other epithelial lined organs (Azcutia et al., 2023).

The highest common L-R score obtained in our analysis was for C3-Itgam interaction. As we show here and previously reported by others, C3 is highly expressed in the murine and bovine lactating mammary gland and expression is considerably increased in response to mammary infection (Salamon et al., 2020). Moreover, we have

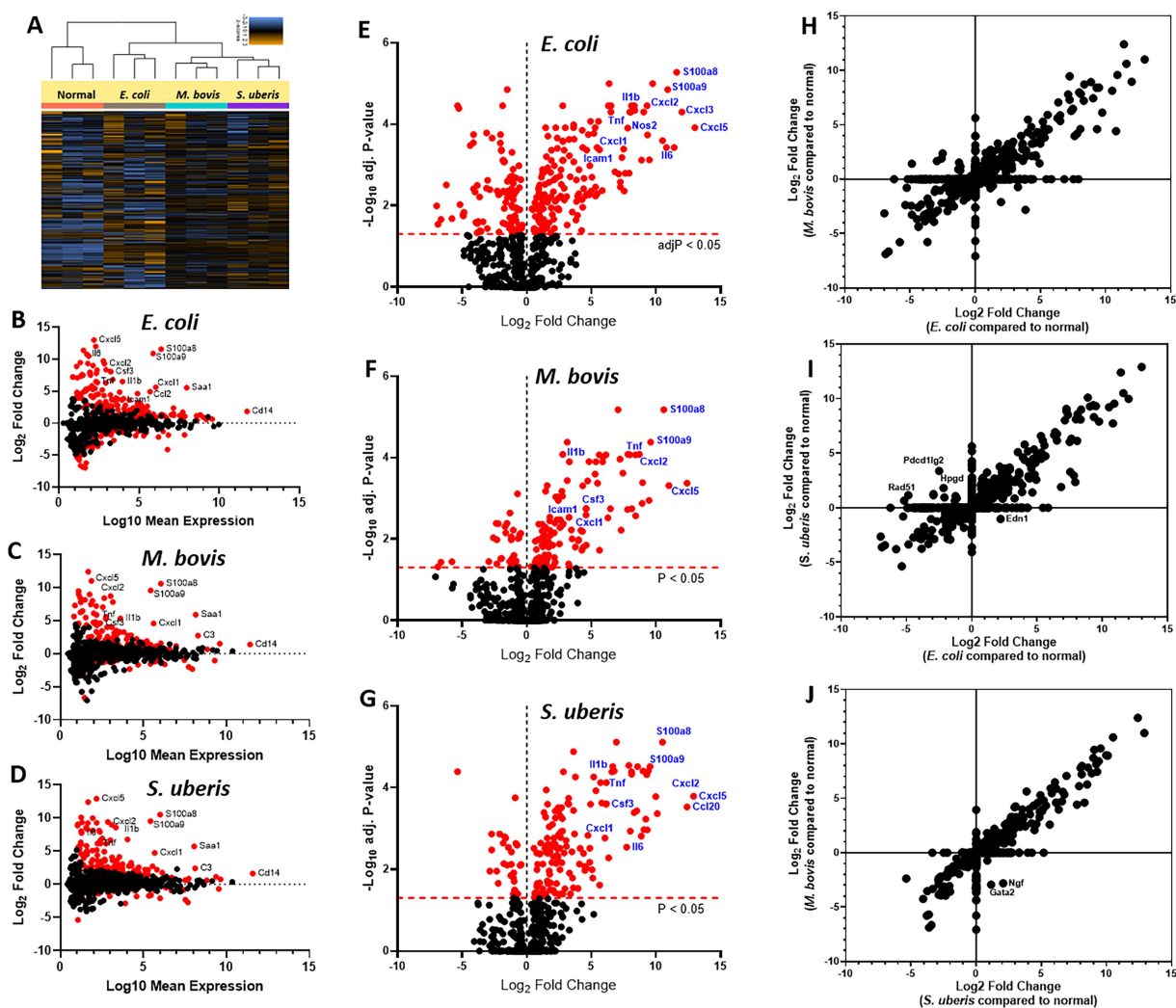


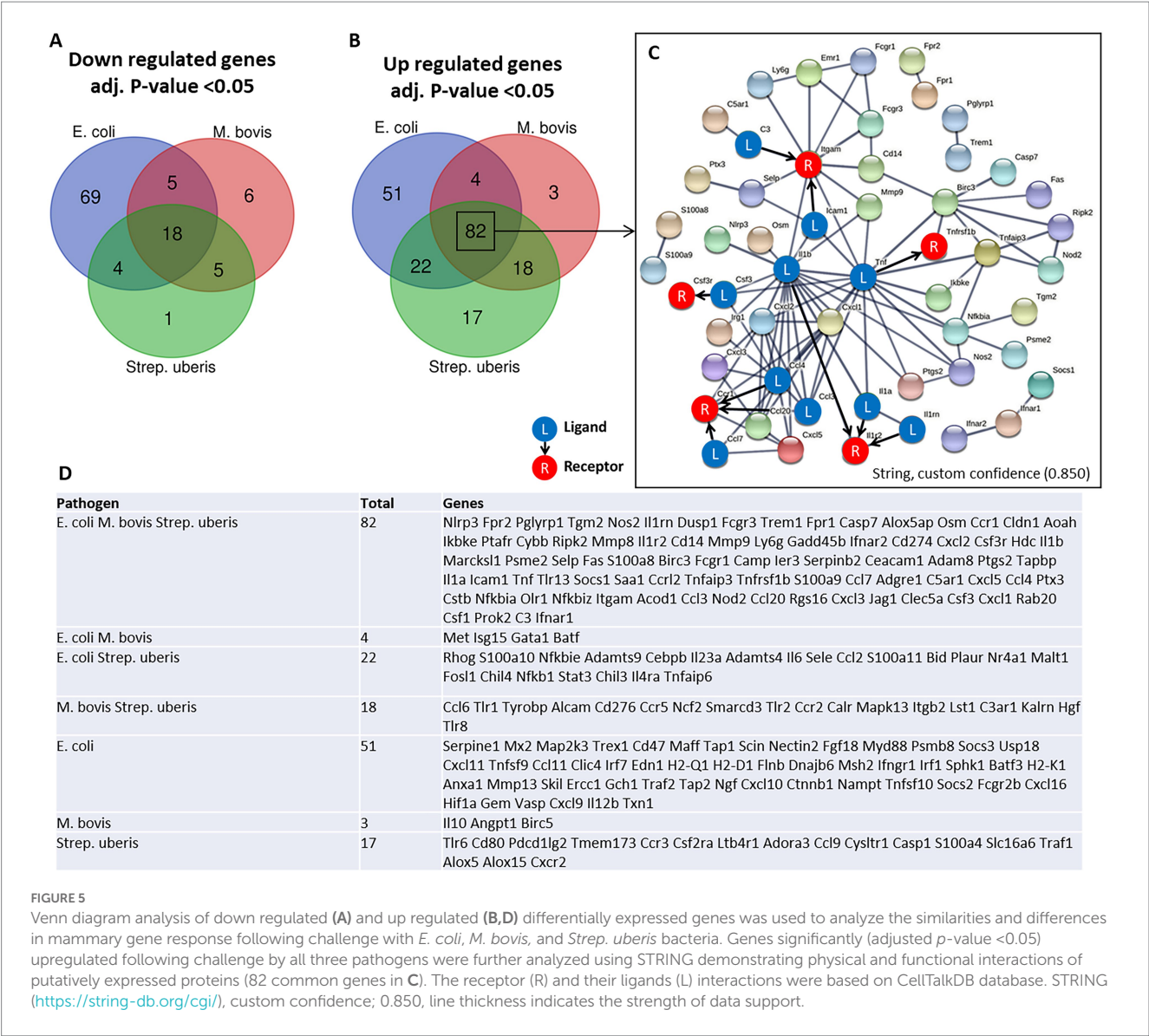
FIGURE 4

Mammary immune profiling in experimental murine mastitis using multiplex gene expression analysis. Lactating BALB/c mice were challenged by intramammary infusion of *E. coli* P4-NR, *M. bovis* PG45, and *Strep. uberis* PS10 bacteria and total RNA was extracted from mammary tissues and profiled using Nanostring nCounter Mouse Myeloid Innate Immunity V2 Panel which includes 754 genes. Following quality check and normalization, expression data presented using cluster analysis (A), MA plots (B–D), Volcano plots (E–G), and correlation plots (H–J). MA plots showing comparison of gene expression between mammary glands challenged with *E. coli* (B), *M. bovis* (C), or *Strep. uberis* (D) and normal control glands. Data represent the combined analysis of three biologically independent samples. The x-axis represents the log₁₀ of mean expression in normal and challenged glands. The y-axis indicates the differences in gene-expression level between infected and non-infected glands (log₂ fold change), larger positive values represent genes with higher expression in infected glands relative to the normal glands and larger negative values represent genes with higher expression in the normal glands relative to the infected glands. Significantly expressed genes (adjusted p -value < 0.05) are highlighted in red, and selected genes are annotated. Volcano plots (E–G) showing fold-change of gene expression in infected glands compared to non-infected normal control glands. The x-axis indicates the log₂ differences in gene-expression level between infected and non-infected glands (y-axis in MA plots). The y-axis shows the $-\log_{10}$ of the adjusted p values for each gene, with larger values indicating greater statistical significance. Those genes showing significantly different expression between infected and normal groups are highlighted in red and the dashed horizontal red line marks the cut-off for p -value lower than 0.05 corresponding to these p -values on the y-axis. Black points represent genes for which there was no significant difference in gene expression. Correlation plots (H–J) present all significantly changed genes (P_{adj} -value < 0.05; $|\log_2$ fold-change| > 1) in either challenged gland, while non-significant log₂ fold-changes are assigned the value of 1 and are located on the x-axis or on the y-axis ($\log_2 = 0$).

previously showed that while elimination of downstream activation and degradation products of C3 (using cobra venom factor treatment) regained mammary fitness of rough strains of *E. coli*, inflammation was not affected (Salamon et al., 2020). Taken together, we can further speculate that there is considerable redundancy in the molecular mechanisms underlying remote activation of neutrophil trafficking in the infected mammary gland and that C3 protein has important roles in this process irrespective of its activation and degradation products. Previous studies, including single-cell RNA sequencing of the mouse

mammary gland, showed that C3 can be expressed and produced by many cell types, including epithelial and myoepithelial cells, macrophages and fibroblasts (Ricklin et al., 2016; Bach et al., 2017; Li et al., 2020).

For now, we can only speculate that many of the upregulated genes observed in our analysis translate into components of the above described process. As previously reported in other tissues (Hyun and Hong, 2017; Girbl et al., 2018; Sekheri et al., 2021), CXCL1 (KC), CXCL2 (MIP2), ICAM-1, ACKR1, Selp (P-selectin),



and Itgam (Cd11b), are all most probably involved in transendothelial neutrophil trafficking in mastitis. Moreover, the chemokine receptor CCR1 and its ligands CCL3 and CCL4, unveiled by our L-R analysis, were previously reported as amplifiers of neutrophil recruitment (Hyun and Hong, 2017). However, gene expression data and pathway analysis need to be validated using protein imaging and intervention studies. For example, our NET gene set analysis was validated by immunofluorescence imaging for the NET marker citrullinated H3 in alveolar neutrophils. However, the relevance of NET formation in the pathogenesis of the disease needs to be evaluated using specific chemical inhibitors and/or genetic manipulation of certain genes in neutrophils. Further validation in dairy animals will be even more difficult. Other interesting pathways that were significantly upregulated by the three pathogens were interferon alpha and gamma response. Noteworthy is a recent single-cell RNA sequencing study showing similar response in recruited inflammatory neutrophils (Grieshaber-Bouyer et al., 2021); moreover, this response might even be related to NET formation (Grunwell et al., 2020; Moreira-Teixeira et al., 2020; Peng et al., 2022). However, the mechanism behind interferon-related

transcripts expression and their role in neutrophil function and immune response remains to be determined.

In conclusion, we established robust and reproducible murine mastitis model systems using important and diverse mammary pathogenic bacteria. Using a newly developed technology, we analyzed the immune genes response to mammary infection in these model systems. We show here that mammary infection with *E. coli*, *M. bovis*, and *Strep. uberis* resulted in activation of conserved core of immune genes and pathways including NET formation. Important limitations of this study were lack of temporal and spatial analysis of disease dynamics. Combining these model systems with current spatially-resolved multi-omics technologies will greatly enhance our understanding of the biology of inflammation in the mammary gland.

Data availability statement

The data presented in the study are deposited in the Gene Expression Omnibus (GEO) repository (link: <https://www.ncbi.nlm.nih.gov/geo/>), accession number GSE225127.

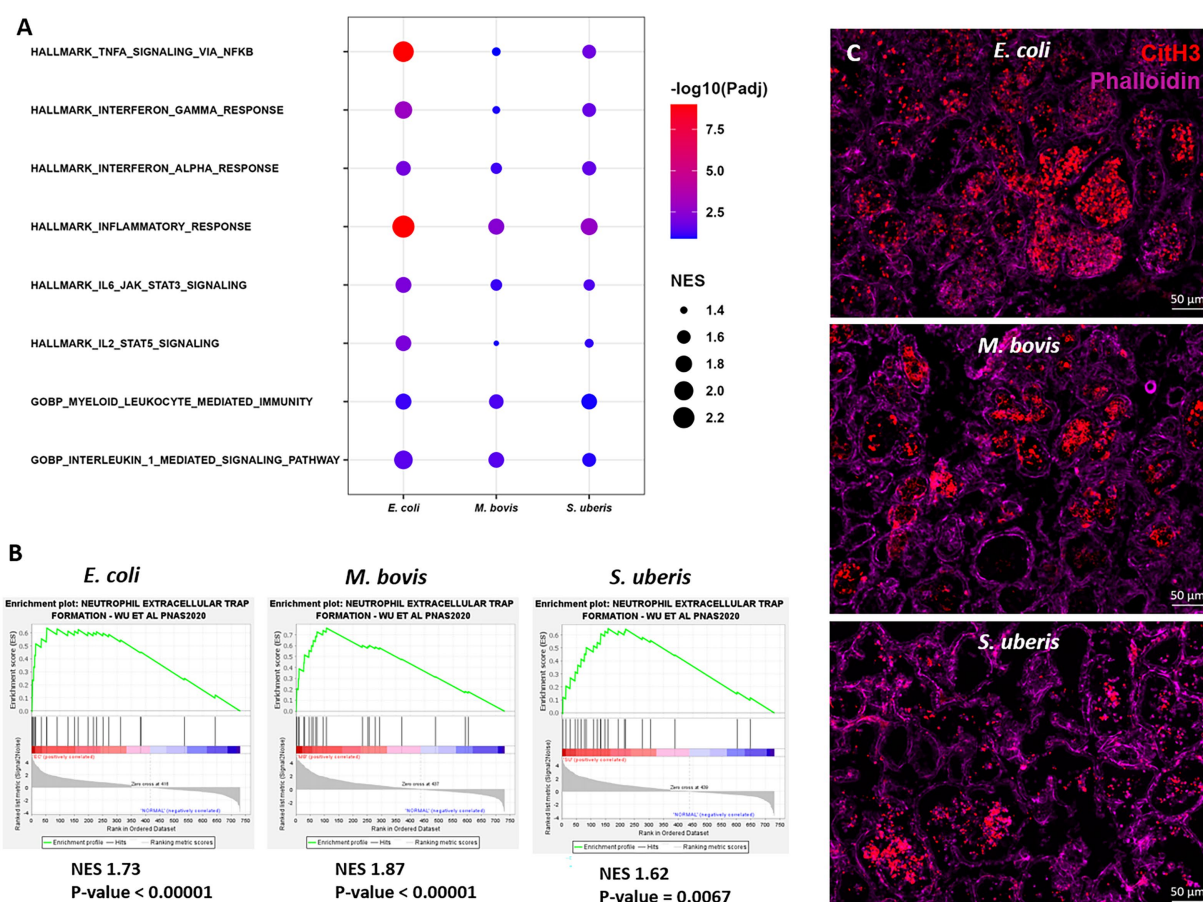


FIGURE 6

Gene set enrichment analysis (GSEA) of mammary gene expression data using HALLMARK and c5GOBP gene sets (A), and neutrophil extracellular trap (NET) gene set (B) comparing infected glands to normal controls. The most enriched HALLMARK and c5GOBP gene sets are presented for *E. coli*, *M. bovis*, and *Strep. uberis* (A). Gene set enrichment plots (Mountain plots in B) showing upregulation of genes associated with NET formation in infected glands. NES, normalized enrichment score. NET GSEA was further validated using immunofluorescence staining for citrullinated histone 3 (CitH3 in C). Representative images of mammary tissue following challenge with *E. coli* (top panel in C), *M. bovis* (middle panel in C) and *Strep. uberis* (bottom panel in C). Epifluorescence microscopic images of phalloidin and anti-CitH3 antibody staining suggesting alveolar neutrophils forming NETs. Scale bars; 50 μ m.

Ethics statement

The IACUC approvals were obtained prospectively from the Ethics Committee for Animal Experimentation, the Hebrew University of Jerusalem.

Author contributions

NS and IL conceived and designed the research. PS and EN-E performed the experimental work. NW performed immunostainings. HS assisted in data analysis and writing of the manuscript. NS took the lead in writing the manuscript. All authors provided critical feedback and helped shape the research, analysis, manuscript, read, and approved the final manuscript.

Funding

This research was funded by US-Israel Binational Agricultural Research and Development fund (BARD), grant number IS-5066-18R and by the Chief Scientist, Ministry of Agriculture and Rural Development, grant number 33-08-0006.

Conflict of interest

The authors declare that the research was conducted in the absence of any commercial or financial relationships that could be construed as a potential conflict of interest.

Publisher's note

All claims expressed in this article are solely those of the authors and do not necessarily represent those of their affiliated organizations, or those of the publisher, the editors and the reviewers. Any product that may be evaluated in this article, or claim that may be made by its manufacturer, is not guaranteed or endorsed by the publisher.

Supplementary material

The Supplementary material for this article can be found online at: <https://www.frontiersin.org/articles/10.3389/fmicb.2023.1126896/full#supplementary-material>

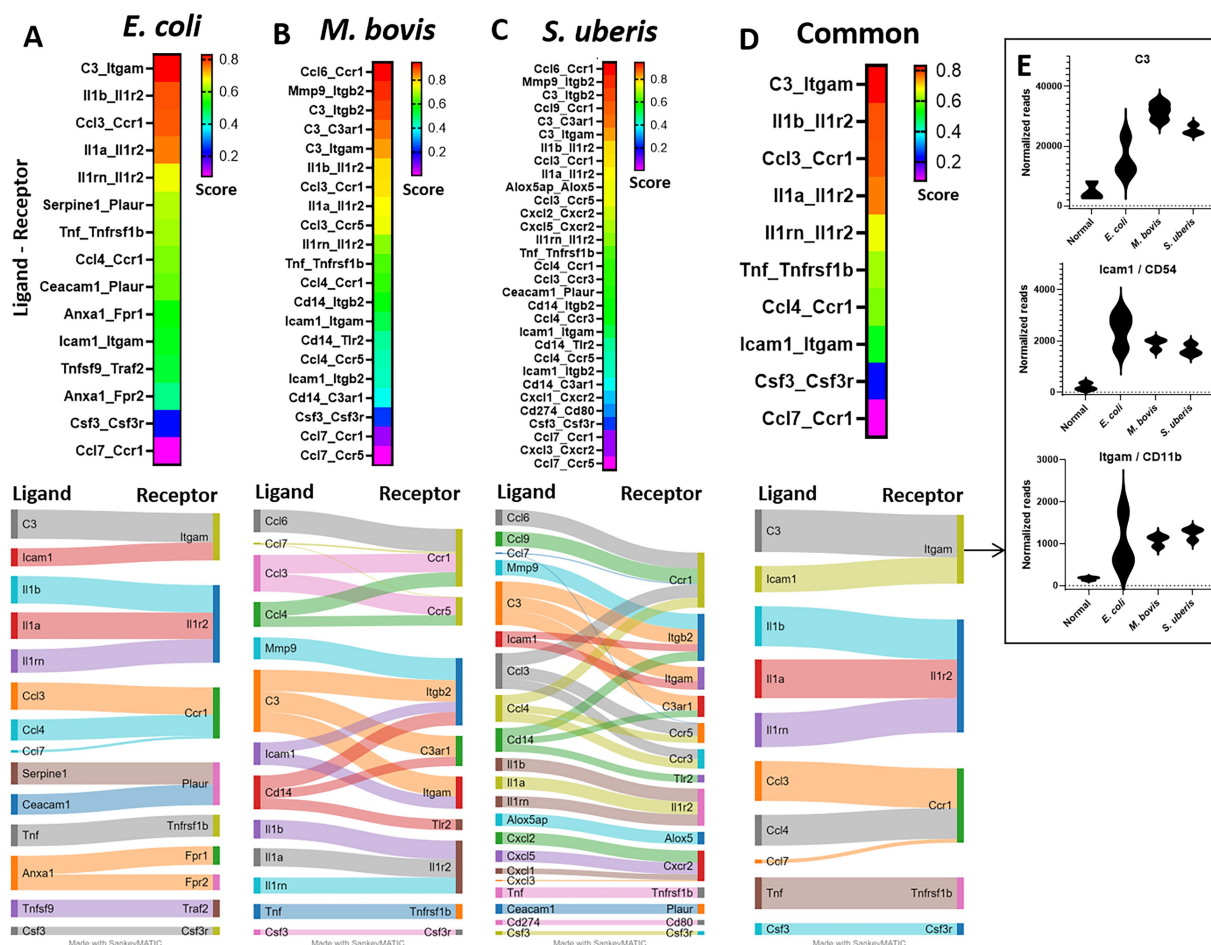


FIGURE 7

Ligand-receptor analysis in *E. coli* (A), *M. bovis* (B), and *Strep. uberis* (C) murine mastitis and common for all three pathogens (D). Mammary tissues were harvested following intramammary (IMM) bacterial challenge, bulk RNA was extracted and gene expression of 734 immune genes was quantified using Nanostring nCounter technology. Ligand-receptor data were obtained from the CellTalkDB database and communication score (CS) was computed for every ligand-receptor pair. CS Correlation coefficients were calculated for each ligand-receptor pair across all data samples and were used as CS for every ligand-receptor pair in the gene expression data. We assumed that a communication pathway is active only when ligand and receptor were both significantly ($P_{adj} < 0.05$) differentially expressed with fold change (FC) greater than 1 (see Supplementary Figure 1). Top ($CS > 0.2$) ligand-receptor interactions were visualized using heatmaps and Sankey diagram. Normalized expressions of the top common R-L pairs; C3 and Icam1 with Itgam, are presented in E.

References

- Anderson, J. C. (1983). The mouse mastitis model: observations relevant to the treatment and control of coliform mastitis. *Vet. Res. Commun.* 7, 223–227. doi: 10.1007/BF02228624
- Anderson, J. C., Howard, C. J., and Gourlay, R. N. (1976). Experimental mycoplasma mastitis in mice. *Infect. Immun.* 13, 1205–1208. doi: 10.1128/iai.13.4.1205-1208.1976
- Armingol, E., Officer, A., Harismendy, O., and Lewis, N. E. (2021). Deciphering cell-cell interactions and communication from gene expression. *Nat. Rev. Genet.* 22, 71–88. doi: 10.1038/s41576-020-00292-x
- Azcutia, V., Kelm, M., Fink, D., Cummings, R. D., Nusrat, A., Parkos, C. A., et al. (2023). Sialylation regulates neutrophil transendothelial migration, CD11b/CD18 activation, and intestinal mucosal inflammatory function. *JCI Insight*. doi: 10.1172/jci.insight.167151 [E-pub ahead of print].
- Bach, K., Pensa, S., Grzelak, M., Hadfield, J., Adams, D. J., Marioni, J. C., et al. (2017). Differentiation dynamics of mammary epithelial cells revealed by single-cell RNA sequencing. *Nat. Commun.* 8, 2128. doi: 10.1038/s41467-017-02001-5
- Benjamini, Y., and Hochberg, Y. (1995). Controlling the false discovery rate: a practical and powerful approach to multiple testing. *J. R. Stat. Soc. Ser. B* 57, 289–300. doi: 10.1111/j.2517-6161.1995.tb02031.x
- Breyne, K., De Vliegher, S., De Visscher, A., Piepers, S., and Meyer, E. (2015). Technical note: a pilot study using a mouse mastitis model to study differences between bovine associated coagulase-negative staphylococci. *J. Dairy Sci.* 98, 1090–1100. doi: 10.3168/jds.2014-8699
- Dyson, R., Charman, N., Hodge, A., Rowe, S. M., and Taylor, L. F. (2022). A survey of mastitis pathogens including antimicrobial susceptibility in southeastern Australian dairy herds. *J. Dairy Sci.* 105, 1504–1518. doi: 10.3168/jds.2021-20955
- Friis, N. (1975). Some recommendations concerning primary isolation of mycoplasma hyopneumoniae and mycoplasma flocculare. *Nordic Vet. Med.* 27, 337–339.
- Fujiwara, T., and Uehara, Y. (1984). The cytoarchitecture of the wall and the innervation pattern of the microvessels in the rat mammary gland: a scanning electron microscopic observation. *Am. J. Anat.* 170, 39–54.
- Gelgie, A. E., Korsa, M. G., and Kerro, D. O. (2022). Mycoplasma bovis mastitis. *Curr. Res. Microb. Sci.* 3, 100123. doi: 10.1016/j.crmicr.2022.100123
- Gherghiceanu, M., and Popescu, L. M. (2005). Interstitial Cajal-like cells (ICLC) in human resting mammary gland stroma. Transmission electron microscope (TEM) identification. *J. Cell. Mol. Med.* 9, 893–910. doi: 10.1111/j.1582-4934.2005.tb00387.x
- Girbl, T., Lenn, T., Perez, L., Rolas, L., Barkaway, A., Thiriot, A., et al. (2018). Distinct compartmentalization of the chemokines CXCL1 and CXCL2 and the atypical receptor ACKR1 determine discrete stages of neutrophil Diapedesis. *Immunity* 49, 1062–1076.e6. doi: 10.1016/j.immuni.2018.09.018
- Grieshaber-Bouyer, R., Radtke, F. A., Cunin, P., Stifano, G., Levescot, A., Vijaykumar, B., et al. (2021). The neutrotime transcriptional signature defines a single continuum of neutrophils across biological compartments. *Nat. Commun.* 12, 2856. doi: 10.1038/s41467-021-22973-9

- Grunwell, J. R., Stephenson, S. T., Mohammad, A. F., Jones, K., Mason, C., Opolka, C., et al. (2020). Differential type I interferon response and primary airway neutrophil extracellular trap release in children with acute respiratory distress syndrome. *Sci. Rep.* 10:19049. doi: 10.1038/s41598-020-76122-1
- Hale, H. H., Helmboldt, C. F., Plastring, W. N., and Stula, E. F. (1962). Bovine mastitis caused by a mycoplasma species. *Cornell Vet.* 52, 582–591.
- Hyun, Y. M., and Hong, C. W. (2017). Deep insight into neutrophil trafficking in various organs. *J. Leukoc. Biol.* 102, 617–629. doi: 10.1189/jlb.1RU1216-521R
- Ingman, W. V., Glynn, D. J., and Hutchinson, M. R. (2015). Mouse models of mastitis – how physiological are they? *Int. Breastfeed. J.* 10:12. doi: 10.1186/s13006-015-0038-5
- Keane, O. M. (2019). Symposium review: Intramammary infections—major pathogens and strain-associated complexity. *J. Dairy Sci.* 102, 4713–4726. doi: 10.3168/jds.2018-15326
- Klein, M., Csöbörnyiová, M., Danišovič, L., Lapides, L., and Varga, I. (2022). Telocytes in the female reproductive system: Up-to-date knowledge, challenges and possible clinical applications. *Life* 12:267. doi: 10.3390/life12020267
- Kobayashi, K., Oyama, S., Uejo, T., Kuki, C., Rahman, M. M., and Kumura, H. (2013). Underlying mechanisms involved in the decrease of milk secretion during *Escherichia coli* endotoxin induced mastitis in lactating mice. *Vet. Res.* 44:119. doi: 10.1186/1297-9716-44-119
- Kucharz, K., Kristensen, K., Johnsen, K. B., Lund, M. A., Lønstrup, M., Moos, T., et al. (2021). Post-capillary venules are the key locus for transcytosis-mediated brain delivery of therapeutic nanoparticles. *Nat. Commun.* 12:4121. doi: 10.1038/s41467-021-24323-1
- Kurban, D., Roy, J. P., Kabera, F., Fréchette, A., Um, M. M., Albaaj, A., et al. (2022). Diagnosing Intramammary infection: meta-analysis and mapping review on frequency and udder health relevance of microorganism species isolated from bovine Milk samples. *Animals* 12:3288. doi: 10.3390/ani12233288
- Leimbach, A., Poehlein, A., Vollmers, J., Görlich, D., Daniel, R., and Dobrindt, U. (2017). No evidence for a bovine mastitis *Escherichia coli* pathotype. *BMC Genomics* 18:359. doi: 10.1186/s12864-017-3739-x
- Li, C. M.-C., Shapiro, H., Tsiobikas, C., Selfors, L. M., Chen, H., Rosenbluth, J., et al. (2020). Aging-associated alterations in mammary epithelia and Stroma revealed by single-cell RNA sequencing. *Cell Rep.* 33:108566
- Liberzon, A., Birger, C., Thorvaldsdóttir, H., Ghandi, M., Mesirov, J. P., and Tamayo, P. (2015). The molecular signatures database Hallmark gene set collection. *Cell Syst.* 1, 417–425. doi: 10.1016/j.cels.2015.12.004
- Livak, K. J., and Schmittgen, T. D. (2001). Analysis of relative gene expression data using real-time quantitative PCR and the 2(-Delta Delta C(T)) method. *Methods* 25, 402–408. doi: 10.1006/meth.2001.1262
- Mignone, J. L., Kukekov, V., Chiang, A. S., Steindler, D., and Enikolopov, G. (2004). Neural stem and progenitor cells in nestin-GFP transgenic mice. *J. Comp. Neurol.* 469, 311–324. doi: 10.1002/cne.10964
- Mintz, D., Salamon, H., Mintz, M., Rosenshine, I., and Shpigel, N. Y. (2019). Intraepithelial neutrophils in mammary, urinary and gall bladder infections. *Vet. Res.* 50:56. doi: 10.1186/s13567-019-0676-5
- Moreira-Teixeira, L., Stimpson, P. J., Stavropoulos, E., Hadebe, S., Chakravarty, P., Ioannou, M., et al. (2020). Type I IFN exacerbates disease in tuberculosis-susceptible mice by inducing neutrophil-mediated lung inflammation and NETosis. *Nat. Commun.* 11:5566. doi: 10.1038/s41467-020-19412-6
- Passe Pereira, H., Lima Verardo, L., Del Cambre, M., Amaral Weller, M., Paula Sbardella, A., Prado Munari, D., et al. (2021). Going further post-RNA-seq: in silico functional analyses revealing candidate genes and regulatory elements related to mastitis in dairy cattle. *J. Dairy Res.* 88, 286–292. doi: 10.1017/S0022029921000571
- Peng, Y., Wu, X., Zhang, S., Deng, C., Zhao, L., Wang, M., et al. (2022). The potential roles of type I interferon activated neutrophils and neutrophil extracellular traps (NETs) in the pathogenesis of primary Sjögren's syndrome. *Arthritis Res. Ther.* 24:170. doi: 10.1186/s13075-022-02860-4
- Radermecker, C., Hego, A., Vanwing, C., and Marichal, T. (2022). Methods to detect neutrophil extracellular traps in asthma. *Methods Mol. Biol.* 2506, 281–295. doi: 10.1007/978-1-0716-2364-0_20
- Rainard, P., Gilbert, F. B., and Germon, P. (2022). Immune defenses of the mammary gland epithelium of dairy ruminants. *Front. Immunol.* 13:1031785. doi: 10.3389/fimmu.2022.1031785
- Ricklin, D., Reis, E. S., Mastellos, D. C., Gros, P., and Lambris, J. D. (2016). Complement component C3 – the “Swiss Army knife” of innate immunity and host defense. *Immunol. Rev.* 274, 33–58. doi: 10.1111/imr.12500
- Rodwell, A., and Whitcomb, R. (1983). Methods for direct and indirect measurement of mycoplasma growth. *Methods Mycoplasma* 1, 185–196. doi: 10.1016/B978-0-12-583801-6.50036-6
- Salamon, H., Nissim-Eliraz, E., Ardronai, O., Nissan, I., and Shpigel, N. Y. (2020). The role of O-polysaccharide chain and complement resistance of *Escherichia coli* in mammary virulence. *Vet. Res.* 15:77. doi: 10.1186/s13567-020-00804-x
- Sanders, N. L., Martin, I. M. C., Sharma, A., Jones, M. R., Quinton, L. J., Bosmann, M., et al. (2022). Neutrophil extracellular traps as an exacerbating factor in bacterial pneumonia. *Infect. Immun.* 90:e0049121. doi: 10.1128/iai.00491-21
- Schneider, P., Re, B., Schouten, I., Nissim-Eliraz, E., Lysnyansky, I., and Shpigel, N. Y. (2022). Lipoproteins are potent activators of nuclear factor kappa B in mammary epithelial cells and virulence factors in mycoplasma bovis mastitis. *Microorganisms* 10:2209. doi: 10.3390/microorganisms10112209
- Sekheri, M., Othman, A., and Filep, J. G. (2021). $\beta 2$ integrin regulation of neutrophil functional plasticity and fate in the resolution of inflammation. *Front. Immunol.* 12:660760. doi: 10.3389/fimmu.2021.660760
- Shao, X., Liao, J., Li, C., Lu, X., Cheng, J., and Fan, X. (2020). CellTalkDB: a manually curated database of ligand–receptor interactions in humans and mice. *Brief. Bioinform.* 22:bbaa269. doi: 10.1093/bib/bbaa269
- Sharifi, S., Pakdel, A., Ebrahimi, M., Reecy, J. M., Fazeli Farsani, S., and Ebrahimie, E. (2018). Integration of machine learning and meta-analysis identifies the transcriptomic bio-signature of mastitis disease in cattle. *PLoS One* 13:e0191227. doi: 10.1371/journal.pone.0191227
- Shoshkes-Carmel, M., Wang, Y. J., Wangenstein, K. J., Tóth, B., Kondo, A., Massasa, E. E., et al. (2018). Subepithelial telocytes are an important source of Wnts that supports intestinal crypts. *Nature* 557, 242–246. doi: 10.1038/s41586-018-0084-4
- Shpigel, N. Y., Levin, D., Winkler, M., Saran, A., Ziv, G., and Bottner, A. (1997). Efficacy of cefquinome for treatment of cows with mastitis experimentally induced using *Escherichia coli*. *J. Dairy Sci.* 80, 318–323.
- Shpigel, N. Y., Winkler, M., Ziv, G., and Saran, A. (1998). Clinical, bacteriological and epidemiological aspects of clinical mastitis in Israeli dairy herds. *Prev. Vet. Med.* 35, 1–9.
- Shwimmer, A., Freed, M., Blum, S., Khatib, N., Weissblit, L., Friedman, S., et al. (2007). Mastitis caused by *Yersinia pseudotuberculosis* in Israeli dairy cattle and public health implications. *Zoonoses Public Health* 54, 353–357. doi: 10.1111/j.1863-2378.2007.01072.x
- Sordillo, L. M., and Nickerson, S. C. (1986). Morphological changes caused by experimental streptococcus uberis mastitis in mice following intramammary infusion of pokeweed mitogen. *Proc. Soc. Exp. Biol. Med.* 182, 522–530.
- Subramanian, A., Tamayo, P., Mootha, V. K., Mukherjee, S., Ebert, B. L., Gillette, M. A., et al. (2005). Gene set enrichment analysis: a knowledge-based approach for interpreting genome-wide expression profiles. *Proc. Natl. Acad. Sci.* 102, 15545–15550. doi: 10.1073/pnas.0506580102
- Szklarczyk, D., Gable, A. L., Lyon, D., Junge, A., Wyder, S., Huerta-Cepas, J., et al. (2018). STRING v11: protein–protein association networks with increased coverage, supporting functional discovery in genome-wide experimental datasets. *Nucleic Acids Res.* 47, D607–D613. doi: 10.1093/nar/gky1131
- Thiriot, A., Perdomo, C., Cheng, G., Novitzky-Basso, I., McArdle, S., Kishimoto, J. K., et al. (2017). Differential DARC/ACKR1 expression distinguishes venular from non-venular endothelial cells in murine tissues. *BMC Biol.* 15:45. doi: 10.1186/s12915-017-0381-7
- Wald, R., Baumgartner, M., Urbantke, V., Stessl, B., and Wittek, T. (2017). Diagnostic accuracy of a standardized scheme for identification of *Streptococcus uberis* in quarter milk samples: a comparison between conventional bacteriological examination, modified Rambach agar medium culturing, and 16S rRNA gene sequencing. *J. Dairy Sci.* 100, 1459–1466. doi: 10.3168/jds.2016-11786
- Warren, S. (2018). Simultaneous, multiplexed detection of RNA and protein on the NanoString[®] nCounter[®] platform. *Methods Mol. Biol.* 1783, 105–120. doi: 10.1007/978-1-4939-7834-2_5
- Weller, M. M. D. C. A., Fonseca, I., Sbardella, A. P., Pinto, I. S. B., Viccini, L. F., Brandão, H. M., et al. (2019). Isolated perfused udder model for transcriptome analysis in response to *Streptococcus agalactiae*. *J. Dairy Res.* 86, 307–314. doi: 10.1017/S0022029919000451
- Wise, K. S., Calcutt, M. J., Foecking, M. F., Röske, K., Madupu, R., and Methé, B. A. (2011). Complete genome sequence of mycoplasma bovis type strain PG45 (ATCC 25523). *Infect. Immun.* 79, 982–983. doi: 10.1128/iai.00726-10
- Wu, M., Chen, Y., Xia, H., Wang, C., Tan, C. Y., Cai, X., et al. (2020). Transcriptional and proteomic insights into the host response in fatal COVID-19 cases. *Proc. Natl. Acad. Sci. U. S. A.* 10, 28336–28343. doi: 10.1073/pnas.2018031117
- Younis, S., Javed, Q., and Blumenberg, M. (2016). Meta-analysis of transcriptional responses to mastitis-causing *Escherichia coli*. *PLoS One* 11:e0148562. doi: 10.1371/journal.pone.0148562



OPEN ACCESS

EDITED BY

Chih-Horng Kuo,
Academia Sinica, Taiwan

REVIEWED BY

Li Xiao,
University of Alabama at Birmingham,
United States
Roger Dumke,
Technical University Dresden, Germany

*CORRESPONDENCE

Tsuyoshi Kenri
✉ kenri@niid.go.jp

[†]Presently retired

RECEIVED 08 April 2023

ACCEPTED 24 May 2023

PUBLISHED 19 June 2023

CITATION

Kenri T, Yamazaki T, Ohya H, Jinnai M, Oda Y, Asai S, Sato R, Ishiguro N, Oishi T, Horino A, Fujii H, Hashimoto T, Nakajima H and Shibayama K (2023) Genotyping of *Mycoplasma pneumoniae* strains isolated in Japan during 2019 and 2020: spread of *p1* gene type 2c and 2j variant strains. *Front. Microbiol.* 14:1202357. doi: 10.3389/fmicb.2023.1202357

COPYRIGHT

© 2023 Kenri, Yamazaki, Ohya, Jinnai, Oda, Asai, Sato, Ishiguro, Oishi, Horino, Fujii, Hashimoto, Nakajima and Shibayama. This is an open-access article distributed under the terms of the [Creative Commons Attribution License \(CC BY\)](https://creativecommons.org/licenses/by/4.0/). The use, distribution or reproduction in other forums is permitted, provided the original author(s) and the copyright owner(s) are credited and that the original publication in this journal is cited, in accordance with accepted academic practice. No use, distribution or reproduction is permitted which does not comply with these terms.

Genotyping of *Mycoplasma pneumoniae* strains isolated in Japan during 2019 and 2020: spread of *p1* gene type 2c and 2j variant strains

Tsuyoshi Kenri^{1*}, Tsutomu Yamazaki², Hitomi Ohya³, Michio Jinnai³, Yoichiro Oda⁴, Sadasaburo Asai⁵, Rikako Sato⁶, Nobuhisa Ishiguro⁶, Tomohiro Oishi⁷, Atsuko Horino¹, Hiroyuki Fujii⁸, Toru Hashimoto⁸, Hiroshi Nakajima^{9†} and Keigo Shibayama¹⁰

¹Department of Bacteriology II, National Institute of Infectious Diseases, Tokyo, Japan, ²Wakaba Children's Clinic, Saitama, Japan, ³Kanagawa Prefectural Institute of Public Health, Kanagawa, Japan, ⁴Chigasaki Municipal Hospital, Kanagawa, Japan, ⁵Asai Children's Clinic, Osaka, Japan, ⁶Department of Pediatrics, Hokkaido University Graduate School of Medicine, Sapporo, Japan, ⁷Department of Clinical Infectious Diseases, Kawasaki Medical School, Okayama, Japan, ⁸Kurashiki Central Hospital, Okayama, Japan, ⁹Okayama Prefectural Institute for Environmental Science and Public Health, Okayama, Japan, ¹⁰Department of Bacteriology, Nagoya University Graduate School of Medicine, Nagoya, Japan

We characterized 118 *Mycoplasma pneumoniae* strains isolated from three areas of Japan (Saitama, Kanagawa, and Osaka) during the period of 2019 and 2020. Genotyping of the *p1* gene in these strains revealed that 29 of them were type 1 lineage (29/118, 24.6%), while 89 were type 2 lineage (89/118, 75.4%), thereby indicating that type 2 lineage was dominant in this period. The most prevalent variant of type 2 lineage was type 2c (57/89, 64%), while the second-most was type 2j, a novel variant identified in this study (30/89, 33.7%). Type 2j *p1* is similar to type 2g *p1*, but cannot be distinguished from reference type 2 (classical type 2) using the standard polymerase chain reaction-restriction fragment length polymorphism analysis (PCR-RFLP) with *HaeIII* digestion. Thus, we used *MboI* digestion in the PCR-RFLP analysis and re-examined the data from previous genotyping studies as well. This revealed that most strains reported as classical type 2 after 2010 in our studies were actually type 2j. The revised genotyping data showed that the type 2c and 2j strains have been spreading in recent years and were the most prevalent variants in Japan during the time-period of 2019 and 2020. We also analyzed the macrolide-resistance (MR) mutations in the 118 strains. MR mutations in the 23S rRNA gene were detected in 29 of these strains (29/118, 24.6%). The MR rate of type 1 lineage (14/29, 48.3%) was still higher than that of type 2 lineage (15/89, 16.9%); however, the MR rate of type 1 lineage was lower than that found in previous reports published in the 2010s, while that of type 2 lineage strains was slightly higher. Thus, there is a need for continuous surveillance of the *p1* genotype and MR rate of *M. pneumoniae* clinical strains, to better understand the epidemiology and variant evolution of this pathogen, although *M. pneumoniae* pneumonia cases have decreased significantly since the COVID-19 pandemic.

KEYWORDS

Mycoplasma pneumoniae, *Mycoplasma pneumoniae*, whole-genome single-nucleotide polymorphism, infectious diseases surveillance, macrolide resistance, antigenic variation, protective immunity, *p1* gene genotyping

1. Introduction

Mycoplasma pneumoniae (*Mycoplasma pneumoniae*) is a cell wall-lacking bacterium that is a common cause of pneumonia and bronchitis in humans. *M. pneumoniae* clinical isolates can be classified into two distinct genetic groups: type 1 and 2 lineages (Xiao et al., 2015; Diaz et al., 2017; Lee et al., 2019; Kenri et al., 2020). Standard genotyping methods developed for *M. pneumoniae*, including multi-locus variable-number tandem repeat analysis (MLVA; Degrange et al., 2009), multi-locus sequence typing (MLST; Brown et al., 2015), and single nucleotide polymorphism (SNP) analysis (Touati et al., 2015; Zhao et al., 2021), can easily discriminate between these two lineages (Supplementary Figure S1). The classical reference strains of the type 1 and 2 lineages are M129 and FH, respectively (GenBank accession nos. U00089 and CP010546, respectively; Lipman et al., 1969; Barile et al., 1988; Himmelreich et al., 1996). The detection rate of type 1 and 2 lineage strains in clinical specimens fluctuates depending on the area and time-point of genotyping research (Pereyre et al., 2007; Dumke et al., 2010; Diaz et al., 2015; Zhao et al., 2019). In Japan, several epidemiological studies have observed that type 1 and 2 lineages alternately become dominant, in cycles of about 10 years (Sasaki et al., 1996; Kenri et al., 2008, 2020). Between the type 1 and 2 lineages, the *p1* (MPN141) and *orf6* (MPN142) genes also exhibit sequence polymorphism (Su et al., 1990; Ruland et al., 1994). The *p1* and *orf6* genes encode the P1 and P40/P90 proteins, respectively, which are components of the adhesin protein complex (nap) and responsible for the infection process and pathogenesis of this bacterium (Waites et al., 2017; Vizarraga et al., 2020). The sequence polymorphism of *p1* and *orf6* can be discriminated using PCR-restriction fragment length polymorphism (RFLP) analysis (Cousin-Allery et al., 2000) or sequencing of the *p1* operon. These analyses enable further classification of *p1* and *orf6* genes, in addition to that of the classical type 1 and 2 sequences of the M129 and FH strains. Several variants of *p1* and *orf6* in the type 1 and 2 lineages are known to date (Kenri et al., 2020; Xiao et al., 2020). These *p1* and *orf6* variants are generated by DNA recombination between repetitive sequences (RepMP elements) in the *M. pneumoniae* genome (Kenri et al., 1999; Hakim et al., 2021). Variations in the *p1* and *orf6* genes cause amino acid substitutions in the P1 and P40/P90 proteins, respectively, and may affect the antigenicity and infectivity of this bacterium, as well as the host immune response. Therefore, it is important to undertake surveillance of new *p1* and *orf6* gene variants.

Macrolides are first-line drugs for the clinical treatment of *M. pneumoniae* pneumonia (Yamazaki and Kenri, 2016). However, macrolide-resistant *M. pneumoniae* (MRMP) strains have spread since the 2000s, especially in East Asian countries (Meyer Sauter et al., 2016; Pereyre et al., 2016; Kim et al., 2022), raising concerns regarding the treatment of *M. pneumoniae* infections. An interesting epidemiological feature of recent MRMP strain profiles is the high macrolide-resistance (MR) rate of type 1 lineage strains, as compared to that of type 2 strains. Most type 1 clinical isolates were MRMPs in the early 2010s, whereas type 2 lineage strains were largely macrolide-susceptible *M. pneumoniae* (MSMP; Liu et al., 2009; Zhao et al., 2019; Kenri et al., 2020; Ishiguro et al., 2021; Nakamura et al., 2021). This may be because of the excessive clinical use of macrolides in the 2000s, when type 1 lineage strains were dominant. Since the late 2010s, type 2 lineage strains have become clinically prevalent in Japan, and most of these type 2 lineage strains are

MSMP. However, in China and South Korea, a gradual increase in the MR rate of the type 2 lineage has been reported in recent years (Wang et al., 2021; Guo et al., 2022; Lee et al., 2022; Wang et al., 2022). Therefore, it is particularly important to monitor the MR rate of the type 2 lineage strains in Japan. In this study, we analyzed the *p1* gene genotype and MR mutations in 118 *M. pneumoniae* strains isolated in Japan during the period of 2019 and 2020.

2. Materials and methods

2.1. *Mycoplasma pneumoniae* isolates

The 118 *M. pneumoniae* strains analyzed in this study are listed in Supplementary Table S1. These strains were isolated from throat swab and sputum specimens by means of culture in PPLO (pleuropneumonia-like organisms) medium, as reported previously (Kenri et al., 2008, 2020). Throat swabs and sputa were collected from patients with acute respiratory infections, between August 2019 and April 2020, from three areas of Japan (Saitama, Kanagawa, and Osaka prefectures). Swabs were collected at the Wakaba Children's Clinic in Saitama, Chigasaki Municipal Hospital and sentinel hospitals for infectious diseases surveillance in Kanagawa, and the Asai Children's Clinic in Osaka. Sputa were collected at Kishiwada Tokushukai Hospital in Osaka. The throat swabs and sputa were collected and analyzed under the approval of the ethics committees of the National Institute of Infectious Diseases (No. 1487) and the Kanagawa Prefectural Institute of Public Health (No. R2-1).

2.2. *p1* typing and detection of MR mutations

p1 genotyping of *M. pneumoniae* isolates was performed using PCR-RFLP analysis, as reported previously (Cousin-Allery et al., 2000). Briefly, *p1* gene sequences containing the RepMP4 or RepMP2/3 regions were amplified using PCR, with the ADH1 (5'-CTGCCTTGTCCAAGTCCACT-3') and ADH2 (5'-AACCTTGTCGGAAGAGCTG-3') or ADH3 (5'-CGAGTTTGCTGCTAACGAGT-3') and ADH4 (5'-CTTGACTGATACCTGTGCGG-3') primer sets (Figure 1A). The amplified fragments were digested using *Hae*III or *Mbo*I restriction enzymes (Takara Bio, Shiga, Japan). To visualize the RFLP patterns for typing, digested fragments were analyzed using 2% agarose-gel electrophoresis. To sequence the *p1* operon, a previously reported method and primer set were used (Katsukawa et al., 2019). The MR of the *M. pneumoniae* isolates was examined by detecting MR mutations in the 23S rRNA gene, using a previously reported method (Matsuoka et al., 2004).

2.3. Genome sequencing and whole-genome single-nucleotide polymorphism (WG-SNP) analysis

Six *M. pneumoniae* strains KPI-025, Y12-4, Y12-24, Y12-38, OA-57, and OA-63 were sequenced in this study (Supplementary Figures S1; Supplementary Table S1). The strains were cultured in 10 mL of PPLO broth, following which the cells were

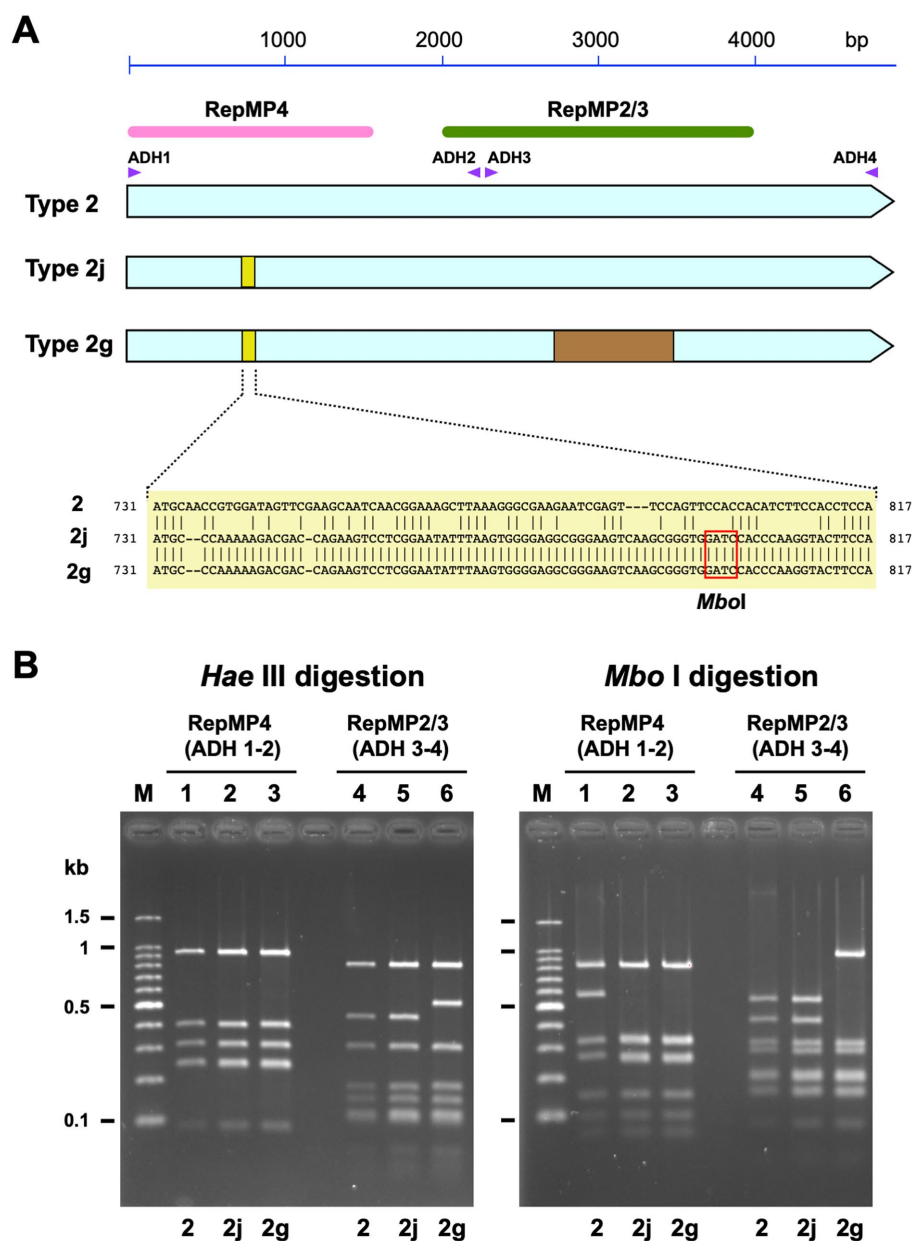


FIGURE 1 Discrimination of type 2 lineage *p1* genes using PCR-RFLP analysis. **(A)** A schematic illustration of type 2 *p1* gene variants. The three light blue arrows indicate type 2, 2j, and 2g genes. The small yellow boxes indicate the location of variation in the type 2j and 2g *p1* genes. The sequences of the variations are shown below. Type 2j and 2g *p1* have an *Mbo*I site in this region. The brown rectangle indicates the location of the variation in the type 2g *p1* gene. The pink and green bars indicate the locations of the RepMP4 and RepMP2/3 elements, respectively. The small purple triangles indicate the positions of ADH1, ADH2, ADH3, and ADH4 primers used for PCR-RFLP analysis. **(B)** Band patterns obtained for PCR-RFLP analysis of type 2, 2j, and 2g *p1* genes upon 2% agarose-gel electrophoresis. The left and the right panels show the *Hae*III and *Mbo*I digestion patterns of the same samples, respectively. The RepMP4 region (ADH1-2 amplicon) of the FH (type 2), Y12-38 (type 2j), and K708 (type 2g) strains have been analyzed in lanes 1, 2, and 3, respectively. The RepMP2/3 region (ADH3-4 amplicon) of the same strains has been analyzed in lanes 4, 5, and 6, respectively. Lane M shows the 100bp ladder DNA size marker.

harvested. Genomic DNA was extracted using the QIAamp DNA Mini Kit (Qiagen, Hilden, Germany). Libraries of 500bp-long genomic DNA inserts were prepared using the Illumina DNA Prep (M) Tagmentation Kit (Illumina, San Diego, CA, United States). Next-generation sequencing was performed at the Genome-Lead Corporation (Kagawa, Japan), using the Illumina MiSeq platform and MiSeq Reagent Micro Kit v2 (Illumina). The obtained paired-end

reads were assembled *de novo* using Shovill v1.1.0,¹ with default parameters. WG-SNP analysis was performed using the CSI Phylogeny 1.4 pipeline² (Kaas et al., 2014). The genome sequences of the type 1

1 <https://github.com/tseemann/shovill>
2 <https://cge.food.dtu.dk/services/CSIPhylogeny/>

strain M129-B7 (GenBank accession no. CP003913) and type 2 strain FH (GenBank accession no. CP017327) were used as reference sequences for the analyses of type 1 and type 2 lineage strains, respectively. Phylogenetic trees were visualized using FigTree v1.4.4 software.³

2.4. Phylogenetic analysis of type 1 lineage strains

MPN295, MPN607, and MPN678 gene fragments were amplified from type 1 *M. pneumoniae* genomic DNA using PCR, with the primer sets listed in Table 1. PCR was performed in multiplex or separately for the three genes. In the multiplex PCR conditions, 4-times higher amounts of the MPN295 primer set than those of the MPN607 and MPN678 primer sets were used in the PCR reaction mixture. The PCR products of the MPN295, MPN607, and MPN678 genes were treated with the restriction enzyme *ApoI* (New England Biolabs, Ipswich, MA, United States) and then analyzed using 2% agarose-gel electrophoresis, to visualize the digestion pattern (see Section 3.3).

2.5. Nucleotide sequence accession numbers

The nucleotide sequences of the type 2j *p1* gene operon of the Y4-20, KT19, and OA-29 strains were deposited in the DDBJ/ENA/GenBank databases, under the accession numbers LC588412, LC588413, and LC588414, respectively. The nucleotide sequence of the type 2b2 *p1* operon of the Y12-24 strain was deposited under the accession number LC753471. Genome sequence data of six *M. pneumoniae* strains, KPI-025, Y12-4, Y12-24, Y12-38, OA-57, and OA-63, were deposited under the accession numbers BSFT01000000, BSFU01000000, BSFV01000000, BSFW01000000, BSFX01000000, and BSFY01000000, respectively.

3. Results

3.1. Identification of a novel *P1* gene variant 2j during *P1* genotyping and MR analysis of *Mycoplasma pneumoniae* isolates collected during the period of 2019 and 2020

We isolated 118 *M. pneumoniae* strains from patients with acute respiratory infections between August 2019 and April 2020 using a culture method. Throat swab and sputum specimens for *M. pneumoniae* isolation were collected from three areas in Japan (Saitama, Kanagawa, and Osaka prefectures; see Section 2; Supplementary Table S1). We analyzed the *p1* gene genotype and MR mutations in these isolates. *P1* genotyping was performed using standard PCR-RFLP analysis, and several specimens were inspected

TABLE 1 PCR primers used for the phylogenetic analysis of type 1 lineage strains.

Primers	Sequence	Amplicon size (bp)
MPN295-F	TTGATTGAATTACTTACCTCAA	150
MPN295-R	TAGTGAACACGCCATAAACA	
MPN607-F	CAGTTAATTACGCAAAAGTTTAG	300
MPN607-R	CAAGGTTAAAGACGAGAAGC	
MPN678-F	GAGGACACTGACACTGAGCG	624
MPN678-R	GCCACTCTTGTCGACTATCAC	

by means of DNA sequencing. During this sequence inspection, we identified a novel *p1* gene variant, which had a minor sequence change in the RepMP4 region of the *p1* gene, as compared to that of the classical type 2 strains (Figure 1). Although this RepMP4 variation was identical to that of the type 2g strain reported previously (Katsukawa et al., 2019), the new variant did not exhibit variation in the RepMP2/3 region, unlike that of type 2g (Figure 1A). We designated this novel variant as type 2j, to distinguish it from classical type 2 and 2g. Type 2j cannot be discriminated from the classical type 2 using PCR-RFLP typing with *HaeIII* digestion, because the sequence change in the RepMP4 region of type 2j and 2g is not recognized by *HaeIII* (Figure 1B, lanes 1–3). Therefore, to distinguish type 2j from classical type 2, we employed *MboI* digestion in the PCR-RFLP genotyping, in addition to *HaeIII* digestion (Figure 1).

The results of *p1* genotyping and MR mutation analysis are shown in Figure 2. Of the 118 isolates, 29 were *p1* gene type 1, 2 were type 2b2, 57 were type 2c, and 30 were type 2j (Figure 2A). No other variants of the type 1 or 2 lineage were detected, including the type 2h and 2i reported recently in the United States (Xiao et al., 2020). This result showed that type 2 lineage strains were clinically prevalent in Japan during the time-period of 2019 and 2020 (89/118, 75.4%). Among the type 2 lineages, the type 2c (57/89, 64%) and type 2j (30/89, 33.7%) strains were the most common. To our knowledge, this is also the first time that type 2b2 has been detected in Japan (Figure 2A). The type 2b2 was named variant 2bv or 2e in the previous reports (Gullsby et al., 2019; Xiao et al., 2020).

Macrolide-resistance mutations in the 23S rRNA gene were detected in 29 isolates (29/118, 24.6%). The MR rate of the type 1 isolates was higher (14/29, 48.3%) than that of the type 2 isolates (15/89, 16.9%; Figure 2A). Two type 1 strains (KP3283 and KP3286) derived from Kanagawa carried the A2064G mutation in the 23S rRNA gene, and one type 2j strain (KT-19) derived from Osaka hospital in 2019 carried the A2063T mutation, while the other 26 MR strains carried the A2063G mutation, including two type 2b2 strains (Figure 2B; Supplementary Figure S1).

The proportion of *p1* genotype and MR rate of isolates varied depending on the area (Figure 2B). In the Osaka clinic, the same number of type 1 and type 2 lineage strains were isolated, whereas only type 2 lineage strains were isolated from the Osaka hospital. The MR rate of type 1 strains was higher in the Saitama clinic (66.7%) than that in the Kanagawa (42.9%) and Osaka (43.8%) clinics. In Osaka hospital, the MR rate of the type 2 lineage was

³ <http://tree.bio.ed.ac.uk/software/figtree>

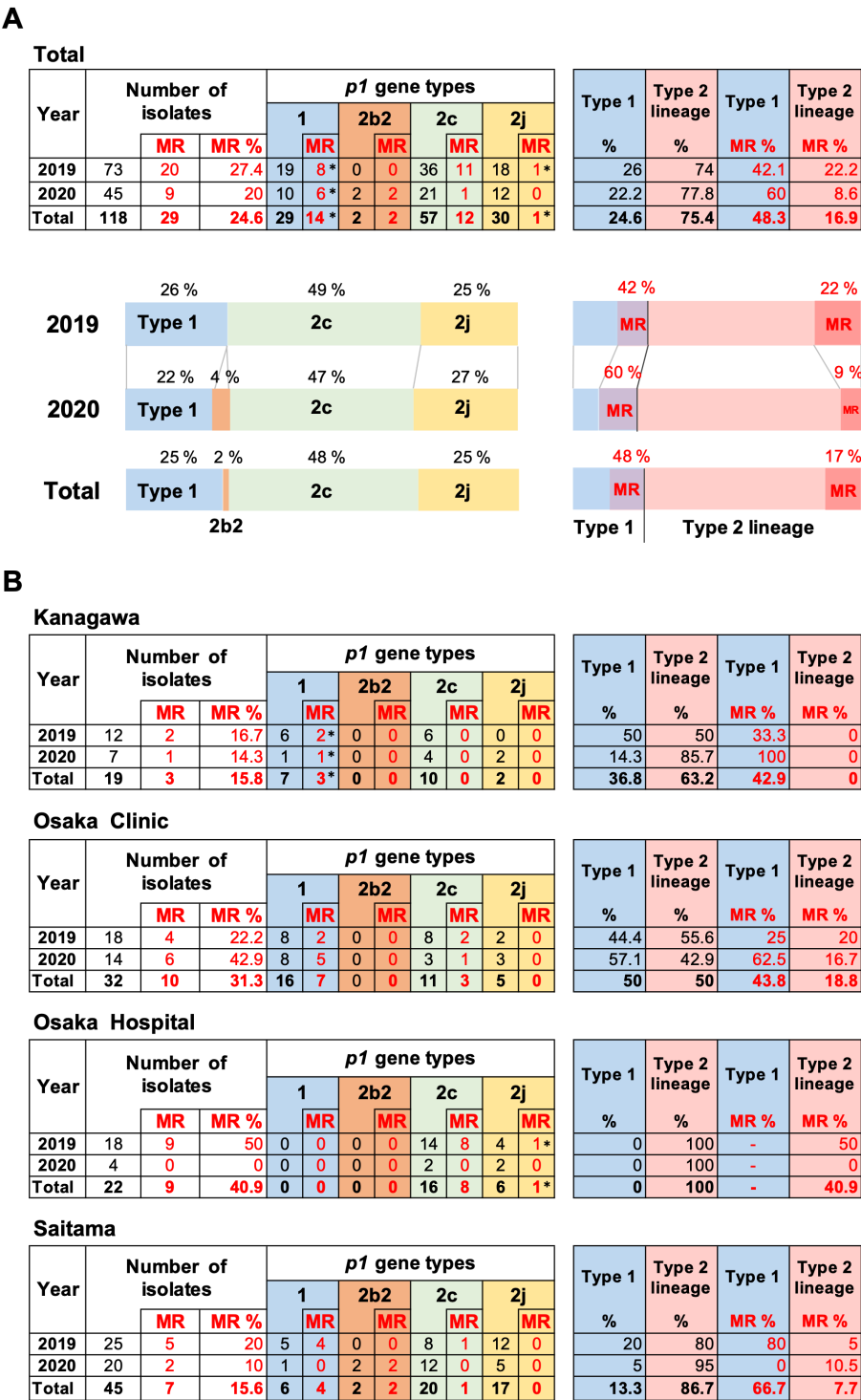


FIGURE 2 Summary of the *p1* genotyping and macrolide resistance (MR) analysis of the 118 *Mycoplasma pneumoniae* strains isolated in this study. (A) Results of *p1* genotyping and MR analysis of the 118 strains isolated in 2019 and 2020. The results have also been represented in the form of graphs. (B) Analysis results shown by collection area of the strains. *Two type 1 strains isolated in Kanagawa in 2019 and 2020 carry a A2064G MR mutation, and one type 2j strain isolated in Osaka hospital in 2019 carries a A2063T MR mutation in the 23S rRNA gene (see Supplementary Table S1). Type 2b2 has also been referred to as type 2e or type 2bv in the reports of other groups (Gullisby et al., 2019; Xiao et al., 2020).

higher (40.9%) than that in the other areas (Figure 2B). We think these differences are probably due to locational deference, property of the specimens (sputa or throat swabs), or medical conditions of patients (Supplementary Table S1). It was also reported that MR rate of isolates tended to be higher in larger hospitals (higher order medical institutions) than in clinics (primary medical institutions) in the previous study in Osaka (Katsukawa et al., 2019).

3.2. Verification of the past genotyping data of type 2 lineage

The unexpectedly high prevalence of type 2j strains and absence of classical type 2 in the *M. pneumoniae* clinical strains isolated in the time-period of 2019 and 2020 made us wonder whether there were unrecognized type 2j strains in the previous genotyping studies. Thus, we re-analyzed the past clinical isolates. In two previous studies (Katsukawa et al., 2019; Kenri et al., 2020), we reported 172 classical type 2 *M. pneumoniae* isolates between 2010 and August 2019. We re-analyzed the *p1* genes of these strains using PCR-RFLP with *MboI* digestion and confirmed that two of these strains in 2010 were classical type 2, whereas the other 170 strains were type 2j (Table 2A). Among these, four draft genome sequenced strains (Y3-12, Y4-15, Y4-20, and Y4-67) from a previous study (Kenri et al., 2020) were also type 2j strains (because complete *p1* gene sequence was not obtained by means of draft genome sequencing, due to the presence of repetitive elements). These four strains clustered with the type 2g strain K708 in the phylogenetic analysis based on WG-SNP, thereby suggesting a close genetic relationship between the type 2g and 2j strains (Supplementary Figure S1). The MLVA and MLST types of these type 2j and 2g strains were 3662 and ST7, respectively.

We also reported *p1* genotyping results of the *M. pneumoniae* DNA in clinical specimens using PCR-based typing methods, without isolating bacteria (Ishiguro et al., 2021; Nakamura et al., 2021). In the Hokkaido prefecture, we reported 38 typing results of classical type 2 *p1*, in the specimens collected between 2016 and 2019 (Ishiguro et al., 2021). Of these specimens, 28 were re-analyzed using PCR-RFLP with *MboI* digestion and *p1* sequencing, and all specimens were confirmed to be type 2j. In the Okayama prefecture, we reported 24 classical type 2 specimens between 2016 and 2018 (Nakamura et al., 2021). Re-analysis of these specimens confirmed that all *p1* genes were type 2j.

We also re-examined the genotyping results before 2003. We reported 183 classical type 2 *M. pneumoniae* strains and specimens between 1976 and 2003 in previous studies (Sasaki et al., 1996; Kenri et al., 2008). Of these, 78 strains were available for re-analysis and examined using PCR-RFLP with *MboI* digestion (Table 2B). In contrast to the re-analysis of strains in the 2010s, no type 2j strain was found among the 78 strains isolated between 1976 and 2003. All 78 strains were classical type 2, suggesting that type 2j strains were not present or were rare before the 2000s (Figure 3; Supplementary Figure S2). This is consistent with lower MR rate of type 2j strains (1.5%, 1/201) compared to that of type 2c (8.1%, 24/295; Supplementary Figure S2). Although when and where the first type 2j strain appeared is unknown, type 2j strains were minor in circulating variants until the middle of 2010s and were not extensively exposed to clinical macrolide treatments in the 2000s.

During this re-analysis of past classical type 2 strains using PCR-RFLP with *MboI*, we noticed a single SNP in *p1* gene that affected *MboI* digestion in the RepMP2/3 region (ADH3-ADH4 amplicon). Some classical type 2 and type 2b strains carry this SNP in the *p1* gene (T to A transversion at the 2,883 nt position corresponds to the FH *p1* gene). This SNP is a useful marker to discriminate strains belonging to the type 2b branch in the phylogenetic tree of the type 2 lineage (Supplementary Figure S1). Strains carrying this SNP exhibited

a PCR-RFLP pattern similar to that of type 2g in the RepMP2/3 region (Supplementary Figure S3).

3.3. Phylogenetic relations between macrolide resistant and susceptible type 1 strains

In this study, the detection rate of type 1 macrolide susceptible (MS) strains was higher (15/29, 51.7%), as compared to that observed in previous studies (Kenri et al., 2020; Ishiguro et al., 2021; Nakamura et al., 2021). Therefore, to explore the phylogenetic relationships between type 1 MR and MS strains, we sequenced the genomes of three type 1 isolates (Y12-4, OA-57, and OA-63) collected in this study, which showed that the MR strain OA-63 belonged to the T1-3R clade of the phylogenetic tree (MLVA type 4572; MLST ST3). In contrast, the MS strains Y12-4 and OA-57 belonged to the T1-2 clade (MLVA type 4573; MLST ST17 and unassigned new ST; Figure 4A; Supplementary Figure S1). These findings suggested that the type 1 MR and MS strains have different phylogenetic backgrounds in this study. To confirm this, we developed a simple phylogenetic analysis method based on the WG-SNP data of 163 type 1 strains (Figures 4B–D; Supplementary Figure S1). We identified three SNPs specific to clades T1-1, T1-2, and T1-3R in the type 1 lineage. Strains belonging to clades T1-1, T1-2, and T1-3R specifically harbored an SNP in the MPN607, MPN678, and MPN295 genes, respectively (Figure 4B). These SNPs were identified using *ApoI* restriction enzyme digestion (Figures 4B–D). Analysis of 22 type 1 strains (isolated in this study at the Osaka and Saitama clinics) showed that 11 MS strains belonged to the T1-2 clade, while 11 MR strains belonged to the T1-3R clade (Figures 4E,F). Empirically, it is known that strains belonging to the T1-2 clade usually have three tandem repeats in the Mpn16 marker of MLVA (Degrange et al., 2009; Supplementary Figure S1); therefore, we also analyzed the MLVA Mpn16 markers of 22 isolates (Supplementary Figure S4). Eleven MS strains harbored three tandem repeats in the Mpn16 region, whereas 11 MR strains had two repeats, further supporting the result that the 11 type 1 MS strains belonged to the T1-2 clade (Supplementary Figure S4). These results suggested that T1-2 clade strains have not acquire MR, as compared to the T1-3R strains in Japan, although a high MR rate of T1-2 clade strains (ST17) was reported in Taiwan (Hung et al., 2021). Probably, T1-2 clade strains had been minor population in Japan and were not exposed to macrolide treatments compared to T1-3R strains in the 2000s. T1-1 or T1-3 clade strains were not found in the 22 type 1 strains in this study (from Osaka and Saitama clinics in 2019 and 2020).

3.4. Changes in the amino acid sequences of P1 and P40/P90 proteins caused by type 2c and 2j variations

This study revealed a high prevalence of type 2c and 2j strains among *M. pneumoniae* isolates in Japan over the recent years. Although the reason for this widespread is unknown, one possible cause is antigenic changes in these variants, particularly in the P1 and

TABLE 2 Re-analysis of type 2 genotyping data of the past reports.

A																						
Year		2010				2015			2016			2017			2018			2019			Total	
Number of strains reported as classical type 2 in previous studies*		2				52			68			18			27			5			172	
Result of re-analysis	Type 2	2				0			0			0			0			0			2	
	Type 2j	0				52			68			18			27			5			170	

B																					
Year		1976	1979	1980	1983	1984	1985	1987	1992	1993	1994	1995	1996	1997	1998	1999	2000	2001	2002	2003	Total
Number of strains or specimens reported as classical type 2 in previous studies**		1	3	19	10	13	2	1	7	5	12	7	13	8	9	1	24	19	22	7	183
Number of strains re-analyzed		1	2	19	9	13	2	1	7	2	3	5	3	3	2	0	0	0	0	6	78
Result of re-analysis	Type 2	1	2	19	9	13	2	1	7	2	3	5	3	3	2	—	—	—	—	6	78
	Type 2j	0	0	0	0	0	0	0	0	0	0	0	0	0	0	—	—	—	—	0	0

*These data were reported in Kenri et al. (2020).
**These data were reported in Sasaki et al. (1996), Kenri et al. (2008) (also see text, Figure 2; Supplementary Figure S2).

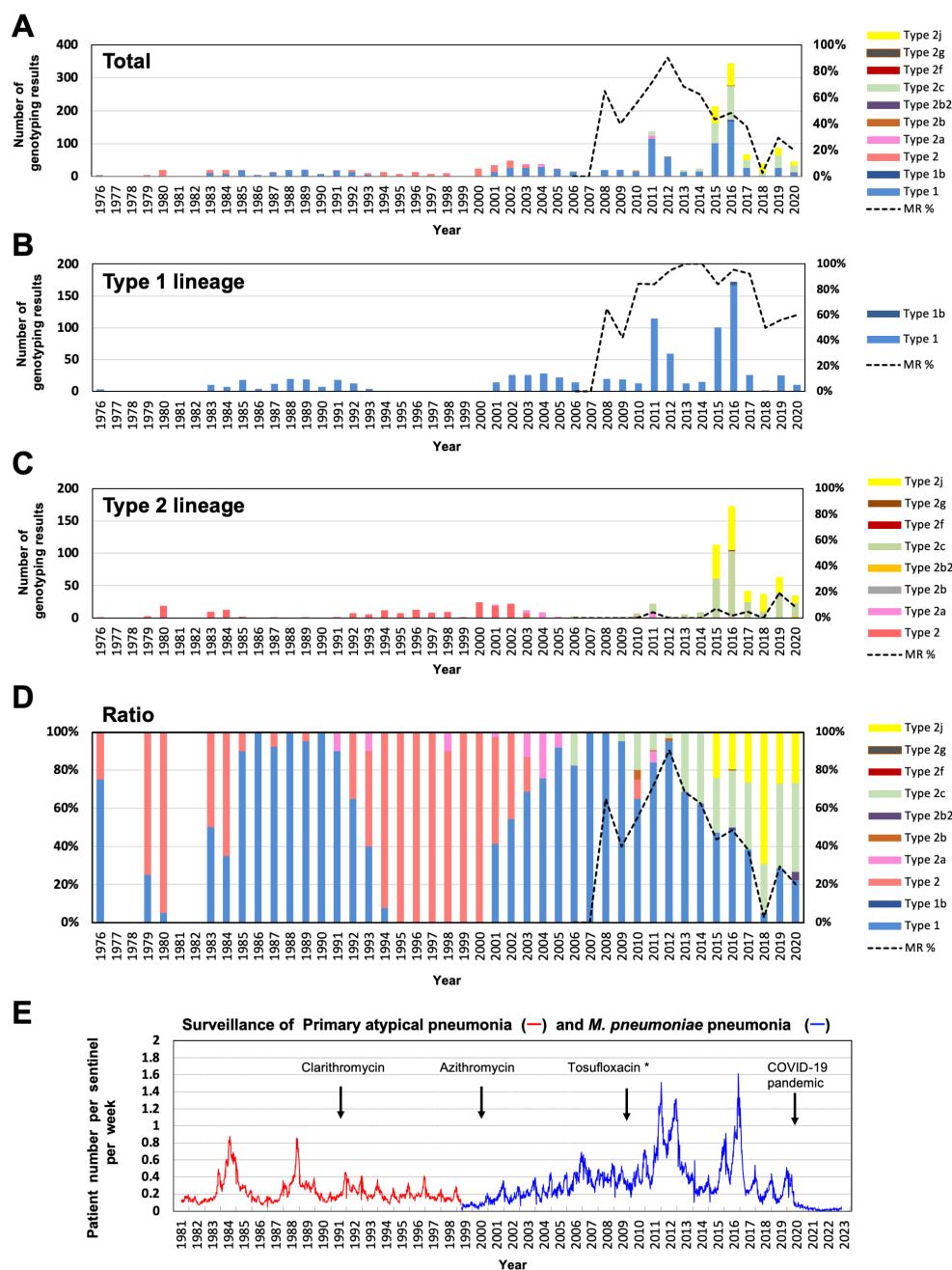


FIGURE 3

Integrated revised data of *M. pneumoniae* genotyping over the past 40 years. (A) Annual typing number and proportion of *p1* gene types. The different *p1* gene variants are shown in different colors. The dotted line shows the MR rate of total isolates after 2006. (B) Annual number of type 1 lineage genotyping results. The dotted line shows the MR rate of type 1 lineage isolates after 2006. (C) Annual number of type 2 lineage genotyping results. The dotted line shows the MR rate of type 2 lineage isolates after 2006. (D) Trend of *p1* gene genotypes (annual ratio of detected genotype). The dotted line shows the MR rate of total isolates after 2006. Detailed data of genotyping and MR analysis are shown in [Supplementary Figure S2](#). (E) Surveillance data of *M. pneumoniae* pneumonia in Japan, obtained from the National Epidemiological Surveillance of Infectious Diseases (<https://www.niid.go.jp/niid/ja/10/2096-weeklygraph/1659-18myco.html>). Surveillance data of primary atypical pneumonia (red line, April 1981–March 1999) and *M. pneumoniae* pneumonia (blue line, after April 1999). The years of introduction of clarithromycin and azithromycin for clinical treatment for *M. pneumoniae* pneumonia in Japan are indicated (Yamazaki and Kenri, 2016). The introduction year of tosufloxacin for children clinical treatments is also indicated. *Tosufloxacin has been officially recommended for pediatric *M. pneumoniae* pneumonia treatment since 2017.

P40/P90 proteins. To further investigate this possibility, we inspected the amino acid substitutions in the P1 and P40/P90 proteins in the type 2c and 2j variants. [Figures 5A,B](#) show the locations of type 2c and 2j variations in P1 and P40/P90 proteins, as compared with those of classical type 1 and 2. Type 2c has variations in the RepMP4 and

RepMP2/3 regions of P1, as compared to those of classical type 2 strains (v1 and v2 in [Figure 5](#)). V1 is only present in type 2c, whereas v2 is found in type 2a strains (Zhao et al., 2011; Kenri et al., 2020). Type 2c strains also had a v3 variation in the RepMP5 region of P40/P90 ([Figure 5](#)). V3 is in the P90 part of P40/P90 and is present in all

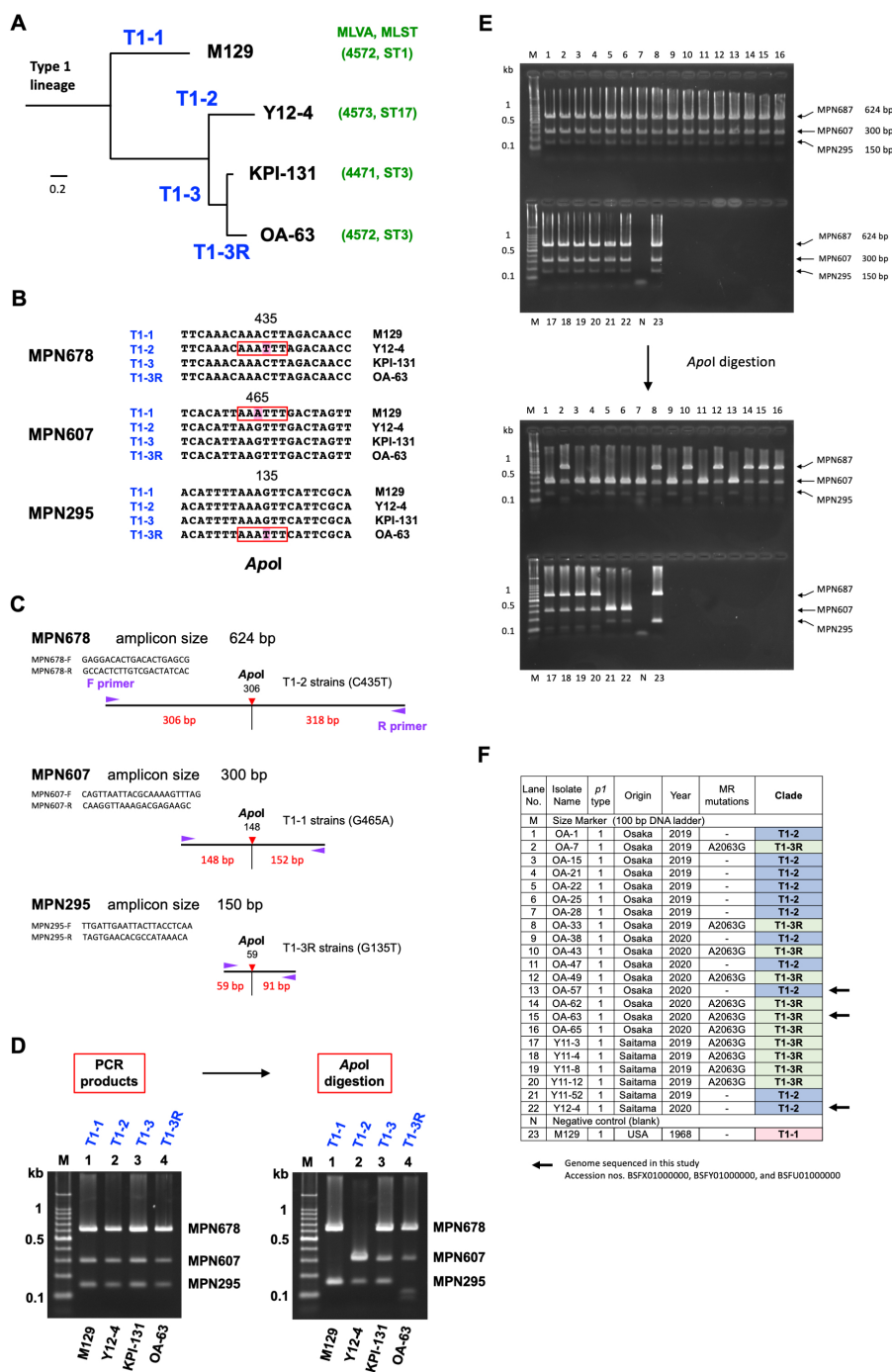


FIGURE 4
Phylogenetic analysis of type 1 lineage strains. (A) Simplified phylogenetic tree of type 1 lineage strains. Four major clades (designated T1-1, T1-2, T1-3, and T1-3R in this study) were identified in the phylogenetic tree of 163 type 1 lineage strains, based on the whole-genome SNPs (Supplementary Figure S1). Representative strains of these 4 clades, M129 (T1-1), Y12-4 (T1-2), KPI-131 (T1-3), and OA-63 (T1-3R) are shown. Y12-4 and OA-63 were genome-sequenced in this study. The MLVA and MLST types of these strains are also shown in green characters in parenthesis. (B) Clade-specific SNPs found in the three genes, MPN678 (C435T), MPN607 (G465A), and MPN295 (G135T). These SNPs are recognized by the restriction enzyme Apol. (C) Scheme of the phylogenetic analysis. PCR primer sequences for amplification of marker genes (MPN295, MPN607, and MPN678) and locations of SNP sites in the amplicons are shown (the primer sequences used for this PCR are given also in Table 1). (D) Discrimination of the phylogenetic clades of the representative type 1 strains (M129, Y12-4, KPI-131, and OA-63) by Apol digestion of the PCR products of MPN678, MPN607, and MPN295 genes. (E) 2% agarose-gel electrophoresis patterns of PCR products from the analyzed strains. Electrophoresis patterns before and after Apol digestion are shown. The lane numbers correspond to the F panel. (F) List of the 22 type 1 *M. pneumoniae* strains analyzed in this study (also see Supplementary Table S1 and the text).

type 2c strains analyzed so far (type 2c *orf6* gene; Supplementary Figure S1). V3 was also found in type 2a strains (MLST, ST14 strains); however, some type 2a strains (MLST, ST2, or ST15 strains) did not have v3 (Supplementary Figure S1). Type 2j P1 has variation in the RepMP4 region (v4 in Figure 5). V4 is located in the region that shows sequence variation between type 1 and 2 lineage

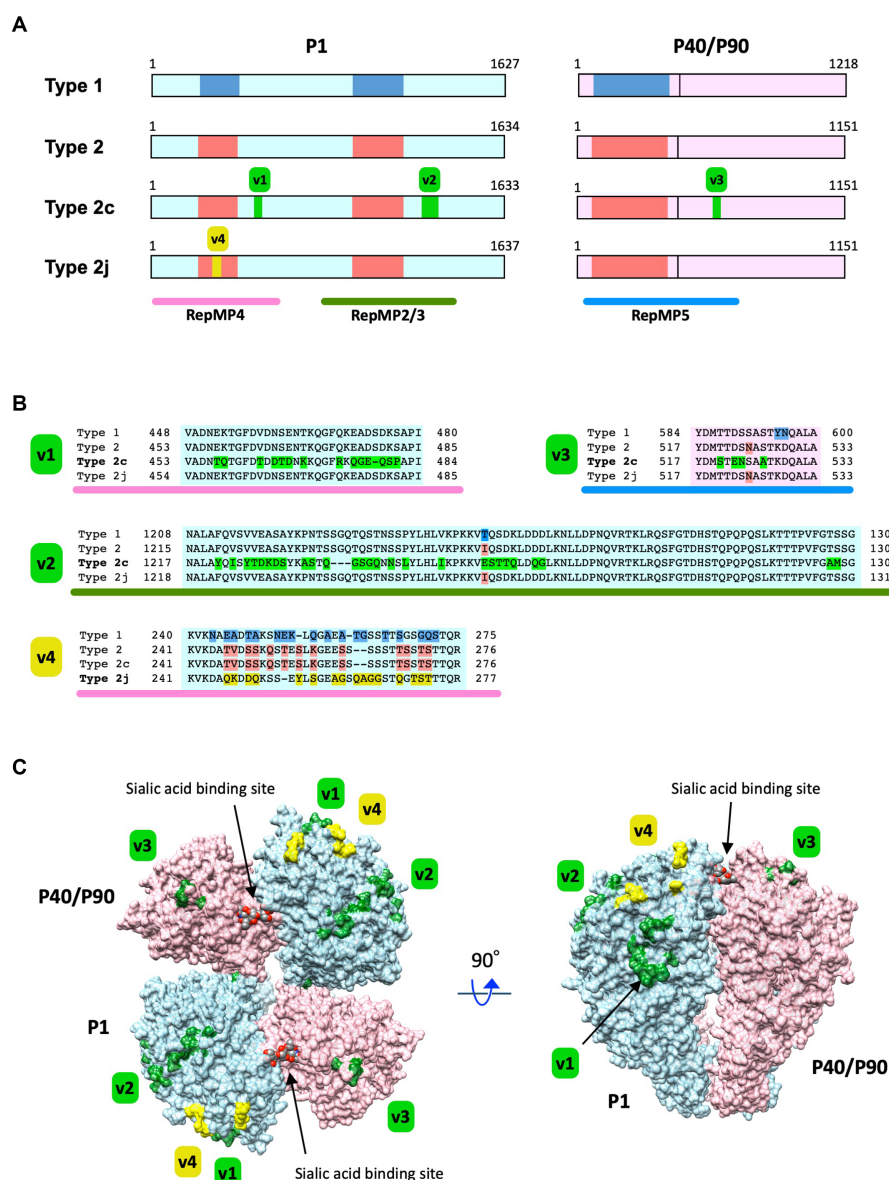


FIGURE 5

Substitutions of the amino acid residues in P1 and P40/P90 proteins caused by type 2c and 2j variations. (A) Locations of the type 2c and 2j variations in the P1 and P40/P90 proteins. The primary structures of the P1 and P40/P90 proteins have been illustrated using light blue and light pink rectangles, respectively. The vertical line in the pink rectangles indicates the cleavage site of P40/P90. The protein type is labeled on the left (Type 1, 2, 2c, and 2j). The blue and red boxes in the rectangles indicate the polymorphic regions between type 1 and 2 lineage sequences. The green boxes (v1–v3) indicate the locations of type 2c variations in the P1 and P40/P90 proteins. The yellow box (v4) indicates the location of the type 2j variation in P1. The RepMP4, RepMP2/3, and RepMP5 repetitive element regions have been indicated using pink, green, and blue bars below, respectively. The illustration has been drawn based on the nucleotide sequence data of type 1, 2, 2c, 2j *p1* and *orf6* genes [GenBank accession nos. M21519 (1054–5937 and 5943–9599), CP010546 (179324–184228 and 184234–187689), AP017319 (179294–184195 and 184201–187656), and LC588412 (1198–6111 and 6117–9572)].

(B) Amino acid sequence alignments of the v1, v2, v3, and v4 variation regions. The variant-specific amino acid substitutions have been shown in different colors. (C) Three-dimensional structure of the P1 and P40/P90 proteins and variation sites. The P1 and P40/P90 molecules are shown as a hetero-tetrameric adhesin protein complex (nap; Vizarraga et al., 2020). The P1 and P40/P90 molecules are colored light blue and light pink, respectively. The positions of amino acid substitution by the type 2c and 2j variations (v1–v4) are displayed on the nap structure (green and yellow). The image was generated using PDB data 6RC9 and 6RJ1, and the UCSF Chimera software v1.14 (Supplementary Video 1).

strains (Figure 5A). The type 2j strains examined had no variation in P40/P90 (Supplementary Figure S1). In v1–v4, some amino acid residues changed their charge and polarity by substitution.

In Figure 5C, the positions of the v1, v2, v3, and v4 variations are displayed in the crystal structures of the P1 and P40/P90 adhesin protein complex (nap). The crystal structures of P1 and P40/P90,

which have been elucidated recently, are type 1 (Vizarraga et al., 2020); however, all P1 and P40/P90 subtypes are most likely to have similar protein conformations. Variations v1, v2, v3, and v4 were largely present at the surface of the P1 and P40/P90 molecules. It is possible that these variations can change the antigenicity of the P1 and P40/P90 proteins, which are responsible for the cytoadherence of *M. pneumoniae*.

4. Discussion

In this study, we showed that type 2 lineage strains were dominant (75.4%, 89/118) among the *M. pneumoniae* isolates collected during the time-period of 2019 and 2020 from patients with respiratory infections in Japan (Figure 1). The most prevalent type 2 lineage was type 2c strain (48% of total isolates, 57/118). Type 2c strains are successful variants that have spread worldwide and are frequently detected in many genotyping studies (Zhao et al., 2011; Edelstein et al., 2016; Gullsby et al., 2019; Kenri et al., 2020; Xiao et al., 2020). Type 2c strains are closely related to type 2a strains, and harbor an additional minor variation in the RepMP4 region of P1 (v1 in Figure 5). Type 2c strains were probably derived from a type 2a strain (MLVA type 3562; MLST ST14; Supplementary Figure S1); however, as compared to that of type 2c, detection of the parent type 2a strain is relatively rare in our epidemiological studies in Japan (Kenri et al., 2020). Another prevalent type 2 lineage strain in this study was type 2j. Type 2j strains may be an intermediate between classical type 2 and type 2g, in variant development (Figure 1). Type 2j *p1* might have been generated by RepMP4 recombination in a type 2 strain (MLVA type 3662; MLST ST7; Supplementary Figure S1). After this event, additional RepMP2/3 recombination occurred in a type 2j strain, resulting in type 2g (Kenri et al., 2020). In contrast to the type 2g strain that was reported in only one isolate in Osaka in 2016 (Katsukawa et al., 2019), type 2j strains have spread widely in Japan and have been clinically prevalent since the middle of the 2010s. To detect type 2j strains, *MboI* digestion should be included in the PCR-RFLP genotyping analysis.

The real factors that contribute to type 2c and 2j becoming prevalent strains are unknown; however, several factors may be involved in this phenomenon, including the growth rate of these variants during infections, evasion of herd immunity by antigenic changes, increase in infectivity or colonization ability, or chance. In terms of antigenic changes, the type 2c and 2j strains have amino acid substitutions at the surface of the P1-P40/P90 adhesin complex (nap; Figure 5). Nap is a major antigen of this bacterium and a target of host protective immunity (Dumke et al., 2008; Zhu et al., 2012a,b). Nap surface variations may affect or disturb host immune recognition and provide advantages for evasion of herd immunity. It is also possible that nap surface variations modify sialic acid binding affinity and change the colonization rate of the bacterium at the host surface. Seroepidemiological studies on the variant P1 and P40/P90 proteins are important to discern whether the type 2c and 2j variations are advantageous for survival of *M. pneumoniae* during infection and for becoming prevalent strains. Furthermore, future studies employing modern structural biology techniques may also provide further insights on the effect of nap variations on epitope recognition by host protective immunity and sialic acid receptor binding.

Explanation of the genotype shift mechanism of clinically prevalent strains in terms of the nap antigenic variations has, however, a contradiction in the type 1 lineage, because the type 1 lineage P1 and P40/P90 proteins are less variable, as compared to those of the type 2 lineage (Supplementary Figure S1). The low variation may be partly due to the lower DNA recombination activity in type 1 cells than in type 2 (Krishnakumar et al., 2010). However, the type 1 P40/P90 protein is approximately 70 amino acids longer than that of the type 2

lineage (Ruland et al., 1994). Furthermore, it is also known that this additional 70 amino acid region is structurally disordered and cannot be elucidated by means of structural analysis (Vizarraga et al., 2020). Although the function of this disordered region of the type 1 P40/P90 protein is unknown, there is a need for evaluation of the role of this region in epitope recognition by host immunity in future studies. *Mycoplasma genitalium* P140 and P110 proteins, the homologs of P1 and P40/P90, respectively, do not have disordered regions, as compared to P1 and P40/P90 (Aparicio et al., 2018, 2020). P140 and P110 frequently generate variations, as compared to P1 and P40/P90 (Wood et al., 2020). Thus, disordered amino acid sequence regions might have advantages in host immune evasion without generating sequence variations.

The total MR rate of the 118 strains analyzed in this study was 24.6% (29/118), which is lower than that observed in previous studies and is mainly due to the increased proportion of MS type 2 lineage strains (Figures 2, 3). However, we also found a decreased MR rate of the type 1 strain (14/29, 48.3%) as compared to that observed in previous reports (Katsukawa et al., 2019; Kenri et al., 2020; Ishiguro et al., 2021; Nakamura et al., 2021). The situation of antimicrobial agents consumption under the National Action Plan on Antimicrobial Resistance (since 2016) may also be involved in these decreasing MR trend. Antimicrobial consumption surveillance data⁴ indicates that macrolide sales in Japan was reduced by 21% in 2021 and 39% in 2020, as compared to that in 2013. In addition, tosufloxacin, a fluoroquinolone antimicrobial has been used for treatments of pediatric *M. pneumoniae* pneumonia when macrolides are not effective (Figure 3E). These factors might have contributed to reduce the MR rate of *M. pneumoniae*. However, our present study also showed that type 1 MS strains were phylogenetically different from MR strains (Figure 4; Supplementary Figure S4). In addition, there was a slight increase in the MR rate of the type 2 lineage (15/89, 16.9%; Figures 2A, 3C). These facts cannot be explained only by reduction of clinical macrolides usage. Thus, continuous monitoring is needed to evaluate and understand the correlations between the MR rate of clinical isolates, drug consumption, and genotype shift of circulating strains. The MR rate of the type 2 lineage remains low in Japan; however, a higher MR rate of the type 2 lineage has recently been reported in China and South Korea (Wang et al., 2021; Guo et al., 2022; Lee et al., 2022; Wang et al., 2022). Therefore, it is particularly important to monitor the MR rate of the type 2 lineage strains in Japan.

Since April 2020, when the COVID-19 pandemic started in Japan, there has been a sharp decline in the incidence of *M. pneumoniae* pneumonia (Figure 3E).⁵ This has made it very difficult to obtain *M. pneumoniae* clinical isolates and carry out epidemiological studies. Although it is unknown when and whether the *M. pneumoniae* infections will reappear after the COVID-19 pandemic, there is a possibility of profile changes in the genotype and MR status of *M. pneumoniae* clinical isolates. Thus, it is important to continue extensive efforts in epidemiological studies on *M. pneumoniae*.

⁴ https://amrccr.ncgm.go.jp/surveillance/Surveillance_en.html

⁵ <https://www.niid.go.jp/niid/ja/10/2096-weeklygraph/1659-18myco.html>

Data availability statement

The datasets presented in this study can be found in online repositories. The names of the repository/repositories and accession number(s) can be found in the article/[Supplementary material](#).

Author contributions

TK, TY, and KS designed the study. TK, TO, and KS obtained funding. TY, HO, MJ, YO, SA, RS, NI, TO, HF, TH, and HN collected the specimens. TK, HO, MJ, RS, AH, and HF performed the experiments. TK analyzed the data and wrote the draft of the manuscript. All authors contributed to the article and approved the submitted version.

Funding

This work was supported by grants from Japan Agency for Medical Research and Development (20jk0210004j0101, 18jk0210004j0101, 17jk0210004j0001, 16jk0210004j0001, and 15jk0210004h0027) and was supported in part by a Grants-in-Aid for Scientific Research (15H01337, 20K08171 and 22K07063) from the Ministry of Education, Culture, Sports, Science, and Technology of Japan.

References

- Aparicio, D., Scheffer, M. P., Marcos-Silva, M., Vizarraga, D., Sprankel, L., Ratera, M., et al. (2020). Structure and mechanism of the nap adhesion complex from the human pathogen *Mycoplasma genitalium*. *Nat. Commun.* 11:2877. doi: 10.1038/s41467-020-16511-2
- Aparicio, D., Torres-Puig, S., Ratera, M., Querol, E., Pinol, J., Pich, O. Q., et al. (2018). *Mycoplasma genitalium* adhesin P110 binds sialic-acid human receptors. *Nat. Commun.* 9:4471. doi: 10.1038/s41467-018-06963-y
- Barile, M. F., Chandler, D. K., Yoshida, H., Grabowski, M. W., Harasawa, R., and Razin, S. (1988). Parameters of *Mycoplasma pneumoniae* infection in Syrian hamsters. *Infect. Immun.* 56, 2443–2449. doi: 10.1128/iai.56.9.2443-2449.1988
- Brown, R. J., Holden, M. T., Spiller, O. B., and Chalker, V. J. (2015). Development of a multilocus sequence typing scheme for molecular typing of *Mycoplasma pneumoniae*. *J. Clin. Microbiol.* 53, 3195–3203. doi: 10.1128/JCM.01301-15
- Cousin-Allery, A., Charron, A., de Barbeyrac, B., Fremy, G., Skov Jensen, J., Renaudin, H., et al. (2000). Molecular typing of *Mycoplasma pneumoniae* strains by PCR-based methods and pulsed-field gel electrophoresis. Application to French and Danish isolates. *Epidemiol. Infect.* 124, 103–111. doi: 10.1017/S0950268899003313
- Degrange, S., Cazanave, C., Charron, A., Renaudin, H., Bebear, C., and Bebear, C. M. (2009). Development of multiple-locus variable-number tandem-repeat analysis for molecular typing of *Mycoplasma pneumoniae*. *J. Clin. Microbiol.* 47, 914–923. doi: 10.1128/JCM.01935-08
- Diaz, M. H., Benitez, A. J., and Winchell, J. M. (2015). Investigations of *Mycoplasma pneumoniae* infections in the United States: trends in molecular typing and macrolide resistance from 2006 to 2013. *J. Clin. Microbiol.* 53, 124–130. doi: 10.1128/JCM.02597-14
- Diaz, M. H., Desai, H. P., Morrison, S. S., Benitez, A. J., Wolff, B. J., Caravas, J., et al. (2017). Comprehensive bioinformatics analysis of *Mycoplasma pneumoniae* genomes to investigate underlying population structure and type-specific determinants. *PLoS One* 12:e0174701. doi: 10.1371/journal.pone.0174701
- Dumke, R., Schurwan, N., and Jacobs, E. (2008). Characterisation of subtype- and variant-specific antigen regions of the P1 adhesin of *Mycoplasma pneumoniae*. *Int. J. Med. Microbiol.* 298, 483–491. doi: 10.1016/j.ijmm.2007.06.002
- Dumke, R., Von Baum, H., Luck, P. C., and Jacobs, E. (2010). Subtypes and variants of *Mycoplasma pneumoniae*: local and temporal changes in Germany 2003–2006 and

Acknowledgments

We are grateful to Chieko Kushibiki of the Kishiwada Tokushukai Hospital for her support in the collection of the *Mycoplasma pneumoniae* strains.

Conflict of interest

The authors declare that the research was conducted in the absence of any commercial or financial relationships that could be construed as a potential conflict of interest.

Publisher's note

All claims expressed in this article are solely those of the authors and do not necessarily represent those of their affiliated organizations, or those of the publisher, the editors and the reviewers. Any product that may be evaluated in this article, or claim that may be made by its manufacturer, is not guaranteed or endorsed by the publisher.

Supplementary material

The Supplementary material for this article can be found online at: <https://www.frontiersin.org/articles/10.3389/fmicb.2023.1202357/full#supplementary-material>

absence of a correlation between the genotype in the respiratory tract and the occurrence of genotype-specific antibodies in the sera of infected patients. *Epidemiol. Infect.* 138, 1829–1837. doi: 10.1017/S0950268810000622

Edelstein, I., Rachina, S., Touati, A., Kozlov, R., Henin, N., Bebear, C., et al. (2016). *Mycoplasma pneumoniae* monoclonal P1 type 2c outbreak, Russia, 2013. *Emerg. Infect. Dis.* 22, 348–350. doi: 10.3201/eid2202.151349

Gullsbj, K., Olsen, B., and Bondeson, K. (2019). Molecular typing of *Mycoplasma pneumoniae* strains in Sweden from 1996 to 2017 and the emergence of a new P1 Cytadhesin gene, variant 2e. *J. Clin. Microbiol.* 57:e00049-19. doi: 10.1128/JCM.00049-19

Guo, Z., Liu, L., Gong, J., Han, N., He, L., Wang, W., et al. (2022). Molecular features and antimicrobial susceptibility of *Mycoplasma pneumoniae* isolates from paediatric inpatients in Weihai, China: characteristics of *M. pneumoniae* in Weihai. *J. Glob. Antimicrob. Resist.* 28, 180–184. doi: 10.1016/j.jgar.2022.01.002

Hakim, M. S., Annisa, L., Jariah, R. O. A., and Vink, C. (2021). The mechanisms underlying antigenic variation and maintenance of genomic integrity in mycoplasma pneumoniae and *Mycoplasma genitalium*. *Arch. Microbiol.* 203, 413–429. doi: 10.1007/s00203-020-02041-4

Himmelreich, R., Hilbert, H., Plagens, H., Pirkel, E., Li, B. C., and Herrmann, R. (1996). Complete sequence analysis of the genome of the bacterium *Mycoplasma pneumoniae*. *Nucleic Acids Res.* 24, 4420–4449. doi: 10.1093/nar/24.22.4420

Hung, H. M., Chuang, C. H., Chen, Y. Y., Liao, W. C., Li, S. W., Chang, I. Y., et al. (2021). Clonal spread of macrolide-resistant *Mycoplasma pneumoniae* sequence type-3 and type-17 with recombination on non-P1 adhesin among children in Taiwan. *Clin. Microbiol. Infect.* 27, 1169.e1–1169.e6. doi: 10.1016/j.cmi.2020.09.035

Ishiguro, N., Sato, R., Kikuta, H., Nakanishi, M., Aoyagi, H., Mori, T., et al. (2021). P1 gene of *Mycoplasma pneumoniae* isolated from 2016 to 2019 and relationship between genotyping and macrolide resistance in Hokkaido, Japan. *J. Med. Microbiol.* 70:001365. doi: 10.1099/jmm.0.001365

Kaas, R. S., Leekitcharoenphon, P., Aarestrup, F. M., and Lund, O. (2014). Solving the problem of comparing whole bacterial genomes across different sequencing platforms. *PLoS One* 9:e104984. doi: 10.1371/journal.pone.0104984

Katsukawa, C., Kenri, T., Shibayama, K., and Takahashi, K. (2019). Genetic characterization of *Mycoplasma pneumoniae* isolated in Osaka between 2011 and 2017:

decreased detection rate of macrolide-resistance and increase of *p1* gene type 2 lineage strains. *PLoS One* 14:e0209938. doi: 10.1371/journal.pone.0209938

Kenri, T., Okazaki, N., Yamazaki, T., Narita, M., Izumikawa, K., Matsuoka, M., et al. (2008). Genotyping analysis of *Mycoplasma pneumoniae* clinical strains in Japan between 1995 and 2005: type shift phenomenon of *M. pneumoniae* clinical strains. *J. Med. Microbiol.* 57, 469–475. doi: 10.1099/jmm.0.47634-0

Kenri, T., Suzuki, M., Sekizuka, T., Ohya, H., Oda, Y., Yamazaki, T., et al. (2020). Periodic genotype shifts in clinically prevalent *Mycoplasma pneumoniae* strains in Japan. *Front. Cell. Infect. Microbiol.* 10:385. doi: 10.3389/fcimb.2020.00385

Kenri, T., Taniguchi, R., Sasaki, Y., Okazaki, N., Narita, M., Izumikawa, K., et al. (1999). Identification of a new variable sequence in the P1 cytoadhesin gene of *Mycoplasma pneumoniae*: evidence for the generation of antigenic variation by DNA recombination between repetitive sequences. *Infect. Immun.* 67, 4557–4562. doi: 10.1128/IAI.67.9.4557-4562.1999

Kim, K., Jung, S., Kim, M., Park, S., Yang, H. J., and Lee, E. (2022). Global trends in the proportion of macrolide-resistant *Mycoplasma pneumoniae* infections: a systematic review and Meta-analysis. *JAMA Netw. Open* 5:e2220949. doi: 10.1001/jamanetworkopen.2022.20949

Krishnakumar, R., Assad-Garcia, N., Benders, G. A., Phan, Q., Montague, M. G., and Glass, J. I. (2010). Targeted chromosomal knockouts in *Mycoplasma pneumoniae*. *Appl. Environ. Microbiol.* 76, 5297–5299. doi: 10.1128/AEM.00024-10

Lee, J. K., Choi, Y. Y., Sohn, Y. J., Kim, K. M., Kim, Y. K., Han, M. S., et al. (2022). Persistent high macrolide resistance rate and increase of macrolide-resistant ST14 strains among *Mycoplasma pneumoniae* in South Korea, 2019–2020. *J. Microbiol. Immunol. Infect.* 55, 910–916. doi: 10.1016/j.jmii.2021.07.011

Lee, J. K., Seong, M. W., Shin, D., Kim, J. I., Han, M. S., Yeon, Y., et al. (2019). Comparative genomics of *Mycoplasma pneumoniae* isolated from children with pneumonia: South Korea, 2010–2016. *BMC Genomics* 20:910. doi: 10.1186/s12864-019-6306-9

Lipman, R. P., Clyde, W. A. Jr., and Denny, F. W. (1969). Characteristics of virulent, attenuated, and avirulent *Mycoplasma pneumoniae* strains. *J. Bacteriol.* 100, 1037–1043. doi: 10.1128/jb.100.2.1037-1043.1969

Liu, Y., Ye, X., Zhang, H., Xu, X., Li, W., Zhu, D., et al. (2009). Antimicrobial susceptibility of *Mycoplasma pneumoniae* isolates and molecular analysis of macrolide-resistant strains from Shanghai, China. *Antimicrob. Agents Chemother.* 53, 2160–2162. doi: 10.1128/AAC.01684-08

Matsuoka, M., Narita, M., Okazaki, N., Ohya, H., Yamazaki, T., Ouchi, K., et al. (2004). Characterization and molecular analysis of macrolide-resistant *Mycoplasma pneumoniae* clinical isolates obtained in Japan. *Antimicrob. Agents Chemother.* 48, 4624–4630. doi: 10.1128/AAC.48.12.4624-4630.2004

Meyer Sauter, P. M., Unger, W. W., Nadal, D., Berger, C., Vink, C., and van Rossum, A. M. (2016). Infection with and carriage of *Mycoplasma pneumoniae* in children. *Front. Microbiol.* 7:329. doi: 10.3389/fmicb.2016.00329

Nakamura, Y., Oishi, T., Kaneko, K., Kenri, T., Tanaka, T., Wakabayashi, S., et al. (2021). Recent acute reduction in macrolide-resistant *Mycoplasma pneumoniae* infections among Japanese children. *J. Infect. Chemother.* 27, 271–276. doi: 10.1016/j.jiac.2020.10.007

Pereyre, S., Charron, A., Renaudin, H., Bebear, C., and Bebear, C. M. (2007). First report of macrolide-resistant strains and description of a novel nucleotide sequence variation in the P1 adhesin gene in *Mycoplasma pneumoniae* clinical strains isolated in France over 12 years. *J. Clin. Microbiol.* 45, 3534–3539. doi: 10.1128/JCM.01345-07

Pereyre, S., Goret, J., and Bebear, C. (2016). *Mycoplasma pneumoniae*: current knowledge on macrolide resistance and treatment. *Front. Microbiol.* 7:974. doi: 10.3389/fmicb.2016.00974

Ruland, K., Himmelreich, R., and Herrmann, R. (1994). Sequence divergence in the ORF6 gene of *Mycoplasma pneumoniae*. *J. Bacteriol.* 176, 5202–9.

Sasaki, T., Kenri, T., Okazaki, N., Iseki, M., Yamashita, R., Shintani, M., et al. (1996). Epidemiological study of *Mycoplasma pneumoniae* infections in Japan based on PCR-restriction fragment length polymorphism of the P1 cytoadhesin gene. *J. Clin. Microbiol.* 34, 447–449. doi: 10.1128/jcm.34.2.447-449.1996

Su, C. J., Chavoya, A., Dallo, S. F., and Baseman, J. B. (1990). Sequence divergency of the cytoadhesin gene of *Mycoplasma pneumoniae*. *Infect. Immun.* 58, 2669–2674. doi: 10.1128/iai.58.8.2669-2674.1990

Touati, A., Blouin, Y., Sirand-Pugnet, P., Renaudin, H., Oishi, T., Vergnaud, G., et al. (2015). Molecular epidemiology of *Mycoplasma pneumoniae*: genotyping using single nucleotide polymorphisms and SNaPshot technology. *J. Clin. Microbiol.* 53, 3182–3194. doi: 10.1128/JCM.01156-15

Vizarraga, D., Kawamoto, A., Matsumoto, U., Illanes, R., Perez-Luque, R., Martin, J., et al. (2020). Immunodominant proteins P1 and P40/P90 from human pathogen *Mycoplasma pneumoniae*. *Nat. Commun.* 11:5188. doi: 10.1038/s41467-020-18777-y

Waites, K. B., Xiao, L., Liu, Y., Balish, M. F., and Atkinson, T. P. (2017). *Mycoplasma pneumoniae* from the respiratory tract and beyond. *Clin. Microbiol. Rev.* 30, 747–809. doi: 10.1128/CMR.00114-16

Wang, X., Li, M., Luo, M., Luo, Q., Kang, L., Xie, H., et al. (2022). *Mycoplasma pneumoniae* triggers pneumonia epidemic in autumn and winter in Beijing: a multicentre, population-based epidemiological study between 2015 and 2020. *Emerg. Microbes. Infect.* 11, 1508–1517. doi: 10.1080/22221751.2022.2078228

Wang, Y., Xu, B., Wu, X., Yin, Q., Wang, Y., Li, J., et al. (2021). Increased macrolide resistance rate of M3562 *Mycoplasma pneumoniae* correlated with macrolide usage and genotype shifting. *Front. Cell. Infect. Microbiol.* 11:675466. doi: 10.3389/fcimb.2021.675466

Wood, G. E., Iverson-Cabral, S. L., Gillespie, C. W., Lowens, M. S., Manhart, L. E., and Totten, P. A. (2020). Sequence variation and immunogenicity of the *Mycoplasma genitalium* MgpB and MgpC adherence proteins during persistent infection of men with non-gonococcal urethritis. *PLoS One* 15:e0240626. doi: 10.1371/journal.pone.0240626

Xiao, L., Ptacek, T., Osborne, J. D., Crabb, D. M., Simmons, W. L., Lefkowitz, E. J., et al. (2015). Comparative genome analysis of *Mycoplasma pneumoniae*. *BMC Genom.* 16:610. doi: 10.1186/s12864-015-1801-0

Xiao, L., Ratliff, A. E., Crabb, D. M., Mixon, E., Qin, X., Selvarangan, R., et al. (2020). Molecular characterization of *Mycoplasma pneumoniae* isolates in the United States from 2012 to 2018. *J. Clin. Microbiol.* 58:e00710-20. doi: 10.1128/JCM.00710-20

Yamazaki, T., and Kenri, T. (2016). Epidemiology of *Mycoplasma pneumoniae* infections in Japan and therapeutic strategies for macrolide-resistant *M. pneumoniae*. *Front. Microbiol.* 7:693. doi: 10.3389/fmicb.2016.00693

Zhao, F., Cao, B., Li, J., Song, S., Tao, X., Yin, Y., et al. (2011). Sequence analysis of the *p1* adhesin gene of *Mycoplasma pneumoniae* in clinical isolates collected in Beijing in 2008 to 2009. *J. Clin. Microbiol.* 49, 3000–3003. doi: 10.1128/JCM.00105-11

Zhao, F., Li, J., Liu, J., Guan, X., Gong, J., Liu, L., et al. (2019). Antimicrobial susceptibility and molecular characteristics of *Mycoplasma pneumoniae* isolates across different regions of China. *Antimicrob. Resist. Infect. Control* 8:143. doi: 10.1186/s13756-019-0576-5

Zhao, F., Zhang, J., Wang, X., Liu, L., Gong, J., Zhai, Z., et al. (2021). A multisite SNP genotyping and macrolide susceptibility gene method for *Mycoplasma pneumoniae* based on MALDI-TOF MS. *iScience* 24:102447. doi: 10.1016/j.isci.2021.102447

Zhu, C., Wang, S., Hu, S., Yu, M., Zeng, Y., You, X., et al. (2012a). Protective efficacy of a *Mycoplasma pneumoniae* PIC DNA vaccine fused with the B subunit of *Escherichia coli* heat-labile enterotoxin. *Can. J. Microbiol.* 58, 802–810. doi: 10.1139/w2012-051

Zhu, C., Wu, Y., Chen, S., Yu, M., Zeng, Y., You, X., et al. (2012b). Protective immune responses in mice induced by intramuscular and intranasal immunization with a *Mycoplasma pneumoniae* PIC DNA vaccine. *Can. J. Microbiol.* 58, 644–652. doi: 10.1139/w2012-041



OPEN ACCESS

EDITED BY

Florence Tardy,
Agence Nationale de Sécurité Sanitaire de
l'Alimentation,
de l'Environnement et du Travail (ANSES),
France

REVIEWED BY

Martijn Zwama,
Osaka University, Japan
Patrice Gaurivaud,
Agence Nationale de Sécurité Sanitaire de
l'Alimentation,
de l'Environnement et du Travail (ANSES),
France

*CORRESPONDENCE

Miklós Gyuranecz
✉ m.gyuranecz@gmail.com

RECEIVED 04 May 2023

ACCEPTED 23 June 2023

PUBLISHED 11 July 2023

CITATION

Nagy EZ, Kovács ÁB, Wehmann E, Bekő K,
Földi D, Bányai K, Kreizinger Z and
Gyuranecz M (2023) Phenotypic and genetic
insights into efflux pump mechanism in
Mycoplasma anserisalpingitidis.
Front. Microbiol. 14:1216893.
doi: 10.3389/fmicb.2023.1216893

COPYRIGHT

© 2023 Nagy, Kovács, Wehmann, Bekő, Földi,
Bányai, Kreizinger and Gyuranecz. This is an
open-access article distributed under the terms
of the [Creative Commons Attribution License
\(CC BY\)](https://creativecommons.org/licenses/by/4.0/). The use, distribution or reproduction
in other forums is permitted, provided the
original author(s) and the copyright owner(s)
are credited and that the original publication in
this journal is cited, in accordance with
accepted academic practice. No use,
distribution or reproduction is permitted which
does not comply with these terms.

Phenotypic and genetic insights into efflux pump mechanism in *Mycoplasma anserisalpingitidis*

Eszter Zsófia Nagy^{1,2}, Áron Botond Kovács^{1,2}, Enikő Wehmann^{1,2},
Katinka Bekő¹, Dorottya Földi^{1,2}, Krisztián Bányai^{1,2,3},
Zsuzsa Kreizinger^{1,4} and Miklós Gyuranecz^{1,2,4,5}

¹Veterinary Medical Research Institute, Budapest, Hungary, ²National Laboratory of Infectious Animal Diseases, Antimicrobial Resistance, Veterinary Public Health and Food Chain Safety, Budapest, Hungary, ³Department of Pharmacology and Toxicology, University of Veterinary Medicine, Budapest, Hungary, ⁴MolliScience Kft., Biatorbágy, Hungary, ⁵Department of Microbiology and Infectious Diseases, University of Veterinary Medicine, Budapest, Hungary

Introduction: *Mycoplasma anserisalpingitidis* is one of the most important waterfowl-pathogenic mycoplasmas. Due to inadequate antibiotic treatment, many strains with high minimal inhibitory concentration (MIC) values for multiple drugs have been isolated lately. Decreased antibiotic susceptibility in several *Mycoplasma* species are known to be associated with mutations in topoisomerase and ribosomal genes, but other strategies such as active efflux pump mechanisms were also described. The scope of this study was the phenotypic and genetic characterization of the active efflux mechanism in *M. anserisalpingitidis*.

Methods: We measured the MIC values in the presence and absence of different efflux pump inhibitors (EPIs), such as carbonyl cyanide m-chlorophenylhydrazine (CCCP), orthovanadate (OV), and reserpine (RSP). Moreover, bioinformatic tools were utilized to detect putative regulatory sequences of membrane transport proteins coding genes, while comparative genome analysis was performed to reveal potential markers of antibiotic resistance.

Results: Out of the three examined EPIs, CCCP decreased the MICs at least two-fold below the original MICs (in 23 cases out of 36 strains). In the presence of OV or RSP, MIC value differences could be seen only if modified dilution series (10% decrease steps were used instead of two-fold dilutions) were applied (in 24/36 cases with OV and 9/36 with RSP). During comparative genome analysis, non-synonymous single nucleotide polymorphisms (nsSNPs) were identified in genes encoding ABC membrane transport proteins, which were displayed in higher percentages in *M. anserisalpingitidis* strains with increased MICs. In terms of other genes, a nsSNP was identified in DNA gyrase subunit A (*gyrA*) gene which can be related to decreased susceptibility to enrofloxacin. The present study is the first to highlight the importance of efflux pump mechanisms in *M. anserisalpingitidis*.

Discussion: Considering the observed effects of the EPI CCCP against this bacterium, it can be assumed, that the use of EPIs would increase the efficiency of targeted antibiotic therapy in the future control of this pathogen. However, further research is required to obtain a more comprehensive understanding of efflux pump mechanism in this bacterium.

KEYWORDS

Mycoplasma sp. 1220, efflux pump inhibitors, antimicrobial resistance, ABC efflux pump, minimal inhibitory concentration

1. Introduction

Mycoplasma anserisalpingitidis is a bacterial pathogen infecting mainly goose, which can cause inflammation of the cloaca and genital tracts (Stipkovits et al., 1986; Hinz et al., 1994; Stipkovits and Kempf, 1996). In three-weeks-old waterfowl, peritonitis and airsacculitis can occur in association with the infection (Stipkovits et al., 1993). Mostly breeding flocks are exposed to this disease, where the morbidity can rise up to even 50–100%. In the affected flocks the egg production is significantly decreased and the embryo mortality can reach up to 40–60% (Dobos-Kovács et al., 2009). Consequently, this pathogen is responsible for significant economic losses (Stipkovits and Szathmari, 2012), which could only be prevented or treated by improving the housing conditions and using antibiotic therapy, as currently no vaccines are available commercially against *M. anserisalpingitidis*. However, many strains with high minimal inhibitory concentration (MIC) values for multiple drugs have been isolated from Europe and China lately (Gróznér et al., 2016; Gyuranecz et al., 2020). So far three main mechanisms of antibiotic resistance have been described in bacteria: modification of target sites by methylation or mutation, drug inactivation and active efflux system (Giedraitienė et al., 2011). Bacterial efflux pumps are responsible for removing toxic substrates from the bacterial cell (Webber, 2003; Poole, 2007). Primary and secondary transporters have been described previously (Marquez, 2005). The group of primary transporters include the ATP-binding cassettes (ABC) and the ABC transporters, which use ATP as energy source. Members of the second group use the proton gradient as a source of energy and are classified into four further families: major facilitator superfamily (MFS), resistance nodulation and cell division family (RND), small multi-drug resistance family (SMR) and multi-drug and toxic compound extrusion family (MATE) (Marquez, 2005).

ATP-binding cassette (ABC) transporters represent one of the largest superfamilies of active membrane transport proteins. They all share the ability to bind and hydrolyze ATP to transport substrates across the lipid bilayer (Higgins, 1992). The primary functions of bacterial ABC transporters are nutrition uptake, as well as the elimination of drugs and metabolic waste (Schneider and Hunke, 1998; Dassa and Bouige, 2001). These transporters exhibit shared structural features, namely two hydrophobic transmembrane domains and two hydrophilic cytoplasmic domains (Linton and Higgins, 1998). Recently, a novel type of ABC transporter called Energy Coupling Factor (ECF) transporters, has been classified as significant in the uptake of micronutrients (Rodionov et al., 2009). The structure of the ECFs contains two nucleotide-binding domains (EcfA and EcfA'), a transmembrane domain (EcfT) and a substrate-binding component (EcfS).

Based on previous studies, efflux pumps have a vital role in low-level antibiotic resistance (Schmalstieg et al., 2012; Antunes et al., 2015). In case of *M. mycoides* subsp. *capri* significant differences were found between the MIC values in the presence or absence of orthovanadate (OV) in case of norfloxacin and ciprofloxacin, but only in strains originally inhibited by lower MICs ($\leq 8 \mu\text{g/mL}$ for norfloxacin and $\leq 1 \mu\text{g/mL}$ for ciprofloxacin and enrofloxacin; Antunes et al., 2015). Similarly in *Mycobacterium* species, only low-level resistance could be inhibited by efflux pump inhibitors (Schmalstieg et al., 2012). Several reviews have recently been published which were dealing with the effect of different efflux pump inhibitors (Raherison et al., 2002; Antunes et al., 2015; Li et al., 2017). In these

studies carbonyl cyanide *m*-chlorophenylhydrazine (CCCP), OV and reserpine (RSP) were used as primary efflux pump inhibitors. CCCP can interfere with the proton gradient, which results in the disruption of the ATP synthesis (Kasianowicz et al., 1984). OV inhibits the ATPase activity (Pezza, 2002), while RSP's mechanism of action is the inhibition of ATP/Mg²⁺ pumps.

Multiple studies have been published that have identified mutations associated with antibiotic resistance in the coding regions (Lupien et al., 2013; Zwama and Nishino, 2021; Waldner et al., 2022) or the promoters (Kaatze et al., 1999; Unemo et al., 2019) of various efflux pump genes in other bacteria. In the mechanism of antibacterial resistance of mycoplasmas, despite the presence of other transport protein families, only the significance of ABC efflux pumps has been previously established (Pereyre et al., 2002; Raherison et al., 2005; Antunes et al., 2015; Chernova et al., 2016). Non-synonymous single nucleotide polymorphisms (nsSNPs) within the regions encoding ABC efflux genes have also been reported in cases of *Mycoplasma bovis* (Waldner et al., 2022) and *Mycoplasma pneumoniae* (Li et al., 2017). The current state of knowledge is limited regarding the regulation of the gene expression—including of ABC efflux genes—in mycoplasmas, because of the reduced genome and low percentage of genes involved in translation and transcription in these bacteria (Madeira and Gabriel, 2007). Previous studies have identified the positions of transcription factors, transcriptional start sites, and core promoter structure in Mollicutes (Lloréns-Rico et al., 2015; Fisunov et al., 2016; Yus et al., 2019), as well as several subsequences of ribosome binding sites (RBSs) in *Mycoplasma* species (Montero-Blay et al., 2019).

The scope of this study was to investigate the activity of ABC efflux pumps in *M. anserisalpingitidis* strains with increased MIC values for the most common antibiotics. Beside examining the effect of three different efflux pump inhibitors (CCCP, OV, RSP) on the MICs, comparative genome analysis was carried out to identify potential mutations involved in antimicrobial resistance. The examinations were focused on identifying non-synonymous mutations in genes previously reported to be associated with antibiotic resistance, as well as in coding genes and putative regulatory sequences of ABC transporter protein coding genes in *M. anserisalpingitidis*.

2. Materials and methods

2.1. Isolate selection

Eleven *M. anserisalpingitidis* clinical isolates were selected for the examinations based on differences in their phenotypic and genetic characteristics which has been previously described (Gróznér et al., 2021; Table 1). In brief, the isolates were cultured in Oxoid Mycoplasma broth medium (Thermo Fisher Scientific, Inc./Oxoid, Inc., Waltham, MA) supplemented with Mycoplasma Supplement G (Thermo Fisher Scientific, Inc./Oxoid, Inc.), 0.5% (wt/vol) sodium pyruvate, 0.5% (wt/vol) glucose, 0.15% L-arginine hydrochloride and 0.05% (wt/vol) phenol red. MIC values of enrofloxacin (group of fluoroquinolones), lincomycin (from lincosamides), tiamulin (from pleuromutilins) and tilmicosin, tylosin, tylvalosin from the group of macrolides were determined with the broth micro-dilution method (Hannan, 2000). Based on the results of the MIC testing, three strains with high and three isolates with low MICs were chosen for each

TABLE 1 Background information about the isolates with high and low MIC values in this study.^{a,b}

GenBank accession number	Strain ID	Initial MIC (μg/mL)						Clade	Subclade	Sample of origin
		Enrofloxacin	Lincomycin	Tiamulin	Tilmicosin	Tylosin	Tylvalosin			
CP042295	ATCC BAA-2147	0.312	1.000	0.312	≤0.250	≤0.250	≤0.250	C	3C	Phallus lymph
Field isolates with low MICs										
SRX9772795	MycAv 65	1.250	2.000	0.312	≤0.250	≤0.250	≤0.250	C	4C	Phallus lymph
SRX9772793	MycAv 63	0.625	0.500	0.156	64.000	4.000	≤0.250	C	6C	Tracheal swab
SRX7583695	MycAv 668	0.312	≤0.250	0.156	≤0.250	≤0.250	≤0.250	C	6C	Cloacal swab
SRX7583629	MycAv 55	2.500	1.000	0.156	≤0.250	≤0.250	≤0.250	C	4C	Ovarian follicles
SRX7583693	MycAv 50	10.000	4.000	0.078	0.500	0.500	≤0.250	B		Phallus
Field isolates with high MICs										
SRX7583639	MycAv 70	5.000	2.000	0.625	>64.000	4.000	≤0.250	B		Phallus lymph
SRX7583671	MycAv 47	5.000	> 128.000	0.625	>64.000	4.000	1.000	C	6C	Lung, air sac
SRX7583648	MycAv 91	5.000	8.000	0.625	≤0.250	≤0.250	≤0.250	C	3C	Phallus
SRX7583635	MycAv 67	5.000	> 128.000	0.625	> 128.000	> 128.000	4.000	C	1C	Phallus lymph
SRX7583636	MycAv 68	2.500	> 128.000	0.625	> 128.000	> 128.000	4.000	C	1C	Phallus lymph
NZ_CP041664.1	MycAv 177	2.500	2.000	0.625	> 128.000	> 64.000	4.000	B		Phallus

Field isolates with low MICs are the parent strains of the *in vitro* cultivated mutants.
^aIsolates with initial MIC values highlighted in bold were submitted to efflux pump inhibition tests with the given antibiotics.
^bThe classification to different clades and subclades are according to Gróznér et al. (2021).

antimicrobial group for further analyses. Overall, six strains exhibited reduced antibiotic susceptibility to multiple widely used antibiotics: MycAv 47, 70 and 91 for enrofloxacin; MycAv 47, 67, and 68 for lincomycin and tiamulin; MycAv 67, 68, and 177 for macrolides. Additionally, five strains showed sensitivity to several antimicrobial agents: MycAv 63, 65, and 668 for enrofloxacin; MycAv 55, 63, and 668 for lincomycin; MycAv 50, 55, and 668 for tiamulin and macrolides (Table 1). The low and high MIC values were determined based on previous studies, as there are no official breakpoints available for veterinary mycoplasmas: low MIC value $\leq 0.5 \mu\text{g/mL}$ for enrofloxacin (Landman et al., 2008), tylvalosin (Behbahan et al., 2008; Ghaleh Gol et al., 2008); $\leq 2 \mu\text{g/mL}$ for lincomycin (Kempf et al., 1988); $\leq 1 \mu\text{g/mL}$ for tylosin (Landman et al., 2008); $\leq 8 \mu\text{g/mL}$ for tilmicosin (Landman et al., 2008); $< 0.625 \mu\text{g/mL}$ for tiamulin (Ghaleh Gol et al., 2008); high MIC value: $\geq 2 \mu\text{g/mL}$ for enrofloxacin (Landman et al., 2008); tylvalosin (Behbahan et al., 2008; Ghaleh Gol et al., 2008); $\geq 8 \mu\text{g/mL}$ for lincomycin (Kempf et al., 1988); $\geq 4 \mu\text{g/mL}$ for tylosin (Landman et al., 2008); $\geq 32 \mu\text{g/mL}$ for tilmicosin (Landman et al., 2008); $\geq 0.625 \mu\text{g/mL}$ for tiamulin (Ghaleh Gol et al., 2008). Whole genome sequences of the isolates were determined on Illumina platform (Illumina, Inc., San Diego, CA, United States) and multilocus sequence typing (MLST) was performed for the genetic characterization of the isolates previously (Gróznier et al., 2021). The selected isolates belong to different clades based on MLST analysis (Table 1; Gróznier et al., 2021).

2.2. Preparation of *in vitro* mutants of low susceptibility to antibiotics

A total of 18 *in vitro* cultivated mutants were selected by serial passages from field isolates inhibited by lower MIC values for the examined antibiotics (Sulyok et al., 2017). The parent strains, the applied antibiotics and the 18 *in vitro* cultivated mutants can be seen in Supplementary Dataset S1. Briefly, two-fold dilution series were made from each antibiotic in sub-inhibitory concentrations for every selected parent strain with low MICs (listed in Table 1 and Supplementary Dataset S1). Enrofloxacin, lincomycin, tiamulin, tilmicosin, tylosin were produced by Vetranal® Sigma-Aldrich, USA and tylvalosin was originated from ECO® Animal Health Ltd., United Kingdom. Stock solutions were diluted in the concentration of 1 mg/mL and aliquots were stored at -70°C . Two-fold dilutions of each antibiotic were freshly prepared in Oxoid Mycoplasma broth medium (Thermo Fisher Scientific) in the range of 0.039–0.156 $\mu\text{g/mL}$ for enrofloxacin and tiamulin, 0.125–0.5 $\mu\text{g/mL}$ for lincomycin and macrolides in the first dilution panel. The selected isolates were incubated in Oxoid Mycoplasma broth medium (Thermo Fisher Scientific) at 37°C for 5 days, and the *M. anserisalpiginidis* cultures changing color (the red media turned yellow) at the highest antibiotic concentrations were inoculated into a fresh, two-fold dilution panel of the antibiotics, with increased concentrations. The serial passages were continued until the strains' MICs reached above the sensitive MIC value determined by previous studies: $\geq 0.5 \mu\text{g/mL}$ for tylvalosin (Ghaleh Gol et al., 2008) and enrofloxacin (Landman et al., 2008), $\geq 1 \mu\text{g/mL}$ for tylosin (Landman et al., 2008), $\geq 8 \mu\text{g/mL}$ for tilmicosin (Landman et al., 2008), $\geq 2 \mu\text{g/mL}$ for lincomycin (Kempf et al., 1988), and $\geq 0.625 \mu\text{g/mL}$ for tiamulin (Ghaleh Gol et al., 2008). However, two (MycAv 63 and 65) of the three selected parent strains' (MycAv

63, 65, 668) MIC values for enrofloxacin were already above 0.5 $\mu\text{g/mL}$, hence it was decided to set a higher threshold of 2 $\mu\text{g/mL}$ for this antibiotic (Landman et al., 2008). In order to reach these MIC values, the sensitive *M. anserisalpiginidis* parent strains (MycAv 50, 55, 63, 65, 668) were submitted to four, increasing dilution series of enrofloxacin, lincomycin, tiamulin, tilmicosin, tylosin, and five, increasing dilution series of tylvalosin supplied liquid medium. *In vitro* developed mutants were passaged once in antibiotic-free medium and the MIC values were determined again (Supplementary Datasets S1,S2).

2.3. MIC testing

Antimicrobial susceptibility was measured by using broth micro-dilution method as described by Hannan (2000). For the MIC testing, twofold dilutions of each antibiotic were freshly prepared in the range of 0.039–10 $\mu\text{g/mL}$ for enrofloxacin and tiamulin and 0.25–64/128 $\mu\text{g/mL}$ for lincomycin, tilmicosin, tylosin and tylvalosin.

M. anserisalpiginidis type strain (ATCC BAA-2147) and five field isolates (the parent strains of the *in vitro* cultivated mutant strains, MycAv 50, 55, 63, 65, 668; Table 1) were used as control and the cultures were adjusted in Oxoid Mycoplasma broth medium (Thermo Fisher Scientific) to 10^5 color changing unit (CCU)/mL. The experiment was carried out on 96-well plate and every experiment was performed in duplicates. The plates were incubated at 37°C and were checked every day for a week or until they did not show further color changes (red to yellow shift) for 2 days. Initial MICs were measured when the growth control changed color.

2.4. Determining the adequate concentrations of the efflux pump inhibitors

Broth micro-dilution assay (Hannan, 2000) was used in order to determine the sensitivity of *M. anserisalpiginidis* to CCCP, OV, and RSP. The efflux pump inhibitors were produced by Vetranal® Sigma-Aldrich, United States. Two-fold dilutions of each efflux pump inhibitor were freshly prepared in the range of 0.191–97.92 $\mu\text{g/mL}$ for CCCP, 0.07–35.84 mM for OV and 0.005–1.28 mg/mL for RSP. *M. anserisalpiginidis* cultures were adjusted in Oxoid Mycoplasma broth medium (Thermo Fisher Scientific) to 10^5 CCU/mL. The experiment was carried out on 96-well plate and every experiment was performed in duplicates. The plates were incubated at 37°C and were checked every day until they did not show further color changes (red to yellow shift). The lowest efflux pump inhibitor concentration at which no color change was detected was considered the lethal dose of the efflux pump. The adequate concentrations of the efflux pump inhibitors to be used in the MIC testing were determined to be at least four-fold below of the lethal concentrations of each efflux pump inhibitors (Raheison et al., 2002; Li et al., 2017).

2.5. MIC testing with efflux pump inhibitors

A modified broth micro-dilution method was used to examine the effect of efflux pump inhibitors (Hannan, 2000; Antunes et al., 2015;

Li et al., 2017). The MIC values against the field isolates (MycAv 47, 70, 91 for enrofloxacin; MycAv 47, 67, 68 for lincomycin and tiamulin, MycAv 67, 68, 177 for macrolides) and *in vitro* cultivated mutant strains with decreased antibiotic susceptibility (MycAv 63-M1, 65-M1, 668-M1 for enrofloxacin, MycAv 55-M2, 63-M2, 668-M2 for lincomycin, MycAv 50-M6, 55-M6, 668-M6 for tiamulin, MycAv 50-M3, 55-M3, 668-M3 for tilmicosin, MycAv 50-M5, 55-M5, MycAv 668-M5 for tylosin, MycAv 50-M4, 55-M4, 668-M4 for tylvalosin) were measured for each antibiotic both in the presence and in the absence of efflux pump inhibitors. A modified dilution series was applied where 10% decrease steps were used instead of two-fold dilutions in order to make a more sensitive system, except for the tests with CCCP (Supplementary Dataset S2). In this case, two-fold dilutions were applicable (applied antibiotic ranges were the same as the ones used for MIC testing of the control strains) due to the strong effect on MIC values which had been experienced during the pilot studies (data not shown). The efflux pump inhibitors were used in the following concentrations: 0.765 µg/mL CCCP, 0.56 mM OV and 0.02 mg/mL RSP. The efflux pump inhibitors were freshly prepared before every experiment and every test was carried out on 96-well plate. The *M. anserisalpinitidis* type strain (ATCC BAA-2147, GenBank accession number CP042295) was used as a quality control. *M. anserisalpinitidis* cultures were diluted in Oxoid Mycoplasma broth medium in the concentration of 10⁵ CCU/mL. The plates were incubated at 37°C and checked after 16, 20, 24, 40, 44, 48, 64, 68, and 72 h of incubation, then on a daily basis for 1 week, or until they did not show further color changes for 2 days. Each experiment was performed in duplicates. Initial MICs were measured when the growth control showed color change.

Two-sample paired (Wilcoxon) signed rank test was used to ascertain whether there is significant difference between MIC values in the presence and absence of each tested efflux pump inhibitor. The (Wilcoxon) signed rank test was performed by R 4.2.1. software (R Core Team, 2022).

2.6. Whole genome sequence determination and analyses of possible antibiotic resistance-associated markers

Genomic DNA of the 18 *in vitro* cultivated mutants (listed in Supplementary Dataset S1) were extracted from 2 mL of logarithmic-phase cultures with the help of a commercial kit (QIAamp DNA Mini Kit, Qiagen Inc., United States) according to the manufacturer's instructions. The whole-genome sequencing was carried out by using NextSeq 500 Illumina equipment (Illumina, Inc., San Diego, CA, United States). The short reads were assembled using SPAdes software version 3.15.4 (Bankevich et al., 2012). The annotation of the genomes was done using Prokaryotic Genome Annotation Pipeline (PGAP) software version 6.3 (Li et al., 2021). The newly assembled genome sequences (Accessibility of the SRA reads: BioProject ID: PRJNA912395) and the field isolates with high MICs were compared to the parent strains of the *in vitro* developed *M. anserisalpinitidis* mutants, and to the type strain (ATCC BAA-2147) with progressive MAUVE algorithm (Darling et al., 2004). SNPs, deletions and insertions were searched by Geneious Prime 2019.2.1 software (Kearse et al., 2012). The putative SNPs were manually reviewed and sorted based on their capability to cause synonymous or non-synonymous

SNP (nsSNP). The functions of those genes which contain nsSNPs were examined with the help of CARD database (Alcock et al., 2019), NCBI nucleotide database (Sayers et al., 2022) and current literature (Google Scholar, using the following key words: "antibiotic resistance" and the gene name or functional group, for example: "gyrA" "antibiotic resistance"). The common nsSNPs were checked in all *M. anserisalpinitidis* strains with publicly available whole genome sequences and MIC data (Gróznier et al., 2022).

2.7. Identifying putative regulatory regions of efflux pump genes

Putative regulatory sequences were identified using the Promotech software version 1.0 (Chevez-Guardado and Peña-Castillo, 2021) and the genome of the *M. anserisalpinitidis* type strain. In order to minimize the number of false positive promoters, the score threshold was suggested to be above 0.6 (Weber et al., 2012; Siqueira et al., 2014; Lloréns-Rico et al., 2015). As the regulatory regions of mycoplasmas are not fully characterized, we established a more stringent threshold for our investigation. Sequences located upstream of an efflux pump coding gene with a score of 0.8 or higher were considered potential regulatory regions involved in efflux pump regulation. The putative regulatory sequences' promoter regions and ribosome-binding sites were determined based on the literature (Lloréns-Rico et al., 2015; Fisunov et al., 2016; Montero-Blay et al., 2019; Yús et al., 2019) and MEME suite software (Bailey et al., 2015). The Promotech-detected potential efflux pump regulatory regions were used as the input for the MEME motif-finding software to identify the putative Pribnow boxes in the sequences.

3. Results

3.1. Efflux pump activity testing of *Mycoplasma anserisalpinitidis* isolates

In this study initial MIC values of 18 *in vitro* cultivated mutants (MycAv 63-M1, 65-M1, 668-M1 for enrofloxacin, MycAv 55-M2, 63-M2, 668-M2 for lincomycin, MycAv 50-M6, 55-M6, 668-M6 for tiamulin, MycAv 50-M3, 55-M3, 668-M3 for tilmicosin, MycAv 50-M5, 55-M5, MycAv 668-M5 for tylosin, MycAv 50-M4, 55-M4, 668-M4 for tylvalosin) and six isolates with decreased antibiotic susceptibility (MycAv 47, 70, 91 for enrofloxacin; MycAv 47, 67, 68 for lincomycin, tiamulin, MycAv 67, 68, 177 for macrolides) were examined in the presence and in the absence of efflux pump inhibitors (Supplementary Dataset S2 and Figures 1, 2). In case of CCCP notable increases were detected in the efficiency of the antibiotics using twofold dilution series.

The MICs for enrofloxacin were halved in all cases out of the three field isolates tested (MycAv 47, 70, 91; Figure 1A); however, the *in vitro* cultivated mutants (MycAv 63-M1, 65-M1, 668-M1) did not show any detectable changes (Figure 2A). The MICs against the *in vitro* mutants with decreased lincomycin susceptibility (MycAv 55-M2, 63-M2, 668-M2) were reduced at least two-fold below (Figure 2B and Supplementary Dataset S2), while there could not be measured any changes in the MICs of clinical isolates of low susceptibility to this agent (MycAv 47, 67, 68 with >128 µg/mL MICs; Figure 1B). The MICs

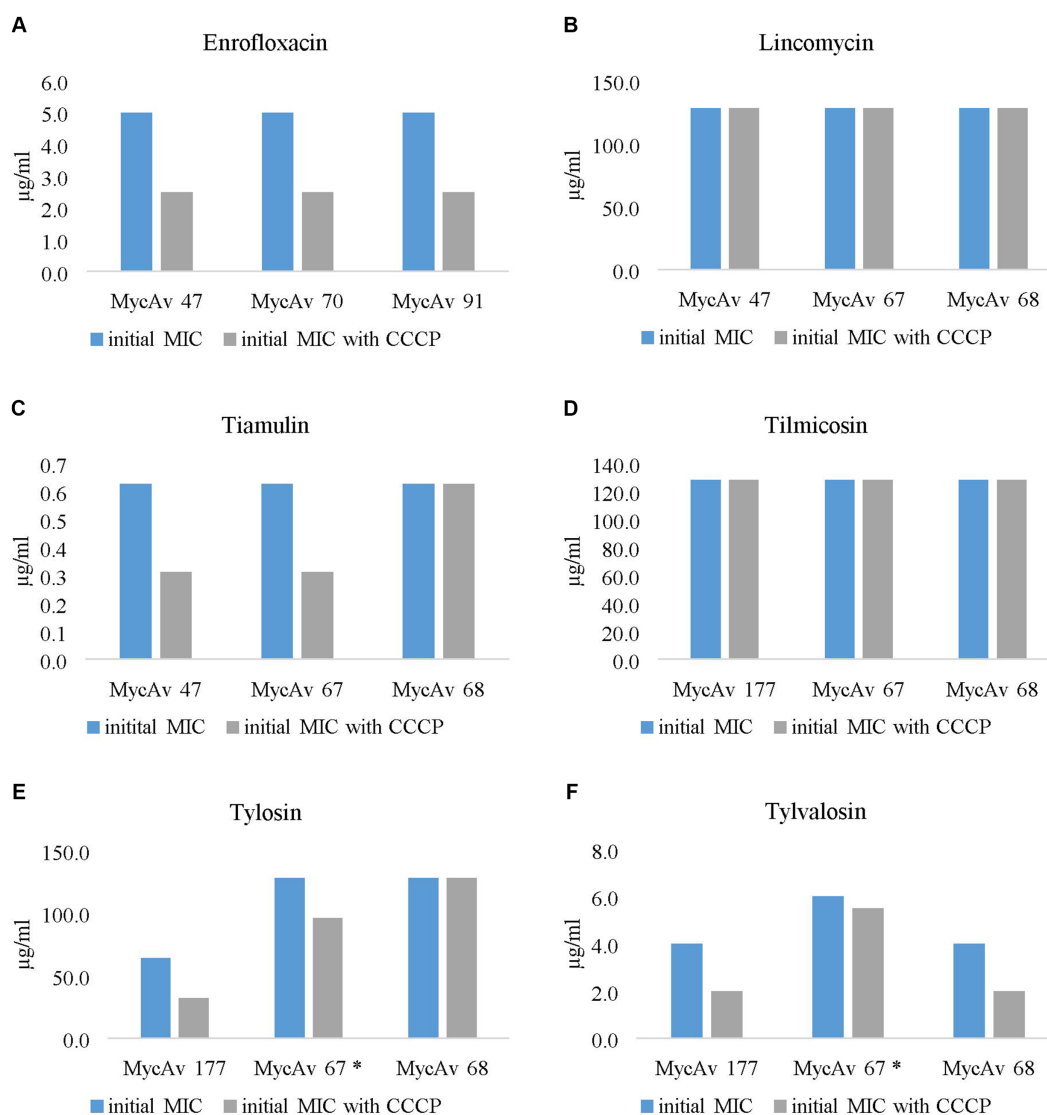


FIGURE 1

The effect of the most successful efflux pump inhibitor (carbonyl cyanide *m*-chlorophenylhydrazine (CCCP)) on the MICs of clinical isolates with decreased antibiotic susceptibility against enrofloxacin (A), lincomycin (B), tiamulin (C), tilmicosin (D), tylosin (E) and tylvalosin (F). In the case of the MIC of MycAv 67 for tylosin and tylvalosin (marked with a star) could be seen differences only in modified dilution series (the concentration ranges used are presented in [Supplementary Dataset S2](#)).

of *in vitro* mutants (MycAv 50-M6, 55-M6, 668-M6) and field isolates (MycAv 47, 67, 68) with decreased susceptibility to tiamulin dwindled at least two-fold below the original values, except in case of MycAv 68 clinical isolate with 0.625 µg/mL original MIC value ([Figure 1C](#) and [Figure 2C](#)). Regarding field isolates with increased MIC values for macrolides (MycAv 67, 68, 177), two-fold MIC decreases could be seen using CCCP in three cases: MIC value of MycAv 177 against tylosin and MycAv 177, 68 against tylvalosin. However, clinical isolates with extremely high MICs (MycAv 177, 67 with >128 µg/mL MIC for tilmicosin and MycAv 68 with >128 µg/mL MICs for tilmicosin and tylosin) did not show any changes ([Figures 1D–F](#)). Additionally, there was a field isolate (MycAv 67 in cases of tylosin and tylvalosin) where we could see differences only in modified dilution series ([Supplementary Dataset S2](#)). In cases of *in vitro* cultivated mutants with decreased susceptibility to macrolides, there were two- (MycAv 50-M3,

MycAv 55-M3, MycAv 50-M4, MycAv 55-M4, MycAv 668-M4, MycAv 50-M5, MycAv 55-M5, MycAv 668-M5) or four-fold (MycAv 668-M3) reductions in the MIC values ([Figures 2D–F](#) and [Supplementary Dataset S2](#)). The difference was statistically significant between the MICs in the presence and absence of CCCP (in twofold dilution series) when all the mutants and field isolates were analyzed together ($p < 0.001$).

In the presence of OV or RSP MIC value differences could be seen only if modified dilution series were used (10% decrease steps were used instead of two-fold dilutions). There were detectable changes in 24 occasions out of the 36 examined combinations with OV ([Supplementary Dataset S2](#)), but these differences were not statistically significant. As for RSP, there were nine detectable, statistically not significant differences out of the 36 combinations ([Supplementary Dataset S2](#)).

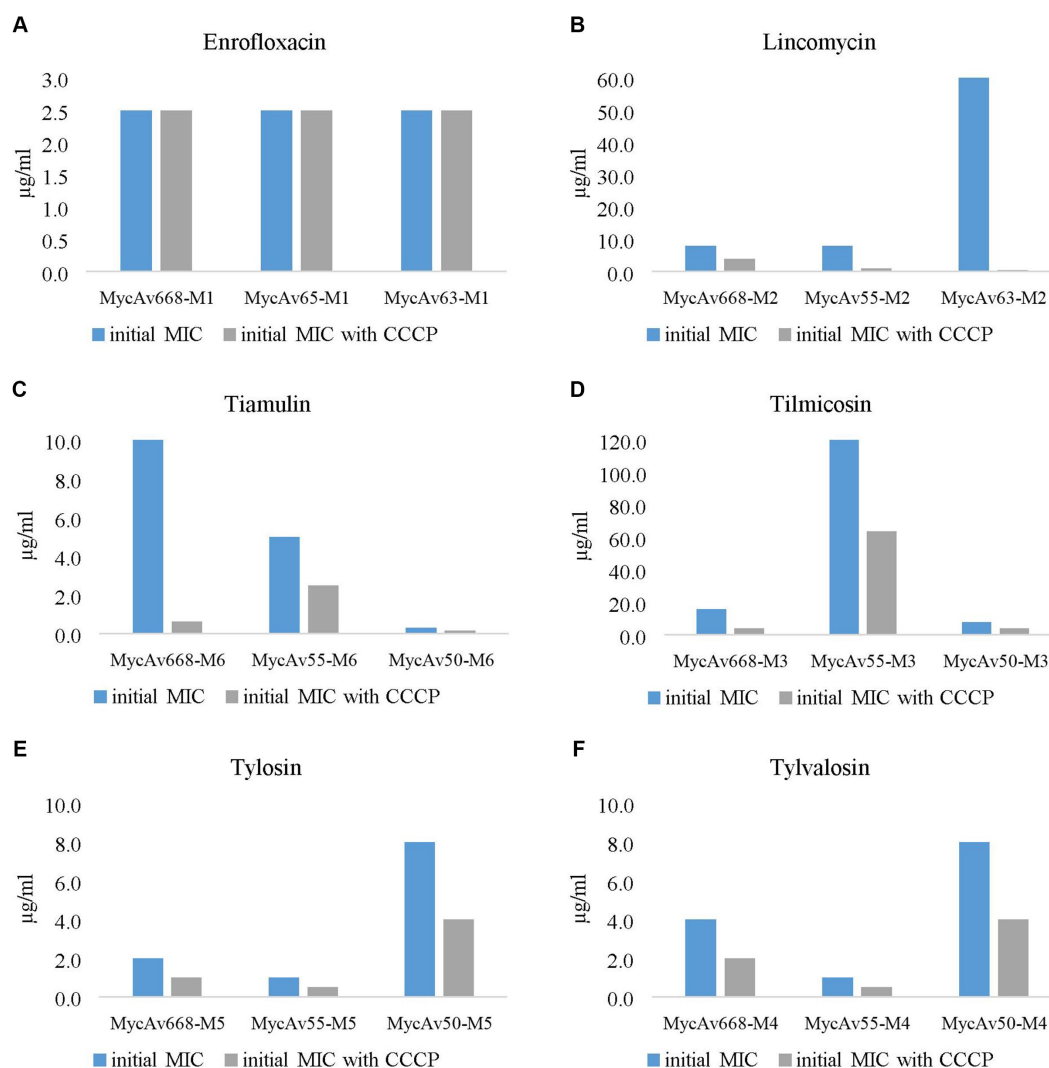


FIGURE 2

The effect of the most successful efflux pump inhibitor [carbonyl cyanide *m*-chlorophenylhydrazine (CCCP)] on the *in vitro* cultivated mutants' MICs for enrofloxacin (A), lincomycin (B), tiamulin (C), tilimicosin (D), tylosin (E) and tylvalosin (F). (the concentration ranges used are presented in [Supplementary Dataset S2](#)).

3.2. Detection of possible antibiotic resistance markers

The 18 *in vitro* cultured mutants (listed in [Supplementary Datasets S1, S2](#), BioProject ID: PRJNA912395) were compared to their parent strains (listed in [Table 1](#) and [Supplementary Dataset S1](#)) to identify novel mutations associated with lower antibiotic susceptibility ([Supplementary Datasets S3, S4](#)). Furthermore, MycAv 47, 67, 68, 70, 91, and 177 (*M. anserisalpiginidis* strains with high MICs for several antibiotics, listed in [Table 1](#)) were compared to the *M. anserisalpiginidis* type strain (ATCC BAA-2147) and the sensitive parent strains (MycAv 50, 55, 63, 65, 668; listed in [Table 1](#) and [Supplementary Datasets S3, S4](#)). ABC family genes that exhibited shared mutations in clinical isolates (or nsSNPs observed in both in clinical and *in vitro* mutants) were analyzed across all available *M. anserisalpiginidis* strains with publicly accessible whole genome sequences and MIC data ([Supplementary Dataset S5](#)).

Gene function predictions, which were based on *M. anserisalpiginidis* type strain (ATCC BAA-2147) gene annotation (GenBank accession number CP042295), showed that most SNPs were located in hypothetical proteins and intergenic regions. Numerous mutations were identified within genes that were previously described as antibiotic resistance-related genes. These genes encode ABC family members ([Supplementary Dataset S3](#)), 23S ribosomal RNA and a topoisomerase coding gene ([Supplementary Dataset S4](#)).

In the present study, numerous nsSNPs were identified in several members of the ABC family, which encompass diverse functions. Clinical isolates with high MIC values (MycAv 47, 67, 68, 70, 91, 177) exhibited nsSNPs within 14 genes that belong to the ABC family: WP_146368471.1, WP_146368786.1, WP_226364443.1, WP_146368361.1, WP_146368222.1, QDY87225.1, WP_146368766.1, WP_146368557.1, WP_146368360.1, WP_146368785.1, WP_146368574.1, WP_146368765.1, WP_146368337.1, WP_146368347.1 ([Supplementary Dataset S3](#)). The functional classification of the proteins was determined through *in silico* methods, utilizing Hidden

Markov Model (HMM) or Subfamily Protein Architecture Labeling Engine (SPARCLE; [Lu et al., 2020](#)) employed by PGAP. Among these genes, WP_146368786.1, WP_146368785.1, and WP_146368557.1 are ABC transporter ATP-binding proteins that potentially serve as ATPase and permease components of an ABC-type multidrug transport system. WP_146368766.1 is an ABC transporter ATP-binding protein, likely functioning as the catalytic subunit of an ATP transporter complex involved in macrolide export. QDY87225.1 and WP_146368347.1 represent ATP-binding cassette domain-containing proteins with potential ATPase activity. Additionally, WP_146368361.1, WP_146368222.1, WP_146368360.1 are ABC transporter permease subunits, while WP_146368765.1 and WP_146368337.1 are ABC transporter permeases, indicating their probable involvement as permease components. Furthermore, nsSNPs were also found in two presumed ATP-binding genes (WP_146368471.1 and WP_226364443.1 ATP-binding cassette domain-containing proteins) and a potential energy-coupling factor transporter ATPase (EcfA, WP_146368574.1). Among these, five probable ABC transporter coding genes (NCBI reference: WP_146368786.1, WP_226364443.1, WP_146368361.1, WP_146368222.1, QDY87225.1) displayed one common mutation among isolates with decreased susceptibility to enrofloxacin, macrolides, lincomycin and tiamulin ([Supplementary Datasets S3, S5](#)).

Regarding *in vitro* cultivated mutants, nsSNPs were identified in three ABC protein coding genes: WP_146368461.1, which encodes an ABC transporter ATP-binding protein and is a potential ATPase component of an ABC-type multidrug transport system; WP_146367439.1, which encodes the energy-coupling factor transporter transmembrane protein EcfT (presumed T component of ECF-type transporters); and WP_146368471.1, an assumed ATP-binding gene encoding an ATP-binding cassette domain-containing protein. Specifically, MycAv 668-M1/2/3/4 exhibited nsSNPs within WP_146368461.1, and MycAv 65-M1 displayed nsSNPs within WP_146367439.1 ([Supplementary Dataset S3](#)). Furthermore, in the case of WP_146368471.1 ATP-binding cassette domain-containing protein nsSNPs were identified both in clinical isolates with decreased antibiotic susceptibility (MycAv 47, 67, 68, 70, 91, 177) and *in vitro* cultivated mutants (listed in [Supplementary Dataset S3](#)). In the field isolates (MycAv 47, 67, 68, 70, 91, 177) either one or both nsSNPs were found at the nucleotide positions 250 and 1,339 (according to the numbering of the concerned gene of the reference strain). On the other hand, in the *in vitro* cultivated mutants, strains with decreased susceptibility to lincosamide, tiamulin and macrolides (MycAv55-M2/3/4/5/6) exhibited a mutation at the nucleotide positions 786 and 789 in the same gene ([Supplementary Dataset S3](#)).

Those ABC transporter protein coding genes that displayed common mutations in clinical isolates (MycAv 47, 67, 68, 70, 91, 177) or both in clinical and *in vitro* developed mutants were examined in all *M. anserisalpinitidis* strains to see any possible patterns among field isolates with low and high MIC values ([Table 2](#) and [Supplementary Dataset S5](#)). The examined nsSNPs could be detected in higher percentages in clinical isolates with decreased antibiotic susceptibility. Most prominent differences were observed in the cases of the ABC transporter ATP-binding protein (WP_146368786.1; a potential ATPase and permease component of an ABC-type multidrug transport system), the ABC transporter permease subunit

(WP_146368222.1) and the ATP-binding cassette domain-containing protein (QDY87225.1) ([Table 2](#) and [Supplementary Dataset S5](#)).

Besides nsSNPs in ABC efflux pump coding genes, different mutations were identified in other genes previously associated with elevated MICs ([Supplementary Dataset S4](#); [Gróznier et al., 2022](#)). In terms of decreased susceptibility to fluoroquinolones, one common nsSNP was found in DNA gyrase subunit A (*gyrA*) gene [in 3/3 field isolates (MycAv 47, 70, 91) and in 2/3 (MycAv 63-M1, 668-M1) *in vitro* mutants] at the nucleotide position 446. Examining this mutation on all *M. anserisalpinitidis* strains with publicly available whole genome sequences and MIC data, there were three types of nsSNPs: strains with extremely high MICs (initial MICs were > 10 µg/mL) and eight strains with elevated MICs (six strains with initial MICs of 5 µg/mL, two strains of 2.5 µg/mL initial MIC values) had an nsSNP at the nucleotide position 446 which altered the original amino acid from Threonine to Isoleucine. Fourteen strains with increased MIC (initial MICs were 5 µg/mL in four cases and 10 strains had 2.5 µg/mL initial MIC value) and three strains with lower MIC (initial MICs were 1.25 µg/mL) displayed Guanine at the nucleotide position 445 which caused a change from Threonine to Alanine. Strains in the third group were inhibited at lower MIC values (initial MICs were < 1.25 µg/mL) and contained Adenine and Cytosine at the nucleotide positions 445 and 446, coding Threonine ([Supplementary Dataset S5](#)).

Evaluating decreased tiamulin susceptibility, *in vitro* cultivated mutants (MycAv 50-M6, 55-M6, 668-M6) displayed mutations in the 23S rRNA gene at different positions (179, 434, 1,502, 1,568, 2,457) according to the numbering of the concerned gene of the type strain, while field isolates (MycAv 47, 67, 68, 70, 177) showed mutations at the nucleotide positions 793, 1,502 and 2067. In terms of the *in vitro* cultivated mutants with higher MIC values for lincomycin (MycAv 55-M2, 63-M2, 668-M2), mutations were determined in the 23S rRNA gene at different positions (179, 434, 1,568, 2067, 2,621). Regarding field isolates with decreased macrolide susceptibility (MycAv 67, 68, 177), three different nsSNPs were identified in the 23S rRNA gene at the nucleotide positions 793, 1,502 and 2067. The same nsSNP at the nucleotide position 793 was also present in three *in vitro* mutants (MycAv668-M3/5, MycAv55-M4), beside others (nucleotide positions 434, 544, 1,502, 1,568). For all strains of this bacterium with publicly available whole genome sequences and MIC data, the nsSNPs in the 23S rRNA gene were analyzed and reported in a previous work ([Gróznier et al., 2022](#)).

3.3. Identifying putative regulatory regions of efflux pump genes

Using the Promotech software, five putative efflux pump regulatory regions were identified related to the following genes: BMP family ABC transporter substrate-binding protein (NCBI reference: QDY86627.1), energy-coupling factor transporter ATPase (QDY86993.1), ATP-binding cassette domain-containing protein (WP_226364443.1), ABC transporter ATP-binding protein (WP_146368785.1), and multidrug transporter MATE (WP_201798414.1). The identified putative regulatory sequences with potential Pribnow box and RBSs ([Figure 3A](#)) showed statistically insignificant *E*-values according to the MEME analyses (*E*-value of the potential RBSs sequences is 0.33 and the *E*-value of the assumed Pribnow box is 2.4;

TABLE 2 The incidence rates of the non-synonymous single nucleotide polymorphisms (nsSNPs) in the ABC efflux pumps among strains with higher (High) and lower (Low) MIC values.^a

Name of the protein	ATP-binding cassette domain-containing protein				ABC transporter ATP-binding protein		ATP-binding cassette domain-containing protein		ABC transporter permease subunit		ABC transporter permease subunit		ATP-binding cassette domain-containing protein	
Accessibility	WP_146368471.1				WP_146368786.1		WP_226364443.1		WP_146368361.1		WP_146368222.1		QDY87225.1	
nsSNP location	250		1,339		1,069		1,494		925		704		667	
	High	Low	High	Low	High	Low	High	Low	High	Low	High	Low	High	Low
Enrofloxacin	33.3% (8/24)	6.3% (1/16)	41.6% (10/24)	6.3% (1/16)	62.5% (15/24)	0.0% (0/16)	58.3% (14/24)	12.5% (2/16)	66.7% (16/24)	12.5% (2/16)	66.7% (16/24)	18.8% (3/16)	54.2% (13/24)	6.3% (1/16)
Tilmicosin	36.8% (7/19)	9.5% (2/21)	36.8% (7/19)	19.0% (4/21)	63.1% (12/19)	14.3% (3/21)	57.9% (11/19)	23.8% (5/21)	63.2% (12/19)	28.6% (6/21)	68.4% (13/19)	23.8% (5/21)	57.9% (11/19)	14.3% (3/21)
Tylosin	35.0% (7/20)	10.0% (2/20)	35.0% (7/20)	20.0% (4/20)	60.0% (12/20)	15.0% (3/20)	60.0% (12/20)	20.0% (4/20)	60.0% (12/20)	25.0% (5/20)	65.0% (13/20)	30.0% (6/20)	55.0% (11/20)	15.0% (3/20)
Tylvalosin	75.0% (3/4)	16.7% (6/36)	50.0% (2/4)	25.0% (9/36)	75.0% (3/4)	33.3% (12/36)	75.0% (3/4)	36.1% (13/36)	75.0% (3/4)	41.7% (15/36)	75.0% (3/4)	44.4% (16/36)	75.0% (3/4)	30.6% (11/36)
Lincomycin	60.0% (3/5)	17.1% (6/35)	80.0% (4/5)	20.0% (7/35)	100.0% (5/5)	28.6% (10/35)	80.0% (4/5)	34.3% (12/35)	100.0% (5/5)	37.1% (13/35)	100.0% (5/5)	40% (14/35)	80.0% (4/5)	28.6% (10/35)
Tiamulin	54.5% (6/11)	10.3% (3/29)	54.5% (6/11)	17.2% (5/29)	63.6% (7/11)	27.6% (8/29)	63.6% (7/11)	31.0% (9/29)	72.7% (8/11)	34.5% (10/29)	81.8% (9/11)	34.4% (10/29)	63.6% (7/11)	24.1% (7/29)

^aExact numbers of the strains that displayed the nsSNP out of every strain with higher and lower MIC values are shown in brackets.

Figures 3B,C). The putative efflux pump regulatory regions of the *M. anserisalpingtonis* type strain were compared to those of all *M. anserisalpingtonis* strains with publicly available whole genome sequences. However, no significant nsSNPs were found in these regions that could potentially contribute to lower antibiotic sensitivity.

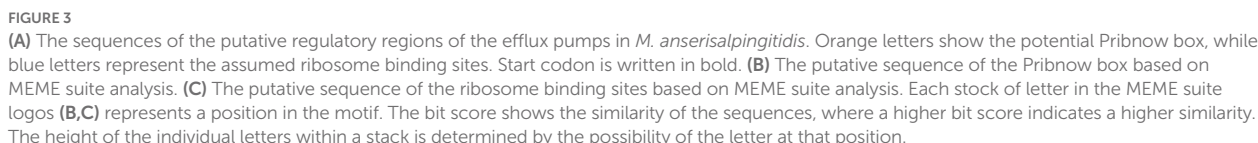
4. Discussion

M. anserisalpingtonis is a common pathogen of geese and it can cause significant economic losses (Dobos-Kovács et al., 2009). Several strains with decreased antibiotic susceptibility were isolated in the past decade (Gróznér et al., 2016; Gyuranecz et al., 2020), which is most probably the consequence of abundant antibiotic usage in the control of *M. anserisalpingtonis* and/or other bacterial infections. The observed high rate of decreased antibiotic susceptibility might be connected with the high genetic variability of this species and capability to rapidly develop resistance to antimicrobials (as was seen in the present study during the development of the mutants with decreased antibiotic susceptibility). In microbes with slightly increased MIC values, the efflux pump mechanism can play an essential role (Schmalstieg et al., 2012), expelling the antibiotics before they reach their targets. Active efflux pump mechanism was identified both in Gram positive and Gram negative bacteria (Van Bambeke et al., 2000), including different *Mycoplasma* species.

The effects of efflux pump inhibitors were also reported in several *Mycoplasma* species formerly (Pereyre et al., 2002; Antunes et al., 2015; Li et al., 2017). In our research, the determination of the MIC values in the presence and absence of different EPIs revealed statistically significant differences when CCCP was applied. The differences between the effectiveness of the particular EPIs can

be explained by their diverse working mechanism. The efflux pump inhibitors can be effective on different types of (primarily and secondarily) efflux pumps, especially the CCCP which can interfere with the proton gradient. This results in the disruption of the ATP synthesis (Kasianowicz et al., 1984) and the inhibition of the proton motive force (PMF) (Pagès et al., 2005). Based on these findings, further examination of the secondary efflux pumps in *M. anserisalpingtonis* can be an area for future research.

In the case of certain strains with extremely high MICs, none of the efflux pump inhibitors were effective (there were seven cases where none of the EPIs were effective out of 11 occasions where *M. anserisalpingtonis* strains have extremely high MICs). In these cases, the lack of detectable effect of the EPIs is explained by that efflux pump mechanism is the first step in the development of antibiotic resistance (Antunes et al., 2015). According to Schmalstieg and co-workers the increasing activity of efflux pumps is a direct response to the sub-inhibitory concentrations of different antibiotics (Schmalstieg et al., 2012). Under the protection of efflux pumps, bacteria can continue replicating and the possibilities of genome mutations are increasing. Eventually, higher-level resistance can emerge due to the mutations. Based on this model, the increasing activity of efflux pumps and the development of higher-level resistance are ordered molecular events in the process of acquiring antibiotic resistance. Additionally, in isolates with high MIC values in the present study (Supplementary Dataset S4) nsSNPs could be identified which were previously described as antibiotic resistance-related markers in *M. anserisalpingtonis* [in the 23S rRNA gene at the nucleotide positions 793 and 2067 (Gróznér et al., 2022)], or which were in genes what contain previously described antibiotic resistance-related markers [DNA gyrase subunit A (*gyrA*) at the nucleotide position 446; Sulyok et al., 2017]. When compared to the *M. anserisalpingtonis* type strain,



Therefore, the present study focused on conducting further comparative genome analysis specifically genes belonging to the ABC superfamily. Based on NCBI database, the *M. anserisalpingitidis* type strain was found to possess a minimum of 37 genes identified as members of the ABC family. Extensive investigation in this study

Additionally, our investigation identified nsSNPs in the energy-coupling factor transporter ATPase (EcfA, WP_146368574.1) and the energy-coupling factor transporter transmembrane protein EcfT (T component of ECF-type transporters, WP_146367439.1). While ECF transporters are primarily recognized for their involvement in micronutrient transport, the potential significance of energy-coupling factor transporter transmembrane protein EcfT in antibiotic resistance has been reported in *M. bovis* (Ledger et al., 2020) and tigecycline resistant *Enterococcus faecalis* (Bai et al., 2022).

Furthermore, certain ABC protein coding gene pairs (WP_146368360.1 and WP_146368361.1, WP_146368765.1 and WP_146368766.1, and WP_146368785.1 and WP_146368786.1) were found to overlap. It is well known that mycoplasmas possess small genomes (less than 1 Mbp), and overlapping genes are believed to be a consequence of evolutionary pressure to reduce the genome size. Previous studies have reported 162 overlapping gene pairs in *M. genitalium* and 203 in *M. pneumoniae* genomes (Fukuda et al., 1999). Additionally, two overlapping ABC protein coding genes associated with ciprofloxacin resistance have been documented (Raherison et al., 2005). Functional roles have been observed for several overlapping genes in prokaryotes (Chen et al., 1990; Inokuchi et al., 2000; Fukuda et al., 2003). However, the gene structure in this context was a result of incidental elongation of coding regions in *M. genitalium* and *M. pneumoniae* (Fukuda et al., 1999). Further research is necessary to fully comprehend the significance of these overlapping ABC protein coding gene in *M. anserisalpinitidis*.

Upon examining the identified nsSNPs in all *M. anserisalpinitidis* strains with publically available whole genome sequences, we found that the nsSNPs were present in higher percentages in field isolates with high MICs, although an exact correlation with the high MIC values could not be established. During this study, we did not examine the consequences of these mutations, such as the possible overexpression of the gene or increased function of the efflux pump, and none of them have been identified so far as potential single-drug resistance (SDR) or multidrug resistance (MDR) marker in mycoplasmas. To ascertain the significance of their role in antibiotic resistance, additional investigations are necessary, including the analysis of gene regulation. Nevertheless, considering that SNPs can occur also in the regulatory elements, we identified putative regulation sequences of the efflux pumps using bioinformatics tools. However, during the comparative genome analysis, no SNPs associated with antibiotic resistance were detected in these regions and E-values of the described Pribnow box and RBSs were not significant either. It is worth mentioning though, that MEME E-values may underestimate the true significance when the input dataset consists of few sequences (specifically, only five in this case; Bailey et al., 2015).

This study revealed active efflux mechanism in *M. anserisalpinitidis* strains for the first time. Efflux pump inhibitors are naturally-generated or synthetic molecules that can inhibit efflux pumps. Utilizing them as adjuvants can restore the effectiveness or increase the potency of antimicrobial agents (Pagès and Amaral, 2009). Although EPIs are great opportunities to fight against antibiotic resistance, the development of commercial EPIs is challenging (AlMatar et al., 2021), and their clinical use warrants further studies. Beside their capability to inhibit the expulsion of most of the clinically important antibiotics from the intracellular environment, there are recent publications about their role in the inhibition of biofilm formation by interfering in the process of releasing the quorum sensing molecules by efflux pumps which facilitate biofilm matrix formation (AlMatar et al., 2021). Based on previous studies (Bekő et al., 2022), biofilm formation can assist *M. anserisalpinitidis* to survive in the environment. Considering the observed effects of the EPI CCCP against *M. anserisalpinitidis* in the present study, and the probable interference with biofilm formation, it is assumed, that the use of EPIs would increase the efficiency of targeted antibiotic therapy in the control of this pathogen.

Data availability statement

The datasets presented in this study can be found in online repositories. The names of the repository/repositories and accession number(s) can be at: <https://www.ncbi.nlm.nih.gov/genbank/>, BioProject ID: PRJNA912395.

Author contributions

EN, EW, KBe, DE, ZK, and MG contributed to conception and design of the study. ÁK, EW, and EN performed the genomic and statistical analysis. KBá carried out the whole genome sequencing. EN wrote the first draft of the manuscript. All authors contributed to manuscript revision, read, and approved the submitted version.

Funding

This work was supported by the KKP19 (129751) grant of the National Research, Development and Innovation Office, Hungary, the SA-27/2021 grant of the Eötvös Loránd Research Network, the Project no. RRF-2.3.1-21-2022-00001 which has been implemented with the support provided by the Recovery and Resilience Facility (RRF), financed under the National Recovery Fund budget estimate, RRF-2.3.1-21 funding scheme and the support provided by the Ministry of Innovation and Technology of Hungary (legal successor: Ministry of Culture and Innovation of Hungary) from the National Research, Development and Innovation Fund, financed under the TKP2021-EGA-01 funding scheme of the National Research, Development and Innovation Office. The funders had no role in study design, data collection and interpretation, or the decision to submit the work for publication.

Conflict of interest

The authors declare that the research was conducted in the absence of any commercial or financial relationships that could be construed as a potential conflict of interest.

Publisher's note

All claims expressed in this article are solely those of the authors and do not necessarily represent those of their affiliated organizations, or those of the publisher, the editors and the reviewers. Any product that may be evaluated in this article, or claim that may be made by its manufacturer, is not guaranteed or endorsed by the publisher.

Supplementary material

The Supplementary material for this article can be found online at: <https://www.frontiersin.org/articles/10.3389/fmicb.2023.1216893/full#supplementary-material>

References

- Alcock, B. P., Raphenya, A. R., Lau, T. T. Y., Tsang, K. K., Bouchard, M., Edalatmand, A., et al. (2019). CARD 2020: antibiotic resistance surveillance with the comprehensive antibiotic resistance database. *Nucleic Acids Res.* 48, D517–D525. doi: 10.1093/nar/gkz935
- AlMatar, M., Albarri, O., Makky, E. A., and Köksal, F. (2021). Efflux pump inhibitors: new updates. *Pharmacol. Rep.* 73, 1–16. doi: 10.1007/s43440-020-00160-9
- Antunes, N. T., Assunção, P., Poveda, J. B., and Tavio, M. M. (2015). Mechanisms involved in quinolone resistance in *Mycoplasma mycoides* subsp. capri. *Vet. J.* 204, 327–332. doi: 10.1016/j.tvjl.2015.04.018
- Bai, B., Chen, C., Zhao, Y., Xu, G., Yu, Z., Tam, V. H., et al. (2022). *In vitro* activity of tigecycline and proteomic analysis of tigecycline adaptation strategies in clinical *Enterococcus faecalis* isolates from China. *J. Glob. Antimicrob. Resist.* 30, 66–74. doi: 10.1016/j.jgar.2022.04.022
- Bailey, T. L., Johnson, J., Grant, C. E., and Noble, W. S. (2015). The MEME suite. *Nucleic Acids Res.* 43, W39–W49. doi: 10.1093/nar/gkv416
- Bankevich, A., Nurk, S., Antipov, D., Gurevich, A. A., Dvorkin, M., Kulikov, A. S., et al. (2012). SPAdes: a new genome assembly algorithm and its applications to single-cell sequencing. *J. Comput. Biol.* 19, 455–477. doi: 10.1089/cmb.2012.0021
- Behbahan, N. G. G., Asasi, K., Afsharif, A. R., and Pourbakhsh, S. A. (2008). Susceptibilities of *Mycoplasma gallisepticum* and *Mycoplasma synoviae* isolates to antimicrobial agents *in vitro*. *Int. J. Poult. Sci.* 7, 1058–1064. doi: 10.3923/ijps.2008.1058.1064
- Bekő, K., Nagy, E. Z., Grözner, D., Kreizinger, Z., and Gyuranecz, M. (2022). Biofilm formation and its impact on environmental survival and antibiotic resistance of *Mycoplasma anserisalpingtonis* strains. *Acta Vet. Hung.* 70, 184–191. doi: 10.1556/004.2022.00029
- Chen, S. M., Takiff, H. E., Barber, A. M., Dubois, G. C., Bardwell, J. C., and Court, D. L. (1990). Expression and characterization of RNase III and era proteins. Products of the rnc operon of *Escherichia coli*. *J. Biol. Chem.* 265, 2888–2895. doi: 10.1016/S0021-9258(19)39884-9
- Chernova, O. A., Medvedeva, E. S., Mouzykantov, A. A., Baranova, N. B., and Chernov, V. M. (2016). Mycoplasmas and their antibiotic resistance: the problems and prospects in controlling infections. *Acta Nat.* 8, 24–34. doi: 10.32607/20758251-2016-8-2-24-34
- Chevez-Guardado, R., and Peña-Castillo, L. (2021). Promotech: a general tool for bacterial promoter recognition. *Genome Biol.* 22:318. doi: 10.1186/s13059-021-02514-9
- Darling, A. C. E., Mau, B., Blattner, F. R., and Perna, N. T. (2004). Mauve: multiple alignment of conserved genomic sequence with rearrangements. *Genome Res.* 14, 1394–1403. doi: 10.1101/gr.2289704
- Dassa, E., and Bouige, P. (2001). The ABC of ABCs: a phylogenetic and functional classification of ABC systems in living organisms. *Res. Microbiol.* 152, 211–229. doi: 10.1016/S0923-2508(01)01194-9
- Dobos-Kovács, M., Varga, Z., Czifra, G., and Stipkovits, L. (2009). Salpingitis in geese associated with *Mycoplasma* sp. strain 1220. *Avian Pathol.* 38, 239–243. doi: 10.1080/03079450902912127
- Fisunov, G. Y., Garanina, I. A., Evsyutina, D. V., Semashko, T. A., Nikitina, A. S., and Govorun, V. M. (2016). Reconstruction of transcription control networks in Mollicutes by high-throughput identification of promoters. *Front. Microbiol.* 7:1977. doi: 10.3389/fmicb.2016.01977
- Fukuda, Y., Nakayama, Y., and Tomita, M. (2003). On dynamics of overlapping genes in bacterial genomes. *Gene* 323, 181–187. doi: 10.1016/j.gene.2003.09.021
- Fukuda, Y., Tomita, M., and Washio, T. (1999). Comparative study of overlapping genes in the genomes of *Mycoplasma genitalium* and *Mycoplasma pneumoniae*. *Nucleic Acids Res.* 27, 1847–1853. doi: 10.1093/nar/27.8.1847
- Ghaleh Gol, N., Asasi, K., Afsharif, A. R., and Pourbakhsh, S. A. (2008). Susceptibilities of *Mycoplasma gallisepticum* and *Mycoplasma synoviae* isolates to antimicrobial agents *in vitro*. *Int. J. Poultry Sci.* 7, 1058–1064. doi: 10.3923/ijps.2008.1058.1064
- Giedraitienė, A., Vitkauskienė, A., Naginienė, R., and Pavilonis, A. (2011). Antibiotic resistance mechanisms of clinically important bacteria. *Medicina* 47, 137–146. doi: 10.3390/medicina47030019
- Grözner, D., Bekő, K., Kovács, Á. B., Mitter, A., Hrivnák, V., Sawicka, A., et al. (2022). Identification and detection of mutations potentially associated with decreased susceptibility to macrolides and lincomycin in *Mycoplasma anserisalpingtonis* isolates. *Vet. Microbiol.* 266:109362. doi: 10.1016/j.vetmic.2022.109362
- Grözner, D., Kovács, Á. B., Wehmann, E., Kreizinger, Z., Bekő, K., Mitter, A., et al. (2021). Multilocus sequence typing of the goose pathogen *Mycoplasma anserisalpingtonis*. *Vet. Microbiol.* 254:108972. doi: 10.1016/j.vetmic.2020.108972
- Grözner, D., Kreizinger, Z., Sulyok, K. M., Rónai, Z., Hrivnák, V., Turcsányi, I., et al. (2016). Antibiotic susceptibility profiles of *Mycoplasma* sp. 1220 strains isolated from geese in Hungary. *BMC Vet. Res.* 12:170. doi: 10.1186/s12917-016-0799-0
- Gyuranecz, M., Mitter, A., Kovács, Á. B., Grözner, D., Kreizinger, Z., Bali, K., et al. (2020). Isolation of *Mycoplasma anserisalpingtonis* from swan goose (*Anser cygnoides*) in China. *BMC Vet. Res.* 16:178. doi: 10.1186/s12917-020-02393-5
- Hannan, P. C. T. (2000). Guidelines and recommendations for antimicrobial minimum inhibitory concentration (MIC) testing against veterinary mycoplasma species. *Vet. Res.* 31, 373–395. doi: 10.1051/vetres:2000100
- Higgins, C. F. (1992). ABC transporters: from microorganisms to man. *Annu. Rev. Cell Biol.* 8, 67–113. doi: 10.1146/annurev.cb.08.110192.000435
- Hinz, K.-H., Pfützner, H., and Behr, K.-P. (1994). Isolation of mycoplasmas from clinically healthy adult breeding geese in Germany. *J. Veterinary Med. Ser. B* 41, 145–147. doi: 10.1111/j.1439-0450.1994.tb00217.x
- Inokuchi, Y., Hirashima, A., Sekine, Y., Janosi, L., and Kaji, A. (2000). Role of ribosome recycling factor (RRF) in translational coupling. *EMBO J.* 19, 3788–3798. doi: 10.1093/emboj/19.14.3788
- Kaatz, G. W., Seo, S. M., and Foster, T. J. (1999). Introduction of a *norA* promoter region mutation into the chromosome of a fluoroquinolone-susceptible strain of *Staphylococcus aureus* using plasmid integration. *Antimicrob. Agents Chemother.* 43, 2222–2224. doi: 10.1128/AAC.43.9.2222
- Kasianowicz, J., Benz, R., and McLaughlin, S. (1984). The kinetic mechanism by which CCCP (carbonyl cyanide-m-chlorophenylhydrazone) transports protons across membranes. *J. Membr. Biol.* 82, 179–190. doi: 10.1007/BF01868942
- Kearse, M., Moir, R., Wilson, A., Stones-Havas, S., Cheung, M., Sturrock, S., et al. (2012). Geneious basic: an integrated and extendable desktop software platform for the organization and analysis of sequence data. *Bioinformatics* 28, 1647–1649. doi: 10.1093/bioinformatics/bts1199
- Kempf, I., Olivier, C., L'hospitalier, R., Guittet, M., and Bennejean, G. (1988). Courte communication: concentrations minimales inhibitrices de 13 antibiotiques vis-à-vis de 21 souches de mycoplasmes des volailles. *Le Point vétérinaire* 20, 83–88.
- Landman, W. J. M., Mevius, D. J., Veldman, K. T., and Feberwee, A. (2008). *In vitro* antibiotic susceptibility of Dutch *Mycoplasma synoviae* field isolates originating from joint lesions and the respiratory tract of commercial poultry. *Avian Pathol.* 37, 415–420. doi: 10.1080/03079450802216637
- Ledger, L., Eidt, J., and Cai, H. Y. (2020). Identification of antimicrobial resistance-associated genes through whole genome sequencing of *Mycoplasma bovis* isolates with different antimicrobial resistances. *Pathogens* 9:588. doi: 10.3390/pathogens9070588
- Li, W., O'Neill, K. R., Haft, D. H., DiCuccio, M., Chetvernin, V., Badretdin, A., et al. (2021). RefSeq: expanding the prokaryotic genome annotation pipeline reach with protein family model curation. *Nucleic Acids Res.* 49, D1020–D1028. doi: 10.1093/nar/gkaa1105
- Li, S. L., Sun, H. M., Zhu, B. L., Liu, F., and And Zhao, H. Q. (2017). Whole genome analysis reveals new insights into macrolide resistance in *Mycoplasma pneumoniae*. *Biomed. Environ. Sci.* 30, 343–350. doi: 10.3967/bes2017.045
- Linton, K. J., and Higgins, C. F. (1998). The *Escherichia coli* ATP-binding cassette (ABC) proteins: *E. coli* ABC proteins. *Mol. Microbiol.* 28, 5–13. doi: 10.1046/j.1365-2958.1998.00764.x
- Lloréns-Rico, V., Lluch-Senar, M., and Serrano, L. (2015). Distinguishing between productive and abortive promoters using a random forest classifier in *Mycoplasma pneumoniae*. *Nucleic Acids Res.* 43, 3442–3453. doi: 10.1093/nar/gkv170
- Lu, S., Wang, J., Chitsaz, F., Derbyshire, M. K., Geer, R. C., Gonzales, N. R., et al. (2020). CDD/SPARCLE: the conserved domain database in 2020. *Nucleic Acids Res.* 48, D265–D268. doi: 10.1093/nar/gkz991
- Lupien, A., Billal, D. S., Fani, F., Soualhine, H., Zhanel, G. G., Leprohon, P., et al. (2013). Genomic characterization of ciprofloxacin resistance in a laboratory-derived mutant and a clinical isolate of *Streptococcus pneumoniae*. *Antimicrob. Agents Chemother.* 57, 4911–4919. doi: 10.1128/AAC.00418-13
- Madeira, H. M. F., and Gabriel, J. E. (2007). Regulation of gene expression in mycoplasmas: contribution from *Mycoplasma hyopneumoniae* and *Mycoplasma synoviae* genome sequences. *Genet. Mol. Biol.* 30, 277–282. doi: 10.1590/S1415-47572007000200016
- Marquez, B. (2005). Bacterial efflux systems and efflux pumps inhibitors. *Biochimie* 87, 1137–1147. doi: 10.1016/j.biochi.2005.04.012
- Montero-Blay, A., Miravet-Verde, S., Lluch-Senar, M., Piñero-Lambea, C., and Serrano, L. (2019). SynMyco transposon: engineering transposon vectors for efficient transformation of minimal genomes. *DNA Res.* 26, 327–339. doi: 10.1093/dnares/dsz012
- Pagès, J.-M., and Amaral, L. (2009). Mechanisms of drug efflux and strategies to combat them: challenging the efflux pump of gram-negative bacteria. *Biochim. Biophys. Acta* 1794, 826–833. doi: 10.1016/j.bbapap.2008.12.011
- Pagès, J.-M., Masi, M., and Barbe, J. (2005). Inhibitors of efflux pumps in gram-negative bacteria. *Trends Mol. Med.* 11, 382–389. doi: 10.1016/j.molmed.2005.06.006
- Pereyre, S., Gonzalez, P., de Barbeyrac, B., Darnige, A., Renaudin, H., Charron, A., et al. (2002). Mutations in 23S rRNA account for intrinsic resistance to macrolides in *Mycoplasma hominis* and *Mycoplasma fermentans* and for acquired resistance to

- macrolides in *M. hominis*. *Antimicrob. Agents Chemother.* 46, 3142–3150. doi: 10.1128/AAC.46.10.3142-3150.2002
- Pezza, R. J. (2002). Vanadate inhibits the ATPase activity and DNA binding capability of bacterial MutS. A structural model for the vanadate–MutS interaction at the Walker a motif. *Nucleic Acids Res.* 30, 4700–4708. doi: 10.1093/nar/gkf606
- Poole, K. (2007). Efflux pumps as antimicrobial resistance mechanisms. *Ann. Med.* 39, 162–176. doi: 10.1080/07853890701195262
- R Core Team (2022). *R: a language and environment for statistical computing*. R Foundation for Statistical Computing, Vienna. Available at: <https://www.R-project.org/>
- Raherison, S., Gonzalez, P., Renaudin, H., Charron, A., Bébér, C., and Bébér, C. M. (2002). Evidence of active efflux in resistance to ciprofloxacin and to ethidium bromide by *Mycoplasma hominis*. *Antimicrob. Agents Chemother.* 46, 672–679. doi: 10.1128/AAC.46.3.672-679.2002
- Raherison, S., Gonzalez, P., Renaudin, H., Charron, A., Bébér, C., and Bébér, C. M. (2005). Increased expression of two multidrug transporter-like genes is associated with ethidium bromide and ciprofloxacin resistance in *Mycoplasma hominis*. *Antimicrob. Agents Chemother.* 49, 421–424. doi: 10.1128/AAC.49.1.421-424.2005
- Rodionov, D. A., Hebbeln, P., Eudes, A., Ter Beek, J., Rodionova, I. A., Erkens, G. B., et al. (2009). A novel class of modular transporters for vitamins in prokaryotes. *J. Bacteriol.* 191, 42–51. doi: 10.1128/JB.01208-08
- Sayers, E. W., Bolton, E. E., Brister, J. R., Canese, K., Chan, J., Comeau, D. C., et al. (2022). Database resources of the national center for biotechnology information. *Nucleic Acids Res.* 50, D20–D26. doi: 10.1093/nar/gkab1112
- Schmalstieg, A. M., Srivastava, S., Belkaya, S., Deshpande, D., Meek, C., Leff, R., et al. (2012). The antibiotic resistance arrow of time: efflux pump induction is a general first step in the evolution of mycobacterial drug resistance. *Antimicrob. Agents Chemother.* 56, 4806–4815. doi: 10.1128/AAC.05546-11
- Schneider, E., and Hunke, S. (1998). ATP-binding-cassette (ABC) transport systems: functional and structural aspects of the ATP-hydrolyzing subunits/domains. *FEMS Microbiol. Rev.* 22, 1–20. doi: 10.1111/j.1574-6976.1998.tb00358.x
- Siqueira, F. M., de Souto Weber, S., Cattani, A. M., and Schrank, I. S. (2014). Genome organization in *Mycoplasma hyopneumoniae*: identification of promoter-like sequences. *Mol. Biol. Rep.* 41, 5395–5402. doi: 10.1007/s11033-014-3411-3
- Stipkovits, L., Glavits, R., Ivanics, E., and Szabo, E. (1993). Additional data on Mycoplasma disease of goslings. *Avian Pathol.* 22, 171–176. doi: 10.1080/03079459308418908
- Stipkovits, L., and Kempf, I. (1996). Mycoplasmoses in poultry. *Rev. Sci. Tech.* 15, 1495–1525. doi: 10.20506/rst.15.4.986
- Stipkovits, L., and Szathmari, S. (2012). Mycoplasma infection of ducks and geese. *Poult. Sci.* 91, 2812–2819. doi: 10.3382/ps.2012-02310
- Stipkovits, L., Varga, Z., Czifra, G., and Dobos-Kovács, M. (1986). Occurrence of mycoplasmas in geese affected with inflammation of the cloaca and phallus. *Avian Pathol.* 15, 289–299. doi: 10.1080/03079458608436289
- Sulyok, K. M., Kreizinger, Z., Wehmann, E., Lysnyansky, I., Bányai, K., Marton, S., et al. (2017). Mutations associated with decreased susceptibility to seven antimicrobial families in field and laboratory-derived *Mycoplasma bovis* strains. *Antimicrob. Agents Chemother.* 61, e01983–e01916. doi: 10.1128/AAC.01983-16
- Unemo, M., Golparian, D., and Eyre, D. W. (2019). “Antimicrobial resistance in *Neisseria gonorrhoeae* and treatment of gonorrhea” in *Neisseria gonorrhoeae methods in molecular biology*. ed. M. Christodoulides (New York, NY: Springer), 37–58.
- Van Bambeke, F., Balzi, E., and Tulkens, P. M. (2000). Antibiotic efflux pumps. *Biochem. Pharmacol.* 60, 457–470. doi: 10.1016/S0006-2952(00)00291-4
- Waldner, M., Kinnear, A., Yacoub, E., McAllister, T., Register, K., Li, C., et al. (2022). Genome-wide association study of nucleotide variants associated with resistance to nine antimicrobials in *Mycoplasma bovis*. *Microorganisms* 10:1366. doi: 10.3390/microorganisms10071366
- Webber, M. A. (2003). The importance of efflux pumps in bacterial antibiotic resistance. *J. Antimicrob. Chemother.* 51, 9–11. doi: 10.1093/jac/dkg050
- Weber, S., Sant’Anna, F. H., and Schrank, I. S. (2012). Unveiling *Mycoplasma hyopneumoniae* promoters: sequence definition and genomic distribution. *DNA Res.* 19, 103–115. doi: 10.1093/dnares/dsr045
- Yus, E., Lloréns-Rico, V., Martínez, S., Gallo, C., Eilers, H., Blötz, C., et al. (2019). Determination of the gene regulatory network of a genome-reduced bacterium highlights alternative regulation independent of transcription factors. *Cell Syst.* 9, 143–158.e13. doi: 10.1016/j.cels.2019.07.001
- Zwama, M., and Nishino, K. (2021). Ever-adapting RND efflux pumps in gram-negative multidrug-resistant pathogens: a race against time. *Antibiotics* 10:774. doi: 10.3390/antibiotics10070774



OPEN ACCESS

EDITED BY

Glenn Francis Browning,
The University of Melbourne, Australia

REVIEWED BY

Patrice Gaurivaud,
Agence Nationale de Sécurité Sanitaire de
l'Alimentation, de l'Environnement et du Travail
(ANSES), France
Joerg Jores,
University of Bern, Switzerland
Joachim Spargser,
University of Veterinary Medicine
Vienna, Austria

*CORRESPONDENCE

Miklós Gyuranecz
✉ m.gyuranecz@gmail.com

RECEIVED 20 April 2023

ACCEPTED 17 July 2023

PUBLISHED 04 August 2023

CITATION

Földi D, Nagy ZE, Belec N, Szeredi L, Földi J,
Kollár A, Tenk M, Kreizinger Z and Gyuranecz M
(2023) Establishment of a *Mycoplasma*
hyorhinis challenge model in 5-week-old
piglets. *Front. Microbiol.* 14:1209119.
doi: 10.3389/fmicb.2023.1209119

COPYRIGHT

© 2023 Földi, Nagy, Belec, Szeredi, Földi,
Kollár, Tenk, Kreizinger and Gyuranecz. This is
an open-access article distributed under the
terms of the [Creative Commons Attribution
License \(CC BY\)](https://creativecommons.org/licenses/by/4.0/). The use, distribution or
reproduction in other forums is permitted,
provided the original author(s) and the
copyright owner(s) are credited and that the
original publication in this journal is cited, in
accordance with accepted academic practice.
No use, distribution or reproduction is
permitted which does not comply with these
terms.

Establishment of a *Mycoplasma hyorhinis* challenge model in 5-week-old piglets

Dorottya Földi^{1,2}, Zsófia Eszter Nagy^{1,2}, Nikolett Belec^{1,2},
Levente Szeredi^{2,3}, József Földi⁴, Anna Kollár^{2,3}, Miklós Tenk^{2,3},
Zsuzsa Kreizinger^{1,2,5} and Miklós Gyuranecz^{1,2,3,5*}

¹Veterinary Medical Research Institute, Budapest, Hungary, ²National Laboratory of Infectious Animal Diseases, Antimicrobial Resistance, Veterinary Public Health and Food Chain Safety, Budapest, Hungary, ³Department of Microbiology and Infectious Diseases, University of Veterinary Medicine, Budapest, Hungary, ⁴EuVet Bt., Gödöllo, Hungary, ⁵MolliScience Kft., Batorbágy, Hungary

Introduction: *Mycoplasma hyorhinis* is an emerging swine pathogen with high prevalence worldwide. The main lesions caused are arthritis and polyserositis, and the clinical manifestation of the disease may result in significant economic losses due to decreased weight gain and enhanced medical costs. We aimed to compare two challenge routes to induce *M. hyorhinis* infection using the same clinical isolate.

Methods: Five-week-old, Choice hybrid pigs were inoculated on 2 consecutive days by intravenous route (Group IV-IV) or by intravenous and intraperitoneal routes (Group IV-IP). Mock-infected animals were used as control (control group). After the challenge, the clinical signs were recorded for 28 days, after which the animals were euthanized. Gross pathological and histopathological examinations, PCR detection, isolation, and genotyping of the re-isolated *Mycoplasma* sp. and culture of bacteria other than *Mycoplasma* sp. were carried out. The ELISA test was used to detect anti-*M. hyorhinis* immunoglobulins in the sera of all animals.

Results: Pericarditis and polyarthritis were observed in both challenge groups; however, the serositis was more severe in Group IV-IV. Statistically significant differences were detected between the challenged groups and the control group regarding the average daily weight gain, pathological scores, and ELISA titers. Additionally, histopathological scores in Group IV-IV differed significantly from the scores in the control group. All re-isolated strains were the same or a close genetic variant of the original challenge strain.

Discussion: Our results indicate that both challenge routes are suitable for modeling the disease. However, due to the evoked more severe pathological lesions and the application being similar to the hypothesized natural route of infection in Group IV-IV, the two-dose intravenous challenge is recommended by the authors to induce serositis and arthritis associated with *M. hyorhinis* infection.

KEYWORDS

challenge, ELISA, infection, *Mycoplasma hyorhinis*, PCR, pig

Introduction

Mycoplasma hyorhinis is an emerging pathogenic bacterium of swine, the distribution of which is considered to be worldwide with a high estimated prevalence (Pieters and Maes, 2019; Roos et al., 2019). *M. hyorhinis* colonizes the upper respiratory tract and tonsil of sows, which are asymptomatic carriers of the bacterium. Piglets get infected directly from the nasal secretions of sows, and later from each other, especially after weaning (Clavijo et al., 2017). Clinical signs usually appear between 3 and 10 weeks of age. Although the susceptibility to the infection decreases after this age, pigs can get infected even up to 16

weeks of age (Martinson et al., 2017). The pathomechanism of systemic spread is still not fully understood. Predisposing factors such as inadequate housing conditions or weaning and decreasing maternal antibodies at ~3 weeks of age can all contribute to the disease (Clavijo et al., 2019).

The first clinical signs appear 3–10 days post-exposure and include fever and lethargy (Gomes Neto, 2012). Later, coughing, labored breathing, and dyspnea can appear due to serofibrinous pleuritis, pericarditis, and peritonitis. Additionally, arthritis with swollen joints and lameness can be observed in pigs (Barden and Decker, 1971). Rarely, *M. hyorhinis* infection causes otitis (Morita et al., 1995), conjunctivitis (Resende et al., 2019), and meningitis (Bünger et al., 2020). Affected pigs show growth retardation, which can be evident even 5 months after infection (Barden and Decker, 1971). As a secondary pathogen, *M. hyorhinis* can aggravate the clinical signs of other infections such as porcine circovirus 2-associated diseases and enzootic pneumonia and is also an important pathogen in the porcine respiratory disease complex (Pieters and Maes, 2019). Decreased weight gain and the cost of medical treatments result in significant economic losses. As no commercial vaccine is available in Europe, prevention mainly relies on decreasing predisposing factors; however, metaphylactic antibiotic treatment is often required.

There are some *M. hyorhinis* challenge models in the literature suggesting different inoculation routes (Lin et al., 2006; Gomes Neto et al., 2014; Lee et al., 2018; Fourour et al., 2019; Merodio et al., 2021). However, not all published models are suitable for vaccine efficacy studies, because with some of the suggested challenge routes not all typical lesions can be induced (Martinson et al., 2018a).

We aimed to compare the effects of experimental infections of two distinct inoculation routes with the same virulent *M. hyorhinis* strain by studying the clinical signs, immune response, and macroscopic and microscopic alterations. Accordingly, the examinations also aimed to establish a challenge model for future vaccine efficacy studies.

Materials and methods

Challenge material

The *M. hyorhinis* isolate used during this study was isolated from the pericardium of a pig affected by pericarditis, originating from Hungary in 2019. The initial isolation was carried out using the filter cloning technique in Mycoplasma Experience Medium (Mycoplasma Experience Ltd., Bletchingley, UK), and the isolate was identified by the partial sequencing of the 16S-23S rRNA intergenic spacer region, using *Mycoplasma* genus-specific primers (Lauerman et al., 1995); the sequencing was performed on an ABI Prism 3100 automated DNA sequencer (Applied Biosystems, Waltham, MA, USA), followed by sequence analysis and BLASTN search (<https://blast.ncbi.nlm.nih.gov/Blast.cgi>). The challenge material was prepared freshly for each challenge day by inoculating the fourth passage of the isolate 48 h prior challenge to Mycoplasma Experience Medium (Mycoplasma Experience) and incubating at 37°C. The color-changed broth was directly used for

the challenge. The viable cell count determination was carried out on the day of the challenge. The number of color-changing units (CCU/ml) was calculated by broth micro-dilution from the highest dilution showing color change (red to yellow shift; Hannan, 2000).

Experimental animals

Sixteen, 4-week-old Choice hybrid piglets were transported to the animal house of the Veterinary Medical Research Institute 6 days prior infection. The animals were obtained from a farm with low *M. hyorhinis* prevalence and high health status (free from brucellosis, leptospirosis, Aujeszky's disease, porcine reproductive and respiratory syndrome, swine dysentery, atrophic rhinitis, *Actinobacillus pleuropneumoniae*, *Mycoplasma hyopneumoniae*, lice, and mange). The *M. hyorhinis*-free status of the piglets was checked before the challenge by real-time PCR testing and *Mycoplasma* culture of nasal swabs.

Upon arrival, the animals were weighed and randomly divided into three groups with similar average weights. The animals were of mixed gender, which was not a factor when the groups were formed. The groups were housed in separate pens of 6 m² each. Humidity and air quality were regulated by the built-in ventilation system, and the age-appropriate temperatures were provided by heating panels. Feed and water were provided *ad libitum*. The experiment was approved by the National Scientific Ethical Committee on Animal Experimentation under reference number: PE/EA/746-7/2021.

Challenge routes

Group IV-IV ($n = 6$) was inoculated by intravenous (IV) route on 0 and 1 day post-infection (0 DPI, 1 DPI) with 10 ml challenge material. Group IV-IP ($n = 6$) was challenged IV on 0 DPI with a 10-ml challenge material and intraperitoneal (IP) route on 1 DPI with a 20-ml challenge material. For the IV inoculation, the external jugular vein was used, while for the IP route, the challenge material was injected into the abdominal cavity in the left lower abdominal quadrant. On 0 DPI, the viable cell count of the challenge strain was 4.6×10^5 CCU/ml, while on 1 DPI, it was 1.2×10^6 CCU/ml. The total challenge dose was 1.66×10^7 CCU/pig and 2.86×10^7 CCU/pig in Group IV-IV and IV-IP, respectively. The controls ($n = 4$) were inoculated by IV route on 0 DPI. Two of these animals were inoculated by the IV route and the remaining two pigs by the IP route on 1 DPI. Animals in the control group received only sterile liquid media in the same volume as the challenged groups.

Clinical observation

The animals were observed daily from settlement until the end of the study, at 28 DPI. Clinical signs of arthritis [swollen joints (mostly detected visually, complemented with palpation) and lameness] and respiratory disease (coughing or labored breath) were recorded. Body temperatures were measured daily from

TABLE 1 Schedule of events, challenge routes, and doses.

Time	Event	Challenge dose
–6 DPI	Arrival of 16 four-week-old piglets Body weight measurement	
–2 DPI	Blood sampling Collection of nasal swabs for PCR and <i>Mycoplasma</i> isolation Body temperature measurement	
–1 DPI	Body temperature measurement	
0 DPI	IV challenge of all groups	10 ml 10 ⁶ CCU/ml challenge material (Groups IV-IV and IV-IP) or 10 ml sterile broth (control group)
1 DPI	IV challenge of group IV-IV and two animals from control group IP challenge of group IV-IP and two animals from control group	IV: 10 ml 10 ⁶ CCU/ml challenge material (group IV-IV) or 10 ml sterile broth (control group) IP: 20 ml 10 ⁶ CCU/ml challenge material (group IV-IP) or 20 ml sterile broth (control group)
0–27 DPI	Daily: - Body temperature measurement - Clinical observations Twice a week: - Body weight measurement - Collection of nasal swabs for PCR and <i>Mycoplasma</i> isolation - Blood sampling	
28 DPI	Euthanasia (after electrical stunning exsanguination was performed) Pathological examination Sample collection for PCR, histopathology, and bacteriology	

IV, intravenous; IP, intraperitoneal; CCU, color changing unit; DPI, days post-infection.

2 days prior challenge. Body weight measurement, blood, and nasal swab sampling were carried out twice a week. Cotton swabs were used for collecting nasal swabs (Swab in tube Alum + Cotton, Deltalab S.L., Barcelona, Spain), and blood was collected from the external jugular vein. The schedule of events is summarized in Table 1. Average daily weight gain (ADWG) was calculated by subtracting the weight measured at arrival (6 days prior challenge, –6 DPI) from the weight measured at 27 DPI and dividing it by the number of days past ($n = 33$).

Isolation, DNA extraction, and PCR

Nasal swabs for *Mycoplasma* isolation and PCR were taken twice a week from all animals throughout the study. Separate swab samples for *Mycoplasma* isolation and PCR were collected during necropsy as well (see below). For *Mycoplasma* isolation, swabs were cut into Mycoplasma liquid media (Mycoplasma Experience Ltd.), and vortex mixed to aid the release of bacteria into the media, which was then filtered using 0.45 μ m pore size filters and incubated at 37°C until color change.

DNA extraction from the swabs and color-changed broths was performed using a ReliaPrep gDNA Tissue Miniprep System (Promega Inc., Madison, USA) according to the manufacturer's instructions. For the *M. hyorhinis* species-specific real-time PCR, previously published (Resende et al., 2019) primers targeting the 16S rRNA gene were optimized. Primer and probe sequences were the following: Forward primer 5'- CGT ACC TAA CCT ACC TTT AAG–3', Reverse primer 5'- TAA TGT TCC GCA CCC C–3', Probe 5'- FAM-CCG GAT ATA GTT ATT TAT CGC ATG AG-BHQ–3'. The PCR was performed using a Bio-Rad C1000 Touch™ Thermal Cycler, CFX96™ Real-Time System (Bio-Rad

Laboratories Inc., USA). The PCR master mix consisted of 6 μ l 2× qPCR BIO Probe Mix No-ROX (PCR Biosystems Ltd., UK), 0.4 μ l of each primer (10 μ M), 0.2 μ l probe, and 2 μ l DNA in the final volume of 12 μ l. PCR conditions were the following: 95°C for 2 min, 45 cycles of 95°C for 5 s, and 60°C for 20 s. In order to test the sensitivity of the developed assays, 10-fold dilutions of the DNA of the type strain (NCTC 10130) were used in the range of 10⁶–10⁰ template copy number/ μ l. Template copy number was calculated with the help of an online tool (<http://cels.uri.edu/gsc/cndna.html>) by measuring the concentration of DNA of pure *M. hyorhinis* culture using a Nanodrop 2000 Spectrophotometer (Thermo Fisher Scientific Inc., USA). The lowest DNA concentration giving a specific signal was considered the detection limit of the assay. The specificity was tested by including *M. hyopneumoniae*, *Mycoplasma hyosynoviae*, and *Mycoplasma flocculare* in the analyses.

Necropsy samples were also tested for the presence of *M. hyopneumoniae* (Wu et al., 2019) and *M. hyosynoviae* (Martinson et al., 2018a) using PCR. *M. hyorhinis* positive isolates were genetically characterized by multi-locus sequence typing (MLST: used as a costly but robust genotyping system) and multiple-locus variable-number tandem-repeat analysis (MLVA: used as a rapid and cheap genotyping system with high-resolution), according to previously published assays (Földi et al., 2020).

Gross pathological examination

Joints of the carpus, elbow, tarsus, and stifle on both sides were opened and examined for signs of arthritis. The thoracic and abdominal cavities (pleura, pericardium, and peritoneum) were checked for serositis. Body condition, skin, subcutaneous tissues, musculoskeletal system, eyes and conjunctiva, nasal, and oral cavity, trachea, lungs, heart, lymph nodes, gastrointestinal system,

liver, spleen, kidney, and brain were also checked for lesions. The scoring system of the gross pathological examination is detailed in [Supplementary Table 1](#). Lesions of joints and serosa were scored to reflect severity based on previously described criteria ([Martinson et al., 2018b](#)). Total scores were calculated by summarizing all organ scores.

Swab samples for bacterial culture, *M. hyorhinis* isolation, and PCR were taken from the conjunctiva, lung, serosa, the four examined joints, and the brain. Joints on both sides were sampled with the same swab. During necropsy, viscose swabs were used (Swab in tube PS + Viscose, Deltalab).

Histological examination

Samples for histopathology were collected from the conjunctiva, choana, tonsilla, trachea, lungs (seven lobes), pericardium, heart, mediastinal and mesenteric lymph nodes, liver, spleen, kidney, joints, and brain (cerebrum, cerebellum, and brain stem). Tissue samples were fixed in 10% formaldehyde and embedded in paraffin, and then, 4 µm thick sections were cut and stained with hematoxylin and eosin (H&E) and examined by light microscope. Given the limited number of examined animals in the present study, the establishment of a general scoring system was not possible. Therefore, lesions were categorized based on the comparison of the severity of the histopathological changes with each other. The criteria of the scoring system used in this study are detailed in [Supplementary Table 2](#).

Bacteriology

The presence of bacterial pathogens other than *Mycoplasma* sp. was tested by culturing the necropsy samples on Columbia sheep blood agar (Biolab Inc., Hungary) and sheep blood agar supplemented with nicotinamide adenine dinucleotide (Sigma-Aldrich Co., USA) at the final concentration of 20 µg/ml. The agar plates were incubated in the presence of 5% CO₂ at 37°C for 48 h.

Serology

Sera were tested in duplicates by an in-house ELISA, using an antigen prepared according to the sarcosyl assay described previously ([Stipkovits et al., 1993](#)). In brief, to prepare the antigen, six clinical isolates of *M. hyorhinis* were propagated ([Supplementary Table 3](#)). After the color changes, the isolates were mixed, washed, and treated with 0.5% sarcosyl. The protein content of the antigen was determined using a Coomassie (Bradford) Protein assay kit (Thermo Fisher Scientific Inc.) according to the manufacturer's instructions.

Furthermore, 96-well ELISA plates were coated with the antigen diluted to the concentration of 1.25 µg/ml in phosphate-buffered saline (PBS, pH 7.4). After blocking with 1% gelatin from cold water fish skin (Sigma-Aldrich Co.), each well was incubated with a serum sample diluted to 1:100 in PBS, followed by a horseradish peroxidase-conjugated rabbit anti-swine

immunoglobulin (Dako A/S, Denmark) diluted to 0.125 µg/ml in PBS. The reaction was visualized with tetramethylbenzidine substrate (TMB, Diavet Ltd., Hungary), and the optical density of the solution was measured at 450 nm using a Multiscan FC reader (Thermo Fisher Scientific Inc.).

Blood samples were centrifuged after collection, and the sera were maintained at −70°C. Each serum sample was thawed only once. Each plate contained a negative control (mix of the sera of each control animal taken at 28 DPI from this study), a positive control (mix of the sera of each animal in Group IV-IV taken at 28 DPI from this study), and a background control, where PBS was measured instead of the serum sample. The mean OD value of the background control was subtracted from the mean OD values of the samples and the controls ([Terato et al., 2016](#)). Samples were considered positive when the OD values were higher than three times the mean OD values of the negative controls ([Lardeux et al., 2016](#)). The mean of all negative controls used in the ELISAs was used to calculate this value.

Statistical analyses

Statistical analyses were accomplished using the R program ([R Core Team, 2021](#)). To compare the effect of the different challenge routes statistical analysis of the ADWG, pathological scores (separately for the joints, serosa of the pericardium, pleura, and peritoneum, and summary of scores), histopathological scores (separately for the joints, serosa of the pericardium, pleura, and peritoneum, and summary of scores), and ELISA results from the last sampling were performed. In the case of the pathological and histopathological scores, first, a Kruskal–Wallis non-parametric ANOVA test was carried out to determine whether the differences among the medians of the three study groups are statistically significant or not. If the results of the Kruskal–Wallis test were significant, Dunn's test was performed to determine exactly which groups are different by making pairwise comparisons between each group. Since multiple groups were considered at the same time, *p*-values were adjusted for multiple comparisons by the Bonferroni method. In the case of the ADWG and the ELISA results, instead of the non-parametric test, a one-way ANOVA followed by Tukey's multiple comparisons of means was performed after the normal distribution of the data was tested using the Shapiro–Wilk normality test.

Results

Clinical observations

No clinical alterations were detected in the control group throughout the study. No body temperature higher than 40.3°C was recorded during the study. One pig in Group IV-IP had a body temperature higher than 40°C on 3 consecutive days (4–6 DPI, [Supplementary Table 4](#)). No respiratory signs were recorded in the challenge groups.

Swollen joints were detected as early as 6 DPI in Group IV-IP and 8 DPI in Group IV-IV. Typically, the first swollen joint was one of the tarsal joints. By 16 DPI, all pigs in Group IV-IP had at

least one swollen joint, three out of six pigs had two swollen tarsi, and in one animal, carpal joints were also affected. In Group IV-IV, by 20 DPI, swollen tarsal joint was observed in four out of six pigs (one side only), and in one animal, both tarsi were affected, while no swollen joints were detected in one pig ([Supplementary Table 5](#)).

Weight gain dynamics of the different groups are shown in [Figure 1](#) and detailed in [Supplementary Table 6](#). The average starting weights of the groups were 10.5 kg (SD 1.2), 10.3 kg (SD 1.2), and 10.3 kg (SD 1.1) in Groups IV-IV, IV-IP, and control, while at the end of the study average body weights of the groups were 18.0, 16.0, and 22.0 kg, respectively. Mean ADWG was 223, 170, and 350 g in Groups IV-IV, IV-IP, and control, respectively. Significant differences in ADWG were detected between control and IV-IV groups ($p = 0.05$) and control and IV-IP groups ($p < 0.01$; [Supplementary Data 1](#)).

Mycoplasma isolation, PCR, and bacteriology

The sensitivity of the reaction with the optimized primers was 10^1 copies/reaction, and no cross-reactions were detected for *M. hyopneumoniae*, *M. hyosynoviae*, and *M. flocculare*.

Nasal swabs of all animals were negative for *M. hyorhinis* by PCR and isolation at the beginning of the study (2 days prior challenge). After the inoculation of the pigs, one sample from each challenged group was positive by isolation which was also positive by PCR either at the same time or at different sampling times. These animals remained PCR positive for 2–4 consecutive sampling points. Furthermore, two animals in Group IV-IV and one animal in Group IV-IP were PCR-positive as well at one sampling point. All nasal samples of the control group were negative by PCR and isolation for *M. hyorhinis* throughout the study ([Supplementary Table 7](#)).

Samples collected from the conjunctiva and meninx during necropsy were negative for the tested mycoplasmas in all animals, while one lung sample in Group IV-IV was positive for *M. hyorhinis* by PCR. Three samples from different serosa (pleura, pericardium, and peritoneum) were positive by PCR as well in Group IV-IV. A high number of joint samples were positive by PCR in both challenged groups. In Group IV-IV, two out of six stifle, four out of six elbow, five out of six tarsus, and four out of six carpus samples were positive for *M. hyorhinis* by PCR. However, in Group IV-IP, two out of six stifle, four out of six elbow, four out of six tarsus, and one out of six carpus samples were positive. All samples from the control group were negative for *M. hyorhinis* ([Supplementary Table 8](#)). *M. hyopneumoniae* or *M. hyosynoviae* were not detected in any samples collected during necropsy.

During the challenge study, two nasal isolates and isolates from six necropsy samples (tarsal, carpal, elbow, and stifle joints) were collected and their genotypes were first determined by MLVA. Two re-isolates in Group IV-IP differed from the challenge strain on one allele (MHR444; [Supplementary Table 9](#)). They were micro-variants due to within-host evolution. The sequence types of these two isolates, two other isolates from the same animals, and one isolate from Group IV-IV were also determined by MLST. All the re-isolated strains showed the same sequence type (ST) with MLST

as the challenge strain (GenBank IDs: OR250721-OR250756). MLST and MLVA trees are shown in [Supplementary Figure 1](#).

None of the cultures of the necropsy samples showed growth of pathogenic bacteria that could also be associated with the lesions, other than *M. hyorhinis*.

Gross pathological examination

Arthritis of at least one joint was observed in all pigs in the challenge groups. Mild-to-severe arthritis was found in all joints examined in one pig and in three joints examined in another pig in Group IV-IV. A single joint was affected in the remaining four animals in this group. Mild-to-severe arthritis was found in three, two, or one joints of two-two pigs in Group IV-IP. Arthritis manifested as serous or purulent inflammation ([Figures 2A, B](#)) and was detected most often in the tarsus (8/12) followed by the elbow (6/12), stifle (5/12), and carpus (4/12) on one or on both sides.

Diffuse, severe, chronic pericarditis presenting a large amount of connective tissue was detected in two animals in both challenge groups ([Figure 2C](#)). Additionally, mild or moderate chronic pleuritis presenting filaments of connective tissues were detected in two animals ([Figure 2D](#)) and mild chronic peritonitis presenting filaments of connective tissues occurred in one other animal in Group IV-IV.

Macroscopic scores of lesions in the affected organs are demonstrated in [Figure 3](#). No gross pathological alterations were found in the remaining organs examined. No gross pathological lesions were detected in any examined organs in the control group. Body condition in all groups was normal. Detailed pathological scores are given in [Supplementary Table 1](#).

Significant differences in pathological scores were detected when scores of joint lesions and total scores of groups were compared. Pathological scores in both challenge groups differed significantly from the control group ($p = 0.03$ and $p = 0.02$ regarding joint lesions, $p = 0.02$ and $p = 0.03$ regarding total scores for Group IV-IV–control group and Group IV-IP–control group, respectively) but not from each other in both cases. No significant difference was found when scores of serosa lesions were compared ([Supplementary Data 1](#)).

Histological examination

The results of the histological examination are summarized in [Supplementary Table 2](#). The main alterations were detected in the joints and in the serosa of parenchymal organs in the thoracic and peritoneal cavities. In the joints, lesions were detected in six out of six animals in Group IV-IV and four out of six animals in Group IV-IP. Joint lesions were evident in several cases only with histological examination. A total of 24 joints presented histological lesions ([Supplementary Table 2](#)), and most of these lesions (16 cases) were given a score of 3 ([Figure 4](#); [Supplementary Table 2](#)). In the joints, inflammation was characterized by infiltration of mononuclear cells and, in more severe cases, hyperplasia of the synoviocytes ([Supplementary Table 2](#)). Lymphoid follicles formed around the blood vessels (four out of six animals in both

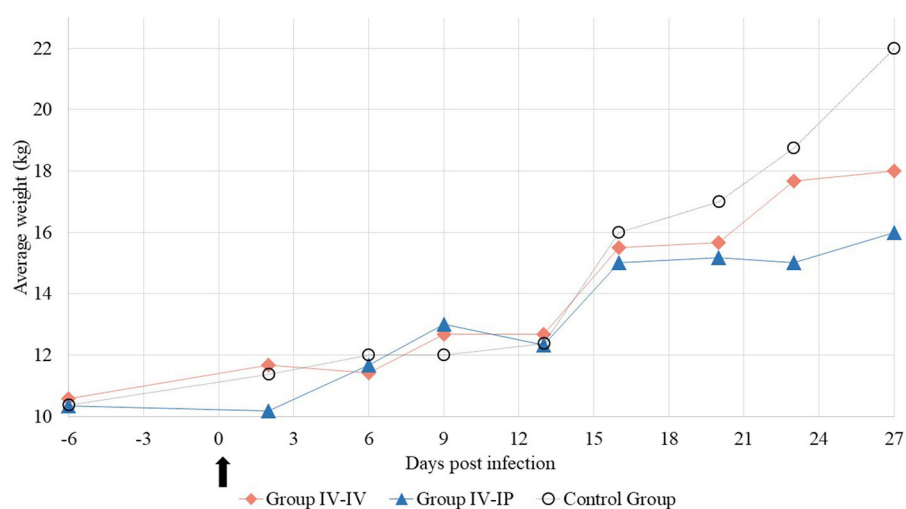


FIGURE 1

Average weight of the study groups at each sampling point. The arrow marks the first day of the challenge.

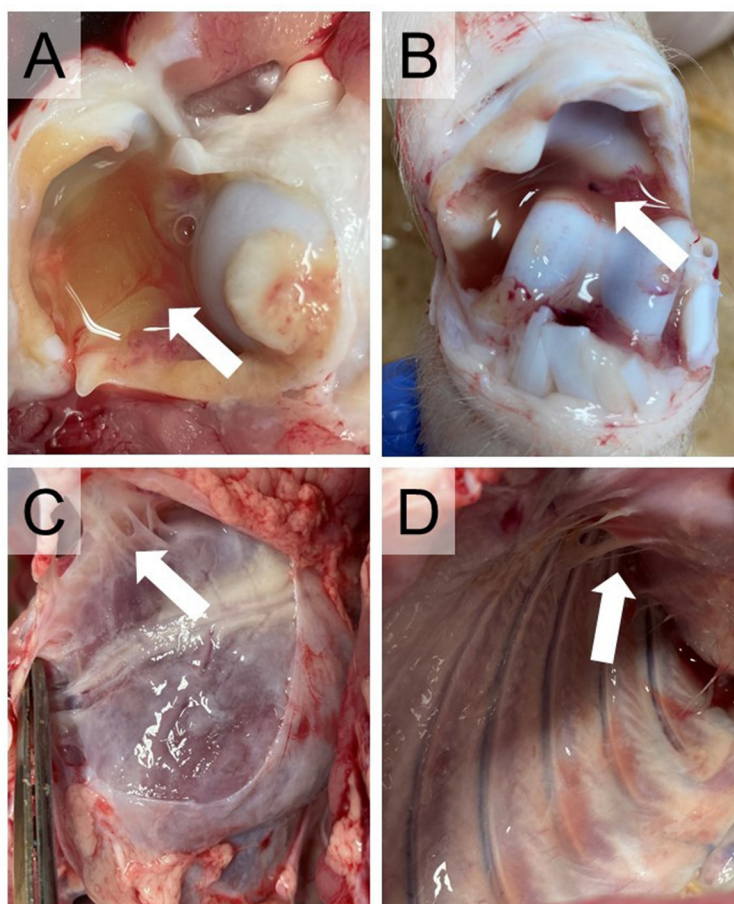


FIGURE 2

Typical lesions of *Mycoplasma hyorhinis* infection. (A) Joint with excess synovial fluid. (B) Serosanguinous synovial fluid. (C) Sero-fibrinous pericarditis. (D) Sero-fibrinous pleuritis.

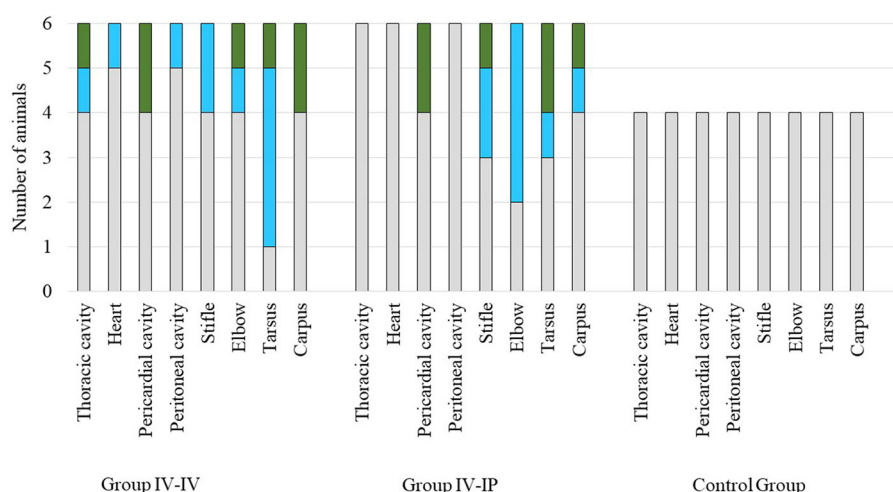


FIGURE 3

Scores of macroscopic lesions of the affected organs of the study groups. Organs were scored between 0 and 2 based on the severity of the lesion, except for the heart where score 1 was given in case of any lesion (Supplementary Table 1). Color codes in the charts: gray indicates the number of animals with a score of 0, blue indicates the number of animals with a score of 1, and green indicates the number of animals with a score of 2. The number of animals in each group is indicated on the Y-axis: the challenge groups consisted of six animals, while the control group involved four animals.

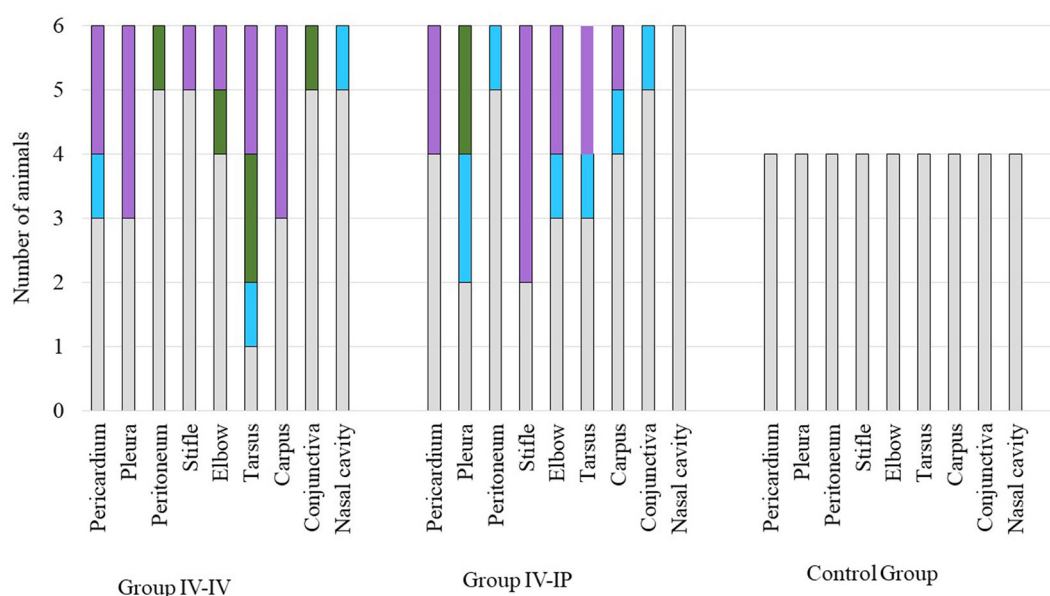


FIGURE 4

Scores of histopathologic lesions of the affected organs. Organs were scored between 0 and 3 based on the severity of the lesion. Color codes in the charts: gray indicates the number of animals with a score of 0 (no lesion), blue indicates the number of animals with a score of 1 (mild lesions), green indicates the number of animals with a score of 2 (moderate lesions), and lilac indicates the number of animals with a score of 3 (severe lesions). The number of animals in each group is indicated on the Y-axis: the challenge groups consisted of six animals, while the control group involved four animals.

Group IV-IV and IV-IP; Figure 5A) and fibrin exudates in the joint cavity were observed in several infected animals (Figure 5B; Supplementary Table 2). One animal in Group IV-IP presented acute-subacute erosive synovitis associated with acute hemorrhages and frequent occurrence of fibrin exudates, blood cells, and neutrophil granulocytes in the joint cavity (Figure 5B). Lesions of the serosal membranes (pleura, pericardium, and peritoneum)

were characterized by the presence of filamentous projections consisting of connective tissue and by different severity of serosal thickening caused by proliferating connective tissue (Figures 4, 6; Supplementary Table 2). Alterations of the pleura were detected in three out of six pigs in Group IV-IV and four out of six pigs in Group IV-IP (Figures 4, 6B). However, lesions of the epi- and pericardium were detected in three out of six animals

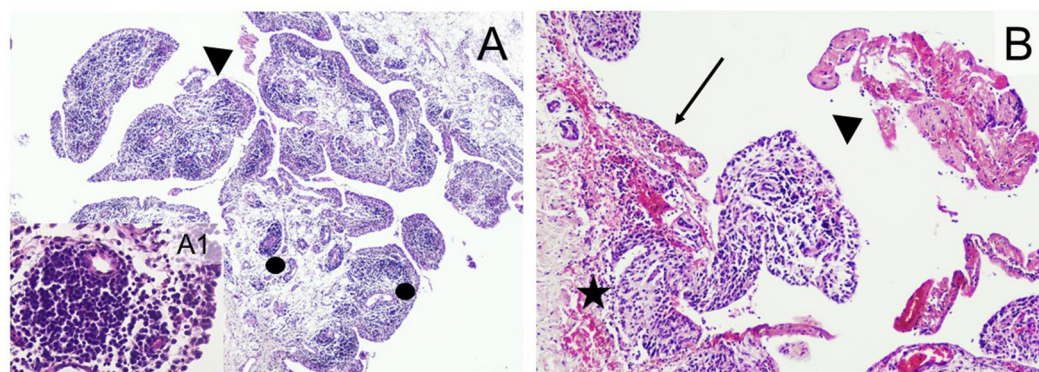


FIGURE 5

Typical histopathological changes in the joints of *Mycoplasma hyorhinis*-infected piglets. (A) Severe arthritis with the formation of perivascular lymphoid follicles (dots) and fibrin exudates in the joint cavity (arrowhead; 40 \times , H&E). A1: Perivascular follicle (400 \times ; H&E). (B) erosive synovitis (arrow) associated with acute hemorrhages (star), frequent occurrence of fibrin exudates, blood cells, and neutrophil granulocytes in the joint cavity (arrowhead; 100 \times ; H&E).

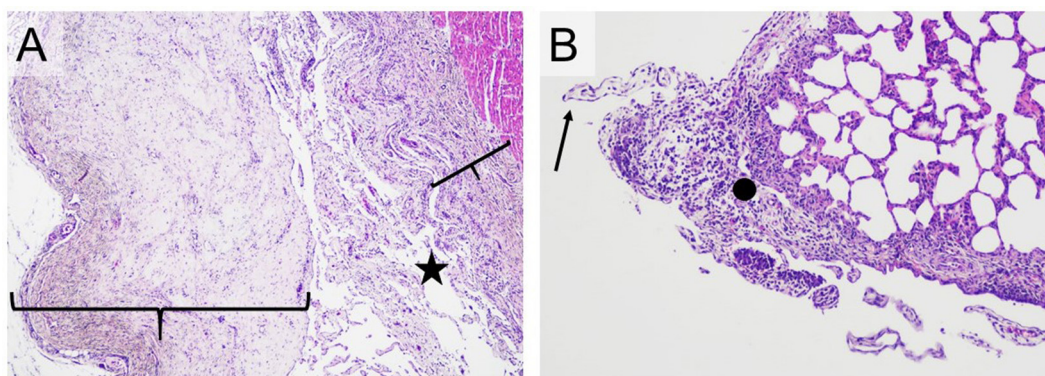


FIGURE 6

Typical histopathological changes in the serosa of *Mycoplasma hyorhinis* infected piglets. (A) A large number of filamentous projections consisting of connective tissue (star) and pronounced thickening of the pericardium and epicardium by proliferating connective tissue (braces; H&E, 40 \times). (B) Filamentous projections consisting of connective tissue (arrow) and focal, moderate thickening of the pleura by proliferating connective tissue with infiltration by mixed inflammatory cells (dot; H&E, 100 \times).

in Group IV-IV and two out of six animals in Group IV-IP (Figures 4, 6A). Finally, lesions of the peritoneum were presented in the capsule of the liver (one out of six animals in Group IV-IV) and the spleen (one animal in both challenge groups). Multinucleated giant cells in the joints in two cases and in the pleura in one of those cases were detected in the animals from Group IV-IV (Supplementary Tables 2, 10). Moreover, in Group IV-IV, one animal showed mild-to-moderate acute rhinitis, and in another case, acute ulcerative conjunctivitis was detected (Supplementary Tables 2, 10). No lesions were detected in the other organs. Combined macroscopic and histopathologic lesion scores with further details of the histopathologic lesions are given in Supplementary Table 10.

Scores of histological lesions of affected organs are shown in Figure 4. Based on the statistical analysis, scores of joints and total scores differed significantly between groups. In both cases, significant differences were detected between Group IV-IV and the control group ($p = 0.04$ regarding joint lesions, $p = 0.04$ regarding total score; Supplementary Data 1).

Serology

All animals were serologically negative for *M. hyorhinis* at the beginning of the study. The positive serological response appeared in Group IV-IP on 5 DPI, and the OD value of one out of six pigs was higher than the set threshold. The positive serological response was recorded in Group IV-IV at the next sampling on 8 DPI. By 28 DPI, all challenged animals were ELISA-positive (Supplementary Table 11). The mean OD values of the groups throughout the study are demonstrated in Figure 7. Significant differences in OD of 28 DPI were detected between the control group and Group IV-IV ($p < 0.01$) and the control group and Group IV-IP ($p < 0.01$; Supplementary Data 1). Animals from the control group remained negative throughout the study.

Discussion

Based on available literature data, the single dose intranasal or intratracheal inoculation with *M. hyorhinis* is not suitable to

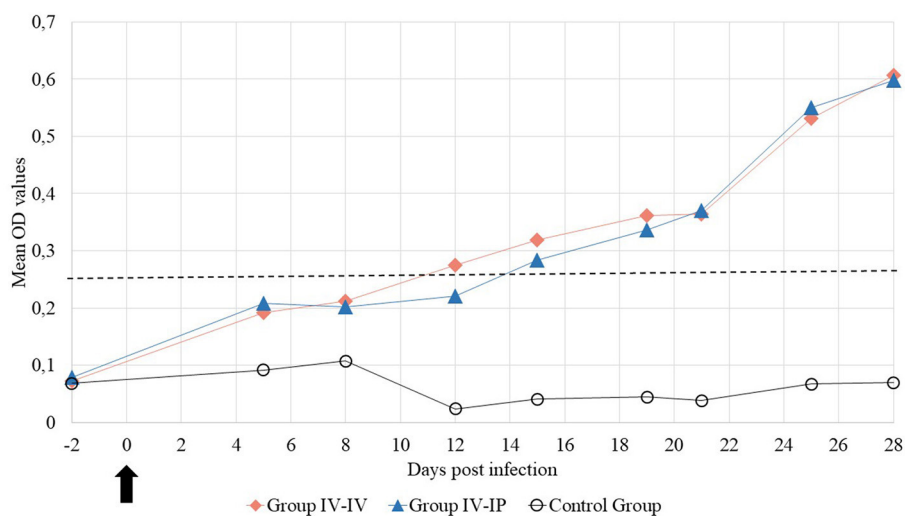


FIGURE 7

Mean optical density (OD) values of the blood samples during the study.

establish a proper challenge model as these routes are usually only suitable to induce one aspect of the infection, mostly polyserositis and lung lesions with little or no serological conversion after infection (Lin et al., 2006; Gomes Neto et al., 2014; Lee et al., 2018; Fourour et al., 2019; Wei et al., 2020). Similarly, intranasal inoculation combined with tonsillar swabbing resulted in low serological conversion with no clinical signs or macroscopic lesions (Merodio et al., 2021). Time of challenge should not have an impact on the results of previous experiments as all studies used pigs at a receptive age (infected mostly at 6 weeks of age (Lin et al., 2006; Gomes Neto et al., 2014; Lee et al., 2018; Fourour et al., 2019; Merodio et al., 2021), or at 10 weeks of age (Wei et al., 2020). Our study plan was based on the study of Martinson et al. (2018a), where one-dose intranasal, intravenous, and intraperitoneal inoculations were compared to two- or three-dose inoculations with combined challenge routes in 7-week-old animals. The results of this study also confirmed that a single dose challenge is not sufficient to induce all typical lesions, with the mildest clinical signs observed in the intranasally infected group. On the other hand, in the intravenously infected group, the rate of pigs with pericarditis and pleuritis was similar to or higher than in the groups with combined challenge routes. The authors suggested the combination of intravenous, intraperitoneal, and intranasal routes on 3 consecutive days to induce both polyserositis and polyarthritis (Martinson et al., 2018a; Wang et al., 2022).

Typical lesions of *M. hyorhinis* infection are considered to be polyserositis and polyarthritis, while the involvement of *M. hyorhinis* in the etiology of lung lesions is still under discussion. Based on literature data, the role of *M. hyorhinis* as a secondary pathogen cannot be neglected in lung lesions as the presence of this pathogen induces more severe lesions in combination with porcine circovirus 2 and *M. hyopneumoniae* (Lee et al., 2016; Luehrs et al., 2017). However, in the challenge studies when both serositis (pericarditis, peritonitis, and pleuritis) and arthritis were induced,

no lesions in the lungs were observed (Martinson et al., 2017, 2018a,b; Wang et al., 2022).

In the present study, two challenge routes were compared by using the same virulent clinical isolate. The double dose IV challenge (which was not mentioned in previous publications) produced equal involvement of joints as the mix of IV-IP route (arthritis of at least one joint was detected in 6/6 animals in both groups), which exceeded the rate of animals affected with arthritis in the previous study (single dose IV challenge resulted in arthritis in only 1/10 animal; Martinson et al., 2018a). The combination of the used infection routes (Group IV-IP) resulted in the earlier appearance of more pronounced clinical signs of arthritis like swollen joints and lameness. In the majority of animals affected with arthritis, the lesions indicated a subacute state of inflammation. Only a single animal in the IV-IP group presented acute inflammation in two joints. On the other hand, in the group which was challenged by the IV route on 2 consecutive days (Group IV-IV), the thoracic and peritoneal cavities were more commonly affected by serositis than in Group IV-IP, with equal involvement of the pericardial cavity in both groups. Most of the rest of the lesions appeared to be chronic in both infected groups. Chronic inflammation of the serosa presents as filamentous projections, serosal thickening, and adhesions between the serosal surfaces, which was detected both in the pericardium, peritoneum, and pleura of the affected animals. The low rate of re-isolation compared to PCR-positive samples also indicates the late phase of infection. Therefore, the reduction of the length of the study is suggested. Based on field observations and data from other challenge studies, the clinical signs gradually start to alleviate 2 weeks after the first clinical signs (Barden and Decker, 1971; Wang et al., 2022). Consequently, the length of the study should be determined based on the appearance of the first clinical signs (5 DPI here) and should be determined 14 days after (approximately 19 DPI in the present case). Genotyping of the re-isolates from the

challenge revealed that the challenge strain was isolated from the affected organs.

Although the natural route of infection is not yet fully understood, the results of the presented and previous challenge models using the IV route indicate that the circulatory system has an important role in the systemic spread of *M. hyorhinis* (Martinson et al., 2018a). In the present study, both applied challenge routes included intravenous infection, and systemic spread of *M. hyorhinis* was obtained in both cases. Furthermore, despite inoculating directly the peritoneum in Group IV-IP, peritonitis was only detected in one animal by histopathology without macroscopic lesions, while in Group IV-IV macroscopic alterations and more pronounced histopathologic lesions of peritonitis were detected. Lesions of the pleura and pericardium were also more severe in Group IV-IV. Nevertheless, as with both challenge methods, the main lesions of *M. hyorhinis* infection were induced, and both models can be recommended for the future study of *M. hyorhinis* infection or vaccine efficacy studies. Considering the hypothesis of the natural spread of the pathogen via the circulatory or lymphatic system and the more severe pathological lesions in Group IV-IV, a two-dose intravenous challenge is recommended by the authors.

Data availability statement

The original contributions presented in the study are included in the article/Supplementary material, further inquiries can be directed to the corresponding author.

Ethics statement

The animal study was reviewed and approved by the National Scientific Ethical Committee on Animal Experimentation under reference number: PE/EA/746-7/2021.

Author contributions

DF: investigation, formal analysis, and writing. ZN, NB, and LS: investigation. JF: supervision. AK and MT: conceptualization. ZK: editing and reviewing. MG: conceptualization, editing and reviewing, funding acquisition, and supervision. All authors contributed to the article and approved the submitted version.

References

- Barden, J. A., and Decker, J. L. (1971). *Mycoplasma hyorhinis* swine arthritis. I. Clinical and microbiologic features. *Arthritis Rheumat.* 14, 193–201. doi: 10.1002/art.1780140202
- Bünger, M., Brunthaler, R., Unterwiesing, C., Loncaric, I., Dippel, M., Ruczizka, U., et al. (2020). *Mycoplasma hyorhinis* as a possible cause of fibrinopurulent meningitis in pigs? - A case series. *Porcine Health Manag.* 6, 38. doi: 10.1186/s40813-020-00178-8
- Clavijo, M. J., Davies, P., Morrison, R., Bruner, L., Olson, S., Rosey, E., et al. (2019). Temporal patterns of colonization and infection with *Mycoplasma hyorhinis* in two swine production systems in the USA. *Vet. Microbiol.* 234, 110–118. doi: 10.1016/j.vetmic.2019.05.021
- Clavijo, M. J., Murray, D., Oliveira, S., and Rovira, A. (2017). Infection dynamics of *Mycoplasma Hyorhinis* in three commercial pig populations. *Vet. Rec.* 181, 68–68. doi: 10.1136/vr.104064
- Földi, D., Beko, K., Felde, O., Kreizinger, Z., Kovács, Á. B., Tóth, F., et al. (2020). Genotyping *Mycoplasma hyorhinis* by multi-locus sequence typing and multiple-locus variable-number tandem-repeat analysis. *Vet. Microbiol.* 249, 108836. doi: 10.1016/j.vetmic.2020.108836

Funding

This study was supported by the Momentum (Lendület) Programme (LP2022-6/2022) of the Hungarian Academy of Sciences and Project no. RRF-2.3.1-21-2022-00001, which has been implemented with the support provided by the Recovery and Resilience Facility (RRF), financed under the National Recovery Fund budget estimate, RRF-2.3.1-21 funding scheme. DF was supported by the New National Excellence Program (ÚNKP-21-3) and the Doctoral Student Scholarship Program of the Co-operative Doctoral Program (KDP-2020) of the Ministry of Innovation and Technology. The funders had no role in study design, data collection and interpretation, or the decision to submit the manuscript for publication.

Acknowledgments

The authors are thankful to Balázs Lajos for his help in providing the animals meeting the study criteria.

Conflict of interest

JF was employed by Euvet Bt. ZK and MG were employed by MolliScience Kft.

The remaining authors declare that the research was conducted in the absence of any commercial or financial relationships that could be construed as a potential conflict of interest.

Publisher's note

All claims expressed in this article are solely those of the authors and do not necessarily represent those of their affiliated organizations, or those of the publisher, the editors and the reviewers. Any product that may be evaluated in this article, or claim that may be made by its manufacturer, is not guaranteed or endorsed by the publisher.

Supplementary material

The Supplementary Material for this article can be found online at: <https://www.frontiersin.org/articles/10.3389/fmicb.2023.1209119/full#supplementary-material>

- Fourour, S., Tocqueville, V., Paboeuf, F., Lediguerher, G., Morin, N., Kempf, I., et al. (2019). Pathogenicity study of *Mycoplasma hyorhinis* and *M. flocculare* in specific-pathogen-free pigs pre-infected with *M. hyopneumoniae*. *Vet. Microbiol.* 232, 50–57. doi: 10.1016/j.vetmic.2019.04.010
- Gomes Neto, J. C. (2012). *Diagnostic and Field Investigations in Mycoplasma hyosynoviae and Mycoplasma hyorhinis* (Graduate Thesis). Iowa State University, Digital Repository. doi: 10.31274/etd-180810-253
- Gomes Neto, J. C., Strait, E. L., Raymond, M., Ramirez, A., and Minion, F. C. (2014). Antibody responses of swine following infection with *Mycoplasma hyopneumoniae*, *M. hyorhinis*, *M. hyosynoviae* and *M. flocculare*. *Vet. Microbiol.* 174, 163–171. doi: 10.1016/j.vetmic.2014.08.008
- Hannan, P. C. T. (2000). Guidelines and recommendations for antimicrobial minimum inhibitory concentration (MIC) testing against veterinary *Mycoplasma* species. *Vet. Res.* 31, 373–395. doi: 10.1051/vetres:2000100
- Kumar, S., Stecher, G., Li, M., Knyaz, C., and Tamura, K. (2018). MEGA X: molecular evolutionary genetics analysis across computing platforms. *Mol. Biol. Evol.* 35, 1547–1549. doi: 10.1093/molbev/msy096
- Lardeux, F., Torrico, G., and Aliaga, C. (2016). Calculation of the ELISA's cut-off based on the change-point analysis method for detection of *Trypanosoma cruzi* infection in Bolivian dogs in the absence of controls. *Mem. Inst. Oswaldo Cruz.* 111, 501–504. doi: 10.1590/0074-02760160119
- Lauerman, L. H., Chilina, A. R., Closser, J. A., and Johansen, D. (1995). Avian mycoplasma identification using polymerase chain reaction amplicon and restriction fragment length polymorphism analysis. *Avian Dis.* 39, 804. doi: 10.2307/1592417
- Lee, J.-A., Hwang, M.-A., Han, J.-H., Cho, E.-H., Lee, J.-B., Park, S.-Y., et al. (2018). Reduction of mycoplasmal lesions and clinical signs by vaccination against *Mycoplasma hyorhinis*. *Vet. Immunol. Immunopathol.* 196, 14–17. doi: 10.1016/j.vetimm.2017.12.001
- Lee, J.-A., Oh, Y.-R., Hwang, M.-A., Lee, J.-B., Park, S.-Y., Song, C.-S., et al. (2016). *Mycoplasma hyorhinis* is a potential pathogen of porcine respiratory disease complex that aggravates pneumonia caused by porcine reproductive and respiratory syndrome virus. *Vet. Immunol. Immunopathol.* 177, 48–51. doi: 10.1016/j.vetimm.2016.06.008
- Lin, J., Chen, S., Yeh, K., and Weng, C. (2006). *Mycoplasma hyorhinis* in Taiwan: diagnosis and isolation of swine pneumonia pathogen. *Vet. Microbiol.* 115, 111–116. doi: 10.1016/j.vetmic.2006.02.004
- Luehrs, A., Siegenthaler, S., Grützner, N., grosse Beilage, E., Kuhnert, P., and Nathues, H. (2017). Occurrence of *Mycoplasma hyorhinis* infections in fattening pigs and association with clinical signs and pathological lesions of Enzootic Pneumonia. *Vet. Microbiol.* 203, 1–5. doi: 10.1016/j.vetmic.2017.02.001
- Martinson, B., Minion, F. C., and Jordan, D. (2018a). Development and optimization of a cell-associated challenge model for *Mycoplasma hyorhinis* in 7-week-old cesarean-derived, colostrum-deprived pigs. *Can. J. Vet. Res.* 82, 12–23.
- Martinson, B., Minion, F. C., Kroll, J., and Hermann, J. (2017). Age susceptibility of caesarian derived colostrum deprived pigs to *Mycoplasma hyorhinis* challenge. *Vet. Microbiol.* 210, 147–152. doi: 10.1016/j.vetmic.2017.09.005
- Martinson, B., Zoghby, W., Barrett, K., Bryson, L., Christmas, R., Minion, F. C., et al. (2018b). Efficacy of an inactivated mycoplasma hyorhinis vaccine in pigs. *Vaccine* 36, 408–412. doi: 10.1016/j.vaccine.2017.11.063
- Merodio, M., McDaniel, A., Poonsuk, K., Magtoto, R., Ferreyra, F. S. M., Meiroz-De-Souza-Almeida, H., et al. (2021). Evaluation of colonization, variable lipoprotein-based serological response, and cellular immune response of *Mycoplasma hyorhinis* in experimentally infected swine. *Vet. Microbiol.* 260, 109162. doi: 10.1016/j.vetmic.2021.109162
- Morita, T., Fukuda, H., Awakura, T., Shimada, A., Umemura, T., Kazama, S., et al. (1995). Demonstration of *Mycoplasma hyorhinis* as a possible primary pathogen for Porcine Otitis media. *Vet. Pathol.* 32, 107–111. doi: 10.1177/030098589503200202
- Pieters, M. G., and Maes, D. (2019). “Mycoplasmosis,” in *Diseases of Swine, 1st Edn.*, eds J. J. Zimmerman, L. A. Karriker, A. Ramirez, K. J. Schwartz, G. W. Stevenson, and J. Zhang (Wiley), 863–883. doi: 10.1002/9781119350927.ch56
- R Core Team (2021). *R: A Language and Environment for Statistical Computing*. Vienna: R Foundation for Statistical Computing. Available online at: <https://www.R-project.org/> (accessed July 27, 2023).
- Resende, T. P., Pieters, M., and Vannucci, F. A. (2019). Swine conjunctivitis outbreaks associated with *Mycoplasma hyorhinis*. *J. Vet. Diagn. Investig.* 31, 766–769. doi: 10.1177/1040638719865767
- Roos, L. R., Surendran Nair, M., Rendahl, A. K., and Pieters, M. (2019). *Mycoplasma hyorhinis* and *Mycoplasma hyosynoviae* dual detection patterns in dams and piglets. *PLoS ONE* 14, e0209975. doi: 10.1371/journal.pone.0209975
- Stipkovits, L., Czifra, G., and Sundquist, B. (1993). Indirect ELISA for the detection of a specific antibody response against *Mycoplasma gallisepticum*. *Avian Pathol.* 22, 481–494. doi: 10.1080/03079459308418937
- Terato, K., Do, C., Chang, J., and Waritani, T. (2016). Preventing further misuse of the ELISA technique and misinterpretation of serological antibody assay data. *Vaccine* 34, 4643–4644. doi: 10.1016/j.vaccine.2016.08.007
- Wang, J., Hua, L., Gan, Y., Yuan, T., Li, L., Yu, Y., et al. (2022). Virulence and inoculation route influence the consequences of *Mycoplasma hyorhinis* infection in bama miniature pigs. *Microbiol. Spectr.* 10, e02493–e02421. doi: 10.1128/spectrum.02493-21
- Wei, Y.-W., Zhu, H.-Z., Huang, L.-P., Xia, D.-L., Wu, H.-L., Bian, H.-Q., et al. (2020). Efficacy in pigs of a new inactivated vaccine combining porcine circovirus type 2 and *Mycoplasma hyorhinis*. *Vet. Microbiol.* 242, 108588. doi: 10.1016/j.vetmic.2020.108588
- Wu, Y., Ishag, H. Z. A., Hua, L., Zhang, L., Liu, B., Zhang, Z., et al. (2019). *Establishment and Application of a Real-Time, Duplex PCR Method for Simultaneous Detection of Mycoplasma hyopneumoniae and Mycoplasma hyorhinis*. *Kafkas Universitesi Veteriner Fakültesi Dergisi*. doi: 10.9775/kvfd.2018.21137



OPEN ACCESS

EDITED BY
Michal Letek,
University of León, Spain

REVIEWED BY
Srishti Baid,
University of Michigan, United States
Tu-Anh Huynh,
University of Wisconsin-Madison, United States
Pierre Alexandre Kaminski,
Institut Pasteur, France

*CORRESPONDENCE
Aiping Wang
✉ pingaw@126.com
Aizhen Guo
✉ aizhen@mail.hzau.edu.cn

RECEIVED 03 July 2023
ACCEPTED 10 November 2023
PUBLISHED 30 November 2023

CITATION
Zhu X, Baranowski E, Hao Z, Li X, Zhao G,
Dong Y, Chen Y, Hu C, Chen H, Citti C,
Wang A and Guo A (2023) An atypical GdpP
enzyme linking cyclic nucleotide metabolism
to osmotic tolerance and gene regulation in
Mycoplasma bovis.
Front. Microbiol. 14:1250368.
doi: 10.3389/fmicb.2023.1250368

COPYRIGHT
© 2023 Zhu, Baranowski, Hao, Li, Zhao, Dong,
Chen, Hu, Chen, Citti, Wang and Guo. This is
an open-access article distributed under the
terms of the [Creative Commons Attribution
License \(CC BY\)](#). The use, distribution or
reproduction in other forums is permitted,
provided the original author(s) and the
copyright owner(s) are credited and that the
original publication in this journal is cited, in
accordance with accepted academic practice.
No use, distribution or reproduction is
permitted which does not comply with these
terms.

An atypical GdpP enzyme linking cyclic nucleotide metabolism to osmotic tolerance and gene regulation in *Mycoplasma bovis*

Xifang Zhu^{1,2,3}, Eric Baranowski⁴, Zhiyu Hao³, Xixi Li³, Gang Zhao³,
Yaqi Dong³, Yingyu Chen³, Changmin Hu³, Huanchun Chen^{3,5,6,7},
Christine Citti⁴, Aiping Wang^{1,2*} and Aizhen Guo^{3,5,6,7*}

¹School of Life Sciences, Zhengzhou University, Zhengzhou, China, ²Longhu Laboratory of Advanced Immunology, Zhengzhou, China, ³The State Key Laboratory of Agricultural Microbiology, College of Veterinary Medicine, Huazhong Agricultural University, Wuhan, China, ⁴IHAP, Université de Toulouse, INRAE, ENVT, Toulouse, France, ⁵Key Laboratory of Preventive Veterinary Medicine in Hubei Province, The Cooperative Innovation Center for Sustainable Pig Production, Wuhan, China, ⁶Key Laboratory of Development of Veterinary Diagnostic Products, Ministry of Agriculture of the People's Republic of China, Wuhan, China, ⁷Hubei International Scientific and Technological Cooperation Base of Veterinary Epidemiology, International Research Center for Animal Disease, Ministry of Science and Technology of the People's Republic of China, Wuhan, China

Nucleotide second messengers play an important role in bacterial adaptation to environmental changes. Recent evidence suggests that some of these regulatory molecular pathways were conserved upon the degenerative evolution of the wall-less mycoplasmas. We have recently reported the occurrence of a phosphodiesterase (PDE) in the ruminant pathogen *Mycoplasma bovis*, which was involved in c-di-AMP metabolism. In the present study, we demonstrate that the genome of this mycoplasma species encodes a PDE of the GdpP family with atypical DHH domains. Characterization of *M. bovis* GdpP (MbovGdpP) revealed a multifunctional PDE with unusual nanoRNase and single-stranded DNase activities. The alarmone ppGpp was found unable to inhibit c-di-NMP degradation by MbovGdpP but efficiently blocked its nanoRNase activity. Remarkably, MbovGdpP was found critical for the osmotic tolerance of *M. bovis* under K⁺ and Na⁺ conditions. Transcriptomic analyses further revealed the biological importance of MbovGdpP in tRNA biosynthesis, pyruvate metabolism, and several steps in genetic information processing. This study is an important step in understanding the role of PDE and nucleotide second messengers in the biology of a minimal bacterial pathogen.

KEYWORDS

Mycoplasma bovis, phosphodiesterase, GdpP, single-stranded DNase, cyclic dinucleotide, ppGpp, osmotic tolerance, gene regulation

1 Introduction

Cyclic nucleotides are important signaling molecules in both prokaryotes and eukaryotes. These second messengers relay signals of extracellular messengers and thus participate in signal transduction. A newly discovered second messenger in bacteria is c-di-AMP (Romling, 2008; Witte et al., 2008), which regulates many cellular processes, including cell size, biofilm formation, potassium ion and carnitine uptake, as well as antibiotic resistance (Ye et al., 2014; Schuster et al.,

2016; Fahmi et al., 2017; Whiteley et al., 2017). Intracellular homeostasis of c-di-AMP is thus crucial for maintaining normal bacterial physiology.

Diadenylate cyclases (DAC) and phosphodiesterases (PDE) are the main proteins involved in c-di-AMP metabolism. DAC are responsible for the synthesis of c-di-AMP through a condensation reaction involving two molecules of ATP or ADP (Bai et al., 2012; Muller et al., 2015; Rosenberg et al., 2015). Several PDE have been identified that catalyze the degradation of c-di-AMP in bacteria, and are generally divided into three protein groups: DhhP, PgpH and GdpP (Huynh and Woodward, 2016; Commichau et al., 2019; He et al., 2020). Originally described in *Borrelia burgdorferi*, DhhP proteins are widely distributed in bacteria. They are characterized by a DHH-DHHA1 domain and have been reported to convert c-di-AMP to phosphoadenylyl adenosine (pApA) or AMP in several species, including *Mycobacterium tuberculosis*, *Mycoplasma pneumonia*, *Staphylococcus aureus*, and *Streptococcus pneumonia* (Cron et al., 2011; Yang et al., 2014; Bowman et al., 2016; Blotz et al., 2017). PgpH proteins contain a His-Asp (HD) domain and have been found to bind c-di-AMP and convert this substrate into pApA in *Listeria monocytogenes* (Huynh et al., 2015). Finally, GdpP proteins are characterized by a PAS/GGDEF motif located upstream of the DHH-DHHA1 domain and possess both PDE and ATPase functions (Rao et al., 2010). This protein family has been found to convert c-di-AMP to pApA, and can slightly degrade ATP to ADP in *Bacillus subtilis*, *Enterococcus faecalis* and *S. aureus* (Rao et al., 2010; Bai et al., 2013; Wang et al., 2017).

Mycoplasmas are wall-less bacteria of the class *Mollicutes*, whose evolution is mainly characterized by genome downsizing (Citti and Blanchard, 2013). Despite a reduced coding capacity, several species are successful pathogens causing debilitating diseases in humans and a wide range of animals including cattle, swine, and avian hosts (Citti et al., 2010). The genome of these minimal, self-replicating bacteria has been used as a model system for the design of synthetic bacterial genomes and the exploration of essential functions in a minimal cell (Hutchison et al., 2016). Yet, nucleotide signaling transduction systems are poorly characterized in these atypical organisms. Recent evidence suggests that nucleotide second messengers, such as (p)ppGpp and c-di-AMP, may play important biological functions in several mycoplasma species including the small ruminant pathogen *Mycoplasma capricolum* and the human pathogen *Mycoplasma pneumoniae* (Glaser et al., 1981; Halbedel et al., 2007; Blotz et al., 2017). In a previous study with the ruminant pathogen *Mycoplasma bovis*, we identified several DHH proteins with PDE and/or nanoRNase activities (Zhu et al., 2020). In the present study, we have used *M. bovis* as a model organism to further analyze genes involved in c-di-AMP metabolism and characterized the enzymatic activity of a putative GdpP PDE encoded by CDS Mbov_0276 (MBOV_RS01380) in strain HB0801. Remarkably, MbovGdpP was found to be a multifunctional enzyme exhibiting a ssDNase activity in addition to the typical PDE function associated with bacterial GdpP and the nanoRNase activity discovered previously (Zhu et al., 2020). The phenotypic characterization of MbovGdpP knock-out mutant identified this protein as important for osmotic tolerance in this species. Finally, the regulatory role played by MbovGdpP was highlighted by transcriptomic analysis revealing an influence of this PDE in tRNA expression, pyruvate metabolism, and several steps in genetic information processing.

2 Materials and methods

2.1 Bacterial strains and culture conditions

Bacterial strains used in this study are listed in [Supplementary Table S1](#). *M. bovis* HB0801 (GenBank sequence CP002058.1; NCBI Reference Sequence NC_018077.1) was grown in pleuropneumonia-like organism (PPLO) medium (BD Company, Sparks, MD, United States) with or without 100 µg/mL gentamicin, as previously described (Han et al., 2015). Mycoplasma titers were determined based on colony counts after 2 to 5 days of incubation at 37°C (Zhu et al., 2020). *Escherichia coli* DH5α and BL21 were grown in Luria Bertani (LB) broth medium with appropriate antibiotics.

2.2 DNA constructions and recombinant protein purification

Since mycoplasmas use UGA as a tryptophan codon, the MbovGdpP nucleotide sequence was modified by converting UGA codons into UGG to avoid premature translation stops in *E. coli*. The modified MbovGdpP nucleotide sequence was synthesized by the Beijing Tianyi Huiyuan Bioscience & Technology Inc. The synthetic gene was digested by *NcoI* and *XhoI* (Takara, Dalian, China), and then was cloned into the plasmid vector pET28b (+) using T4 DNA Ligase (Takara, Dalian, China) to generate plasmid pMbovGdpP ([Supplementary Table S1](#)). DNA constructions were validated by DNA sequencing before transformation into *E. coli* BL21 for protein expression. Recombinant proteins were purified with the nickel affinity chromatography method using 1 L of *E. coli* cultures ([Supplementary Table S1](#)) induced by 0.8 mM b-D-1-thiogalactopyranoside (IPTG) for 20 h at 16°C. Purified recombinant proteins were analyzed by SDS-PAGE, and their concentration was determined by using the BCA protein assay kit (Thermo Fisher Scientific, Waltham, MA, United States). Purified proteins were stored at −80°C.

2.3 Enzymatic activity assays

The ssDNA was synthesized by the Wuhan TsingKe Biological Technology Inc. with the sequence listed in [Supplementary Table S1](#). For ssDNase assay, 5 µM recombinant proteins were incubated with ssDNA at 37°C overnight in 20 mM Tris-HCl (pH 7.0) containing 2.5 mM MnCl₂. The reaction was stopped by boiling for 10 min. After centrifuging at 20,800 × g, samples were analyzed by electrophoresis on 12% polyacrylamide gels and stained with ethidium bromide before visualization with an imaging system (ProteinSimple, Santa Clara, CA, United States). For enzymatic degradation efficiency assays, 50 µM c-di-AMP, 50 µM pApA, and 10 µM ssDNA were used as substrates to measure PDE, nanoRNase, and ssDNase activities, respectively. The reaction mixtures were incubated from 0 to 240 min at 37°C and analyzed by HPLC, as previously described. Briefly, the soluble components were separated on an RP C18 column (250 × 4.6 mm id, 5 µm; Thermo Fisher Scientific, Waltham, MA, United States). The mobile phase consisted of 90% phosphate buffer (30 mM K₂HPO₄, 20 mM KH₂PO₄; pH 6.0) and 10% methanol at a flow rate of 1 mL/min. The wavelength of the UV detector was set up

at 254 nm and the injection volume of the autosampler was 10 μ L. For ssDNase activity, the incubation time was extended to 480 min, and reaction mixtures were analyzed by polyacrylamide gels. The conversion rate c-di-AMP was calculated by converting the corresponding HPLC peak regions to concentrations according to the standard curve.

2.4 ppGpp inhibition assay

To test the ability of ppGpp in inhibiting the MbovGdpP PDE activity, the reaction mixture containing 50 μ M c-di-AMP was incubated with increasing concentrations of ppGpp (0 to 200 μ M; Biolog, Bremen, Germany). The reaction products were analyzed by HPLC.

2.5 Osmotic tolerance

Tolerance to osmotic stress was carried out in axenic conditions. Briefly, *M. bovis* (10⁴ CFUs) was grown in PPLO medium containing increasing concentrations of KCl or NaCl (0 to 250 mM; Sinopharm, Shanghai, China). Mycoplasma titers were determined each 12 h incubation at 37°C.

2.6 RNA isolation and quantitative RT-PCR

Mycoplasma cells were harvested from 3 mL of PPLO cultures by centrifugation at 12,000 \times g for 5 min. Total RNA was isolated from *M. bovis* pellets using the TRIzol reagent (Invitrogen Corporation, Carlsbad, CA, United States) (Flores-Valdez et al., 2018). RNA was stored at -80°C. Quantitative RT-PCR was performed as described (Zhu et al., 2021).

2.7 Transcriptome analysis of differential expressed genes

The expression profiles of differentially expressed genes of *M. bovis* were determined by RNA-sequencing (RNA-seq). The cDNA libraries were constructed by using TruSeq Stranded Total RNA with Ribo-Zero Gold (Illumina, San Diego, CA, United States) according to the manufacturer's instructions. The quality and purity of RNA samples were determined with an Agilent Technologies 2100 Bioanalyzer (Agilent, Santa Clara, CA, United States). The RNA-seq library was sequenced on an Illumina HiSeq X10 sequencer (Illumina, San Diego, CA, United States) to generate paired-end (2 \times 150 bp) reads. Raw reads generated during high-throughput sequencing were fastq format sequences. High-quality clean reads were generated by using Trimmomatic software to remove the linker and filtered out low-quality bases, N-bases or low-quality reads. Rockhooper2 was used to align clean reads to the *M. bovis* HB0801 genome (NCBI Reference Sequence NC_018077.1). Both *M. bovis* wild-type strain and mutant were set up for 3 biological replicates. Differentially expressed genes (DEGs) were defined by 1.5-fold change with a *p*-value <0.05, a commonly used cut-off value in transcriptomic studies (Pletzer et al., 2020; Brochado et al., 2021; Tremblay et al.,

2021). RNA-seq data (raw fastq files and read counts) are deposited in the Gene Expression Omnibus (GEO) repository under accession number GSE233141.

2.8 Bioinformatic analysis

Protein sequences alignments between RecJ and RecJ-like proteins were performed using National Center for Biotechnology Information (NCBI) Cobalt multiple alignment tool¹ combined with ESPript 3.0 software.²

2.9 Statistical analysis

Statistical analyses were performed with SPSS software (SPSS, Inc., Chicago, IL, United States). The unpaired student's *t*-test was used for the comparisons of two groups, while one-way ANOVA was used for multiple comparison. The differences were considered to be significant when *p*-value was lower than 0.05.

3 Results

3.1 Single-stranded DNase activity of MbovGdpP

Unlike typical members of the GdpP family, such as *B. subtilis* GdpP, MbovGdpP is only characterized by a GGDEF-like motif and a DHH-DHHA1 domain, but no PAS motif (Figure 1). Yet, sequence comparison with other members of the DHH superfamily revealed similarity with prokaryotic subfamily I members including cyclic nucleotide phosphodiesterase, nanoRNases, and exonuclease RecJ (Srivastav et al., 2019; Wang et al., 2020). In particular, MbovGdpP sequence alignment with RecJ and RecJ-like proteins revealed an important level of similarity (Supplementary Figure S1). This led us to test the ssDNase activity of MbovGdpP with a synthetic oligonucleotide (Supplementary Table S1). The MbovGdpP_{120–666} and MbovGdpP_{158–666} were successfully expressed in *E. coli*, and the molecular weight of these proteins were 61.8 kDa and 57.0 kDa, respectively (Supplementary Figure S2). Polyacrylamide gel electrophoresis (PAGE) revealed a progressive degradation of the ssDNA concentration upon incubation with a recombinant MbovGdpP having the N-terminal transmembrane domain deleted amino acid residues 0 to 119 (MbovGdpP_{120–666}) (Zhu et al., 2020), but not with the truncated MbovGdpP_{158–666} having the N-terminal region deleted up to amino acid 157 (Zhu et al., 2020) (Figures 1A–C). The catalytic efficiency of MbovGdpP on ssDNA was estimated to be less than 0.02 μ M L⁻¹ min⁻¹, with a nearly complete degradation of ssDNA within 480 min. These data suggest that MbovGdpP has ssDNase activity and that amino-acid residues 120–158 are essential for MbovGdpP ssDNase activity.

1 <https://www.ncbi.nlm.nih.gov/tools/cobalt>

2 <http://esprict.ibcp.fr/ESPript/ESPript/>

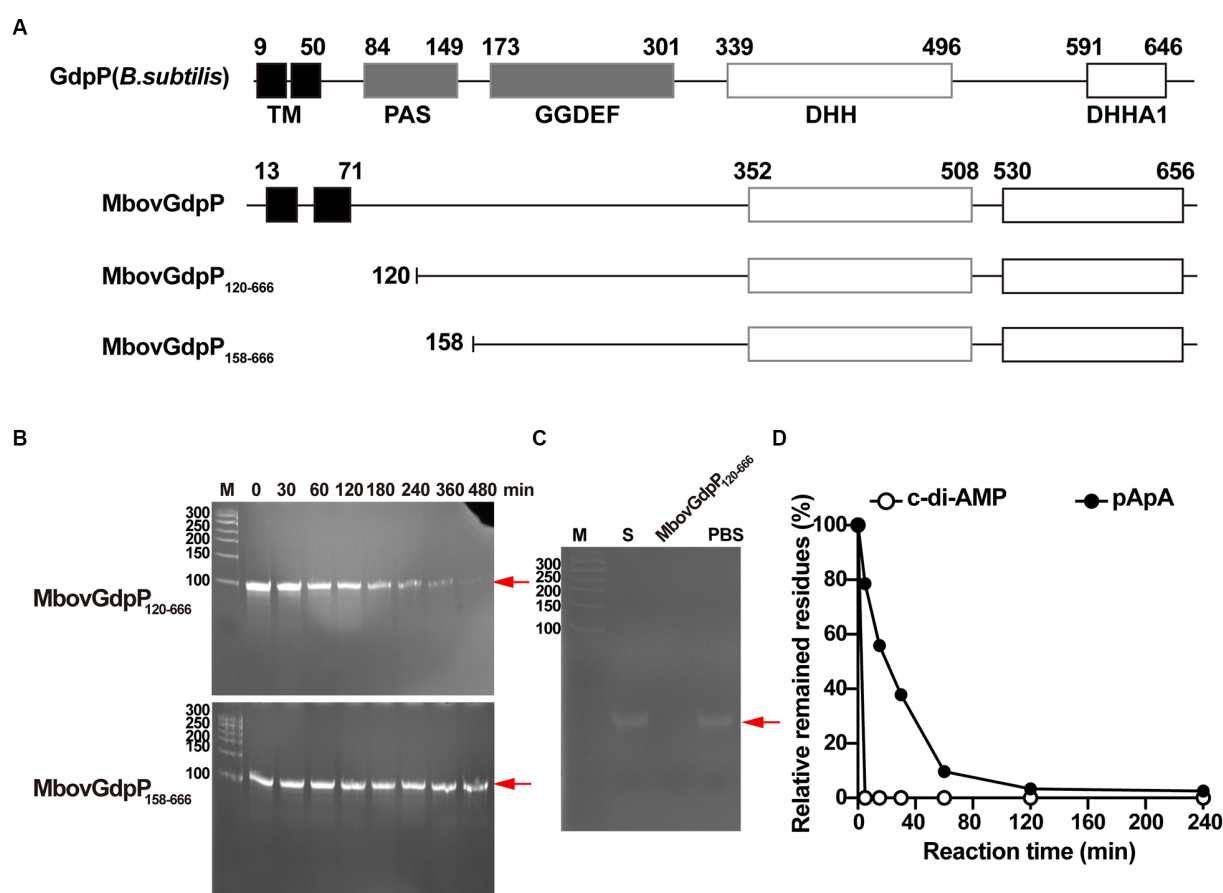


FIGURE 1

Enzymatic efficiency of MbovGdpP in degrading various substrates. (A) Schematic diagram of typical GdpP of *B. subtilis*, MbovGdpP, and truncated MbovGdpP₁₂₀₋₆₆₆ and MbovGdpP₁₅₈₋₆₆₆. In MbovGdpP₁₂₀₋₆₆₆, the deleted region spans amino acids 1 to 119, while in MbovGdpP₁₅₈₋₆₆₆, the deletion spans amino acids 1 to 157. (B) Polyacrylamide gel analysis of ssDNA degradation upon incubation with MbovGdpP₁₂₀₋₆₆₆ (upper panel) and truncated MbovGdpP₁₅₈₋₆₆₆ (lower panel). The red arrow indicates the position of the ssDNA following 0, 30, 60, 120, 180, 240, 360, and 480 min of incubation. The Lane M is the DNA ladder. (C) Using MbovGdpP₁₂₀₋₆₆₆ as a control to analyze the catalyzation activity on ssDNA after 480 min. M: 50 bp DNA ladder; S: ssDNA in H₂O; PBS: ssDNA in PBS. (D) HPLC analysis of c-di-AMP and pApA degradation by MbovGdpP₁₂₀₋₆₆₆. The incubation time ranged from 0–240 min. The y-axis indicates the proportion of remaining c-di-AMP or pApA in the reacted system relative to initial concentration of c-di-AMP or pApA. The results displayed are from a typical experiment. The concentration of MbovGdpP₁₂₀₋₆₆₆ and MbovGdpP₁₅₈₋₆₆₆ used in present study were 5 μ M, the concentration of ssDNA was 10 μ M, while both c-di-AMP or pApA were 50 μ M.

3.2 c-di-AMP and pApA degradation by MbovGdpP

To further characterize MbovGdpP enzymatic activity, we have analyzed the degradation efficiency of c-di-AMP and pApA upon incubation with the recombinant protein MbovGdpP. Quantitative analyses revealed a complete degradation of c-di-AMP and pApA within 5 min and 120 min, respectively (Figure 1D). The catalytic rate of MbovGdpP on c-di-AMP and pApA was nearly 10 μ M L⁻¹ min⁻¹ and 0.42 μ M L⁻¹ min⁻¹, respectively. These results suggest that c-di-AMP and pApA may be the preferential substrates of MbovGdpP when compared to ssDNA.

3.3 NanoRNase but not phosphodiesterase activity of MbovGdpP is inhibited by ppGpp

To test the capacity of ppGpp to inhibit MbovGdpP enzymatic activities, c-di-AMP degradation was analyzed following complete

and incomplete reaction conditions. Data revealed that c-di-AMP degradation into AMP includes the formation of a pApA intermediate (Figures 2A,B). Remarkably, HPLC analysis only identified the accumulation of the pApA intermediate product upon c-di-AMP degradation in the presence of ppGpp, even after overnight incubation (Figures 2C–F). This result indicates that ppGpp is only able to inhibit the nanoRNase activity of MbovGdpP, but not its PDE activity. Altogether, these data highlight the unique enzymatic properties of MbovGdpP.

3.4 MbovGdpP enhances *Mycoplasma bovis* resistance to K⁺ stress

Deletion of GdpP can alter bacterial resistance to osmotic stress (Pham et al., 2018; Teh et al., 2019). In the present study, *M. bovis* resistance to salt stress was tested by using the MbovGdpP knock-out mutant T6.290 (Zhu et al., 2020). When compare to wild-type strain HB0801, T6.290 growths in PPLO medium containing increasing

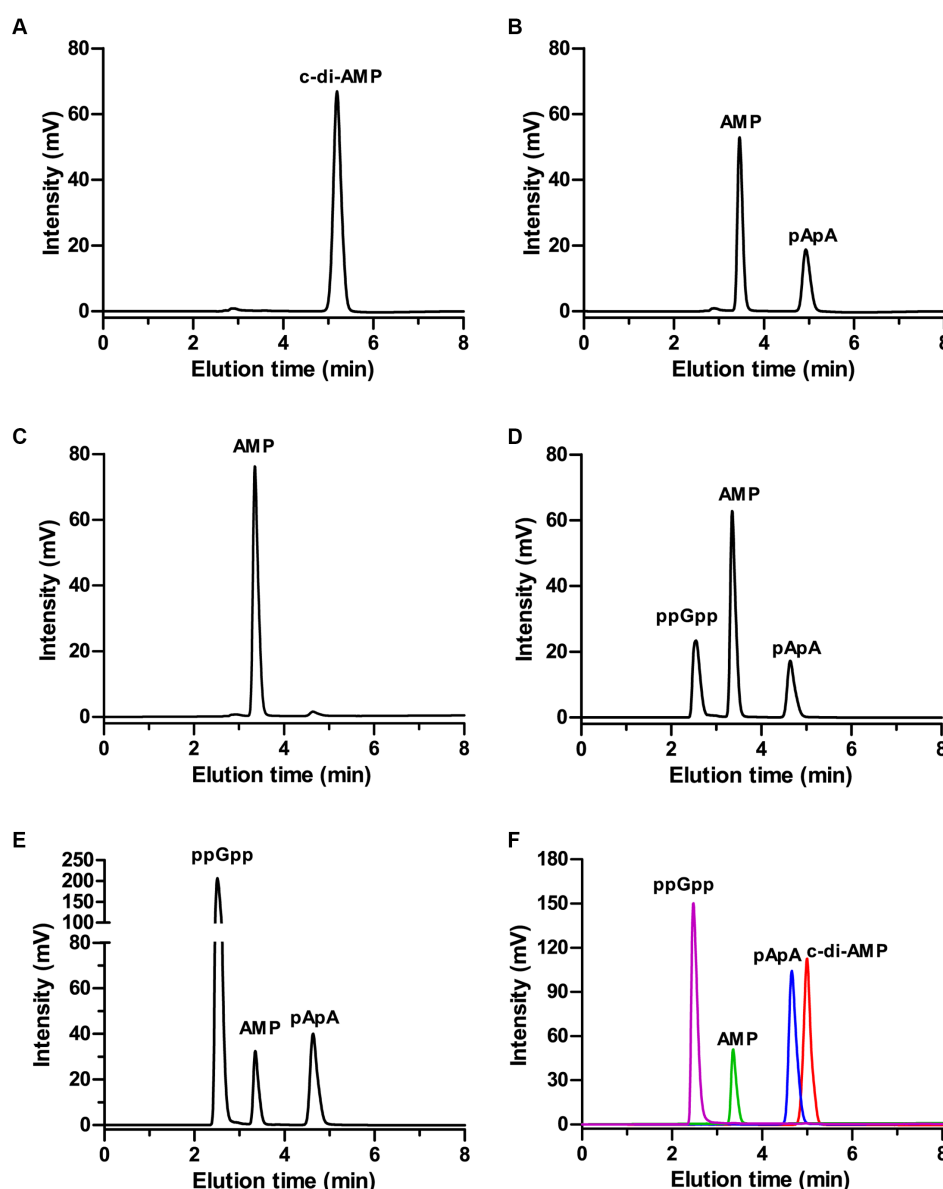


FIGURE 2

Inhibition of MbovGdpP enzymatic activities by ppGpp. (A,B) HPLC analysis of c-di-AMP degradation by MbovGdpP in 0 min (A) and 30 min (B); (C–E) HPLC analysis of c-di-AMP degradation by MbovGdpP in the presence of 0 mM (C), 50 mM (D) and 200 mM (E) of ppGpp. (F) Elution time of ppGpp (pink), c-di-AMP (red), pApA (blue) and AMP (green) standards. The concentration of MbovGdpP and c-di-AMP were 5 μ M and 50 μ M, respectively.

concentrations of KCl/NaCl was found to be affected by KCl concentrations higher or equal to 50 mM, but not by NaCl (Figure 3). This result indicates that MbovGdpP may play important role in *M. bovis* resistance to potassium (K^+) stress.

3.5 MbovGdpP plays an important role in tRNA biosynthesis and pyruvate metabolism

To better understand the role of MbovGdpP in cellular processes, RNA-seq was used to determine the transcriptional profile of T6.290 and HB0801 grown to the stationary phase. Differential gene expression analysis identified up to 161 genes with significant changes

in T6.290, with 74 mRNA up-regulated and 87 down-regulated (Figure 4A and Supplementary Table S2). The accuracy of RNA-seq was further validated by qRT-PCR. Upregulated ($n=8$) and down-regulated ($n=10$) genes were selected among the most significant differentially expressed genes (DEGs) in T6.290. The qRT-PCR analysis confirmed changes in mRNA levels for 17 out of the 18 genes selected, including 9 up-regulated genes Mbov_0022 (deoxyguanosine kinase), Mbov_0023 (deoxyguanosine kinase), Mbov_0147 (hypothetical protein), Mbov_0215 (hypothetical protein), Mbov_0426 (glycine cleavage system protein H), Mbov_0476 (PTS sugar transporter subunit IIA), Mbov_0523 (DNA-binding protein WhiA), Mbov_0709 (DNA adenine methylase), Mbov_0725 (Cof-type HAD-IIB family hydrolase), and 8 down-regulated genes Mbov_0049 (hypothetical protein), Mbov_0242 (S8 family peptidase),

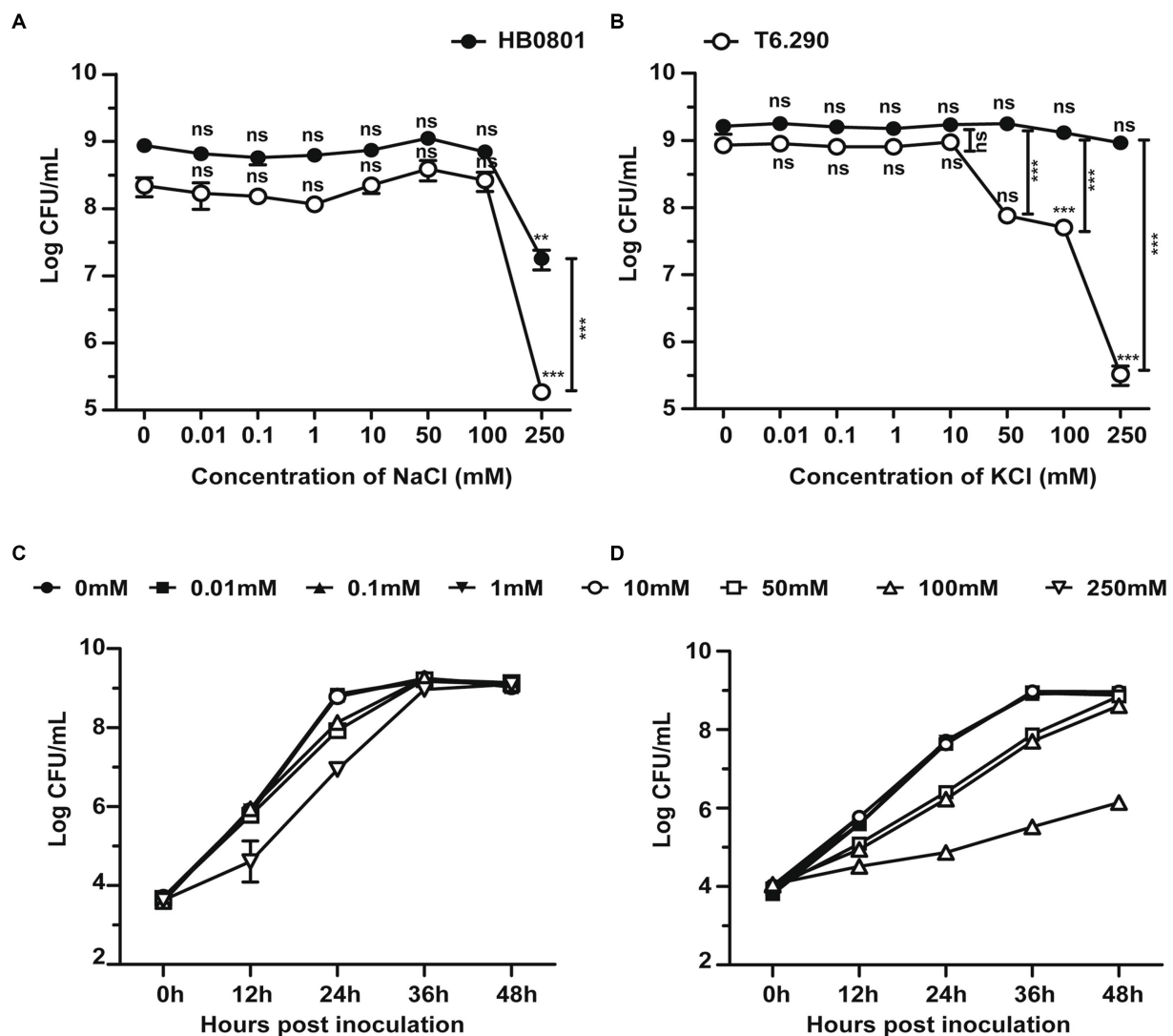


FIGURE 3

The osmotic tolerance of *M. bovis* is impaired in MbovGdpP knock-out mutants. Growth of MbovGdpP knock-out mutant (T6.290) and parental strain (HB0801) in PPLO medium in the presence of increasing concentration of Na⁺ (A) and K⁺ (B). Mycoplasma titers were determined after 48 h of incubation. Growth curve of HB0801 (C) and T6.290 (D) in PPLO medium under different KCl concentrations. The data are presented as the means of three independent assays. Standard deviations are indicated by error bars. *p*-values are indicated by asterisks (***p* < 0.01, ****p* < 0.001, ns = *p* > 0.05).

Mbov_0277 (50S ribosomal protein L9), Mbov_0278 (replicative DNA helicase), Mbov_0279 (DUF21 domain-containing protein), Mbov_0292 (variable surface lipoprotein), Mbov_0395 (hypothetical protein), Mbov_0639 (hypothetical protein) (Figure 4B).

Interestingly, tRNA accounted for over 26% (23/87) of the down-regulated genes (Table 1), representing 67% of the total number of tRNA genes (23/34). The tRNA Arg, Gly, Ile, Leu, Lys, Met, Ser, Thr, and Trp are encoded by more than one gene. Among them, 7 tRNA genes (tRNA Arg, Leu, Lys, Met, Ser, Thr, and Trp) were down-regulated, while tRNA Gly and Ile remained unchanged. The remaining tRNAs (*n* = 9) were encoded by one gene, among them, six were differentially expressed in T6.290. These results indicate that MbovGdpP plays an important role in tRNA biosynthesis which may further influence gene expression in *M. bovis*.

Up to 57 DEGs in T6.290 were of unknown functions. GO enrichment was carried out to analyze the functions of the 81 remaining

DEGs in T6.290. According to GO annotation, DEGs significantly enriched were involved in biological process (cell septum assembly), and molecular function (nucleoside kinase activity and nucleotidyltransferase activity) (Figure 5). KEGG pathway analysis revealed many DEGs participating in genetic information processing including translation, replication and repair (Figure 6A) and a vast group of DEGs participating in metabolism such as nucleotide, amino acid, cofactors and vitamins, as well as carbohydrate metabolism (Figure 6A). Up to 7 DEGs were involved in central metabolism including upregulated genes Mbov_0150 (Phosphate acetyltransferase, Pta), Mbov_0151 (Acetate kinase, AckA) and Mbov_0312 (Alcohol dehydrogenase, Adh), as well as down-regulated genes Mbov_0155 (Pyruvate kinase, Pk), Mbov_0160 (Lactate dehydrogenase, LdhA), Mbov_0286 (NADH oxidase (NOXASE), HcaD) and Mbov_0338 (Alcohol dehydrogenase, Adh) (Figure 6B). Among them, 4 genes (Mbov_0150, Mbov_0151, Mbov_0155 and Mbov_0160) are involved in pyruvate metabolism (Figure 6C). Indeed,

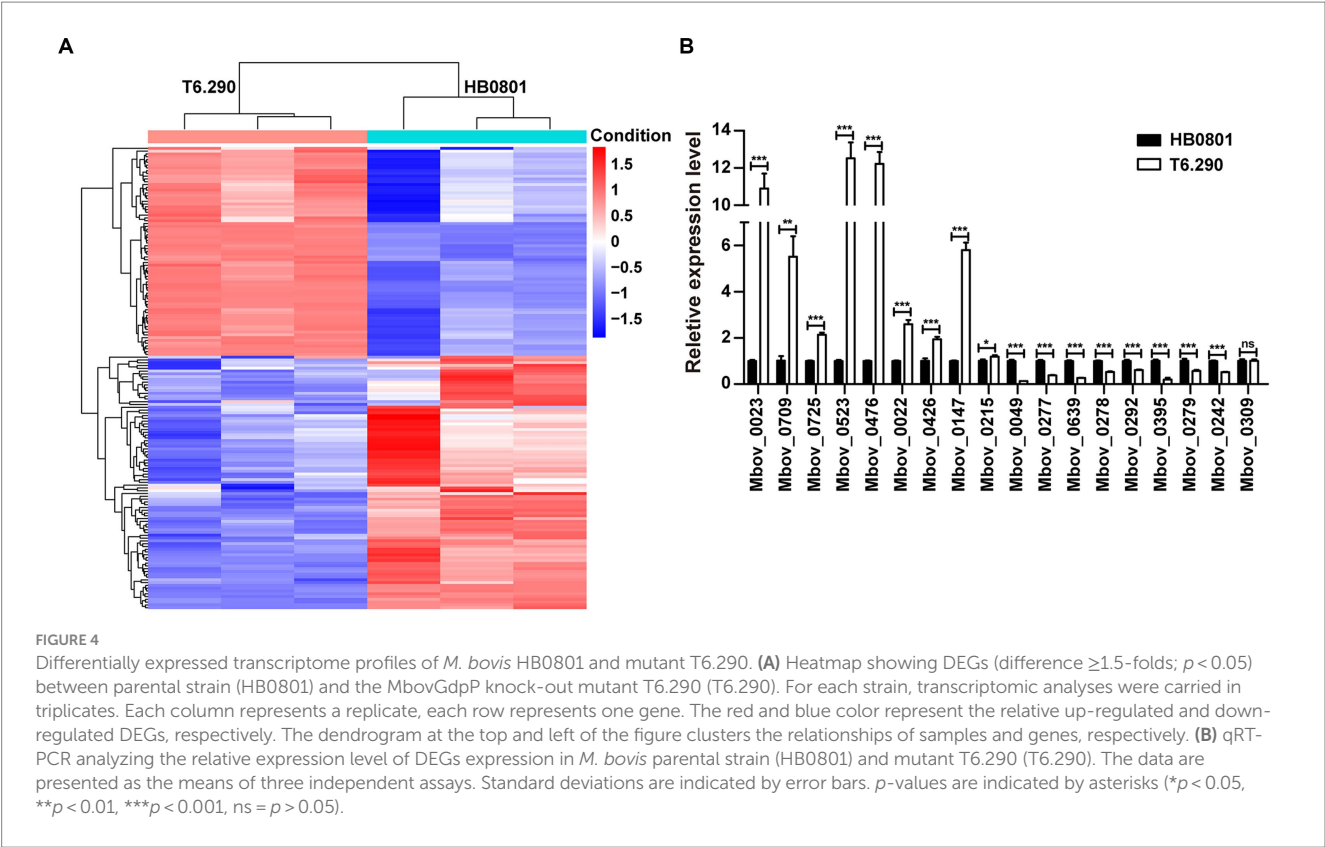


TABLE 1 Differential expressed tRNA genes in *M. bovis* MbovGdpP knock-out mutant T6.290.

Gene	Product	Seq.	Position	Fold changes	p -value
Mbov_tRNA15	tRNA-Asn	gtt	301681–301683	0.512231	0.008801
Mbov_tRNA9	tRNA-Met	cat	289713–289715	0.503700	0.003385
Mbov_tRNA34	tRNA-Trp	cca	474372–474445	0.493298	0.031258
Mbov_tRNA29	tRNA-Thr	cgt	952332–952405	0.489691	0.002568
Mbov_tRNA17	tRNA-Val	tac	301808–301883	0.488978	0.012596
Mbov_tRNA18	tRNA-Thr	tgt	301886–301961	0.463227	0.002711
Mbov_tRNA14	tRNA-Phe	gaa	290143–290218	0.437130	0.013866
Mbov_tRNA27	tRNA-Leu	caa	971964–972047	0.429675	0.002130
Mbov_tRNA12	tRNA-Met	cat	289982–290057	0.423892	0.013597
Mbov_tRNA30	tRNA-Ser	cga	912775–912864	0.418897	0.015990
Mbov_tRNA16	tRNA-Glu	ttc	301729–301804	0.412727	0.001471
Mbov_tRNA19	tRNA-Leu	tag	301970–302054	0.410065	0.002163
Mbov_tRNA28	tRNA-Trp	tca	955330–955404	0.403808	0.004407
Mbov_tRNA13	tRNA-Asp	gtc	290062–290138	0.365602	0.017434
Mbov_tRNA26	tRNA-Thr	ggt	951789–951864	0.362123	0.000132
Mbov_tRNA25	tRNA-Lys	ctt	934711–934786	0.356144	0.007747
Mbov_tRNA22	tRNA-Ser	gct	627996–628088	0.354050	0.023577
Mbov_tRNA31	tRNA-His	gtg	888380–888455	0.312977	0.027021
Mbov_tRNA11	tRNA-Ser	tga	289859–289951	0.309675	0.001887
Mbov_tRNA5	tRNA-Arg	tct	85616–85692	0.286589	0.000341
Mbov_tRNA6	tRNA-Arg	cct	85759–85834	0.281319	0.002602
Mbov_tRNA2	tRNA-Leu	taa	3026–3100	0.276278	0.000535
Mbov_tRNA24	tRNA-Lys	ttt	801958–802033	0.268189	0.000199

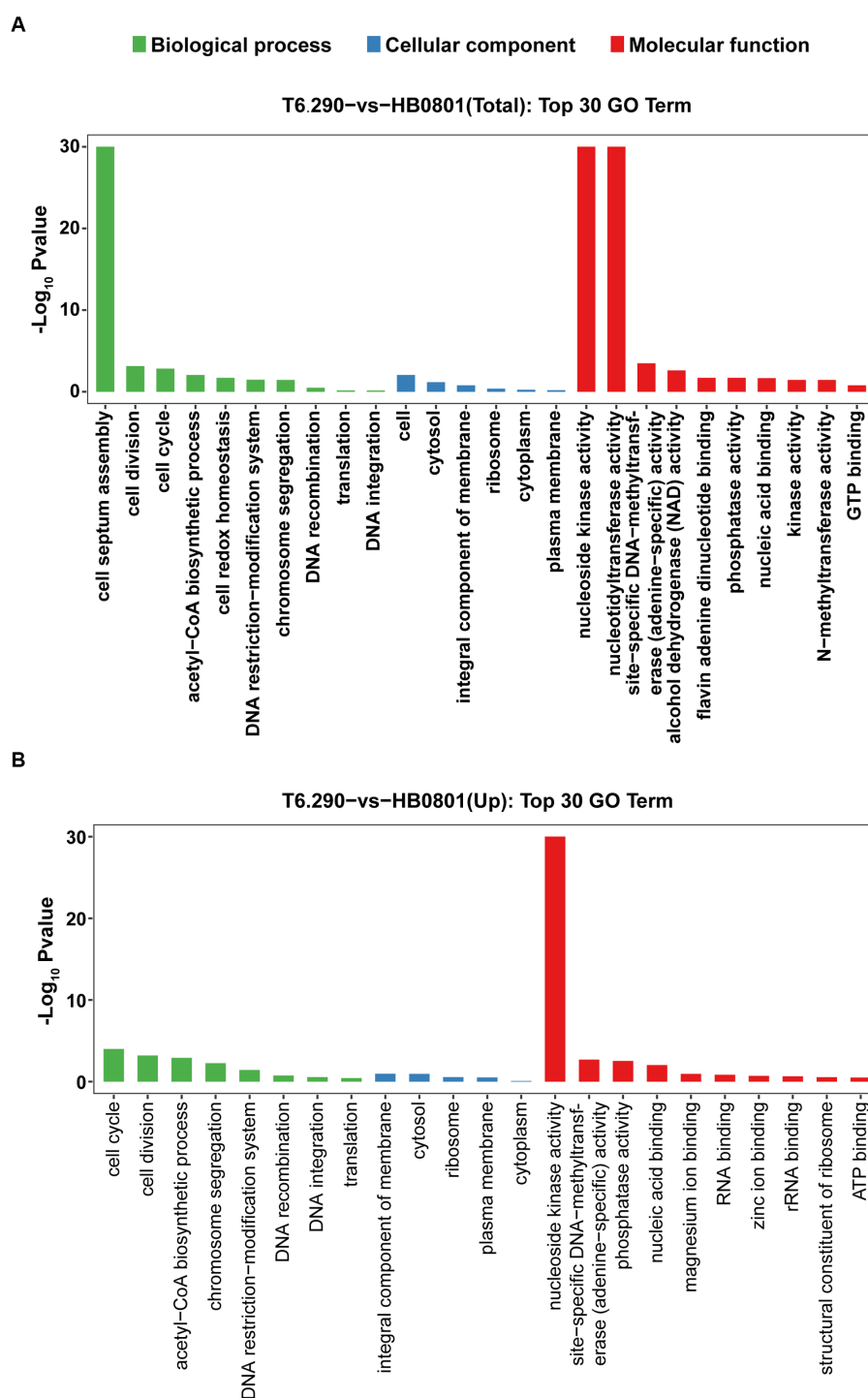


FIGURE 5

Mapping of DEGs by Gene Ontology (GO) function. The top 30 GO term enrichment analysis of total DEGs (A) and up-regulated mRNA (B) between HB0801 parental strain and T6.290 mutant.

genes involved in acetate production were up-regulated in the mutant, while genes that participate in the production of lactate were down-regulated. The Mbov_0286 product is the NADH oxidase (NOXASE) which is involved in the H_2O_2 production. These data illustrate the broad transcriptomic response of mycoplasma cells to the loss of GdpP activity and indirectly the central regulatory role played by GdpP and its secondary messenger substrates in the biology of *M. bovis*.

4 Discussion

Cyclic-di-AMP homeostasis is essential for bacterial growth and virulence, as both the accumulation and depletion of this signaling molecule are detrimental to the bacteria (Corrigan and Grundling, 2013; Mehne et al., 2013; Whiteley et al., 2015). The PDEs of the GdpP family play a central role in the metabolism of this second

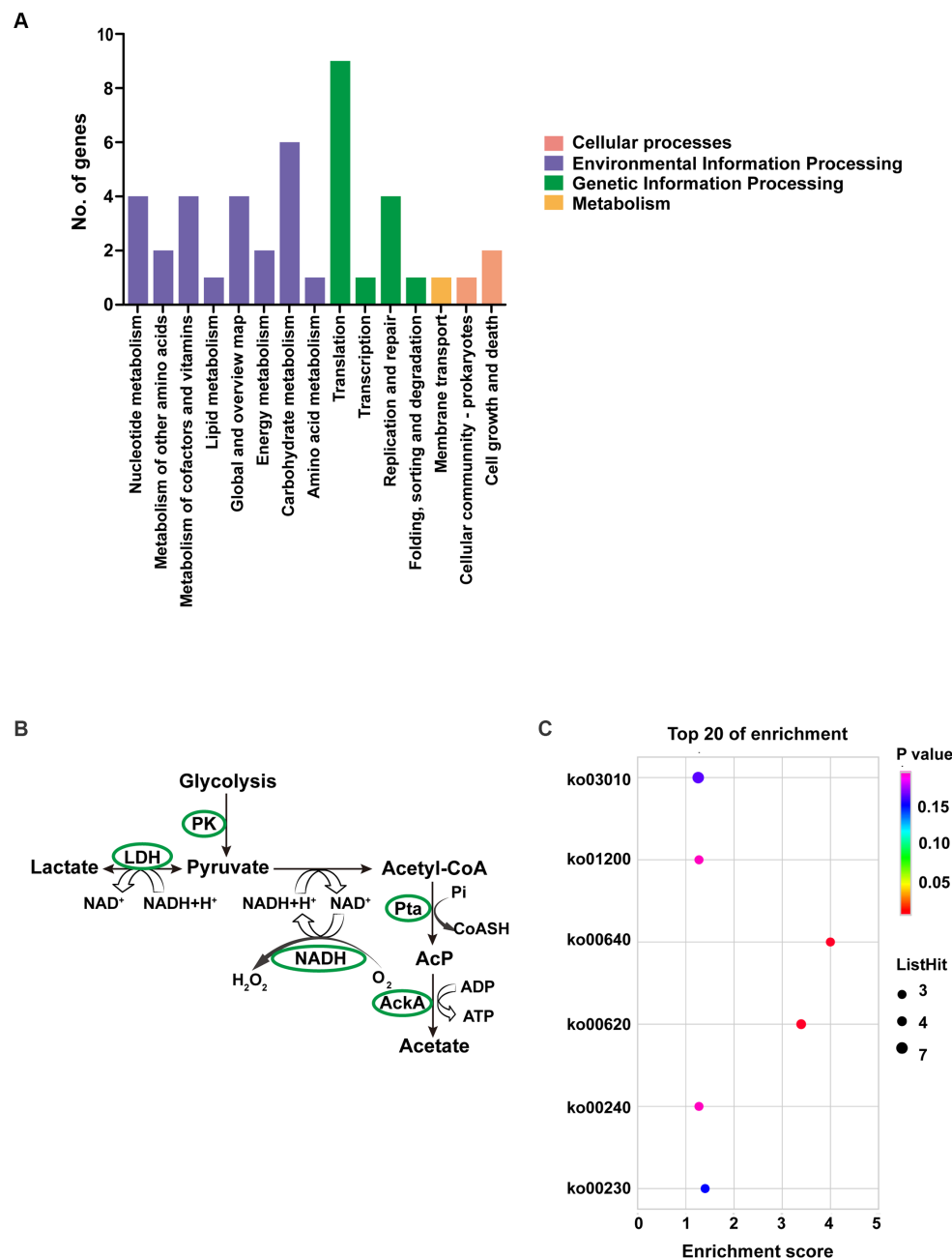


FIGURE 6

Pathway analyses of DEGs of *M. bovis* HB0801 and mutant T6.290. (A) KEGG pathway enrichment of DEGs. (B) DEGs involved in pyruvate metabolism pathway. (C) KEGG enrichment of top 20 metabolism pathway of DEGs.

messenger (Rao et al., 2010; Du et al., 2014; Wang et al., 2017). Remarkably, MbovGdpP was found to be a multifunctional enzyme exhibiting ssDNase activity in addition to the typical PDE function associated with bacterial GdpP and the nanoRNase activity (Zhu et al., 2020). However, despite showing similarity with exonuclease RecJ, nanoRNA and c-di-AMP may be the preferred substrates of MbovGdpP, since the enzyme only displayed a limited ssDNase activity. However, a quantification of catalytic efficiencies for each substrate is needed to confirm this hypothesis. Long incubation times needed to observe ssDNA degradation raised questions regarding the origin of the ssDNase activity, with possible contamination of

recombinant MbovGdpP proteins with a ssDNase from *E. coli*. However, this hypothesis was ruled out by the catalytically dead recombinant protein MbovGdpP_{158–666}, which excluded any contamination with *E. coli* ssDNase. This unusual PDE activity, which was only previously reported for the ssDNA exonuclease RecJ (Han et al., 2006; Handa et al., 2009; Zhang et al., 2022), suggests a possible role of MbovGdpP in nucleotide recycling. Indeed, cyclic dinucleotide PDE and nanoRNase activities were recently found essential for nucleotide recycling in *M. bovis* (Zhu et al., 2020). Remarkably, extracellular DNA was recently identified as a nutritional limiting factor for *M. bovis* proliferation under cell culture

conditions and cytotoxicity of this pathogenic species. Altogether, these results point towards nucleotide metabolism as strategic for *M. bovis* interaction with host cells (Zhu et al., 2019, 2020). Far from its classical role in the storage of genetic information, DNA is also pivotal for bacterial physiology. In several species, such as *Vibrio cholera*, *Pseudomonas aeruginosa*, *Shewanella*, *Serratia marcescens* and *S. aureus*, eDNA can be degraded into nucleotides, which are further used as phosphate, carbon and nitrogen sources (Beliaeva et al., 1976; Pinchuk et al., 2008; Gumpenberger et al., 2016; McDonough et al., 2016; Vorkapic et al., 2016; Lewenza et al., 2020). More interestingly, the extracellular DNase MbovNase and MnuA were recently identified as a virulence factor in *M. bovis* (Zhang et al., 2016; Mitiku et al., 2018) and a key element for this pathogen to escape neutrophil extracellular traps (NETs) (Zhang et al., 2016; Mitiku et al., 2018).

The ability to withstand external pressures, such as salt and other osmotic stresses, is critical for mycoplasmas that lack a cell wall. Our results suggest that osmotic tolerance may be regulated by MbovGdpP in *M. bovis*. This result is consistent with the role of c-di-AMP specific PDEs in classical bacteria. Indeed, deletion of GdpP can lead to hypersensitivity to Na⁺ and/or K⁺ salts in several species including *Listeria monocytogenes*, *Lactococcus lactis*, *Bacillus anthracis*, *S. aureus*, and *Streptococcus gallolyticus subsp. gallolyticus* (Smith et al., 2012; Moscoso et al., 2016; Pham et al., 2018; Teh et al., 2019; Hu et al., 2020; Schwedt et al., 2023).

In *L. monocytogenes*, GdpP is linking cyclic nucleotide metabolism to osmotic tolerance by regulating intracellular c-di-AMP levels. Indeed, this secondary messenger was found to bind to several target proteins and regulate their activities (Schwedt et al., 2023). In *S. aureus*, the osmosensitive phenotype was associated with altered expression of osmotic receptors such as K⁺ and glycine-betaine transporters (Moscoso et al., 2016; Schuster et al., 2016; Zeden et al., 2018). Whether these osmotic receptors are involved in the osmotic tolerance of *M. bovis* is unknown, but the cytosolic regulatory protein KtrC, a protein found associated with Ktr ion transporters in other bacteria, is one of the c-di-AMP receptors in *M. pneumoniae* (Blotz et al., 2017).

Potassium is essential for cell survival and physiology, such as osmoregulation, pH homeostasis, regulation of protein synthesis, enzyme activation, membrane potential adjustment, and electrical signaling (Binepal et al., 2016; Stautz et al., 2021). For example, the growth of *S. mutans* is sensitive to extracellular K⁺ availability, and low or high K⁺ concentrations result in delayed bacterial growth (Binepal et al., 2016). In *B. subtilis*, the concentration of extracellular K⁺ is reported to influence biofilm formation (Fall et al., 2006; Lopez et al., 2010). In the foodborne pathogen *Salmonella enterica*, high environmental K⁺ concentrations increased the expression of virulence factors and host cell invasion (MacGilvary et al., 2019). The physiological relevance of potassium stress in *M. bovis* remains to be further investigated. Interestingly, several mycoplasma species, including *M. bovis*, have the ability to invade host cells and to survive intracellularly (van der Merwe et al., 2010; Burki et al., 2015; Mizuki et al., 2015; Niller et al., 2017; Nishi et al., 2021). Upon cell invasion, bacteria have to face important changes in potassium concentration, which vary from 4 mM K⁺ in host blood and tissue fluid to 150 mM K⁺ in the cytoplasm (Xue et al., 2011; Stautz et al., 2021). Whether MbovGdpP may facilitate cell invasion by *M. bovis* remains largely unknown.

The nucleotide ppGpp is a signaling molecule involved in the bacterial response to nutrient starvation (Chatterji and Ojha, 2001; Kalia et al., 2013). As reported, the intracellular ppGpp in bacteria can rapidly accumulate up to a millimolar level under starvation conditions (Potrykus and Cashel, 2008; Srivatsan and Wang, 2008). In several bacterial species, such as *B. subtilis*, *S. aureus* and *E. faecalis* (Rao et al., 2010; Corrigan et al., 2015; Wang et al., 2017), up to 1 mM of ppGpp was used to confirm that this molecule can inhibit the PDE activity of GdpP, which covered the concentration used in our study. Remarkably, ppGpp was found to inhibit the nanoRNase activity of MbovGdpP, but not its PDE activity. This suggests that PDE and nanoRNase activities may be mediated by different catalytic sites in MbovGdpP, and that ppGpp may competitively bind to the nanoRNase active site.

c-di-AMP-specific PDE can have an important impact on gene expression (Zarrella et al., 2020; Zhu et al., 2020). Interestingly, our study highlighted an altered expression of tRNA in the MbovGdpP knock-out mutant. In *L. monocytogenes*, lacking c-di-AMP lead to the accumulation of alarmone molecular (p)ppGpp (Peterson et al., 2020), according to the report in *E. coli* and *M. capricolum*, the accumulation of ppGpp and pppGpp would further influence the stability of tRNA (Glaser et al., 1981; Fernandez-Coll and Cashel, 2020). Thus we speculate that ppGpp may play a bridge connecting c-di-AMP and tRNA levels in *M. bovis*.

A considerable number of DEGs in the MbovGdpP knock-out mutant were associated with replication, recombination, repair and translation. These data were consistent with the association of the DHH superfamily with a broad range of cellular processes (Srivastav et al., 2019). KEGG analysis further revealed an influence of MbovGdpP on pyruvate metabolism genes and energy production (Hegde et al., 2015). The down-regulation of energy-producing genes in the MbovGdpP knock-out mutant may have important implications *in vivo*, as suggested by the growth-deficient phenotype exhibited by this mutant cell under cell culture conditions (Zhu et al., 2020).

While identifying the role of multifunctional genes in minimal bacteria, this study further illustrates the necessity of nucleotide metabolism in maintaining the normal physiological activities of mycoplasmas.

Data availability statement

The data presented in the study are deposited in the Gene Expression Omnibus (GEO) repository, accession number GSE233141 (<https://www.ncbi.nlm.nih.gov/geo/query/acc.cgi?acc=GSE233141>).

Author contributions

AG, XZ, and EB designed the study and wrote the main manuscript text. XZ, EB, ZH, XL, GZ, and YD contributed in collecting and analyzing the data. All authors contributed to the article and approved the submitted version.

Funding

This work was supported by the Youth Program of the National Natural Science Foundation of China [32102668], China Postdoctoral

Science Foundation [2021M692937], the National Natural Science Foundation of China (NSFC) [31772745], Special Fund for Chinese Agricultural Research System (Beef/yaks) [CARS-37], Special Fund for National Distinguished Scholars in Agricultural Research and Technical Innovative Team and the Fundamental Research Funds for the Central Universities [2013QC001], and financial support from the INRAE and ENVt.

Conflict of interest

The authors declare that the research was conducted in the absence of any commercial or financial relationships that could be construed as a potential conflict of interest.

References

- Bai, Y., Yang, J., Eisele, L. E., Underwood, A. J., Koestler, B. J., Waters, C. M., et al. (2013). Two DHH subfamily 1 proteins in *Streptococcus pneumoniae* possess cyclic di-AMP phosphodiesterase activity and affect bacterial growth and virulence. *J. Bacteriol.* 195, 5123–5132. doi: 10.1128/JB.00769-13
- Bai, Y., Yang, J., Zhou, X., Ding, X., Eisele, L. E., and Bai, G. (2012). *Mycobacterium tuberculosis* Rv3586 (DacA) is a diadenylate cyclase that converts ATP or ADP into c-di-AMP. *PLoS One* 7:e35206. doi: 10.1371/journal.pone.0035206
- Beliaeva, M. I., Kapranova, M. N., Vitol, M., Golubenko, I. A., and Leshchinskaia, I. B. (1976). Nucleic acids utilized as the Main source of bacterial nutrition. *Mikrobiologiya* 45, 420–424.
- Binepal, G., Gill, K., Crowley, P., Cordova, M., Brady, L. J., Senadheera, D. B., et al. (2016). Trk2 potassium transport system in streptococcus mutans and its role in potassium homeostasis, biofilm formation, and stress tolerance. *J. Bacteriol.* 198, 1087–1100. doi: 10.1128/JB.00813-15
- Blotz, C., Treffon, K., Kaever, V., Schwede, F., Hammer, E., and Stulke, J. (2017). Identification of the components involved in cyclic di-AMP signaling in *Mycoplasma pneumoniae*. *Front. Microbiol.* 8:1328. doi: 10.3389/fmicb.2017.01328
- Bowman, L., Zeden, M. S., Schuster, C. F., Kaever, V., and Grundling, A. (2016). New insights into the cyclic di-adenosine monophosphate (C-di-AMP) degradation pathway and the requirement of the cyclic dinucleotide for acid stress resistance in *Staphylococcus aureus*. *J. Biol. Chem.* 291, 26970–26986. doi: 10.1074/jbc.M116.747709
- Brochado, O., Martinez, I., Berenguer, J., Medrano, L., Gonzalez-Garcia, J., Jimenez-Sousa, M. A., et al. (2021). HCV eradication with IFN-based therapy does not completely restore gene expression in PBMCs from HIV/HCV-coinfected patients. *J. Biomed. Sci.* 28:23. doi: 10.1186/s12929-021-00718-6
- Burki, S., Gaschen, V., Stoffel, M. H., Stojiljkovic, A., Frey, J., Kuehni-Boghenbor, K., et al. (2015). Invasion and persistence of *Mycoplasma bovis* in embryonic calf turbinates. *Vet. Res.* 46:53. doi: 10.1186/s13567-015-0194-z
- Chatterji, D., and Ojha, A. K. (2001). Revisiting the stringent response, ppGpp and starvation signaling. *Curr. Opin. Microbiol.* 4, 160–165. doi: 10.1016/S1369-5274(00)00182-X
- Citti, C., and Blanchard, A. (2013). Mycoplasmas and their host: emerging and re-emerging minimal pathogens. *Trends Microbiol.* 21, 196–203. doi: 10.1016/j.tim.2013.01.003
- Citti, C., Nouvel, L. X., and Baranowski, E. (2010). Phase and antigenic variation in mycoplasmas. *Future Microbiol.* 5, 1073–1085. doi: 10.2217/fmb.10.71
- Commichau, F. M., Heidemann, J. L., Ficner, R., and Stulke, J. (2019). Making and breaking of an essential poison: the cyclases and phosphodiesterases that produce and degrade the essential second messenger cyclic di-AMP in bacteria. *J. Bacteriol.* 201:e00462. doi: 10.1128/JB.00462-18
- Corrigan, R. M., Bowman, L., Willis, A. R., Kaever, V., and Grundling, A. (2015). Cross-talk between two nucleotide-signaling pathways in *Staphylococcus aureus*. *J. Biol. Chem.* 290, 5826–5839. doi: 10.1074/jbc.M114.598300
- Corrigan, R. M., and Grundling, A. (2013). Cyclic di-AMP: another second messenger enters the fray. *Nat. Rev. Microbiol.* 11, 513–524. doi: 10.1038/nrmicro3069
- Cron, L. E., Stol, K., Burghout, P., van Selm, S., Simonetti, E. R., Bootsma, H. J., et al. (2011). Two DHH subfamily 1 proteins contribute to pneumococcal virulence and confer protection against pneumococcal disease. *Infect. Immun.* 79, 3697–3710. doi: 10.1128/IAI.01383-10
- Du, B., Ji, W., An, H., Shi, Y., Huang, Q., Cheng, Y., et al. (2014). Functional analysis of c-di-AMP phosphodiesterase, GdpP, in *Streptococcus suis* serotype 2. *Microbiol. Res.* 169, 749–758. doi: 10.1016/j.micres.2014.01.002
- Fahmi, T., Port, G. C., and Cho, K. H. (2017). c-di-AMP: an essential molecule in the signaling pathways that regulate the viability and virulence of gram-positive bacteria. *Genes* 8:197. doi: 10.3390/genes8080197
- Fall, R., Kearns, D. B., and Nguyen, T. (2006). A defined medium to investigate sliding motility in a *Bacillus subtilis* flagella-less mutant. *BMC Microbiol.* 6:31. doi: 10.1186/1471-2180-6-31
- Fernandez-Coll, L., and Cashel, M. (2020). Possible roles for basal levels of (P)Pppp: growth efficiency vs. surviving stress. *Front. Microbiol.* 11:592718. doi: 10.3389/fmicb.2020.592718
- Flores-Valdez, M. A., Pedroza-Roldan, C., Aceves-Sanchez, M. J., Peterson, E. J. R., Baliga, N. S., Hernandez-Pando, R., et al. (2018). The BCGΔBCG1419c vaccine candidate reduces lung pathology, IL-6, TNF-α, and IL-10 during chronic TB infection. *Front. Microbiol.* 9:1281. doi: 10.3389/fmicb.2018.01281
- Glaser, G., Razin, A., and Razin, S. (1981). Stable RNA synthesis and its control in *Mycoplasma capricolum*. *Nucleic Acids Res.* 9, 3641–3646. doi: 10.1093/nar/9.15.3641
- Gumpenberger, T., Vorkapic, D., Zingl, F. G., Pressler, K., Lackner, S., Seper, A., et al. (2016). Nucleoside uptake in vibrio cholerae and its role in the transition fitness from host to environment. *Mol. Microbiol.* 99, 470–483. doi: 10.1111/mmi.13143
- Halbedel, S., Eilers, H., Jonas, B., Busse, J., Hecker, M., Engelmann, S., et al. (2007). Transcription in *Mycoplasma pneumoniae*: analysis of the promoters of the ackA and ldh genes. *J. Mol. Biol.* 371, 596–607. doi: 10.1016/j.jmb.2007.05.098
- Han, E. S., Cooper, D. L., Persky, N. S., Sutera, V. A., Whitaker, R. D., Montello, M. L., et al. (2006). RecJ exonuclease: substrates, products and interaction with SSB. *Nucleic Acids Res.* 34, 1084–1091. doi: 10.1093/nar/gkj503
- Han, X., Khan, F. A., Zhu, X., Zhang, R., Mustafa, R., Hu, C., et al. (2015). Establishment of an antibody avidity test to differentiate vaccinated cattle from those naturally infected with *Mycoplasma bovis*. *Vet. J.* 203, 79–84. doi: 10.1016/j.tvjl.2014.10.032
- Handa, N., Morimatsu, K., Lovett, S. T., and Kowalczykowski, S. C. (2009). Reconstitution of initial steps of dsDNA break repair by the RecF pathway of *E. coli*. *Genes Dev.* 23, 1234–1245. doi: 10.1101/gad.1780709
- He, J., Yin, W., Galperin, M. Y., and Chou, S. H. (2020). Cyclic di-AMP, a second messenger of primary importance: tertiary structures and binding mechanisms. *Nucleic Acids Res.* 48, 2807–2829. doi: 10.1093/nar/gkaa112
- Hegde, S., Rosengarten, R., and Chopra-Dewasthaly, R. (2015). Disruption of the pdhB pyruvate dehydrogenase [corrected] gene affects Colony morphology, *in vitro* growth and cell invasiveness of *Mycoplasma agalactiae*. *PLoS One* 10:e0119706. doi: 10.1371/journal.pone.0119706
- Hu, J., Zhang, G., Liang, L., Lei, C., and Sun, X. (2020). Increased excess intracellular cyclic di-AMP levels impair growth and virulence of *Bacillus anthracis*. *J. Bacteriol.* 202:e00653. doi: 10.1128/JB.00653-19
- Hutchison, C. A., Chuang, R. Y., Noskov, V. N., Assad-Garcia, N., Deerinck, T. J., Ellisman, M. H., et al. (2016). Design and synthesis of a minimal bacterial genome. *Science* 351:aad6253. doi: 10.1126/science.aad6253
- Huynh, T. N., Luo, S., Pensinger, D., Sauer, J. D., Tong, L., and Woodward, J. J. (2015). An HD-domain phosphodiesterase mediates cooperative hydrolysis of c-di-AMP to affect bacterial growth and virulence. *Proc. Natl. Acad. Sci. U. S. A.* 112, E747–E756. doi: 10.1073/pnas.1416485112
- Huynh, T. N., and Woodward, J. J. (2016). Too much of a good thing: regulated depletion of c-di-AMP in the bacterial cytoplasm. *Curr. Opin. Microbiol.* 30, 22–29. doi: 10.1016/j.mib.2015.12.007

Publisher's note

All claims expressed in this article are solely those of the authors and do not necessarily represent those of their affiliated organizations, or those of the publisher, the editors and the reviewers. Any product that may be evaluated in this article, or claim that may be made by its manufacturer, is not guaranteed or endorsed by the publisher.

Supplementary material

The Supplementary material for this article can be found online at: <https://www.frontiersin.org/articles/10.3389/fmicb.2023.1250368/full#supplementary-material>

- Kalia, D., Merey, G., Nakayama, S., Zheng, Y., Zhou, J., Luo, Y., et al. (2013). Nucleotide, c-di-GMP, c-di-AMP, cGMP, cAMP, (p)ppGpp signaling in bacteria and implications in pathogenesis. *Chem. Soc. Rev.* 42, 305–341. doi: 10.1039/c2cs35206k
- Lewenza, S., Johnson, L., Charron-Mazenod, L., Hong, M., and Mulcahy-O'Grady, H. (2020). Extracellular DNA controls expression of *Pseudomonas aeruginosa* genes involved in nutrient utilization, metal homeostasis, acid Ph tolerance and virulence. *J. Med. Microbiol.* 69, 895–905. doi: 10.1099/jmm.0.001184
- Lopez, D., Gontang, E. A., and Kolter, R. (2010). Potassium sensing histidine kinase in *Bacillus subtilis*. *Methods Enzymol.* 471, 229–251. doi: 10.1016/S0076-6879(10)71013-2
- MacGillvary, N. J., Kevorkian, Y. L., and Tan, S. (2019). Potassium response and homeostasis in *Mycobacterium tuberculosis* modulates environmental adaptation and is important for host colonization. *PLoS Pathog.* 15:e1007591. doi: 10.1371/journal.ppat.1007591
- McDonough, E., Kamp, H., and Camilli, A. (2016). *Vibrio cholerae* phosphatases required for the utilization of nucleotides and extracellular DNA as phosphate sources. *Mol. Microbiol.* 99, 453–469. doi: 10.1111/mmi.13128
- Mehne, F. M., Gunka, K., Eilers, H., Herzberg, C., Kaever, V., and Stulke, J. (2013). Cyclic di-AMP homeostasis in *Bacillus subtilis*: both lack and high level accumulation of the nucleotide are detrimental for cell growth. *J. Biol. Chem.* 288, 2004–2017. doi: 10.1074/jbc.M112.395491
- Mitiku, F., Hartley, C. A., Sansom, F. M., Coombe, J. E., Mansell, P. D., Beggs, D. S., et al. (2018). The major membrane nuclease MnuA degrades neutrophil extracellular traps induced by *Mycoplasma bovis*. *Vet. Microbiol.* 218, 13–19. doi: 10.1016/j.vetmic.2018.03.002
- Mizuki, H., Kawamura, T., and Nagasawa, D. (2015). In situ immunohistochemical detection of intracellular *Mycoplasma salivarium* in the epithelial cells of oral leukoplakia. *J. Oral Pathol. Med.* 44, 134–144. doi: 10.1111/jop.12215
- Moscoco, J. A., Schramke, H., Zhang, Y., Tosi, T., Dehbi, A., Jung, K., et al. (2016). Binding of cyclic di-AMP to the *Staphylococcus aureus* sensor kinase KdpD occurs via the universal stress protein domain and downregulates the expression of the Kdp potassium transporter. *J. Bacteriol.* 198, 98–110. doi: 10.1128/JB.00480-15
- Muller, M., Deimling, T., Hopfner, K. P., and Witte, G. (2015). Structural analysis of the diadenylate cyclase reaction of DNA-integrity scanning protein A (DisA) and its inhibition by 3'-dATP. *Biochem. J.* 469, 367–374. doi: 10.1042/BJ20150373
- Niller, H. H., Masa, R., Venkei, A., Meszaros, S., and Minarovits, J. (2017). Pathogenic mechanisms of intracellular bacteria. *Curr. Opin. Infect. Dis.* 30, 309–315. doi: 10.1097/QCO.0000000000000363
- Nishi, K., Gondaira, S., Fujiki, J., Katagata, M., Sawada, C., Eguchi, A., et al. (2021). Invasion of *Mycoplasma bovis* into bovine synovial cells utilizing the clathrin-dependent endocytosis pathway. *Vet. Microbiol.* 253:108956. doi: 10.1016/j.vetmic.2020.108956
- Peterson, B. N., Young, M. K. M., Luo, S., Wang, J., Whiteley, A. T., Woodward, J. J., et al. (2020). (p)ppGpp and c-di-AMP homeostasis is controlled by CbpB in *Listeria monocytogenes*. *mBio* 11:e01625. doi: 10.1128/mBio.01625-20
- Pham, H. T., Nhiep, N. T. H., Vu, T. N. M., Huynh, T. N., Zhu, Y., Huynh, A. L. D., et al. (2018). Enhanced uptake of potassium or glycine betaine or export of cyclic-di-AMP restores osmoregulation in a high cyclic-di-AMP *Lactococcus lactis* mutant. *PLoS Genet.* 14:e1007574. doi: 10.1371/journal.pgen.1007574
- Pinchuk, G. E., Ammons, C., Culley, D. E., Li, S. M., McLean, J. S., Romine, M. F., et al. (2008). Utilization of DNA as a sole source of phosphorus, carbon, and energy by *Shewanella* spp.: ecological and physiological implications for dissimilatory metal reduction. *Appl. Environ. Microbiol.* 74, 1198–1208. doi: 10.1128/AEM.02026-07
- Pletzer, D., Blimkie, T. M., Wolfmeier, H., Li, Y., Baghela, A., Lee, A. H. Y., et al. (2020). The stringent stress response controls proteases and global regulators under optimal growth conditions in *Pseudomonas aeruginosa*. *mSystems* 5:e00495. doi: 10.1128/mSystems.00495-20
- Potrykus, K., and Cashel, M. (2008). (p)ppGpp: still magical? *Annu. Rev. Microbiol.* 62, 35–51. doi: 10.1146/annurev.micro.62.081307.162903
- Rao, F., See, R. Y., Zhang, D., Toh, D. C., Ji, Q., and Liang, Z. X. (2010). YybT is a signaling protein that contains a cyclic dinucleotide phosphodiesterase domain and a GGDEF domain with ATPase activity. *J. Biol. Chem.* 285, 473–482. doi: 10.1074/jbc.M109.040238
- Romling, U. (2008). Great times for small molecules: c-di-AMP, a second messenger candidate in bacteria and archaea. *Sci. Signal.* 1:pe39. doi: 10.1126/scisignal.133pe39
- Rosenberg, J., Dickmanns, A., Neumann, P., Gunka, K., Arens, J., Kaever, V., et al. (2015). Structural and biochemical analysis of the essential diadenylate cyclase CdaA from *Listeria monocytogenes*. *J. Biol. Chem.* 290, 6596–6606. doi: 10.1074/jbc.M114.630418
- Schuster, C. F., Bellows, L. E., Tosi, T., Campeotto, I., Corrigan, R. M., Freemont, P., et al. (2016). The second messenger c-di-AMP inhibits the osmolyte uptake system OpuC in *Staphylococcus aureus*. *Sci. Signal.* 9:ra81. doi: 10.1126/scisignal.aaf7279
- Schwedt, I., Wang, M., Gibhardt, J., and Commichau, F. M. (2023). Cyclic di-AMP, a multifaceted regulator of central metabolism and osmolyte homeostasis in *Listeria monocytogenes*. *MicroLife* 4:uqad005. doi: 10.1093/femsl/uqad005
- Smith, W. M., Pham, T. H., Lei, L., Dou, J., Soomro, A. H., Beatson, S. A., et al. (2012). Heat resistance and salt hypersensitivity in *Lactococcus lactis* due to spontaneous mutation of llmg_1816 (gdpP) induced by high-temperature growth. *Appl. Environ. Microbiol.* 78, 7753–7759. doi: 10.1128/AEM.02316-12
- Srivastav, R., Sharma, R., Tandon, S., and Tandon, C. (2019). Role of DHH superfamily proteins in nucleic acids metabolism and stress tolerance in prokaryotes and eukaryotes. *Int. J. Biol. Macromol.* 127, 66–75. doi: 10.1016/j.ijbiomac.2018.12.123
- Srivatsan, A., and Wang, J. D. (2008). Control of bacterial transcription, translation and replication by (p)ppGpp. *Curr. Opin. Microbiol.* 11, 100–105. doi: 10.1016/j.mib.2008.02.001
- Stautz, J., Hellmich, Y., Fuss, M. F., Silberberg, J. M., Devlin, J. R., Stockbridge, R. B., et al. (2021). Molecular mechanisms for bacterial potassium homeostasis. *J. Mol. Biol.* 433:166968. doi: 10.1016/j.jmb.2021.166968
- Teh, W. K., Dramsi, S., Tolker-Nielsen, T., Yang, L., and Givskov, M. (2019). Increased intracellular cyclic di-AMP levels sensitize *Streptococcus gallolyticus* subsp. *Gallolyticus* to osmotic stress and reduce biofilm formation and adherence on intestinal cells. *J. Bacteriol.* 201:e00597. doi: 10.1128/JB.00597-18
- Tremblay, P. G., Fortin, C., and Sirard, M. A. (2021). Gene cascade analysis in human granulosa tumor cells (KGN) following exposure to high levels of free fatty acids and insulin. *J. Ovarian Res.* 14:178. doi: 10.1186/s13048-021-00934-6
- van der Merwe, J., Pryslak, T., and Perez-Casal, J. (2010). Invasion of bovine peripheral blood mononuclear cells and erythrocytes by *Mycoplasma bovis*. *Infect. Immun.* 78, 4570–4578. doi: 10.1128/IAI.00707-10
- Vorkapic, D., Pressler, K., and Schild, S. (2016). Multifaceted roles of extracellular DNA in bacterial physiology. *Curr. Genet.* 62, 71–79. doi: 10.1007/s00294-015-0514-x
- Wakamatsu, T., Kim, K., Uemura, Y., Nakagawa, N., Kuramitsu, S., and Masui, R. (2011). Role of RecJ-like protein with 5'-3' exonuclease activity in oligo(deoxy) nucleotide degradation. *J. Biol. Chem.* 286, 2807–2816. doi: 10.1074/jbc.M110.161596
- Wang, X., Davlieva, M., Reyes, J., Panesso, D., Arias, C. A., and Shamoo, Y. (2017). A novel phosphodiesterase of the GdpP family modulates cyclic di-AMP levels in response to cell membrane stress in daptomycin-resistant enterococci. *Antimicrob. Agents Chemother.* 61:e01422. doi: 10.1128/AAC.01422-16
- Wang, W., Ma, L., Wang, L., Zheng, L., and Zheng, M. (2020). RecJ from *Bacillus halodurans* possesses endonuclease activity at moderate temperature. *FEBS Lett.* 594, 2303–2310. doi: 10.1002/1873-3468.13809
- Whiteley, A. T., Garelis, N. E., Peterson, B. N., Choi, P. H., Tong, L., Woodward, J. J., et al. (2017). c-di-AMP modulates *Listeria monocytogenes* central metabolism to regulate growth, antibiotic resistance and osmoregulation. *Mol. Microbiol.* 104, 212–233. doi: 10.1111/mmi.13622
- Whiteley, A. T., Pollock, A. J., and Portnoy, D. A. (2015). The PAMP c-di-AMP is essential for *Listeria monocytogenes* growth in rich but not minimal media due to a toxic increase in (p)ppGpp. [corrected]. *Cell Host Microbe* 17, 788–798. doi: 10.1016/j.chom.2015.05.006
- Witte, G., Hartung, S., Buttner, K., and Hopfner, K. P. (2008). Structural biochemistry of a bacterial checkpoint protein reveals diadenylate cyclase activity regulated by DNA recombination intermediates. *Mol. Cell* 30, 167–178. doi: 10.1016/j.molcel.2008.02.020
- Xue, T., You, Y., Hong, D., Sun, H., and Sun, B. (2011). The *Staphylococcus aureus* KdpDE two-component system couples extracellular K⁺ sensing and Agr signaling to infection programming. *Infect. Immun.* 79, 2154–2167. doi: 10.1128/IAI.01180-10
- Yang, J., Bai, Y., Zhang, Y., Gabrielle, V. D., Jin, L., and Bai, G. (2014). Deletion of the cyclic di-AMP phosphodiesterase gene (cnpB) in *Mycobacterium tuberculosis* leads to reduced virulence in a mouse model of infection. *Mol. Microbiol.* 93, 65–79. doi: 10.1111/mmi.12641
- Ye, M., Zhang, J. J., Fang, X., Lawlis, G. B., Troxell, B., Zhou, Y., et al. (2014). DhhP, a cyclic di-AMP phosphodiesterase of *Borrelia burgdorferi*, is essential for cell growth and virulence. *Infect. Immun.* 82, 1840–1849. doi: 10.1128/IAI.00030-14
- Zarrella, T. M., Yang, J., Metzger, D. W., and Bai, G. (2020). Bacterial second messenger cyclic di-AMP modulates the competence state in *Streptococcus pneumoniae*. *J. Bacteriol.* 202:e00691. doi: 10.1128/JB.00691-19
- Zeden, M. S., Schuster, C. F., Bowman, L., Zhong, Q., Williams, H. D., and Grundlein, A. (2018). Cyclic di-adenosine monophosphate (c-di-AMP) is required for osmotic regulation in *Staphylococcus aureus* but dispensable for viability in anaerobic conditions. *J. Biol. Chem.* 293, 3180–3200. doi: 10.1074/jbc.M117.818716
- Zhang, L., Lin, T., Yin, Y., and Chen, M. (2022). Biochemical and functional characterization of a thermostable RecJ exonuclease from *Thermococcus gammatolerans*. *Int. J. Biol. Macromol.* 204, 617–626. doi: 10.1016/j.ijbiomac.2022.02.033
- Zhang, H., Zhao, G., Guo, Y., Menghuar, H., Chen, Y., Chen, H., et al. (2016). *Mycoplasma bovis* MBOV_RS02825 encodes a secretory nuclease associated with cytotoxicity. *Int. J. Mol. Sci.* 17:628. doi: 10.3390/ijms17050628
- Zhu, X., Baranowski, E., Dong, Y., Li, X., Hao, Z., Zhao, G., et al. (2020). An emerging role for cyclic dinucleotide phosphodiesterase and nanoRNase activities in *Mycoplasma bovis*: securing survival in cell culture. *PLoS Pathog.* 16:e1008661. doi: 10.1371/journal.ppat.1008661
- Zhu, X., Dordet-Frisoni, E., Gillard, L., Ba, A., Hygonenq, M. C., Sagne, E., et al. (2019). Extracellular DNA: A nutritional trigger of *Mycoplasma bovis* cytotoxicity. *Front. Microbiol.* 10:2753. doi: 10.3389/fmicb.2019.02753
- Zhu, T., Liu, H., Su, L., Xiong, X., Wang, J., Xiao, Y., et al. (2021). MicroRNA-18b-5p downregulation favors *Mycobacterium tuberculosis* clearance in macrophages via HIF-1 α by promoting an inflammatory response. *ACS Infect. Dis.* 7, 800–810. doi: 10.1021/acinfecdis.0c00650



OPEN ACCESS

EDITED BY

Glenn Francis Browning,
The University of Melbourne, Australia

REVIEWED BY

Ján Matiašovic,
Veterinary Research Institute (VRI), Czechia
Patrice Gaurivaud,
Agence Nationale de Sécurité Sanitaire de
l'Alimentation, de l'Environnement et du
Travail (ANSES), France

*CORRESPONDENCE

Jingyu Wang
✉ wjingyu2004@126.com

RECEIVED 09 November 2023

ACCEPTED 26 December 2023

PUBLISHED 09 January 2024

CITATION

Han S, Wang Y, Wang L, Chang W, Wen B,
Fang J, Hou X, Qi X and Wang J (2024)
Mycoplasma synoviae LP78 is a fibronectin/
plasminogen binding protein, putative
adhesion, and potential diagnostic antigen.
Front. Microbiol. 14:1335658.
doi: 10.3389/fmicb.2023.1335658

COPYRIGHT

© 2024 Han, Wang, Wang, Chang, Wen, Fang,
Hou, Qi and Wang. This is an open-access
article distributed under the terms of the
[Creative Commons Attribution License
\(CC BY\)](https://creativecommons.org/licenses/by/4.0/). The use, distribution or reproduction
in other forums is permitted, provided the
original author(s) and the copyright owner(s)
are credited and that the original publication
in this journal is cited, in accordance with
accepted academic practice. No use,
distribution or reproduction is permitted
which does not comply with these terms.

Mycoplasma synoviae LP78 is a fibronectin/plasminogen binding protein, putative adhesion, and potential diagnostic antigen

Shuizhong Han¹, Ying Wang², Lizhen Wang¹, Wenchi Chang¹,
Bo Wen¹, Junyang Fang¹, Xiaolan Hou¹, Xuefeng Qi¹ and
Jingyu Wang^{1*}

¹College of Veterinary Medicine, Northwest A&F University, Yangling, China, ²College of Food and
Drugs, Luoyang Polytechnic, Luoyang, China

Mycoplasma synoviae (*M. synoviae*) is one of the major poultry pathogens causing infectious synovitis, airsacculitis, a high incidence of shell breakage, and egg production loss. However, the pathogenesis of *M. synoviae* remains unclear. Adhesion of mycoplasmas to host cells is a crucial step in infection and colonization. The purpose of this study was to determine the adhesive function of a putative P80 family lipoprotein (LP78) and evaluate its application in the detection of antibodies against *M. synoviae*. Recombinant LP78 (rLP78) was expressed in the supernatant component of *Escherichia coli* and mouse anti-rLP78 serum was prepared. Bioinformatic analysis and western blotting results revealed that LP78 was conservative among *M. synoviae* strains. It was distributed not only in the cytoplasm but also on the membrane of *M. synoviae* through western blotting and indirect immunofluorescence (IFA). The adherence of *M. synoviae* to DF-1 cells was significantly inhibited by mouse anti-rLP78 serum ($p < 0.01$). IFA revealed that rLP78 adhered to DF-1 cells, and this adherence was prevented by mouse anti-rLP78 serum. Furthermore, rLP78 was found to bind to the DF-1 cells membrane proteins in a dose-dependent manner by enzyme-linked immunosorbent assay (ELISA). Screening of DF-1 cells membrane proteins by western blotting showed that proteins with molecular weight of 35–40 kDa and 55–70 kDa bound to rLP78. Moreover, rLP78 was identified to be a fibronectin/plasminogen binding protein. The sensitivity and specificity of rLP78-based iELISA were 85.7 and 94.1%, respectively. The maximum dilution of positive serum (HI titer, 1:128) detected via rLP78-based iELISA was 1:6,400, whereas that detected using a commercial ELISA kit was 1:12,800–1:25,600. Both rLP78-based iELISA and the commercial ELISA kit detected seroconversion after 7 days of challenge and immunization. No cross-reactivity with positive sera against other avian pathogens was observed in rLP78-based iELISA. Collectively, these results indicate that LP78 is a fibronectin/plasminogen-binding adhesion protein of *M. synoviae* and a potential diagnostic antigen. The present study will facilitate a better understanding of the pathogenesis of *M. synoviae* and the development of new diagnostic.

KEYWORDS

Mycoplasma synoviae, LP78, adhesion, fibronectin, plasminogen, ELISA, antibody

Introduction

Mycoplasma synoviae (*M. synoviae*) is one of the most important poultry pathogens, leading significant economic losses to the poultry industry worldwide. *M. synoviae* infection can cause infectious synovitis, airsacculitis, a high incidence of shell breakage, and egg production loss (Kleven et al., 1975; Cisneros-Tamayo et al., 2020). Substantial variations in pathogenicity and tissue tropism are observed among *M. synoviae* isolates, and some strains cause no infection whereas others cause respiratory disease or synovitis (Lockaby et al., 1998; Lockaby and Hoerr, 1999). It is challenging to diagnose *M. synoviae* infection on-site, especially when additional respiratory agents are present (Kleven et al., 1975; Hopkins and Yoder, 1982). Furthermore, breeder hens infected with *M. synoviae* can spread the disease vertically to progeny and laterally through direct contact via the respiratory tract (Feberwee et al., 2021). Upon infection, *M. synoviae* can persistently colonize the tracheas of chickens, even throughout the production period (Olson and Kerr, 1967). In some continents, the seroprevalence of *M. synoviae* exceeds 70% in layer flocks, and the clinical and economic relevance of *M. synoviae* is superior to that of *Mycoplasma gallisepticum* (*M. gallisepticum*) (Landman, 2014; Cortes et al., 2021). However, the pathogenesis and possible virulence factors of *M. synoviae* are not yet fully known.

Adhesion of mycoplasmas to host cells is recognized as the primary requisite for infection and successful colonization (Razin and Jacobs, 1992). The loss of adhesion capacity leads to loss of infectivity, whereas reversion to cytoadhering phenotype is accompanied by recovering infectivity and virulence (Krause et al., 1982, 1983). Therefore, cytoadhesins play a significant role in determining the virulence of mycoplasmas. Due to the lack of cell walls, the mycoplasmas membrane components are in direct contact with the cell membranes of the host and are responsible for adherence. The non-specific initial stage of the adhesion process is determined by the microorganisms' structure. The second stage entails the correctly binding of the microorganism-specific ligands to the relevant host cell receptors, primarily via the surface proteins (Razin and Jacobs, 1992). Variable lipoprotein hemagglutinin (vLhA), enolase, pyruvate dehydrogenase alpha (PdhA) and beta (PdhB) subunits, dihydrolipoamide dehydrogenase (PdhD), NADH oxidase and other surface proteins from *M. synoviae* have been identified to be involved in adhesion (Noormohammadi et al., 1997; Bao et al., 2014, 2021; Hu et al., 2022; Qi et al., 2022). Additionally, most microorganisms bind to a range of host extracellular matrix (ECM) components, such as fibronectin (Fn), collagen, elastin, and laminin via interactions between microbial adhesins and host cell receptors (Chagnot et al., 2012). Fn is a multifunctional glycoprotein with a high molecular weight. It can be found as an insoluble multimer in conjunction with the surfaces of eukaryotic cell, the ECM, and the basement membrane (BM), or as a soluble dimer in majority of body fluids (Henderson et al., 2011). Furthermore, bacterial can degrade tissue barriers formed by ECM and BM through fibrinolysis, which is one of the most important factors in the pathogenesis of bacterial infection. Plasminogen (Plg) is cleaved to generate active plasmin, which plays an important role in the fibrinolysis system (Bhattacharya et al., 2012). *M. synoviae* can be detected in a variety of internal organs, including trachea, lung, air sac, joint, and so on (Lockaby et al., 1998). Fn-binding proteins (FnBPs) and Plg-binding proteins (PlgBPs) are present in many

species of bacteria. The inactivation or mutation of some FnBPs genes decrease the adherence or virulence (Cloward and Krause, 2009; Henderson et al., 2011; Zhao et al., 2017; Liu et al., 2023). PlgBPs will enhance the conversion of Plg to plasmin, allowing bacteria to invade more easily (Li et al., 2022; Liu et al., 2023). Until now, the binding abilities of enolase, PdhA and PdhB subunits, PdhD and NADH oxidase to Fn and Plg have been determined. In addition to the above-mentioned proteins, other proteins in *M. synoviae* may also contribute to the cytoadhesion and possess Fn/Plg-binding abilities. Therefore, it is important to identify and characterize membrane-associated proteins involved in adherence and Fn/Plg-binding, since this may assist to shed light on the pathogenesis of *M. synoviae*.

Usually, adhesins are exposed on the mycoplasma cell surface and have the ability to elicit humoral responses, and then could potentially be used as a diagnostic tool. For the control and elimination of *Mycoplasma* infection, flocks should be maintained free of *Mycoplasma* infection by implementing an effective biosecurity program and a consistently applied monitoring system. Serological assays are widely used for preliminary diagnosis of *M. synoviae* infection. Until now, several serological tests, including serum plate agglutination (SPA), hemagglutination inhibition (HI), and enzyme-linked immunosorbent assay (ELISA), have been developed for monitoring flocks and detecting the outbreak of *M. synoviae* infection (Vardaman and Yoder, 1969; Thornton, 1978; Opitz et al., 1983). ELISA has been reported to have higher specificity than SPA and higher sensitivity than HI (Opitz et al., 1983). Several ELISAs based on whole cells or membrane proteins have been developed to detect antibodies against *M. synoviae* (Opitz et al., 1983; Higgins and Whithear, 1986; Opitz and Cyr, 1986). However, the cross-reactivity of these ELISAs with *M. gallisepticum* and non-specific reactions impede the development of specific serodiagnostic tests (Opitz et al., 1983; Higgins and Whithear, 1986; Opitz and Cyr, 1986). ELISA based on MSPB, the amino-terminal end of vLhA, has demonstrated good correlation with SPA without any cross-reactivity with sera against *M. gallisepticum* (Noormohammadi et al., 1999). However, a high degree of amino acid variations is observed in MSPB across strains, which affects the sensitivity of ELISA (Noormohammadi et al., 1998, 2002). Therefore, identifying novel antigens for the diagnosis of *M. synoviae* infection is necessary.

In previous study, LP78 is identified to be one of the major immunogenic proteins of *M. synoviae* and is annotated to be a P80 family lipoprotein (Bercic et al., 2008). Lipoproteins play important roles in the pathogenicity and virulence in some pathogenic mycoplasmas, and some are associated with adherence (Narat et al., 1998; Browning et al., 2011; Xiong et al., 2016). Nevertheless, few studies have been reported on the functions of LP78. We previously produced recombinant LP78 (rLP78) in *E. coli*, and the rLP78 was strongly recognized by *M. synoviae* convalescent serum. This promoted us to consider the potential roles of LP78 in cytoadherence, Fn/Plg-binding, and serological detection.

In this study, we demonstrated that LP78 is a surface located protein on *M. synoviae* and is involved in cytoadhesion with Fn/Plg-binding activities. In addition, the LP78-based ELISA showed a good performance in the diagnosis of anti-*M. synoviae* antibodies. The findings of this study may facilitate a better understanding of the pathogenesis of *M. synoviae* and improve the serological diagnosis of *M. synoviae* infection.

Materials and methods

Bacterial strains, cell line, growth conditions, and sera

Five *M. synoviae* strains, including Strain W1, YL, HN, M6, and Q9 were isolated from chickens with severe airsacculitis or synovitis in China during 2021 to 2022. The isolates were propagated in modified Frey's medium at 37°C with 5% CO₂. The *E. coli* strains DH5 α and BL21 (DE3) were grown in Luria–Bertani (LB) broth or on solid media. A continuous cell line of chicken embryo fibroblasts (DF-1 cells) was obtained from the American Type Culture Collection (Manassas, VA, United States) and grown in Dulbecco's modified Eagle's medium (DMEM; Gibco, Carlsbad, CA, United States) containing 10% fetal bovine serum (FBS; Gibco), 100 IU/mL of penicillin, and 100 μ g/mL of streptomycin at 37°C with 5% CO₂. Mouse anti-*M. synoviae* polyclonal antibody was produced in female BALB/c mice by the inoculation of a commercial inactivated *M. synoviae* vaccine (YBF-MS1 strain) (Yebio Bioengineering, co., Ltd. of Qingdao, China) via muscular routine. Convalescent sera samples were collected from commercial poultry farms with known *Mycoplasma* infection status and confirmed by a commercial *M. synoviae* antibody test kit (IDEXX, Westbrook, Maine, USA). Chicken sera against other avian pathogens, including *M. gallisepticum*, *Haemophilus paragallinarum* (Hpg), newcastle disease virus (NDV), avian influenza virus (AIV), infectious bronchitis virus (IBV), and infectious bursal disease virus (IBDV), were preserved in our laboratory.

Bioinformatic analysis

The full-length sequence of the gene encoding LP78 (MSH_01690) in *M. synoviae* strain MS-H was obtained from the GenBank database (accession number: AWL84125). Molecular weight (Mw) of LP78 (MSH_01690) was computed by ExPASy proteomics tool.¹ BLASTP² was used to carry out amino acid identity matches with sequences retrieved from NCBI database. SignalP-5.0 Server³ was conducted to predict the presence of signal peptide. Prediction of transmembrane helices was performed with TMHMM Server V. 2.0.⁴ CELLO⁵ was employed to predict protein subcellular localization. The protein sequence was submitted to the VaxiJen v2.0 server⁶ to identify antigenicity and its adhesin probability was calculated through Vaxign.⁷

Amplification of the *lp78* gene and mutagenesis via overlap-extension PCR

The *lp78* gene contains six UGA codons that are interpreted as tryptophan codons in *M. synoviae* but as stop codons in *E. coli*. Seven

primer pairs designed and synthesized by Tsingke Biotechnology Co., Ltd. (Beijing, China) were used to clone and mutate *lp78*. The primer sequences are shown in [Supplementary Table S1](#). The genomic DNA of *M. synoviae* strain MS-H (Bioproperties Ltd., Ringwood, Victoria, Australia) was extracted using the TIANamp Bacteria DNA Kit (Tiangen, Beijing, China). Sequences that contained tryptophan codons (TGA) were subjected to site-directed mutagenesis to TGG via overlap-extension PCR. In the first PCR run, the seven primer pairs were used to amplify the genomic DNA. Seven fragments of 99 bp, 126 bp, 552 bp, 482 bp, 611 bp, 129 bp, and 398 bp in size were obtained ([Supplementary Figure S1A](#)). The amplified fragments were collected using the TIANgel Purification Kit (Tiangen, Beijing, China) and used as templates in the second PCR run. The *lp78*-1-F/ *lp78*-7-R primers were used to amplify *lp78* gene and a fragment of 2,235 bp was obtained ([Supplementary Figure S1B](#)). The reaction mixture had a final volume of 50 μ L, including 2 μ L of each primer, 25 μ L of 2 \times PrimeSTAR Max Premix (Takara Biomedical Technology (Beijing) Co., Ltd., China), 19 μ L of ultrapure water, and 2 μ L of template DNA. The PCR conditions were as follows: 94°C for 10 min; 35 cycles of 95°C for 30 s, 55°C for 30 s, 72°C for 60 s, and 72°C for 10 min. The PCR product was applied to gene sequencing by Tsingke Biotechnology Co., Ltd. (Beijing, China). The mutated gene (2,235 bp) was cloned into the pET-28a (+) vector and transformed into *E. coli* DH5 α and BL21 (DE3) competent cells using the heat shock method.

Expression, purification, and identification of rLP78

E. coli BL21 (DE3) cells containing the recombinant plasmid were cultured in LB broth supplemented with kanamycin (50 μ g/mL) at 37°C on a shaker at 200 rpm. The cells were incubated with 1-mM isopropyl β -D-1-thiogalactopyranoside (IPTG) at 22°C for 12 h. After induction, rLP78 was successfully expressed in *E. coli*, and 80-kDa protein was existed mainly in the supernatant of the bacterial lysate ([Supplementary Figure S2](#)). After centrifugation at 5,000 rpm for 10 min, the cell pellets were harvested and washed twice with tris–HCl (0.02 mol/L, pH 8.0). The cell pellets were sonicated on ice with 5-s pulses at 15-s intervals. After centrifugation, the supernatant containing the recombinant protein (rLP78) was added to an affinity chromatography column prepacked with Ni-NTA His-Bind® Resin (Huiyan bio, Wuhan, China), and the recombinant protein was eluted using a linear gradient of 20–500 mM of imidazole. The recombinant protein was analyzed on 12% sodium dodecyl sulfate–polyacrylamide gels (SDS-PAGE), and its reactivity with anti-His-tag monoclonal antibody (Boster, Hubei, China) and mouse anti-*M. synoviae* polyclonal antibody were determined via western blotting. The concentration of rLP78 was determined using a BCA Protein Assay kit (Beyotime, China).

Preparation of antisera against rLP78 in mice

Female BALB/c mice aged 8 weeks were subcutaneously injected with 30 μ g of rLP78 emulsified with Montanide™ ISA 206 VG adjuvant (Seppic, Shanghai, China) at an equal ratio (w/w) at multiple points in the back. A booster dose was injected on days 14 and 28 after the first immunization. Blood samples were collected from the

1 <https://web.expasy.org/protscale/>

2 <https://blast.ncbi.nlm.nih.gov/>

3 <https://services.healthtech.dtu.dk/services/SignalP-5.0/>

4 <https://services.healthtech.dtu.dk/services/TMHMM-2.0/>

5 <http://cello.life.nctu.edu.tw/>

6 <http://www.ddg-pharmfac.net/vaxijen/VaxiJen/VaxiJen.html>

7 <https://violinet.org/vaxign/>

retro-orbital sinus after 2 weeks of the last booster immunization. A specific antibody against rLP78 in sera was evaluated via indirect ELISA (iELISA) and the ELISA titer was 1:100,000. The protocols were approved by the Ethics Committee of Animal Experimentation of Northwest A&F University (No. 220412).

Conservation of LP78 in different *Mycoplasma synoviae* strains

The presence of the lp78 gene and its expression in other *M. synoviae* strains was investigated by PCR and western blotting. Briefly, *M. synoviae* strains W1, YL, HN, M6, and Q9 were harvested from broth cultures by centrifugation at 12,000 rpm and washed three times with PBS. The whole genome was extracted and applied to PCR amplification using lp78-1-F/ lp78-7-R primers. The PCR products were sequenced and then compared with *M. synoviae* strain MS-H.

For western blotting, the whole cell lysates were separated via SDS-PAGE (12% gels) and transferred to a PVDF membrane. The membrane was blocked with 10% skim milk in TBS (0.02 mol/L Tris, 0.15 mol/L NaCl, pH 7.4) containing 0.05% Tween-20 (TBST) for 2 h at room temperature. After washing with TBST, the membrane was incubated with mouse anti-rLP78 polyclonal antibody (1:500), followed by HRP-conjugated goat anti-mouse antibody (1:10,000) (Boster, Hubei, China). The signals were developed with an enhanced chemiluminescence (ECL) reagent (Millipore, Billerica, MA, United States).

Subcellular localization of LP78 in *Mycoplasma synoviae*

To determine the distribution of LP78 in *M. synoviae*, a western blotting and an indirect immunofluorescence assay (IFA) were performed. For western blotting, the membrane and cytoplasmic proteins of the *M. synoviae* strain W1 were extracted using a protein extraction kit (Beyotime, China) according to the manufacturer's instructions. The proteins were separated via SDS-PAGE (12% gels) and transferred to a PVDF membrane. The membrane was blocked with 10% skim milk in TBS (0.02 mol/L, pH 7.4) containing 0.05% Tween-20 (TBST) for 2 h at room temperature. The membrane was washed thrice with TBST and incubated with mouse anti-rLP78 polyclonal antibody (1:500) for 2 h at room temperature. Subsequently, it was washed thrice with TBST and incubated with HRP-conjugated goat anti-mouse antibody (1:10,000) (Boster, Hubei, China) at room temperature for 2 h. The protein band was visualized using an enhanced chemiluminescence (ECL) reagent (Millipore, Billerica, MA, United States).

For IFA, *M. synoviae* strain W1 was grown in modified Frey's medium at 37°C with 5% CO₂. At the log-phase, *M. synoviae* cells were harvested and washed three times with PBS. Afterwards, the cells were incubated with a 1:200 dilution of mouse anti-rLP78 polyclonal antibody or pre-immune serum overnight at 4°C. After washing, the cells were incubated with 1:500 dilution of FITC-labeled goat anti-mouse IgG (Boster, Hubei, China) for 1 h, and then visualized under a fluorescence microscope (Zeiss, Jena, Germany).

Inhibition of *Mycoplasma synoviae* adherence to cells by mouse anti-rLP78 serum

For the adherence inhibition assay, *M. synoviae* W1 strain cells (1×10^7 CCU/ml) were washed three times with PBS, and then incubated with mouse anti-rLP78 or nonimmune serum (1:20 dilution) at 37°C for 1 h. DF-1 cells were seeded into 24-well cell plates and grown to a confluent monolayer. After washing three times with PBS, DF-1 cells were blocked with 5% bovine serum protein (BSA) at 37°C for 30 min. Subsequently, *M. synoviae* cells pretreated with serum were added to the wells and incubated at 37°C for 1 h. The unbound *M. synoviae* cells were removed by washing three times with PBS. Then, the DF-1 cells were digested with 0.25% trypsin, followed by bacterial genome extraction using the TIANamp Bacteria DNA Kit (Tiangen, Beijing, China). The amounts of *M. synoviae* were determined by quantitative real-time PCR using primers targeting the 16S rRNA gene (217 bp) as described previously (Raviv and Kleven, 2009). The DNA copies were calculated according to the standard curve plotting the Ct values against 10-fold serial dilutions of the standard plasmid.

Adhesion of rLP78 to host cells

An indirect immunofluorescence assay (IFA) was used to determine the adhesion of rLP78 to DF-1 cells. Briefly, DF-1 cells were cultured in a 96-well cell culture dish in DMEM medium for 24 h, and then fixed with 4% paraformaldehyde. After blocking with 5% BSA, the cells were incubated with 10 µg of rLP78 for 1 h. After washing to remove nonadherent proteins, the bound protein was stained with anti-His-tag monoclonal antibody (1:1,000 dilution) (Boster, Hubei, China) at 37°C for 1 h, followed by FITC-labeled goat anti-mouse IgG (1:500 dilution) (Boster, Hubei, China) for 1 h. Finally, the cell nuclei were stained with DAPI, and the immunofluorescence was detected using a fluorescence microscope (Zeiss, Jena, Germany). For the adherence inhibition assays, 100 µg/mL of rLP78 was incubated with mouse anti-rLP78 serum, or nonimmune serum (1:10 dilution) at 37°C for 1 h. Then, the mixtures were added to the fixed DF-1 cells as described above.

Binding of rLP78 to cell membrane proteins

The ability of rLP78 to bind cell membrane proteins were determined by a microtiter plate adhesion assay (MPAA) and western blotting as previously described (Li et al., 2022; Peng, et al., 2023). For MPAA, membrane and cytoplasmic proteins were extracted from 2×10^7 DF-1 cells using a commercial kit (Beyotime, China) according to the manufacturer's instructions. Microtiter ELISA plate was coated with 5 µg/mL of cell membrane proteins, cytoplasmic proteins, or BSA diluted in sodium carbonate buffer (pH 9.6) and incubated overnight at 4°C. After blocking with 5% skim milk in PBST for 2 h at 37°C, different concentrations of rLP78 (ranging from 0.78 µg/mL to 100 µg/mL) were added and incubated for 2 h at 37°C. Unbound proteins were removed by washing with PBST, and adherence was evaluated by adding 100 µL of anti-His-tag monoclonal antibody (1:1,000 dilution)

(Boster, Hubei, China) followed by 100 μ L of HRP-conjugated goat anti-mouse IgG (1:10,000 dilution) (Boster, Hubei, China). Finally, the optical density (OD) values of the solutions were measured at 450 nm. For the adherence inhibition assay, 100 μ g/mL of recombinant protein was mixed with mouse anti-rLP78 serum at various dilutions (ranging from 1:10 to 1:2,560) and incubated for 1 h at 37°C before being added to the wells.

For western blotting, the DF1 cell membrane and cytosolic proteins were separated by 12% SDS-PAGE and then transferred onto PVDF membranes. After blocking with 5% skim milk, the membrane was incubated with rLP78 (20 μ g/mL) overnight at 4°C. After washing three times with TBST, the membrane was incubated with a 1:500 dilution of mouse anti-rLP78 polyclonal antibody at 37°C for 2 h. After washing three times with TBST, a 1:10,000 dilution of HRP-conjugated goat anti-mouse IgG (Boster, Hubei, China) was added and incubated at 37°C for 1 h.

Binding activities of rLP78 to human fibronectin (hFn) and human plasminogen (hPlg)

The binding activities of rLP78 to hFn or hPlg were determined by ELISA and western blotting. For ELISA analysis, microtiter ELISA plates were coated with 100 μ L of hFn or hPlg (Sigma-Aldrich, Burlington, MA, United States) at 5 μ g/mL, and incubated overnight at 4°C. After blocking with 5% skim milk, 100 μ L of rLP78 at different concentrations (ranging from 1.56 μ g/mL to 100 μ g/mL) was added and incubated for 2 h at 37°C. After being washed with PBST, the plates were treated with 100 μ L of anti-His-tag monoclonal antibody (1:1,000 dilution) (Boster, Hubei, China), followed by 100 μ L of HRP-conjugated goat anti-mouse IgG (1:10,000 dilution) (Boster, Hubei, China). Finally, the optical density (OD) values of the solutions were measured at 450 nm.

For western blotting, rLP78 was separated by 12% SDS-PAGE and transferred onto PVDF membranes. After blocking with 10% skim milk, the membrane was incubated with 5 μ g/mL hFn or hPlg, followed by incubation with rabbit anti-fibronectin antibody or rabbit anti-plasminogen antibody (1:1,000 dilution) (Boster, Hubei, China) as the primary antibody, and HRP-conjugated goat anti-rabbit IgG (1:10,000 dilution) (Boster, Hubei, China) as the secondary antibody.

Sensitivity, specificity, and reproducibility of rLP78-based iELISA

For the development of rLP78-based iELISA, the optimal coating concentration of rLP78 and optimal dilution ratios of the tested sera were determined by a checkerboard titration method. The cut-off value of iELISA was determined by testing 83 serum samples collected from chickens that were free of *M. synoviae* infection. The S/P cut-off value was expressed as the mean S/P of 83 negative sera samples plus 3 standard deviations (SDs) to ensure 99% confidence for negative sera samples in this range.

To determine the sensitivity and specificity of rLP78-based iELISA, a total of 170 serum samples collected from chickens with known *M. synoviae* infection status were detected using both rLP78-based iELISA and a commercial ELISA kit (IDEXX, Westbrook,

Maine, USA). The sensitivity and specificity of rLP78-based iELISA were calculated relative to those of the commercial ELISA kit. To determine the lowest detection limit, three serum samples (HI titer, 1:128) were serially diluted 2-fold from 1:100 to 1:51,200, and cross-reactivity of rLP78-based iELISA with positive sera against other avian pathogens, including *M. gallisepticum*, *Hpg*, NDV, AIV, IBV, and IBDV, was measured.

The reproducibility of rLP78-based iELISA was evaluated by testing 10 serum samples (five positive and five negative samples). Within-run precision was assessed in three plates in one run, and between-run precision was assessed in three runs. The mean OD, SD, and coefficient of variation (CV) were calculated for each test.

Detection of antibody response against *Mycoplasma synoviae* in experimentally infected and immunized chickens

To investigate the antibody response against *M. synoviae* in chickens, 135 sequential chicken serum samples were detected using rLP78-based iELISA and a commercial ELISA kit (IDEXX, Westbrook, Maine, United States). Among the 135 serum samples, 90 samples were collected from 10 chickens infected with *M. synoviae* W1 (1×10^8 CCU/mL) via tracheal routine, whereas 45 serum samples were collected from 5 chickens immunized with the commercial inactivated *M. synoviae* vaccine (YBF-MS1 strain) (Yebio Bioengineering, co., Ltd. of Qingdao, China) via muscular routine. The samples were collected at 0, 3, 7, 10, 14, 21, 28, 42, and 60 days after challenge or immunization.

Statistical analysis

Statistical analyses were performed using IBM SPSS Statistics 20 (Armonk, NY, United States). Values given in the text are the mean \pm SD from the experiment. Graphs were prepared in GraphPad Prism 8.0 (San Diego, CA, United States).

Results

Bioinformatic analysis

The full length of *lp78* gene in *M. synoviae* strain MS-H was 2,310 bp. The ORF was predicted to encode a 770-amino-acid protein with a molecular mass of 84 kDa containing six Trp residues (positions 53, 86, 264, 415, 610, 645), all encoded by TGA codons. The LP78 protein sequence was predicted to possess a signal peptide (cleavage site between amino acid position 24 and 25), but lack a classical transmembrane domain, and be an outer membrane protein. Comparison of the LP78 protein sequences in the databases found identities of 98.7% with strain 53 (AAZ43746.2), 97.4% with strain WVU1853 (AAZ43746.2), native strains SD2 (UZW64787.1), and HN01 (QGL45032.1), and 99.3% with native strains FJ-01 (QXV99750.1) and ZX313 (UZW64085.1). LP78 was predicted to have an antigenicity score of 0.643 (the threshold score for antigenicity is 0.4), and an adhesion score of 0.785 (the threshold score for adhesion is 0.51).

Purification and identification of rLP78

The recombinant protein was purified using the Ni-NTA His-Bind® Resin column and a band with a molecular weight of 80 kDa was observed in the elution (Figure 1A). In addition, the recombinant protein was quantified via western blotting using an anti-His-tag monoclonal antibody (Figure 1B) and mouse anti-*M. synoviae* sera (Figure 1C). The concentration of the recombinant protein was estimated to be 1.5 mg/mL.

Conservation of LP78 in different *Mycoplasma synoviae* field strains

The conservation of LP78 was identified by PCR and western blotting. As shown in Figure 2A, a fragment of 2,235 bp was detected from the five *M. synoviae* field strains by PCR. After sequencing, a high identity (98.7–97.4%) was found between the five *M. synoviae* strains and strain MS-H. In addition, an 80-kDa protein band was specifically recognized by mouse anti-rLP78 polyclonal antibodies in the five strains (Figure 2B). The bands were in accordance with the theoretical molecular mass of rLP78, which indicated the LP78 was expressed by all strains examined.

Subcellular localization of LP78 in *Mycoplasma synoviae*

Western blotting and IFA was performed to determine the distribution of LP78 in *M. synoviae* using mouse anti-rLP78 polyclonal

antibody. Western blotting showed that LP78 was found to be located both on the membrane and in the cytoplasm of *M. synoviae* (Figure 3A). In particular, a stronger band was observed for cytoplasmic proteins than for membrane proteins, indicating that LP78 was primarily located in the cytoplasm of *M. synoviae*. IFA demonstrated that *M. synoviae* cells stained with fluorescein isothiocyanate when incubated with mouse anti-rLP78 polyclonal antibody, but no when incubated with pre-immune serum (Figure 3B).

Adherence inhibition of *Mycoplasma synoviae* to DF-1 cells using antibodies against rLP78

The antibody inhibition assay was carried out to assess the contribution of LP78 in *M. synoviae* cytoadhesion. Compared with the nonimmune serum group, the number of *M. synoviae* attached to DF-1 cells was greatly reduced after treatment with anti-rLP78 serum ($p < 0.05$) (Figure 4). The result implied that LP78 plays an important part in *M. synoviae* adherence to DF-1 cells.

Adherence of rLP78 to DF-1 cells

The adherence of rLP78 to DF-1 cells was visualized by IFA. As shown in Figure 5A, rLP78 was able to adhere to DF-1 cells. No adherence was observed for the control (Figure 5B). Additionally, rLP78 adhered to DF-1 cells was effectively inhibited by mouse anti-rLP78 serum (Figure 5C), whereas nonimmunized mouse serum did not inhibit adherence to DF-1 cells (Figure 5D).

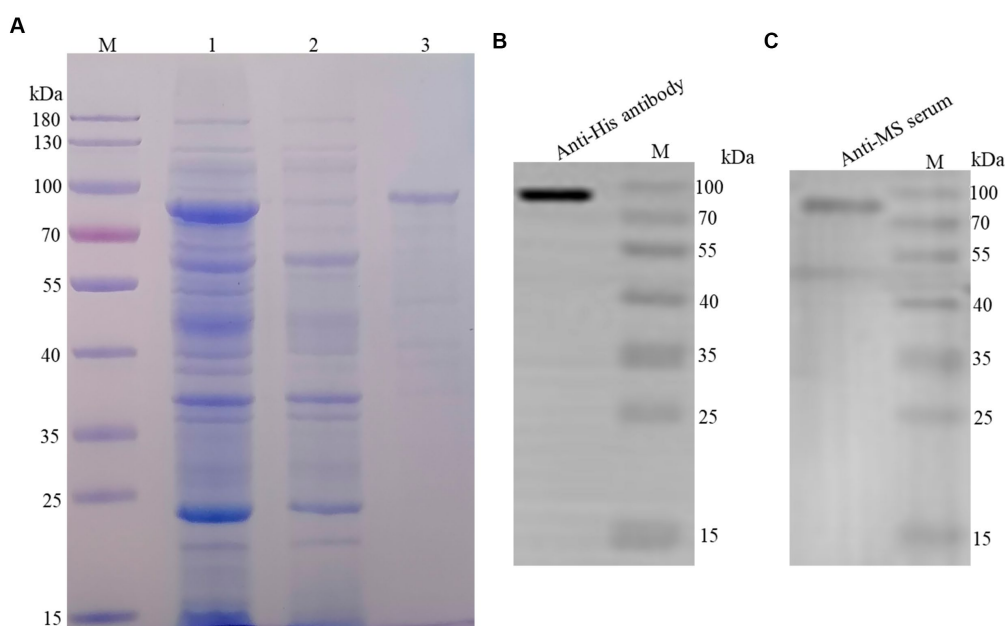


FIGURE 1

Purification and identification of rLP78. (A) SDS-PAGE analysis of the purification of rLP78 by Ni²⁺ column. Lane M, protein molecular weight marker; Lane 1, the supernatant of the whole bacterial lysate; Lane 2, elution with 50 mM of imidazole; Lane 3, elution with 500 mM of imidazole. (B) Western blotting analysis of the purified rLP78 using anti-His-tag monoclonal antibody. (C) Western blotting analysis of the purified rLP78 using mouse anti-*M. synoviae* polyclonal antibodies.

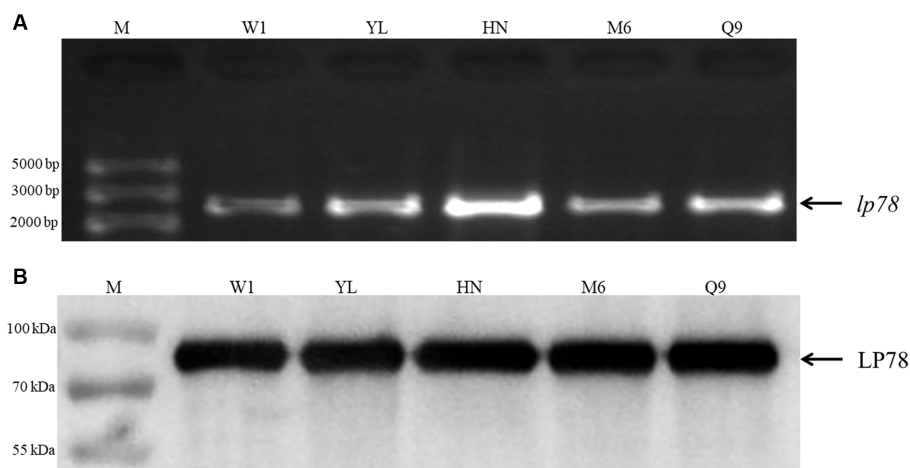


FIGURE 2

Identification of LP78 in different *M. synoviae* strains. (A) Amplification of *lp78* gene in different *M. synoviae* strains. Genomic DNA was extracted from *M. synoviae* cultures and used as templates. (B) Immunoblot analysis of the expression of LP78 in different *M. synoviae* strains. Whole cell protein from different *M. synoviae* strains cells were separated by 12% SDS-PAGE and transferred to a PVDF membrane. The membrane was incubated with mouse anti-rLP78 polyclonal antibody, followed by HRP-conjugated goat anti-mouse antibody.

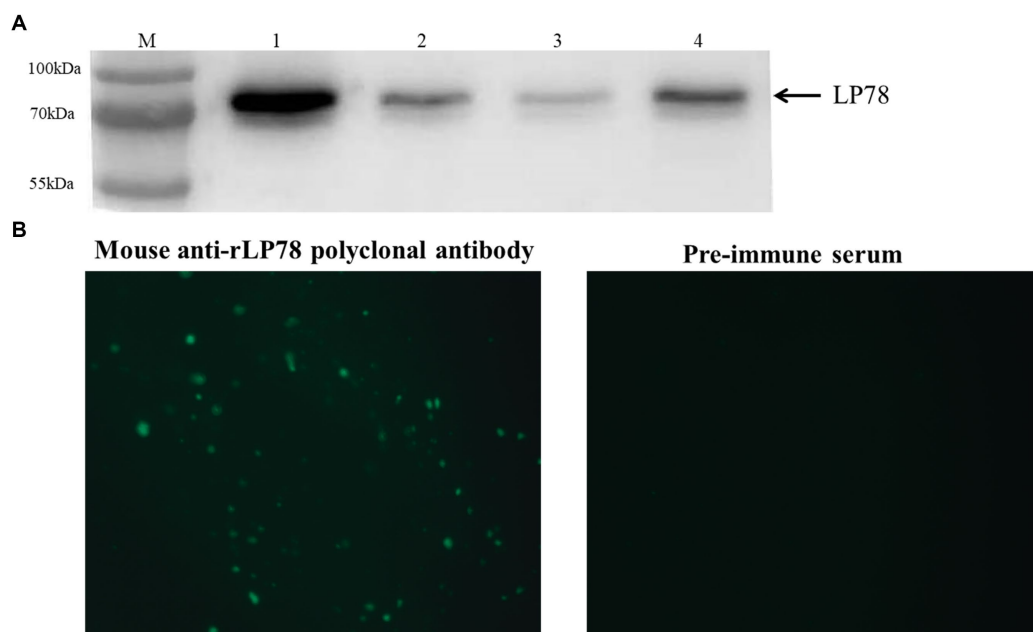


FIGURE 3

Subcellular localization of LP78 in *M. synoviae* by western blotting and IFA using mouse anti-rLP78 serum. (A) Western blotting analysis. Lanes 1: rLP78; Lane 2: Cytosolic proteins; Lane 3: Membrane proteins; Lane 4: Total cellular proteins. (B) IFA of *M. synoviae* cells incubated with mouse anti-rLP78 polyclonal antibody and pre-immune serum.

Binding of rLP78 to cell membrane proteins

The binding activity of rLP78 to DF-1 cells was quantitatively determined by MPAA and western blotting. As shown in Figure 6A, rLP78 bound to the membrane and cytosolic proteins of DF-1 cells in a dose-dependent manner from 6.25 µg/mL to 100 µg/mL ($p < 0.05$). The binding was significantly inhibited by anti-rLP78 serum in a

dose-dependent manner (Figure 6B) ($p < 0.05$). When the antibody levels decreased, the OD_{450nm} values gradually increased. In the membrane protein incubated with mouse anti-rLP78 polyclonal antibody, two bands were observed: one between 35 kDa and 40 kDa and the other between 55 kDa and 70 kDa (Figure 7A). The two bands were also found in the cytosolic protein (Figure 7A). The DF1 cell membrane and cytosolic proteins were successfully extracted, with no contamination from other fractions (Figures 7B,C).

Binding ability of rLP78 to hFn and hPlg

The binding ability of rLP78 to hFn and hPlg was determined by ELISA and western blotting. ELISA results showed that rLP78 bound to immobilized hFn (Figure 8A) or hPlg (Figure 8B) in a

dose-dependent manner and the OD_{450nm} values of rLP78 were significantly higher than BSA ($p < 0.05$). To further confirm the specific interaction between rLP78 and hFn or hPlg, western blotting was performed. After rLP78 was transferred to PVDF membranes, hFn or hPlg was added. The bound hFn or hPlg was detected with rabbit anti-fibronectin antibody (Figure 8C) or rabbit anti-plasminogen antibody (Figure 8D) at the site corresponding to the band of purified rLP78. No obvious interactions between hFn or hPlg and BSA were observed.

Sensitivity, specificity, and reproducibility of rLP78-based iELISA

The checkerboard titration results showed that the optimal coating concentration of rLP78 was 1 µg/mL and the optimal dilution ratios of the tested sera were 1:600 for rLP78-based iELISA (Supplementary Figure S3). The cut-off value of iELISA was calculated to be 0.341. Serum samples from infected or immunized chickens were considered positive for *M. synoviae* infection when the S/p value was ≥ 0.341 ; otherwise, they were considered negative.

The sensitivity and specificity of rLP78-based iELISA and a commercial ELISA kit were compared in 170 clinical serum samples. Of the 119 positive serum samples identified using the commercial kit, 102 samples were classified as positive using rLP78-based iELISA (Table 1). Of the 51 negative serum samples identified using the

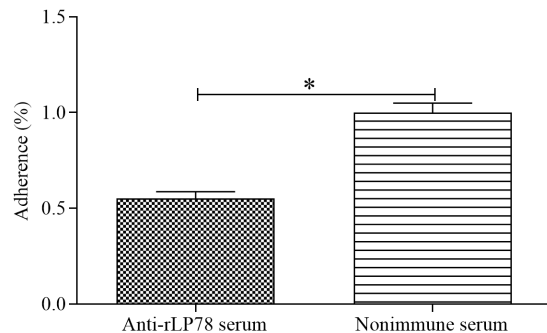


FIGURE 4
Adherence inhibition of *M. synoviae* to DF-1 cells by anti-rLP78 serum. *M. synoviae* cells were pre-incubated with anti-rLP78 serum, and then the mixtures were added to DF-1 cells. The amounts of bound *M. synoviae* were determined by qPCR. Adhesion rate: number of *M. synoviae* in the cells incubated with anti-rLP78 serum/number of *M. synoviae* in the cells incubated with nonimmune serum. Data are expressed as the mean \pm SD of samples in triplicate. * $p < 0.05$.

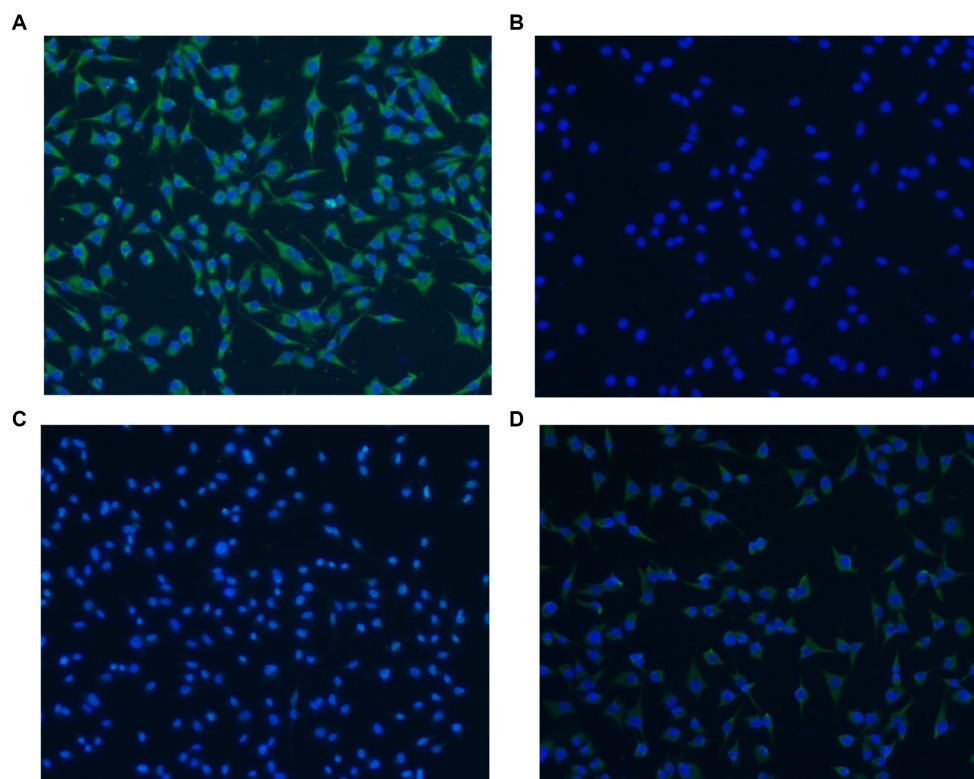


FIGURE 5
Adherence of rLP78 to DF-1 cells detected by IFA. DF-1 cells were incubated with rLP78 (A) or pET-28a control protein (B). Bound proteins were detected by an anti-His-tagged monoclonal antibody and immunostained with FITC-conjugated goat anti-mouse IgG. (C) Mouse anti-rLP78 serum inhibited rLP78 adherence. (D) Nonimmunized mouse serum showed no inhibition of rLP78 adherence to DF-1 cells. Cell nuclei were labeled with 4,6-diamidino-2-phenylindole (DAPI).

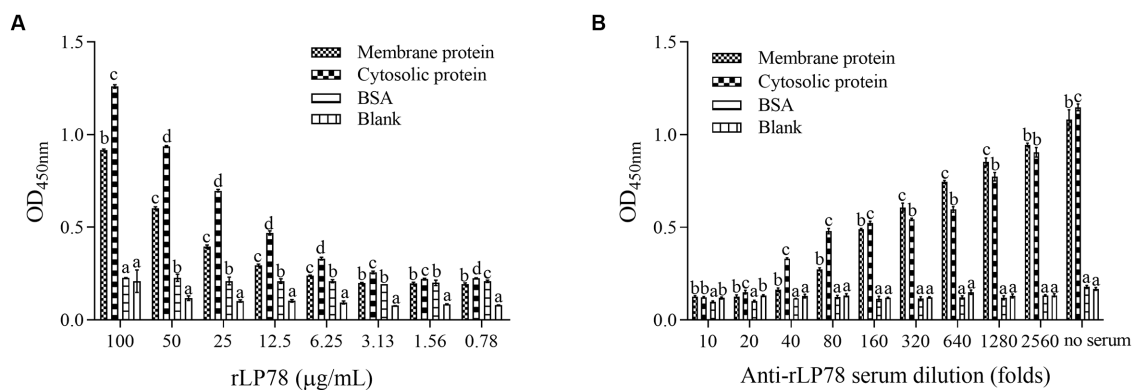


FIGURE 6

Activity of rLP78 to adhere to membrane proteins of DF-1 cells. Microtiter ELISA plates were coated with the extracted membrane protein, cytosolic protein or BSA. (A) Different concentrations of rLP78 were added to individual wells. Bound proteins were detected using a mouse anti-His-tag monoclonal antibody. (B) Adherence of rLP78 (100 µg/mL) to membrane proteins of DF-1 cells was inhibited by mouse anti-LP78 serum and further detected using goat anti-mouse IgG. Bars represent the mean \pm standard deviation of the OD_{450nm} values of samples in triplicate. The differences were compared between each group. The same letter indicates no obvious difference ($p > 0.05$); different letters indicate a significant difference ($p < 0.05$).

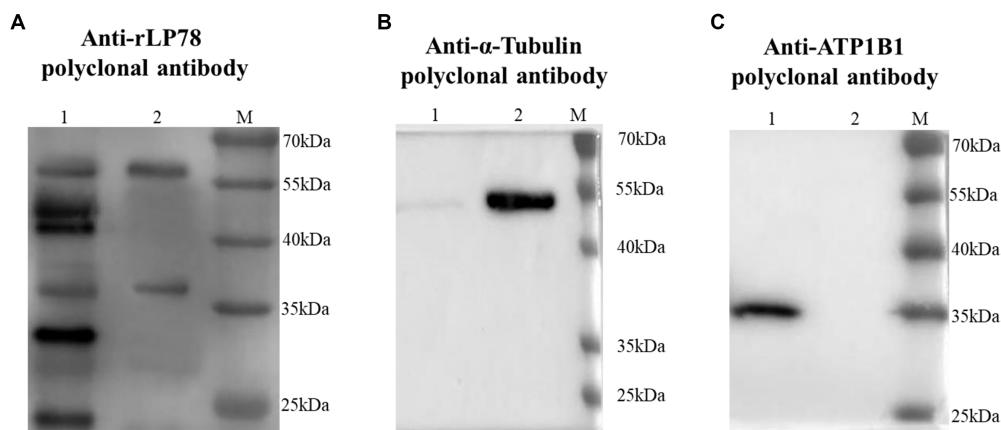


FIGURE 7

Screening of DF1 cells membrane proteins that bound to rLP78 by western blotting. DF1 cells cytosolic protein (lane 1) and cells membrane protein (lane 2) were transferred to PVDF membranes and incubated with rLP78 (20 µg/mL). Subsequently, the membranes were incubated with mouse anti-rLP78 polyclonal antibody (A), rabbit anti-α-Tubulin polyclonal antibody (B), and rabbit anti-ATP1B1 polyclonal antibody (C).

commercial kit, 48 samples were classified as negative using rLP78-based iELISA (Table 1). The results of rLP78-based iELISA and the commercial ELISA kit were inconsistent in 20 samples. Therefore, the total agreement between rLP78-based iELISA and the commercial ELISA kit was 88.2%, with the sensitivity and specificity of rLP78-based iELISA being 85.7 and 94.1%, respectively. For different dilutions of positive sera (HI titer, 1:128), positive reactions were observed at the dilution of 1:6,400 in rLP78-based iELISA and at the dilution of 1:12,800 or 1:25,600 in the commercial kit (Figure 9A).

To verify the cross-reactivity of rLP78-based iELISA, it was used to detect sera against *M. gallisepticum*, *Hpg*, AIV, NDV, IBV, and IBDV. All samples yielded a negative result, indicating that rLP78-based iELISA had no cross-reactivity with the tested sera (Figure 9B). The reproducibility of rLP78-based iELISA was determined by calculating the CV of the OD values of 10 serum samples. The inter-assay CV of the 10 samples ranged from 4.2 to 6.8%, whereas the intra-assay CV ranged from 3.1 to 8.9%.

Antibody response against *Mycoplasma synoviae* in experimentally infected and immunized chickens

To test the antibody response of iELISA, 90 infected serum samples and 45 immunized serum samples collected from chickens between 0 and 60 days were tested. The results of both rLP78-based iELISA and the commercial ELISA kit showed that the chickens seroconverted on day 7 after experimental infection, with a positive rate of 4/10 and 9/10, respectively (Figure 10A). All chickens seroconverted on day 10 after experimental infection and remained positive until day 60 after infection. In chickens immunized with the *M. synoviae* bacterin, the two ELISAs detected seroconversion on day 7 after immunization, with a positive rate of 1/5 for iELISA and 2/5 for the commercial kit (Figure 10B). Both ELISAs detected seroconversion at a positive rate of 5/5 on day 14 after immunization and remained positive until day 60 after immunization.

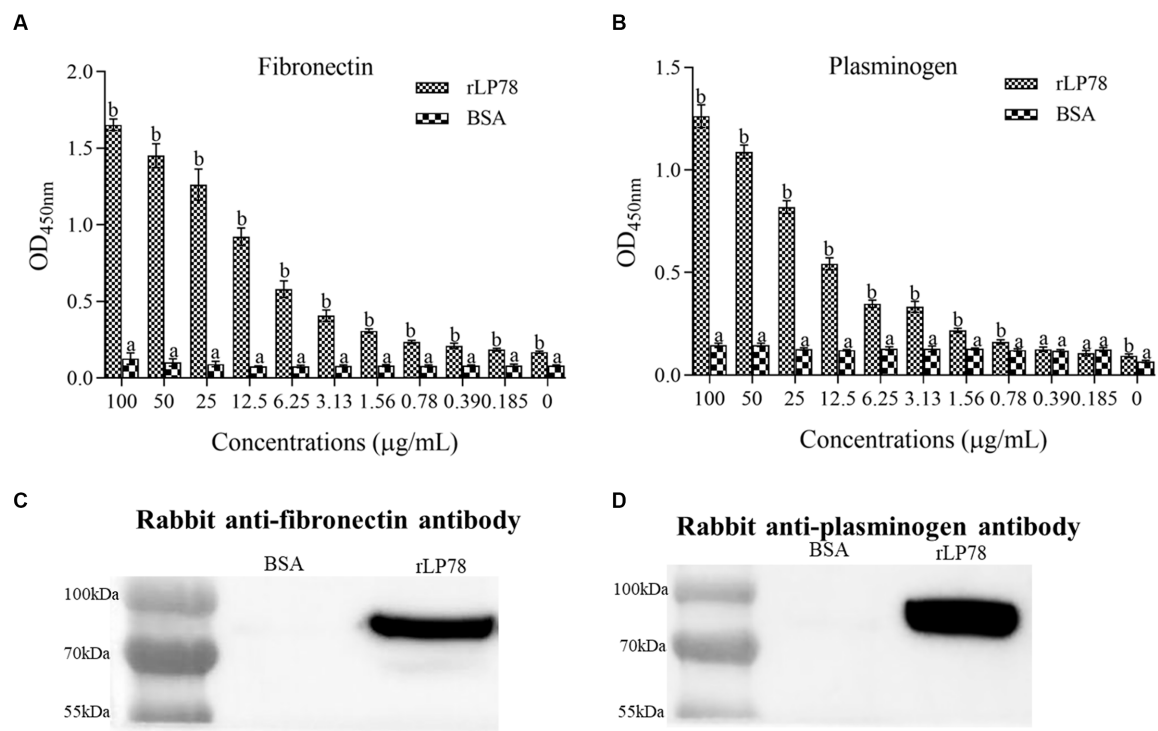


FIGURE 8 Binding ability of rLP78 to human fibronectin (hFn) and human plasminogen (hPlg). The binding ability of rLP78 to hFn (**A**) or hPlg (**B**) was identified by ELISA. The plates were coated with 5 µg/mL of hFn or hPlg. Different concentrations of rLP78 or BSA were added to individual wells. Bound proteins were detected using a mouse anti-His-tag monoclonal antibody. Bars represent the mean ± standard deviation of the OD values of samples in triplicate. The differences were compared between each group. The same letter indicates no obvious difference ($p > 0.05$); different letters indicate a significant difference ($p < 0.01$). Binding ability of rLP78 to hFn (**C**) or hPlg (**D**) was confirmed by western blotting. Bound hFn was determined by rabbit anti-hFn antibody or rabbit anti-plasminogen antibody. BSA was chosen as negative control.

TABLE 1 Determination of sensitivity and specificity of rLP78 iELISA.

		IDEXX ELISA		Sensitivity(%)	Specificity (%)	Accuracy(%)
		Positive	Negative			
rLP78 ELISA	Positive	102	3	85.7% (102/119)	94.1% (48/51)	88.2% (150/170)
	Negative	17	48			
	Total	119	51			

Discussion

In recent years, the incidence of *M. synoviae* infection has increased and led to serious economic losses in the poultry industry worldwide. Attachment of mycoplasmas to host cells is a crucial step in colonization and subsequent infection, which is predominantly mediated by membrane proteins and lipoproteins (Lockaby et al., 1999; Browning et al., 2011). Various membrane-associated proteins, including vlhA, enolase, PdhA and PdhB subunits, PdhD and NADH oxidase, are involved in *M. synoviae* cytoadhesion (Noormohammadi et al., 1997; Bao et al., 2014, 2021; Hu et al., 2022; Qi et al., 2022). *Mycoplasma* lipoproteins have been demonstrated to exert a variety of effects during infection and interaction with the hosts, including immunomodulatory, antigenic variation, transporter operation, and cytoadhesion (Athamna et al., 1997; Browning et al., 2011;

Christodoulides et al., 2018). LP78 belongs to P80 family lipoprotein with undefined functions.

Comparison of the LP78 protein sequences in the databases revealed a high level of identity (97.4 to 99.3%). The conservation was confirmed by detecting LP78 among different native field strains. In addition, high levels of antibodies against LP78 were found in the *M. synoviae*-infected chicken serum and field serum through LP78-based iELISA. The findings imply LP78 plays an important role during infection. Bioinformatics analysis demonstrated that LP78 is located on the cell membrane surface of *M. synoviae* with a signal peptide but lack membrane-spanning domains. Western blotting and IFA results in the current investigation revealed that LP78 is exposed to the surface. Other mycoplasmas surface-exposed proteins were also shown to be lack of classical membrane-spanning domains (May et al., 2006; Guo et al., 2017; Chen et al., 2018). In addition, LP78 was also

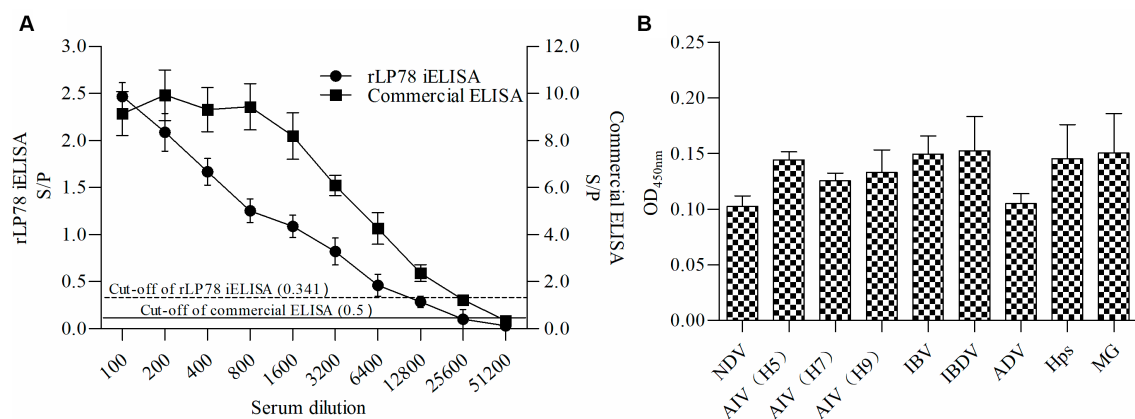


FIGURE 9

Sensitivity and specificity of rLP78 iELISA. **(A)** Determination of the largest dilution of positive chicken serum for anti-*M. synoviae* antibodies. The HI titer of chicken anti-*M. synoviae* serum was 1:128. **(B)** The cross-reactivity of rLP78 iELISA with antibodies against other avian pathogens, including NDV, AIV (H5, H7, H9), IBV, IBDV, ADV, Hps, and MG. Bars represent the mean \pm standard deviations of the S/p values or OD_{450nm} values of samples ($n = 3$). The full line and dashed line represent the cut-off of rLP78-based iELISA ($S/p \geq 0.341$ is positive, otherwise, is negative) and commercial ELISA ($S/p > 0.5$ is positive, otherwise, is negative), respectively.

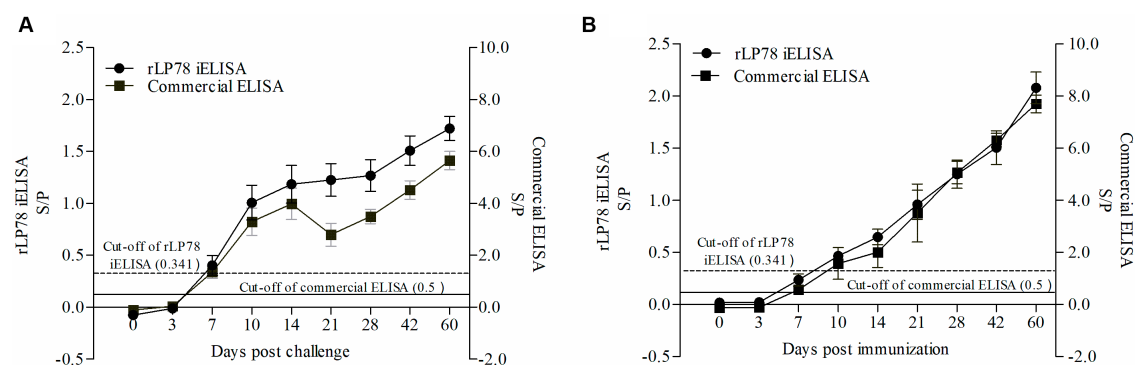


FIGURE 10

Detection of antibody response against *M. synoviae*. **(A)** Serum samples were collected from 10 chickens infected by *M. synoviae* at 0–60 days after inoculation. **(B)** Serum samples were collected from 5 chickens immunized with inactivated *M. synoviae* vaccine at 0–60 days after inoculation. The full line and dashed line represent the cut-off of rLP78-based iELISA ($S/p \geq 0.341$ is positive, otherwise, is negative) and commercial kit ($S/p > 0.5$ is positive, otherwise, is negative), respectively. Bars represent the mean \pm standard deviations of the S/p values of samples in each group.

found in cytoplasmic fractions, it will be meaningful to investigate its functions in the cytoplasm. A signal peptide was found in LP78 by bioinformatics analysis, which suggests LP78 has secretory proteins characteristics. However, it has not been verified that LP78 is a secreted protein in a previous study (Rebollo Couto et al., 2012).

Although *M. synoviae* is mostly considered to be an extracellular pathogen, it can adhere to and subsequently invade erythrocytes, synovial sheath cells, and chicken embryonic fibroblast cells (Dusanic et al., 2009; Xu et al., 2020). Adherence of rLP78 to DF-1 cells was visualized by IFA, and the adherence was effectively inhibited by anti-rLP78 serum. The MPAA results showed that rLP78 bound to the membrane proteins of DF-1 cells in a dose-dependent manner and that the binding was inhibited by anti-rLP78 serum, further supporting the adherence. Furthermore, the adherence of *M. synoviae* to DF-1 cells was significantly reduced following pretreatment with anti-rLP78 serum. These provide additional evidences that LP78 contributes to the adhesion of *M. synoviae* to cells. However,

anti-rLP78 serum only partially prevented adhesion to DF-1 cells. The fact that mycoplasmas cytodherence is a complex, multifactorial process involving numerous membrane proteins and cytoskeletal elements (Razin and Jacobs, 1992). In addition to LP78, other proteins have also been proven to contribute to the adhesion process of *M. synoviae*, such as vlhA, enolase, PdhA, PdhB, PdhD and NADH oxidase (Noormohammadi et al., 1997; Bao et al., 2014, 2021; Hu et al., 2022; Qi et al., 2022). It has been established that vlhA facilitates *M. synoviae* attachment to sialylated receptors on host cells (May et al., 2014). Further research should be carried out on the receptors that are mediated by LP78.

Although *M. synoviae* has been shown to invade host cells, its mechanism remains unclear. In previous studies, enolase, PdhA, PdhB, PdhD and NADH oxidase from *M. synoviae* have been identified as FnBPs and PlgBPs (Bao et al., 2014, 2021; Hu et al., 2022; Qi et al., 2022). The binding of FnBPs to Fn mediates not only the adherence of microorganism to extracellular matrices but also to the

surface of host cells. It is now established that Fn can act as a molecular bridge between the FnBPs on the surface of microorganisms and the integrin on host cells (Henderson et al., 2011). This complex induces integrin clustering and triggers the actin cytoskeleton to be reorganized, which will assist in the internalization of microorganisms and facilitate cell invasion (Henderson et al., 2011). Additionally, the blocking of Fn significantly decreases the adherence of microorganisms to host cells (Yu et al., 2018). Apart from degradation of fibrin clot in fibrinolysis, plasmin degrades various ECMs and connective tissue components, including fibronectin and laminin (Bhattacharya et al., 2012). Traditionally, the activation pathway of Plg depends on tissue plasminogen activator (tPA) and urokinase (uPA). A few bacterial species, such as *streptococci*, can produce activator, which may be employed to activate the host Plg (Verhamme et al., 2015). In most bacterial species, Plg can be recruited from the surrounding environment to the bacterial surface and then promoted to be converted into plasmin (Raymond et al., 2015). In the present study, LP78 was identified to be PlgBPs. Whether the binding of LP78 would increase the susceptibility of Plg to be activated by tPA should be investigated further. The finding will contribute to understanding the mechanism of *M. synoviae* cell invasion.

Since LP78 is an immunodominant antigen found on the surface of *M. synoviae*, it may be used as a diagnostic antigen. Owing to its high sensitivity and ease of use, ELISA is an efficient alternative to SPA and HI tests for screening large numbers of serum samples. In a study, an ELISA was developed based on a protein fraction (p46–52) that was extracted from the Triton X-114 detergent phase and further purified via ion exchange chromatography (Gurevich et al., 1995). The results of this ELISA were highly consistent with those of the SPA test (Gurevich et al., 1995). A Dot-ELISA was developed based on the p41 antigen purified via SDS-PAGE, and was found to be more sensitive than HI (Avakian and Kleven, 1990). Although ELISA based on purified native antigens are sensitive, the production of sufficient and consistent antigens is expensive. Alternatively, an iELISA developed using recombinant MSPB protein expressed in *E. coli* showed good performance in the detection of anti-*M. synoviae* antibodies (Noormohammadi et al., 1999). In this study, we established and evaluated rLP78-based iELISA. Compared with a commercial ELISA kit, rLP78-based iELISA demonstrated less sensitivity in the detection of *M. synoviae*-positive serum samples. This result was consistent with that of the detection of different dilutions of *M. synoviae*-positive sera. Positive reactions were observed at the maximum dilution of 1:6,400 in rLP78-based iELISA and at the maximum dilution of 1:12,800 and 1:25,600 in the commercial ELISA kit. However, rLP78-based iELISA could detect seroconversion in 4/10 chickens on day 7 after experimental infection, with all chickens showing positive reactions between 10 and 60 days. These findings indicate that rLP78-based iELISA can be used in the diagnosis of early-stage *M. synoviae* infection. No cross-reactivity of rLP78-based iELISA was observed with other poultry pathogens, especially *M. gallisepticum*-positive serum samples. Therefore, LP78 is a good candidate for the development of diagnostic tests for *M. synoviae* infection. The prevalence of *M. synoviae* infection in Chinese commercial poultry farms was investigated using rLP78-based iELISA. The total seropositive rate

of the tested samples was 58.77%, with the highest rate (74.91%) (Supplementary Table S2). A serological survey of *M. synoviae* infection was conducted in China during 2010–2015, and the seropositive rates in different provinces ranged from 24.70 to 57.20% (Xue et al., 2017). The results suggest that *M. synoviae* infection is a serious concern in China at present. In addition to routine serological monitoring, biosecurity, vaccination, and antibiotic administration are important measures for the control of *M. synoviae* infection (Kleven, 2008).

Conclusion

In summary, the present study demonstrated that LP78 is a conservative, surface-exposed *M. synoviae* putative adhesion with Fn/Plg-binding activity, making it a good candidate for the development of diagnostic tests for *M. synoviae* infection.

Data availability statement

Publicly available datasets were analyzed in this study. This data can be found at: <https://www.ncbi.nlm.nih.gov/nucleotide/CP021129>.

Ethics statement

The animal study was approved by the Ethics Committee of Animal Experimentation of Northwest A&F University. The study was conducted in accordance with the local legislation and institutional requirements.

Author contributions

SH: Data curation, Formal analysis, Investigation, Writing – original draft. YW: Data curation, Formal analysis, Software, Writing – review & editing. LW: Supervision, Writing – review & editing. WC: Data curation, Formal analysis, Investigation, Writing – review & editing. BW: Supervision, Writing – review & editing. JF: Data curation, Formal analysis, Investigation, Writing – review & editing. XH: Data curation, Writing – review & editing. XQ: Supervision, Writing – review & editing. JW: Conceptualization, Funding acquisition, Project administration, Writing – review & editing.

Funding

The author(s) declare financial support was received for the research, authorship, and/or publication of this article. This research was supported by the National Natural Science Foundation of China [32172843].

Conflict of interest

The authors declare that the research was conducted in the absence of any commercial or financial relationships that could be construed as a potential conflict of interest.

Publisher's note

All claims expressed in this article are solely those of the authors and do not necessarily represent those of their affiliated

organizations, or those of the publisher, the editors and the reviewers. Any product that may be evaluated in this article, or claim that may be made by its manufacturer, is not guaranteed or endorsed by the publisher.

Supplementary material

The Supplementary material for this article can be found online at: <https://www.frontiersin.org/articles/10.3389/fmicb.2023.1335658/full#supplementary-material>

References

- Athamna, A., Rosengarten, R., Levisohn, S., Kahane, I., and Yogev, D. (1997). Adherence of *Mycoplasma gallisepticum* involves variable surface membrane proteins. *Infect. Immun.* 65, 2468–2471. doi: 10.1128/IAI.65.6.2468-2471.1997
- Avakian, A. P., and Kleven, S. H. (1990). Evaluation of sodium dodecyl sulfate-polyacrylamide gel electrophoresis purified proteins of *Mycoplasma gallisepticum* and *M. synoviae* as antigens in a dot-enzyme-linked immunosorbent assay. *Avian Dis.* 34, 575–584. doi: 10.2307/1591247
- Bao, S., Ding, X., Yu, S., Xing, X., and Ding, C. (2021). Characterization of pyruvate dehydrogenase complex E1 alpha and beta subunits of *Mycoplasma synoviae*. *Microb. Pathog.* 155:104851. doi: 10.1016/j.micpath.2021.104851
- Bao, S., Guo, X., Yu, S., Ding, J., Tan, L., Zhang, F., et al. (2014). *Mycoplasma synoviae* enolase is a plasminogen/fibrinogen binding protein. *BMC Vet. Res.* 10:223. doi: 10.1186/s12917-014-0223-6
- Bercic, R. L., Slavec, B., Lavric, M., Narat, M., Bidovec, A., Dovc, P., et al. (2008). Identification of major immunogenic proteins of *Mycoplasma synoviae* isolates. *Vet. Microbiol.* 127, 147–154. doi: 10.1016/j.vetmic.2007.07.020
- Bhattacharya, S., Ploplis, V. A., and Castellino, F. J. (2012). Bacterial plasminogen receptors utilize host plasminogen system for effective invasion and dissemination. *J. Biomed. Biotechnol.* 2012:482096. doi: 10.1155/2012/482096
- Browning, G. F., Marends, M. S., Noormohammadi, A. H., and Markham, P. F. (2011). The central role of lipoproteins in the pathogenesis of mycoplasmoses. *Vet. Microbiol.* 153, 44–50. doi: 10.1016/j.vetmic.2011.05.031
- Chagnot, C., Listrat, A., Astruc, T., and Desvaux, M. (2012). Bacterial adhesion to animal tissues: protein determinants for recognition of extracellular matrix components. *Cell. Microbiol.* 14, 1687–1696. doi: 10.1111/cmi.12002
- Chen, X., Huang, J., Zhu, H., Guo, Y., Khan, F. A., Menghwar, H., et al. (2018). P27 (MBOV_RS03440) is a novel fibronectin binding adhesin of *Mycoplasma bovis*. *Int. J. Med. Microbiol.* 308, 848–857. doi: 10.1016/j.ijmm.2018.07.006
- Christodoulides, A., Gupta, N., Yacoubian, V., Maithel, N., Parker, J., and Kelesidis, T. (2018). The role of lipoproteins in *Mycoplasma*-mediated immunomodulation. *Front. Microbiol.* 9:1682. doi: 10.3389/fmicb.2018.01682
- Cisneros-Tamayo, M., Kempf, I., Coton, J., Michel, V., Bougeard, S., De Boisseson, C., et al. (2020). Investigation on eggshell apex abnormality (EAA) syndrome in France: isolation of *Mycoplasma synoviae* is frequently associated with *Mycoplasma pullorum*. *BMC Vet. Res.* 16:271. doi: 10.1186/s12917-020-02487-0
- Cloward, J. M., and Krause, D. C. (2009). *Mycoplasma pneumoniae* J-domain protein required for terminal organelle function. *Mol. Microbiol.* 71, 1296–1307. doi: 10.1111/j.1365-2958.2009.06602.x
- Cortes, V., Sevilla-Navarro, S., Garcia, C., Tudon, A., Marin, C., and Catala-Gregori, P. (2021). Seroprevalence and prevalence of *Mycoplasma synoviae* in laying hens and broiler breeders in Spain. *Poult. Sci.* 100:100911. doi: 10.1016/j.psj.2020.11.076
- Dusanic, D., Bercic, R. L., Cizelj, I., Salmic, S., Narat, M., and Bencina, D. (2009). *Mycoplasma synoviae* invades non-phagocytic chicken cells in vitro. *Vet. Microbiol.* 138, 114–119. doi: 10.1016/j.vetmic.2009.02.014
- Ferberwee, A., De Wit, S., and Dijkman, R. (2021). Clinical expression, epidemiology, and monitoring of *Mycoplasma synoviae* immunogenic surface proteins and their potential use as antigens in the enzyme-linked immunosorbent assay. *Avian Pathol.* 51, 2–18. doi: 10.1080/03079457.2021.1944605
- Guo, Y., Zhu, H., Wang, J., Huang, J., Khan, F. A., Zhang, J., et al. (2017). TrmFO, a fibronectin-binding adhesin of *Mycoplasma bovis*. *Int. J. Mol. Sci.* 18:1732. doi: 10.3390/ijms18081732
- Gurevich, V. A., Ley, D. H., Markham, J. F., Whithear, K. G., and Walker, I. D. (1995). Identification of *Mycoplasma synoviae* immunogenic surface proteins and their potential use as antigens in the enzyme-linked immunosorbent assay. *Avian Dis.* 39, 465–474. doi: 10.2307/1591797
- Henderson, B., Nair, S., Pallas, J., and Williams, M. A. (2011). Fibronectin: a multidomain host adhesin targeted by bacterial fibronectin-binding proteins. *FEMS Microbiol. Rev.* 35, 147–200. doi: 10.1111/j.1574-6976.2010.00243.x
- Higgins, P. A., and Whithear, K. G. (1986). Detection and differentiation of *Mycoplasma gallisepticum* and *M. synoviae* antibodies in chicken serum using enzyme-linked immunosorbent assay. *Avian Dis.* 30, 160–168. doi: 10.2307/1590628
- Hopkins, S. R., and Yoder, H. W. Jr. (1982). Influence of infectious bronchitis strains and vaccines on the incidence of *Mycoplasma synoviae* airsacculitis. *Avian Dis.* 26, 741–752. doi: 10.2307/1589860
- Hu, Z., Li, H., Zhao, Y., Wang, G., Shang, Y., Chen, Y., et al. (2022). NADH oxidase of *Mycoplasma synoviae* is a potential diagnostic antigen, plasminogen/fibrinogen binding protein and a putative adhesin. *BMC Vet. Res.* 18:455. doi: 10.1186/s12917-022-03556-2
- Kleven, S. H. (2008). Control of avian mycoplasma infections in commercial poultry. *Avian Dis.* 52, 367–374. doi: 10.1637/8323-041808-Review.1
- Kleven, S. H., Fletcher, O. J., and Davis, R. B. (1975). Influence of strain of *Mycoplasma synoviae* and route of infection on development of synovitis or airsacculitis in broilers. *Avian Dis.* 19, 126–135. doi: 10.2307/1588963
- Krause, D. C., Leith, D. K., and Baseman, J. B. (1983). Reacquisition of specific proteins confers virulence in *Mycoplasma pneumoniae*. *Infect. Immun.* 39, 830–836. doi: 10.1128/iai.39.2.830-836.1983
- Krause, D. C., Leith, D. K., Wilson, R. M., and Baseman, J. B. (1982). Identification of *Mycoplasma pneumoniae* proteins associated with hemadsorption and virulence. *Infect. Immun.* 35, 809–817. doi: 10.1128/iai.35.3.809-817.1982
- Landman, W. J. M. (2014). Is *Mycoplasma synoviae* outrunning *Mycoplasma gallisepticum*? A viewpoint from the Netherlands. *Avian Pathol.* 43, 2–8. doi: 10.1080/03079457.2014.881049
- Li, Y., Wang, J., Liu, B., Yu, Y., Yuan, T., Wei, Y., et al. (2022). DnaK functions as a moonlighting protein on the surface of *Mycoplasma hyorhinis* cells. *Front. Microbiol.* 13:842058. doi: 10.3389/fmicb.2022.842058
- Liu, S., Li, Z., Lan, S., Hao, H., Jin, X., Liang, J., et al. (2023). LppA is a novel plasminogen receptor of *Mycoplasma bovis* that contributes to adhesion by binding the host extracellular matrix and annexin A2. *Vet. Res.* 54:107. doi: 10.1186/s13567-023-01242-1
- Lockaby, S. B., and Hoerr, F. J. (1999). Virulence of *Mycoplasma synoviae* in poultry: a review. *Worlds Poult. Sci. J.* 55, 175–185. doi: 10.1079/WPS19990012
- Lockaby, S. B., Hoerr, F. J., Lauerman, L. H., and Kleven, S. H. (1998). Pathogenicity of *Mycoplasma synoviae* in broiler chickens. *Vet. Pathol.* 35, 178–190. doi: 10.1177/030098589803500303
- Lockaby, S. B., Hoerr, F. J., Lauerman, L. H., Smith, B. F., Samoylov, A. M., Toivio-Kinnucan, M. A., et al. (1999). Factors associated with virulence of *Mycoplasma synoviae*. *Avian Dis.* 43, 251–261. doi: 10.2307/1592615
- May, M., Dunne, D. W., and Brown, D. R. (2014). A sialoreceptor binding motif in the *Mycoplasma synoviae* adhesin VlhA. *PLoS One* 9:e110360. doi: 10.1371/journal.pone.0110360
- May, M., Papazisi, L., Gorton, T. S., and Geary, S. J. (2006). Identification of fibronectin-binding proteins in *Mycoplasma gallisepticum* strain R. *Infect. Immun.* 74, 1777–1785. doi: 10.1128/IAI.74.3.1777-1785.2006
- Narat, M., Bencina, D., Kleven, S. H., and Habe, F. (1998). The hemagglutination-positive phenotype of *Mycoplasma synoviae* induces experimental infectious synovitis in chickens more frequently than does the hemagglutination-negative phenotype. *Infect. Immun.* 66, 6004–6009. doi: 10.1128/IAI.66.12.6004-6009.1998
- Noormohammadi, A. H., Browning, G. F., Jones, J., and Whithear, K. G. (2002). Improved detection of antibodies to *Mycoplasma synoviae* vaccine MS-H using an autologous recombinant MSPB enzyme-linked immunosorbent assay. *Avian Pathol.* 31, 611–617. doi: 10.1080/0307945021000024553

- Noormohammadi, A. H., Markham, P. F., Duffy, M. F., Whithear, K. G., and Browning, G. F. (1998). Multigene families encoding the major hemagglutinins in phylogenetically distinct mycoplasmas. *Infect. Immun.* 66, 3470–3475. doi: 10.1128/IAI.66.7.3470-3475.1998
- Noormohammadi, A. H., Markham, P. F., Markham, J. F., Whithear, K. G., and Browning, G. F. (1999). *Mycoplasma synoviae* surface protein MSPB as a recombinant antigen in an indirect ELISA. *Microbiology (Reading)* 145, 2087–2094. doi: 10.1099/13500872-145-8-2087
- Noormohammadi, A. H., Markham, P. F., Whithear, K. G., Walker, I. D., Gurevich, V. A., Ley, D. H., et al. (1997). *Mycoplasma synoviae* has two distinct phase-variable major membrane antigens, one of which is a putative hemagglutinin. *Infect. Immun.* 65, 2542–2547. doi: 10.1128/IAI.65.7.2542-2547.1997
- Olson, N. O., and Kerr, K. M. (1967). The duration and distribution of synovitis-producing agent in chickens. *Avian Dis.* 11, 578–585. doi: 10.2307/1588298
- Opitz, H. M., and Cyr, M. J. (1986). Triton X-100-solubilized *Mycoplasma gallisepticum* and *M. synoviae* ELISA antigens. *Avian Dis.* 30, 213–215. doi: 10.2307/1590636
- Opitz, H. M., Duplessis, J. B., and Cyr, M. J. (1983). Indirect micro-enzyme-linked immunosorbent assay for the detection of antibodies to *Mycoplasma synoviae* and *M. gallisepticum*. *Avian Dis.* 27, 773–786. doi: 10.2307/1590321
- Peng, K., Liao, Y., Li, X., Zeng, D., Ye, Y., Chen, L., et al. (2023). Vimentin is an attachment receptor for *Mycoplasma pneumoniae* P1 protein. *Microbiol. Spectr.* 11:e0448922. doi: 10.1128/spectrum.04489-22
- Qi, J., Wang, Y., Li, H., Shang, Y., Gao, S., Ding, C., et al. (2022). *Mycoplasma synoviae* dihydroliipoamide dehydrogenase is an immunogenic fibronectin/plasminogen binding protein and a putative adhesin. *Vet. Microbiol.* 265:109328. doi: 10.1016/j.vetmic.2021.109328
- Raviv, Z., and Kleven, S. H. (2009). The development of diagnostic real-time TaqMan PCRs for the four pathogenic avian mycoplasmas. *Avian Dis.* 53, 103–107. doi: 10.1637/8469-091508-Reg.1
- Raymond, B. B., and Djordjevic, S. (2015). Exploitation of plasmin(ogen) by bacterial pathogens of veterinary significance. *Vet. Microbiol.* 178, 1–13. doi: 10.1016/j.vetmic.2015.04.008
- Razin, S., and Jacobs, E. (1992). *Mycoplasma* adhesion. *J. Gen. Microbiol.* 138, 407–422. doi: 10.1099/00221287-138-3-407
- Rebollo Couto, M. S., Klein, C. S., Voss-Rech, D., and Terenzi, H. (2012). Extracellular proteins of *Mycoplasma synoviae*. *ISRN Vet. Sci.* 2012:802308. doi: 10.5402/2012/802308
- Thornton, G. A. (1978). A comparison of three *Mycoplasma synoviae* rapid plate agglutination antigens in experimental *M. synoviae* infection in chickens. *Avian Pathol.* 7, 123–130. doi: 10.1080/03079457808418264
- Vardaman, T. H., and Yoder, H. W. Jr. (1969). Preparation of *Mycoplasma synoviae* hemagglutinating antigen and its use in the hemagglutination-inhibition test. *Avian Dis.* 13, 654–661. doi: 10.2307/1588539
- Verhamme, I. M., Panizzi, P. R., and Bock, P. E. (2015). Pathogen activators of plasminogen. *J. Thromb. Haemost.* 13, S106–S114. doi: 10.1111/jth.12939
- Xiong, Q., Wang, J., Ji, Y., Ni, B., Zhang, B., Ma, Q., et al. (2016). The functions of the variable lipoprotein family of *Mycoplasma hyorhinis* in adherence to host cells. *Vet. Microbiol.* 186, 82–89. doi: 10.1016/j.vetmic.2016.01.017
- Xu, B., Liu, R., Ding, M., Zhang, J., Sun, H., Liu, C., et al. (2020). Interaction of *Mycoplasma synoviae* with chicken synovial sheath cells contributes to macrophage recruitment and inflammation. *Poult. Sci.* 99, 5366–5377. doi: 10.1016/j.psj.2020.08.003
- Xue, J., Xu, M. Y., Ma, Z. J., Zhao, J., Jin, N., and Zhang, G. Z. (2017). Serological investigation of *Mycoplasma synoviae* infection in China from 2010 to 2015. *Poult. Sci.* 96, 3109–3112. doi: 10.3382/ps/pex134
- Yu, Y., Wang, H., Wang, J., Feng, Z., Wu, M., Liu, B., et al. (2018). Elongation factor Thermo unstable (EF-Tu) moonlights as an adhesin on the surface of *Mycoplasma hyopneumoniae* by binding to fibronectin. *Front. Microbiol.* 9:974. doi: 10.3389/fmicb.2018.00974
- Zhao, G., Zhang, H., Chen, X., Zhu, X., Guo, Y., He, C., et al. (2017). *Mycoplasma bovis* NADH oxidase functions as both a NADH oxidizing and O(2) reducing enzyme and an adhesin. *Sci. Rep.* 7:44. doi: 10.1038/s41598-017-00121-y



OPEN ACCESS

EDITED BY

Christine Citti,
Institut National de recherche pour l'agriculture,
l'alimentation et l'environnement (INRAE),
France

REVIEWED BY

Rosario Gil,
University of Valencia, Spain
Isabel Gordo,
Gulbenkian Institute of Science (IGC), Portugal

*CORRESPONDENCE

Sébastien Rodrigue,
✉ Sebastien.Rodrigue@usherbrooke.ca

RECEIVED 29 November 2023

ACCEPTED 24 January 2024

PUBLISHED 09 February 2024

CITATION

Matteau D, Duval A, Baby V and Rodrigue S
(2024), *Mesoplasma florum*: a near-minimal
model organism for systems and
synthetic biology.
Front. Genet. 15:1346707.
doi: 10.3389/fgene.2024.1346707

COPYRIGHT

© 2024 Matteau, Duval, Baby and Rodrigue. This
is an open-access article distributed under the
terms of the [Creative Commons Attribution
License \(CC BY\)](#). The use, distribution or
reproduction in other forums is permitted,
provided the original author(s) and the
copyright owner(s) are credited and that the
original publication in this journal is cited, in
accordance with accepted academic practice.
No use, distribution or reproduction is
permitted which does not comply with these
terms.

Mesoplasma florum: a near-minimal model organism for systems and synthetic biology

Dominick Matteau¹, Anthony Duval¹, Vincent Baby² and
Sébastien Rodrigue^{1*}

¹Département de biologie, Université de Sherbrooke, Sherbrooke, QC, Canada, ²Centre de diagnostic
vétérinaire de l'Université de Montréal, Université de Montréal, Saint-Hyacinthe, QC, Canada

Mesoplasma florum is an emerging model organism for systems and synthetic biology due to its small genome (~800 kb) and fast growth rate. While *M. florum* was isolated and first described almost 40 years ago, many important aspects of its biology have long remained uncharacterized due to technological limitations, the absence of dedicated molecular tools, and since this bacterial species has not been associated with any disease. However, the publication of the first *M. florum* genome in 2004 paved the way for a new era of research fueled by the rise of systems and synthetic biology. Some of the most important studies included the characterization and heterologous use of *M. florum* regulatory elements, the development of the first replicable plasmids, comparative genomics and transposon mutagenesis, whole-genome cloning in yeast, genome transplantation, in-depth characterization of the *M. florum* cell, as well as the development of a high-quality genome-scale metabolic model. The acquired data, knowledge, and tools will greatly facilitate future genome engineering efforts in *M. florum*, which could next be exploited to rationally design and create synthetic cells to advance fundamental knowledge or for specific applications.

KEYWORDS

Mesoplasma florum, Mollicutes, synthetic biology, systems biology, minimal genome

Introduction

Mollicutes form a group of bacteria characterized by the absence of a cell wall and exceptionally small genomes. During the past decades, the field of molecular and cellular biology experienced significant advances, leading to a heightened interest for this class of bacteria. As new molecular data was generated, more particularly about the mycoplasmas, the idea that these microorganisms could actually be the simplest self-replicating life forms existing on Earth was becoming increasingly plausible (Morowitz and Tourtellotte, 1962; Morowitz, 1984). The minimal genome concept started to emerge: what is the smallest set of genes required for autonomous life, and what functions do they encode? Are there many or only one possible combination of genes composing a minimal genome? If we could understand the function of every single gene in a cell, we would have a better

Abbreviations: GEM, Genome-scale model; PEG, Polyethylene glycol; *oriC*, Chromosomal origin of replication; WGC, Whole genome cloning; iTSS, Internal transcription start site; ALE, Adaptive laboratory evolution.

comprehension of the most fundamental principles of life (Peterson et al., 2001; Glass et al., 2017; Lachance et al., 2019). Just as the study of the hydrogen atom was fundamental in developing the laws of quantum physics, examining the simplest autonomous cells presented itself as the most logical starting point for this endeavor (Morowitz and Tourtellote, 1962; Morowitz, 1984). An impressive number of Mollicutes species were isolated during the 1980s and 1990s, including many species associated with plants and insects (Whitcomb and Tully, 1995; Pettersson and Johansson, 2002). Unlike most mycoplasmas, which are typically parasitic, many of these species appeared to be commensals, coexisting in a mutually beneficial relationship with a variety of animal hosts. Many of these isolates also showed no strict requirement of sterols or cholesterol for growth *in vitro*, and were initially regrouped under the genus name *Acholeplasma* (Tully, 1979; Tully, 1983; Tully et al., 1990; Tully et al., 1993). This was the case for *Mesoplasma florum*, a bacterium that has become an interesting model organism for the fields of systems and synthetic biology.

What is *Mesoplasma florum*?

M. florum is a small (0.5–0.6 μm), ovoid, near-minimal and non-pathogenic bacterium of the Mollicutes class (Figure 1A) initially described for the first time as *Acholeplasma florum* in 1984 by McCoy and colleagues (McCoy et al., 1984). The species was named after its recovery site—the flowers of healthy plants found in Florida, United States. *M. florum* L1, the type strain of the species, was isolated from flowers of a lemon tree (*Citrus limon*) (McCoy et al., 1980; McCoy et al., 1984). Since *M. florum* grew in culture media without sterols it was originally classified in the genus *Acholeplasma* (Tully, 1979; Tully, 1983; Clark et al., 1986; Tully et al., 1990). However, this species was reassigned to the *Mesoplasma* genus in 1993 according to new physiological and molecular evidence, including phylogenetic clustering based on 16S rRNA sequence analysis (Tully et al., 1993). *M. florum* is in fact closely related to a phylogenetically distinct group of mycoplasmas called the mycoides cluster (Figure 1B). This cluster notably includes *Mycoplasma mycoides* and *Mycoplasma capricolum*, two well-known model organisms for the fields of systems and synthetic biology (Sirand-Pugnet et al., 2007; Glass et al., 2017; Lachance et al., 2019). Yet, in contrast to *M. mycoides* and *M. capricolum*, *M. florum* has never been associated with any disease, and no virulence factor has been identified in its genome. As for other members of the class Mollicutes, *M. florum* does not have a cell wall and its genome is particularly small, varying from 738,512 (BARC 787) to 830,640 bp (W20) depending on the exact strain, with an average GC content of about 27% (Baby et al., 2018b). *M. florum* genes are predominantly oriented according to the direction of DNA replication, frequently expressed as polygenic transcriptional units, and occupy most of the genome space, typical of bacterial genomes (Baby et al., 2018b; Matteau et al., 2020). This bacterium also uses an alternative genetic code (the *Mycoplasma* and *Spiroplasma* code) in which the canonical UGA stop codon rather codes for the incorporation of a tryptophan (Navas-Castillo et al., 1992). This distinctive feature is also present in mycoplasmas of the mycoides cluster as well as in the phylogenetically related Mollicute *Spiroplasma citri*, the causative agent of the Citrus stubborn disease (Saglio et al., 1973).

Among all previously isolated *M. florum* strains, the L1 strain is the most extensively studied. Compared to most Mollicutes, *M. florum* L1 shows a remarkably fast growth rate, corresponding to a doubling time of ~32 min at the optimal growth temperature (34°C) (Matteau et al., 2020). In comparison, *M. mycoides* subspecies *capri* has a doubling time of ~60 min in similar conditions (Gibson et al., 2010; Hutchison et al., 2016), whereas for *M. capricolum* subspecies *capricolum* and *Mycoplasma pneumoniae* this value is estimated to be around 90 min and 8–20 h, respectively (Seto and Miyata, 1998; Yus et al., 2009; Wodke et al., 2013). Since Mollicutes have experienced massive gene loss events through evolution, they have lost the capacity to synthesize many metabolites, resulting in an important simplification of their metabolism (Sirand-Pugnet et al., 2007). In *M. florum*, for example, most of the biosynthesis occurs through salvage pathways, and the energy production relies exclusively on glycolysis and fermentation since no respiratory system is present (Lachance et al., 2021). Consequently, this bacterium, as for most Mollicutes, requires a very rich medium to palliate its metabolic deficiencies *in vitro*. The most common growth medium for *M. florum* is the ATCC 1161, a complex and undefined medium containing horse serum, yeast extract, and heart infusion broth. Other similar media such as SP5 have also been used (Whitcomb et al., 1982; McCoy et al., 1984; Pollack and Williams, 1996; Matteau et al., 2015; Matteau et al., 2020; Baby et al., 2018a). *M. florum* L1 colonies display the typical Mollicutes “fried-egg” appearance on solid medium (Figure 1A) (McCoy et al., 1984; Tully et al., 1994; Labroussaa et al., 2016), and batch cultures growing in ATCC 1161 display the four typical bacterial growth phases (lag, exponential, stationary, and decline), reaching up to $\sim 10^{10}$ cells/mL at the end of the exponential growth phase (Matteau et al., 2015; Matteau et al., 2020). *M. florum* growth rate is however highly limited by the concentration of horse serum and yeast extract present in the medium, clearly demonstrating the dependance of this bacterium on pre-assembled building blocks for its metabolism (Lachance et al., 2021). The end of the exponential phase also coincides with an important drop in the pH of the medium, most likely due to the accumulation of lactate and acetate fermentation products (Pollack and Williams, 1996; Matteau et al., 2020; Lachance et al., 2021). This decrease in the medium’s pH is likely to be responsible for the progressive death of the *M. florum* cell population after the stationary phase. Indeed, no significant mortality is observed when the exponential phase is maintained using a continuous culture device (Matteau et al., 2015).

Where does *M. florum* primarily live?

M. florum is hypothesized to live primarily inside the gastrointestinal tract of insects, which would provide continuous access to complex nutrients such as sugars, lipids, peptides, and other metabolites required for growth. The continuous flow of the digestive tract would also prevent the accumulation of fermentation products and the possible acidification of the milieu, acting similar to a continuous culture device (Matteau et al., 2015). This natural habitat would also explain the presence of this bacterium on plant surfaces as insects would carry them from site to site and excrete the microbe through their feces (Whitcomb et al., 1982; McCoy et al., 1984; Tully et al., 1990). The extracellular polysaccharide layer

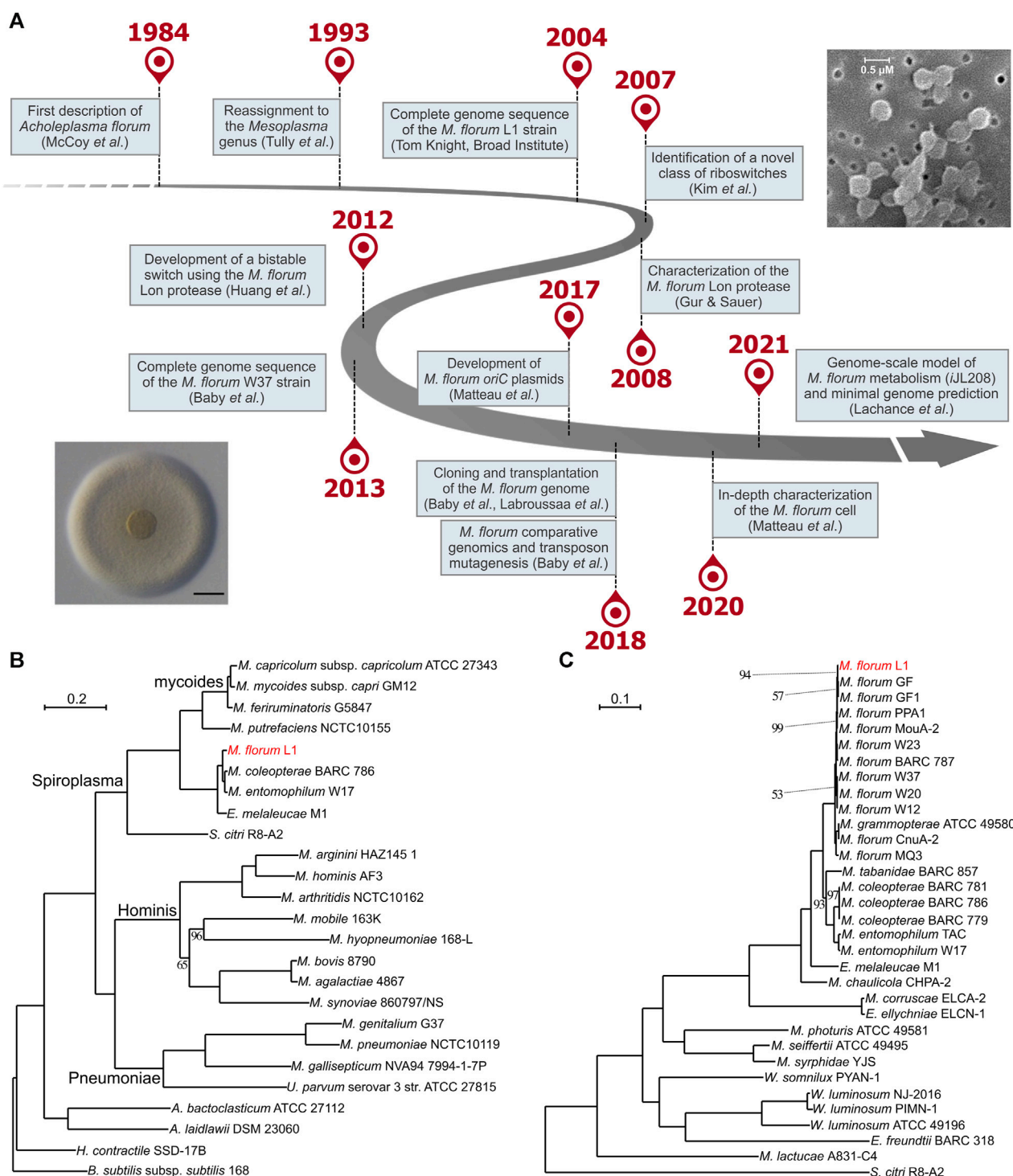


FIGURE 1

Forty years of research on *Mesoplasma florum*. (A) Important milestones in *M. florum* research timeline. Representative picture of an *M. florum* L1 colony displaying the typical “fried-egg” morphology (adapted from Labroussaa et al., 2016, Vol. 44, No. 17, pp. 8501–8511, by permission of Oxford University Press; scale bar: 100 μ m) as well as *M. florum* L1 cells observed by scanning electron microscopy (Baby et al., 2013) are also depicted. (B) and (C) Maximum-likelihood phylogenetic trees of the Mollicutes (B) and the *Mesoplasma/Entomoplasma* genera (C) inferred using concatenated alignments of 109 and 229 conserved proteins, respectively. Trees were constructed using RAxML (Stamatakis, 2014) with 150 bootstrap replicates as determined using the autoFC bootstopping criterion. Bootstrap replicate values are of 100 unless specified otherwise. *Bacillus subtilis* and *S. citri* were used as outgroups. See Table 1 for additional information on strains and genomes included in the *Mesoplasma/Entomoplasma* phylogenetic tree.

TABLE 1 List of *Mesoplasma* and *Entomoplasma* strains with genome assemblies deposited on the RefSeq database.

Organism name	Previous names	Strain name	Original reference	Isolation source	Source details	RefSeq accessiona	Submitter	Submission date	Assembly level	Length (bp)
<i>Entomoplasma ellychniae</i>	<i>Mycoplasma ellychniae</i>	ELCN-1	Tully et al. (1989)	<i>Ellychnia corrusca</i>	Hemolymph of firefly beetle	GCF_002930155.1	Academia Sinica	15/02/2018	Contig	900,037
<i>Entomoplasma freundtii</i>	-	BARC 318 (ATCC 51999)	Tully et al. (1998)	<i>Coleoptera Cicindelidae</i>	Green tiger beetle gut tissue	GCF_002804205.1	Academia Sinica	04/12/2017	Complete	838,114
<i>Entomoplasma melaleucae</i>	<i>Mycoplasma melaleucae</i>	M1 (ATCC 49191)	Tully et al. (1990b)	<i>Melaleuca quinquenervia</i>	Surface of tropical plant flower	GCF_002804105.1	Academia Sinica	04/12/2017	Complete	845,295
<i>Mesoplasma chauliocola</i>	-	CHPA-2 (ATCC 49578)	Tully et al. (1987); Tully et al. (1994)	<i>Chauliognathus pennsylvanicus</i>	Gut of goldenrod soldier beetle	GCF_002290085.1	Ginkgo Bioworks Inc	12/09/2017	Complete	854,780
<i>Mesoplasma coleopterae</i>	-	BARC 779 (ATCC 49583)	Tully et al. (1994)	<i>Chauliognathus sp</i>	Gut of adult soldier beetles	GCF_002804245.1	Academia Sinica	04/12/2017	Complete	800,407
<i>Mesoplasma coleopterae</i>	<i>Mesoplasma florum</i>	BARC 781	Unpublished	Beetle	-	GCF_002999455.1	Universite de Sherbrooke	14/03/2018	Chromosome	803,948
<i>Mesoplasma coleopterae</i>	<i>Mesoplasma florum</i>	BARC 786	Unpublished	Beetle	-	GCF_002999395.1	Universite de Sherbrooke	14/03/2018	Chromosome	765,660
<i>Mesoplasma corruscae</i>	-	ELCA-2 (ATCC 49579)	Tully et al. (1987); Tully et al. (1994)	<i>Ellychnia corrusca</i>	Gut of an adult firefly beetle	GCF_002930145.1	Academia Sinica	15/02/2018	Contig	839,085
<i>Mesoplasma entomophilum</i>	<i>Acholeplasma entomophilum</i>	TAC (ATCC 43706)	Clark et al. (1986)	<i>Tabanus catenatus</i>	Gut of tabanid fly	GCF_002749675.1	Ginkgo Bioworks Inc	03/11/2017	Complete	847,967
<i>Mesoplasma entomophilum</i>	<i>Mesoplasma florum</i> ; <i>Acholeplasma florum</i> ; <i>Acholeplasma entomophilum</i>	W17	Whitcomb et al. (1982)	<i>Aster sp</i>	Surface of plant flower	GCF_002999315.1	Universite de Sherbrooke	14/03/2018	Chromosome	787,107
<i>Mesoplasma florum</i>	<i>Acholeplasma florum</i>	L1 (ATCC 33453)	McCoy et al. (1984)	<i>Citrus limon</i>	Surface of plant flower	GCF_000008305.1	Broad Institute	19/07/2004	Complete	793,224
<i>Mesoplasma florum</i>	<i>Acholeplasma florum</i> ; <i>Acholeplasma entomophilum</i>	W37	Whitcomb et al. (1982)	<i>Solidago sp</i>	Surface of plant flower	GCF_000479355.1	Universite de Sherbrooke	24/10/2013	Complete	825,824
<i>Mesoplasma florum</i>	<i>Acholeplasma florum</i>	GF1	Whitcomb et al. (1982)	<i>Citrus limon</i>	Surface of plant flower	GCF_002504365.1	Ginkgo Bioworks Inc	10/10/2017	Complete	807,195
<i>Mesoplasma florum</i>	-	PPA1	Unpublished	<i>Calliandra haematocephalus</i>	Surface of plant flower	GCF_002504385.1	Ginkgo Bioworks Inc	10/10/2017	Complete	820,043

(Continued on following page)

TABLE 1 (Continued) List of *Mesoplasma* and *Entomoplasma* strains with genome assemblies deposited on the RefSeq database.

Organism name	Previous names	Strain name	Original reference	Isolation source	Source details	RefSeq accessiona	Submitter	Submission date	Assembly level	Length (bp)
<i>Mesoplasma florum</i>	-	BARC 787	Unpublished	Unspecified insect	-	GCF_002999435.1	Universite de Sherbrooke	14/03/2018	Complete	738,512
<i>Mesoplasma florum</i>	<i>Acholeplasma florum</i>	CNUA-2	Tully et al. (1987)	<i>Coleoptera: Cantharidae</i>	Gut of soldier beetle	GCF_002999275.1	Universite de Sherbrooke	14/03/2018	Complete	813,801
<i>Mesoplasma florum</i>	-	GF	Unpublished	-	-	GCF_002999355.1	Universite de Sherbrooke	14/03/2018	Chromosome	792,347
<i>Mesoplasma florum</i>	-	MouA-2	Unpublished	<i>Monobia quadridens</i>	Vespid wasp	GCF_002999255.1	Universite de Sherbrooke	14/03/2018	Complete	781,099
<i>Mesoplasma florum</i>	<i>Acholeplasma florum</i>	MQ3 (MQ-3)	Clark et al. (1986)	<i>Monobia quadridens</i>	Gut of a Vespid wasp	GCF_002999415.1	Universite de Sherbrooke	14/03/2018	Complete	793,277
<i>Mesoplasma florum</i>	<i>Acholeplasma florum</i>	W20	Whitcomb et al. (1982)	<i>Aster simplex</i>	Surface of plant flower	GCF_002999375.1	Universite de Sherbrooke	14/03/2018	Chromosome	830,640
<i>Mesoplasma florum</i>	<i>Acholeplasma florum</i>	W23	Whitcomb et al. (1982)	<i>Helianthus annuus</i>	Surface of plant flower	GCF_002999295.1	Universite de Sherbrooke	14/03/2018	Complete	773,885
<i>Mesoplasma florum</i>	<i>Acholeplasma florum</i>	W12	Whitcomb et al. (1982)	<i>Chrysanthamnus sp</i>	Surface of plant flower	GCF_003006095.1	Universite de Sherbrooke	16/03/2018	Chromosome	829,202
<i>Mesoplasma grammopterae</i>	-	GRUA-1 (ATCC 49580)	Tully et al. (1987); Tully et al. (1994)	<i>Grammoptera sp</i>	Gut of adult long-horned beetle	GCF_000701525.1	DOE Joint Genome Institute	11/06/2014	Scaffold	806,944
<i>Mesoplasma lactucae</i>	<i>Mycoplasma lactucae</i>	831-C4 (ATCC 49193)	Rose et al. (1990)	<i>Lactuca sativa</i>	Surface of lettuce plant	GCF_002441935.1	Ginkgo Bioworks Inc	04/10/2017	Complete	837,471
<i>Mesoplasma photuris</i>	-	PUPA-2 (ATCC 49581)	Tully et al. (1987); Tully et al. (1994)	<i>Photuris sp</i>	Gut of firefly larva	GCF_000702725.1	DOE Joint Genome Institute	11/06/2014	Contig	778,966
<i>Mesoplasma seiffertii</i>	<i>Acholeplasma seiffertii</i>	F7 (ATCC 49495)	Bonnet et al. (1991)	<i>Citrus senensis</i>	Surface of sweet orange flower	GCF_000518725.1	DOE Joint Genome Institute	13/01/2014	Scaffold	977,957
<i>Mesoplasma syrphidae</i>	-	YJS (ATCC 51578)	Tully et al. (1994)	<i>Diptera: Syrphidae</i>	Gut of an adult yellowjacket-like syrphid fly	GCF_002843565.1	Ginkgo Bioworks Inc	17/12/2017	Complete	908,214
<i>Mesoplasma tabanidae</i>	-	BARC 857 (ATCC 49584)	Tully et al. (1994)	<i>Tabanus abactor</i>	Gut of adult horse fly	GCF_002804025.1	Academia Sinica	04/12/2017	Complete	846,907
<i>Williamsoniiplasma lucivorax</i>	<i>Entomoplasma lucivorax</i> ; <i>Mycoplasma lucivorax</i>	PIPN-2 (ATCC 49196)	Williamson et al. (1990)	<i>Photinus pyralis</i>	Gut of an adult firefly beetle	GCF_000518285.1	DOE Joint Genome Institute	13/01/2014	Scaffold	11,03,092

(Continued on following page)

TABLE 1 (Continued) List of Mesoplasma and Entomoplasma strains with genome assemblies deposited on the RefSeq database.

Organism name	Previous names	Strain name	Original reference	Isolation source	Source details	RefSeq accessiona	Submitter	Submission date	Assembly level	Length (bp)
Williamsoniitiplasma luminosum	Entomoplasma luminosum; Mycoplasma luminosum	PIMN-1 (ATCC 49195)	Williamson et al. (1990)	Photinus marginalis	Gut of an adult firefly beetle	GCF_002803985.1	Academia Sinica	04/12/2017	Complete	10,31,560
Williamsoniitiplasma luminosum	Entomoplasma luminosum; Mycoplasma luminosum	NJ-2016	Unpublished	Photinus pyralis	Gut of an adult firefly beetle	GCA_003013295.1	Photinus pyralis genome working group	21/03/2018	Complete	10,29,845
Williamsoniitiplasma somnilux	Entomoplasma somnilux; Mycoplasma somnilux	PYAN-1 (ATCC 49194)	Williamson et al. (1990)	Pyrractonema angulata	Pupal gut of the firefly beetle	GCF_002804005.1	Academia Sinica	04/12/2017	Complete	868,413

aWhen more than one genome assemblies were available, the most complete assembly was selected. If assembly levels were identical, then the first submitted assembly was chosen.

surrounding *M. florum* cells, which was shown to occupy for up to 5% of the total *M. florum* biomass, probably contributes to the survivability of this microorganism on plant surfaces (Matteau et al., 2020; Lachance et al., 2021). Mainly composed of galactose and glucose, this capsule-like structure might provide a physical protection against desiccation, and therefore participate in the dissemination of *M. florum* across insect populations. The possibility that *M. florum* uses plants as secondary hosts like some pathogenic spiroplasmas seems rather unlikely since no such observation has ever been reported and *M. florum* has never been isolated in the context of a plant disease.

The full range of hosts susceptible to *M. florum* colonization and the possibility of a predominant association with specific insect types are still not well-defined. Although a few strains were directly recovered from the gut content of insects such as soldier beetles (*Cantharidae*) as well as Vespid wasps (*Monobia quadridens*) (Clark et al., 1986; Tully et al., 1987), most of the previously described *M. florum* strains were originally isolated from plant flowers (Table 1). This prevents their direct association with an insect host. Still, the isolation source of closely related species, especially species of the *Mesoplasma* and *Entomoplasma* genera, suggests that *M. florum* could potentially be found in a wide variety of insects, including firefly beetles (*Ellychnia corrusca*), goldenrod soldier beetles (*Chauliognathus pennsylvanicus*), as well as tabanid (*Tabanus catenatus*) and syrphid (*Syrphidae*) flies (Clark et al., 1986; Tully et al., 1987; Tully et al., 1989; Tully et al., 1994). Furthermore, *Mesoplasma* and *Entomoplasma* have intermixed relationships and recent phylogenetic data suggest that they should no longer be taxonomically separated (Gasparich and Chih-Horng, 2019) (Figure 1C).

While we cannot completely rule out the possibility that *M. florum* could be pathogenic in certain hosts or under yet unidentified circumstances, its ecological niche seems quite different from related pathogenic mycoplasmas of the mycoides cluster. Since the growth of *M. florum* is dramatically impaired at 37°C (McCoy et al., 1984; Matteau et al., 2020), the probability that it infects warm-blooded animals similar to *M. mycoides* or *M. capricolum* is indeed very low. Recent data suggest that mycoplasmas of the mycoides cluster rather gained the ability to infect animals like other mycoplasmas through convergent evolution, in which a common ancestor experienced important gene losses and acquisitions, notably by exchanging genes with the Hominis and Pneumoniae lineages (Lo et al., 2018). Whether *M. florum* simply benefits from its hosts or rather perform advantageous metabolic activities, for example, by degrading or secreting particular metabolites in the gut, remains also to be determined. It has been shown that some bacteria of the *Entomoplasmatales* clade play important roles in the digestive system of attine fungus-farming leaf-cutting ants (Sapountzis et al., 2015; Sapountzis et al., 2018). In any cases, *M. florum* or its predecessor had to adapt and develop strategies to compete for the available resources. Its small size might in fact be advantageous in that context. With an average cell diameter of 0.5–0.6 µm (Figure 1A), *M. florum* is estimated to have a total cell volume of only 0.08–0.10 µm³, which is nearly 50 times smaller than *Escherichia coli* (Volkmer and Heinemann, 2011; Dai and Zhu, 2018; Matteau et al., 2020). This causes *M. florum* cells to have a surface area to volume ratio approximately 2.5 times higher than *E. coli*, as well as a relatively higher biomass fraction allocated to

lipids (~18%). These characteristics probably facilitate the importation of complex nutrients from the environment that are required for biosynthesis reactions and ATP production. Given its scavenger lifestyle, nutrient acquisition certainly occupies a critical role in *M. florum* metabolism. Transport reactions actually represent about a third (84/277) of the total number of reactions included in the recently published genome-scale model (GEM) of *M. florum* (Lachance et al., 2021). This is also reflected by the capacity of *M. florum* L1 to import and process various sugars, including glucose, fructose, sucrose, trehalose, and maltose (Lachance et al., 2021). Since the glycolysis is the only way of producing ATP in *M. florum*, being able to degrade various sugars might be important to survive in the insect gut, especially if the hosts diet is variable across individuals or between feeding periods. Interestingly, genes responsible for carbohydrate transport and metabolism are among the most variable between *M. florum* strains (Baby et al., 2018b), suggesting that some strains might be more fit to certain diets. Since the phylogeny of those strains could not be linked to their geographical origin or isolation source (Baby et al., 2018b), nutritional preferences of *M. florum* primary hosts could be one of many important actors driving the evolution of this species.

Another important consideration about very small cells is the limited amount of material that their volume can accommodate. This is well exemplified by the very small genomes of Mollicutes, which can be as small as 580 kbp in the case of *Mycoplasma genitalium* (Su and Baseman, 1990; Fraser et al., 1995). At 0.5–0.6 µm of diameter, *M. florum* cells are in fact only 5,000 to 6,000 times larger than a hydrogen atom, and weight just about 100 fg (Morowitz and Tourtellotte, 1962; Morowitz, 1984; Sundararaj et al., 2004; Matteau et al., 2020). With only ~800 kbp, the *M. florum* chromosome obviously requires fewer nucleotides and most probably less energy than for *E. coli* to replicate, especially since both organisms have approximately the same number of genome copies per cell (Bionumbers, 2015; Matteau et al., 2020). The number of RNA and protein molecules is also much lower in *M. florum* compared to *E. coli*, corresponding to roughly 10 times fewer molecules per cell for both constituents. Yet, if we normalize these values per unit of volume, *M. florum* and *E. coli* show similar proteins and RNA concentrations (Sundararaj et al., 2004; Milo, 2013; Bionumbers, 2015; Matteau et al., 2020). Combined with the low metabolic cost predicted for *M. florum* biomass synthesis reactions, which are mainly fueled by the import, assembly, and rearrangement of premade molecular building blocks, these physical limitations might decrease the amount of energy needed to complete a round of cellular division. This probably contributes to the fast growth rate of *M. florum*, and could explain why little amounts of sugars are sufficient to sustain its growth *in vitro* (Lachance et al., 2021). The main protease responsible for the degradation of incomplete proteins that are expressed from mRNA lacking stop codons is also 8 to 16 times more processive in *M. florum* compared to *E. coli* (Gur and Sauer, 2008). This could allow a more efficient recycling of the amino acids incorporated into incomplete proteins. This protease (Lon) was notably used in metabolic engineering applications (Zhou et al., 2023) as well as to develop artificial gene circuits in other bacteria (Huang et al., 2012; Cameron and Collins, 2014; Sakkos et al., 2021; Szydlo et al., 2022). Of course, other factors most likely come into play to explain the fast-growing phenotype of *M. florum* compared to other

Mollicutes. Not spending resources and energy on the expression of virulence factors is probably one of them. Allocating most of its resources on protein expression might also help, as nearly half of all protein molecules present in the *M. florum* cell are associated with translation and other related processes (Matteau et al., 2020; Lachance et al., 2021). More precisely, the estimated ribosome concentration in *M. florum* is roughly ten times higher than the values reported for *M. pneumoniae*, but comparable to concentrations estimated in *M. mycoides* and *E. coli* (Sundararaj et al., 2004; Kühner et al., 2009; Yus et al., 2009; Bakshi et al., 2012; Wodke et al., 2013; Breuer et al., 2019; Matteau et al., 2020). Rather than adopting complex survival strategies like *M. pneumoniae* and other slow-growing pathogenic mycoplasmas, *M. florum* appears to focus on rapid biomass production to thrive in its natural environment. The reconstruction of a GEM that accounts for protein expression constraints (ME-model) (Lloyd et al., 2018) and its comparison with protein abundances previously estimated for *M. florum* might provide additional clues on the relationship between protein allocation and growth rate in Mollicutes.

Is the genome of *M. florum* minimal?

Although the *M. florum* genome has been streamlined by evolution (Sirand-Pugnet et al., 2007), previous studies showed that it is not minimal, at least not under laboratory conditions (Baby et al., 2018b; Lachance et al., 2021). Even if Mollicutes have some of the smallest genomes found in nature, a considerable fraction of their genome is dispensable in rich media. Most non-essential elements consist of genes or regulatory elements important for fitness and robustness of the cells in their natural habitat, which generally provide much more challenging and variable physicochemical conditions compared to laboratory settings. In *M. genitalium*, for example, approximately 100 of its 485 predicted protein-coding genes were found to be non-essential using random transposon mutagenesis experiments (Hutchison et al., 1999; Glass et al., 2006). Another good example is JCVI-syn3.0, the currently closest approximation of a minimal organism (Hutchison et al., 2016). This artificial bacterium harbors a synthetic chromosome of only 531 kbp and 438 protein-coding genes based on the *M. mycoides* subspecies *capri* genome, which represents an impressive reduction of roughly 50% compared to the original sequence. Still, around 25% of the remaining genes in JCVI-syn3.0 and derivative strains are of unknown function (Hutchison et al., 2016; Glass et al., 2017; Breuer et al., 2019), highlighting our current gap of knowledge in the biology of even the simplest forms of life.

What could be the *M. florum* minimal genome, and would it be any different from JCVI-syn3.0? In *M. florum*, essential genes have been studied using two different but complementary methods, i.e., comparative genomics and random transposon mutagenesis (Baby et al., 2018b). By comparing the genomic sequence of 13 *M. florum* strains, two main groups were revealed, one comprising most of the *M. florum* representatives (10/13), and a second one containing only three strains, namely, W17, BARC 781, and BARC 786. Interestingly, these three strains were recently renamed based on their average nucleotide identity with other *Mesoplasma* species (Table 1). Nonetheless, the genomes of W17,

BARC 781, and BARC 786 were found to be highly syntenic with the other representatives, and a core set of 546 homologous gene cluster families was observed in all compared genomes (Baby et al., 2018b). This corresponds to approximately 80% of all protein coding genes present in each strain, which was found to vary between 651 and 740 among strains. Unsurprisingly, more than 25% of the conserved *M. florum* genes are related to translation, a functional category that was observed to be significantly enriched in the core genome compared to the entire gene sets. Still, transposon mutagenesis performed in the *M. florum* L1 strain showed that a total of 430 genes out of 720 can be interrupted by transposon, including 320 core genes (Baby et al., 2018b). No transposon was observed in the remaining 290 genes, which are most likely essential in *M. florum* L1 or could have been missed given the transposon insertion density of the study. The number of putatively essential genes was however increased to 332 upon re-analysis of the transposition insertion data by considering the insertion position of the transposons within *M. florum* open-reading frames (Lachance et al., 2021). All analyzed genomes were predicted to encode 29 tRNA genes, as well as two virtually identical copies of the rRNA gene loci, although one copy is probably sufficient for growth (Asai et al., 1999; Hutchison et al., 2016).

Gene conservation and essentiality data have been used to propose minimal genome scenarios for *M. florum* L1. One scenario would be to remove all non-core genes from its genome, which should yield a ~645 kbp genome coding for 585 genes if all intergenic and non-coding elements are retained (Baby et al., 2018b). However, 25 non-core protein coding genes were identified to be essential for *M. florum* L1 in ATCC 1161 medium. Including these genes in the minimal genome design would thus increase the chances of producing a viable cell. The 110 genes interrupted by transposons and absent from the core genome thus represent interesting first-step candidates for genome streamlining. Yet, this genome would probably be far from minimal since a majority (~55%) of core genes can be interrupted by transposons without severely impacting *M. florum* growth. On the other hand, keeping only the genes in which no transposon was detected is a dubious strategy since synthetic lethality interactions are likely to occur, resulting in a non-viable cell when certain combinations of genes are simultaneously deleted. Given the phylogenetic proximity between *M. florum* and *M. mycoides* (Figure 1B), another possible scenario would be to include the 409 *M. florum* L1 protein-coding genes in which an ortholog was found in JCVI-syn3.0. Intriguingly, this Syn3.0 inspired minimal genome would contain 401 of the 585 *M. florum* L1 core genes, but would lack 57 genes identified as essential in *M. florum* (Baby et al., 2018b). Conversely, 69 gene families unique to *M. mycoides* JCVI-syn3.0 would not be present in that design.

Even if we combine the 57 essential genes found only in *M. florum* L1 with the 409 protein-coding genes shared between *M. florum* and JCVI-syn3.0, it remains difficult to predict if this synthetic design will be viable. Genome design rules remain poorly understood, and most synthetic genome projects rely on trial-and-error approaches, involving long and fastidious rounds of optimization. For instance, to create JCVI-syn3.0, it took not only many rounds of genome design, transposon mutagenesis, and debugging, but also an extensive knowledge of the biochemical data available in the literature as well as an impressive amount of

time and resources (Sleator, 2010; Sleator, 2016; Hutchison et al., 2016). Systems biology approaches that can integrate multiple layers of information and systematically evaluate genome designs represent promising tools in that context (Chalkley et al., 2019; Rees-Garbutt et al., 2020a; Rees-Garbutt et al., 2020b). Such approaches were recently used to further explore the minimal gene set of *M. florum* and compare it with JCVI-syn3.0 (Lachance et al., 2021). This required the reconstruction of a high-quality metabolic GEM for *M. florum*, consisting of 370 reactions, 208 genes, and 351 metabolites (iJL208). This model was experimentally validated using growth data on various sugars as well as gene expression and essentiality data, which were all in good agreement with the model predictions (Lachance et al., 2021). Gene essentiality data and metabolic constraints defined by the model allowed the prediction of a 562 kbp minimal genome containing 535 protein-coding genes. Since this prediction also considered the 387 previously identified *M. florum* transcription units (Matteau et al., 2020), its viability is more likely than previously mentioned hypothetical scenarios. Interestingly, this minimal genome contains 97 more protein-coding genes than JCVI-syn3.0, which could be due to real biological differences between the two organisms or simply be caused by prediction inaccuracies given the current gaps of knowledge in *M. florum* and Mollicutes biology. While this prediction shares 343 protein-coding genes with JCVI-syn3.0, it contains 129 genes unique to *M. florum* as well as 63 genes exclusively shared with JCVI-syn1.0, the parent strain of JCVI-syn3.0. This suggests that different minimal genome compositions probably exist, even for closely related species. However, most genes unique to *M. florum* are currently of unknown function, which complicates further investigation. Still, many protein-coding genes unique to *M. florum* or shared with JCVI-syn1.0 are associated with metabolic functions, notably transport and carbohydrate metabolism (Lachance et al., 2021). We can therefore imagine that different pathways could be used by minimal genomes to produce energy and fulfill cellular needs. Some minimal genome configurations could thus be more optimal than others. Indeed, 19 genes initially discarded in JCVI-syn3.0 were later reintroduced to resolve important morphological and growth defects, creating a more robust cell named JCVI-syn3A (Breuer et al., 2019; Pelletier et al., 2021). Among these genes, two are present in the minimal *M. florum* genome prediction. However, the construction of synthetic *M. florum* genomes will ultimately be needed to test and validate these computational predictions.

Can we engineer the genome of *M. florum*?

The *M. florum* genome engineering toolbox is not as sophisticated as those available for *E. coli* or *Saccharomyces cerevisiae*. However, there is a growing number of methods that can be used for modifying the *M. florum* genome. Given its relative simplicity, Tn5 transposon mutagenesis was the first approach used in *M. florum* (Baby et al., 2018b). This system had previously been used in many bacterial species, including *M. mycoides* (Goryshin et al., 2000; Karas et al., 2014; Hutchison et al., 2016). Given the natural *M. florum* antibiotic susceptibility profile (Matteau et al., 2017), the widely used *tetM* gene conferring resistance to

tetracycline was chosen as the selection marker in the transposon. The transformation of this transposon by electroporation resulted in tetracycline resistant *M. florum* colonies on ATCC 1161 plates (Baby et al., 2018b). Despite of a relatively high variability in the method efficiency, this allowed the creation of a collection comprising 2,806 individually picked transposon insertion mutants in which 430 of the 720 *M. florum* genes were found to be interrupted (Baby et al., 2018b; Lachance et al., 2021). Similar to the *E. coli* Keio collection (Baba et al., 2006), this library of gene-inactivated *M. florum* mutants represents an invaluable resource to study the biology of this near-minimal bacterium, especially for finding function to currently unassigned genes. This approach could also be repeated using different growth conditions to obtain additional information on the function of specific genes.

Another way to deliver genetic material into the genome is through the transformation of plasmids. Unfortunately, no natural plasmid has yet been reported to replicate in *M. florum*, and artificial plasmids developed in *M. mycoides*, *M. capricolum*, and *S. citri* have been shown to be incompatible with this species (Matteau et al., 2017). These plasmids harbor a partial or complete copy of the host chromosomal origin of replication (*oriC*) to replicate in their host. The *oriC* contains short DNA sequences known as DnaA boxes essential for the recognition by the DnaA protein, which is responsible for initiating DNA replication in bacteria (Messer, 2002). In Mollicutes, DnaA boxes are generally located within the two intergenic regions flanking the *dnaA* gene (Cordova et al., 2002; Lartigue et al., 2003; Ishag et al., 2017; Matteau et al., 2017). Artificial plasmids have recently been constructed using the *M. florum* predicted *oriC* (Matteau et al., 2017). The *tetM* gene was included in all tested *M. florum oriC* plasmids. While both intergenic regions surrounding the *dnaA* gene were shown to be essential for replication, contrasting with observations in *S. citri* (Lartigue et al., 2002), the presence of a copy of the *dnaA* gene was not. Plasmids containing both *dnaA* intergenic regions (pMfT-o3 and pMfT-o4) were stably maintained for more than 85 generations with or without antibiotics selection. Interestingly, *M. florum oriC* plasmids could successfully be transformed by electroporation or polyethylene glycol (PEG) transformation, as well as by conjugation from an *E. coli* strain using the RP4 system (Matteau et al., 2017). These plasmids allowed the validation of two additional selection markers, *pac* and *aadA1*, conferring resistance to puromycin and streptomycin/spectinomycin, respectively. While the *pac* marker had previously been used in other Mollicutes (Algire et al., 2009; Krishnakumar et al., 2010; Maglennon et al., 2013), this was the first reported use of the *aadA1* marker in a Mollicutes species. The functionality of this cassette also confirmed the recognition of P_{N25} promoter by the *M. florum* σ^{70} factor (Brunner and Bujard, 1987), which had not been used in the context of the *tetM* marker. This result is consistent with the sequence of the *M. florum* consensus promoter, which is, similar to *E. coli*, characterized by a strongly conserved -10 box of sequence TAWAAT (Matteau et al., 2020). However, in *M. florum*, the -35 box is highly degenerated. The *M. florum oriC* plasmids represent basic molecular tools that will help the validation of additional DNA parts in this bacterium, as well as facilitate the development of more sophisticated approaches to engineer its genome.

Since *oriC* plasmids are replicated using the same mechanism as the chromosome, they are maintained at very low copy numbers in

the cells. In *M. florum*, these plasmids are estimated to be present at 1 or 2 copies per cell (Matteau et al., 2017). In addition, their homology with the endogenous *oriC* region causes frequent recombination events with the host chromosome, a tendency also observed with *M. florum oriC* plasmids. While in some cases the integrated DNA cargo can interfere with the normal replication of the chromosome, this property can be exploited for genome engineering purposes. This was well demonstrated by the whole genome cloning (WGC) of the *M. florum* chromosome in the yeast *S. cerevisiae* (Labroussaa et al., 2016; Baby et al., 2018a) (Figure 2A). In that context, sequences enabling replication, partitioning, and selection in yeast were first introduced into the *M. florum* chromosome by the recombination of an *oriC* plasmid derivative. Following transformation in yeast, this allowed the *M. florum* chromosome to be replicated as a practically inert extrachromosomal element, with only minor impact on the yeast growth and cell cycle. WGC in yeast offers the opportunity to use the vast and well characterized molecular toolbox available in this model organism. For instance, the natural capacity of yeast to perform efficient homologous recombination was used to replace the duplicated *oriC* region resulting from the recombination of the *oriC* derivative plasmid by an *URA3* cassette (Baby et al., 2018a). Since many Mollicutes lack efficient molecular tools to modify their genome, WGC in yeast has been performed for several species, including *M. mycoides* and *M. genitalium* (Labroussaa et al., 2019). This procedure is at the heart of the strategy used to create JCVI-syn1.0 and JCVI-syn3.0 (Gibson et al., 2010; Hutchison et al., 2016). Whole genomes cloned and engineered in yeast must however be transplanted into a suitable recipient bacterium to assess their viability, a delicate procedure known as genome transplantation (Lartigue et al., 2007; Labroussaa et al., 2019) (Figure 2A). Due to its remarkable capacity to recognize the *oriC* region of other Mollicutes species, *M. capricolum* is generally used for this task (Lartigue et al., 2003; Lartigue et al., 2007; Labroussaa et al., 2016). Following transplantation and selection, the *M. capricolum* genome is replaced by the donor genome, and individual transplants can be recovered for validation and characterization. While many aspects of genome transplantation are still puzzling, the phylogenetic distance between the donor and recipient bacteria is known to play a critical role in the overall efficiency of the method (Labroussaa et al., 2016). Sharing ~92% identity on the core proteome with *M. capricolum*, *M. florum* appears to be the most phylogenetically distant organism for which the transplantation with this recipient bacterium is possible (Baby et al., 2018a). Indeed, attempts to transplant the genome of *S. citri* and *S. floricola* have failed, and genome transplantation of more distant Mollicutes species such as *M. genitalium* and *M. hominis* has never been reported, albeit their genomes have been successfully cloned in yeast (Labroussaa et al., 2016; Labroussaa et al., 2019). Apart from the phylogenetic distance, other factors such as the concentration and quality of donor genomic DNA as well as the presence of mobile genetic elements or restriction-modification systems are also known to affect the success of the procedure (Lartigue et al., 2007; Gibson et al., 2010; Labroussaa et al., 2016; Labroussaa et al., 2019). The topology of the transplanted genomes might also be important as supercoiled DNA seems to drastically increase the transformability of large DNA molecules in *E. coli* (Mukai et al., 2020; Yoneji et al., 2021; Fujita et al., 2022).

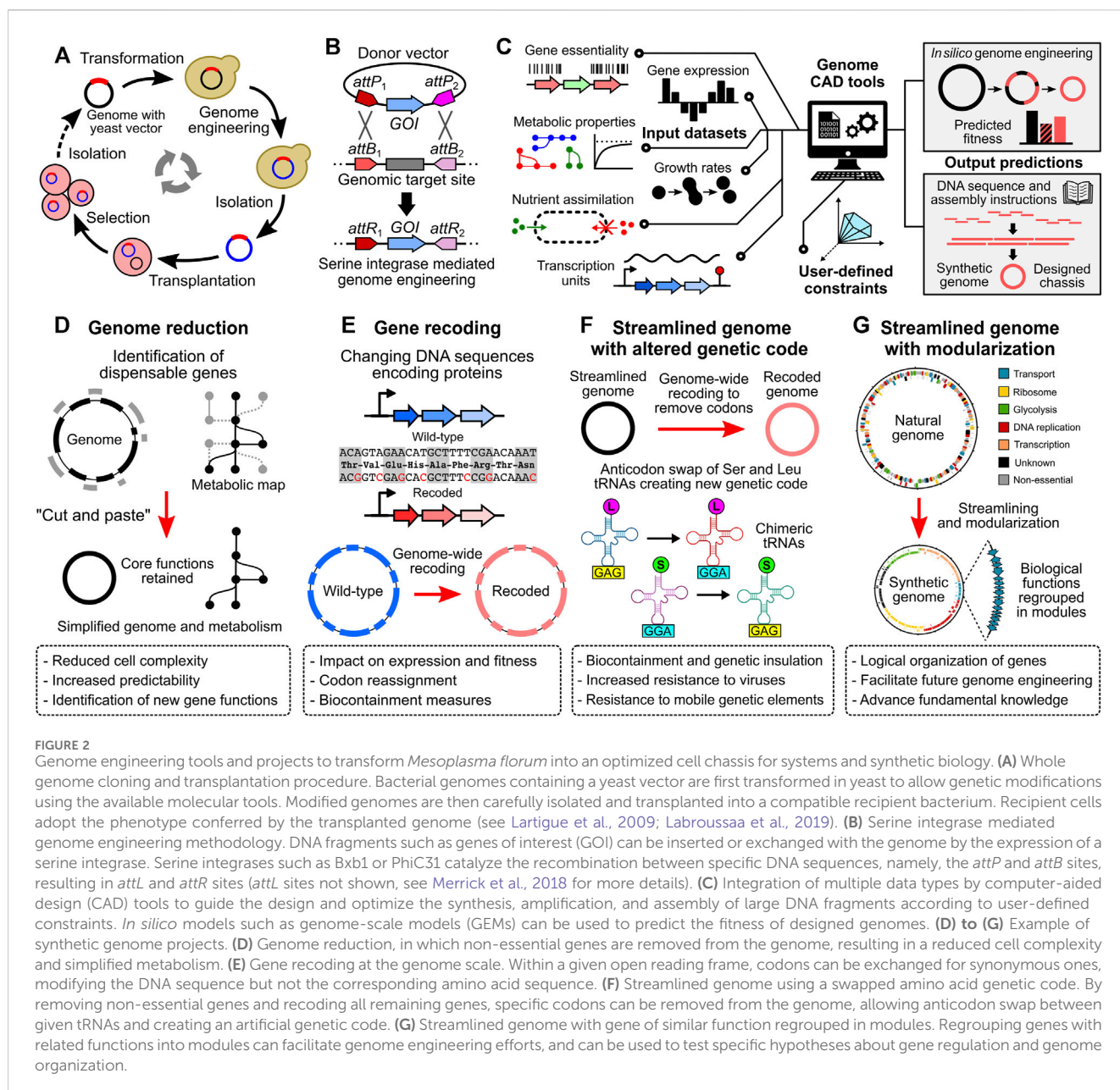


FIGURE 2

Genome engineering tools and projects to transform *Mesoplasma florum* into an optimized cell chassis for systems and synthetic biology. (A) Whole genome cloning and transplantation procedure. Bacterial genomes containing a yeast vector are first transformed in yeast to allow genetic modifications using the available molecular tools. Modified genomes are then carefully isolated and transplanted into a compatible recipient bacterium. Recipient cells adopt the phenotype conferred by the transplanted genome (see Lartigue et al., 2009; Labroussaa et al., 2019). (B) Serine integrase mediated genome engineering methodology. DNA fragments such as genes of interest (GOI) can be inserted or exchanged with the genome by the expression of a serine integrase. Serine integrases such as Bxb1 or PhiC31 catalyze the recombination between specific DNA sequences, namely, the *attP* and *attB* sites, resulting in *attL* and *attR* sites (*attL* sites not shown, see Merrick et al., 2018 for more details). (C) Integration of multiple data types by computer-aided design (CAD) tools to guide the design and optimize the synthesis, amplification, and assembly of large DNA fragments according to user-defined constraints. *In silico* models such as genome-scale models (GEMs) can be used to predict the fitness of designed genomes. (D) to (G) Example of synthetic genome projects. (D) Genome reduction, in which non-essential genes are removed from the genome, resulting in a reduced cell complexity and simplified metabolism. (E) Gene recoding at the genome scale. Within a given open reading frame, codons can be exchanged for synonymous ones, modifying the DNA sequence but not the corresponding amino acid sequence. (F) Streamlined genome using a swapped amino acid genetic code. By removing non-essential genes and recoding all remaining genes, specific codons can be removed from the genome, allowing anticodon swap between given tRNAs and creating an artificial genetic code. (G) Streamlined genome with gene of similar function regrouped in modules. Regrouping genes with related functions into modules can facilitate genome engineering efforts, and can be used to test specific hypotheses about gene regulation and genome organization.

What could be the next steps in *M. florum* research?

Expanding the available molecular toolbox should certainly be one of the key priorities to fully harness the potential of *M. florum* for systems and synthetic biology. Even if the transplantation of the *M. florum* genome is possible (Figure 2A), the very low efficiency and high variability associated with this method using *M. florum* constitutes an important limitation to the in-yeast genome engineering strategy. It is not rare to obtain less than 10 *M. florum* transplants per experiment, or even no transplant at all (Labroussaa et al., 2016; Baby et al., 2018a). Further investigations are therefore required to enable rapid and easy prototyping of the *M. florum* genome cloned in yeast. Finding a new compatible recipient strain phylogenetically closer to *M. florum* than *M. capricolum* could in principle improve transplantation rates. Alternatively, targeted

engineering of the recipient strain could also favor the recognition and boot-up of the transplanted genome. Nevertheless, genome transplantation remains a complex and delicate procedure. Complementary approaches should therefore be developed to facilitate the genetic modification of *M. florum*. Methods using serine integrases (Merrick et al., 2018) to efficiently exchange or insert DNA fragments at specific positions in the genome (Figure 2B) could prove very useful for *M. florum* since Tn5 transposons insert randomly and current *oriC* plasmids tend to recombine only at the *oriC* region. Another option would be to adapt the well-known recombineering technique by properly expressing proteins of the λ -Red system (Datsenko and Wanner, 2000) or the GP35 recombinase, which was recently demonstrated to be functional in *M. pneumoniae* (Piñero-Lambea et al., 2020; Piñero-Lambea et al., 2022). This approach could even be coupled with the expression of the CRISPR-Cas9 system to

further stimulate DNA recombination by cutting *M. florum*'s genome and counter-selecting unmodified or incorrectly repaired cells. Unlocking the CRISPR-Cas9 technology in *M. florum* would be a significant asset for future research on this bacterium, with a wide array of potential applications (Adli, 2018; Mariscal et al., 2018; Pickar-Oliver and Gersbach, 2019). Yet, heterologous proteins such as Cas9 must be sufficiently expressed in the host to display desired effect. On the other hand, constitutive or uncontrolled expression of many proteins is known to cause toxicity and can affect cell viability. Unfortunately, as of now not even a handful of promoters have been tested and validated on synthetic constructs introduced in *M. florum* (Matteau et al., 2017), none of which are inducible. Testing additional promoters -natural or synthetic- and combining them with other regulatory elements enabling strong activation or tight repression would unlock several methods (Kim et al., 2007; Breton et al., 2010; Domin et al., 2017; Etzel and Mörl, 2017; Ruegg et al., 2018; Piñero-Lambea et al., 2020). In addition, comparing these results with published transcriptional data would provide valuable information about the DNA sequences enabling strong transcription in this organism.

By increasing the molecular toolbox available in *M. florum*, performing large or extensive genome modifications and testing new hypotheses will become significantly easier. Combined with the most recent gene synthesis and high-throughput DNA assembly technologies (Gibson et al., 2010; Hughes and Ellington, 2017; Juhas and Ajioka, 2017; Schindler et al., 2018; Hoose et al., 2023), genome engineering projects could be undertaken (Figures 2D–G). For example, minimal genomes are powerful tools to study fundamental aspects of life, and constitute interesting cell chassis to learn genome design principles and develop promising applications in synthetic biology (Morowitz, 1984; Glass et al., 2017; Lachance et al., 2019). Their limited complexity increases predictability using modeling approaches and decreases the chance of unexpected interactions between artificial gene circuits and native host functions. Stripping the *M. florum* genome near its minimum would reduce the number of genes without any assigned function, and slightly decrease the costs associated with genome synthesis projects. Moreover, the comparison between a minimal *M. florum* genome and JCVI-syn3.0 could provide invaluable information about the different strategies used by bacteria to fulfill essential functions. Still, to enable rapid construction and testing of synthetic *M. florum* genomes, additional tools should be developed to integrate multiple data sources and properly guide the design as well as optimize the synthesis, amplification, and assembly of large DNA fragments (Figure 2C). With an efficient *M. florum* genome prototyping platform in hands, other exciting genome-wide projects could also become more realistic. Entire genome fractions could be recorded, separately or in combination with genome reduction efforts, to systematically investigate the impact of several parameters such as the GC content or the removal of internal transcription start sites (iTSSs) (Matteau et al., 2020) on gene expression and cell fitness (Figure 2E). Engineered or minimal *M. florum* cells will probably be sub-optimal at first, as observed with JCVI-syn3.0 and many other genome-reduced bacteria (Iwade et al., 2011; Karcagi et al., 2016; Breuer et al., 2019; Pelletier et al., 2021; Dervyn et al., 2023). Artificial cells could next be subjected to adaptive laboratory evolution (ALE) for fine-tuning and selection of the most adapted mutants (Dragosits and Mattanovich, 2013; Sandberg et al., 2019). This strategy could be

performed without adding any mutagenic compound or plasmid (Badran and Liu, 2015) given the particularly high DNA replication error rate of *M. florum* (Sung et al., 2012; Lynch et al., 2016). Interestingly, ALE experiments performed on JCVI-syn3A cultures led to growth rate improvements of >15%, corresponding to a doubling time of ~80 min (Sandberg et al., 2023). The resulting *M. florum* mutants could be compared with ALE evolved JCVI-syn3A strains to see if they share similar mutation profiles and growth rates. Rare codons could also be systematically removed from the *M. florum* genome (Isaacs et al., 2011; Fredens et al., 2019), allowing codon reassignment and strict biocontainment measures. Artificial genetic codes could be developed and tested by swapping tRNA anticodons, thereby improving resistance to viruses and mobile genetic elements (Zürcher et al., 2022; Nyerges et al., 2023) (Figure 2F). Genes with related functions could be regrouped into modules, reorganizing and streamlining the entire genome for engineering purposes (Hutchison et al., 2016; Coradini et al., 2020) (Figure 2G). Large genome portions could be inverted to study the importance of DNA orientation at large-scale. Every predicted transcriptional regulator could be tagged for genome-wide binding site assays, enabling high-throughput experimental determination of transcription regulation networks (Matteau and Rodrigue, 2015; Rossi et al., 2018). Protein sequences of entire pathways could be replaced by more or less phylogenetically related homologs to study protein compatibility and create chimeric genomes with enhanced properties. Guided by predictive tools such as the iJL208 GEM (Rees-Garbutt et al., 2020b; Rees-Garbutt et al., 2020a; Lachance et al., 2021), new metabolic capacities or biosynthetic pathways could be introduced by testing a large number of protein variants in parallel and finding the most optimal sequence combination for *M. florum* (Emanuel et al., 2017; Schubert et al., 2021). Synthetic genomics unlocks new possibilities that were simply not technically feasible not so long ago. As we move forward, the frontiers of biology will be redefined, allowing us to pursue and test hypotheses that long remained out of reach, thereby enhancing our comprehension of life at a deeper level.

Author contributions

DM: Investigation, Writing—original draft, Writing—review and editing. AD: Investigation, Writing—original draft. VB: Investigation, Writing—original draft. SR: Funding acquisition, Resources, Writing—review and editing.

Funding

The author(s) declare financial support was received for the research, authorship, and/or publication of this article. This work was supported by a Discovery grant (RGPIN-2020-06151) from the Natural Sciences and Engineering Research Council (NSERC) of Canada.

Conflict of interest

The authors declare that the research was conducted in the absence of any commercial or financial relationships that could be construed as a potential conflict of interest.

Publisher's note

All claims expressed in this article are solely those of the authors and do not necessarily represent those of their affiliated

References

- Adli, M. (2018). The CRISPR tool kit for genome editing and beyond. *Nat. Commun.* 9, 1911. doi:10.1038/s41467-018-04252-2
- Algire, M. A., Lartigue, C., Thomas, D. W., Assad-Garcia, N., Glass, J. I., and Merryman, C. (2009). New selectable marker for manipulating the simple genomes of *Mycoplasma* species. *Antimicrob. Agents Chemother.* 53, 4429–4432. doi:10.1128/AAC.00388-09
- Asai, T., Zaporozhets, D., Squires, C., and Squires, C. L. (1999). An *Escherichia coli* strain with all chromosomal rRNA operons inactivated: complete exchange of rRNA genes between bacteria. *Proc. Natl. Acad. Sci. U. S. A.* 96, 1971–1976. doi:10.1073/pnas.96.5.1971
- Baba, T., Ara, T., Hasegawa, M., Takai, Y., Okumura, Y., Baba, M., et al. (2006). Construction of *Escherichia coli* K-12 in-frame, single-gene knockout mutants: the Keio collection. *Mol. Syst. Biol.* 2, 2006.0008. doi:10.1038/msb4100050
- Baby, V., Labrousseau, F., Brodeur, J., Matteau, D., Gourgues, G., Lartigue, C., et al. (2018a). Cloning and transplantation of the *Mesoplasma florum* genome. *ACS Synth. Biol.* 7, 209–217. doi:10.1021/acssynbio.7b00279
- Baby, V., Lachance, J.-C., Gagnon, J., Lucier, J.-F., Matteau, D., Knight, T. F., et al. (2018b). Inferring the minimal genome of *Mesoplasma florum* by comparative genomics and transposon mutagenesis. *mSystems* 3, 001988–e217. doi:10.1128/mSystems.00198-17
- Baby, V., Matteau, D., Brodeur, J., and Rodrigue, S. (2013). *Whole genome sequencing and comparative genomics of the near-minimal bacterium Mesoplasma florum: first steps towards a simplified chassis for synthetic biology*. Ottawa, Canada: Conférence Annuelle de la Société Canadienne des Microbiologistes.
- Badran, A. H., and Liu, D. R. (2015). Development of potent *in vivo* mutagenesis plasmids with broad mutational spectra. *Nat. Commun.* 6, 8425–8510. doi:10.1038/ncomms9425
- Bakshi, S., Siryaporn, A., Goulian, M., and Weisshaar, J. C. (2012). Superresolution imaging of ribosomes and RNA polymerase in live *Escherichia coli* cells. *Mol. Microbiol.* 85, 21–38. doi:10.1111/j.1365-2958.2012.08081.x
- Bonnet, F., Saillard, C., Vignault, J. C., Garnier, M., Carle, P., Bove, J. M., et al. (1991). *Acholeplasma seiffertii* sp. nov., a mollicute from plant surfaces. *Int J Syst Microbiol.* 40 (1), 45–49. doi:10.1099/00207713-41-1-45
- Bionumbers (2015). What is the macromolecular composition of the cell. Available at: <http://book.bionumbers.org/what-is-the-macromolecular-composition-of-the-cell/> (Accessed March 19, 2019).
- Breton, M., Sagné, E., Duret, S., Béven, L., Citti, C., and Renaudin, J. (2010). First report of a tetracycline-inducible gene expression system for mollicutes. *Microbiology* 156, 198–205. doi:10.1099/mic.0.034074-0
- Breuer, M., Earnest, T. M., Merryman, C., Wise, K. S., Sun, L., Lynott, M. R., et al. (2019). Essential metabolism for a minimal cell. *Elife* 8, e36842–e36877. doi:10.7554/elife.36842
- Brunner, M., and Bujard, H. (1987). Promoter recognition and promoter strength in the *Escherichia coli* system. *EMBO J.* 6, 3139–3144. doi:10.1002/j.1460-2075.1987.tb02624.x
- Cameron, D. E., and Collins, J. J. (2014). Tunable protein degradation in bacteria. *Nat. Biotechnol.* 32, 1276–1281. doi:10.1038/nbt.3053
- Chalkley, O., Purcell, O., Grierson, C., and Marucci, L. (2019). The genome design suite: enabling massive *in-silico* experiments to design genomes. *bioRxiv*, doi:10.1101/681270
- Clark, T. B., Tully, J. G., Rose, D. L., Henegar, R., and Whitcomb, R. F. (1986). *Acholeplasmas* and similar nonsterol-requiring mollicutes from insects: missing link in microbial ecology. *Curr. Microbiol.* 13, 11–16. doi:10.1007/BF01568152
- Coradini, A. L. V., Hull, C. B., and Ehrenreich, I. M. (2020). Building genomes to understand biology. *Nat. Commun.* 11, 6177–6211. doi:10.1038/s41467-020-19753-2
- Cordova, C. M. M., Lartigue, C., Sirand-Pugnet, P., Renaudin, J., Cunha, R. A. F., and Blanchard, A. (2002). Identification of the origin of replication of the *Mycoplasma pulmonis* chromosome and its use in *oriC* replicative plasmids. *J. Bacteriol.* 184, 5426–5435. doi:10.1128/JB.184.19.5426-5435.2002
- Dai, X., and Zhu, M. (2018). High osmolarity modulates bacterial cell size through reducing initiation volume in *Escherichia coli*. *mSphere* 3, 004300–e518. doi:10.1128/mSphere.00430-18
- Datsenko, K. A., and Wanner, B. L. (2000). One-step inactivation of chromosomal genes in *Escherichia coli* K-12 using PCR products. *Proc. Natl. Acad. Sci. U. S. A.* 97, 6640–6645. doi:10.1073/pnas.120163297
- Dervyn, E., Planson, A. G., Tanaka, K., Chubukov, V., Guérin, C., Derozier, S., et al. (2023). Greedy reduction of *Bacillus subtilis* genome yields emergent phenotypes of high resistance to a DNA damaging agent and low evolvability. *Nucleic Acids Res.* 51, 2974–2992. doi:10.1093/nar/gkad145
- Domin, G., Findeiß, S., Wachsmuth, M., Will, S., Stadler, P. F., and Mörl, M. (2017). Applicability of a computational design approach for synthetic riboswitches. *Nucleic Acids Res.* 45, 4108–4119. doi:10.1093/nar/gkw1267
- Dragosits, M., and Mattanovich, D. (2013). Adaptive laboratory evolution - principles and applications for biotechnology. *Microb. Cell Fact.* 12, 64–17. doi:10.1186/1475-2859-12-64
- Emanuel, G., Moffitt, J. R., and Zhuang, X. (2017). High-throughput, image-based screening of pooled genetic-variant libraries. *Nat. Methods* 14, 1159–1162. doi:10.1038/nmeth.4495
- Etzel, M., and Mörl, M. (2017). Synthetic riboswitches: from plug and pray toward plug and play. *Biochemistry* 56, 1181–1198. doi:10.1021/acs.biochem.6b01218
- Fraser, C. M., Gocayne, J. D., White, O., Adams, M. D., Clayton, R., Fleischmann, R. D., et al. (1995). The minimal gene complement of *Mycoplasma genitalium*. *Science* 270, 397–403. doi:10.1126/science.270.5235.397
- Fredens, J., Wang, K., de la Torre, D., Funke, L. F. H., Robertson, W. E., Christova, Y., et al. (2019). Total synthesis of *Escherichia coli* with a recoded genome. *Nature* 569, 514–518. doi:10.1038/s41586-019-1192-5
- Fujita, H., Osaku, A., Sakane, Y., Yoshida, K., Yamada, K., Nara, S., et al. (2022). Enzymatic supercoiling of bacterial chromosomes facilitates genome manipulation. *ACS Synth. Biol.* 11, 3088–3099. doi:10.1021/acssynbio.2c00353
- Gasparich, G. E., and Chih-Horng, K. (2019). Genome analysis-based union of the genus *Mesoplasma* with the genus *Entomoplasma*. *Int. J. Syst. Evol. Microbiol.* 69, 2735–2738. doi:10.1099/ijsem.0.003548
- Gibson, D. G., Glass, J. I., Lartigue, C., Noskov, V. N., Chuang, R.-Y. Y., Algire, M. A., et al. (2010). Creation of a bacterial cell controlled by a chemically synthesized genome. *Science* 329, 52–56. doi:10.1126/science.1190719
- Glass, J. I., Merryman, C., Wise, K. S., Iii, C. A. H., and Smith, H. O. (2017). Minimal cells — real and imagined. *Cold Spring Harb. Perspect. Biol.* 1, 0238611–a23912. doi:10.1101/cshperspect.a023861
- Glass, J. I., Assad-Garcia, N., Alperovich, N., Yooshep, S., Lewis, M. R., Maruf, M., et al. (2006). Essential genes of a minimal bacterium. *Proc. Natl. Acad. Sci. U. S. A.* 103, 425–430. doi:10.1073/pnas.0510013103
- Goryshin, I. Y., Jendrisak, J., Hoffman, L. M., Meis, R., and Reznikoff, W. S. (2000). Insertional transposon mutagenesis by electroporation of released Tn5 transposition complexes. *Nat. Biotechnol.* 18, 97–100. doi:10.1038/72017
- Gur, E., and Sauer, R. T. (2008). Evolution of the *ssrA* degradation tag in *Mycoplasma*: specificity switch to a different protease. *Proc. Natl. Acad. Sci. U. S. A.* 105, 16113–16118. doi:10.1073/pnas.0808802105
- Hoose, A., Vellacott, R., Storch, M., Freemont, P. S., and Ryadnov, M. G. (2023). DNA synthesis technologies to close the gene writing gap. *Nat. Rev. Chem.* 7, 144–161. doi:10.1038/s41570-022-00456-9
- Huang, D., Holtz, W. J., and Maharbiz, M. M. (2012). A genetic bistable switch utilizing nonlinear protein degradation. *J. Biol. Eng.* 6, 9–13. doi:10.1186/1754-1611-6-9
- Hughes, R. A., and Ellington, A. D. (2017). Synthetic DNA synthesis and assembly: putting the synthetic in synthetic biology. *Cold Spring Harb. Perspect. Biol.* 9, a023812. doi:10.1101/cshperspect.a023812
- Hutchison, C. A., Chuang, R. Y., Noskov, V. N., Assad-Garcia, N., Deerinc, T. J., Ellisman, M. H., et al. (2016). Design and synthesis of a minimal bacterial genome. *Science* 351, aad6253–11. doi:10.1126/science.aad6253
- Hutchison, C. A., III, Peterson, S. N., Gill, S. R., Cline, R. T., White, O., Fraser, C. M., et al. (1999). Global transposon mutagenesis and a minimal *Mycoplasma genome*. *Science* 286, 2165–2169. doi:10.1126/science.286.5447.2165
- Isaacs, F. J., Carr, P. A., Wang, H. H., Lajoie, M. J., Sterling, B., Kraal, L., et al. (2011). Precise manipulation of chromosomes *in vivo* enables genome-wide codon replacement. *Science* 333, 348–353. doi:10.1126/science.1205822
- Ishag, H. Z. A., Xiong, Q., Liu, M., Feng, Z., and Shao, G. (2017). Development of *oriC*-plasmids for use in *Mycoplasma hyorhinis*. *Sci. Rep.* 7, 10596–10610. doi:10.1038/s41598-017-10519-3
- Iwade, Y., Honda, H., Sato, H., Hashimoto, M., and Kato, J. (2011). Oxidative stress sensitivity of engineered *Escherichia coli* cells with a reduced genome. *FEMS Microbiol. Lett.* 322, 25–33. doi:10.1111/j.1574-6968.2011.02331.x

- Juhas, M., and Ajioka, J. W. (2017). High molecular weight DNA assembly *in vivo* for synthetic biology applications. *Crit. Rev. Biotechnol.* 37, 277–286. doi:10.3109/07388551.2016.1141394
- Karas, B. J., Wise, K. S., Sun, L., Craig Venter, J., Glass, J. I., Hutchison, C. A., et al. (2014). Rescue of mutant fitness defects using *in vitro* reconstituted designer transposons in *Mycoplasma mycoides*. *Front. Microbiol.* 5, 369–9. doi:10.3389/fmicb.2014.00369
- Karcagi, I., Draskovits, G., Umenhoffer, K., Fekete, G., Kovács, K., Méhi, O., et al. (2016). Indispensability of horizontally transferred genes and its impact on bacterial genome streamlining. *Mol. Biol. Evol.* 33, 1257–1269. doi:10.1093/molbev/msw009
- Kim, J. N., Roth, A., and Breaker, R. R. (2007). Guanine riboswitch variants from *Mesoplasma florum* selectively recognize 2'-deoxyguanosine. *Proc. Natl. Acad. Sci. U. S. A.* 104, 16092–16097. doi:10.1073/pnas.0705884104
- Krishnakumar, R., Assad-garcia, N., Benders, G. A., Phan, Q., Montague, M. G., and Glass, J. I. (2010). Targeted chromosomal knockouts in *Mycoplasma pneumoniae*. *Appl. Environ. Microbiol.* 76, 5297–5299. doi:10.1128/AEM.00024-10
- Kühner, S., Van Noort, V., Betts, M. J., Leo-Madas, A., Batisse, C., Rode, M., et al. (2009). Proteome organization in a genome-reduced bacterium. *Science* 326, 1235–1240. doi:10.1126/science.1176343
- Labroussaa, F., Baby, V., Rodrigue, S., and Lartigue, C. (2019). Whole genome transplantation: bringing natural or synthetic bacterial genomes back to life. *Médecine/Sciences* 35, 761–770. doi:10.1051/medsci/2019154
- Labroussaa, F., Lebaudy, A., Baby, V., Gourgues, G., Matteau, D., Vashee, S., et al. (2016). Impact of donor-recipient phylogenetic distance on bacterial genome transplantation. *Nucleic Acids Res.* 44, 8501–8511. doi:10.1093/nar/gkw688
- Lachance, J.-C., Matteau, D., Brodeur, J., Lloyd, C., Mih, N., King, Z. A., et al. (2021). Genome-scale metabolic modeling reveals key features of a minimal gene set. *Mol. Syst. Biol.* 17, 1–20. doi:10.15252/msb.202010099
- Lachance, J.-C., Rodrigue, S., and Palsson, B. O. (2019). Synthetic Biology: minimal cells, maximal knowledge. *Elife* 8, 1–4. doi:10.7554/elife.45379
- Lartigue, C., Blanchard, A., Renaudin, J., Thiaucourt, F., and Sirand-Pugnet, P. (2003). Host specificity of mollicutes *oriC* plasmids: functional analysis of replication origin. *Nucleic Acids Res.* 31, 6610–6618. doi:10.1093/nar/gkg848
- Lartigue, C., Duret, S., Garnier, M., and Renaudin, J. (2002). New plasmid vectors for specific gene targeting in *Spiroplasma citri*. *Plasmid* 48, 149–159. doi:10.1016/S0147-619X(02)00121-X
- Lartigue, C., Glass, J. I., Alperovich, N., Pieper, R., Parmar, P. P., Hutchison, C. A., et al. (2007). Genome transplantation in bacteria: changing one species to another. *Science* 317, 632–638. doi:10.1126/science.1144622
- Lartigue, C., Vashee, S., Algire, M. A., Chuang, R. Y., Benders, G. A., Ma, L., et al. (2009). Creating bacterial strains from genomes that have been cloned and engineered in yeast. *Science* 325, 1693–1696. doi:10.1126/science.1173759
- Lloyd, C. J., Ebrahim, A., Yang, L., King, Z. A., Catoiu, E., O'Brien, E. J., et al. (2018). COBRAme: a computational framework for genome-scale models of metabolism and gene expression. *PLoS Comput. Biol.* 14, e1006302. doi:10.1371/journal.pcbi.1006302
- Lo, W. S., Gasparich, G. E., and Kuo, C. H. (2018). Convergent evolution among ruminant-pathogenic *Mycoplasma* involved extensive gene content changes. *Genome Biol. Evol.* 10, 2130–2139. doi:10.1093/gbe/evy172
- Lynch, M., Ackerman, M. S., Gout, J. F., Long, H., Sung, W., Thomas, W. K., et al. (2016). Genetic drift, selection and the evolution of the mutation rate. *Nat. Rev. Genet.* 17, 704–714. doi:10.1038/nrg.2016.104
- Maglennon, G. A., Cook, B. S., Matthews, D., Deeney, A. S., Bossé, J. T., Langford, P. R., et al. (2013). Development of a self-replicating plasmid system for *Mycoplasma hyopneumoniae*. *Vet. Res.* 44, 63–10. doi:10.1186/1297-9716-44-63
- Mariscal, A. M., Kakizawa, S., Hsu, J. Y., Tanaka, K., González-González, L., Broto, A., et al. (2018). Tuning gene activity by inducible and targeted regulation of gene expression in minimal bacterial cells. *ACS Synth. Biol.* 7, 1538–1552. doi:10.1021/acssynbio.8b00028
- Matteau, D., Baby, V., Pelletier, S., and Rodrigue, S. (2015). A small-volume, low-cost, and versatile continuous culture device. *PLoS One* 10, e0133384. doi:10.1371/journal.pone.0133384
- Matteau, D., Lachance, J.-C., Grenier, F., Gauthier, S., Daubenspeck, J. M., Dybvig, K., et al. (2020). Integrative characterization of the near-minimal bacterium *Mesoplasma florum*. *Mol. Syst. Biol.* 16, 98444–e9925. doi:10.15252/msb.20209844
- Matteau, D., Pepin, M., Baby, V., Gauthier, S., Arango Giraldo, M., Knight, T. F., et al. (2017). Development of *oriC*-based plasmids for *Mesoplasma florum*. *Appl. Environ. Microbiol.* 83, 033744–e3416. doi:10.1128/AEM.03374-16
- Matteau, D., and Rodrigue, S. (2015). "Precise identification of DNA-binding proteins genomic location by exonuclease coupled chromatin immunoprecipitation (ChIP-exo)," in *DNA-protein interactions SE - 11 methods in molecular biology*. Editors B. P. Leblanc and S. Rodrigue (New York: Springer), 173–193. doi:10.1007/978-1-4939-2877-4_11
- McCoy, R. E., Basham, H. G., Tully, J. G., and Rose, D. L. (1980). "Isolation of a new *Acholeplasma* from flowers in Florida," in *Third conference of the international organization for mycoplasmaology*. Custer, South Dakota, USA: (ICSP).
- McCoy, R. E., Basham, H. G., Tully, J. G., Rose, D. L., Carle, P., Bové, J. M., et al. (1984). *Acholeplasma florum*, a new species isolated from plants. *Int. J. Syst. Bacteriol.* 34, 11–15. doi:10.1099/00207713-34-1-11
- Merrick, C. A., Zhao, J., and Rosser, S. J. (2018). Serine integrases: advancing synthetic biology. *ACS Synth. Biol.* 7, 299–310. doi:10.1021/acssynbio.7b00308
- Messer, W. (2002). The bacterial replication initiator DnaA. DnaA and *oriC*, the bacterial mode to initiate DNA replication. *FEMS Microbiol. Rev.* 26, 355–374. doi:10.1111/j.1574-6976.2002.tb00620.x
- Milo, R. (2013). What is the total number of protein molecules per cell volume? A call to rethink some published values. *BioEssays* 35, 1050–1055. doi:10.1002/bies.201300066
- Morowitz, H. J. (1984). The completeness of molecular biology. *Isr. J. Med. Sci.* 20, 750–753.
- Morowitz, H. J., and Tourtellotte, M. E. (1962). The smallest living cells. *Sci. Am.* 206, 117–126. doi:10.1038/scientificamerican0362-117
- Mukai, T., Yoneji, T., Yamada, K., Fujita, H., Nara, S., and Su'etsugu, M. (2020). Overcoming the challenges of megabase-sized plasmid construction in *Escherichia coli*. *ACS Synth. Biol.* 9, 1315–1327. doi:10.1021/acssynbio.0c00008
- Navas-Castillo, J., Laigret, F., Tully, J., and Bové, J.-M. (1992). Le mollicute *Acholeplasma florum* possède un gène du système phosphoenolpyruvate sucrophosphotransférase et il utilise UGA comme codon tryptophane. *Comptes Rendus l'Académie Des. Sci. - Ser. III* 315, 43–48.
- Nyerges, A., Vinke, S., Flynn, R., Owen, S. V., Rand, E. A., Budnik, B., et al. (2023). A swapped genetic code prevents viral infections and gene transfer. *Nature* 615, 720–727. doi:10.1038/s41586-023-05824-z
- Pelletier, J. F., Sun, L., Wise, K. S., Assad-Garcia, N., Karas, B. J., Deerinck, T. J., et al. (2021). Genetic requirements for cell division in a genomically minimal cell. *Cell* 184, 2430–2440. doi:10.1016/j.cell.2021.03.008
- Peterson, S. N., Fraser, C. M., and Claire, M. (2001). The complexity of simplicity. *Genome Biol.* 2, 1–2002. doi:10.1016/S0378-4754(97)00044-X
- Pettersson, B., and Johansson, K.-E. (2002). "Taxonomy of mollicutes," in *Molecular biology and pathogenicity of mycoplasmas*. Editors S. Razin and R. Herrmann (New York (USA): Springer), 1–30.
- Pickar-Oliver, A., and Gersbach, C. A. (2019). The next generation of CRISPR–Cas technologies and applications. *Nat. Rev. Mol. Cell Biol.* 20, 490–507. doi:10.1038/s41580-019-0131-5
- Piñero-Lambea, C., Garcia-Ramallo, E., Martinez, S., Delgado, J., Serrano, L., and Lluch-Senar, M. (2020). *Mycoplasma pneumoniae* genome editing based on oligo recombineering and cas9-mediated counterselection. *ACS Synth. Biol.* 9, 1693–1704. doi:10.1021/acssynbio.0c00022
- Piñero-Lambea, C., Garcia-Ramallo, E., Miravet-Verde, S., Burgos, R., Scarpa, M., Serrano, L., et al. (2022). SURE editing: combining oligo-recombineering and programmable insertion/deletion of selection markers to efficiently edit the *Mycoplasma pneumoniae* genome. *Nucleic Acids Res.* 50, e127. doi:10.1093/nar/gkac836
- Pollack, J., Williams, M., Banzon, J., Jones, M. A., Harvey, L., and Tully, J. G. (1996). Comparative metabolism of *Mesoplasma*, *Entomoplasma*, *mycoplasma*, and *Acholeplasma*. *Int. J. Cell. Physiol.* 46, 885–890. doi:10.1099/00207713-46-4-885
- Rees-Garbutt, J., Chalkley, O., Landon, S., Purcell, O., Marucci, L., and Grierson, C. (2020a). Designing minimal genomes using whole-cell models. *Nat. Commun.* 11, 836–912. doi:10.1038/s41467-020-14545-0
- Rees-Garbutt, J., Rightmyer, J., Karr, J. R., Grierson, C., and Marucci, L. (2020b). Furthering genome design using models and algorithms. *Curr. Opin. Syst. Biol.* 24, 120–126. doi:10.1016/j.coisb.2020.10.007
- Rose, D. L., Kocka, J. P., Somerson, N. L., Tully, J. G., Whitcomb, R. F., Carle, P., et al. (1990). *Mycoplasma lactuca* sp. nov., a sterol-requiring mollicute from a plant surface. *Int. J. Syst. Bacteriol.* 40 (2), 138–42. doi:10.1099/00207713-40-2-138
- Rossi, M. J., Lai, W. K. M., and Pugh, B. F. (2018). Simplified ChIP-exo assays. *Nat. Commun.* 9, 2842–2913. doi:10.1038/s41467-018-05265-7
- Ruegg, T. L., Pereira, J. H., Chen, J. C., DeGiovanni, A., Novichkov, P., Mutalik, V. K., et al. (2018). Jungle Express is a versatile repressor system for tight transcriptional control. *Nat. Commun.* 9, 3617–3713. doi:10.1038/s41467-018-05857-3
- Saglio, P., Lhospital, M., Laflèche, D., Dupont, G., Bové, J. M., Tully, J. G., et al. (1973). *Spiroplasma citri* gen. and sp. n.: a mycoplasma-like organism associated with "stubborn" disease of Citrus. *Int. J. Syst. Bacteriol.* 23, 191–204. doi:10.1099/00207713-23-3-191
- Sakkos, J. K., Hernandez-Ortiz, S., Osteryoung, K. W., and Ducat, D. C. (2021). Orthogonal degen system for controlled protein degradation in cyanobacteria. *ACS Synth. Biol.* 10, 1667–1681. doi:10.1021/acssynbio.1c00035
- Sandberg, T. E., Salazar, M. J., Weng, L. L., Palsson, B. O., and Feist, A. M. (2019). The emergence of adaptive laboratory evolution as an efficient tool for biological discovery and industrial biotechnology. *Metab. Eng.* 56, 1–16. doi:10.1016/j.ymben.2019.08.004
- Sandberg, T. E., Wise, K. S., Dalldorf, C., Szubin, R., Feist, A. M., Glass, J. I., et al. (2023). Adaptive evolution of a minimal organism with a synthetic genome. *iScience* 26, 107500. doi:10.1016/j.isci.2023.107500

- Sapountzis, P., Zhukova, M., Hansen, L. H., Sørensen, S. J., Schiøtt, M., and Boomsma, J. J. (2015). Acromyrmex leaf-cutting ants have simple gut microbiota with nitrogen-fixing potential. *Appl. Environ. Microbiol.* 81, 5527–5537. doi:10.1128/AEM.00961-15
- Sapountzis, P., Zhukova, M., Shik, J. Z., Schiøtt, M., and Boomsma, J. J. (2018). Reconstructing the functions of endosymbiotic mollicutes in fungus-growing ants. *Elife* 7, e39209–e39231. doi:10.7554/eLife.39209
- Schindler, D., Dai, J., and Cai, Y. (2018). Synthetic genomics: a new venture to dissect genome fundamentals and engineer new functions. *Curr. Opin. Chem. Biol.* 46, 56–62. doi:10.1016/j.cbpa.2018.04.002
- Schubert, M. G., Goodman, D. B., Wannier, T. M., Kaur, D., Farzadfard, F., Lu, T. K., et al. (2021). High-throughput functional variant screens via *in vivo* production of single-stranded DNA. *Proc. Natl. Acad. Sci. U. S. A.* 118, e2018181118. doi:10.1073/pnas.2018181118
- Seto, S., and Miyata, M. (1998). Cell reproduction and morphological changes in *Mycoplasma capricolum*. *J. Bacteriol.* 180, 256–264. doi:10.1128/JB.180.2.256-264.1998
- Sirand-Pugnet, P., Citti, C., Barré, A., and Blanchard, A. (2007). Evolution of mollicutes: down a bumpy road with twists and turns. *Res. Microbiol.* 158, 754–766. doi:10.1016/j.resmic.2007.09.007
- Sleator, R. D. (2010). The story of *Mycoplasma mycoides* JCVI-syn1.0. *Bioeng. Bugs* 1, 231–232. doi:10.4161/bbug.1.4.12465
- Sleator, R. D. (2016). JCVI-syn3.0 – a synthetic genome stripped bare. *Bioengineered* 7, 53–56. doi:10.1080/21655979.2016.1175847
- Stamatikis, A. (2014). RAXML version 8: a tool for phylogenetic analysis and post-analysis of large phylogenies. *Bioinformatics* 30, 1312–1313. doi:10.1093/bioinformatics/btu033
- Su, C. J., and Baseman, J. B. (1990). Genome size of *Mycoplasma genitalium*. *Genome Size Mycoplasma genitalium* 172, 4705–4707. doi:10.1128/jb.172.8.4705-4707.1990
- Sundararaj, S., Guo, A., Habibi-Nazhad, B., Rouani, M., Stothard, P., Ellison, M., et al. (2004). The CyberCell Database (CCDB): a comprehensive, self-updating, relational database to coordinate and facilitate *in silico* modeling of *Escherichia coli*. *Nucleic Acids Res.* 32, D293–D295. doi:10.1093/nar/gkh108
- Sung, W., Ackerman, M. S., Miller, S. F., Doak, T. G., and Lynch, M. (2012). Drift-barrier hypothesis and mutation-rate evolution. *Proc. Natl. Acad. Sci. U. S. A.* 109, 18488–18492. doi:10.1073/pnas.1216223109
- Szydlo, K., Ignatova, Z., and Gorochowski, T. E. (2022). Improving the robustness of engineered bacteria to nutrient stress using programmed proteolysis. *ACS Synth. Biol.* 11, 1049–1059. doi:10.1021/acssynbio.1c00490
- Tully, J., Rose, D., Whitcomb, R. F., Hackett, K. J., Clark, T. B., Henegar, R. B., et al. (1987). Characterization of some new insect-derived achleplasmas. *Isr. J. Med. Sci.* 23, 699–703.
- Tully, J. G. (1979). Special features of the achleplasmas. *Mycoplasmas* 1, 431–449. doi:10.1016/b978-0-12-078401-1.50022-4
- Tully, J. G. (1983). The Emmy Klieneberger-Nobel Award lecture. Reflections on recovery of some fastidious mollicutes with implications of the changing host patterns of these organisms. *Yale J. Biol. Med.* 56, 799–813.
- Tully, J. G., Bove, J. M., Laigret, F., and Whitcomb, R. F. (1993). Revised taxonomy of the class mollicutes: proposed elevation of a monophyletic cluster of arthropod-associated mollicutes to ordinal rank (*Entomoplasmatales* ord. Nov.), with provision for familial rank to separate species with nonhelical morphology. *Entom. Int. J. Syst. Bacteriol.* 43, 378–385. doi:10.1099/00207713-43-2-378
- Tully, J. G., Rose, D. L., Hackett, K. J., Whitcomb, R. F., Carle, P., Bove, J. M., et al. (1989). *Mycoplasma ellychniae* sp. nov., a sterol-requiring mollicute from the firefly beetle *Ellychnia corrusca*. *Int. J. Syst. Bacteriol.* 39, 284–289. doi:10.1099/00207713-39-3-284
- Tully, J. G., Whitcomb, R. F., Hackett, K. J., Rose, D. L., Henegar, R. B., Bove, J. M., et al. (1994). Taxonomic descriptions of eight new non-sterol-requiring Mollicutes assigned to the genus *Mesoplasma*. *Int. J. Syst. Bacteriol.* 44, 685–693. doi:10.1099/00207713-44-4-685
- Tully, J. G., Whitcomb, R. F., Rose, D. L., Hackett, K. J., Edward, C. L. A. R. K., Henegar, R. B., et al. (1990a). Current insight into the host diversity of achleplasmas. *Zentralblatt für Bakteriologie* 20, 461–467.
- Tully, J. G., Rose, D. L., McCoy, R. E., Carle, P., Bove, J. M., Whitcomb, W. G., et al. (1990b). *Mycoplasma melaleuca* sp. nov., a sterol-requiring mollicute from flowers of several tropical plants. *Int J Syst Bacteriol.* 40 (2), 143–7. doi:10.1099/00207713-40-2-143
- Tully, J. G., Whitcomb, R. F., Hackett, K. J., Williamson, D. L., Laigret, F., Carle, P., et al. (1998). *Entomoplasma freundtii* sp. nov., a new species from a green tiger beetle (Coleoptera: Cicindelidae). *Int J Syst Bacteriol.* 48 (4), 1197–204. doi:10.1099/00207713-48-4-1197
- Volkmer, B., and Heinemann, M. (2011). Condition-Dependent cell volume and concentration of *Escherichia coli* to facilitate data conversion for systems biology modeling. *PLoS One* 6, e23126–6. doi:10.1371/journal.pone.0023126
- Whitcomb, R., and Tully, J. (1995). Revised minimum standards for description of new species of the class mollicutes (division tenericutes). *J. Syst.* 45, 605–612. doi:10.1099/00207713-45-3-605
- Whitcomb, R. F., Tully, J. G., Rose, D. L., Stephens, E. B., Smith, A., McCoy, R. E., et al. (1982). Wall-less prokaryotes from fall flowers in Central United States and Maryland. *Curr. Microbiol.* 7, 285–290. doi:10.1007/bf01566864
- Williamson, D. L., Tully, J. G., Rose, D. L., Hackett, K. J., Henegar, R., Carle, P., et al. (1990). *Mycoplasma somnifera* sp. nov., *Mycoplasma luminis* sp. nov., and *Mycoplasma lucivorax* sp. nov., new sterol-requiring mollicutes from firefly beetles (Coleoptera: Lampyridae). *Int J Syst Bacteriol.* 40 (2), 160–4. doi:10.1099/00207713-40-2-160
- Wodke, J. A. H., Pucha, J., Lluch-Senar, M., Marcos, J., Yus, E., Godinho, M., et al. (2013). Dissecting the energy metabolism in *Mycoplasma pneumoniae* through genome-scale metabolic modeling. *Mol. Syst. Biol.* 9, 653. doi:10.1038/msb.2013.6
- Yoneji, T., Fujita, H., Mukai, T., and Suetsugu, M. (2021). Grand scale genome manipulation via chromosome swapping in *Escherichia coli* programmed by three one megabase chromosomes. *Nucleic Acids Res.* 49, 8407–8418. doi:10.1093/nar/gkab298
- Yus, E., Maier, T., Michalodimitrak, K., van Noort, V., Yamada, T., Chen, W. H., et al. (2009). Impact of genome reduction on bacterial metabolism and its regulation. *Science* 326, 1263–1268. doi:10.1126/science.1177263
- Zhou, Q., Wu, Y., Deng, J., Liu, Y., Li, J., Du, G., et al. (2023). Combinatorial metabolic engineering enables high yield production of α -arbutin from sucrose by biocatalysis. *Appl. Microbiol. Biotechnol.* 107, 2897–2910. doi:10.1007/s00253-023-12496-2
- Zürcher, J. F., Robertson, W. E., Kappes, T., Petris, G., Elliott, T. S., Salmond, G. P. C., et al. (2022). Refactored genetic codes enable bidirectional genetic isolation. *Science* 378, 516–523. doi:10.1126/science.add8943



OPEN ACCESS

EDITED BY
Michal Letek,
University of León, Spain

REVIEWED BY
Ciaran Skerry,
University of Maryland, United States
Catherine Chaput,
NEC Laboratories Europe, Germany

*CORRESPONDENCE
Haixia Luo
✉ haixia.luo@foxmail.com
Min Li
✉ limingfm@126.com

RECEIVED 26 February 2024
ACCEPTED 13 May 2024
PUBLISHED 28 May 2024

CITATION
Wang Y, Ma C, Hao X, Wang W, Luo H and
Li M (2024) Identification of *Mycoplasma
pneumoniae* proteins interacting with NOD2
and their role in macrophage inflammatory
response.
Front. Microbiol. 15:1391453.
doi: 10.3389/fmicb.2024.1391453

COPYRIGHT
© 2024 Wang, Ma, Hao, Wang, Luo and Li.
This is an open-access article distributed
under the terms of the [Creative Commons
Attribution License \(CC BY\)](#). The use,
distribution or reproduction in other forums is
permitted, provided the original author(s) and
the copyright owner(s) are credited and that
the original publication in this journal is cited,
in accordance with accepted academic
practice. No use, distribution or reproduction
is permitted which does not comply with
these terms.

Identification of *Mycoplasma pneumoniae* proteins interacting with NOD2 and their role in macrophage inflammatory response

Yongyu Wang^{1,2}, Chunji Ma^{1,2,3}, Xiuqing Hao¹, Weili Wang^{1,2},
Haixia Luo^{1,2*} and Min Li^{1,2*}

¹Life Science School, Ningxia University, Yinchuan, China, ²Key Laboratory of Ministry of Education for Conservation and Utilization of Special Biological Resources in Western China, Ningxia University, Yinchuan, China, ³Ningxia Polytechnic College, Yinchuan, China

Mycoplasma pneumoniae (*M. pneumoniae*, Mp) is a cell wall-deficient microorganism known to cause chronic respiratory infections in both children and adults. Nucleotide-binding oligomerization domain-containing protein 2 (NOD2) is an intracellular pattern recognition receptor primarily responsible for identifying muramyl dipeptide (MDP) found in bacterial cell walls. Previous experiments have demonstrated that *Mycoplasma ovipneumoniae* induces macrophage autophagy through NOD2. In this study, we conducted RNA-seq analysis on macrophages infected with *M. pneumoniae* and observed an up-regulation in the expression of genes associated with the NOD2 signaling pathway. Mechanistic investigations further revealed the involvement of the NOD2 signaling pathway in the inflammatory response of macrophages activated by *M. pneumoniae*. We utilized GST pull-down technology in conjunction with liquid chromatography–tandem mass spectrometry (LC–MS/MS) to pinpoint the *M. pneumoniae* proteins that interact with NOD2. Additionally, co-immunoprecipitation (Co-IP) and immunofluorescence co-localization techniques were used to confirm the interaction between DUF16 protein and NOD2. We found that DUF16 protein can enter macrophages and induce macrophage inflammatory response through the NOD2/RIP2/NF- κ B pathway. Notably, the region spanning amino acids 13–90 was identified as a critical region necessary for DUF16-induced inflammation. This research not only broadens our comprehension of the recognition process of the intracellular receptor NOD2, but also deepens our understanding of the development of *M. pneumoniae* infection.

KEYWORDS

Mycoplasma pneumoniae, DUF16, macrophages, NOD2, NF- κ B, inflammation

1 Introduction

M. pneumoniae is a minute organism with a small genome. It is the smallest self-replicating prokaryotic organism that can live independently without a cell wall (Shimizu, 2015; Kenri, 2023). *M. pneumoniae* is a well-known pathogen responsible for community-acquired pneumonia (CAP) and can also invade the respiratory tract (Kumar, 2018),

leading to laryngitis, pharyngitis, bronchitis, atypical pneumonia, and aggravation of asthma. Additionally, *M. pneumoniae* is capable of causing extrapulmonary complications (Tsai et al., 2021). In recent years, there has been a significant increase in the number of patients with refractory *M. pneumoniae* pneumonia (RMPP) (Tong et al., 2022). Unfortunately, the treatment effectiveness has declined noticeably, and there have been frequent reports of fatal cases, which has garnered considerable attention (Lee et al., 2018). Our understanding of the invasive nature and intracellular parasitism of *M. pneumoniae* in the host remains limited. Consequently, the pathogenic mechanism of *M. pneumoniae* continues to elude us.

Macrophages, as the body's primary defense against pathogenic bacteria, play a critical role in the innate immune response by engaging in phagocytosis, bacterial destruction, and antigen presentation to ward off infections (Cole et al., 2014; Shamaei and Mirsaedi, 2021). Through pattern recognition receptors (PRRs), macrophages can identify pathogen-associated molecular patterns (PAMPs) that stimulate an immune response (Takeuchi and Akira, 2010). Studies have indicated that *M. pneumoniae* can provoke a robust inflammatory reaction by activating Toll-like receptors (TLR2, TLR4) (Shimizu, 2016; de Groot et al., 2022). Unlike typical bacteria, mycoplasmas lack cell walls and lack inflammation-inducing endotoxins such as lipopolysaccharide (LPS) (Kenri, 2023; Lanao et al., 2024). Accordingly, lipoproteins in *M. pneumoniae* have been pinpointed as the agents responsible for instigating inflammation, as they trigger the immune response through TLR2 and TLR4 (Shimizu et al., 2005, 2014; Shimizu, 2016). Yet, the precise mechanism by which these lipoproteins interact with pattern recognition receptors remains incompletely elucidated, leaving unanswered queries as to the potential activation of similar receptors by other proteins. Consequently, further research is necessary to unravel the interplay between *M. pneumoniae* and the body's PRRs and to discover novel therapeutic targets.

The NOD-like receptor (NLR) family, composed of NLRs, RLRs, and ALRs subfamilies, represents the largest group of pattern recognition receptors within the human body (Wicherska-Pawłowska et al., 2021). These receptors are distributed across various tissues and cells and play a crucial role in maintaining overall health. Nucleotide-binding oligomerization domain-containing protein 2 (NOD2) is a critical intracellular pattern recognition receptor (PRR) belonging to the NLRs (Domínguez-Martínez et al., 2018; Godkowicz and Druszczyńska, 2022). The structural components of this particular entity are unique, consisting of a C-terminal domain rich in leucine repeats (LRR), a central domain for binding nucleotides (NBD), and two CARD domains at the N-terminus for the activation and recruitment of caspases (Trindade and Chen, 2020). The C-terminal LRR domain is responsible for recognizing bacterial peptidoglycans (Alipoor and Mirsaedi, 2021). The central NBD domain regulates the oligomerization of ATP-dependent receptors and also serves in detecting the C-terminal domain (Strober et al., 2006). The N-terminal CARDS are involved in regulating intracellular signaling pathways such as apoptosis, autophagy, and inflammation (Alipoor and Mirsaedi, 2021). NOD2 acts as a sensor for discerning muramyl dipeptide (MDP) derived from in bacterial cell walls. Upon recognition of MDP, the NOD2 CARD domains recruit and activate serine/threonine kinase receptor-interacting protein 2 (RIP2). This activation process initiates the movement of NF- κ B into the nucleus,

leading to the transcription and expression of various inflammatory factors (Caruso et al., 2014; Negroni et al., 2018).

Based on the aforementioned interaction between *Mycoplasma* and pattern recognition receptors, it is hypothesized that *M. pneumoniae* has the ability to activate macrophage NOD2, thereby inducing a macrophage inflammatory response. It is postulated that the virulence proteins associated with *M. pneumoniae* may have a significant impact on this mechanism. In our previous study we discovered that *M. ovipneumoniae* can induce macrophage autophagy through NOD2 (Luo et al., 2020). However, it is unclear the mechanism of *mycoplasma* on the activation NOD2 and its interaction with inflammatory in macrophage. The initial findings of our research revealed the specific factor in *M. pneumoniae* that triggers NOD2 activation, as well as its domain's role in the inflammatory response triggered by *M. pneumoniae*.

2 Materials and methods

2.1 *Mycoplasma pneumoniae* culture, count and extraction

The FH strain of *M. pneumoniae* (ATCC 15531) was acquired from the American Type Culture Collection (ATCC) in Rockville, MD, United States, and was grown in a broth resembling pleuropneumonia-like organisms (PPLO) by BD Biosciences, located in the USA. The *M. pneumoniae* was then cultured at a temperature of 37°C for a minimum of 7 days until there was a noticeable shift in the color of the medium from red to a yellowish-orange hue.

M. pneumoniae was quantified using Color-changing units (CCU). Twelve sterile EP tubes were labeled with numbers 1 to 12. Each EP tube was filled with 900 μ L of *Mycoplasma* complete medium. Tube 1 received 100 μ L of the *Mycoplasma* solution to be tested, which was then mixed. Then, 100 μ L of the mixed liquid in tube 1 was transferred to tube 2, and this process was repeated until tube 11. Tube 12 served as the negative control. The 12 EP tubes were incubated in a 5% CO₂ incubator at 37°C for 7–10 days. The last tube to turn yellow indicated the *M. pneumoniae* CCU. After centrifugation at 10,000 \times g for 10 min, the supernatant was discarded, and the precipitated bacteria were suspended and washed once with sterile PBS solution. After another round of centrifugation, the supernatant was discarded, and the bacteria were left to precipitate for further use.

2.2 Recombinant protein expression and purification

E. coli BL21 (DE3) was maintained by the laboratory. The LRR protein was tagged with a GST tag, while DUF16 was tagged with a His tag. The following procedure was used to purify GST-LRR, GST-Tag and His-DUF16 proteins. The appropriate plasmid was introduced into *E. coli* BL21 (DE3) by transformation, and the expression of the mutant protein was induced by adding IPTG to 0.6 mM. The cells were grown at 37°C for 12 h and harvested. The cell pellet was resuspended in buffer PBS. The cells were lysed by sonication, and GST-LRR, GST-Tag or His-DUF16 was purified over an BeaverBeads™ GSH and Ni-NTA column (beaverbio, China)

according to the manufacturer's instructions. The eluted fractions were separated on a 12% SDS-PAGE to confirm the purity of the protein.

2.3 Cell culture and stimulation

293 T cells and RAW264.7 monocytes from the Chinese Academy of Sciences cell bank in Shanghai, China were utilized in our research after confirming their mycoplasma contamination-free status. Specifically, RAW264.7 monocytes and 293 T cells were maintained in DMEM medium (HyClone, United States) supplemented with 10% FBS and 1% penicillin-streptomycin at 37°C with 5% CO₂. Upon reaching the logarithmic growth phase, macrophages were seeded in 6-well plates at a concentration of 1×10^6 /ml and allowed to proliferate overnight. Subsequently, the cells were exposed to varying concentrations of Mp or recombinant proteins at designated time points.

2.4 Cell viability and cytotoxicity assay

The Cell Counting Kit-8 (CCK-8, KeyGEN BioTECH, Nanjing, China) assay was employed to assess cell proliferation, in accordance with the instructions provided by the manufacturer. RAW264.7 cells (8,000 per well) were plated in 96-well dishes, utilizing the same techniques outlined earlier for MΦ differentiation. To establish the multiplicity of infection (MOI), MΦs were exposed to varying MOI levels of 0, 10, 20, 40, 80, and 160 over a 24-h period after infection with *M. pneumoniae*. To evaluate Mp's impact on MΦs, cells were exposed to *M. pneumoniae* at different time points ranging from 0 to 96 h, based on the results of the MOI analysis from the preceding step. Cell viability was gaged following the manufacturer's instructions for the cell counting kit-8, with absorbance readings taken at 490 nm using a fluorescence microplate reader (PerkinElmer, United States).

2.5 RNA extraction, library construction and sequencing

RNA extraction was carried out with the Trizol reagent kit according to the manufacturer's instructions. The RNA quality was assessed using the Agilent 2100 Bioanalyzer and validated by RNase-free agarose gel electrophoresis. Subsequently, eukaryotic mRNA was isolated using Oligo (dT) beads and then fragmented into shorter segments with fragmentation buffer before being reverse transcribed into cDNA using the NEB Next Ultra RNA Library Prep Kit for Illumina. The resulting double-stranded cDNA fragments underwent end repair, addition of an A base, and ligation to Illumina sequencing adapters. After purification with AMPure XP Beads, the ligated fragments were size-selected via agarose gel electrophoresis and amplified by PCR. The cDNA library obtained was then sequenced on an Illumina Novaseq6000 platform by Gene Denovo Biotechnology Co. in Guangzhou, China.

2.6 Enrichment analysis

Enrichment analysis is a common method used in omics research to gain insight into the functional tendencies of a gene set. Two

popular methods for enrichment analysis include gene ontology (GO) enrichment analysis and Kyoto Encyclopedia of Genes and Genomes (KEGG) enrichment analysis. GO, established by the Gene Ontology Consortium, is a database aimed at defining the functions of gene products. Through GO enrichment analysis, researchers can assess how enriched differential genes are in terms of specific GO terms, with more significant enrichments represented by darker colors. On the other hand, KEGG, founded in 1995, is a comprehensive database that integrates information on genomics, chemicals, and systemic functionalities. This database enables the prediction of protein interaction networks involved in various cellular processes. By performing KEGG pathway enrichment analysis, researchers can annotate the functions of differentially expressed genes and gain insights into the relevant pathways and functions associated with these genes.

2.7 Small interfering RNA transfection

Small interference reagents, including siNC and siNOD2, were procured from Guangzhou Ruibo Biotechnology Co., Ltd. siNC serves as a universal negative control for siNOD2, with a sequence that shows no similarity to the human, rat, and mouse transcriptomes. The specific sequence details of siNC have not been made public by the company at this moment. The target sequence of siNOD2#1 is: GCAACAGCGTGGGTGATAA, the target sequence of siNOD2#2 is: GCACAGAGTTGCAACTGAA, and the target sequence of siNOD2#3 is: GCGAGCACTTCCATTCCAT. RAW264.7 cells underwent transfection with siNOD2-1, siNOD2-2, siNOD2-3 (50 nM) or a negative control siRNA (si-NC) (50 nM) using Lipofectamine™ 2000 Transfection Reagent (Invitrogen Inc., Carlsbad, CA, United States). The cells were seeded in a 6-well plate per group and placed in an incubator at 37°C with 5% CO₂ until reaching 80% confluence. The cell transfection was carried out in strict adherence to the Lipofectamine 2000 Transfection Reagent operational guidelines. The efficacy of knockdown was validated through western blot analysis 24 h post transfection.

2.8 ELISA assay

The cell supernatants were centrifuged at 12,000 × g and 4°C for 5 min to remove any cellular debris before being analyzed using mouse IL-1β, TNF-α, IL-6, IL-8, and IL-8 ELISA kits from Boster in China following the instructed procedures. The absorbances of the samples were measured at 450 nm using a fluorescence microplate reader made by PerkinElmer in the United States.

2.9 Construction of plasmids, protein production and GST pull-down assays

Primer sequences were designed using the PCR-based Accurate Synthesis (PAS) method, incorporating the protective base synthesis gene LRR at both ends. The recombinant plasmid pGEX-4 T-1-LRR resulted from ligating the primers within the EcoRI (GAATTC)-XhoI (CTCGAG) sites of the pGEX-4 T-1 vector. Insertion of the full-length NOD2-LRR domain from mice into the pGEX-4 T-1 vector enabled

protein production in *Escherichia coli*. Transformation of the resulting plasmid DNA into BL21 (DE3) cells (TIANGEN BIOTECH (BEIJING) Co., LTD.) was followed by induction of protein expression at 16°C for 12 h upon addition of isopropyl- β -D-thiogalactoside (IPTG) to a final concentration of 0.1 mM. Subsequent steps included cell collection by centrifugation, washing, and storage at -80°C . Protein purification involved incubating supernatants with glutathione-Sepharose resin (Amersham Pharmacia, Piscataway, NJ) for 2 h, followed by centrifugation at 500 rpm for 2 min at 4°C . The resin was rinsed with a buffer containing 1 mM PMSE, 1% Triton, 50 mM Tris-HCl, and 100 mM NaCl, followed by elution of proteins using 15 mM glutathione. The proteins were validated through SDS-PAGE analysis and Western blotting with the anti-GST antibody from Proteintech. To assess binding, 500 μL of the refined GST-LRR extract was combined with Tris-NaCl buffer-washed glutathione-Sepharose resin. As a control, GST protein was utilized. *M. pneumoniae* whole cell lysates were mixed with the resin and left to incubate overnight with gentle rotation at 4°C . The resin was then collected and washed thrice using Tris-NaCl buffer. Following a brief boiling, SDS-containing gel loading buffer (100 μL) was introduced to the resin. Samples (10 μL) were subjected to SDS-PAGE electrophoresis, protein silver staining, and Western blotting employing anti-GST antibodies.

2.10 nanoLC-MS/MS

In this investigation, a total of 1 microgram of peptides were separated and examined utilizing a nano-UPLC (EASYnLC1200) linked to a Q Exactive HFX Orbitrap device (Thermo Fisher Scientific) with a nano electrospray ion source. The process of separation included the utilization of a reversed-phase column (100 micrometers ID \times 15 cm, ReprosilPur 120 C18AQ, 1.9 micrometers, Dr. Maisch) and mobile solutions containing H₂O with 0.1% formic acid, 2% acetonitrile (solvent A) and 80% acetonitrile, 0.1% formic acid (solvent B). The specimen was separated utilizing a 60-min gradient at a flow rate of 300 nanoliters per minute. The B gradient was varied as follows: 2–5% for 2 min, 5–22% for 44 min, 22–45% for 10 min, 45–95% for 2 min, and 95% for 2 min. Acquisition of data was carried out using Data-Dependent Acquisition (DDA) in both profile and positive modes with an Orbitrap analyzer. The resolution for MS1 analysis was set at 120,000 (@200 m/z) over a range of 350–1,600 m/z. In comparison, MS2 analysis was performed at a resolution of 15,000 with a dynamic initial mass. For MS1, the automatic gain control (AGC) target was 3E6 with a maximum injection time (IT) of 50 ms, while for MS2, it was set to 1E5 with a maximum IT of 110 ms. The 20 most intense ions were subjected to HCD fragmentation with a normalized collision energy (NCE) of 27% within an isolation window of 1.2 m/z. Dynamic exclusion was applied with a time window of 45 s, and single-charged and over 6-charged ions were excluded from the DDA process.

2.11 Bioinformatics analysis

The proteins identified were classified and annotated functionally through the utilization of the Gene Ontology (GO) analysis tool within the Database for Annotation, Visualization, and Integrated

Discovery (DAVID). Analysis of pathways was carried out with the KEGG pathway database. Furthermore, the software Ingenuity Pathway Analysis (IPA) was used for the analysis of Diseases and Functions.

2.12 Protein Annotation

The Uniprot database¹ was used for genome annotation of 12 differential proteins. The virulence function of 12 proteins was predicted through VirulentPred² online software.

2.13 Plasmid transfection

RAW264.7 cells ($0.5\text{--}2 \times 10^5/\text{well}$) were seeded in 24-well plates to achieve a confluence of 90–95% at the time of transfection. Each plasmid was diluted separately in 50 μL OptiPro SFM and mixed gently. 2 μL of each Lipofectamine2000 CD (ThermoFisher, United States) reagent was diluted in each tube in 50 μL LOptiPro SFM. The cells were incubated at room temperature for 5 min. After 5 min of incubation, diluted DNA and Lipofectamine 2000CD reagent (total volume per tube = 100 μL) were combined. Mix gently and incubate at room temperature for 20 min (the solution may become cloudy). 100 μL of the complex was added to Wells containing cells and medium. Shake the dish back and forth and mix lightly. Cells were incubated in a CO₂ incubator for 48 h at 37°C before determined protein expression.

2.14 Western blot

The purified protein solution was mixed with 6 \times protein loading buffer (obtained from TransGen in China) and subsequently subjected to denaturation by heating at 100°C for a duration of 10 min. The RIPA Lysis buffer was used to lyse total protein from 264.7 cells, following which 40 μg of total proteins were subjected to sodium dodecyl sulfate-polyacrylamide gel electrophoresis (SDS-PAGE). These proteins were then transferred onto a PVDF nitrocellulose membrane. The next step involved blocking the membrane with a solution of 5% non-fat milk that contained 0.2% Tween-20 in 1 \times PBS for a period of 1.5 h at room temperature. The membranes were incubated overnight at 4°C with these primary antibodies: NOD2, RIPK2, total NF- κB , Phospho-NF- κB p65 (Ser536), Phospho-IKB α p-IKB α (Ser32/Ser36), IKB α , and β -actin (all sourced from Affinity Biosciences, China); Flag-tag, GST-tag, and His-tag (all obtained from Proteintech, China). Subsequently, the membranes underwent incubation with a secondary antibody conjugated with horseradish peroxidase (HRP) for 2 h at room temperature. The protein of interest was then visualized using an enhanced chemiluminescence (ECL) reagent and GE Image Quant LAS 600. The intensity of the bands was measured through densitometric analysis using Image J software. Each experiment was carried out three times to ensure accuracy and reliability.

1 <https://www.uniprot.org/>

2 <http://bioinfo.icgeb.res.in/virulent/>

2.15 Statistical analysis

All data were analyzed using GraphPad Prism 8 software. Each experiment was repeated a minimum of 3 times. The data were analyzed using ANOVA and Tukey's test. And expressed as the mean \pm SD. Significance levels were indicated as * $p < 0.05$, ** $p < 0.01$, *** $p < 0.001$, and ns for not significant.

3 Results

3.1 Transcriptome analysis of *Mycoplasma pneumoniae*-infected macrophages

In order to investigate the transcriptome of *M. pneumoniae*-infected macrophages, we conducted experiments to determine the optimal post-infection time and dose using CCK8. Our results indicated a notable decrease in macrophage viability with increasing MOI values, with a significant decrease observed at MOI=10:1 (Figure 1A). Further analysis showed that after infecting macrophages with *M. pneumoniae* (MOI=10:1) for 6h and 12h, there was no significant change in macrophage viability. However, as the infection duration increased, macrophage viability began to decrease significantly after 24h (Figure 1B). The same experimental results were also obtained through fluorescence microscopy (Figures 1C,D). After infecting macrophages with *Mycoplasma pneumoniae* at a dose of MOI=10 for 24h, it was observed that the majority of cells remained viable (green). Consequently, we established an infection dose of MOI=10 and an infection duration of 24h as the standardized experimental conditions for further analysis. From three independent experiments, we obtained a total of 277,293,446 raw sequencing, encompassing both *M. pneumoniae*-infection and uninfected RAW264.7 cells. Our analysis identified 806 differentially expressed genes in response to *M. pneumoniae* infection based on FDR and log2 fold change criteria ($FDR < 0.05$ and $|\log_2 fc| > 2$). KEGG Pathway analysis demonstrated that the top 20 enriched pathways associated with *M. pneumoniae* infection predominantly involved NOD-like receptor signaling pathway, Toll-like receptor signaling pathway, and other pathways (Figure 1E). To better illustrate the regulatory role of NOD-like receptor signaling pathways in *M. pneumoniae* infection, we analyzed and identified differential genes enriched in these pathways. We found that the expression of genes such as NOD2, IL-1 β , and TNF- α in the NOD-like signaling pathway was up-regulated (Figure 1F). qPCR technology was utilized to confirm the expression of key genes in the NOD2 signaling pathway 24h post-infection of macrophages with *M. pneumoniae*. In comparison to the control group, *M. pneumoniae* infection led to a notable upregulation in the transcription levels of genes like NOD2, RIP2, and TNF- α (see Figure 1G; Supplementary Figure S1). These data collectively suggest the involvement of the NOD2 signaling pathway in the inflammatory response of mouse macrophages induced by *M. pneumoniae*.

3.2 NOD2 activate *Mycoplasma pneumoniae* induced macrophage inflammatory

Our Transcriptome results revealed a notable focus on the NOD-like receptor signaling pathway during *M. pneumoniae* infection.

In the NOD-like signaling pathway, NOD1 primarily detects γ -D-glutamo-diaminopimelic acid (iE-DAP) in the bacterial cell wall, whereas NOD2 primarily recognizes muramyl dipeptide (MDP). Upon activation, NOD1 and NOD2 recruit downstream receptor-interacting serine-threonine protein 2 (RIP2) through CARD-CARD interaction. RIP2, along with E3 ligases cIAP1, cIAP2, and XIAP, form a polyubiquitin scaffold that recruits TAK1 and IKK, leading to NF- κ B activation. NF- κ B then triggers the expression of inflammatory cytokines and genes involved in nitric oxide (NO) production. The downstream signaling pathways of NOD1 and NOD2 exhibit significant similarities. To verify the activation of NOD2 induced in macrophage inflammation, we assessed the expression of NOD1 and NOD2-related genes in RAW264.7 cells following a 24-h infection of *M. pneumoniae*. Our experimental results demonstrate that *M. pneumoniae* infection induces a notable upregulation of NOD2, p-RIP2, and p-NF- κ B p65 expression in macrophages when compared to uninfected cells (control). This is similar to the effect observed with MDP, a NOD2 activator (Figures 2A–E). Conversely, there was no significant alteration in the expression of NOD1 in macrophages (Figure 2B). These results confirmed that *M. pneumoniae* can activate NOD2. Small interfering (siRNA)-NOD2 was utilized to downregulate NOD2 expression in order to investigate the impact of NOD2 on inflammation induction in *M. pneumoniae*-infected cells over a 24-h period. The findings revealed that all three small interfering RNAs successfully achieved NOD2 knockdown, with siNOD2-3 demonstrating the most effective interference effect (Figures 2F,G). Consequently, siNOD2-3 was selected for further experiments. Inflammatory factors TNF- α , IL-6, IL-8, and IL-1 β were assessed using ELISA. The results show that both *M. pneumoniae* and MDP treated RAW264.7 cells showed markedly increased expression of TNF- α , IL-6, IL-8, and IL-1 β compared to siRNA-control (siNC) (Figures 2H–K). knock downing NOD2 expression via siRNA significantly suppressed the *M. pneumoniae* induced the expression of TNF- α , IL-6, IL-8, and IL-1 β comparing with siNC+Mp treatment (Figures 2H–K). Thus, these collective findings indicate that *M. pneumoniae*-induced inflammatory was mediated by the activation of NOD2.

3.3 *Mycoplasma pneumoniae* DUF16 interacted with NOD2

To identify the precise protein from *M. pneumoniae* that activates NOD2, we expressed NOD2 LRR domain tagged it with GST (LRR-GST) using an *E. coli* expression system (Figure 3A). Purified LRR-GST fusion protein purification magnetic beads were used to pull down the LRR-GST interaction protein from lysed *M. pneumoniae*. Purified GST was used as control. Silver staining revealed discernible bands in the LRR-GST efflux fluid group (LRR-GST-elution) compared to the control group (GST-elution) (Figure 3B). Subsequent elution protein samples using LC-MS/MS identified a total of 39 *M. pneumoniae* proteins. Twelve *M. pneumoniae* proteins that potentially interact with NOD2 were identified in the LRR-GST group (Figure 3C). Information of these proteins regarding the names, subcellular localization, functions, and virulence effects of these proteins was obtained in Table 1. Subcellular localization analysis revealed that out of the 12 differential proteins, four were membrane proteins, five were intracellular proteins, and three had unknown localization. Virulence protein prediction indicated that six proteins have virulence functions.

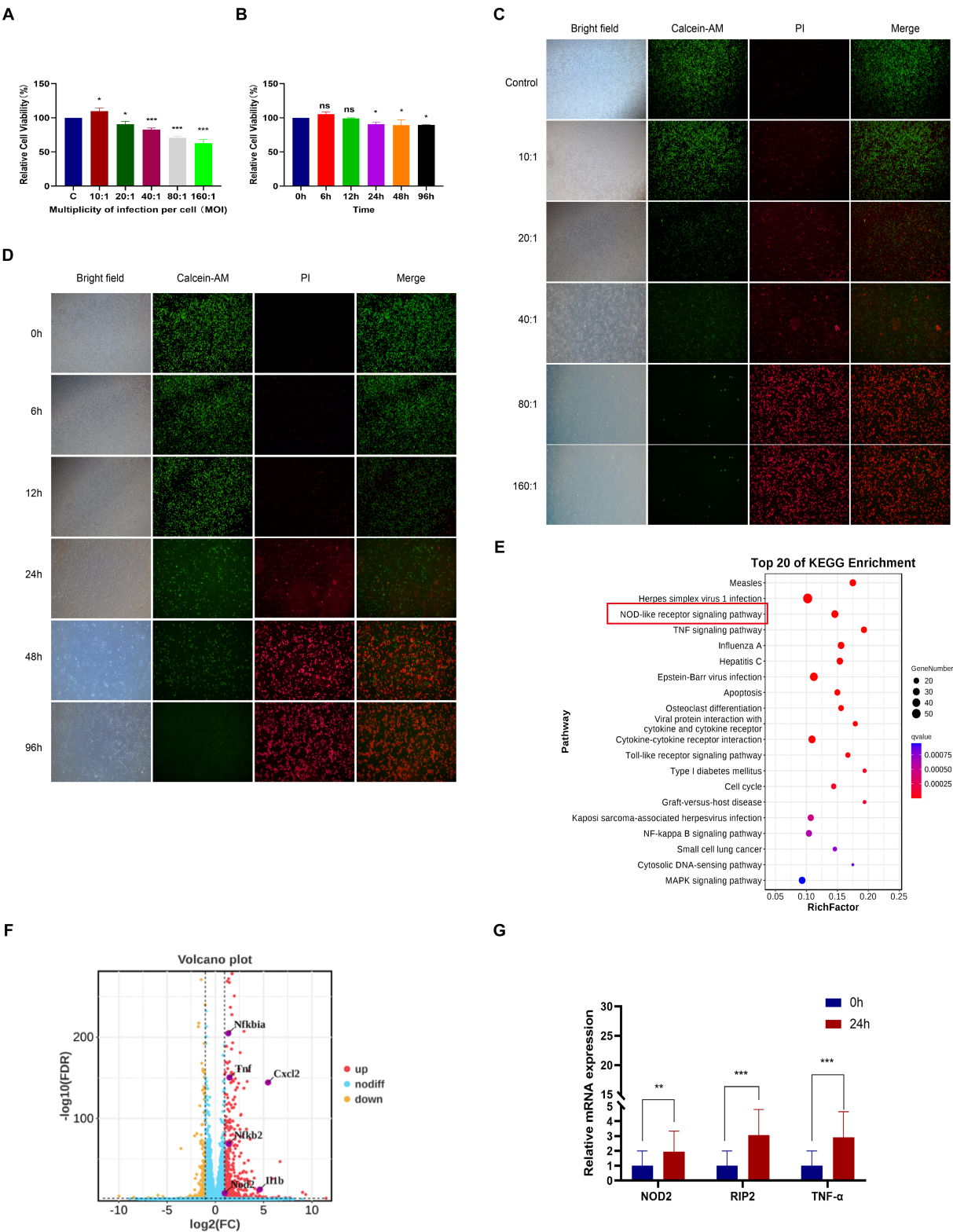


FIGURE 1 RNA-seq analysis of macrophages from mice infected with *M. pneumoniae*. **(A)** CCK-8 detection results after Mp infected RAW264.7 cells at different MOIs for 24 h. **(B)** CCK-8 detection results of RAW264.7 cells infected with Mp (MOI = 10) for different times. **(C)** The results were observed by immunofluorescence after Mp infected RAW264.7 cells at different MOIs for 24 h. **(D)** Immunofluorescence observation results of RAW264.7 cells infected with Mp (MOI = 10) for different times. **(E)** KEGG enrichment analysis diagram of differentially expressed genes. **(F)** Volcano plot of differentially expressed genes between the infected group and the control group. **(G)** qPCR validation of NOD2 signaling pathway-related gene expression in RNA-Seq. The data represent three independent treatments, and *p*-values were calculated using the one-way ANOVA test. SD, error bars; ns, not significant; **p* < 0.05, ***p* < 0.01, ****p* < 0.001.

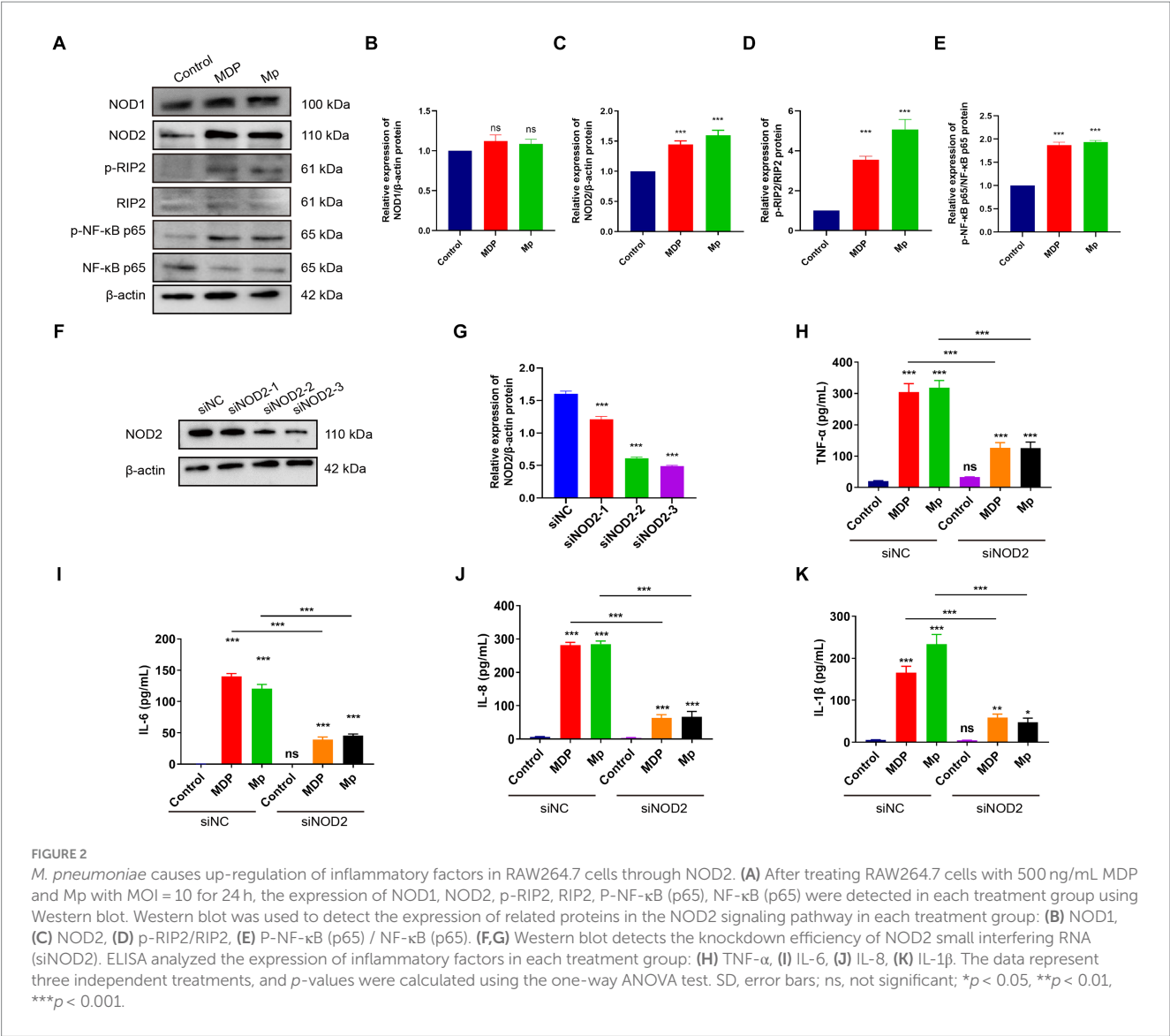


TABLE 1 12 *M. pneumoniae* proteins.

Accession	Protein name	Subcellular location	VirulentPred
P75089	Fructose-bisphosphate aldolase	Cytoplasm	Non-Virulent
A0A0H3DPP5	30S ribosomal protein S17	Cytoplasm	Virulent
A0A449A1T4	DUF16 family-like protein	Uncharacterized	Virulent
A0A0H3DP25	30S ribosomal protein S5	Cytoplasm	Virulent
A0A449A0G9	Uncharacterized protein	Cell membrane	Non-Virulent
A0A449A0R9	Pyruvate dehydrogenase E1 component subunit alpha	Cytoplasm	Non-Virulent
A0A449A0P5	Pyruvate dehydrogenase E1 component, beta subunit	Cytoplasm	Non-Virulent
A0A449A0R7	Dihydropolyl dehydrogenase	Uncharacterized	Non-Virulent
A0A7I8HMOV6	P1 adhesin type 2 g2	Cell membrane	Virulent
A0A7I8HMI2	P40/P90 adhesin	Cell membrane	Virulent
A0A449A1T5	MG032/MG096/MG288 family 2	Uncharacterized	Non-Virulent
P75295	Uncharacterized protein MPN_491	Cell membrane	Virulent

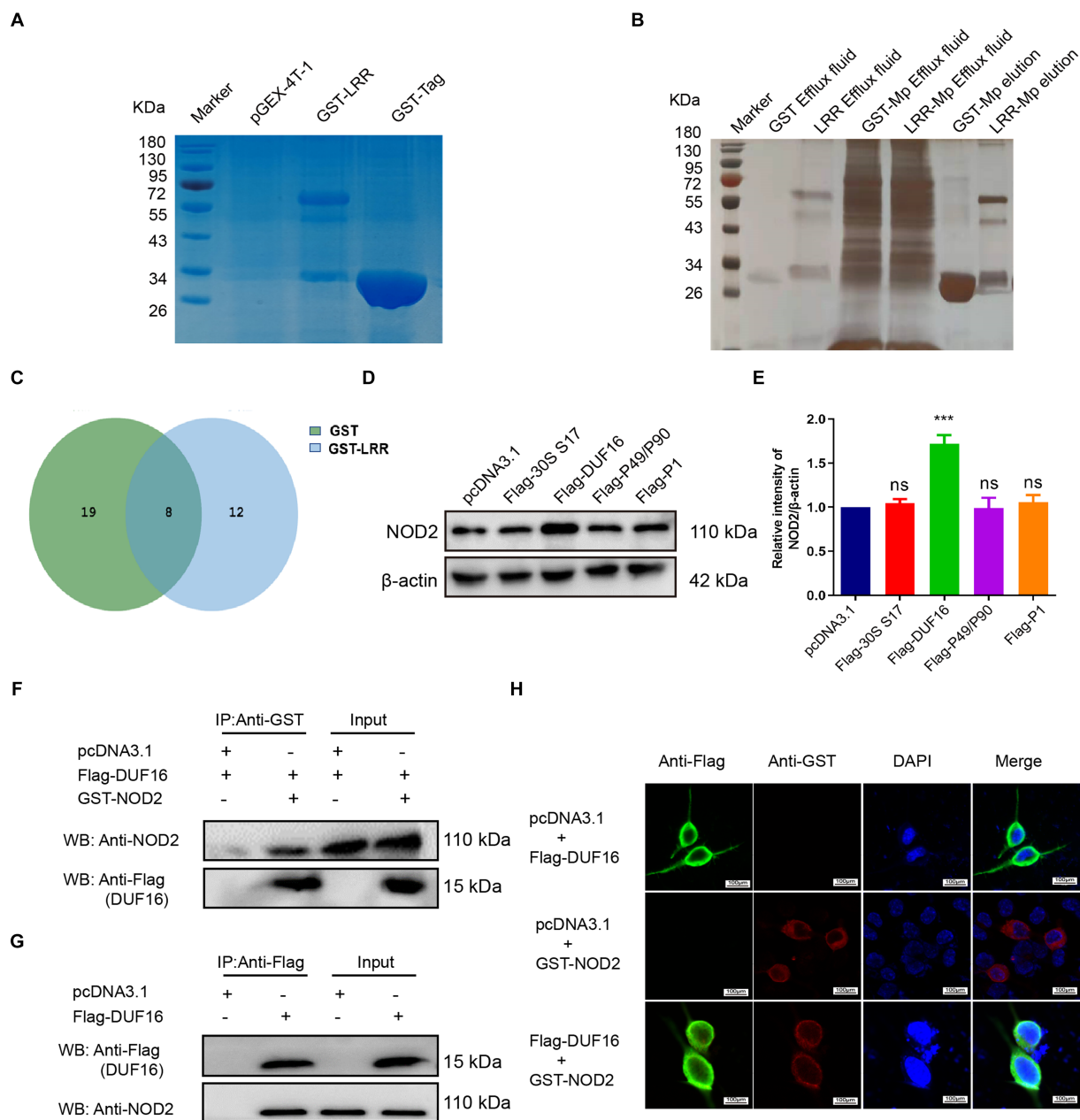


FIGURE 3

Screening and identification of *M. pneumoniae* proteins that interact with NOD2. (A) SDS-PAGE analysis of purified GST-tagged protein and GST-LRR protein. (B) Silver staining detection pictures of each group after GST pull-down. (C) Venn diagram of differential proteins in elution samples from the GST and GST-LRR groups. (D) After the eukaryotic plasmids of four Mp proteins (30S ribosomal protein S17, DUF16 family-like protein, P1 adhesin type 2g2, and P40/P90 adhesin) were transfected into RAW264.7 cells for 48 h, the protein expression was identified by Western blot. (E) Histogram of NOD2 expression in each transfection group. (F) Co-precipitation of NOD2 protein with recombinant DUF16 in 293T cell lysate. (G) Co-precipitation (Internal reverse IP) of NOD2 protein with DUF16 in RAW264.7 cell lysate. (H) Confocal microscopy analysis was carried out for demonstrating colocalization of NOD2 (red fluorescence) and DUF16 (green fluorescence). The data represent three independent treatments, and *p*-values were calculated using the one-way ANOVA test. SD, error bars; ns, not significant; ****p* < 0.001.

We identified 4 proteins that may activate NOD2 through information such as subcellular localization, virulence function prediction, and biological function of 12 proteins. For further verification, we selected the four most likely proteins: 30S ribosomal protein S17(30S), DUF16 family-like protein (DUF16), P1 adhesin type 2g2 (P1), and P40/P90 adhesin (P40/P90). We transfected S17(30S), DUF16, P1 and P40/P90 into RAW264.7 (Supplementary Figure S2), and identified the expression of NOD2 in transfected cells, we found that only RAW264.7

cell transfected with DUF16 trigger the overexpression of NOD2 (Figures 3D,E). It indicates that DUF16 might be the specific protein in *M. pneumoniae* for the activation of NOD2. To further validate the interaction between DUF16 and NOD2, we Co-transfection of 293T cells with the DUF16 tagged with Flag (Flag-DUF16) and NOD2 tagged with GST. Co-IP revealed the presence of DUF16 only in the presence of NOD2 (Figure 3F). The same results were found in RAW264.7 transfected with DUF16 (Figure 3G). Additionally,

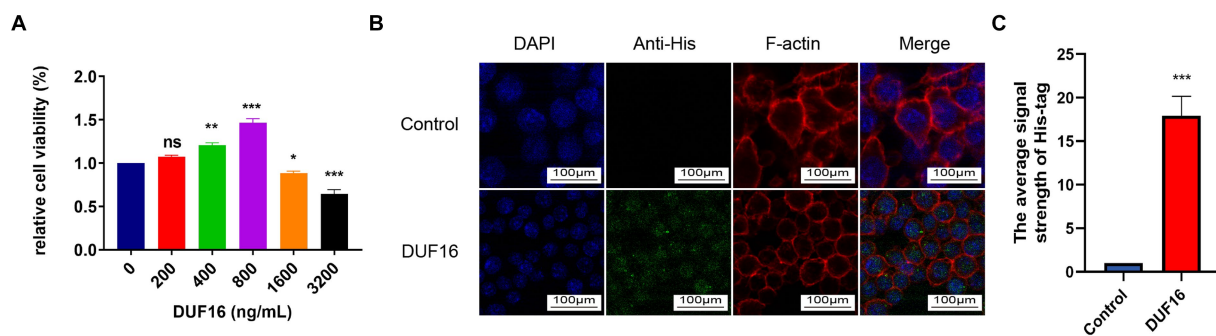


FIGURE 4

DUF16 protein can be phagocytosed by RAW264.7 cells. (A) After RAW264.7 cells were treated with different concentrations of His-DUF16 recombinant protein for 24 h, Cell Counting Kit-8 was used to detect cell viability. (B) His-DUF16 protein is phagocytosed by RAW264.7 cells. (C) Histogram of His-DUF16 content in each treatment group. The data represent three independent treatments, and *p*-values were calculated using the one-way ANOVA test. SD, error bars; ns, not significant; **p* < 0.05, ***p* < 0.01, ****p* < 0.001.

co-localization analysis via laser confocal microscopy showed DUF16 and NOD2 co-localizing in the cytoplasm in 293T cells transfected with DUF16 and NOD2 (Figure 3H). Thus, our findings support that the DUF16 protein of *M. pneumoniae* interacts with the host cell NOD2.

3.4 DUF16 protein can be phagocytosed by macrophages

To study the function of DUF16 protein, we obtained recombinant DUF16 (His-DUF16) protein using the *E. coli* expression system (Supplementary Figure S3). The concentration of DUF16 treatment in subsequent experiments was determined by assessing the relative cell viability of DUF16-treated macrophages using CCK8. Our results showed that DUF16 significantly reduced the viability of uninfected cells at a concentration of 1,600 ng/mL (Figure 4A). We determined the concentration of DUF16 treatment in subsequent experiments to be 1,600 ng/mL. NOD2 is an intracellular Pattern Recognition Receptor. therefore, we performed colocalization analysis of recombinant DUF16 protein and RAW264.7 cells using immunofluorescence to confirm whether macrophages can phagocytose DUF16. Our results revealed the presence of DUF16 protein (green fluorescence) in the cytoplasm of RAW264.7 cells in the experimental group, while no green fluorescence signal was observed in the control group (Figure 4B). It shown that macrophages are capable of phagocytosing DUF16 protein.

3.5 DUF16 induces macrophage inflammatory response through NOD2/RIP2/NF-κB

To investigate the pro-inflammatory effects of DUF16 on macrophages through NOD2, we utilized small interfering (siRNA)-NOD2 to downregulate NOD2 expression for a 12-h duration. Subsequently, RAW264.7 cells were treated with DUF16 protein for 24h. The levels of inflammatory cytokines, including IL-1β, IL-6, IL-8, and TNF-α, were quantified using ELISA (Figures 5A–D). The results demonstrated a significant reduction in the expression of

inflammatory factors upon NOD2 suppression compared to the control group. Additionally, DUF16 displayed a notable ability to enhance the expression of inflammatory factors in macrophages, similar to the effects observed with MDP (NOD2 activator). NOD2 knockdown significantly reduced the expression of inflammatory factors induced by DUF16. Interestingly, even when NOD2 was knocked down and cells were treated with DUF16 domain proteins, the secretion of inflammatory factors persisted, suggesting the possible involvement of other pattern recognition receptors such as TLRs. These findings indicate that DUF16 protein can stimulate macrophages to secrete inflammatory factors via NOD2. To investigate the involvement of the NOD2/RIP2/NF-κB signaling pathway in DUF16-induced macrophage inflammation, we utilized siRNA-NOD2 to knock down NOD2. Macrophages were then treated with DUF16 for 24h, and the expressions of NOD2, p-RIP2, RIP2, p-NF-κB p65, NF-κB p65, p-IKB α, and IKB α were assessed. The results indicated that the DUF16 upregulated the expression of NOD2, p-RIP2, p-NF-κB p65, and p-IKB α in the macrophage NOD2 signaling pathway, while downregulating the expression of IKBα. Moreover, NOD2 knockdown diminished the impact of DUF16 on the elevated expression of p-RIP2, p-NF-κB p65 and p-IKB α compared to the siNC+DUF16 group (Figures 5E–I). These findings suggest that DUF16 elicits cellular inflammatory responses through the NOD2/RIP2/NF-κB signaling pathway.

3.6 13–90 aa is a critical region for DUF 16 function

To identify the specific region where DUF16 interacts with the host protein NOD2 to induce cellular inflammation, we conducted a multiple sequence alignment of various proteins within the DUF16 family using the Clustal Omega tool.³ Our analysis revealed a conserved region in the DUF16 protein family (Supplementary Figure S4). In order to further investigate whether DUF16 activates NOD2 through this conserved structural region, we designed and constructed different

³ <https://www.ebi.ac.uk/Tools/msa/clustalo/>

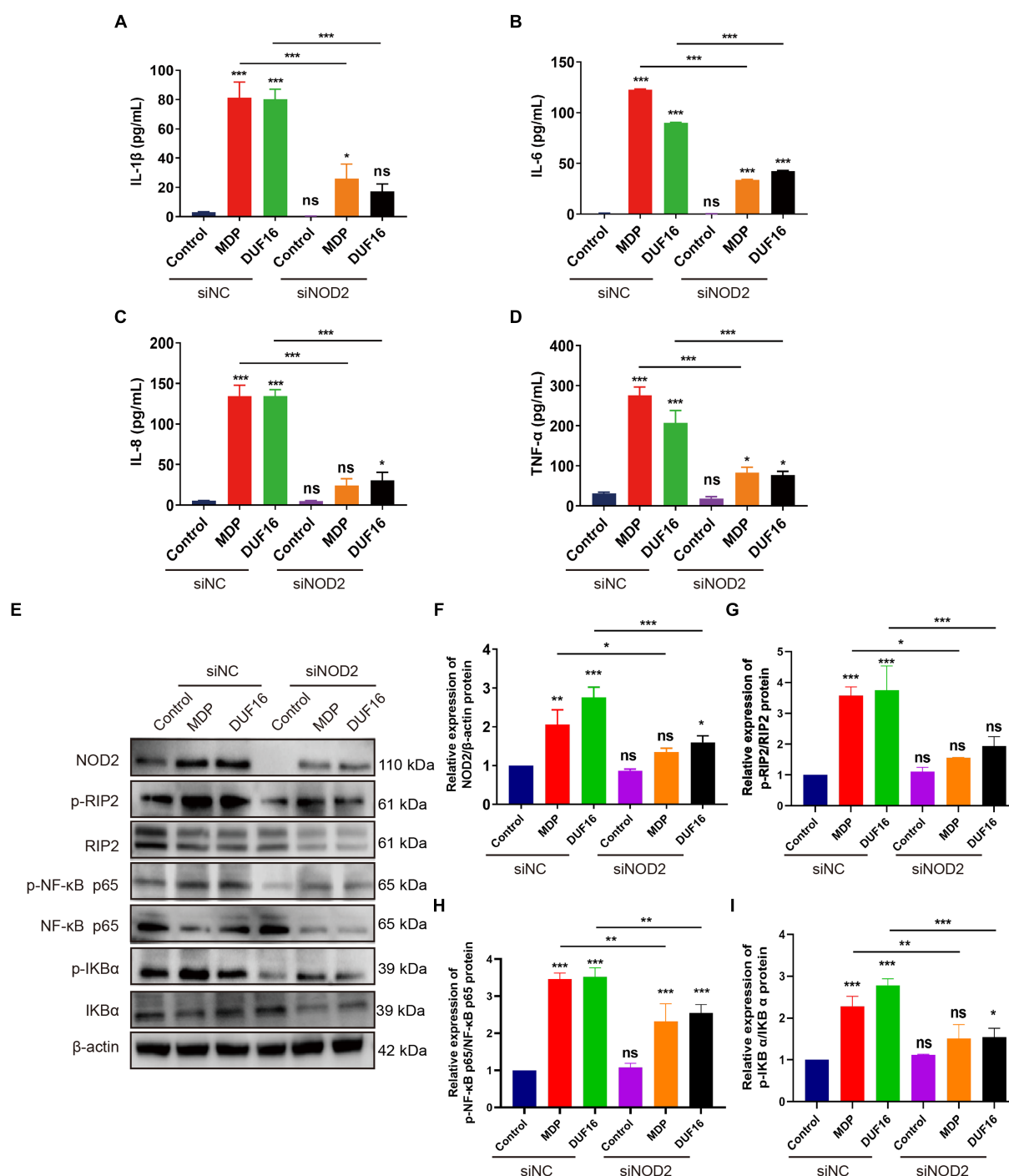


FIGURE 5

DUF16 protein induces an inflammatory response in mouse macrophages through NOD2. ELISA analyzed the expression of inflammatory factors in each treatment group: (A) IL-1 β , (B) IL-6, (C) IL-8, (D) TNF- α . (E) The expression changes of NOD2, p-RIP2, RIP2, P-NF- κ B (p65), NF- κ B (p65), p-IKB α , and IKB α were detected using Western blot analysis in RAW264.7 cells induced by His-DUF16 (1,600 ng/mL) protein and MDP (500 ng/mL). Histogram of protein expression of NOD2 signaling pathway in cells of each treatment group detected by Western blot analysis: (F) NOD2, (G) p-RIP2/RIP2, (H) P-NF- κ B (p65) / NF- κ B (p65), (I) p-IKB α /IKB α . The data represent three independent treatments, and p -values were calculated using the one-way ANOVA test. SD, error bars; ns, not significant; * p < 0.05, ** p < 0.01, *** p < 0.001.

truncated versions of DUF16 (Figure 6A). These truncated constructs were then transfected into RAW264.7 cells, and the subsequent expression of NOD2 in the transfected cells was assessed using Western blotting. The results revealed that both Flag- Δ 1 (1-90 aa) and Flag- Δ 3 (13-276 aa) significantly increased the expression of NOD2 in

macrophages compared to RAW264.1 cells transfected with pCDN3.1 (control) (Figures 6B,C). However, transfection of RAW264.7 cells with Flag- Δ 2 (91-276 aa) did not induce the expression of NOD2. These findings suggest that the 13-90 fragment of DUF16 is critical for NOD2 activation. To further confirm the key interaction areas between

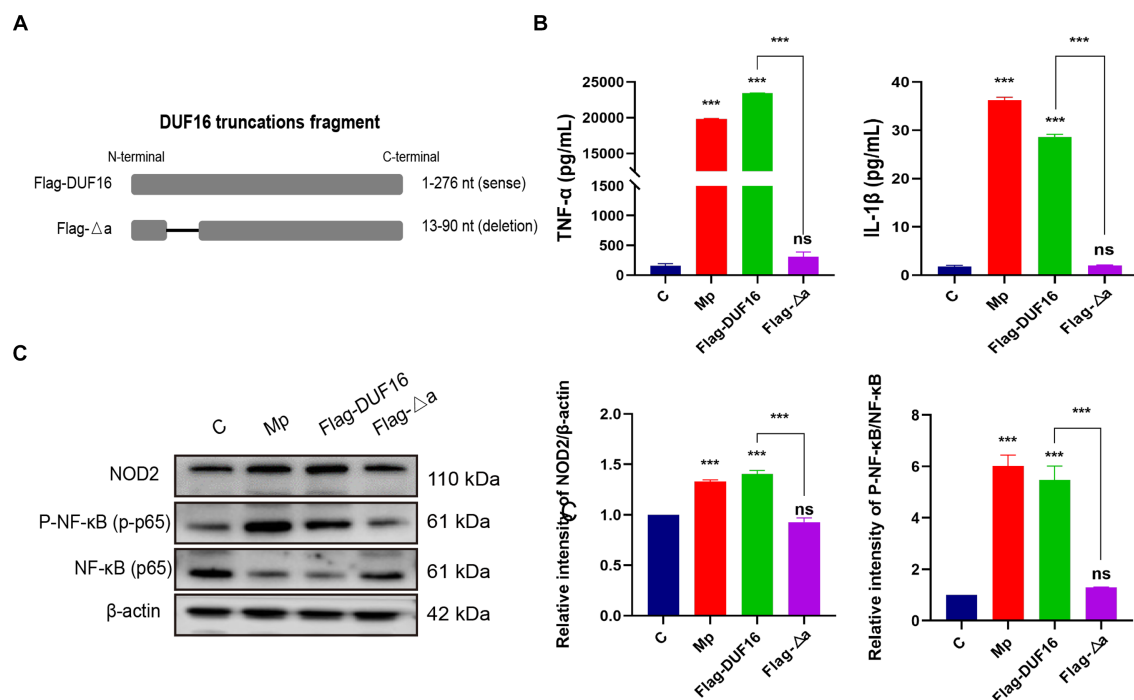


FIGURE 7

13–90 aa is a critical region for DUF 16 to trigger cellular NOD2-mediated inflammatory responses. (A) A truncated expression vector was designed and constructed based on the DUF16 interaction region. (B) After RAW264.7 cells were treated with Mp, DUF16 or Flag-Δa, respectively, for 24 h, TNF-α and IL-1β in the cell supernatants of each group were detected by ELISA. (C) The expression changes of NOD2, RIP2, p-NF-κB p65, NF-κB p65 were detected using Western blot analysis in RAW264.7 cells induced by 4 treatment groups (Control, Mp, DUF16 and Flag-Δa). The data represent three independent treatments, and *p*-values were calculated using the one-way ANOVA test. SD, error bars; ns, not significant; ****p* < 0.001.

DUF16 and NOD2, Flag-Δ1 (1–90 aa), Flag-Δ2 (91–276 aa), Flag-Δ3 (13–276 aa), and GST-NOD2 were co-transfected into 293T (Figures 6D,F,H) or RAW264.7 (Figures 6E,G,I) cells, followed by Co-IP verification. The results showed that both Flag-Δ1 (1–90 aa) and Flag-Δ3 (13–276 aa) interacted with NOD2, while Flag-Δ2 (91–276 aa) could not interact with NOD2. These findings indicate that the DUF16 (13–90 aa) region plays a critical role as a phase activator of NOD2 in macrophages.

3.7 DUF16 Δ13–90 region is crucial for NOD2/RIP2/NF-κB include inflammatory in macrophage

To further investigate the function of the critical region of DUF 16, we constructed a truncation mutant (Flag-Δa) of this region, as shown in Figure 7A. The truncated construct was then transfected into RAW264.7 cells for 48 h, while *M. pneumoniae* and DUF16 proteins were used to treat macrophages for 24 h, respectively. Subsequent expression of NOD2 in cells from each treatment group was assessed using Western blotting. The experimental results revealed that both *M. pneumoniae* and DUF16 significantly increased the expression of TNF-α and IL-1β in macrophages (Figure 7B). In contrast, Flag-Δa did not show the same effect after transfection into macrophages. Additionally, Western blot analysis demonstrated that both *M. pneumoniae* and DUF16 significantly increased the expression of RIP2 and P-NF-κB p65 in the macrophage NOD2 signaling pathway (Figure 7C). On the other hand, Flag-Δa did not show such an effect.

These results indicate that the 13–90 amino acid region plays a critical role in DUF16-induced inflammation.

4 Discussion

M. pneumoniae, an atypical microorganism without a cell wall, is a key contributor to community-acquired pneumonia (CAP). The initial immune response against this pathogen is mediated by pattern recognition receptors of the innate immune system. Previous studies have predominantly focused on the interplay between *M. pneumoniae* and Toll-like receptors (TLRs) (Shimizu, 2015; Shimizu, 2016). TLR2, TLR6 (or TLR1), and TLR4 can detect mycoplasma lipoproteins via their extracellular leucine repeats, leading to the induction of macrophage autophagy and the production of pro-inflammatory cytokines like IL-1β and TNF-α (Shimizu, 2016). Our study indicates that infection with *M. pneumoniae* in mouse macrophages leads to the increased expression of genes associated with the NOD2 signaling pathway and the release of inflammatory cytokines (see Figures 1, 2). This strongly implies the involvement of the NOD2 pathway in the macrophage inflammatory response triggered by *M. pneumoniae*. This discovery is consistent with our prior finding that *Mycoplasma ovipneumoniae* induces macrophage autophagy through NOD2. NOD proteins encompass NOD1 and NOD2, belonging to a class of intracellular pattern recognition receptor proteins. Both NOD1 and NOD2 are capable of detecting bacterial peptidoglycan fragments, leading to the activation of pro-inflammatory and antibacterial responses. NOD1 and NOD2 show similarities in structure and signaling pathways. Our experimental results found that

M. pneumoniae seems to activate NOD2 but not NOD1. However, further experimental studies are required to confirm this finding.

NOD2, a critical intracellular receptor for pattern recognition (PRR) within the NOD-like family of receptors, is produced by different types of cells, such as T cells, B cells, and macrophages (Al Nabhani et al., 2017). NOD2 detects bacterial PAMPs including muramyl dipeptide (Mukherjee et al., 2019), leading to the induction of host cell inflammation. Interestingly, NOD2 has also been found to detect microorganisms that lack cell walls, such as single-stranded RNA viruses and parasites, triggering an inflammatory response in host cells (Sabbah et al., 2009; Al Nabhani et al., 2017; Kuss-Duerkop and Kestra-Gounder, 2020). Despite lacking a cell wall, mycoplasmas possess several virulence factors, including adhesins, glycolipids, toxic metabolites, community-acquired respiratory distress syndrome (CARDS) toxins, capsular polysaccharides, and numerous cell surface antigens, as well as putative lipoprotein-coding genes in their genome (Cloward and Krause, 2009; Lluch-Senar et al., 2015; Shimizu, 2015; Chaudhry et al., 2016). This indicates that the absence of a cell wall in *M. pneumoniae* does not imply the absence of the bacterial intracellular pathway for muropeptides. Based on this information, we hypothesized that cell surface antigens and putative mycoplasmal lipoproteins of *M. pneumoniae* could act as ligands for NOD2 activation. Previous studies have shown an interaction between *Mycoplasma hyopneumoniae* lipoprotein Mhp390 and host NOD1, where binding to Mhp390 can stimulate pro-inflammatory cytokines production in PAMs, such as TNF- α (Liu et al., 2022). In this study, we employed pull-down combined with MS technology to screen and identify 12 potential interacting proteins with NOD2. Using various techniques, we confirmed that DUF16 can penetrate macrophages and activate the NOD2/RIP2/NF- κ B signaling pathway, resulting in macrophage inflammatory response through its interaction with the NOD2 protein (Figures 3–6). Notably, this study is the first to identify DUF16 from *M. pneumoniae* as a specific protein that interacts with NOD2.

The DUF16 family consists of 33 members, with 26 members exclusively found in *M. pneumoniae*. Among the 88 hypothetical proteins of *M. pneumoniae*, 26 proteins are part of the DUF16 family and have conserved regions ranging from 13 bp to 90 bp (Shin et al., 2006). It is worth noting that all DUF16 family members in *M. pneumoniae* are considered essential genes (Shin et al., 2006). However, the specific function of the DUF16 protein remains poorly understood. Our research findings indicate that the DUF16 protein can activate NOD2 in macrophages, leading to an inflammatory response.

We have also observed that the 13 bp–90 bp region of the DUF16 protein is crucial for NOD2 activation. Deletion of this region results in the loss of NOD2-induced macrophage inflammation. These findings raise several important questions. Do other types of mycoplasma trigger macrophage NOD2-dependent inflammatory responses using similar proteins? Can mycoplasma induce macrophage inflammatory responses through other pattern recognition receptors? Can the DUF16 protein be utilized as a novel immune activator for the development of new vaccines? Further investigation is required to address these questions. The emergence of clinically significant acquired macrolide resistance has become a global concern and poses challenges in the treatment of *M. pneumoniae* pneumonia. Extensive research is urgently needed to understand the pathogenesis of *M. pneumoniae*, identify novel causative factors, develop advanced detection methods, and design effective vaccines. We hope that our research can provide valuable insights into these areas.

This study revealed that *M. pneumoniae* can trigger NOD2-dependent inflammatory reactions in macrophages. Furthermore, we discovered a new virulence factor in *M. pneumoniae* called the DUF16 protein. This specific protein triggers the inflammatory reaction in macrophages by activating the NOD2/RIP2/NF- κ B signaling pathway. These discoveries present new opportunities for identifying molecular targets for detecting *M. pneumoniae* and offer a starting point for exploring its mechanisms of infection and disease development.

Data availability statement

The original contributions presented in the study are publicly available. This data can be found in the NCBI BioProject repository, accession number PRJNA1111650.

Author contributions

YW: Data curation, Formal analysis, Investigation, Software, Writing – original draft, Methodology, Writing – review & editing. CM: Writing – review & editing. XH: Methodology, Writing – review & editing. WW: Formal analysis, Methodology, Writing – review & editing. HL: Conceptualization, Formal analysis, Supervision, Writing – original draft, Writing – review & editing. ML: Supervision, Funding acquisition, Writing – review & editing.

Funding

The author(s) declare that financial support was received for the research, authorship, and/or publication of this article. This study is supported by grants from National Natural Foundation of China (grant number NSFC 32370198 and NSFC U22A20505).

Acknowledgments

We express our gratitude to all the fellow researchers at the Key Laboratory of the Ministry of Education for the Conservation and Utilization of Unique Biological Resources in Western China.

Conflict of interest

The authors declare that the research was conducted in the absence of any commercial or financial relationships that could be construed as a potential conflict of interest.

Publisher's note

All claims expressed in this article are solely those of the authors and do not necessarily represent those of their affiliated organizations, or those of the publisher, the editors and the reviewers. Any product

that may be evaluated in this article, or claim that may be made by its manufacturer, is not guaranteed or endorsed by the publisher.

Supplementary material

The Supplementary material for this article can be found online at: <https://www.frontiersin.org/articles/10.3389/fmicb.2024.1391453/full#supplementary-material>

References

- Al Nabhani, Z., Dietrich, G., Hugot, J. P., and Barreau, F. (2017). Nod2: the intestinal gate keeper. *PLoS Pathog.* 13:e1006177. doi: 10.1371/journal.ppat.1006177
- Alipour, S. D., and Mirsaedi, M. (2021). Inborn errors in the Lrr domain of Nod2 and their potential consequences on the function of the receptor. *Cells* 10:2031. doi: 10.3390/cells10082031
- Caruso, R., Warner, N., Inohara, N., and Núñez, G. (2014). Nod1 and Nod2: signaling, host defense, and inflammatory disease. *Immunity* 41, 898–908. doi: 10.1016/j.immuni.2014.12.010
- Chaudhry, R., Ghosh, A., and Chandolia, A. (2016). Pathogenesis of *Mycoplasma Pneumoniae*: an update. *Indian J. Med. Microbiol.* 34, 7–16. doi: 10.4103/0255-0857.174112
- Cloward, J. M., and Krause, D. C. (2009). *Mycoplasma Pneumoniae* J-domain protein required for terminal organelle function. *Mol. Microbiol.* 71, 1296–1307. doi: 10.1111/j.1365-2958.2009.06602.x
- Cole, J., Aberdein, J., Jubrail, J., and Dockrell, D. H. (2014). The role of macrophages in the innate immune response to streptococcus pneumoniae and *Staphylococcus Aureus*: mechanisms and contrasts. *Adv. Microb. Physiol.* 65, 125–202. doi: 10.1016/b.sampbs.2014.08.004
- de Groot, R. C. A., Zhu, H., Hoogenboezem, T., de Bruijn, A., Eenjes, E., 't Jong, A. E. J., et al. (2022). *Mycoplasma Pneumoniae* compared to *Streptococcus Pneumoniae* avoids induction of proinflammatory epithelial cell responses despite robustly inducing Th2 signaling. *Infect. Immun.* 90:e0012922. doi: 10.1128/iai.00129-22
- Dominguez-Martínez, D. A., Núñez-Avellaneda, D., Castañón-Sánchez, C. A., and Salazar, M. I. (2018). Nod2: activation during bacterial and viral infections, polymorphisms and potential as therapeutic target. *Rev. Invest. Clin.* 70, 18–28. doi: 10.24875/ric.17002327
- Godkovicz, M., and Druszczyńska, M. (2022). NOD1, NOD2, and NLRC5 receptors in antiviral and antimycobacterial immunity. *Vaccine* 10:1487. doi: 10.3390/vaccines10091487
- Kenri, T. (2023). Genetic manipulation of *Mycoplasma Pneumoniae*. *Methods Mol. Biol. (Clifton, NJ)* 2646, 347–357. doi: 10.1007/978-1-0716-3060-0_29
- Kumar, S. (2018). *Mycoplasma Pneumoniae*: a significant but underrated pathogen in Paediatric community-acquired lower respiratory tract infections. *Indian J. Med. Res.* 147, 23–31. doi: 10.4103/ijmr.IJMR_1582_16
- Kuss-Duerkop, S. K., and Keestra-Gounder, A. M. (2020). Nod1 and Nod2 activation by diverse stimuli: a possible role for sensing pathogen-induced endoplasmic reticulum stress. *Infect. Immun.* 88:e00898-19. doi: 10.1128/iai.00898-19
- Lanao, A. E., Chakraborty, R. K., and Pearson-Shaver, A. L. (2024). "Mycoplasma infections" in *Statpearls* (Treasure Island, FL: StatPearls Publishing Ineligible companies. Disclosure: Rebanta Chakraborty declares no relevant financial relationships with ineligible companies. Disclosure: Anthony Pearson-Shaver declares no relevant financial relationships with ineligible companies).
- Lee, H., Yun, K. W., Lee, H. J., and Choi, E. H. (2018). Antimicrobial therapy of macrolide-resistant *Mycoplasma Pneumoniae* pneumonia in children. *Expert Rev. Anti-Infect. Ther.* 16, 23–34. doi: 10.1080/14787210.2018.1414599
- Liu, W., Jiang, P., Yang, K., Song, Q., Yuan, F., Liu, Z., et al. (2022). *Mycoplasma Hyopneumoniae* infection activates the Nod1 signaling pathway to modulate inflammation. *Front. Cell. Infect. Microbiol.* 12:927840. doi: 10.3389/fcimb.2022.927840
- Lluch-Senar, M., Cozzuto, L., Cano, J., Delgado, J., Llórens-Rico, V., Pereyre, S., et al. (2015). Comparative "-omics" in *Mycoplasma Pneumoniae* clinical isolates reveals key virulence factors. *PLoS One* 10:e0137354. doi: 10.1371/journal.pone.0137354
- Luo, H., Wu, X., Xu, Z., Hao, X., Wang, Y., and Li, M. (2020). Nod2/C-Jun Nh(2)-terminal kinase triggers *Mycoplasma Ovipneumoniae*-induced macrophage autophagy. *J. Bacteriol.* 202:e00689-19. doi: 10.1128/jb.00689-19
- Mukherjee, T., Hovingh, E. S., Foerster, E. G., Abdel-Nour, M., Philpott, D. J., and Girardin, S. E. (2019). Nod1 and Nod2 in inflammation, immunity and disease. *Arch. Biochem. Biophys.* 670, 69–81. doi: 10.1016/j.abb.2018.12.022
- Negróni, A., Pierdomenico, M., Cucchiara, S., and Stronati, L. (2018). Nod2 and inflammation: current insights. *J. Inflamm. Res.* 11, 49–60. doi: 10.2147/jir.S137606
- Sabbah, A., Chang, T. H., Harnack, R., Frohlich, V., Tominaga, K., Dube, P. H., et al. (2009). Activation of innate immune antiviral responses by Nod2. *Nat. Immunol.* 10, 1073–1080. doi: 10.1038/ni.1782
- Shamaei, M., and Mirsaedi, M. (2021). Nontuberculous mycobacteria, macrophages, and host innate immune response. *Infect. Immun.* 89:e0081220. doi: 10.1128/iai.00812-20
- Shimizu, T. (2015). Pathogenic factors of *Mycoplasma*. *Nihon Saikingaku Zasshi* 70, 369–374. doi: 10.3412/jsb.70.369
- Shimizu, T. (2016). Inflammation-inducing factors of *Mycoplasma Pneumoniae*. *Front. Microbiol.* 7:414. doi: 10.3389/fmicb.2016.00414
- Shimizu, T., Kida, Y., and Kuwano, K. (2005). A Dipalmitoylated lipoprotein from *Mycoplasma Pneumoniae* activates Nf-kappa B through Tlr1, Tlr2, and Tlr6. *J. Immunol. (Baltimore, Md: 1950)* 175, 4641–4646. doi: 10.4049/jimmunol.175.7.4641
- Shimizu, T., Kimura, Y., Kida, Y., Kuwano, K., Tachibana, M., Hashino, M., et al. (2014). Cytoadherence of *Mycoplasma Pneumoniae* induces inflammatory responses through autophagy and toll-like receptor 4. *Infect. Immun.* 82, 3076–3086. doi: 10.1128/iai.01961-14
- Shin, D. H., Kim, J. S., Yokota, H., Kim, R., and Kim, S. H. (2006). Crystal structure of the Duf16 domain of Mpn010 from *Mycoplasma Pneumoniae*. *Protein Sci.* 15, 921–928. doi: 10.1110/ps.051993506
- Strober, W., Murray, P. J., Kitani, A., and Watanabe, T. (2006). Signalling pathways and molecular interactions of Nod1 and Nod2. *Nat. Rev. Immunol.* 6, 9–20. doi: 10.1038/nri1747
- Takeuchi, O., and Akira, S. (2010). Pattern recognition receptors and inflammation. *Cell* 140, 805–820. doi: 10.1016/j.cell.2010.01.022
- Tong, L., Huang, S., Zheng, C., Zhang, Y., and Chen, Z. (2022). Refractory *Mycoplasma Pneumoniae* pneumonia in children: early recognition and management. *J. Clin. Med.* 11:2824. doi: 10.3390/jcm11102824
- Trindade, B. C., and Chen, G. Y. (2020). Nod1 and Nod2 in inflammation and infectious diseases. *Immunol. Rev.* 297, 139–161. doi: 10.1111/imr.12902
- Tsai, T. A., Tsai, C. K., Kuo, K. C., and Yu, H. R. (2021). Rational stepwise approach for *Mycoplasma Pneumoniae* pneumonia in children. *J. Microbiol. Immunol. Infect.* 54, 557–565. doi: 10.1016/j.jmii.2020.10.002
- Wicherska-Pawlowska, K., Wróbel, T., and Rybka, J. (2021). Toll-like receptors (TLRs), NOD-like receptors (NLRs), and RIG-I-like receptors (RLRs) in innate immunity. TLRs, NLRs, and RLRs ligands as immunotherapeutic agents for hematopoietic diseases. *Int. J. Mol. Sci.* 22:13397. doi: 10.3390/ijms222413397

Frontiers in Microbiology

Explores the habitable world and the potential of microbial life

The largest and most cited microbiology journal which advances our understanding of the role microbes play in addressing global challenges such as healthcare, food security, and climate change.

Discover the latest Research Topics

[See more →](#)

Frontiers

Avenue du Tribunal-Fédéral 34
1005 Lausanne, Switzerland
frontiersin.org

Contact us

+41 (0)21 510 17 00
frontiersin.org/about/contact

